A Clinician's Contribution to Biomedical Engineering in Experimental Echocardiography

The studies presented in this dissertation were financially supported by:

- La Fondation Bekales, Vaduz, Liechtenstein,
- La Fondation Vésale, Hôpital Saint Pierre, Bruxelles,
- Research Fellowship of the European Society of Cardiology,
- The Belgian American Educational Foundation, Brussels,
- The North Atlantic Treaty Organization, Brussels,
- National Aeronautics and Space Administration (grant NCC9-60), Houston,
- Institute for the Promotion of Innovation by Science and Technology in Flanders
- Interuniversity Cardiology Institute of the Netherlands (ICIN)
- Dutch Technology Foundation (STW)

Cover illustration: The montage, prepared by Jan Tuin, Thoraxcentre, Rotterdam, shows some biomedical engineering projects in which the author has been involved. The picture illustrates an electrocardiographic system that he built in 1983 using Fischertechnik™. The incrustations on the paper roll illustrate intravascular ultrasound (IVUS) developments of the last 5 years. On the first IVUS cross section, 32, 16 and 8 Gy isodoses (in purple) were computed for an Ir^{192} γ-source placed in the same position as the IVUS catheter (16 Gy was prescribed 2 mm off source centre). On the next IVUS, the same isodoses in yellow were computed for a Sr/Y^{90} β-source (see part 4). Next, a palpogram demonstrates the stiffness of a coronary plaque. A computer simulation demonstrated a similar low strain in the plaque, color-coded in red, from 1 to 3 o'clock and high strain values (in green) at the shoulders of the plaque (see part 3). Finally, one example of the IVUS flowmetry method is demonstrated (see part 2).

ISBN: 90-9015130-3

Printed by: AstraZeneca

A Clinician's Contribution to Biomedical Engineering in Experimental Echocardiography

Een klinische bijdrage aan technologische ontwikkelingen in de experimentele echocardiografie

PROEFSCHRIFT

ter verkrijging van de graad van doctor
aan de Erasmus Universiteit Rotterdam
op gezag van de Rector Magnificus
Prof.dr.ir. J.H. van Bemmel
en volgens besluit van het College voor Promoties

De openbare verdediging zal plaatsvinden op
woensdag 26 september 2001 om 15.45 uur

door

Stéphane Guy Carlier

geboren te Ath, België

PROMOTIECOMMISSIE

PROMOTOREN:	Prof.dr.ir. N. Bom Prof.dr. P.W. Serruys
OVERIGE LEDEN:	Dr.ir. A.F.W. van der Steen (tevens co-promotor) Prof.dr. J.R.T.C. Roelandt Prof. J.D. Thomas, MD Prof.dr.ir. P. Verdonck

Support by AstraZeneca Belgium for the publication of this thesis is gratefully acknowledged.

Generous sponsoring by Jomed / EndoSonics, Guidant, Cordis, Boston Scientific and Novoste is gratefully acknowledged.

To the women I did not love the way they deserved it,
because I was running too much for this project
and Corine, my best sister, alas was among them;

To Tina, who had the endurance to run with me
and who has the courage to give us another challenge now;

To my parents, who did everything they could for this achievement;

CONTENTS

INTRODUCTION

INTRODUCTION

The research of this thesis has been focused on the biomedical engineering aspects of new techniques of echocardiography. In close collaboration with the engineers of the Experimental Echocardiography Department of the Thoraxcentre, Erasmus University, Rotterdam, new methods to measure coronary blood flow and arterial wall elasticity with intravascular ultrasound (IVUS) have been developed. We have also investigated the clinical application of these measurements and have tried to improve traditional techniques based on intracoronary Doppler wires. In another field, we have developed a method to determine the radiation dose delivered in the wall of coronary arteries treated with brachytherapy, in collaboration with the Emory University, Atlanta, GA. This method utilizes 3-dimensional IVUS reconstruction combined with radiotherapy treatment planning. Finally, the tools developed for the recording of the signals of intracoronary Doppler wires have been adapted, during a stay at the Cleveland Clinic Foundation, OH, for the study of left ventricular mechanics and the compliance of the large arteries. This has been achieved by simultaneous acquisition of non-invasive pressure (with tonometry) and flow (with transthoracic Doppler echocardiography) signals. The fruits of an old and close collaboration with the Institute Biomedical Technology of the Ghent University can also be found in different chapters. This work is subdivided in five major parts, and a detailed introductory chapter precedes each one.

What is biomedical engineering?

Following the report of a panel of experts of the NIH (National Institutes of Health), biomedical engineering is rooted in physics, mathematics, chemistry, biology and life sciences. It is the application of a systematic, quantitative and integrative way of thinking about and approaching solutions to problems that are important to biology, medical research and population studies. The NIH definition is the following: "Bioengineering integrates physical, chemical or mathematical sciences and engineering principles for the study of biology, medicine, behavior or health. It advances fundamental concepts, creates knowledge from the molecular to the organ systems levels, and develops innovative biologics, material, processes, implants, devices, and informatics approaches for the prevention, diagnosis, and treatment of disease, for patient rehabilitation, and for improving health."

Biomedical engineering is the fastest growing specialty at engineering schools today. In the United States alone, there are 10,000 companies specializing in medical devices, diagnostic products and health information systems, creating opportunities for many of these new engineers. Efforts span from using engineering principles to help decipher the intricacies of cell signaling, to developing new imaging technologies. Bioengineering-related research projects require a multidisciplinary team of engineers, computer scientists, mathematicians, physicists, physicians and biologists to work on biological problems. As an illustration, table 1 summarizes the ever-expanding number of different societies where "bioengineers" can be found, and their related peer-review journals.

Table 1: Bioengineering and biomedical societies and journals (focusing on ultrasound)

Acoustical Society of America	Journal of the Acoustical Society of America
American Association for the Advancement of Science	Science
American Medical Informatics Association	Journal of the American Medical Informatics Association
American Society of Mechanical Engineers	Journal of Biomechanical Engineering Annual Reviews
Association for the Advancement of Medical Instrumentation	Biomedical Instrumentation and Technology
Biomedical Engineering Society	Annals of Biomedical Engineering Biomedical Engineering Society Bulletin
Biophysical Society	Biophysical Journal
Controlled Release Society	Journal of Controlled Release
European Federation of Societies For Ultrasound in Medicine and Biology	European Journal of Ultrasound
International Federation for Medical and Biological Engineering	IFBME news and clinical engineering update Medical and Biological Engineering and Computing
International Society for Optical Engineering	Journal of Biomedical Optics
Institute of Electrical and Electronics Engineers	IEEE EMBS Book Series IEEE Engineering in Medicine and Biology Magazine IEEE Transactions on Biomedical Engineering IEEE Transactions on Medical Imaging IEEE Transactions on Neural Systems and Rehabilitation IEEE Transactions on Ultrasonics, Ferroelectrics and Frequency Control
National Science Foundation	NSF Engineering Senior Design Projects to Aid the Disabled
Society for Biomaterials	Journal of Biomedical Materials Research
World Federation for Ultrasound in Medicine and Biology	Ultrasound in Medicine and Biology
Others	Annual Reviews in Biomedical Engineering Biomaterials Clinical Biomechanics Dental Materials Journal of Biomechanics Medical Engineering and Physics Ultrasonics Ultrasonic Imaging

The most important areas of biomedical engineering are thought to be computational science, imaging and tissue engineering:

Genome: the genome project, the increasing demand of gene sequencing and the functional genomics application, studying how genes are turned on and off and how proteins interact, require the most powerful computers available to present, manipulate, visualize, understand or exchange these data. Other bioengineering developments that require similar extensive number-crunching performances include artificial sight, life-support in hostile environments such as space flights, and nanotechnologies;

Imaging: visualization needs range from three-dimensional x-ray crystallography to functional imaging of organs, with the integration of the fourth dimension: movement over time. The visualization of the results of any bio-engineering project requires graphical representations of the data too numerous to be only reported in tables and listings;

Tissue engineering: in conventional biology, molecular regulation of cell behavior has been studied. However, now, with tissue engineering, research is focused on ways to modify these

molecular regulations with polymeric materials. Possible applications range from gene therapy (embedding gene sequences in microcapsules designed to enter specific cells) to artificial organs.

Numerous other research topics in bioengineering are given in table 2. Most of them require extensive signal processing for EEG, ECG, biorythms, MRI, X-rays acquisition, presentation and interpretation.

Table 2: Bioengineering topics

Biomedical Engineering	Signal processing Modeling Bioelectronics Devices Electromagnetic fields Optics Lasers and electro-optics Intelligence systems DNA sequencing
Rehabilitation Engineering	Brain-computer interfaces Functional neuromuscular stimulation EMG and EEG studies Posture and gait Wheelchairs and seating Sensory substitution
Medical Imaging	Ultrasound imaging X-ray Magnetic resonance imaging Optical imaging Computed tomography Single photon emission computed tomography Electron microscopy Image processing (segmentation, compression...) Image guided surgery

There was little activity in biomedical engineering before World War II and little communication or interaction existed between the engineer and the life scientist. However, there were exceptions and the studies of Aristotle (384-322 BC) or Leonardo da Vinci (1452-1519) on the movements of animals and of the human body can be seen as the foundations of biomechanics, one of the major field of bioengineering and rehabilitation medicine today. It is very difficult to define when bioengineering really begun. Galileo Galilei (1564-1642) was first a student of medicine before becoming a famous physicist and could be considered as one of the first bioengineers: he discovered the constancy of the period of the pendulum, and used the pendulum to measure the pulse rate of people, expressing the results quantitatively in terms of the length of a pendulum synchronous to the heart. William Harvey (1578-1658), probably a disciple of Galileo, was influenced by his theories in biomechanics and his principles of measurements. By measuring the capacity of the heart, he estimated that the heart beats were pumping more than 200 liters of blood in one hour, and he could only conclude that the circulation was a necessary condition for the function of the heart. However, bioengineering really took off only in the 1950's with a strong influence of electrical engineers in the medical and life-support fields. Medical instrumentation and medical electronics were the major areas of research, but also applications in biological modeling, blood-flow dynamics, prosthetics, biomechanics, biological heat transfer and biomaterials increased steadily. Early developments started from specific desire such as the need for surgeons to bypass the heart or the

need to take over the function of failing kidneys. The early contacts established between physicians or physiologists and engineers were personal. The communication between them was immediately recognized as a problem. Most of these engineers had just had a minimal exposure to life science and biology during their curriculum. It is only much later, when recognizing a need to assist in overcoming the communication barrier as well as to prepare engineers for the future, that engineering schools developed curricula in biomedical engineering. The other way to be directly involved in biomedical engineering is reflected by this thesis: a clinician, during and after his medical school and clinical fellowship, tries to understand how the biological systems are working, as well as the devices used to measure these activities. By keeping a close collaboration and dialogue with engineers, new tools can be developed that will remain focused on clinically relevant problems. Finally, a MD arguing some expertise in bioengineering is perhaps only someone who can help clinical and engineering experts, living in completely different worlds, to communicate.

Outline of the thesis:

The first part of this thesis focuses on measurements of the coronary blood flow and pressure using conventional 0.014" wires and is introduced in **chapter 1** by a review of different developments in this field. In **chapter 2**, we investigate the determinants of the coronary flow and resistance reserve in a population of patients where histologic studies of the microvascular bed were possible. Capillary density was measured from surgical specimens of patients with hypertrophic cardiomyopathy and cardiac biopsies in transplant recipients served as the control group. In **chapter 3**, we present the development of an acquisition system for the combined recording of raw Doppler signals together with physiological signals such as an ECG or pressure recordings. This system, which improves the archiving and post-processing of intracoronary Doppler measurements, facilitates the evaluation of parameters combining pressure and flow measurements. In **chapter 4**, we compare the cost-effectiveness of a strategy of balloon angioplasty guided by Doppler flow velocity and angiography with a strategy of primary stenting. The patients randomized to provisional angioplasty were further sub-randomized, after optimization, to either additional stenting or termination of the procedure to further investigate what could be optimal. Optimal results, initially based on a previous study, were defined as a coronary flow reserve >2.5 and a diameter stenosis ≤ 35%. In **chapter 5**, we test *in vitro* whether the fractional flow reserve (FFR), a physiological index based on coronary pressure measurements recently introduced for the assessment of coronary stenoses and interventions, can discriminate between suboptimally and optimally deployed stents. We performed quantitative angiography as well as IVUS in order to determine which imaging technique best correlated to the FFR results.

Chapter 6 explains the principles of a new methodology developed in our laboratory and introduces the second part of this thesis, describing the simultaneous combined assessment of morphological and physiological parameters with one IVUS catheter. Flow velocity is estimated from the decorrelation of successive radiofrequency (RF) traces. Validations of these measurements, based on a rotating scanner, that were performed in a carotid pig model are presented in **chapter 7**. In **chapter 7b** preliminary clinical data are further illustrated by a case report. In **chapter 8**, the disturbances in the 3-D velocity profile induced by the catheter in the coronary lumen are evaluated by applying computational fluid dynamics. The latest developments and *in vitro* calibration of the

IVUS flow method using an array catheter are reported in **chapter 9**. In this chapter we analyse the influence of factors such as the catheter ring-down (the artefact related to its vibration after electrical excitation), the catheter eccentricity, noise.

Part three of this thesis deals with a new method developed for measuring the local elastic properties of coronary arteries using intravascular ultrasound. In **chapter 10** the principles of coronary elastography are introduced. We give an overview of the innovative developments and applications of this rapidly growing field, including the potential to detect vulnerable plaques. The feasibility to perform these measurements during percutaneous interventions is reported in **chapter 11**. A simplified method of elastography, called palpography, potentially more robust in a clinical setting, and faster to process, is introduced in **chapter 12**.

The fourth part of this dissertation is related to the use of radioactive sources in interventional cardiology (coronary brachytherapy) to decrease the restenosis process. In **chapter 13**, we stress the importance of IVUS imaging in coronary brachytherapy. We illustrate the different applications of IVUS in assessing vascular remodeling, in helping the prescription of an optimal dose and in assessing the vessel wall dosimetry. In **chapter 14**, we emphasize our contribution in this field, with the development of 3-dimensional dosimetry and the evaluation of dose volume histograms. We have investigated, by computer simulation, the different existing modalities in brachytherapy (centered- or non-centered b- and g-sources) and the influence of their respective use on the homogeneity of the dose distribution across the arterial wall. We demonstrate that 3-d dosimetry is a valuable tool to understand IVUS (**chapter 15**) and quantitative coronary angiography (**chapter 16**) outcomes of patients treated with brachytherapy.

The last part of this thesis summarizes non-coronary applications based on transthoracic echocardiography. The principles of this important imaging modality in cardiology are given in **chapter 17**. The tools developed for the recordings of invasive Doppler and pressure signals have been applied to non-invasive transthoracic Doppler echocardiography. In **chapter 18**, we develop a combined acquisition of of non-invasive pressure and flow data for the assessment of the compliance of the large arteries using the pulse pressure method, which had been previously only investigated in animals using invasive recordings. Considering the limitations of carotid tonometry, we have investigated the changes of the arterial pressure contour wave between the carotid and radial sites in order to preferentially use this site. The transfer function that we could characterize is reported in **chapter 19**. Finally, in **chapter 20**, we demonstrate an original evaluation of ventricular contractility based on the determination of left ventricular peak power during supine exercise. In the studied population, the derived contractile reserve index correlated well with the simultaneously measured peak oxygen consumption (VO_2).

PART 1

Intracoronary Doppler and Pressure Measurements

Chapter 1

Intracoronary Doppler and pressure monitoring.

SG Carlier, C Di Mario, M J Kern, PW Serruys.

E Topol (ed), Textbook of Interventional Cardiology (3rd ed), 1998; p 748-781.

CHAPTER 40

Stéphane G. Carlier / Carlo Di Mario / Morton J. Kern
Patrick W. Serruys

Intracoronary Doppler and Pressure Monitoring

Andreas Grüntzig performed the first percutaneous transluminal coronary angioplasty (PTCA) in 1977 using 4-French dilation catheters with a double lumen, allowing on one side balloon inflation and on the other side pressure recordings. He described trans-stenotic pressure gradient measurements as a guide to the progress of the dilation.[1] At that time, pressure gradient measurements were routinely performed and used to monitor the intervention and to assess the final results: a residual trans-stenotic gradient less than 20 mm Hg was considered optimal.[2] However, with technical developments such as the flexible-tipped guidewire introduced in the lumen previously used to measure pressure and the low-profile balloons, pressure recordings were more difficult to perform. Moreover, the relations among the measured pressure gradient, the diameter stenosis, and the lesion length were imprecisely known, and they depended on the presence of the catheter itself in the stenosis.[3] Finally, pressure gradient had a limited prognostic value and distal pressure recordings were abandoned because the pressure channel was eliminated to improve the crossing profile of the balloons and because of the advent of quantitative coronary angiography (QCA).

In parallel, attempts were made to mount piezoelectric crystal at the tip of catheters[4, 5] to characterize coronary blood flow, but the partial obstruction of the coronary ostium by those relatively large catheters limited their clinical use. With the development of parameters to assess the functional significance of a stenosis from its geometry with QCA,[6] many interventional cardiologists considered that the available anatomic information was sufficient and that these attempts to perform physiologic pressure and flow recordings were only for research purposes.

The limitations of QCA for the physiologic assessment of intermediate coronary lesions in unselected patients with extensive coronary atherosclerosis have now been recognized[7, 8]; the haziness of the borders of the vessel after PTCA also limits the use of QCA to assess the acute results of an intervention. On the other hand, technical improvements have allowed the development of miniaturized pressure and Doppler transducers, mounted on 0.014-in. guidewires, which alleviate the initial fluid dynamics problems. The clinical importance of the coronary flow reserve (CFR) distal to a stenosis, derived from Doppler recording, or the myocardial fractional flow reserve (FFR_{myo}), derived from pressure recordings, are explained in this chapter.

Recently, the association of a CFR greater than 2.5 and a diameter stenosis less than 35% has been demonstrated as a prognostic factor for the recurrence of symptoms and the restenosis rate in patients undergoing PTCA.[9] The safety of not performing an angioplasty for intermediate stenosis without a functional significant severity assessed by flow or pressure measurements has also been demonstrated.[10, 11] This new interest in pressure and flow recordings illustrates one more example of the swing back of the pendulum, a commonly seen process in interventional cardiology.

INTRACORONARY DOPPLER PROBES

Principles of Doppler Velocimetry

An observer moving toward a sound source hears a tone with higher frequency than at rest; an observer moving away from the source hears a tone of lower frequency. This change in frequency is called the *Doppler effect* after Christian Johann Doppler (1803 to 1853), an Austrian physicist who was the first to describe this phenomenon. This principle is applied in practice by mounting a piezoelectric crystal that emits and receives high-frequency sounds on the tip of an intravascular catheter. The blood flow velocity alters the return frequency, causing the Doppler shift. Electronic circuits performing spectral analysis of the received signal allow continuous determination of the Doppler shift and of blood flow velocity, based on the following Doppler equation:

$$V = (F_i - F_0) \cdot C/(2 \cdot F_0 \cdot \cos(\phi))$$

where V = velocity of blood flow, F_0 = transmitting (transducer) frequency, F_i = returning frequency, C = constant: speed of sound in blood, and ϕ = angle of incidence.

Maximum velocity can be recorded, provided the transducer beam is nearly parallel to blood flow and ϕ is zero so that the cosine (ϕ) is 1. With continuous-wave Doppler, the signal reflects all the flow velocities encountered by the exploring ultrasound beam. In contrast, a pulsed-wave Doppler permits determination of both magnitude and direction of the flow changes at a predetermined distance from the transducer. Intracoronary Doppler has several advantages for the assessment of the coronary circulation. Doppler flowmeters directly measure the red blood cell velocity so that flow markers are not required, allowing a continuous assessment of flow. Since the catheter can be selectively inserted in epicardial vessels, regional measurements are possible. There is a direct relation between velocity and volumetric flow, where blood flow = vessel cross-sectional area × mean flow velocity. The differences or changes in Doppler coronary flow velocities, thus, can be used to represent changes in absolute coronary flow, provided the cross-sectional area remains constant. Intracoronary Doppler, however, also has several limitations. The method is extremely "space dependent" and may be affected by the stenosis geome-

try as well as by the intracoronary velocity profile.[4] The angle existing between the piezoelectric crystal and the main stream of the blood is critical for the estimation of flow velocity.[12] In addition, the sampling volume can be rather limited and does not necessarily represent the mean velocity of the blood stream.[13] Finally, the catheter itself changes the velocity profile in the arterial lumen, and this velocity profile is not constant during the pulsatile-flow condition of a cardiac cycle.

Doppler Probes Mounted on Angiographic Catheters

The first attempts to record Doppler tracings at the ostium of the native coronary vessels were performed with a 20-MHz piezoelectric crystal mounted at the tip of a standard S-French Sones catheter[13] and later on a Judkins catheter.[5]

With these systems, however, no selective measurements were made in the vessel(s) of interest, and a contamination of the coronary flow due to aortic components was present. The presence of the relatively large catheter in the coronary ostium was partly limiting the coronary blood flow, especially during hyperemia.

Intracoronary Doppler Catheters

At the University of Iowa, special suction-mounted epicardial Doppler probes were designed for intraoperative and experimental use,[14] and an evaluation of relative flow changes was performed.[15] Changes in coronary blood flow velocity measured with this intravascular ultrasonic flowmeter correlated well with flow measurement performed with microspheres and electromagnetic flowmeters.[15, 16]

With this system, a selective intracoronary measurement of flow velocities became possible during cardiac catheterization. Further technical development allowed an easier and safer integration of Doppler measurements in the catheterization laboratory during coronary interventions, owing to the availability of an internal lumen for a movable guidewire in the second-generation catheters.

Subselective Doppler recordings using a circular end-mounted crystal on a flexible 3-French catheter amenable to guidewire insertion were later described by Sibley and associates.[17] In this system, the angle between the ultrasonic beam and the centerline of the intravascular flow profile was minimized.

The flow stream interference due to the presence of the catheter in the blood stream is of concern if velocities close to the transducer have to be measured. Tadaoka and colleagues[18] reported that in an in vitro model, a blunt or M-shaped velocity profile, depressed at the centerline, is present several millimeters distal to the catheter tip, resulting in underestimation of flow velocity away from the transducer. A distance of at least 10 catheter diameters was required to have a complete restoration of the flow-velocity profile.

A prototype series of coronary balloon catheters with an end-mounted 20-MHz Doppler crystal has been evaluated in our laboratory.[19] The system allowed the recording of high-quality Doppler tracings distal to the stenosis before, during, and after balloon inflation. The maximal hyperemic velocity after balloon inflation was found to be a useful guide for the assessment of the result of angioplasty.

Doppler Guidewire Probes

Although side- and end-mounted Doppler catheters have been used extensively in research cardiac catheterization laboratories, mainly for assessing relative changes of coronary velocities, several limitations have prevented their widespread clinical application.

1. Catheters with a 1-mm diameter are unlikely to be an obstacle to flow in proximal coronary arteries with a 3- to 4-mm diameter. However, across or distal to a stenotic segment, the obstruction due to the catheter may induce marked reduction or disappearance of the anterograde flow.
2. The catheters had to be inserted before and after coronary interventions, resulting in repeated and complex exchange procedures and in the inability to monitor coronary blood flow velocities during the most critical phases of the procedure.
3. Their small sample volume required an optimal position inside the vessel to record a high-quality signal, including the highest blood velocities. Their maximal recording velocity was 110 cm/sec, limiting the measurements across a stenosis. Moreover, only zero-crossing (ZC) detectors were available with these Doppler probes.

The *Doppler guidewire* is a 0.014-in.-diameter, 175-cm-long, flexible, and steerable guidewire with handling characteristics similar to traditional angioplasty guidewires. The latest "wide-beam" model has a 12-MHz piezoelectric ultrasound transducer integrated onto the tip. It has a minimal cross-sectional area of 0.1 mm^2, which is 12% of the cross-sectional area of a 1-mm catheter. The cross-sectional area of the Doppler guidewire causes a 9% area reduction of a circular lumen of 1.2-mm diameter, whereas a 1-mm diameter catheter induces a 70% obstruction. The wire creates less disturbance of the flow profile distal to its tip when placed within a vessel and can be passed into smaller coronary arteries without creating significant stenoses. The flexibility and steerability of the Doppler guidewire are designed for crossing intracoronary arterial obstructions and maintaining a stable, prolonged placement in the distal portion of the coronary artery during coronary angioplasty procedures. When a Doppler-tipped guidewire is substituted for a standard angioplasty guidewire, phasic coronary flow-velocity measurements are easily incorporated into an angioplasty procedure without adding unnecessary technical maneuvers. In the latest model, the forward-directed ultrasound beam diverges at 35 degrees from the Doppler transducer, so that the Doppler sample volume is approximately 0.65-mm thick × 3.1-mm diameter when maintained 5.2 mm beyond the transducer, distal to the area of flow-velocity profile distortion induced by the Doppler guidewire.[18] This broad ultrasound beam provides a relatively large area of insonification, sampling a large portion of the flow-velocity profile (Fig. 40-1). An adjustable pulse-repetition frequency of 16 to 94 kHz, pulse duration of 0.83 μsec, and sampling delay of 0.5 μsec provides satisfactory parameters for spectral signal analysis. The signal transmitted from the piezoelectric transducer is processed from the quadrature Doppler audio signal by a real-time spectral analyzer using on-line fast Fourier transformation (FFT), providing a scrolling gray scale spectral display. The frequency response of this system calculates approximately 90 spectra per second. The spectral analysis of the signal and the Doppler audio signals are videorecorded for later review. Simultaneous electrocardiogram and blood pressure are displayed with the spectral velocity. We have recently demonstrated the feasibility of recording the quadrature signals with an independent PC-based analogic to digital acquisition system for archiving and postprocessing of such Doppler spectra.[20]

The Doppler flowwire (FloWire, Cardiometrics, Inc., Mountain View, CA) has been validated during intravascular measurement of coronary arterial flow velocity by Doucette and coworkers.[21] The Doppler flow-velocity signal was recorded in model tubes with pulsatile blood flow in straight tubes, with internal diameters varying from 0.79 to 4.76 mm. The peak

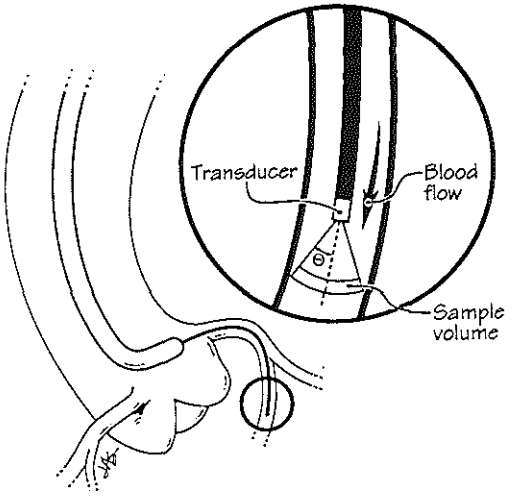

FIGURE 40-1. Diagram showing the large sample volume of a Doppler guidewire anterogradely inserted into the left anterior descending coronary artery. The ultrasound beam opens at 15 degrees from the Doppler crystal to obtain a larger Doppler sample volume. (From Ofili EO, Labovitz AJ, Kern MJ: Coronary flow velocity dynamics in normal and diseased arteries. Am J Cardiol 17:3D–9D, 1993.)

spectral flow velocity was linearly related to absolute flow velocity measured by on-line electromagnetic flowmeters. Quantitative volumetric flow was calculated from vessel cross-sectional area and mean flow velocity. The average peak velocity was less accurate in larger tubes (> 7.5 mm), and a slightly reduced correlation with absolute flow was observed in some tortuous model segments. In four canine circumflex coronary arteries, the electromagnetic flow probe and the Doppler guidewire also demonstrated high correlations in both the proximal and distal segments. Using QCA to determine arterial diameter, absolute volume flows were closely correlated. Measurements were not significantly affected by increasing heart rates to 150 beats/min in the canine model. These data indicated that the Doppler guidewire accurately measures phasic flow-velocity patterns and linearly tracks changes in flow rates in small, predominantly straight coronary arteries.

The in vivo studies established several important features applicable to patient use.[22] The Doppler guidewire could be easily steered in the proximal and distal branches of the coronary arterial tree. The phasic velocity recordings had a high signal-to-noise ratio and were satisfactory for prolonged monitoring periods, with a good separation of forward and reverse flows. Low-frequency wall motion artifacts were occasionally encountered and could be minimized by repositioning of the guidewire.

Comparison studies were performed using an 8-French Judkins Doppler catheter.[23] There was no significant difference between the Doppler guidewire and Doppler catheter mean velocities and coronary vasodilator reserve.

The safety of the instrumentation of normal and mildly diseased coronary arteries with the Doppler guidewire during diagnostic coronary angiography was assessed in 120 patients. No complications related to the use of the guidewire were observed immediately after the procedure and at 6-month follow-up.[24]

Analysis of the Doppler Signal: Advantages of the Spectral Analysis

Simple, straightforward Doppler velocity registrations can be obtained with a ZC detector. The interval between each pair of adjacent ZCs of the same polarity is measured and the Doppler frequency shift is calculated. This method was implemented on most of the first generation of Doppler catheters. Although inexpensive, simple, and convenient, this technique is less accurate than spectral signal analysis in areas of disturbed flow and is unable to detect the peak velocities.[12] The different frequencies corresponding to the velocities of the scatters are best examined by a full-power spectrum provided by FFT, which also has the advantage of distinguishing laminar from disturbed turbulent flow patterns, and which can detect the maximal Doppler shift.

Comparison of ZC detectors and FFT has been performed in vitro and in animal models.[18, 25–28] ZC detectors underestimated consistently the true velocity measured with FFT but seemed sufficiently reliable for the evaluation of relative flow changes.

Comparison in patients has been reported by Di Mario and coworkers.[29] The mean velocity measured with a ZC detector (Millar MVD 20) was compared with the FFT-derived time-averaged maximal and mean velocities in the same period in 19 patients. There were large differences between the paired measurements, suggesting that the two techniques of analysis are not interchangeable. Furthermore, only the spectral analysis allowed the detection of frequency aliasing during recordings within a stenosis. Large differences between flow-velocity measurements obtained with ZC and FFT were also observed by Piek and associates.[30]

CORONARY BLOOD FLOW-VELOCITY PATTERNS

Pulsatile Characteristics of Coronary Flow

The pulsatility of coronary arterial flow was described by Scaramucci in the late seventeenth century.[31] In contrast with the flow characteristics of most arterial districts, arterial coronary blood flow has a distinctive and unique phasic pattern. Blood flow is higher in diastole and lower in systole. Large differences, however, are present between the flow pattern in the left (LCA) and in the right coronary artery (RCA) (Fig. 40-2). An opposite flow pattern is present in the coronary veins, which are characterized by a predominant systolic component, by flow variations during the cardiac cycle synchronous with the right atrial pressure waves, and by large phasic changes due to respiration. These opposite flow changes during the cardiac cycle can be explained only by assuming the presence of a blood reservoir between the arterial and venous sides of the coronary circulation (intramyocardial capacitance). The classic experiments of Sabiston and Gregg confirmed that the systolic reduction of arterial coronary flow results from the contraction of the heart, with a squeezing of the capillary network.[32] More recently, an increased systolic stiffness of the cardiac myocytes has been considered a possible alternative. The different patterns of flow during the cardiac cycle in the LCAs and the RCAs is in part attributable to the greater systolic compressive force of the left ventricle or to the higher stiffness of the left ventricular myocytes during the contractile phase. Both theories can then explain the presence of a reversal of flow during systole in some patients with severe aortic valve stenosis or obstructive hypertrophic cardiomyopathy.[33–35]

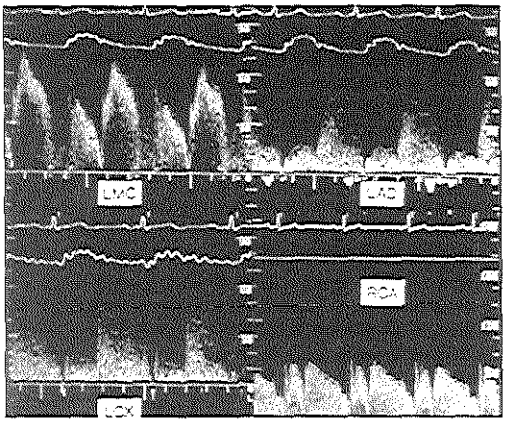

FIGURE 40-2. Flow-velocity measurements obtained in the left main coronary artery (LMC) and the proximal segments of the left anterior descending (LAD), left circumflex (LCX), and right coronary artery (RCA) of a patient without epicardial coronary stenoses. Note the prevalent diastolic component and the similar pattern and maximal velocity observed in the LAD and LCX arteries.

Normal Blood Flow Velocity and Flow Pattern

Knowledge of normal flow-velocity range and of signal characteristics in normal proximal and distal coronary arteries is an essential prerequisite for the evaluation of the flow-velocity changes in patients with coronary lesions. To define the normal range of coronary flow velocity, the time-averaged blood flow velocity was measured in 81 proximal coronary arteries without hemodynamically significant coronary stenosis.[35] A Doppler guidewire was advanced into a straight, smooth and regular proximal segment of the studied artery. An on-line measurement of time-averaged peak blood flow velocity and mean diastolic-to-systolic velocity ratio is automatically available in the previously described Doppler guidewire system. The videorecorded Doppler spectra were also traced using a digitizing tablet. The systolic and diastolic components were defined based on the simultaneously recorded electrocardiogram (QRS complex), aortic pressure (dicrotic notch), and flow changes (Fig. 40-3). A repeated independent analysis of 10 Doppler tracings from the same observer or from a second observer showed less than 5% interobserver and intraobserver variability for all the analyzed parameters. The time-averaged peak velocity was 23 ± 11 cm/sec (mean ± SD of all the arterial segments). A large range of velocity (9 to 61 cm/sec) was observed. Maximal blood flow velocity was 42 ± 17 cm/sec (range, 14 to 82 cm/sec).

The differences in flow velocity and pattern between proximal and distal segments have also been investigated in 55 angiographically normal, proximal, and distal coronary arteries[35] and are summarized in Table 40-1. Proximal and distal velocities in each artery were not different at baseline or hyperemia. All three coronary arteries showed a diastolic-predominant pattern in both proximal and distal arterial segments. This pattern was less marked in the RCA, which had a significantly lower peak diastolic-to-systolic flow-velocity ratio compared with the left anterior descending (LAD) coronary artery. The LAD had higher hyperemic diastolic velocities. CFR (hyperemic-to-basal flow-velocity ratio) was similar in all three arteries. Thus, proximal and distal normal native coronary arteries have similar relative flow-velocity parameters and vasodilator reserve, with a diastolic-predominant pattern. The diastolic-to-systolic flow-velocity ratio greater than 1.5 is maintained in both the proximal and distal segments in patients without hemodynamically significant coronary stenosis and with normal left ventricles. The minor reduction in flow velocity observed when advancing the Doppler probe from proximal to distal is somewhat surprising when the large reduction of the corresponding cross-sectional area and, consequently, coronary flow is considered. The maintenance of flow velocity across the length of the epicardial artery is the result of the gradually diminishing vessel area as volumetric flow is distributed to side branches along the proximal-to-distal vessel course. Anatomically, the division of the coronary arteries is extremely irregular, with the presence of small transmural arteries directly branching from the major epicardial arteries and of a nonsymmetric division of the mother vessel into numerous smaller daughter branches. Strahler ordering and fractal models have been proposed to describe the heterogene-

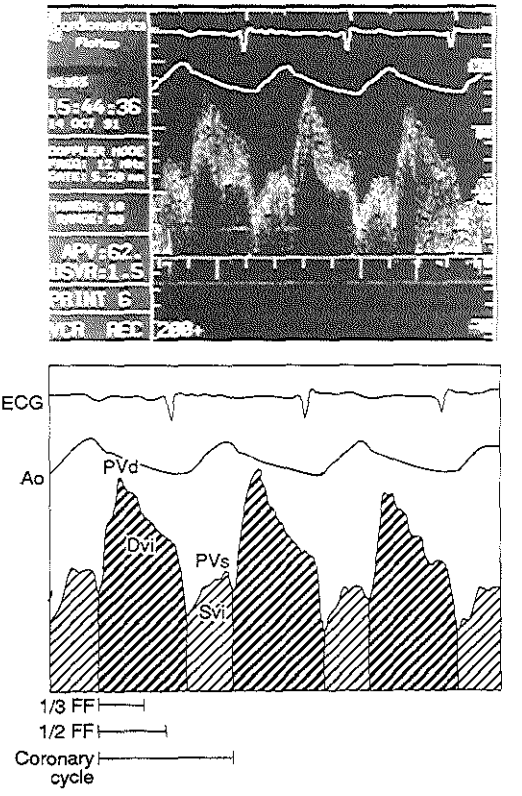

FIGURE 40-3. *Top panel*, Flow-velocity recording in a proximal left anterior descending coronary artery. Note the prominent diastolic component. The diastolic-to-systolic flow-velocity ration (DSVR) automatically calculated on-line and displayed in the top figure is based on the ratio between mean diastolic and systolic flow velocity. *Bottom panel*, The comparison between diastolic and systolic component can be based on the peak velocity in diastole and systole (PVd and PVs) or, more correctly, on the flow integrals (Dvi/Svi). ECG, electrocardiogram; Ao, aorta; 1/3 FF, one third flow fraction. (From Ofili EO, Labovitz AJ, Kern MJ: Coronary flow velocity dynamics in normal and diseased arteries. Am J Cardiol 17:3D–9D, 1993.)

TABLE 40–1. BASELINE AND HYPEREMIA VELOCITY PARAMETERS IN INDIVIDUAL CORONARY ARTERIES

	BASELINE			HYPEREMIA‡		
	LAD	LCX	RCA	LAD	LCX	RCA
Proximal						
Peak D Vel	49 ± 20	40 ± 15	37 ± 12	104 ± 28†	79 ± 20	72 ± 13
Mean Vel	31 ± 15	25 ± 8	26 ± 7	66 ± 18†	50 ± 14	48 ± 13
D Vel Int	18 ± 11*	13 ± 5	11 ± 4	37 ± 55†	27 ± 12	22 ± 9
1/3 FF (%)	45 ± 4*	44 ± 5	40 ± 5	44 ± 5	43 ± 6	41 ± 4
D/S	2.0 ± 0.5*	1.8 ± 0.7	1.5 ± 0.5	2.0 ± 0.5	1.9 ± 0.6	1.9 ± 0.8
Distal						
Peak D Vel	35 ± 16	35 ± 8	28 ± 8	70 ± 17	71 ± 22	67 ± 16
Mean Vel	23 ± 11	21 + 6	21 ± 9	45 ± 12	45 ± 12	42 ± 9
D Vel Int	13 ± 9	10 ± 3	8 ± 5	9 ± 6	11 ± 8	9 ± 2
1/3 FF (%)	46 ± 2	45 ± 9	39 ± 6	45 ± 3	42 ± 7	40 ± 9
D/S	2.4 ± 0.8*	2.1 ± 0.8	1.4 ± 0.3	2.2 ± 1.0	1.9 ± 0.8	1.6 ± 0.3

*LAD versus RCA ($P < .05$).
†LAD versus LCX and RCA ($P < .05$).
‡All three coronary arteries had significantly higher absolute velocity parameters during hyperemia ($P < .001$).
Note: Anova: Scheffe F test only test used for comparison.
D, diastolic; D/S, peak diastolic/systolic velocity; D Vel Int, diastolic flow-velocity integral (U); Vel, velocity (cm/sec); 1/3 FF, one third flow fraction; LAD, left anterior descending coronary artery; LCX, left circumflex coronary artery; RCA, right coronary artery.
From Ofili EO, Labovitz AJ, Kern MJ: Coronary flow-velocity dynamics in normal and diseased arteries. Am J Cardiol 17:3D–9D, 1993.

ity of the vessel distribution, analogous to other physiologic structures such as the airways of the lung.[36]

When only the increase of the total arterial cross-sectional area between mother and daughter vessels in large epicardial arteries is considered, a progressive moderate increase is observed, in accordance with the principles of limited/adaptive vascular shear stress, of minimum vascular volume at bifurcations, and of minimum viscous energy loss. After three-dimensional reconstruction of the arterial tree, Seiler and colleagues[37] calculated a ratio between the area of the mother vessel and the mean of the areas of the daughter vessels of 1.647, similar to the ratio predicted based on the previously mentioned principles (1.588).

Consequently, the cross-sectional area increases by a factor of 1.214 per bifurcation so that the large increase in cross-sectional area between the coronary entrance arteries and the capillary bed can be explained only by the larger number of consecutive bifurcations. These considerations explain why only a moderate decrease, inversely proportional to the moderate increase in total cross-sectional area, occurs from proximal to distal in the coronary arterial tree. Flow velocity, therefore, is relatively uniform in the epicardial arteries of the same patient, and a rapid decrease indicates redistribution of flow in the lower-resistance branches proximal to a flow-limiting coronary stenosis.

Vascular Resistance in Proximal and Distal Coronary Segments

The differential characterization of blood flow velocity and vascular resistance between proximal and distal normal epicardial human arteries has been examined by Ofili and coworkers.[38] Using mean and peak velocity and cross-sectional area of the proximal and distal segments, coronary volumetric blood flow and vascular resistances were computed. Mean velocity and CFR were similar for all three native arteries and were preserved from proximal to distal coronary segments. Volumetric flow decreased from proximal to distal segments. The demonstration of an inverse and curvilinear polynomial relationship between volumetric flow and vascular resistance agrees with the theoretical and animal models of coronary physiologic characteristics and suggests a nadir of coronary vascular resistance below which coronary flow can no longer decrease. For the three coronary arteries, the distal coronary flow velocity reserve and coronary volumetric flow were similar at 55 ± 45, 51 ± 25, and 64 ± 35 mL/min for the LAD, circumflex, and RCAs respectively. CFR for the same vessels was 2.5, 2.6, and 2.4, respectively. Although the flow-volume gradient (ratio of proximal to distal flow) was 2.9, 2.5, and 3.1 for the LAD, circumflex, and RCAs, respectively, the decrement in distal volumetric flow was expected for the branching myocardium receiving the appropriate myocardial blood supply. The vascular resistance was significantly greater in the distal than in the proximal coronary segments for each vessel: on average, 2.7 ± 1.8 versus 0.8 ± 0.4. Volumetric flow, as expected, diminishes from proximal to distal regions primarily because of the gradual reduction in vessel cross-sectional area with increasing total arterial perfusion area through branching vessel systems. The nonlinear inverse relation between absolute coronary blood flow and coronary vascular resistance in proximal and distal segments has been previously identified by coronary physiologists in models, suggesting that at low levels of coronary vascular resistance, further decreases do not necessarily result in increases in coronary blood flow.

Flow Velocity in Saphenous Veins and Mammary Arteries Used as Coronary Conduits

The saphenous vein grafts have a predominantly diastolic flow, similar to the flow in native coronary arteries.[39] In the proximal saphenous veins used as aortocoronary bypass, however, large high-peaked systolic waves may be present, probably reflecting the high distensibility of these long, thin-walled vascular conduits, with a higher vascular capacitance than the shorter and smaller native coronary arteries. In the proximal segment of in situ internal thoracic (mammary) arteries anastomosed to coronary arteries, the phasic blood flow velocity resembles that of the subclavian artery,[39, 40] with a predominant systolic peak velocity (diastolic-to-systolic mean velocity ratio = 0.6 ± 0.2). The velocity pattern changes in the distal internal mammary artery near the coronary anastomosis with a predominant diastolic flow showing diastolic velocities similar to those recorded in native coronary arteries.[39, 41] A peculiar characteristic of saphenous veins used as sequential conduits is the sudden decrease

in velocity observed distal to a coronary anastomosis, in contrast with the progressive velocity decrease observed from proximal to distal in native coronary arteries. The low flow velocity consequent to the inability to adjust the caliber according to flow demand may explain why saphenous vein grafts are more prone to accelerated atherosclerosis than are native coronary arteries or mammary arteries used as coronary bypass. The low flow velocity and shear rate may facilitate thrombosis and greater interactions between blood elements and intimal surface.

Variations in Normal Coronary Vasodilatory Reserve

Variations in CFR, defined as the ratio of maximal coronary flow in hyperemia to baseline flow, in multiple arteries in large numbers of patients in the cardiac catheterization laboratory have led to controversy regarding normal values. This issue is especially pertinent for assessing the significance of coronary stenosis in patients with angiographically near-normal coronary arteries and early atherosclerotic disease who may have concomitant impairment of the microcirculation. To assess the spectrum of CFR responses found in adult patients undergoing cardiac catheterization, CFR was measured in 410 coronary arteries in 214 patients comprising three groups: atypical chest pain syndrome (n = 85) and angiographically normal coronary arteries; coronary artery disease and angiographically normal vessels (n = 21); and angiographically normal transplant recipients (n = 108).[42]

Intracoronary flow velocity was measured with an 0.018-in. Doppler flowwire. Maximal hyperemia was stimulated with intracoronary adenosine (12 to 18 μg bolus) and CFR was computed as hyperemia ÷ basal average peak (mean) velocity (Fig. 40-4). Because bolus adenosine does not increase vessel cross-sectional area,[43] coronary flow-velocity reserve as the ratio of maximal hyperemic mean flow velocity to basal mean flow velocity was used as a surrogate for CFR.

CFR (Table 40-2), on average, in normal patients with chest pain syndromes was approximately 2.9 ± 0.6, and similar in the angiographically normal artery in patients with coronary artery disease (2.5 ± 0.95); both values were higher than the poststenotic diseased-vessel CFR (1.8 ± 0.6). Transplant arteries had the highest CFR (3.1 ± 0.9). Among different normal arteries, there was no difference in CFR for circumflex, RCA, or LCAs. Regional differences were not present, suggesting that relative CFR should be 1.0 ± 0.2. These data should be considered for studies involving assessment of coronary microcirculation in patients in the cardiac catheterization laboratory. Microcirculatory abnormalities may be differentiated from abnormal CFR due to stenosis using relative coronary vasodilatory reserve.[44]

Erbel and associates[45] have reported CFR values in angiographically normal coronary arteries in which intravascular ultrasound (IVUS) was performed to further classify patients with early atherosclerosis. Of 44 patients, 16 (group 1) had a normal

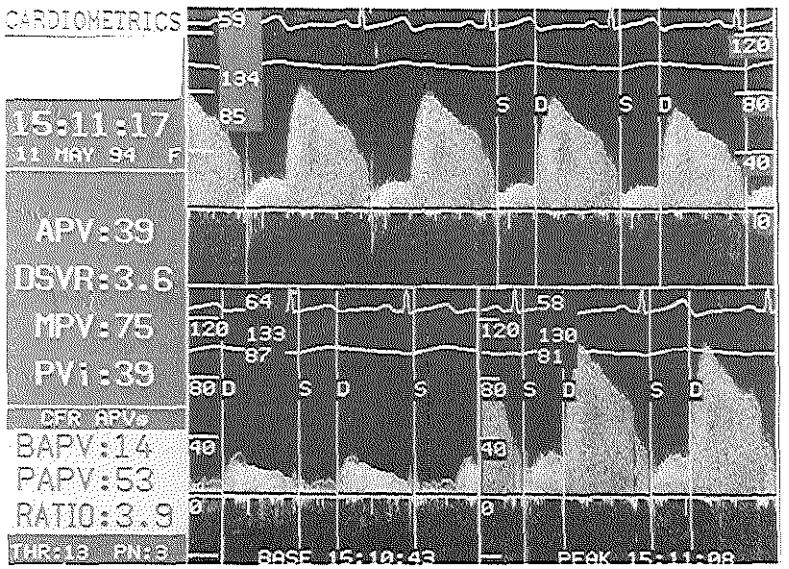

FIGURE 40-4. Spectral coronary flow velocity signals used in the calculation of coronary vasodilatory reserve. The display screen is split into top and bottom, which is then subdivided into left and right panels. *Top section*, Continuous-phasic flow velocity during hyperemia. The velocity scale is 0 to 120 cm/sec. Electrocardiogram and arterial pressure are the top two tracings. S and D indicate systolic and diastolic periods. The heart rate and systolic and diastolic pressures are shown as the numbers in the gray box at the upper left corner of the flow panel. *Bottom left and right panels*, Coronary flow velocity at baseline and at peak hyperemia is shown in the lower panel of the split screen. The same velocity scale is used in the upper panel. APV, average peak velocity; DSVR, diastolic-to-systolic velocity ratio; MPV, maximal peak velocity; PVi, peak velocity integral; CFR, coronary flow reserve. Coronary vasodilatory reserve is calculated from basal average peak velocity (BAPV) of 14 cm/sec and peak average peak velocity (PAPV) of 53 cm/sec to produce a coronary vasodilatory reserve ratio of 3.9 (shown in the lower far left light gray panel).

TABLE 40–2. CORONARY FLOW RESERVE IN ANGIOGRAPHICALLY NORMAL ARTERIES

GROUP NO., DESCRIPTION	NO. OF ARTERIES STUDIES	ARTERY			SEX	
		LAD	RCA	CFX	Men	Women
1. Normal	150	2.68	2.81	2.39†	2.69	2.51‡
2. NL/AB	20/20	2.76/1.78*	2.42/1.85*	2.42/1.85*	2.44/1.79*	2.53/1.81*‡
3. Transplant recipients	280	3.04*	3.29*	3.06*	3.09*	3.09*

* $P < 0.05$ vs. other groups.
† $P < 0.05$ vs. LAD, RCA.
‡ $P < 0.05$ vs. men.
LAD, left anterior descending artery; RCA, right coronary artery; CFX, circumflex coronary artery.
From Kern MJ, Aguirre FV, Bach RG, et al: Variations in normal coronary vasodilatory reserve by artery, sex, status post transplantation, and remote coronary disease (abstract). Circulation 90:I-154, 1994.

coronary morphology by IVUS and a CFR greater than 3.0 (mean = 5.3 ± 1.8), and 7 (group 2) had a normal IVUS appearance but a reduced CFR (2.1 ± 0.4). Plaque formation was found in a total of 21 patients. Mean plaque sizes were 3.6 ± 1.6 mm^2 for the patients with a CFR greater than 3 (group 3), and 5.0 ± 2.3 mm^2 in those having a reduced CFR (group 4). The authors concluded that only 36% of the patients with normal angiograms were true normal, that 48% exhibited an early stage of coronary atherosclerosis, and that the patients in group 2 might be considered as syndrome X. These data were in agreement with earlier reports of abnormal CFR in patients with angina but normal coronary angiography.[40–49]

Relative Coronary Flow Reserve

Absolute CFR is the summation of the conduit and microcirculatory response. CFR is similar among the three major vessel territories, and the ratio of CFR in any two territories is 1.0 ± 0.2.[42] Relative CFR ($CFR_{TARGET}/CFR_{REFERENCE}$) in patients with coronary artery disease should exclude the differences attributable to microvascular disease and different hemodynamic states for serial studies. Baumgart and colleagues[50] compared FFR_{MYO}, derived from intracoronary pressure measurements (see following paragraph) to relative flow reserve (computed as $CFR_{TARGET}/CFR_{REFERENCE}$). The correlation coefficient for FFR_{MYO} versus absolute CFR was $r = 0.045$ compared with the correlation for relative flow reserve ($r = 0.95$) for stenoses severity ranging between 50% and 95% diameter narrowed.

Similarly, Uren and coworkers[51] demonstrated the difference between FFR_{MYO} and absolute CFR in 11 stenosis in three experimental canine models. The stenoses were created with a cuff occluder and the percent area stenosis was evaluated with QCA. FFR_{MYO} correlated better than absolute CFR for stenosis severity in both absolute (minimum luminal diameter [MLD]) and relative (percent diameter) values.

These preliminary data indicated that relative flow reserve had an excellent correlation with FFR_{MYO} and that absolute flow reserve had a poor correlation because of the unexpected and unpredictable abnormalities of microcirculation. The relative CFR seems to be more appropriate for lesion specificity than absolute CFR, and its application will likely facilitate improved decision making using coronary Doppler measurements. Figure 40–5*A* and *B* demonstrate the use of relative flow reserve.

Calculation of Volume Flow from Flow-Velocity Measurements

Two crucial steps are required to accurately calculate absolute (volume) flow from flow-velocity measurements: the calcu-

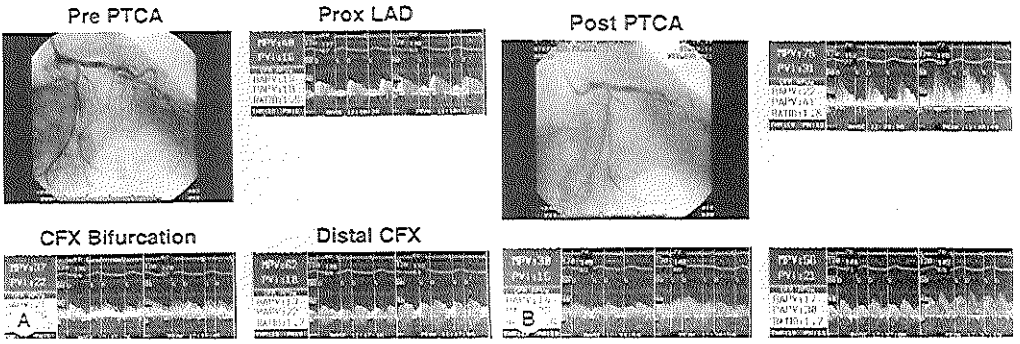

FIGURE 40–5. *A*, Demonstration of the value of relative coronary flow reserve in a patient undergoing percutaneous transluminal coronary angioplasty (PTCA). An 82-year-old woman had severe circumflex coronary artery stenosis and progressive angina pectoris despite medical therapy. Coronary flow velocity was measured in the proximal left anterior descending (Prox LAD), the distal circumflex (Distal CFX), and the obtuse marginal branch beyond the stenosis. The coronary flow reserve in the proximal LAD was 1.5, in the distal normal circumflex was 1.2, and in the distal circumflex in the normal segment was 1.7. Relative coronary flow reserve preangioplasty was 1.2/1.7 = 0.70. *B*, After angioplasty, coronary flow reserve was 1.8 in the normal reference LAD, 1.6 in the target obtuse marginal branch, and 1.7 in the adjacent reference zone. Relative coronary flow reserve increased to 0.9. This patient had coexisting microvascular disease. See Figure 40–4 legend for additional abbreviations.

lation of the mean blood flow velocity in a given vascular cross-section, and the accurate measurement of the cross-sectional area at the site of the measurement.

Assessment of Mean Blood Flow Velocity

The measurement of the mean blood flow velocity requires an adequate Doppler sampling of the peak flow region within a vessel, with the ultrasound beam optimally aligned parallel with the centerline of flow, and with the entire flow profile or at least a significant proportion that includes the maximal velocity insonified. The physical presence of the Doppler probe should not modify the velocity profile at the site of the Doppler sample volume and a spectral analysis of the Doppler frequency should give the different velocities in the sample volume, including the maximal velocity.

Although theoretically possible,[52] several technical shortcomings limit the practical usefulness of the measurement of mean blood flow velocity from the velocity spectrum. A different approach is based on the use of the maximal blood flow velocity that is less sensitive to the presence of noise and is more easily included in the sample volume based on the earlier-described characteristics of the Doppler flowwire. Mean blood flow velocity can be estimated from the maximal blood flow velocity assuming Poiseuille's flow using the equation describing the velocity of a laminar flow field:

$$V_{MAX} = \Delta P/4\ \mu L \times r^2, \quad (1)$$

in which V_{MAX} is the maximal velocity of the flow, ΔP is the pressure gradient in the vascular segment of length L, μ is blood flow viscosity, r is the radius, and L is the length in millimeters of the considered segment. Under the assumed conditions and if mean velocity times cross-sectional area (A) equals blood flow (Q), from the Poiseuille equation it follows that:

$$V_{MEAN} = Q/A = (\Delta P \pi r^4/8\ \mu L)/A, \quad (2)$$

with $A = \pi r^2$, Equation 2 can be simplified to:

$$V_{MEAN} = \Delta P r^2/8\ \mu L = V_{MAX}/2. \quad (3)$$

An important limitation to the applicability of this formula is that the velocity profile is assumed to be parabolic and fully developed. The distance L necessary to allow the full development of a parabolic flow profile is defined by the equation[53]:

$$L = (0.03\ R_E)d, \quad (4)$$

where R_E is the Reynolds number and d is the diameter of the conduit. Consequently, the velocity measurement should be taken at a distance of four to six times the vessel diameter to allow a complete development of the velocity profile at the Reynolds numbers present in normal epicardial coronary arteries (150 to 200). The same issues must be considered when sampling velocity distal to major bifurcations of the vessel or stenotic segments. The non-newtonian characteristics of blood and the pulsatility of the flow induce a blunted velocity profile so that the mean blood flow velocity may be underestimated by $V_{MAX}/2$.[54–56] Validation studies have shown a high correlation both in vitro and in vivo between volumetric flow measured with an electromagnetic flowmeter[21] or with a transit-time ultrasound flowmeter[57] and flow derived from Doppler measurements obtained with the Doppler guidewire probe, using for the calculation of the blood flow:

cross-sectional area × average peak velocity × 0.5

Conversely, other in vitro and in vivo data using a 3-French Doppler system or Doppler wire also demonstrated good correlation between the flow calculated as cross-sectional area × average peak velocity and the measured flow.[26, 58–60] Since in most of the recordings in human coronary arteries the assumption of a parabolic velocity profile is rarely encountered, no definitive value can be defined. However, in most clinical situations it is the ratio of the hyperemic flow over the baseline flow that is clinically relevant. When a constant velocity profile at the sampling site is assumed, there is then a simplification of the variable related to the velocity profile for the calculation of the coronary flow reserve.

Assessment of the Cross-Sectional Area at the Site of the Doppler Sample Volume

A high-quality angiogram, suitable for measurements of the cross-section at the site of the Doppler sample volume, can be performed almost simultaneously with the acquisition of the Doppler recording with the Doppler flowwire. However, more accurate measurements are obtained when the probe is positioned in an arterial segment of uniform caliber so that a mean cross-sectional area over a short arterial segment immediately distal to the Doppler probe can be obtained.

An alternative method is the combination of intracoronary Doppler and bidimensional IVUS imaging. A continuous recording of high-quality echographic cross-sections, suitable for automated QCA, can be achieved with the modern ultrasound imaging catheters. Linker[61] and Eichhorn[59] and their colleagues described this approach using sequentially a 3-French Doppler catheter and then an IVUS catheter. The introduction of the Doppler guidewire allowed then simultaneous assessments. The slightly different position of the Doppler sample volume and of the echographic cross-section and the potential electrical interference are minor limitations of this approach. Since the first data reported by Sudhir and coworkers in dogs,[62] this method has been used mainly in studies of the coronary endothelial function: simultaneous changes in luminal size and in coronary blood flow velocities during the pharmacologic provocation with acetylcholine can be monitored.[63–64] Coronary blood flow and CFR using this method have been recently reported by Caracciolo and coworkers[65] in a population of 36 angiographically normal orthotopic heart transplant recipients. In this study, it was demonstrated that the epicardial intimal thickening does not diminish conduit and resistance vessel response during endothelial-independent vasodilator administration of adenosine or nitroglycerin.

ASSESSMENT OF STENOSIS SEVERITY

Poststenotic Coronary Blood Flow-Velocity Patterns

Severe coronary stenoses are characterized by three major alterations in the intracoronary flow-velocity pattern. These changes are discussed in the following sections.

Diastolic-to-Systolic Velocity Ratio

Previous investigators documented a reduction in the diastolic-to-systolic coronary flow ratio distal to experimental stenoses in animal models.[25, 66–68] Intraoperative studies confirmed a reduction in diastolic flow velocity and unchanged systolic flow velocity during graft occlusion.[25, 68] Abnormal arteries show a reduction of diastolic flow velocity with relatively preserved systolic flow velocity. The systolic-predominant pattern was seen in more than 50% of abnormal arteries and in none of the

normal arteries.[69, 70] There is a normalization of the diastolic-to-systolic velocity ratio after angioplasty.[71-73]

Proximal-to-Distal Flow-Velocity Ratio

The distal flow-velocity parameters in normal compared with abnormal arteries showed a distinct pattern of abnormality, with significantly lower mean velocity, peak diastolic velocity, and peak systolic velocity in the abnormal arteries compared with the normal arteries.

Impaired Coronary Blood Flow Reserve

A blunted hyperemic response of the distal abnormal arteries compared with normal is also characteristic of hemodynamically significant lesions. Since the original work of Gould and colleagues,[74] the assessment of CFR has been viewed as a method to establish the severity of a stenosis located in one of the major epicardial vessels. It is assumed that the reduction in hyperemic flow through the stenotic lesion would be an indicator of stenosis severity. This assumption is derived from the complex hemodynamic principles regulating the coronary circulation. At rest, flow is independent from the driving pressure over a wide range (60 to 180 mm Hg) of physiologic pressures, a phenomenon classically described as autoregulation of the coronary circulation. During maximal vasodilation, flow becomes linearly related to the driving pressure.[75] The presence of a flow-limiting stenosis in a major epicardial vessel generates a pressure drop across the stenotic lesion that is the result of viscous and turbulent resistances, so that the driving pressure distal to the stenosis decreases exponentially in response to the flow increase.[76]

The CFR concept is appealing to the clinician because it constitutes a functional surrogate to the anatomic description of the lesions located in the epicardial vessels. Many investigators have shown in animal experiments that a decrease in flow reserve may discriminatingly detect lesions of increasing severity.[77] Although the concept may be easily and accurately applied in an optimal physiologic situation in humans,[78, 79] it should be recognized that CFR is influenced by several factors independent from the hydrodynamic characteristics of the stenotic lesion. Since flow reserve is by definition a ratio, similar values may be obtained at different levels of resting and hyperemic flow. Changes in basal resting flow without changes in hyperemic flow would considerably affect the ratio. Furthermore, any factors affecting the hyperemic pressure-flow relationship would likewise modify the flow reserve and thereby change the assessment of the severity of the coronary lesion under study. The hyperemic pressure-flow relationship is influenced by factors such as heart rate, preload, myocardial hypertrophy, contractility, or disease of the microvasculature.[75, 80] This has been demonstrated in open-chest dogs[81] and in different studies in patients.[82-85]

Effects of the Pharmacologic Agents Used to Induce Maximal Hyperemia

An increase in coronary blood flow can be observed either during reactive hyperemia induced by transluminal occlusion or by pharmacologically induced hyperemia. Widely used vasodilator agents are dipyridamole, nitroglycerin, papaverine, and adenosine. The hyperosmolar ionic and low-osmolar nonionic contrast media cannot be used, because they do not produce maximal vasodilation.[86] Nitrates have a predominant effect on large conductance vessels, so that the flow changes due to peripheral vasodilation are partially masked by the large simultaneous increase in cross-sectional area in the proximal arterial segments. Continuous infusion of an adequate dose of dipyridamole results in maximal coronary vasodilation, but it has the disadvantage of a long duration of action, which makes the repeated assessment of the coronary hyperemic response of the coronary vascular bed or the assessment of different coronary vascular bed response during the same procedure impossible.

Bookstein and Higgins[86] have shown in dogs that the hyperemic response after an intracoronary bolus injection of adenosine triphosphate or papaverine is of the same magnitude as that occurring after a 15-second occlusion of the coronary artery. The dose range of intracoronary papaverine needed to produce maximal coronary vasodilation has been established in humans by Wilson and White.[87] Selective intracoronary infusion of papaverine produced a maximal hyperemic response in most coronary arteries (80%) after 8 mg and in all coronary arteries after 12 mg. Papaverine in this dose range (8 to 12 mg) produced a response equal to that of an intravenous infusion of dipyridamole in a dose of 0.56 to 0.84 mg/kg of body weight.

The coronary vasodilation after intravenous or intracoronary adenosine is of a comparable magnitude to that observed after papaverine. The time from intracoronary injection of adenosine to peak hyperemia, as well as the total duration of the hyperemic response, is about four times shorter than that of papaverine.[88] Furthermore, adenosine does not prolong the QT interval and avoids the potentially dangerous ventricular arrhythmias observed after papaverine.[89] Wilson and associates[90] reported that an intracoronary bolus or infusion of adenosine increases coronary velocity to levels similar to those recorded after papaverine without significant systemic effects or symptoms. Adenosine can also be administered intravenously. Kern and colleagues have shown that a continuous intravenous infusion of 140 $\mu g \cdot kg^{-1} \cdot min^{-1}$ induces maximal coronary vasodilation in most patients.[91] Development of mild hypotension, bradycardia, or first- or second-degree atrioventricular block or symptoms (flushing, chest discomfort, headache, dyspnea) rarely requires discontinuation of the infusion.[92] In view of the extremely high safety profile of adenosine, this agent is the pharmacologic stimulus of choice.

Effect of the Pharmacologic Agent Used to Induce Hyperemia on Stenosis Geometry

The ideal vasodilator should dilate exclusively the resistance vessels without affecting the geometry of the flow-limiting stenosis in the epicardial coronary artery. Gould and Kelley found important changes in stenosis geometry caused by papaverine-induced hyperemia in dogs.[93] Zijlstra and coworkers[94] have reported an increase in the cross-sectional area of the stenosis. Since change in vessel caliber caused by the coronary vasodilator (dipyridamole, papaverine, or adenosine) may alter the pressure-flow relationship, administration of nitrates before the measurement of CFR is strongly advocated to negate the epicardial vasodilator action of the drugs used for the induction of maximal hyperemia.

Differences in Proximal and Distal Coronary Flow Reserve

Because of the influence of low resistance and prestenotic branches, differences in proximal and poststenotic flow velocity have been observed and attributed to the branching circulation.[8, 95, 96] Donohue and associates have reported in 101 patients simultaneous measurements of pressure gradient and of proximal and distal CFR.[97] In the diseased vessels, the proximally measured CFR was not statistically different for any translesional gradient. The distal CFR was significantly lower in arteries with a gradient greater than 20 mm Hg (1.4 ± 0.6 vs. 2.1 ± 0.7). The poststenotic flow reserve is thus a better descriptor of the severity of a coronary stenosis, the proximal flow reserve being influenced by the branching and prestenotic diversion of flow to regions with lower resistance.

Effect of Heart Rate, Arterial Pressure, and Ventricular Preload

The coronary flow-velocity reserve is estimated by the ratio of peak-to-resting flow velocity. One of the potential problems of this measurement is that the flow-velocity ratio can be affected by a change in resting flow velocity caused either by factors increasing myocardial oxygen consumption (e.g., thyrotoxicosis) or by factors producing a resting high-flow state (e.g., anemia). CFR measurements are highly reproducible in the absence of conditions known to affect resting or hyperemic coronary blood flow, but increases in heart rate or preload reduced CFR because resting coronary blood flow velocity increased. In contrast, changes in mean arterial pressure do not alter CFR because of similar increase in resting and hyperemic blood flow.[92–94] De Bruyne and colleagues[95] have recently analyzed the short-term reproducibility of CFR measurements. CFR was measured twice at 3-minute intervals and under atrial pacing and nitroprusside and then dobutamine administration. The coefficient of variation of CFR was 10.5% between the two baseline measurements. CFR did not change during infusion of nitroprusside but decreased during atrial pacing and dobutamine infusion.

Interpretation of CFR measurements should thus account for the variable hemodynamic conditions at which the flow-velocity measurements are obtained.

Technical Factors Influencing the Accuracy of Doppler-Based Coronary Flow Reserve

There is a possible induction of flow obstruction due to the large guiding catheter engaged in the coronary ostium: in an ostium of 3 mm in diameter, the tip of an 8-French guiding catheter occupies 77% of the luminal area.[98] With a blood collection method, it was demonstrated that the maximal flow through the side holes of such a catheter does not exceed 80 mL/min. It is thus advocated that when impedance of the flow could occur, after selective injection of the vasodilator, the catheter should be immediately pulled out from the ostium without moving the Doppler probe. A careful monitoring of the pressure waveform recorded through the guiding catheter can facilitate the detection of damping of velocity (Fig. 40-6). Use of diagnostic coronary catheters (5 or 6 French) is an easier alternative possibility to prevent flow obstruction.

Side holes permit continued blood flow, but there is an unpredictable amount of adenosine being lost in the aorta during intracoronary bolus injection that influences the measurement of CFR.[99] A larger dose (up to 36 μg) should be used to assess CFR when guiding catheters with side holes are used.

Finally, when the signal-to-noise ratio of the received Doppler signal is low, the automatic contour detection implemented in this system fails to recognize the true maximal velocity profile. This can occur in up to 16% of the cases.[100] Manual retracing with an off-line system for the calculation of the average peak velocity and the CFR is necessary. We have demonstrated recently that digitization of the raw Doppler signal associated with automatic off-line processing allows a better evaluation of maximal flow.[101]

Long-term Variability of Coronary Flow Reserve

Di Mario and coworkers[100] analyzed long-term changes in baseline and hyperemic intracoronary flow velocity and CFR in angiographically normal arteries. Baseline and hyperemic velocities were similar between baseline assessment and after 6 months, but the agreement between successive measurements was rather poor. The long-term reproducibility was improved when flow velocity was normalized for the cross-sectional area at the site of measurements. To improve the reproducibility of the measurements, the use of intracoronary nitrates is recommended to reduce the velocity changes related to changes of the cross-sectional area at the site of the Doppler sample volume.

Application of the Continuity Equation in Coronary Stenosis

The continuity equation states that in a tube without branches, the velocity-area product at any point is equal to the velocity-area product at any other point in the tube. The conti-

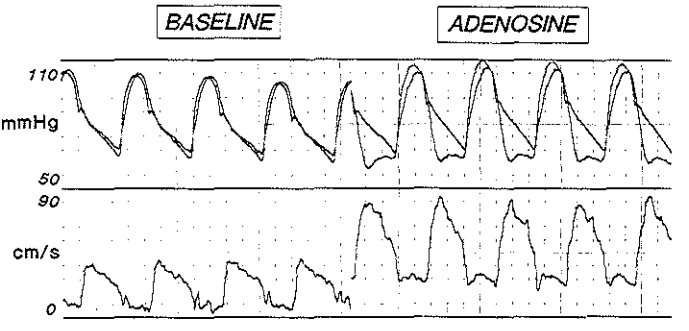

FIGURE 40-6. In the upper part of the illustrations, note the simultaneous recording of the pressure in the ascending aorta (tip manometry) and of the proximal coronary pressure (fluid-filled 8-French guiding catheter at the ostium of the left coronary artery). At baseline the two tracings are superimposed, indicating that the voluminous guiding catheter does not impede the flow in the mainstem of the left coronary artery. The intracoronary administration of 18μg of adenosine induces the development of a pressure gradient between the aorta and left main coronary artery, generated by the presence of the guiding catheter. Note the ventricularization of the proximal coronary pressure and, in the lower part of the illustration, the simultaneous changes in flow velocity recorded using a Doppler guidewire positioned in the proximal left anterior descending artery. (From Serruys PW, Di Mario C, Meneveau N, et al: Intracoronary pressure and flow velocity from sensor-tip guidewires: A new methodological comprehensive approach for the assessment of coronary hemodynamics before and after coronary interventions. Am J Cardiol 17:41D–53D, 1993.)

nuity equation is a principle largely applied for the calculation of cardiac valve areas in echocardiography.[102] Miniaturization of the Doppler probes has allowed the application of this principle for the assessment of the severity of coronary artery stenoses. In vitro studies in hydraulic models of coronary stenoses have shown an excellent correlation between this method and true cross-sectional area of stenosis.[103] Similar results were obtained in animal experiments[47] and in humans for the assessment of moderate (<50% diameter) coronary stenoses, using 3-French intracoronary Doppler catheters that cannot, however, be used in severe coronary stenoses.[104]

The feasibility of measuring maximal jet velocity within a stenosis with the Doppler guidewire was tested in 52 consecutive patients, in a total of 61 arteries, prior to coronary angioplasty.[105] Based on the continuity equation, percentage cross-sectional area stenosis was calculated as:

$$\%CSA\ St = (1 - APV\ Ref/APV\ St) \times 100,$$

where St = stenosis, Ref = reference segment, CSA = cross-sectional area, and APV = average peak velocity.

An increase in flow velocity advancing the guidewire into the stenosis was observed in 17 arteries. Only in 10 cases (16%), however, was the quality of the Doppler recording sufficient to allow the measurement of the time-averaged peak velocity. In these cases, the time-averaged peak velocity increased from 15 ± 5 cm/sec to 110 ± 34 cm/sec from the reference normal segment to the stenosis. A marked decrease was observed in the angiographically measured cross-sectional areas (7.75 ± 2.55 mm^2 vs. 1.05 ± 0.61 mm^2 for the reference and stenosis areas, respectively). Consequently, comparable volumetric flow values were calculated in the stenosis and in the reference segment from the corresponding flow-velocity and cross-sectional area measurements. The percentage reduction of cross-sectional area calculated from the QCA measurements and from the Doppler flow-velocity measurements were significantly correlated. But the application of the continuity equation for the assessment of stenosis severity has significant practical and theoretical limitations. The first problem is the choice of the reference "normal" segment. Epicardial and IVUS have confirmed the pathology findings showing that diffuse or focal intimal thickening is present in angiographically normal arterial segments.[106, 107] If the flow-velocity measurement is obtained in a segment already narrowed by the atherosclerotic wall encroachment, the percentage cross-sectional area stenosis calculated from the velocity measurements will underestimate the stenosis severity. In the presence of severe stenoses, the flow is preferentially diverted to the prestenotic branches so that distal flow is reduced, resulting in a high proximal-to-distal flow-velocity ratio. The reference flow velocity in a segment distal to the stenosis should thus be used. Another important limitation is related to the measurement of the flow velocity in the stenosis, where the velocity profile is modified (in the presence of abrupt changes of vascular diameter stenosis, a vascular segment four to six times longer than the vascular diameter is required to reconstitute a fully developed parabolic profile).[53] Therefore, for short stenoses, the use of the maximal velocity may underestimate the percentage cross-sectional area stenosis. But the most important practical limitation to the applicability of the continuity equation for severe coronary lesions is the possibility of obtaining Doppler recordings suitable for quantitization only in a minority of the study population. The appropriate orientation of the Doppler sample volume in the narrow tapering segment immediately proximal to the lesion is difficult, resulting in inability to capture the small stenotic jet. Extensive manipulation or tip reshaping of the Doppler guidewire may yield a higher acquisition rate of jet velocity signals in the stenosis but is associated with a potential risk of wall dissection before access to the distal vessel has been secured.

Translesional Pressure—The Fractional Coronary Flow Reserve

After the initial description by Andreas Grüntzig of the use of the translesional pressure gradient for the assessment of the success of an angioplasty,[1] pressure measurements were progressively abandoned.

From translesional pressure measurements made with a guidewire transducer during maximal hyperemia, a new concept for the determination of coronary blood flow, the FFR_{MYO} has emerged.[108] When blood flows from the proximal to the distal part of the normal epicardial coronary artery, virtually no energy is lost and, therefore, the pressure remains constant throughout the conduit. In the case of epicardial coronary narrowing, potential energy is transformed in kinetic energy and in heat when blood traverses the lesion. The resultant pressure drop reflects the total loss of energy. To maintain resting myocardial perfusion at a constant level, a decrease in myocardial resistance will compensate for any resistance of flow due to the epicardial narrowing. Arteriolar resistance decreases to maintain the flow. The decrease in myocardial resistance reserve is proportional to the resistance that can be computed from the pressure gradient-flow relation and, hence, the pressure at constant maximal flow can represent an index of the physiologic consequences of a given coronary narrowing on the myocardium.

The maximal myocardial blood flow in the presence of a stenosis is reduced relative to expected normal flow in the absence of a stenosis and can be expressed as a fraction of its normal expected value, if there was no lesion. This value, called FFR_{MYO}, can be derived from pressure data alone separately for the myocardium, the epicardial coronary artery, and the collateral supply, based on several assumptions regarding translesional pressure measured during maximal hyperemia.[108, 109] The proposed equations have been derived from a theoretical model of the coronary circulation and have been validated experimentally in instrumented dogs, and later in humans, by the comparison with myocardial flow measured by positron emission tomography (PET).[110] During maximal hyperemia (with papaverine or adenosine), coronary resistance is at the lowest level and remains constant, so that flow is directly related to the measured pressure gradient. The total myocardial blood flow (Q) in an area de-served by a coronary artery with a stenosis is the sum of the flow through the stenosis (Q_S) and the collateral flow (Q_C). The FFR_{MYO} is defined as the ratio of the measured flow (Q) over the maximal flow that should be present without any stenosis (Q^N)[108, 111]:

$$FFR_{MYO} = Q/Q^N = \frac{(P_D - P_V)/R}{(P_A - P_V)/R}$$

with P_A = mean arterial pressure; P_V = mean venous pressure; P_D = mean pressure distal to the stenosis, and R = the resistance of the myocardial vascular bed. Because this resistance is assumed constant,

$$FFR_{MYO} = \frac{(P_D - P_V)}{(P_A - P_V)} = 1 - \frac{\Delta P}{(P_A - P_V)} \sim = \frac{P_D}{P_A}$$

with P_V assumed low and constant. FFR_{MYO} can thus be estimated as the ratio between the mean distal coronary blood pressure (using ultrathin pressure transducers) over the mean aortic blood pressure (measured by the guiding catheter). For a normal vessel, FFR_{MYO} is unequivocally equal to 100%. Since

each myocardial territory serves as its own control, it is a lesion-specific index independent of the microcirculation, heart rate, blood pressure, and other hemodynamic variables, and it can be applied in multivessel disease.

Fractional collateral flow reserve (FFR_{COLL}) and fractional coronary flow reserve (FFR_{COR}) are calculated with similar equations:

$$FFR_{COR} = 1 - \Delta P/(P_A - P_W)$$

$$FFR_{COLL} = FFR_{MYO} - FFR_{COR}$$

with P_W = the coronary wedge pressure measured distally when the PTCA balloon is inflated in the artery.

Thanks to the development of miniaturized pressure transducers, the mean trans-stenotic pressure gradient ΔP can be measured without a significant overestimation of the true pressure gradient.[112] Investigated pressure wires were 0.015-in. fluid filled[113] or high-fidelity 0.018-in. tip pressure transducers based on optic fibers (Pressure Guide, RadiMedical Systems, Uppsala, Sweden).[114, 115]

Technical Limitations to Pressure Guidewires

The Radi and Premo pressure guides and the Tracker catheter produce excellent phasic signals. The Premo Wire (fluid-filled pressure monitoring guidewire) produces damped pressure tracings owing to its small inner lumen. However, all three systems reliably reflect mean pressures. The evaluation of pressure gradients is valuable only if a reliable pressure tracing can be obtained. The reliability of pressure gradients is questioned when one is dealing with small vessels (<2.5-mm diameter), acute artery bends, or multiple lesions in a vessel. An artifactual pressure drop due to obstruction of the tip of the pressure catheter is highly unlikely when the catheter is aligned in a normal and relatively straight segment of a coronary artery. In contrast with angioplasty catheters, the pressure measurements made with guidewires and Tracker catheters are not generally affected by tortuosity of a proximal artery segment.

Clinical Significance of Pressure Gradients

The risk of abrupt closure and restenosis increases with high residual pressure gradients after angioplasty.[4, 116] A persistent postprocedure pressure gradient, especially if the angiographic result is suboptimal, is an indication for further balloon inflations (either prolonged inflations or up-sizing of the balloon) or stent. A pressure gradient of less than 15 mm Hg has been considered a successful postangioplasty result.[116] However, investigations have identified limitations in using the resting pressure gradient alone to assess the potential for ischemia due to a given stenosis.[117, 118]

In its initial clinical validation, FFR_{MYO} has been compared with the relative flow reserve (RFR) measured by ^{15}O-labeled water and PET and to QCA.[110] Isolated proximal discrete stenosis of the LAD coronary artery were investigated. FFR_{MYO} and RFR were realized 24 hours apart. They were measured during maximal vasodilation under adenosine (140 $\mu g \cdot kg^{-1} \cdot min^{-1}$ intravenous). RFR was defined as the ratio of the maximal achievable absolute flow in the anterior region to the maximal achievable absolute flow in the lateral region. PET RFR and FFR_{MYO} were highly correlated, while the correlation between indices derived from QCA and RFR was markedly weaker.

To define the threshold of FFR_{MYO} below which inducible ischemia is present Pijls[109] and De Bruyne[119] and their associates conducted independent, but parallel and complementary, investigations. Pijls and coworkers studied 60 patients accepted for a single-vessel PTCA who had a positive exercise test in the preceding 24 hours. FFR_{MYO} was measured before and 15 minutes after PTCA and the exercise test was repeated after 1 week. If the second exercise test had reverted to normal after PTCA, FFR_{MYO} values were associated with inducible ischemia. All, except two, FFR_{MYO} measurements greater than 0.74 were not associated with ischemia, and all FFR_{MYO} 0.74 or less were related to inducible ischemia. In normal coronary arteries, FFR_{MYO} was 0.98 ± 0.03. De Bruyne and coworkers[119] studied FFR_{MYO} in 60 patients with one isolated lesion in one major coronary artery who had a maximal exercise test 6 hours before catheterization. ST segment depression was compared to FFR_{MYO}, ΔP_{MAX}, and ΔP_{REST}. Intersection of sensitivity and specificity curves were at 87%, 83%, and 75%, respectively, for FFR_{MYO} = 0.66, ΔP_{MAX} = 31 mm Hg, and ΔP_{REST} = 12 mm Hg. No abnormal test was present for FFR_{MYO} greater than 0.72. FFR_{MYO} has also been compared to the results of dobutamine echocardiography in 75 patients with normal left ventricular function and single-vessel coronary artery disease[120]; the degree of dobutamine-induced dys-synergy correlated significantly with the QCA data, but the correlation was markedly better with FFR_{MYO}. All but one patient with an FFR_{MYO} greater than 0.75 had a normal stress test result.

Among the most important reports of FFR_{MYO} is that of Pijls and colleagues,[121] who compared FFR_{MYO} with the unique ischemic standard of common noninvasive testing modalities in 45 patients with moderate coronary stenoses and chest pain syndromes. When the FFR_{MYO} was lower than 0.75 (21 patients), reversible myocardial ischemia was demonstrated unequivocally on at least one noninvasive test (bicycle exercise testing, thallium scintigraphy, stress echocardiography with dobutamine), and all these positive test results were reverted after PTCA or coronary artery bypass grafting (CABG). In 21 of 24 patients with an FFR_{MYO} greater than 0.75, all the test were negative, with no demonstration of ischemia, and no revascularization procedure was performed. None were required after 14 months of follow-up. The sensitivity of FFR_{MYO} in the identification of reversible ischemia was 88%, the specificity was 100%, the positive predictive value was 100%, the negative predicted value was 88%, and the accuracy was 93%.

De Bruyne and associates[85] demonstrated also in humans that FFR_{MYO} is independent of hemodynamic conditions: changes in heart rate by pacing, in contractility by dobutamine infusion, and in blood pressure by nitroprusside infusion did not alter FFR_{MYO}. The coefficient of variability between two consecutive measurements was 4.2%, lower than 17.7% for the CFR measured with a Doppler wire.

Fractional and Coronary Flow Reserves and Myocardial Perfusion Imaging

To assess the relationship among radionuclide perfusion imaging, poststenotic coronary flow velocity, and translesional pressure gradients using flow-velocity guidewires and 2.7-French fluid-filled tracking catheters, Tron and colleagues investigated 68 arteries in 59 patients, at baseline and during maximal hyperemia (intracoronary [ic] adenosine).[122] FFR_{MYO} of 0.7 or less had positive and negative predictive values for perfusion imaging defects of 71% and 57%, respectively. Poststenotic flow reserve (>2.0 units) had a positive and negative predictive values of 88% and 74%, respectively.

The pressure measuring catheter used in this study was larger than a pressure guidewire and likely induced a systematic increase in hyperemic pressure gradients. CFR had a higher positive and negative predictive value than FFR_{MYO} for the perfusion imaging results. It should not be surprising that myocardial perfusion responses are not translated into directly measured translesional pressure gradient since distal myocardial bed resistance may be variable or impaired and not accounted for in the

primary assumptions of this methodology. The use of translesional gradients has important value for determining lesion significance, especially when distal myocardial flow reserve is impaired.

Simultaneous Measurement of Flow Velocity and Trans-Stenotic Pressure Gradient

Assessment of Coronary Stenosis Using Sensor-Tip Pressure and Doppler Wires

Trans-stenotic blood flow velocity and pressure gradient are the parameters used to define the hemodynamics of a stenosis.[113] Combined use of sensor-tip pressure and Doppler guidewires has been evaluated in 21 patients.[125] Flow-velocity and poststenotic pressure recordings were obtained distal to the stenosis, both in baseline conditions and after intracoronary bolus injection of papaverine.

The maximal hyperemic trans-stenotic gradient showed a significant inverse correlation with the simultaneously measured hyperemic coronary flow. Patients with nonsignificant stenoses were identified by the presence of hyperemic trans-stenotic gradients less than 20 mm Hg associated with a maximal coronary flow greater than 150 mL/min or a CFR less than 2. At the other extreme, the presence of large trans-stenotic gradients during hyperemia associated with a low maximal hyperemic flow identified the most severe stenoses.

The simultaneous measurement of the trans-stenotic pressure gradient and flow velocity has several practical advantages. The possible misinterpretation of a low-flow increase during maximal vasodilation is avoided because the simultaneous presence of a high-pressure gradient discriminates a low-flow increase due to a hemodynamically severe stenosis from a reduction of the maximal trans-stenotic flow increase due to impairment of the distal vasodilatory mechanisms or to competition of flow through a well-developed collateral circulation. Conversely, when a low-maximal flow is present owing to factors not dependent on the stenosis resistance, the measurement of a low trans-stenotic pressure gradient can be misleading and the presence of a significant stenosis cannot be ruled out.

Instantaneous Hyperemic Coronary Pressure-Gradient/Flow-Velocity Relation

The trans-stenotic pressure-gradient/flow-velocity relation has been analyzed from digitized pressure and flow velocity during mid-diastole in 15 patients.[125]

A clear Doppler envelope allowing a reliable automatic detection of the hyperemic diastolic peak velocity during four consecutive beats was obtained in 12 of 15 cases (80%). A linear relation between trans-stenotic gradient and flow velocity was observed in 5 of 12 patients (42%) (Fig. 40-7). In the remaining 7 patients, a quadratic equation had the best fitting for the data obtained. In all but one case an intercept close to 0 (within ±10 mm Hg) was observed. Steeper increases of the trans-stenotic pressure gradient at a given flow increase were measured in the arteries with the most severe reduction in luminal cross-sectional area.

Although the maximal flow and, consequently, the maximal trans-stenotic gradient is determined also by factors independent from the stenosis resistance, the pressure-gradient/flow-velocity relation is intimately correlated with the stenosis hemodynamics. Two approaches are available to assess the slope of the pressure-gradient/flow-velocity relation. The first is based on the measurement of the changes of the mean trans-stenotic pressure and flow velocity from baseline conditions to maximal hyperemia.[124] A technically more complex approach is based

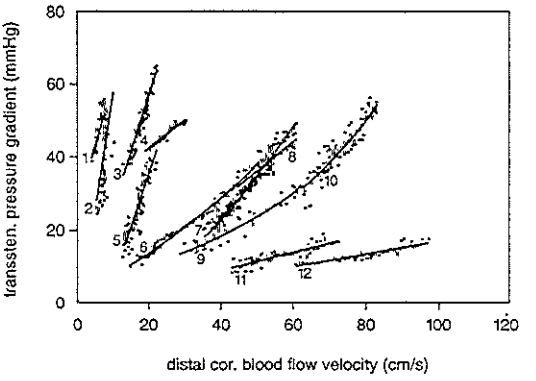

FIGURE 40-7. Instantaneous hyperemic diastolic pressure-gradient/flow-velocity relation for 12 stenoses of increasing hemodynamic severity (from right to left and from bottom to top). MLCSA, minimum luminal cross-sectional area.

NO.	CATH. NO.	MLCSA (mm^2)	EQUATION
1	92707	0.21	$y = 21 + 3.72x$
2	92999	0.33	$y = -6 + 5.76x$
3	921858	1.16	$y = 2 + 2.01x + 0.0275x^2$
4	921132	0.49	$y = 25 + 0.79x$
5	920922	0.82	$y = 2 + 0.11x + 0.073x^2$
6	922047	0.83	$y = 1.6 + 0.50x + 0.0035x^2$
7	930201	1.72	$y = -4 + 0.28x + 0.009x^2$
8	920908	0.83	$y = -4 + 0.76x$
9	921502	0.36	$y = 9 + 0.0055x^2$
10	921504	1.19	$y = -0.1 + 0.0074x^2$
11	921448	4.61	$y = -1 + 0.23x$
12	921330	2.09	$y = 5 + 0.0011x^2$

on the assessment of the instantaneous pressure-gradient/flow-velocity relation during the progressive flow decrease in mid to late diastole. The advantage of an assessment based on instantaneous instead of mean gradient/flow changes during the cardiac cycle is that the phases of acceleration/deceleration of flow, influenced by factors unrelated to stenosis resistance, can be eliminated from the analysis. The pressure-gradient/flow-velocity relation can also be studied during a prolonged cardiac arrest induced with a high-dose intracoronary bolus of adenosine during papaverine-induced maximal hyperemia (Fig. 40-8). In principle, however, the pressure-gradient/flow-velocity relation is independent from the hemodynamic conditions of assessment, including the maximal level of flow and pressure gradient, and could give sufficient information to characterize stenosis severity also in resting conditions.

Mancini and coworkers[125] have validated in dogs the slope of the instantaneous pressure-flow relation as an index of coronary stenosis. This relation was compared with a microsphere-derived index of myocardial conductance. The instantaneous hyperemic flow versus pressure index demonstrated no dependence on heart rate, left ventricular end-diastolic pressure, mean aortic pressure, or inotropic changes.[81, 126, 127] The decrease in flow-pressure slope with the presence of stenoses of increasing severity correlated well with the transmural and the subendocardial microsphere-derived measurements.

The feasibility and the reproducibility of the assessment of the slope of the instantaneous diastolic relation between coronary flow velocity and aortic pressure during maximal hyperemia (IHDVPS) have been investigated in 95 patients.[128] It is postulated that the changes in coronary blood velocities re-

corded by the Doppler wire are directly, and only, related to changes in flow (assuming a constant velocity profile and a constant coronary diameter), to derive Mancini's index from velocity-pressure relation. In the arteries with less than 30% diameter stenosis, blood flow velocity was measured in a regular straight proximal-middle segment of the artery where an optimal Doppler signal could be obtained. The Doppler signal was acquired distal to the stenosis using a Doppler guidewire. The proximal coronary pressure was measured through the guiding catheter. Linear regression analysis was used to assess the slope of the digitized pressure-velocity relation ($cm \cdot sec^{-1} \cdot mm\ Hg^{-1}$) in four consecutive beats during maximal coronary vasodilation. A clear Doppler envelope allowing a reliable automatic detection of the hyperemic diastolic peak velocity during four consecutive beats was obtained in 79 (83%) of 95 patients. A CFR greater than 2 and an IHDVPS greater than 1 were present in 5 (21%) and 3 (12%), patients with greater than 30% diameter stenosis. In the normal group, a CFR and an IHDVPS equal to or less than these levels were observed in 4 (7%) and 8 (14%) arteries, respectively. Using these arbitrarily defined cutoff values, CFR and IHDVPS correctly identified 79% and 88% of the arteries with greater than 30% diameter stenosis and excluded the presence of a stenosis in 93% and 86% of the 55 control arteries (NS). On average, the beat-to-beat variability of the pressure-velocity slope was 15 ± 8%.

A possible limitation of IHDVPS is the dependence of the hyperemic pressure-velocity slope from the cross-sectional area, as expected for an index reflecting coronary conductance. The inability to normalize coronary flow for the perfused myocardial mass limits the comparability of measurements performed in vessels of different dimensions. However, coronary flow velocity shows only a moderate decrease from large epicardial arteries to the more distal branches, suggesting that a comparison remains possible in normal-sized proximal/middle epicardial arteries. The analysis of the pressure-velocity relation of long diastolic pauses suggested that the linearity of the pressure/flow-velocity relation observed during normal sinus beats cannot be extrapolated over a larger range of pressures and flow velocity, probably because of a significant reduction of arterial cross-section at low distending pressures. This technique, therefore, cannot be used for an accurate estimation of the zero-flow pressure.

De Bruyne and colleagues[85] have compared the feasibility and variability of IHDVPS, CFR, and FFR_{MYO}. Both CFR and FFR_{MYO} could be calculated in all cases, but IHDVPS could only be calculated in 82 (79%) of the 104 investigated patients. CFR was sensitive to hemodynamic changes (atrial pacing, dobutamine infusion). Conversely, IHDVPS and FFR_{MYO} were not influenced. Coefficients of variation between two consecutive measurements were 4.2% for FFR_{MYO}, significantly lower than 17.7% and 24.7%, for CFR and IHDVPS, respectively.

Quantitative Coronary Angiography, Translesional Pressure, and Flow Velocity

The imperfect nature of angiography in assessing the functional significance of coronary stenoses, mostly attributable to large interobserver and intraobserver variability, has been well documented. QCA was developed to overcome the limitations of visual interpretation, and its accuracy and reproducibility have been demonstrated.[129] On the basis of stenosis geometry and fundamental fluid dynamic equations, QCA methods have been able to provide mathematically derived translesional pressure gradients and coronary blood flow. QCA-derived hemodynamic data also provide an estimate of flow reserve attributed to the coronary lesion (stenotic flow reserve).[130] Translesional pressure gradients are generated from fluid-dynamic formulas validated in experimental models.[6] These parameters were correlated only with functional indexes of coronary stenoses in selected patients with limited coronary atherosclerosis,[78,131] but not when extensive atherosclerosis was present.[7,8]

Comparison of QCA with pressure gradients and coronary flow measurements with a Doppler wire has been performed in several studies. Donohue and coworkers[97] have measured CFR, translesional gradient at rest with a 2.2-French infusion catheter, and QCA (Philips DCI or ImageComm [Statview System, Sunnyvale, CA] systems) in 33 patients.[97] There was a weak correlation between angiographic lesion severity and corresponding gradients, and in the 40% to 60% angiographically intermediate range, there was no correlation between lesion diameter narrowing and gradient.

Angiographically severe (concentric, >80%) lesions generally had significant (>30 mm Hg) gradients. However, the limitations of angiography are well known for both operator and technical factors, making lesion interpretation difficult and, at times, impossible. When studies of stenosis severity are reviewed, often a single "worst-case" view will be reported. An eccentric lesion with one view of 80% and one view of 40% may not be associated with a translesional gradient. Conversely, a moderate concentric lesion can frequently be associated with a significant gradient.

More recently, Tron and associates measured translesional hemodynamics in the same arteries in which QCA pressure and flow were measured (Philips DCI-ACA).[132] Stenotic flow reserve and baseline and maximal translesional pressure gradients were calculated from the worst QCA projection. Translesional pressure gradients were measured with a 2.7-French fluid-filled tracking catheter. Intracoronary Doppler flow velocities at rest and during maximal hyperemia (ic adenosine) were measured with a Doppler wire in 28 arteries from 25 patients. The results of this study indicated that QCA did not correlate with measured gradients at baseline or at maximal hyperemia. No correlation was found between QCA-predicted stenotic flow reserve

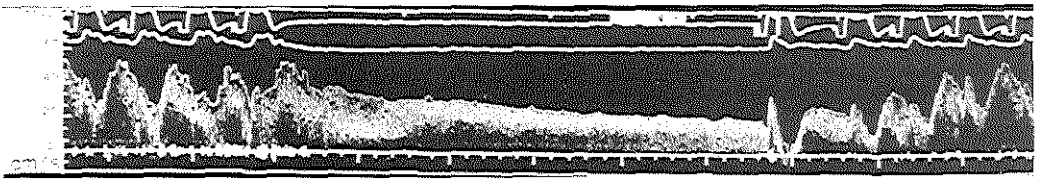

FIGURE 40–8. Prolonged diastolic pause induced by the intracoronary injection of 3 mg of adenosine during maximal hyperemia induced by papaverine. A progressive decrease of flow velocity and aortic pressure is observed during the 6 seconds of cardiac arrest. In the first beats, induced by ventricular pacing, note the pressure of a large systolic flow component indicating refilling of the capacitance of the epicardial coronary artery. The dotted tracing at the top of the Doppler envelope indicates the instantaneous peak velocity (automatically detected online and used for the analysis of the pressure/velocity relation).

and measured CFR. For intermediately severe angiographic stenoses, no correlation existed among measured pressure gradient, CFR, lesion diameter, or cross-sectional area. This study suggests that because of inherent limitations of angiography, state of the distal bed, and assumptions of the physiologic state for fluid dynamic equations, QCA-derived parameters of translesional physiology particularly relevant for interventional decisions do not correlate with directly measured translesional pressure and flow. But a limitation in this study could be the use of a 2.7-French device to measure distal coronary pressure, which could overestimate the true pressure gradient.

In a more recent study, QCA has been compared with FFRMYO determined with a 0.015-in. fluid-filled pressure monitoring guidewire (Premo wire).[155] Quantitative assessment of stenosis geometry was performed on-line using the ACA system. Before angioplasty, QCA was obtained in 105 patients, and after the procedure, pressure measurements and QCA were performed again in 52 patients. With pooled preangioplasty and postangioplasty results, a curvilinear relation was found between diameter stenosis and myocardial flow reserve, and between MLD and myocardial flow reserve, in agreement with previously published data.[134] A linear equation was also found between angiographic stenosis flow reserve and FFRMYO. This study demonstrated that in an unselected cohort scheduled for PTCA, an overall correlation exists between QCA measurements and FFRMYO. There was a rather large dispersion of the data; nevertheless, the diagnostic accuracy of an MLD of less than 1.5 mm and a diameter stenosis greater than 50% in detecting lesions associated with an FFRMYO of less than 0.72 were 92% and 89%, respectively.

Perfusion Imaging and Poststenotic Coronary Blood Flow

Clinical decisions for coronary interventions are often based on the results of out-of-laboratory physiologic testing such as stress thallium perfusion myocardial imaging. Because the physiologic assessment of angiographically intermediate stenoses remains problematic, functional measurements of poststenotic intracoronary flow velocity reserve may be useful in clinical decision making. However, the correlation between poststenotic CFR and hyperemic myocardial perfusion scintigraphic imaging was lacking. Miller and colleagues[8] studied 33 patients to correlate stress myocardial perfusion imaging using technetium 99m sestamibi with poststenotic coronary flow reserve in patients with angiographically intermediate stenoses. A Kappa statistic measuring the strength of correlation among the velocity, imaging, and QCA variables was computed. QCA stenosis severity (≥ 50% diameter stenosis) and poststenotic coronary flow velocity reserve of 2.0 or less were correlated in 20 of 27 patients. Perfusion imaging abnormalities and coronary angiographic stenosis severity were correlated in 28 of 33 patients. The strongest correlation was noted between hyperemic poststenotic flow velocity reserve and sestamibi perfusion imaging in 24 of 27 patients. Nearly all patients with abnormal distal hyperemic flow velocity values had corresponding reversible myocardial perfusion tomographic imaging defects. The high correlation between two different physiologic techniques to assess myocardial perfusion in the poststenotic region suggests that clinical decisions can be made in the laboratory in a fashion similar to out-of-laboratory testing. The physiologic assessment of coronary stenoses, especially those of angiographically intermediate severity, may be improved by the use of poststenotic flow velocity measurements when perfusion imaging has not or cannot be performed.

A similar correspondence between poststenotic CFR and myocardial perfusion imaging has been described by Joye and coworkers,[95] who compared single-photon emission-computed tomographic (SPECT) thallium imaging to CFR in 30 patients with intermediate coronary stenoses. The poststenotic flow reserve and SPECT thallium studies were compared with blinded interpretation of the results. A CFR of 2.0 or less was considered abnormal. The sensitivity, specificity, and overall predictive accuracy of Doppler-derived CFR with stress SPECT thallium 201 results were 94%, 95%, and 94%, respectively. More recently, Miller and associates[135] have correlated regional myocardial blood flow (RMBF) derived from $[^{15}O]H_2O$ PET with directly measured poststenotic intracoronary Doppler flow velocity under basal conditions and dipyridamole-induced hyperemia in 11 patients. There was a highly significant correlation between Doppler-derived CFR and PET-derived myocardial perfusion reserve (MPR). There was a trend toward a correlation between Doppler-derived CFR and MLD, but no correlation was found between PET-derived perfusion reserve and MLD or diameter stenosis. This demonstrates that the correlation of two physiologic endpoints of coronary blood flow more accurately reflects the functional severity of coronary stenoses than does angiography alone. These physiologic techniques provide objective evidence of lesion significance, which is useful to support the decision for coronary revascularization interventions.

To address the relationship between artery stenosis and distal coronary blood flow, 35 patients with single-vessel coronary artery disease underwent $[^{15}O]H_2O$ PET assessment of coronary blood flow at rest and during hyperemia (intravenous adenosine 140 $\mu g \cdot kg^{-1} \cdot min^{-1}$ or dipyridamole 0.56 mg/kg).[136] Twenty-one patients were studied as age match-control subjects. The results indicated that basal myocardial blood flow (1.14 ± 0.42 $mL \cdot min^{-1} \cdot g^{-1}$) was similar between patients 1.13 ± 0.26 mL $min^{-1} \cdot g^{-1}$) and controls. However, during hyperemia, myocardial blood flow was lower in patients (2.10 vs. 3.37 $mL \cdot min^{-1} \cdot g^{-1}$. Basal flow remained unchanged regardless of stenosis severity for diameter stenosis ranging from 17% to 87%. Flow during hyperemia was inversely correlated with the degree of stenosis severity and directly correlated with MLD. CFR declined with diameter narrowing greater than 40% and approached unity at stenosis severity of 80% or greater. These data are important relative to assessment of coronary blood flow in patients undergoing coronary interventions that use angiographic endpoints. Physiologic considerations using intracoronary Doppler techniques can identify residual luminal narrowing of 40% or greater not appreciated by angiography.[137]

INTRACORONARY DOPPLER IN THE ASSESSMENT OF CORONARY INTERVENTIONS

Since the advent of coronary angioplasty, the assessment of the acute results of interventions has been a source of debate and discussion. In recent years, major efforts were made to accurately measure the luminal area of the stenotic lesion before and after coronary angioplasty using QCA with computer-based automatic edge detection.[129, 138, 139] However, for the evaluation of the angioplasty results, this technique has inherent limitations. The disruption of the internal wall of the vessel following the barotrauma of angioplasty cannot be easily delineated by contour detection of the shadowgram obtained with coronary angiography.[140] These limitations have prompted investigators to use alternative methods based on the functional assessment of angioplasty results.[19, 141] The availability of the Doppler angioplasty guidewire and pressure wires allows continuous monitoring of blood flow during a routine angioplasty and assessment of the results of this intervention.

Balloon Coronary Angioplasty

One of the earliest experiences in balloon PTCA was a study of 35 patients performed in our laboratory.[71] The angioplasty guidewire was successfully used to cross the stenosis in 32 (89%) of 36 arteries. A flow-velocity recording was obtained distal to the stenosis, both in baseline conditions and during hyperemia (ie bolus injection of papaverine: 8 mg for the RCA and 12.5 mg for the LCA and saphenous vein bypass graft). Intracoronary nitrates were used before the injection of papaverine to induce a maximal coronary vasodilation and avoid changes in cross-sectional area between baseline and postpapaverine assessment. The Doppler guidewire was left in place distal to the lesion during the dilation procedure. The Doppler signal was continuously acquired during balloon inflation and after deflation to monitor the development of collateral flow, the restoration of flow after balloon deflation, the phase of postocclusive reactive hyperemia and, incidentally, the development of flow-limiting complications. Monitoring coronary blood flow during intracoronary interventions has potential advantages as an early indicator of acute closure, thrombus formation, or vasospasm. These events currently are detected only by repeated angiography. The quality of angiography and the clinical effects of increased radiographic contrast media administration are obvious but unavoidable limitations. During balloon inflation a complete disappearance of flow was observed in 26 arteries (81%). In the remaining six cases (19%), the flow velocity progressively increased during inflation, with a negative flow-velocity signal in five patients indicating recruitment of collateral coronary flow. The restoration of anterograde flow could be immediately detected during the deflation of the balloon, before the disappearance of the electrocardiographic changes or of the symptoms. In three cases (9%) a sudden decrease in blood flow velocity was the first warning signal that a flow-limiting wall dissection developed after angioplasty.

Cyclic Flow Variations as a Predictor of Intracoronary Thrombus Formation After Angioplasty

In animal models with an artificially created coronary stenosis and intracoronary thrombus, cyclic coronary blood flow variations can be abolished with antiplatelet or antithrombotic agents.[142-145] Similar cyclic flow variations have been reported to occur in patients during coronary angioplasty.[146] Cyclic flow variations in an artery with the potential for intraluminal thrombus formation appear to be a marker of continued prothrombotic activity that, despite adequate anticoagulation, may result in failure of the procedure.

The endothelial damage associated with severe coronary stenosis usually results in a cyclic pattern of flow reductions and restorations related to recurrent episodes of platelet aggregation and subsequent dislodgement of thrombus.[147,148] When platelets aggregate, vasoconstrictor substances, including serotonin and thromboxane A_2, are known to change vessel caliber, promote rheologic disturbances, and induce further platelet aggregation and thrombus formation.[149-152] In patients, cyclic flow variations measured in the distal coronary artery bed may be the result of mechanical vasoconstrictor and platelet aggregatory effects.

The detection of intracoronary thrombus may be obscured by angiographic difficulties related to the mechanical disruption of the coronary intimal surface. Monitoring coronary blood flow velocity in patients at risk for intracoronary thrombus may provide an early indication of unsatisfactory dilation or of the need for increased heparin or thrombolytic therapy prior to the potentially serious management problems of abrupt artery closure.

The abrupt changes in flow velocity observed during the development of coronary spasm or of severe flow-limiting dissection and the persistent flow decrease in the presence of a significant elastic recoil[153] can be distinguished from the cyclic flow variations due to the formation of thrombi.[154]

A recent prospective investigation including the first 102 patients of the Doppler Endpoints Balloon Angioplasty Trial Europe (DEBATE) study (described in the following paragraph) has recently highlighted the relation between the presence of cyclic flow variation after angioplasty and immediate complications.[155] In 94 patients (92%), a stable and reliable Doppler signal could be recorded for 15 minutes after the procedure. Cyclic flow variation defined as a gradual decline in flow over several minutes followed by sudden restoration to higher values was observed in 4 patients. In 3 patients, immediate complication occurred: 2 intracoronary thrombosis and 1 acute closure. None of the 90 patients without cyclic flow variation had an acute closure during their hospital stay. This demonstrates that coronary cyclic flow after angiographically successful elective PTCA is rare (4.3%) but highly sensitive for the prediction of abrupt occlusion, in agreement with the observation of Kern and associates,[156] who found a higher prevalence of such events, but in a more heterogenous population, including acute myocardial infarction, atherectomy, urgent stenting, and desobstruction procedures.

Assessment of Results

In our preliminary study,[71] for the 29 coronary arteries without acute complication, baseline average peak velocity increased significantly from 16 ± 9 cm/sec before PTCA to 27 ± 14 cm/sec after PTCA. A more than twofold increase was observed for the average peak velocity recorded at the maximal effect of papaverine (27 ± 17 cm/sec before PTCA and 60 ± 28 cm/sec after PTCA). The cross-sectional area at the site of the Doppler recording showed a nonsignificant change before and after coronary angioplasty, suggesting that the velocity changes reflected a true flow increase after PTCA in baseline and hyperemic conditions. CFR, as a ratio of the hyperemic-to-baseline flow-velocity measurements, showed a moderate but significant increase after PTCA (from 1.75 ± 0.55 to 2.39 ± 0.75).

Segal and colleagues[69] have also reported their results after balloon angioplasty in 38 patients. Twelve patients without significant coronary artery disease served as a control group. Following angioplasty, the time-averaged peak velocity in the distal vessel increased from 19 ± 12 to 35 ± 16 cm/sec ($P < 0.01$), whereas in the proximal vessel velocity increased to a lesser extent (34 ± 18 cm/sec before angioplasty versus 41 ± 14 cm/sec after angioplasty; $P = 0.04$). CFR did not increase significantly after angioplasty, whether measured in either the distal or proximal coronary artery. Similar findings have been reported by Ofili and coworkers[70] before and after angioplasty in 32 patients. After angioplasty, improvement in the diastolic-to-systolic velocity ratio and increases in the total velocity integral and in the peak diastolic velocity during hyperemia in the distal region were noted.

In the peripheral circulation, a categorical cutoff criterion based on Doppler measurements (maximal velocity after nitroglycerin distal to the stenosis ≥48 cm/sec) predicted 32 of 34 cases with a successful procedure based on angiography, IVUS, and clinical results.[157]

These data suggested that measurement of distal velocity variables after coronary balloon angioplasty provides important information concerning the immediate physiologic outcome of the procedure. However, acute changes in resting blood flow together with changes in the anatomy of the stenotic lesion and

concomitant persistent modifications of the hyperemic pressure-velocity relationship should be considered when CFR is used for the assessment of the functional results.[69, 70, 158, 159] The aforementioned considerations are schematically illustrated in Figure 40-9.

Heller and colleagues have reported original data regarding the RCA: rest average peak velocity, measured with a Doppler wire, did not decrease distal to the stenoses (23.3 ± 9.4 cm/sec proximal vs. 20.2 ± 11.1 cm/sec distal), proximal-to-distal velocity ratio was 1.4 ± 0.9 before angioplasty and did not significantly decrease after angioplasty, and diastolic-predominant flow after angioplasty was not observed in the proximal or distal RCA, but was present in the posterolateral and posterior descending coronary arteries.[160]

Clinical Outcome of Deferring Angioplasty Based on Normal Translesional Hemodynamics

The clinical significance of intermediate coronary stenoses on angiography frequently requires adjunctive noninvasive stress testing. Direct translesional flow measurements now available correlate well with myocardial perfusion imaging studies and may assist in clinical decision making. A prospective study was performed to determine the feasibility, safety, and outcome of deferring angioplasty in patients with such lesions.[10] Translesional pressure and flow velocity data were obtained with a 2.7-French infusion catheter and a Doppler wire in 88 patients for 100 lesions (26 single-vessel and 74 multivessel lesions). The mean diameter stenosis by QCA was 54 ± 7% (range 40% to 74%). Predetermined normal values of translesional flow velocity (proximal-to-distal average peak velocity ratio) of less than 1.7 or a pressure gradient less than 25 mm Hg, or both, were required to defer angioplasty. Patient follow-up ranged from 6 to 30 months (mean 9 ± 5 months). The translesional hemodynamics of the deferred angioplasty group were similar to those of a normal reference group. By study design, translesional pressure gradient in the deferred group was 10±9 mm Hg compared with 45 ± 22 mm Hg in the angioplasty group. At follow-up 4, 6, 0, and 2 patients in the deferred angioplasty group required subsequent angioplasty, required bypass surgery, had a myocardial infarction, or died, respectively. One death

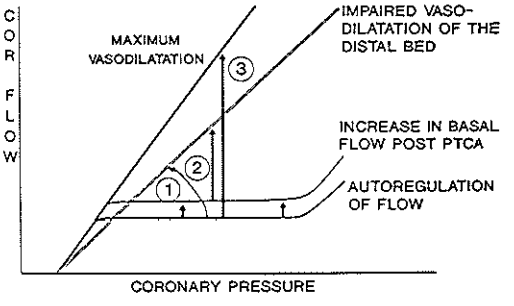

FIGURE 40-9. Pressure/flow relationship in resting and hyperemic conditions. The curved line indicates the flow increase in the presence of a flow-limiting stenosis. Two confounding factors may preclude the assessment of the improvement (3) of coronary flow reserve following a percutaneous transluminal coronary angioplasty (PTCA) procedure: an increase in resting blood flow (1) and/or acute or chronic changes in the pressure-flow relationship during hyperemia (2). (From Serruys PW, Di Mario C, Meneveau N, et al: Intracoronary pressure and flow velocity from sensor-tip guidewires: A new methodological comprehensive approach for the assessment of coronary hemodynamics before and after coronary interventions. Am J Cardiol 17:41D-53D, 1993.)

was related to angioplasty of a nontarget lesion, and one death was the result of ventricular fibrillation in a patient with severe multivessel disease 12 months after lesion assessment. In the 10 patients later requiring coronary revascularization, only six procedures were performed on previously assessed target arteries that had a normal flow. Of the six procedures, four had conversion from normal to abnormal flow pattern. No patient had a complication of translesional flow or pressure measurements. The investigators concluded that the safety, feasibility, and clinical output of deferring angioplasty of coronary stenoses associated with normal translesional hemodynamic variables were satisfactory. This assessment has since been further validated in other centers.[161-166]

Similar results have been reported using FFRMYO[164]: in 100 consecutive patients in whom angioplasty was deferred because measured FFRMYO was 0.75 or greater, the MLD was 1.68 ± 0.44 mm and the percentage diameter stenosis was 46.8 ± 9.4%. During a follow-up of 18 ± 3 months, 2 patients died from noncardiac causes and 89 remained free of any events. In the 9 patients with coronary events, 2 had an infarction, 4 had unstable angina followed by PTCA, 2 had elective PTCA, and 1 had elective CABG (but the last 3 were because of disease progression in other vessels). A prospective, randomized trial (DEFER) evaluating the safety of this approach is ongoing.

Given the practice of performing angioplasty without ischemic testing or when ischemic testing is inconclusive, translesional hemodynamic data can identify patients in whom it is safe to forego coronary intervention. Coupled with the correlation of poststenotic flow reserve with scintigraphic stress imaging, lesion assessment in the cardiac catheterization laboratory can now become a cost-effective method to assess patients before intervention.

Prognostic Value of Intracoronary Flow Velocity and Diameter Stenosis in Assessing the Outcome of Coronary Balloon Angioplasty

Until recently, no appropriately sized and prospectively conducted study had assessed the value of flow-velocity indices in predicting immediate complications and the recurrence of stenosis and symptoms after PTCA. The aim of the DEBATE study was to identify Doppler flow-velocity indices predictive of the short- and long-term clinical outcome after angioplasty. The hypothesis was that a normalization of flow-velocity patterns and rheology within the dilated segment would have a favorable impact on the restenosis process. The study population consisted of 297 patients undergoing balloon angioplasty of a single major native coronary artery.[9] Flow-velocity measurements were realized with the Doppler wire in a proximal normal vessel segment, and distal to the lesion, in baseline conditions, and after intracoronary administration of adenosine (12 μg in the RCA and 18 μg in the LCA). Proximally and distally, a distance from the stenosis greater than five times the vessel diameter was maintained to avoid prestenotic acceleration of flow or poststenotic turbulent flow. Recommendations were given to disengage (whenever possible) the guiding catheter from the ostium at the time of hyperemia to avoid impedance of the maximal flow. At the end, flow-velocity recordings were obtained in the same position as before dilation. Assessment of the angioplasty procedure was based only on angiographic criteria (diameter stenosis <50%), using at least two cite angiograms in orthogonal projections. At 1 month of follow-up, the patient's anginal status was determined using the Canadian Cardiovascular Society Angina Classification and, whenever possible, a symptom-limited bicycle stress test was also performed. At 6 months, anginal status was re-evaluated and a control QCA (using the same projection) was made. All the QCA measurements were performed off-line with the CAAS II system (Pie

Medical, The Netherlands) by an independent core laboratory, which was blinded to the clinical and the Doppler information.

Because of bail-out stenting or protocol violation, matched recordings of preprocedure and postprocedure CFR were available in 225 patients leaving the hospital without any major adverse cardiac event. A complete set of recordings preprocedure and postprocedure of the CFR, the ratio of average diastolic-to-average systolic velocities and the proximal-to-distal velocity flow ratio were available in total in 187 patients. A summary of angiographic and flow measurements is illustrated in Figure 40–10. Diameter stenosis decreased from 62 mm ± 9% to 37 ± 8%. Distal CFR significantly increased from 1.60 ± 0.62 before PTCA to 2.74 mm ± 0.94 after the procedure. No difference was present between the RCAs and the LCAs. Distal baseline diastolic-to-systolic velocity ratio increased from 1.71 ± 0.65 to 2.06 mm ± 0.92 postprocedure. Pre-PTCA diastolic-to-systolic velocity ratio was significantly lower in the RCA compared to the LCA (1.44 ± 0.35 vs. 1.82 ± 0.71), and the diastolic-to-systolic velocity ratio remained unchanged in the RCA after the procedure, confirming the observation of Heller and associates.[160]

After 4 weeks, 82% of patients were free of symptoms and ischemic events, whereas 18% experienced either typical chest pain or had an electrocardiographic positive exercise test. At 6 months, 224 patients (99.6% of the eligible population) were monitored for the occurrence of any adverse major cardiac event: no death or myocardial infarction occurred and 166 patients had no target lesion revascularization (TLR). At the same time, 204 patients (91% of the eligible population) underwent clinical evaluation and a bicycle test and 123 were free of angina and/or ischemia. Control angiography was done in 202 patients: 130 had no restenosis.

Patients with or without symptoms and/or ischemia 1 month after PTCA had similar angiographic measurements after PTCA. However, among them, distal postangioplasty CFR was significantly lower (2.38 ± 0.74) compared with the asymptomatic patients (2.82 ± 0.95). The diastolic-to-systolic velocity and proximal-to-distal ratios were similar and thus had no prognostic values. After 6 months' follow-up, angiographic measurements were not different between patients with or without TLR, whereas distal CFR was significantly higher (2.80 ± 0.95) in patients without TLR compared with those with TLR (2.50 ± 0.77). Postprocedural diameter stenosis was significantly higher in patients with angiographic restenosis at 6 months (41 ± 8%) compared with patients free from restenosis (35 ± 8%). Receiver operating characteristic curves analysis showed that postprocedural CFR appears to have a modest prognostic value in predicting the incidence of symptoms and/or ischemia at 4 weeks. Prognostic value for symptoms and/or ischemia and for TLR at 6 months was weaker, with an optimal prognostic cut-off of approximately CFR = 2.5. Diameter stenosis had a reasonable prognostic value in predicting angiographic restenosis and symptoms and/or ischemia recurrence at 6 months, with an optimal cut-off value of 35%. Multivariate logistic regression demonstrated that CFR and diameter stenosis had significant independent prognostic value, which permitted categorization of the population into subgroups: those with or without a CFR of 2.5 or less and those with or without a diameter stenosis of 35% or less. The subset with the best outcome was the one characterized by a CFR of greater than 2.5 and a diameter stenosis of 35% or less (n = 44). Compared with the three other pooled groups (n = 158), early recurrence of ischemia was present in 10% versus 19% (P = 0.15) of the patients, late recurrence in 23% versus 47% (P = 0.005), TLR in 16% versus 34% (P = 0.02), and restenosis rate in 16% versus 41% (P = 0.002).

This study demonstrated that flow-velocity parameters recorded at the time of the procedure are the most important prognostic indicators of early clinical recurrence, whereas diameter stenosis is a better predictive marker of angiographic restenosis. The combination of a CFR of greater than 2.5 and a diameter stenosis of 35% or less is a predictor of 6 months' recurrence of symptoms and TLR. A patient with a diameter stenosis of less than 35% will have a 26% incidence of events at 6 months, a patient with a CFR of greater than 2.5 will have a 24% incidence of events, but a patient with a diameter stenosis of 35% or less and a CFR of greater than 2.5 will have the best long-term result, with an event rate of 16%, comparable to results so far obtained with stents.[165] In this trial, 20% to 25% of the population did not need further therapy to achieve a clinical outcome similar to those observed after stenting. The cost effectiveness of a therapeutic policy in which no stent is implanted when the criteria of CFR greater than 2.5 and diameter stenosis of 35% or less are present after conventional balloon angioplasty is being investigated in a new ongoing trial: DEBATE II.

The DESTINI study is also a trial of provisional stenting in which CFR and residual diameter stenosis after PTCA are used for clinical decision making.[166] The initial results have shown that 50% of the 305 lesions treated with Doppler and QCA-guided balloon angioplasty received a stent because the functional or angiographic endpoints were not met. In both the patients receiving a stent and the patients remaining in the PTCA group, the incidence of inhospital adverse events was lower than 4%.

Nonballoon Coronary Interventions

Stent Implantation

Angiography has clear limitations in the assessment of the hemodynamic severity of a dissection after balloon angioplasty.

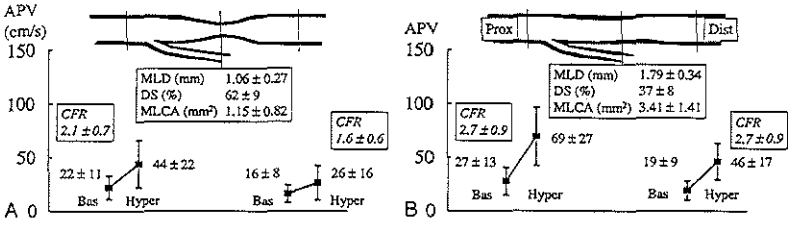

FIGURE 40–10. Summary of the acute angiographic and velocity measurements obtained pre-PTCA *(A)* and post-PTCA *(B)* procedure in the DEBATE study in 225 patients: minimum (B) luminal diameter (MLD), diameter stenosis (DS) and minimum luminal cross-sectional area (MLCA) by densitometry, and average peak velocity (APV) in baseline condition (Bas) and during hyperemia (Hyper), proximally and distally to the lesion. MLD increased from 1.06 ± 0.27 to 1.7 ± 0.34 mm, with a decrease in DS from 62 ± 9% to 37 ± 8%. Distal coronary flow reserve (CFR) increased from 1.6 ± 0.6 to 2.7 ± 0.9. PTCA, percutaneous transluminal coronary angioplasty.

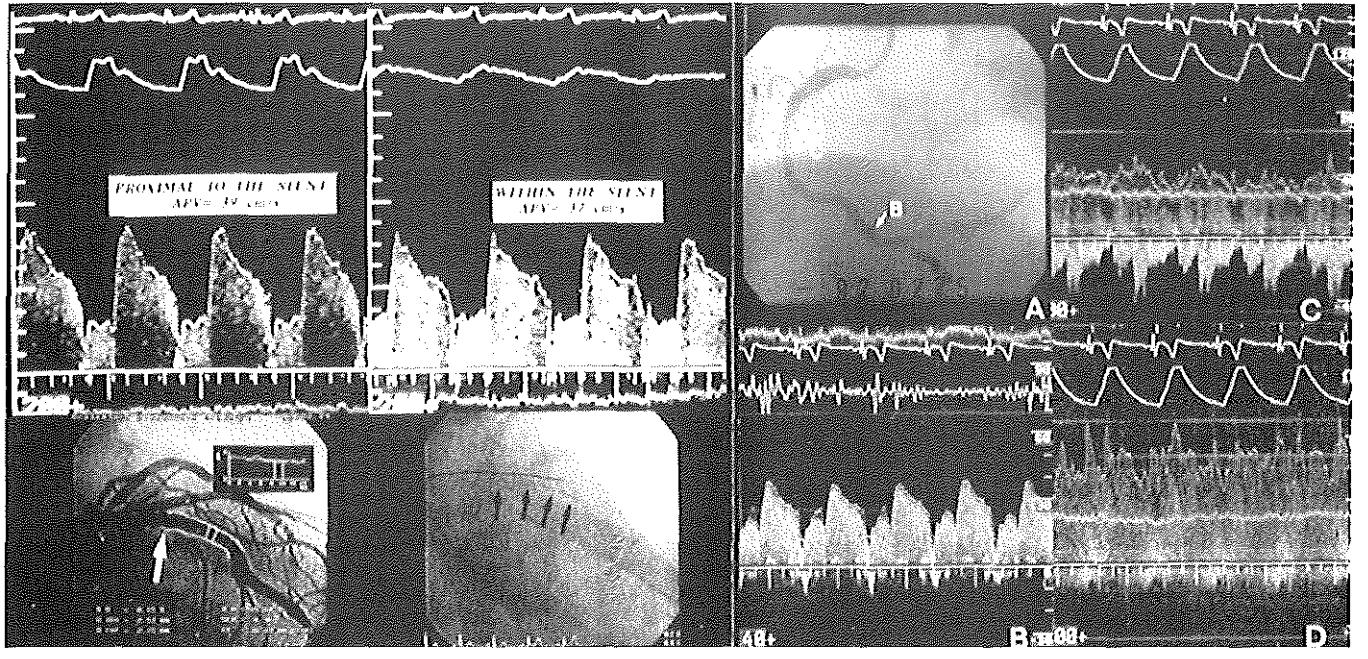

FIGURE 40–11. *A*, Flow-velocity recordings immediately distal and within a stented coronary segment. Note that the maximal velocity and velocity pattern are unchanged proximal to the stent *(upper left panel)* and within the stent *(upper right panel)*. In the lower left panel, an arrow indicates the position of the Doppler sample volume proximal to the stent and two lines indicate the sample volume within the stent. In the fluoroscopic image in the lower right panel, arrows indicate the poorly radiopaque stent. *B*, Flow-velocity recordings distal *(B)* and within *(C,D)* a coronary stenosis after coronary balloon angioplasty. In the right upper panel *(A)* the position of the velocity recordings distal to the stenosis is indicated with an arrow and, more proximally, the tip of the Doppler guidewire is positioned in the segment treated with balloon dilation. Note the marked increase in flow velocity from the distal reference segment *(B)* to the dilated stenosis *(C,D)*, with an almost continuous flow and a negative velocity component probably indicating a retrograde filling of the angiographically visible dissection.

Intracoronary Doppler can detect the presence of an impaired flow distal to the dissection requiring treatment with coronary stenting.[167] Stent implantation is the only coronary intervention inducing a complete normalization of the arterial cross-sectional area in most cases. This provides a unique opportunity to verify whether a complete flow normalization occurs after the arterial geometry normalization following stenting.

Coronary artery lumen enlargement with stenting, improving coronary blood flow, has reduced the historically high restenosis rate of balloon angioplasty.[168, 169] Reduced restenosis is related to blocking elastic recoil, as well as improved blood rheology.[170, 171] Coronary blood flow reserve after balloon angioplasty has been persistently abnormal in more than 50% of patients, attributed to microcirculatory abnormality and/or inadequate epicardial lumen expansion not identified by successful angiography.[158, 159]

A possible method of assessing the adequacy of the arterial conduit obtained after stent implantation is the measurement of flow velocity immediately distal, within, and proximal to the stent. The presence of an unchanged velocity and velocity pattern directly demonstrates, based, on the continuity equation, the normalization of flow dynamics (Fig. 40-11).

Several authors have reported a statistically significant increase in the CFR distal to a stenosis (dCFR) measured after stent implantation, compared with the dCFR measured after the angioplasty, but in rather small series of patients.[172-175] A recent analysis[175] of the first 27 patients who required a stent implantation for a nonoptimal angiographic result after PTCA in the DEBATE study has demonstrated similar results: after PTCA, MLD increased from 1.05 ± 0.23 mm to 1.77 ± 0.31 mm, and after stent implantation, it increased to 2.57 ± 0.35 mm. At the same time, dCFR significantly increased from 1.38 ± 0.4 before the procedure to 1.82 ± 0.43 after PTCA, and to 2.57 ± 0.56 after stenting. A similar improvement in the fluid dynamic properties of stented epicardial vessels has been measured with pressure wires by the assessment of the FFRMYO.[176]

Role of Coronary Lumen Enlargement in Improving Coronary Blood Flow After Balloon Angioplasty and Stenting

A combined IVUS and Doppler flow imaging study to demonstrate the role of the conduit lumen on coronary blood flow after balloon angioplasty and coronary stenting was performed in 42 patients.[137] Data were collected before and after angioplasty and again after stent placement. A subset of 17 patients underwent IVUS examination of the target and reference segments after each intervention. The angiographic percent diameter stenosis decreased from 84 ± 13% to 37 ± 18% after angioplasty and to 8 ± 8% after stenting. CFR was minimally changed from 1.70 ± 0.79 at baseline to 1.89 ± 0.56 after angioplasty and increased to 2.49 ± 0.68 after stent placement, a value similar to that of the reference vessel of 2.61 ± 0.46 (Fig. 40-12). Comparing stenting and postangioplasty results, IVUS cross-sectional area was 8.39 ± 2.09 versus 5.10 ± 2.03 mm² ($P < 0.01$). Increasing CFR was correlated with increasing lumen cross-sectional area as determined by IVUS and angiography (Fig. 40-13) and QCA percent area stenosis. The relative CFR ($CFR_{TARGET}/CFR_{REFERENCE}$) was 0.65 ± 0.03 before angioplasty, significantly increasing to 0.72 ± 0.21 after angioplasty and normalizing to 1.03 ± 0.3 after stenting (normal relative CFR should be 1.0 ± 0.2).

For the entire subset of patients, the IVUS imaging data demonstrated that total vessel cross-sectional area was similar for the reference segments before and after angioplasty and

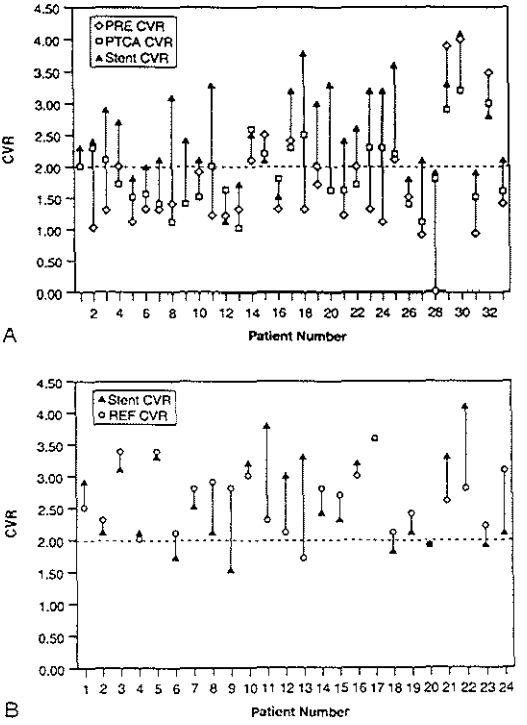

FIGURE 40-12. *A*, Individual patient data for coronary flow reserve (CVR) measurements before (diamonds) and after (squares) percutaneous transluminal coronary angioplasty (PTCA) and again after stent placement (triangles). *B*, CVR in the reference segment (circle) versus the stent segment (triangles). (From Kern MJ, DuPouy P, Drury JH, et al: Role of coronary artery lumen enlargement in improving coronary blood flow after balloon angioplasty and stenting: A combined intravascular ultrasound Doppler flow and imaging study. J Am Coll Cardiol 29:1520-1527, 1997. Reprinted with permission from the American College of Cardiology.)

stenting (16 ± 3 mm²), but there was an 80 ± 59% increase in lumen area from 5.1 to 8.39 mm² after stenting.

Although angiography has been used to guide the endpoint decision of coronary angioplasty, the relationship of CFR to residual conduit lumen cross-sectional narrowing suggests than an endpoint decision based solely on anatomy may be incomplete in some cases. Stenting appears to normalize absolute CFR in most patients. For those with CFR of less than 2.0, stenting normalized relative CFR in 95% of patients.

These data indicated that increases in CFR were associated with increases in coronary lumen cross-sectional area in most patients. The data further suggest that impaired CFR after angioplasty is more often related to the degree of residual narrowing than the occurrence of microvascular flow impairment. These data also support a physiologically complemented approach to balloon angioplasty that may improve procedural outcome decisions for provisional stenting.

Directional Coronary Atherectomy

The clinical application of intracoronary Doppler for the assessment of directional atherectomy was limited in the early

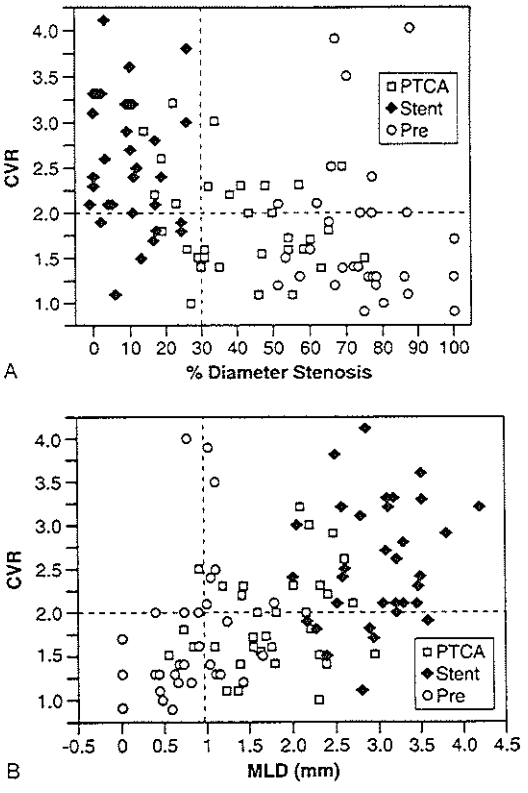

FIGURE 40-13. *A*, Relationship between percent diameter stenosis and coronary flow reserve (CVR). *B*, Minimum luminal diameter (MLD) and CVR for the prestent patients (circles), the post-PTCA results (squares), and the poststent results (diamonds). PTCA, percutaneous transluminal coronary angioplasty. (From Kern MJ, DuPouy P, Drury JH, et al: Role of coronary artery lumen enlargement in improving coronary blood flow after balloon angioplasty and stenting: A combined intravascular ultrasound Doppler flow and imaging study. J Am Coll Cardiol 29:1520-1527, 1997. Reprinted with permission from the American College of Cardiology.)

days because of a practical limitation related to the incompatibility of the 0.018-in. Doppler guidewire with the lumen of the devices used, which is now solved with the 0.014-in. model. Nevertheless, observations have confirmed the potential usefulness of intracoronary Doppler,[177] but massive release of local vasoactive factors due to extensive wall damage could hamper an acute restoration of a normal coronary flow reserve.

Rotational Coronary Atherectomy

Rotational atherectomy is being performed with increasing frequency in distinct subsets of patients with lesion characteristics unfavorable for either conventional balloon angioplasty or directional atherectomy. Although satisfactory angiographic luminal enlargement can be accomplished with rotational ablation alone, documentation of the physiologic influence of this technique and the beneficial effect of adjunctive angioplasty were lacking. Khoury and associates[178] and, more recently, Bowers and colleagues,[179] have investigated this issue. Khoury and associates studied 14 arteries treated by percutaneous transluminal coronary rotational atherectomy (PTCRA) followed by angioplasty in 13 patients. MLD measured by quantitative angiography increased after PTCRA from 0.7 ± 0.4 mm to 1.9 ± 0.4 mm, and a further significant increase was obtained after adjunctive balloon angioplasty (2.4 ± 0.5 mm). Distal to the stenosis, coronary blood flow at baseline, measured with a Doppler wire, was 47 ± 23 mL/min and 57 ± 38 mL/min during hyperemia (ic adenosine). After PTCRA, coronary blood flow increased to 104 ± 59 mL/min at baseline and to 132 ± 73 mL/min during hyperemia. Adjunctive angioplasty did not significantly increase baseline and hyperemic flow compared with PTCRA (84 ± 40 mL/min and 143 ± 81 mL/min, respectively). Poststenotic flow reserve, not significantly increased after PTCRA alone (1.1 ± 0.2 versus 1.3 ± 0.3), significantly increased after adjunctive balloon angioplasty (1.6 ± 0.3). Similar measurements were found by Bowers and coworkers[179] in a series of 22 patients. They reported a significant increase in MLD from 0.8 ± 0.1 to 1.5 ± 0.2 after Rotablator atherectomy, and a further increase to 2.0 ± 0.1 mm after adjunctive balloon angioplasty. There was a nonsignificant increase in baseline and hyperemic distal average peak velocities. There was a significant increase, versus baseline, in distal average peak velocity to 39.5 ± 3.7 cm/sec (53.4 cm/sec during hyperemia) after adjunctive PTCA. There was no statistically significant increase in the CFR after Rotablator or after balloon angioplasty.

The mechanism of rotational atherectomy relies on plaque pulverization and embolization of microparticles, usually small enough to pass through the capillary circulation, that are removed by the reticuloendothelial system.[180] These two studies demonstrate that after rotational atherectomy and adjunctive balloon angioplasty, although a luminal enlargement is obtained and coronary blood flow is improved, with a restoration of the diastolic predominant pattern in the LCA, there is a persistent impairment of CFR. Further studies are required to understand the possible underlying causes: residual stenosis of the epicardial conduit arteries, secondary impairment of the microcirculation, or transient secondary increase in basal flow velocity.

Laser-Assisted Angioplasty

Explosive gas bubble formation represents a mechanism of tissue ablation during laser application, explaining the persistent high incidence of laser-induced dissections.[181] The use of intracoronary Doppler in combination with a laser catheter has shown acoustic disruption of the Doppler signal that was temporarily limited to the period of active laser firing, thus confirming that gas formation is a normal operative mechanism of tissue ablation in vivo during Excimer laser angioplasty, carrying a potential risk of wall dissection.[182]

After multiple passages of laser probes, the obtained luminal enlargement is insufficient in most cases to restore a normal flow velocity both in coronary and peripheral arteries. After completion of the procedure with balloon angioplasty, a normalization of the indices reflecting flow dynamics across the stenosis was observed.[74] Similar results have been confirmed in peripheral and coronary arteries by Isner and colleagues.[183]

INTRACORONARY DOPPLER AS A RESEARCH TOOL FOR THE STUDY OF CORONARY CIRCULATION

Doppler Coronary Flow Velocity and Acute Myocardial Infarction

Physiology of Acute Myocardial Infarction

Coronary blood flow can be accurately measured using intracoronary Doppler blood flow velocity and compared with semiquantitative but clinically predictive Thrombolysis in Myocardial

Infarction (TIMI) angiographic flow, an established standard of reperfusion therapies. To address the relationship of TIMI flow-to-flow velocity, coronary flow velocity was measured before and after primary or rescue angioplasty using a Doppler wire in 41 patients with acute myocardial infarction.[184] TIMI angiographic flow grade was assessed by two independent observers and also quantitated by frames-to-opacification method from cinefilm. Before angioplasty, 34 patients had TIMI grade 0 or 1, 5 patients had TIMI grade 2, and 3 patients had TIMI grade 3 flow in the infarcted artery. Following angioplasty, diameter stenosis improved from 95 ± 7% to 22 ± 10%. One patient had TIMI grade 1, 5 patients had TIMI grade 2, and 35 patients had TIMI grade 3 flow. Poststenotic flow velocity increased from 6.6 ± 6.1 cm/sec to 20.0 ± 11.1 cm/sec following angioplasty. Before angioplasty there were no statistical differences between poststenotic flow velocity values among infarct vessels with TIMI grade 0, 1, or 2; however, TIMI grade 3 had higher flow velocity (9.4 ± 5 cm/sec vs. 16 ± 5.4 cm/sec). Postangioplasty flow velocity correlated with angiographic frame count. However, for TIMI grade 3, there was a large overlap with low TIMI ≤2 flow velocity (<20 cm/sec), despite frames-to-opacification below 60 (Fig. 40-14).

These results indicate that semiquantitative TIMI perfusion grades are distinguished by differences in coronary flow velocity, with TIMI grade ≤2 consistently associated with low flow values. On average, TIMI grade 3 flow velocity is higher than TIMI grades ≤2 flow, but there is a substantial overlap with low flow values of TIMI ≤2 flow. Quantitative assessment of flow velocity after reperfusion could potentially establish important physiologic correlations among clinical outcomes after various reperfusion therapies.

Impaired Coronary Flow Reserve After Myocardial Infarction: Residual Stenosis, Microcirculatory Stunning, or Both?

CFR in target regions after myocardial infarction is frequently impaired. Whether the abnormal CFR is related to residual stenosis severity and potential myocardial viability (microcirculatory integrity) was examined by Claeys and associates.[185] Distal coronary blood flow velocity before and after angioplasty in 36 patients 13 ± 7 days after acute myocardial infarction was examined, and 38 patients with similar coronary artery disease but without myocardial infarction served as controls. Residual coronary stenosis severity was analyzed by QCA and infarct size was assessed by myocardial perfusion scintigraphy. For similar degrees of angiographic stenosis severity preangioplasty and postangioplasty, CFR was significantly lower in patients with myocardial infarction compared with controls without myocardial infarction (1.22 ± 0.26 vs. 1.50 ± 0.45 and 1.72 ± 0.43 vs. 2.21 ± 0.74, respectively, before and after PTCA). Although CFR increased significantly after successful angioplasty in both groups, abnormal CFR was present in 80% of infarct patients and 44% of patients without infarct. Angiographic stenosis severity was the most important determinant of CFR in both study groups. The investigators concluded that CFR is significantly lower in patients with recent myocardial infarction both before and after intervention. In addition to the presence of postreperfusion coronary microcirculatory responses, CFR is related mainly to stenosis severity rather than to residual myocardial viability. These findings suggest that limiting residual luminal narrowing by stenting in acute myocardial infarction may immediately improve the physiologic responses.

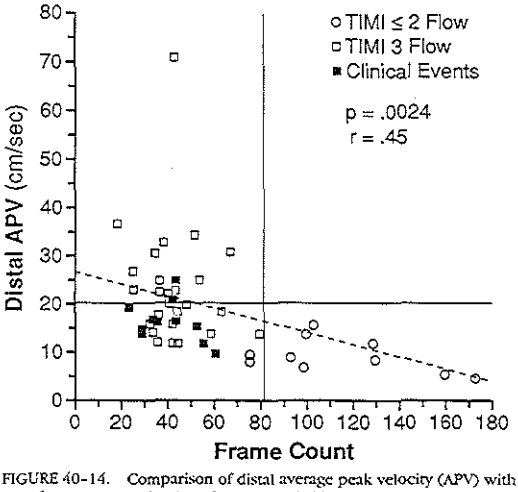

FIGURE 40-14. Comparison of distal average peak velocity (APV) with cine frames-to-opacification (frame count): TIMI 3 flow (open squares), TIMI ≤2 (circles), and clinical events (solid squares). There is a correlation between distal APV and the frame count. Postmyocardial infarction (solid squares) occurred in 9 of 11 patients with TIMI flow <20 cm/sec. (From Kern MJ, DuPuoy P, Drury JH, et al: Determination of angiographic [TIMI grade] blood flow by intracoronary Doppler flow velocity during acute myocardial infarction. Circulation 94:1545-1552, 1996.)

Postmyocardial Infarction Risk Prediction

Intracoronary Doppler assessment of poststenotic reperfusion CFR may be useful as a marker of postinfarction risk. Miller and colleagues[186] examined coronary Doppler flow and postmyocardial infarction risk stratification markers in 41 consecutive patients after primary angioplasty. Coronary flow was measured 15 minutes after the intervention and SPECT perfusion imaging and stress electrocardiographic ST segment changes were measured 3 weeks following myocardial infarction. The infarct-related artery diameter stenosis decreased from 97 ± 8% to 24 ± 10% with an improvement in TIMI grade flow from 0.5 to 2.8. Average peak velocity increased from 7 ± 6 to 19 ± 8 cm/sec. Postangioplasty, CFR was 1.6 ± 0.6 and left ventricular ejection fraction was 48 ± 14%. At a follow-up period of 19 ± 12 months, a multivariate regression revealed that following successful primary angioplasty for acute myocardial infarction, coronary flow-velocity reserve failed to predict future cardiac events, whereas residual postperfusion left ventricular ejection fraction and SPECT perfusion imaging had incrementally defined prognostic events. It should not be surprising that immediate postinfarction CFR is impaired and that the 3-week follow-up result may have significance for myocardial reperfusion benefit.

Study of Collateral Circulation

Flow-Velocity Measurements in the Recipient Vessel

Quantification of coronary collateral flow has been performed in experimental animal studies by direct measurement of retrograde flow and pressure[187, 188] or radionuclide microsphere flow techniques.[189-191] In patients, only a qualitative and subjective angiographic determination of mature epicardial collateral channels[192, 193] or acutely recruitable collateral vessels during angioplasty[194-197] has been achieved. The use of a Doppler guidewire permits quantitative measurement of coronary blood flow velocity beyond severe and totally occluded arterial segments[22, 198] so that collateral flow velocity can be measured. Although acutely recruitable and mature collateral flow has been shown during

angioplasty by both hemodynamic (coronary occlusion wedge pressure)[199, 200] and angiographic methods,[192, 197] neither technique is sufficiently quantitative to assess collateral function during hemodynamic or pharmacologic perturbations. During routine coronary angioplasty, retrograde collateral flow velocity, observed during multiple coronary balloon inflations as a reproducible phenomenon, is associated with acutely recruited angiographic collateral supply.[22, 198] To assess quantification of the coronary collateral circulation, flow-velocity data were obtained during angioplasty and compared with both angiographic grade of collateral flow and the spectrum of normal antegrade flow patterns.

Twenty-one patients undergoing routine coronary angioplasty had evidence of angiographically established collateral flow (n = 10) or had acutely recruitable collateral flow velocity during balloon inflation (n = 11).[201]

After a lesion was crossed with the guidewire and balloon catheter, the balloon was inflated and flow-velocity data were continuously recorded before, during, and for 120 seconds after balloon deflation. Collateral blood flow was defined as retrograde or persistent antegrade flow during balloon occlusion. A typical retrograde collateral flow-velocity response is shown in Figure 40-15. In some patients, continuous antegrade flow during total arterial occlusion of balloon inflation was recorded. These patients had septal to LAD or LAD to posterolateral branch flow, wherein the flow was measured distal to the contralateral collateral input origin.

The angiographic collateral supply was assigned a collateral score based on opacification according to Rentrop and coworkers,[196, 197] whereby a score of 3 is dense, 2 is moderate, 1 is faint, and 0 is no visible filling of collateral channels.

Retrograde collateral flow was observed in 17 patients. There were no differences between left-to-right collateral flow patterns and no difference between systolic or diastolic velocity between the RCA or the LCA. There was a poor correlation between magnitude of collateral flow velocity and angiographic score.

The coronary collateral flow-velocity response was characterized by flow reversal or persistent antegrade flow during coronary balloon occlusion.[22, 198] The phasic nature of the reversed flow pattern appeared related to source artery and pathway of the collateral channels. Large, completely epicardial collaterals with grade 3 angiographic flow had the most clearly demarcated phasic components. Coronary flow velocity reversal was identified showing peak negative flow velocities of 10 to 25 cm/sec and flow patterns that recurred during multiple balloon occlusions. At the conclusion of the angioplasty, restoration of the normal coronary flow-velocity pattern was clearly evident.

The quantitative nature of collateral flow velocity provides an excellent tool to evaluate pharmacologic interventions postulated to alter collateral supply, such as was reported by Donohue and associates.[202]

Several potential applications are immediately apparent for collateral flow measurement in patients with ischemic heart disease. The documentation of collateral flow in patients in whom angiographic appearance is poor or absent might provide an increased margin of safety for patients undergoing coronary angioplasty. A Doppler guidewire may identify patients in whom adequate collateral flow may obviate more invasive and potentially complicating hemodynamic support measures.

Measurement of Flow Velocity in the Donor Vessel

As described in the previous section, flow-velocity changes in the recipient vessel during coronary occlusion provide infor-

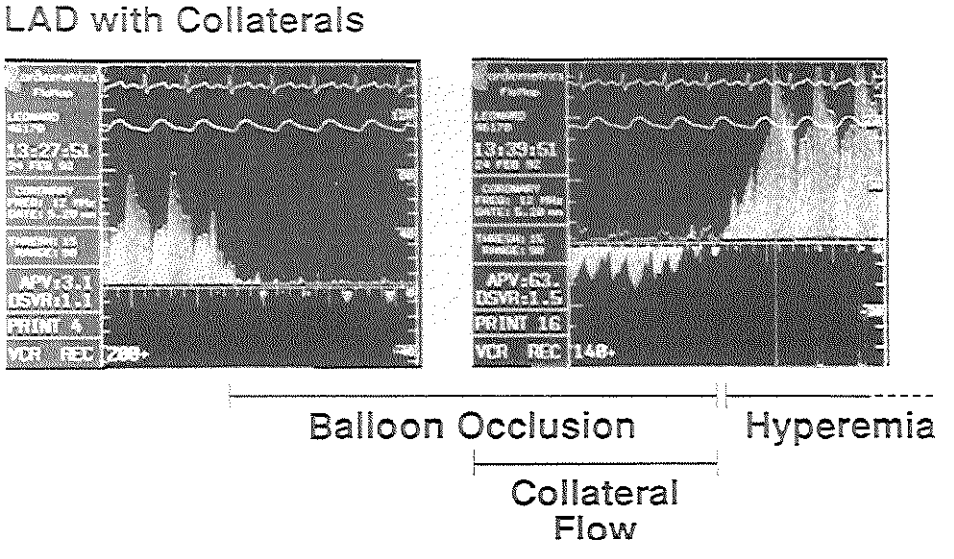

FIGURE 40-15. Spectral velocity (scale 0 to 200 cm/sec) showing normal antegrade (upward directed from base) flow pattern with phasic systolic and diastolic flow prior to coronary balloon occlusion. At balloon occlusion, coronary flow goes to zero. After 10 seconds, collateral flow appears as reversed flow toward the guidewire tip (inverted phasic signal beneath the baseline). On balloon deflation, antegrade flow is restored with postischemic hyperemia. During balloon occlusion, the collateral flow velocity can be quantitated. (From Kern MJ, Donohue TJ, Bach RG, et al: Quantitating coronary collateral flow velocity in patients during coronary angioplasty using a Doppler guidewire. Am J Cardiol 17:34D–40D, 1993.)

mation on collateral flow in a semiquantitative fashion. Experimental data, however, have indicated that flow-velocity alterations of the contralateral artery during sudden coronary occlusion can be used for assessment of collateral flow.[205] Collateral vascular growth was induced in these experiments by repeated brief coronary occlusions. After collateral vessels had developed, a reduction of electrocardiographic and hemodynamic signs of ischemia during coronary occlusion was noted, related to a transient increase in flow velocity of the contralateral artery. A model was developed to express the growth of the collateral circulation in terms of flow and resistance in the setting of coronary angioplasty. It was based on recordings in 23 patients with single-vessel disease.[50]

Angiography of the contralateral artery was performed before and during balloon coronary occlusion to assess recruitability of collateral vessels using Rentrop's classification.[196] Flow-velocity assessment of the contralateral artery was performed with a 3-French Doppler catheter (model DC-201, Millar Instruments, Inc.) during the second and subsequent balloon inflations.

Assessment of flow-velocity changes in the contralateral artery by spectral analysis was performed by determining maximal diastolic flow velocity before (V_1), during (V_2), and after (V_3) balloon inflation. Collateral flow was determined by the decrease of maximal diastolic flow velocity after balloon deflation (V_2 to V_3), expressed as a percentage of the maximal diastolic flow velocity before balloon inflation (V_2 to V_3/V_1), according to a previously described method.[197] Flow-velocity changes of the contralateral artery were used, in combination with the aortic and coronary wedge pressure, to calculate the relative resistance of the collateral vascular bed.[204, 205]

The transient flow-velocity increase of the contralateral artery during coronary occlusion was significantly less in the eight patients without collateral vessels, as compared with the patients with collateral vessels. A lower ratio between resistance of the collateral vessels and arteriolar resistance of the donor artery was observed in the presence of collateral vessels during coronary occlusion. Furthermore, when collateral vessels were present during coronary occlusion, the coronary wedge pressure was higher (24 ± 6 mm Hg vs. 40 ± 14 mm Hg) and less severe electrocardiographic signs of ischemia were observed.

The positive predictive value of a low relative collateral vascular resistance (ratio between the resistance of the collateral vessels and arteriolar resistance of the donor artery <10), a contralateral flow-velocity change greater than or equal to 10%, or a coronary wedge pressure greater than 30 mm Hg, for the presence of collateral vessels during coronary occlusion was 100%, 100%, and 78%, respectively. The negative predictive value was 88%, 80%, and 55%, respectively.

The authors concluded that collateral vessels are important for prevention of electrocardiographic signs of ischemia during 1-minute coronary occlusion. The beneficial effect of collateral vessels is exerted by a significant increase in flow of the contralateral artery in combination with a reduced resistance of the collateral vascular bed. Flow-velocity assessment of the contralateral artery is a technique providing quantitative information on the development of the collateral vascular bed in obstructive coronary artery disease. Similar results were also reported by Yamada[206] and Bach[207] and their associates.

More recently, Piek and colleagues[208] studied the clinical, angiographic, and hemodynamic predictors of recruitable collateral flow using this method in 105 patients. Duration of angina (≥3 months), lesion severity, and proximal lesion location were independent factors positively associated with recruitability of collateral vessels in a multivariate logistic analysis, with an overall predictive accuracy of 80%. Conversely, nitrates exerted an independent negative effect. Presence of recruitable collateral vessels during balloon inflation resulted in a higher coronary wedge-to-aortic pressure ratio (0.35 ± 0.13 vs. 0.27 ± 0.12), a lower relative collateral vascular resistance (6.7 ± 7.4 vs. 21.3 ± 10), and a reduction of electrocardiographic signs of ischemia. However, the relative collateral vascular resistance was the best predictor for recruitability of collateral vessels compared with the other variables related to collateral vascular growth.

Measurement of Flow Velocity in the Donor and the Recipient Vessels

Tron and coworkers[209] examined the flow-velocity patterns of human coronary collateral circulation and characterized the ipsilateral coronary blood flow during coronary angioplasty. In 49 patients, angiographic collateral filling was categorized by the Rentrop grading system and by anatomic pathway (epicardial, intramyocardial, or unknown, that was acutely recruited). Collateral blood flow velocity was measured distal to the balloon-occluded segment during balloon inflation. Collateral blood flow velocity was characterized as predominantly systolic or diastolic flow, biphasic or monophasic (only systolic or diastolic), and antegrade or retrograde. Biphasic flow was found in 47% of the patients, and predominantly systolic flow signal was seen in 73%. Epicardial collateral pathways had the highest total flow-velocity integral. There were no differences in the flow-velocity integrals among the Rentrop angiographic grades of collateral filling.

Piek and associates[210] have also reported a comparison of collateral vascular responses assessed in the donor and the recipient coronary artery during transient coronary occlusion in 57 patients with single-vessel disease. Flow analysis was performed with a Doppler catheter in the contralateral donor artery or the ipsilateral recipient artery or both using a Doppler catheter or wire. Ischemia was evaluated by ST segment shift on a 12-lead electrocardiogram at 1 minute of coronary occlusion. Recruitable collateral flow was present in 39 patients and was associated with an increase in blood flow velocity in the donor artery and in the recipient artery, related to a reduced relative collateral vascular resistance. Collateral flow in the recipient artery was a better predictor for ischemia than was collateral flow in the donor artery or angiographic grading of collateral vessels.

Pharmacologic Modulation of Human Collateral Vascular Resistance

Piek and colleagues[211] recently evaluated the pharmacologic responsiveness of the coronary collateral circulation in patients with recruitable or spontaneously visible collateral vessels during balloon coronary occlusion using a Doppler wire in the recipient coronary artery distal to the balloon. In 38 patients, one guiding catheter was used for the introduction of the Doppler wire and the balloon in the recipient artery and another guiding catheter was used for angiography of the donor coronary artery and the administration of adenosine (12 to 18 μg) or nitroglycerin (0.2 mg). Diastolic blood flow-velocity integral (dVi), aortic (Pao) and coronary wedge (Pw) pressures were used to compute the collateral vascular resistance index

$$R_{COLL} = (P_{AO} - P_W)/dVi$$

and the peripheral vascular resistance index of the recipient coronary artery

$$R4 = P_W/dVi$$

Using these definitions, the coronary wedge/aortic pressure ratio can be expressed by

$$Pw/Pao = R4/(Rcoll + R4)$$

The effect of bolus injections of adenosine and nitroglycerin in the donor vessel on these variables was assessed during balloon inflations. In patients with recruitable collateral vessels, there was no change in dVi and Pw-to-Pao ratio with adenosine or nitroglycerin. In patients with spontaneously visible collateral vessels, dVi increased after adenosine and nitroglycerin. The Pw-to-Pao ratio remained unchanged, but Rcoll and R4 decreased. This study was the first one to directly assess the pharmacologic responsiveness of the collateral circulation. It demonstrated that coronary collateral blood flow can be increased with adenosine and nitroglycerin in patients with single-vessel disease when spontaneously visible collateral vessels are visible. This effect is a result of a reduction in the collateral vascular resistance and peripheral vascular resistance of the recipient coronary artery. Because of the importance of the collateral vessels in the outcome of acute coronary syndromes, these findings might stimulate further research for the evaluation of other pharmacologic agents that are effective in modulating coronary collateral vascular resistance.

Coronary Blood Flow Velocity During Aortic Balloon Counterpulsation

Controversy exists regarding the ability of intra-aortic balloon pumping to increase coronary blood flow in patients with obstructive coronary artery disease. To assess the effects of intra-aortic balloon pumping on coronary hemodynamics, coronary blood flow velocity was measured with a Doppler guidewire in 15 patients who received an intra-aortic balloon pump for typical clinical indications.[212, 213] In nine patients before angioplasty, peak diastolic coronary flow velocity beyond the stenosis was unaffected by intra-aortic balloon pumping. After angioplasty, the improved coronary luminal diameter narrowing was associated with increased distal flow, further increased with intra-aortic balloon pumping. In the five normal reference arteries, intra-aortic balloon pumping increased flow.

These data demonstrated a lack of significant flow improvement beyond the most critical stenoses with intra-aortic balloon pumping, despite augmented diastolic pressure and the unequivocal restoration and intra-aortic balloon pump-mediated augmentation of both proximal and distal coronary blood flow velocity after amelioration of severe coronary obstructions in patients after successful coronary angioplasty. The question of whether a 25% augmentation of distal mean coronary flow by intra-aortic balloon pumping provides substantial clinical benefit cannot be completely answered. However, a modest increase in distal velocity often is accompanied by a shift in the phasic relationship of flow, with a decrement in systolic flow and a significant increase in diastolic flow. Previous studies have demonstrated that subendocardial perfusion occurs during diastolic epicardial coronary flow and that the systolic component provides little contribution to subendocardial perfusion. By shifting flow to diastole, the physiologic benefit of increased flow may be more dramatic than can be inferred from a 25% increase in mean flow. Enhanced coronary blood flow velocity in the setting of angioplasty for acute myocardial infarction may assist in maintaining or promoting a reduced incidence of postprocedural abrupt closure when intra-aortic balloon pumping is used as adjunctive therapy.[214, 215]

More recently, Bach and coworkers[216] studied the effects of aortic counterpulsation on coronary flow through coronary perfusion balloon catheters. Intra-aortic balloon pumping increased average peak and mean diastolic velocities. The investigators concluded that intra-aortic balloon pumping significantly augmented distal coronary blood flow during balloon pumping, which may provide a mechanism to further reduce ischemia and increase the safety of high-risk coronary angioplasty in patients with hypotension who require perfusion balloon catheters.

Assessment of Endothelial Function

The in vitro observations of Furchgott and Zawadzki[217] and the in vitro and in vivo reports from the group of Moncada[218, 219] have shown that an endothelium-derived relaxing factor, identified as nitric oxide,[218] modulates vascular tone in response to physiologic and pathologic stimuli (e.g., increase in wall shear stress, serotonin, bradykinin, sympathetic stimulation, acetylcholine, endotoxins). Endothelial damage, leading to a decreased formation or release of nitric oxide from its precursor L-arginine, or reduced penetration due to the presence of subendothelial intimal thickening, is a possible explanation of the impairment of endothelium-mediated vasodilation observed in patients with systemic hypertension,[220] hypercholesterolemia, diabetes mellitus,[221] and atherosclerosis.[222]

The presence of paradoxic vasoconstriction induced by acetylcholine has been shown in coronary patients at sites of severe stenosis or moderate wall irregularities[223] and in angiographically normal segments.[224–226] Coronary spasm after acetylcholine infusion has also been demonstrated in patients with variant angina, with and without angiographically visible changes.[227, 228] The observed vasoconstriction or vasodilation after acetylcholine is the net effect of the conflicting action of this substance on the endothelial cells (stimulation to the release of endothelium-derived relaxing factor) and on the smooth muscle cells (vasoconstriction due to the direct effect on the cholinergic receptors). With the use of intracoronary Doppler, an impairment of the endothelium-derived vasodilation was observed also after physiologic stimuli such as the increase in blood flow.[229–231] The flow-dependent vasodilation is an essential mechanism of adjustment of coronary tone to prevent endothelial damage due to a pathologic increase in wall shear stress. An abnormal vasoconstriction in response to sympathetic stimulation[232] or release of platelet-derived vasoconstrictors[233, 234] was observed if the direct effect of these substances on the muscular media was not antagonized by a preserved endothelium-mediated vasodilation. Nitric oxide has also a powerful antiaggregatory activity. Yao and associates[235] showed a protective effect of endogenous nitric oxide in the prevention of cyclic flow variations due to platelet aggregation at the site of the endothelial injury. Garg and Hassid[236] demonstrated also that nitric oxide inhibits smooth muscle cell proliferation. Endothelial dysfunction, therefore, not only potentially aggravates ischemia in patients with coronary atherosclerosis but also increases the risk of endothelial injury and impairs the antithrombotic reaction, thus facilitating the development of acute coronary syndromes and the release of platelet-derived growth factors that may predispose to progression of atherosclerosis. An impairment of endothelium-mediated vasodilation has been shown in patients with risk factors for coronary atherosclerosis but without angiographically visible atherosclerotic changes.[225, 237] A possible limitation of these studies is the poor sensitivity of angiography in the detection of early atherosclerotic changes. More recently, the presence of endothelial dysfunction also in patients with structurally normal coronary arteries but with hypertension, hyperlipidemia, family history of coronary diseases, or a history of smoking has been confirmed using two-dimensional intracoronary ultrasound.[238] A progressive impairment of endothelial function was observed in patients with different stages of atherosclerosis. A complete loss of endothelium-mediated vasodila-

tion was present in arteries with angiographically visible atherosclerotic changes, whereas a more selective impairment was present in angiographically normal arteries of patients with hypercholesterolemia, showing normal responses after flow increase and abnormal vasoconstriction after acetylcholine.[239]

The possible presence of opposite effects of acetylcholine infusion on epicardial and resistance coronary arteries has been reported by Hodgson and Marshall.[239] The observed increase in coronary flow after acetylcholine was prevented by the pretreatment with methylene blue, an inhibitor of endothelium-derived relaxing factor. Zeiher and coworkers[240] reported a significantly lower flow increase after acetylcholine in patients with coronary artery disease than in control subjects. These findings confirmed previous experimental results showing that the impairment of endothelial function in atherosclerotic arteries may involve also the coronary microcirculation.[241-245] The presence of an impaired endothelium-dependent vasodilation of the resistance vessels may induce or facilitate the development of myocardial ischemia in response to neurohumoral stimulation or increased myocardial work.

Using two-dimensional intracoronary ultrasound and Doppler measurements, Reddy and associates[63] have demonstrated that patients with one or more risk factors had an abnormal epicardial artery cross-sectional area vasoconstriction response to acetylcholine infusion. However, the patients who presented minimal disease on ultrasound (intimal thickening or small eccentric plaque) did not respond differently from the patients without demonstrable disease on ultrasound.

The effect of the subselective intracoronary infusion of increasing doses of acetylcholine was studied in our laboratory in coronary arteries without significant coronary stenosis (< 30% diameter stenosis) in 29 patients undergoing PTCA of a different artery.[244] The changes in coronary diameter over a proximal/middle segment and a distal segment of the studied artery were assessed with QCA and correlated with the changes in tone of the resistance vessels, which in turn was assessed from the flow velocity continuously monitored using an intracoronary Doppler guidewire. All vasoactive medications, with the exclusion of short-acting sublingual nitrates, were withheld at least 48 hours before the catheterization.

A significant increase in flow velocity was observed within 30 seconds after the beginning of the infusion of the two highest concentrations of acetylcholine (10^{-7} and 10^{-6} M) in most cases. Cyclic variations of flow velocity were observed in the following minutes despite the constant rate of infusion and the stable hemodynamic conditions. A large increase was observed after papaverine injection, with a peak velocity 2.8 ± 0.8 times higher than in basal conditions. The injection of the two lowest concentrations of acetylcholine induced a moderate but significant reduction of the mean cross-sectional area in both the proximal and the distal segments. A larger decrease was observed after the highest concentration of acetylcholine (−24 ± 20%), at which almost all the studied arteries showed a variable degree of vasoconstriction. In no cases was a greater than 75% mean cross-sectional area reduction observed. A normal vasodilation of the studied artery was observed after bolus injection of an endothelium-independent vasodilator such as isosorbide dinitrate (+16 ± 26%).

A significant increase in coronary flow was observed only after the maximal concentration of acetylcholine (+43 ± 83%), but with a large interindividual variability. At the peak concentration of acetylcholine, 10 patients showed a decrease in absolute flow and an increase in coronary resistance. The flow velocity, cross-sectional area, and flow changes after acetylcholine showed no correlation with age, sex, presence of systemic hypertension, total cholesterol, high-density lipoprotein (HDL) cholesterol, HDL cholesterol-to-total cholesterol ratio, plasma triglycerides, type of studied artery, and basal coronary luminal diameter. The presence of wall irregularities was associated with a larger decrease in luminal cross-sectional area and a smaller flow increase after the last concentration of acetylcholine.

Acetylcholine is the prototype and the most frequently used pharmacologic stimulus, with a primary endothelium-independent contractile action on the vascular smooth muscle cells and an opposite endothelium-mediated vasodilatory activity that is predominant in normal conditions and at physiologic concentrations.[245, 246] Acetylcholine was used in the in vitro experiments in which the role of intact endothelium in the regulation of vascular tone was established[247] and in the first in vivo studies showing that acetylcholine induces severe vasospasm in human coronary arteries with significant stenoses.[225] The induction of an endothelium-dependent vasodilation in canine femoral[247] and coronary[248] arteries after the application of acetylcholine on the arterial adventitia suggests a role of acetylcholine, the mediator of the parasympathetic stimulation, in the modulation of vascular tone. The predominance of the parasympathetic activity has been advocated to explain the circadian rhythm of acute coronary syndromes such as vasospastic angina and myocardial infarction. Selective intracoronary infusion of acetylcholine elicited vascular responses comparable to those observed after serotonin, a substance that is released after intracoronary platelet activation and that may contribute to the development of myocardial ischemia in acute coronary syndromes.[238, 249-251]

Experimental data have demonstrated that atherosclerotic animals show an abnormal endothelium-dependent vasodilation of the coronary resistance arteries despite the absence of structural atherosclerotic lesions.[241] The comparison of the flow response to acetylcholine in patients with coronary artery disease and in control subjects has confirmed an impaired flow increase in the coronary patients, despite the absence of significant lesions of the epicardial coronary arteries.[240] In this study, a large variability in the flow changes was observed after the highest doses of acetylcholine. A dose-dependent vasodilation after acetylcholine was present in most cases, with flow increase up to three times the baseline flow. In 10 patients, however, a flow decrease was observed after the maximal concentration of acetylcholine. No clinical or angiographic predictors of these large individual differences could be observed. A reduction of the endothelium-dependent relaxation is present in animals fed an atherogenic diet with a high content of cholesterol.[252, 253] In hypercholesterolemic patients without angiographic evidence of coronary artery disease, an impaired endothelium-mediated vasodilation of the epicardial coronary arteries and of the resistance coronary vessels has been demonstrated.[226, 237] Thirteen of the studied patients had a total cholesterol level of 6.4 mmol/L (250 mg/dL) or higher. This study showed no significant differences in terms of flow increase and vascular diameter changes after acetylcholine. The importance of the relative amount of HDL and low-density lipoprotein cholesterol has recently been reported to correlate more closely than total cholesterol with the degree of impairment of the endothelium-mediated vasodilation.[254] In the study group, however, the additional use of the HDL-to-total cholesterol ratio did not individuate a subset of patients with a different response to acetylcholine.

The flow increase or flow resistance decrease after the maximal concentration of acetylcholine showed only a poor correlation with the corresponding cross-sectional area changes. The discrepancy between flow and cross-sectional area changes after acetylcholine reflects a different response of the conductance and resistance arteries to acetylcholine. The large arteries are the preferential target of the atherosclerotic process. At this level the presence of intimal thickening may constitute a barrier

to the diffusion of nitric oxide from the endothelial cells to the muscular media.[245] A macrophagic infiltration or the presence of a lipidic component of the intimal plaque may also accelerate the degradation of nitric oxide and prevent its action on the underlying muscular layer.[245] The importance of these mechanisms in atherosclerotic human arteries is indirectly confirmed by the possible development of focal vasoconstriction observed after acetylcholine also in arteries with minimal wall irregularities. Myocardial perfusion is regulated predominantly by resistance arteries less than 200 μm in diameter.[255] These arteries do not show signs of atherosclerotic involvement at histology, suggesting that biochemical or ultrastructural changes are the most likely mechanisms underlying the abnormal endothelium-dependent relaxation.

These observations have potential clinical implications. A prolonged treatment aimed at the regression of the atherosclerotic intimal changes may be required to restore an impaired endothelium-mediated response when the presence of an intimal barrier is the main operative mechanism.[256] On the contrary, acute pharmacologic interventions or a short-lasting treatment may be sufficient to normalize the endothelial function when metabolic abnormalities are involved, as occurs for the microcirculation. The possibility of normalizing the endothelial response in hypercholesterolemia with a short-term infusion of L-arginine has been shown in animal experiments[257] as well as in human coronary arteries.[258] Similarly, different classes of drugs have shown the ability to restore a normal endothelium-mediated vascular reactivity in experimental animals.[259–261] In humans, beneficial effects on endothelial function, evaluated by a reduction of acetylcholine-induced vasoconstriction, have been demonstrated for inhibitors of HMG-CoA reductase[262–264] and with angiotensin-converting enzyme inhibitor.[265] The possibility of delaying or even reversing the atherosclerotic process and improving endothelial function is being studied in different ongoing trials by the combined use of intravascular ultrasound, QCA, and flow measurements with Doppler wire.

FUTURE DIRECTIONS

New Intracoronary Volumetric Blood Flow Measurement Method with Intravascular Ultrasound

Because of the already discussed limitations of true volumetric flow estimation from the combined use of Doppler wire flow measurements and angiographically derived cross-sectional area evaluation, an alternative method has recently been developed in our laboratory. This method is based on a unique feature of the IVUS technique: the direction of blood flow is almost normal to the imaging plane, and when blood particles move across it, the received radiofrequency echo signals decor-

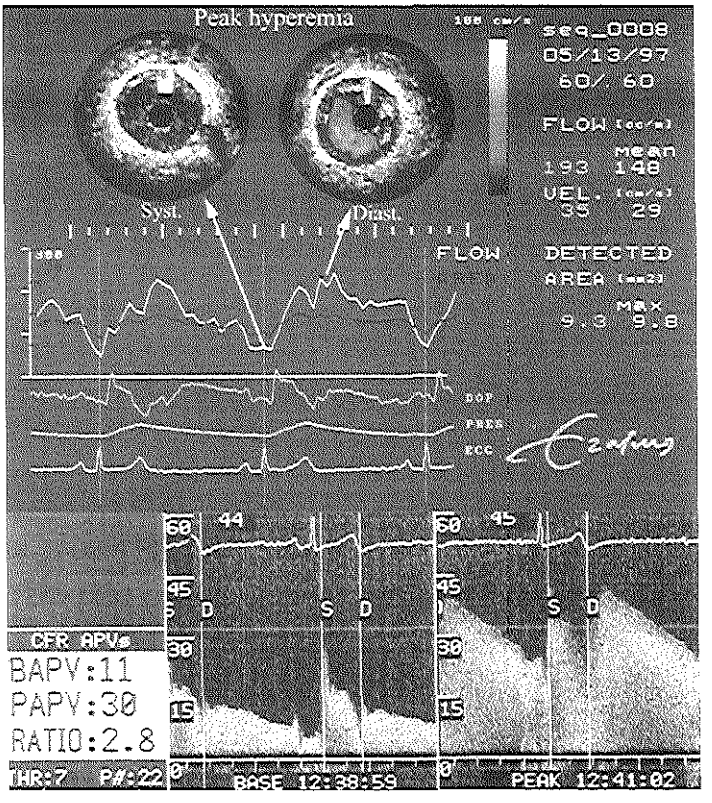

FIGURE 40-16. Volumetric blood flow measurement in a right coronary artery with an intravascular ultrasound (IVUS) catheter using the analysis of the decorrelation of the radiofrequency signals. *Top right*, A conventional IVUS image with the calculated coronary blood flow velocities in diastole superimposed over the cross-sectional area. The color scheme used goes from dark red (10 cm/sec) to yellow (100 cm/sec). *Top left*, The decrease of coronary flow in systole can be visualized with lower velocities recorded over the arterial lumen. The calculated flow from the 60 consecutively acquired frames is plotted (in white) below, together with the instantaneous peak Doppler velocity (DOP) (in blue, measured with a Doppler wire advanced 3 cm more distally in the artery), the aortic blood pressure (PRES) and the electrocardiogram (ECG). This recording was made during an intravenous infusion of adenosine. The corresponding Doppler spectrum is at the bottom right. The Doppler average peak velocity was 30 cm/sec. The coronary cross-sectional area measured with quantitative coronary angiography at the level of the tip of the Doppler wire was 7.42 mm^2. The Doppler-derived coronary blood flow (134 mL/min) is in agreement with the mean flow measured with the IVUS radiofrequency processing (148 mL/min). The coronary flow reserve derived from the IVUS method was 3 (baseline flow not illustrated: 48 mL/min), close to the Doppler estimation: 2.8 (lower left corner). See color plate 2.

relate at a rate proportional to flow velocities.[266] Blood flow velocity is estimated by decorrelation processing on a series of acquired radiofrequency signals. Characterization of the relationship between the correlation of echo signals and the scatterer motion across the ultrasound beam has been evaluated.[267]

For 100 angular positions over the cross-sectional arterial lumen area, the decorrelation rate is estimated in small (~200 μm) consecutive range windows, and the derived local transverse velocity is plotted using a color-coded scale, as illustrated in Figure 40-16. Volume flow is calculated by integrating the local transverse velocity with its corresponding area element over the complete imaging plane. Because the motion of wall tissues has much lower velocity than blood, the contribution of tissue velocities can be automatically removed by setting a threshold, and thus, no contour tracing of the arterial lumen is needed. Although the catheter modifies the velocity profile, because all the velocities in the imaging plane are integrated, the true volumetric flow across this plane can be estimated.[268] Figure 40-16 shows, during intravenous administration of adenosine ($140\ \gamma \cdot kg^{-1} \cdot min^{-1}$), the maximal flow present in diastole (top right) and the lower flow in systole (top left) in an RCA of a patient. The good phasic response of this method can be appreciated with the simultaneously acquired instantaneous peak velocity measured with a Doppler wire 3 cm more distally (blue curve). The mean flow measured was 148 mL/min, in agreement with the flow estimated with the Doppler recording (134 mL/min, shown in the bottom of the figure). This method has been calibrated in vitro on a flow phantom and in a carotid porcine model[269] using an electromagnetic flowmeter. This method, presently under clinical evaluation in our laboratory, offers a unique opportunity to simultaneously assess physiologic and anatomic parameters in coronary arteries with the same catheter and should be useful during coronary interventions.

CONCLUSIONS

The last few years have seen rapid advances in coronary Doppler and pressure probes technology and the development of new approaches to the interpretation of intracoronary hemodynamic measurements. A complex technique reserved to a few research laboratories has been transformed into a reliable diagnostic tool that can be used for the assessment of stenosis severity, for the evaluation of the results of coronary interventions, and for the study of coronary circulation. Combined flow and imaging ultrasound can be applied for measurement of absolute coronary flow as well as for the simultaneous study of morphologic and functional characteristics of the coronary system. The development of combined Doppler-pressure sensors on guidewires should facilitate a more complete assessment of stenosis hemodynamics.

Technical improvements alone, however, are insufficient. Knowledge of the recent advances in coronary flow physiology is a prerequisite for the interpretation of the flow-velocity changes and the development and the application of new methodologic approaches. A close collaboration between clinicians and basic scientists is essential for the future development of these techniques in the study of coronary artery disease.

Presently, with the refinements of pressure and Doppler guidewire technology, the superiority of one technique is not established, because pressure and flow represent the two sides of the same coin—that of coronary flow resistance. Ambiguous values obtained with one technique can be reduced or eliminated using the corresponding alternative method. In the 25% of the current angioplasty population with stable chest pain syndromes in whom evidence of ischemia is lacking, using coronary physiology, one might modify a widely practiced dictum, "When in doubt, dilate" to "When in doubt, measure and decide."[270]

ACKNOWLEDGMENTS: The contribution of the medical, technical, and nursing staffs of the Catheterization Laboratory of the Thoraxcenter and of the G. Mudd Catheterization Laboratory of the St. Louis University is gratefully acknowledged, as well as the contribution of Drs. R. Krams, C. J. Slager, R. L. Kirkeeide, G. B. J. Mancini, and J. J. Piek.

References

1. Grüntzig AR, Senning A, Siegenthaler WE: Nonoperative dilatation of coronary artery stenosis. N Engl J Med 301:61-68, 1979.
2. Rothman MT, Baim DS, Simpson JB, Harrison DC: Coronary hemodynamics during percutaneous transluminal coronary angioplasty. Am J Cardiol 49:1615-1622, 1982.
3. Anderson HV, Roubin GS, Leimgruber PP, et al: Measurement of transstenotic pressure gradient during percutaneous transluminal coronary angioplasty. Circulation 73:1223-1230, 1986.
4. Kilpatrick D, Webber S: Intravascular blood velocity in simulated coronary artery stenoses. Cathet Cardiovasc Diagn 12:317, 1986.
5. Kern M, Courtois M, Ludbrook P: A simplified method to measure coronary blood flow velocity in patients: Validation and application of a new Judkins-style Doppler-tipped angiographic catheter. Am Heart J 120:1202, 1990.
6. Gould K, Kelley K, Bolson E: Experimental validation of quantitative coronary arteriography for determining pressure-flow characteristics of coronary stenosis. Circulation 66:930-937, 1982.
7. Legrand V, Mancini G, Bates E, et al: Comparative study of coronary flow reserve, coronary anatomy, and results of radionuclide exercise tests in patients with coronary artery disease. J Am Coll Cardiol 8:1022-1032, 1986.
8. Miller D, Donohue T, Younis L, et al: Correlation of pharmacological 99mTc-sestamibi myocardial perfusion imaging with poststenotic coronary flow reserve in patients with angiographically intermediate coronary artery stenoses. Circulation 89:2150-2160, 1994.
9. Serruys P, Di Mario C, Piek J, et al: Prognostic value of intracoronary flow velocity and diameter stenosis in assessing the short- and long-term outcome of coronary balloon angioplasty: The DEBATE study. Circulation 96:3369, 1997.
10. Kern MJ, Donohue TJ, Aguirre FV, et al: Clinical outcome of deferring angioplasty in patients with normal translesional pressure-flow velocity measurements. J Am Coll Cardiol 25:178-187, 1995.
11. Pijls NHJ, de Bruyne B, Peels K, et al: Measurement of fractional flow reserve to assess the functional severity of coronary artery stenoses. N Engl J Med 334:1703-1708, 1996.
12. Hatle L, Angelsen B: Physics of blood flow. *In* Hatle L, Angelsen B (eds): *Doppler Ultrasound in Cardiology*: Philadelphia, Lea & Febiger, 1982, pp 8-31.
13. Hartley C, Cole J: An ultrasonic-pulsed Doppler system for measuring blood flow in small vessels. J Appl Physiol 37:626, 1974.
14. Wright CB, Doty DB, Eastham CL: Measurement of coronary reactive hyperemia with a Doppler probe: Intraoperative guide to hemodynamically significant lesions. J Thorac Cardiovasc Surg 80:888, 1980.
15. Wilson RF, Laughlin DE, Ackell PH, et al: Transluminal, subselective measurement of coronary artery blood flow velocity and vasodilator reserve in man. Circulation 72:82, 1985.
16. Marcus M: The Coronary Circulation in Health and Disease. New York, McGraw-Hill, 1983, p 23.
17. Sibley DH, Millar HD, Hartley CJ, Whitlow PL: Subselective measurement of coronary blood flow velocity using a steerable Doppler catheter. J Am Coll Cardiol 8:1332, 1986.
18. Tadaoka S, Kigiyama M, Hiramatsu O, et al: Accuracy of 20-MHz Doppler catheter coronary artery velocimetry for measurement of coronary blood flow velocity. Cathet Cardiovasc Diagn 19:205, 1990.
19. Serruys PW, Juilliere Y, Zijlstra F, et al: Coronary blood flow veloc-

ity during percutaneous transluminal coronary angioplasty as a guideline for assessment of functional result. Am J Cardiol 61:253, 1988.
20. Carlier SG, Frinking P, Krams R, et al: Improvement of coronary flow studies by the acquisition of raw Doppler signals and the use of echocontrast enhancement. Eur Heart J 18(abst suppl):151, 1997.
21. Doucette JW, Corl PD, Payne HM, et al: Validation of a Doppler guidewire for intravascular measurements of coronary artery flow velocity. Circulation 85:1899–1911, 1992.
22. Ofili EO, Kern MJ, Tatineni S, et al: Detection of coronary collateral flow by a Doppler-tipped guidewire during coronary angioplasty. Am Heart J 222:221, 1991.
23. Ofili EO, Karim AM, Kern MJ, et al: Simultaneous comparison of intracoronary spectral and zero-cross-flow velocity measurements by Doppler guidewire and catheter techniques. J Am Coll Cardiol 17:124A, 1991.
24. Mechem CJ, Kern MJ, Aguirre F, et al: Safety and outcome of angioplasty guidewire Doppler instrumentation in patients with normal or mildly diseased coronary arteries. Circulation 86:I-323, 1992.
25. Kajiya F, Ogasawara Y, Tsujioka K, et al: Evaluation of human coronary blood flow with an 80-channel 20-MHz pulsed Doppler velocimeter and zero-cross and Fourier transform methods during cardiac surgery. Circulation 74(suppl II):III-53, 1986.
26. Sudhir K, Hargrave VK, Johnson EL, et al: Measurement of volumetric coronary blood flow with a Doppler catheter: Validation in an animal model. Am Heart J 124:870–875, 1992.
27. Johnson EL, Yock PG, Hargrave VK, et al: Assessment of severity of coronary stenoses using a Doppler catheter: Validation of a method based on the continuity equation. Circulation 80:625, 1989.
28. Tanouchi J, Kitabatake A, Ishihara K, et al: Experimental validation of Doppler catheter technique using fast Fourier spectrum analysis for measuring coronary flow velocity. Circulation 80(suppl II):II-566, 1989.
29. Di Mario C, Roelandt JRTC, de Jaegere P, et al: Limitations of the zero-crossing detector in the analysis of intracoronary Doppler: A comparison with fast Fourier analysis of basal, hyperemic, and transstenotic blood flow velocity measurements in patients with coronary artery disease. Cathet Cardiovasc Diagn 28:56, 1993.
30. Piek JJ, Koolen JJ, Metting van Rijn AC, et al: Spectral analysis of flow velocity in the contralateral artery during coronary angioplasty: A new method for assessing collateral flow. J Am Coll Cardiol 21:1574–1582, 1993.
31. Scaramucci J: De Motu Cordis, Theorema Sextum. *In* Scaramucci J (ed): *Theorematа Familiaria de Physico-Medicis Lucubrationibus Iucta Leges Mecanicas.* Urbino, 1695, pp 70–81.
32. Sabiston DC Jr, Gregg DE: Effect of cardiac contraction on coronary blood flow. Circulation 15:14, 1957.
33. Akasaka T, Yoshikawa J, Yoshida K, Maeda K: Systolic coronary flow reversal associated with abnormal diastolic flow dynamics in patients with aortic stenosis assessed by a coronary Doppler catheter. Circulation 84:II-372, 1991.
34. Memmola C, Iliceto S, Carella L, et al: Assessment of coronary blood flow velocity characteristics in hypertrophic obstructive cardiomyopathy by transesophageal echo Doppler. Circulation 86:I-725, 1992.
35. Ofili EO, Labovitz AJ, Kern MJ: Coronary flow dynamics in normal and diseased arteries. Am J Cardiol 71:3D, 1993.
36. Spaan JAE: Structure and function of the coronary arterial tree. *In* Spaan JAE (ed): *Coronary blood flow: Mechanics, distribution, and control.* Boston, Kluwer Academic, 1991, pp 37–67.
37. Seiler C, Kirkeeide RL, Gould KL: Basic structure-function relations of the epicardial coronary vascular tree. Circulation 85:1987, 1992.
38. Ofili EO, Kern MJ, St Vrain JA, et al: Differential characterization of blood flow, velocity, and vascular resistance between proximal and distal normal epicardial human coronary arteries: Analysis by intracoronary spectral flow velocity. Am Heart J 130:37–46, 1995.
39. Bach RG, Kern MJ, Donohue T, et al: Comparison of arterial and venous coronary bypass conduits: Analysis of intravessel blood flow velocity characteristics. Circulation 86:I-181, 1992.
40. Pezzano A, Cali G, Cataldo G, et al: Evaluation of postoperative flow of internal mammary coronary graft by two-dimensional and color-Doppler echocardiography. J Am Coll Cardiol 19:298A, 1992.
41. Takayama T, Suma J, Wanibuchi Y, et al: Physiological and pharmacologic responses of arterial graft flow after coronary artery bypass grafting measured with an implantable ultrasonic Doppler miniprobe. Circulation 86:II-217, 1992.
42. Kern MJ, Bach RG, Mechem CJ, et al: Variations in normal coronary vasodilatory reserve stratified by artery, gender, heart transplantation, and coronary artery disease. J Am Coll Cardiol 28:1154–1160, 1996.
43. Caracciolo EA, Wolford TL, Underwood RD, et al: Influence of intimal thickening on coronary blood flow responses in orthotopic heart transplant recipients: A combined intravascular Doppler and ultrasound imaging study. Circulation 92(suppl II):II-182–II-190, 1995.
44. Kern MJ, Donohue TJ, Bach RG, et al: Assessment of intermediate coronary stenosis by relative coronary flow velocity reserve. J Am Coll Cardiol 29(suppl A):21A, 1997.
45. Erbel R, Ge J, Bockisch A, et al: Value of intracoronary ultrasound and Doppler in the differentiation of angiographically normal coronary arteries: A prospective study in patients with angina pectoris. Eur Heart J 17:880–889, 1996.
46. Cannon RO, Schenke WH, Leon MB, et al: Limited coronary flow reserve after dipyridamole in patients with ergonovine-induced coronary vasoconstriction. Circulation 75:163–174, 1987.
47. Quyyumi AA, Cannon RO III, Panza JA, et al: Endothelial dysfunction in patients with chest pain and normal coronary arteries. Circulation 86:1864–1871, 1992.
48. Holdright DR, Lindsay DC, Clarke D, et al: Coronary flow reserve in patients with chest pain and normal coronary arteries. Br Heart J 70:513–519, 1993.
49. Chauhan A, Mullins PA, Petch MC, Schofield PM: Is coronary flow reserve in response to papaverine really normal in syndrome X? Circulation 89:1998–2004, 1994.
50. Baumgart D, Haude M, Liu F, et al: Fractional velocity reserve—a new index for stenosis severity assessment with good correlation to fractional flow reserve. J Am Coll Cardiol 29(suppl A):126A, 1997.
51. Uren NG, Schwarzacher SP, Whitbourn R, et al: Fractional vs. coronary flow reserve: Comparison of guidewire-based measurements of coronary stenosis (abstract). J Am Coll Cardiol 29(Suppl A):125A, 1997.
52. Evans DH, Schlindwein FS, Levene MI: The relationship between time-averaged intensity-weighted mean velocity and time-averaged maximum velocity in neonatal cerebral arteries. Ultrasound Med Biol 15:429, 1989.
53. Caro CG, Pedley TJ, Schroter RC, Seed WA: Flow in pipes and around objects. *In* Caro CG, Schroter RC, Seed WA (eds): *The Mechanics of the Circulation.* New York, Oxford University Press, 1978, pp 44–73.
54. Ling SC, Atabek HB, Fry DL, et al: Application of heated-film velocity and shear probes to hemodynamic studies. Circ Res 23:789, 1968.
55. Ritter M, Vassalli G, Kiowski W, et al: How does the velocity profile affect the assessment of coronary reserve? In vitro evaluation by Doppler catheter. Eur Heart J, 16(abst suppl):P1190, 1995.
56. Asakura T, Karino T: Flow patterns and spatial distribution of atherosclerotic lesions in human coronary arteries. Circ Res 66:1045–1066, 1990.
57. Chou TM, Sudhir K, Iwanaga S, et al: Measurement of volumetric coronary blood flow by simultaneous intravascular two-dimensional and Doppler ultrasound: Validation in an animal model. Am Heart J 128:237–243, 1994.
58. Labovitz AJ, Anthonis DM, Cravens TL, Kern MJ: Validation of volumetric flow measurements by means of a Doppler-tipped coronary angioplasty guidewire. Am Heart J 126:1456–1461, 1993.
59. Eichhorn EJ, Alvarez LG, Jessen ME, et al: Measurement of coronary and peripheral artery flow by intravascular ultrasound and pulsed Doppler velocimetry. Am J Cardiol 70:542–545, 1992.
60. Grayburn PA, Willard JE, Haagen DR, et al: Measurement of coronary flow using high-frequency intravascular ultrasound imaging and pulsed Doppler velocimetry: In vitro feasibility studies. J Am Soc Echocardiogr 5:5–12, 1992.
61. Linker DT, Torp H, Groenningsaether A, et al: Instantaneous arterial flow estimated with an ultrasound imaging and Doppler catheter. Circulation 80:II-580, 1989.
62. Sudhir K, McGreggor JS, Barbant SD, et al: Assessment of coronary

conductance and resistance vessel reactivity in response to nitroglycerine, ergonovine, and adenosine: In vivo studies with simultaneous intravascular two-dimensional and Doppler ultrasound. J Am Coll Cardiol 21:1261–1268, 1993.
63. Reddy KG, Nair RN, Sheehan HM, Hodgson JM: Evidence that selective endothelial dysfunction may occur in the absence of angiographic or ultrasound atherosclerosis in patients with risk factors for atherosclerosis. J Am Coll Cardiol 24:833–843, 1994.
64. Sudhir K, McGregor JS, Amidon TM, et al: Differential contribution of nitric oxide to regulation of vascular tone in coronary conductance and resistance arteries: Intravascular ultrasound studies. Am Heart J 127:858–865, 1994.
65. Caracciolo EA, Wolford TL, Underwood RD, et al: Influence of intimal thickening on coronary blood flow responses in orthotopic heart transplant recipients: A combined intravascular Doppler and ultrasound imaging study. Circulation 92:II-182–II-190, 1995.
66. Furuse A, Klopp EH, Brawley RK, Gott VL: Hemodynamic determinations in the assessment of distal coronary artery disease. J Surg Res 19:25, 1975.
67. Wiesner TF, Levesque MJ, Rooz E, Nerem RM: Epicardial coronary blood flow, including the presence of stenoses and aorto-coronary bypasses: II. Experimental and comparison parametric investigations. Trans ASME 110:144, 1988.
68. Kajiya F, Ogasawara Y, Tsujioka K, et al: Analysis of flow characteristics in poststenotic regions of the human coronary artery during bypass graft surgery. Circulation 76:1092, 1987.
69. Segal J, Kern MJ, Scott NA, et al: Alterations of phasic coronary artery flow velocity in man during percutaneous coronary angioplasty. J Am Coll Cardiol 20:276, 1992.
70. Ofili EO, Kern MJ, Labovitz AJ, et al: Analysis of coronary blood flow velocity dynamics in angiographically normal and stenosed arteries before and after endoluminal enlargement by angioplasty. J Am Coll Cardiol 21:308, 1992.
71. Serruys PW, Di Mario C, Meneveau N, et al: Intracoronary pressure and flow velocity with sensor-tip guidewires: A new methodological comprehensive approach for the assessment of coronary hemodynamics before and after coronary interventions. Am J Cardiol 71:41D, 1993.
72. Dirschinger J, Dennig K, Hall D, Rudolph W: Intracoronary blood flow velocity profile in patients with coronary artery disease. Circulation 86:I-587, 1992.
73. Segal J: Applications of coronary flow velocity during angioplasty and other coronary interventional procedures. Am J Cardiol 71:17D, 1993.
74. Gould KL, Lipscomb K, Hamilton GW: Physiologic basis for assessing critical coronary stenosis: Instantaneous flow response and regional distribution during coronary hyperemia as measures of coronary flow reserve. Am J Cardiol 33:87, 1974.
75. Klocke FJ: Measurements of coronary flow reserve: Defining pathophysiology versus making decisions about patient care. Circulation 76:245, 1987.
76. Sugawara M: Stenosis: Theoretical background. *In* Sugawara M, Kajiya F, Kitabatake A, Matsuo H (eds): *Blood Flow in the Heart and Large Vessels*. New York, Springer-Verlag, 1989, p 91.
77. Gould KL, Kirkeeide RL, Buchi M: Coronary flow reserve as a physiologic measure of stenosis severity. J Am Coll Cardiol 15:459, 1990.
78. Wilson RF, Marcus ML, White CW: Prediction of the physiologic significance of coronary arterial dimensions by quantitative lesion geometry in patients with limited coronary artery disease. Circulation 75:723–732, 1987.
79. Harrison DG, White CW, Hiratzka LF, et al: The value of lesional cross-sectional area determined by quantitative coronary angiography in assessing the physiologic significance of proximal left anterior descending coronary artery stenoses. Circulation 69:111, 1984.
80. Klocke FJ: Cognition in the era of technology: "Seeing the shades of gray." J Am Coll Cardiol 16:763, 1990.
81. Cleary RM, Ayon D, Moore NB, et al: Tachycardia, contractility, and volume loading alter conventional indexes of coronary flow reserve, but not the instantaneous hyperemic flow versus pressure slope index. J Am Coll Cardiol 20:1261–1269, 1992.
82. McGinn AL, White CW, Wilson RF: Interstudy variability of coronary flow reserve. Circulation 81:1319–1330, 1990.
83. Rossen JD, Winniford MD: Effects of increases in heart rate and arterial pressure on coronary flow reserve in humans. J Am Coll Cardiol 21:343–348, 1993.
84. Hongo M, Nakatsuka T, Watanabe N, et al: Effects of heart rate on phasic coronary blood flow pattern and flow reserve in patients with normal coronary arteries: A study with an intravascular Doppler catheter and spectral analysis. Am Heart J 127:545–551, 1994.
85. De Bruyne B, Bartunek J, Sys SU, et al: Simultaneous coronary pressure and flow velocity measurements in humans: Feasibility, reproducibility, and hemodynamic dependence of coronary flow velocity reserve, hyperemic flow versus pressure slope index, and fractional flow reserve. Circulation 94:1842–1849, 1996.
86. Bookstein JJ, Higgins CB: Comparative efficacy of coronary vasodilatory methods. Invest Radiol 12:121, 1977.
87. Wilson RF, White CW: Intracoronary papaverine: An ideal coronary vasodilator for studies of the coronary circulation in conscious humans. Circulation 73:444, 1986.
88. Zijlstra F, Juilliére Y, Serruys PW, Roelandt JRTC: Value and limitations of intracoronary adenosine for the assessment of coronary flow reserve. Cathet Cardiovasc Diagn 15:76, 1988.
89. Wilson RF, White CW: Serious ventricular dysrhythmias after intracoronary papaverine. Am J Cardiol 62:1301, 1988.
90. Wilson RF, Wyche K, Christensen BV, et al: Effects of adenosine on human coronary circulation. Circulation 82:1595–1606, 1990.
91. Kern MJ, Deligonul U, Aguirre F, Hilton TC: Intravenous adenosine: Continuous-infusion and low-dose bolus administration for determination of coronary vasodilator reserve in patients with and without coronary artery disease. J Am Coll Cardiol 18:718, 1991.
92. Abreu A, Mahmarian JJ, Nishimura S, Verani MS: Tolerance and safety of pharmacologic coronary vasodilation with adenosine in association with thallium 201 scintigraphy in patients with suspected coronary artery disease. Am J Cardiol 18:730, 1991.
93. Gould KL, Kelley KO: Physiological significance of coronary flow velocity and changing stenosis geometry during coronary vasodilation in awake dogs. Circ Res 50:695, 1982.
94. Zijlstra F, Reiber JHC, Serruys PW, et al: Does intracoronary papaverine dilate epicardial coronary arteries? Implications for assessment of coronary flow reserve. Cathet Cardiovasc Diagn 14:1, 1987.
95. Joye JD, Schulman DS, Lasorda D, et al: Intracoronary Doppler guidewire versus stress single-photon emission computed tomographic thallium 201 imaging in assessment of intermediate coronary stenoses. J Am Coll Cardiol 24:940–947, 1994.
96. Heller LL, Lewis BS, Silver KH, et al: Proximal coronary flow reserve does not reflect coronary flow reserve distal to significant stenoses. Circulation 90:I-227, 1994.
97. Donohue TJ, Kern MJ, Aguirre FV: Assessing the hemodynamic significance of coronary artery stenoses: Analysis of translesional pressure-flow velocity relations in patients. J Am Coll Cardiol 22:449–458, 1993.
98. De Bruyne B, Stockbroeckx J, Demoor D, et al: Role of side holes in guiding catheters: Observations on coronary pressures and flows. Cathet Cardiovasc Diagn 33:145–152, 1994.
99. Abizaid A, Kornowski R, Mintz GS, et al: Influence of guiding catheter selection on the measurement of coronary flow reserve. Am J Cardiol 79:703–704, 1997.
100. Di Mario C, Gil R, Serruys PW: Long-term reproducibility of coronary flow velocity measurements in patients with coronary artery disease. Am J Cardiol 75:1177–1180, 1995.
101. Carlier SG, Gordov E, Gailly E, et al: Acquisition of raw intracoronary Doppler signal for better characterization of flows. Comput Cardiol 1996, p 205.
102. Hatle L, Angelsen B: Pulsed and continuous-wave Doppler in diagnosis and assessment of various heart lesions. *In* Hatle L, Angelsen B (eds): *Doppler Ultrasound in Cardiology*: Philadelphia, Lea & Febiger, 1985, p 97.
103. Blasini R, Schad H, Huttl S, et al: Intracoronary Doppler catheter: Determination of the cross-sectional area of coronary artery stenoses by improved frequency analysis. Eur Heart J 13(abst suppl):362, 1992.
104. Nakatami S, Yamagishi M, Tamai J, et al: Quantitative assessment of coronary artery stenosis by intravascular Doppler catheter technique. Circulation 85:1786, 1992.
105. Di Mario C, Meneveau N, Gil R, et al: Maximal blood flow velocity in severe coronary stenoses measured with a Doppler guidewire. Am J Cardiol 71:54D, 1993.

106. Nissen SE, Gurley JC, Grines CL, et al: Intravascular ultrasound assessment of lumen size and wall morphology in normal subjects and patients with coronary artery disease. Circulation 84:1087, 1991.
107. St Goar FG, Pinto FJ, Alderman EL, et al: Intravascular ultrasound of angiographically normal coronary arteries: An in vivo comparison with quantitative angiography. J Am Coll Cardiol 18:952, 1991.
108. Pijls NHJ, van Son JAM, Kirkeeide RL, et al: Experimental basis of determining maximum coronary, myocardial, and collateral blood flow by pressure measurements for assessing functional stenosis severity before and after percutaneous transluminal coronary angioplasty. Circulation 86:1354–1367, 1993.
109. Pijls NHJ, Van Gelder B, Van der Voort P, et al: Fractional flow reserve: A useful index to evaluate the influence of an epicardial coronary stenosis on myocardial blood flow. Circulation 92:318–319, 1995.
110. De Bruyne B, Baudhuin T, Melin JA, et al: Coronary flow reserve calculated from pressure measurements in humans: Validation with positron emission tomography. Circulation 89:1013–1022, 1994.
111. De Bruyne B, Paulus WJ, Pijls NHJ: Rationale and application of coronary transstenotic pressure gradient measurements. Cathet Cardiovasc Diagn 33:250–261, 1994.
112. De Bruyne B, Pijls NHJ, Paulus WJ, et al: Transstenotic coronary pressure gradient measurement in humans: In vitro and in vivo evaluation of a new pressure monitoring angioplasty guidewire. J Am Coll Cardiol 22:119–126, 1993.
113. De Bruyne B, Sys SU, Heyndrickx GR: Percutaneous transluminal coronary angioplasty catheters versus fluid-filled pressure monitoring guidewires for coronary pressure measurements and correlation with quantitative coronary angiography. Am J Cardiol 72:1101–1106, 1993.
114. Emanuelsson H, Dohnal M, Lamm C, Tenerz L: Initial experiences with a miniaturized pressure transducer during coronary angioplasty. Cathet Cardiovasc Diagn 24:137–143, 1991.
115. Lamm C, Dohnal M, Serruys PW, Emanuelsson H: High-fidelity translesional pressure gradients during percutaneous transluminal coronary angioplasty: Correlation with quantitative coronary angiography. Am Heart J 126:66–75, 1993.
116. Hodgson JM, Reinert S, Most AS, Williams DO: Prediction of long-term clinical outcome with final translesional pressure gradient during coronary angioplasty. Circulation 74:563–566, 1986.
117. Serruys PW, Wijns W, Reiber JHC, et al: Values and limitations of transstenotic pressure gradients measured during percutaneous coronary angioplasty. Herz 10: 337–342, 1985.
118. Leiboff R, Bren G, Katz R, et al: Determinants of transstenotic gradients observed during angioplasty: An experimental model. Am J Cardiol 52:1311, 1983.
119. De Bruyne B, Bartunek J, Sys SU, Heyndrickx GR: Relation between myocardial fractional flow reserve calculated from coronary pressure measurements and exercise-induced myocardial ischemia. Circulation 92:39–46, 1995.
120. Bartunek J, Marwick TH, Rodrigues ACT, et al: Dobutamine-induced wall motion abnormalities: Correlations with myocardial fractional flow reserve and quantitative coronary angiography. J Am Coll Cardiol 27:1429–1436, 1996.
121. Pijls NHJ, De Bruyne B, Peels K, et al: Measurement of fractional flow reserve to assess the functional severity of coronary artery stenoses. N Engl J Med 334:1703–1708, 1996.
122. Tron C, Donohue TJ, Bach RG, et al: Comparison of pressure-derived fractional flow reserve with poststenotic coronary flow velocity reserve for prediction of stress myocardial perfusion imaging results. Am Heart J 130:723–733, 1995.
123. Di Mario C, Gil R, de Feyter P, et al: Utilization of translesional hemodynamics: Comparison of pressure and flow methods in stenosis assessment in patients with coronary artery disease. Cathet Cardiovasc Diagn 38:189–201, 1996.
124. Zijlstra F, Serruys PW: Intracoronary blood flow velocity and transstenotic pressure gradient in an awake human being during coronary vasodilatation. J Intervent Cardiol 1:1, 1988.
125. Mancini GBJ, Cleary RM, DeBoe SF, et al: Instantaneous hyperemic flow-versus-pressure slope index: Microsphere validation of an alternative to measures of coronary flow reserve. Circulation 80:941, 1989.
126. Mancini GBJ, Cleary RM, DeBoe SF: Instantaneous hyperemic flow-versus-pressure slope index: Microsphere validation of an alternative to measures of coronary flow reserve. Circulation 84:862–870, 1991.
127. Cleary RM, Moore NB, DeBoe SF, Mancini GBJ: Sensitivity and reproducibility of the instantaneous hyperemic flow-versus-pressure slope index compared to coronary flow reserve for the assessment of stenosis severity. Am Heart J 126:57–65, 1993.
128. Di Mario C, Krams R, Gil R, Serruys PW: Slope of the instantaneous hyperemic diastolic coronary flow velocity-pressure relation: A new index for assessment of the physiological significance of coronary stenosis in humans. Circulation 90:1215–1224, 1994.
129. Reiber JHC, Serruys PW, Kooijman CJ, et al: Assessment of short-, medium-, and long-term variations in arterial dimensions from computer-assisted quantification of coronary angiograms. Circulation 71:280–288, 1985.
130. Kirkeeide RL, Gould KL, Parsel L: Assessment of coronary stenosis by myocardial perfusion imaging during pharmacologic coronary vasodilatation: VII. Validation of coronary flow reserve as a single integrated functional measure of stenosis severity reflecting all its geometric dimensions. J Am Coll Cardiol 7:103–113, 1986.
131. Zijlstra F, Van Ommeren J, Reiber JHC, Serruys PW: Does quantitative assessment of coronary artery dimensions predict the physiologic significance of a coronary stenosis? Circulation 75:1154–1161, 1987.
132. Tron C, Kern MJ, Donohue TJ, et al: Comparison of quantitative angiographically derived and measured translesion pressure and flow velocity in coronary artery disease. Am J Cardiol 75:111–117; 1995.
133. Bartunek J, Sys SU, Heyndrickx GR, et al: Quantitative coronary angiography in predicting functional significance of stenoses in an unselected patient cohort. J Am Coll Cardiol 26:328–334, 1995.
134. Wijns W, Serruys PW, Reiber JH, et al: Quantitative angiography of the left anterior descending coronary: Correlations with pressure gradient and results of exercise thallium scintigraphy. Circulation 71: 273–279, 1985.
135. Miller DD, Donohue TJ, Wolford TL, et al: Assessment of blood flow distal to coronary artery stenoses: Correlations between myocardial positron emission tomography and poststenotic intracoronary Doppler flow reserve. Circulation 94:2447–2454, 1996.
136. Uren NG, Melin JA, De Bruyne B, et al. Relation between myocardial blood flow and the severity of coronary artery stenosis. N Engl J Med 330:1782–1788, 1994.
137. Kern MJ, Dupouy P, Drury JH, et al: Role of coronary artery lumen enlargement in improving coronary blood flow after balloon angioplasty and stenting: A combined intravascular ultrasound Doppler flow and imaging study. J Am Coll Cardiol 29:1520–1517, 1997.
138. De Cesare NB, Williamson PR, Moore NB, et al: Establishing comprehensive, quantitative criteria for detection of restenosis and remodelling after percutaneous transluminal coronary angioplasty. Am J Cardiol 69:77, 1992.
139. Serruys PW, Foley DP, de Feyter PJ: Restenosis after coronary angioplasty: A proposal of new comparative approaches based on quantitative angiography. Br Heart J 68:417–422, 1992.
140. Serruys PW, Reiber JHC, Wijns W, et al: Assessment of percutaneous transluminal coronary angioplasty by quantitative coronary angiography: Diameter versus densitometric area measurements. Am J Cardiol 54:482, 1984.
141. Marcus ML, Armstrong ML, Heistad DD, et al: A comparison of three methods of evaluating coronary obstructive lesions: Postmortem arteriography, pathological examination, and measurement of regional myocardial perfusion during maximal vasodilation. Am J Cardiol 49:1699, 1982.
142. Folts JD, Gallagher K, Rowe GG: Blood flow reductions in stenosed canine coronary arteries: Vasospasm or platelet aggregation? Circulation 65:248, 1982.
143. Bush LR, Campbell WB, Buja LM, et al: Effects of the selective thromboxane synthetase inhibitor dazoxiben on variations in cyclic blood flow in stenosed canine coronary arteries. Circulation 65:248, 1984.
144. Ashton JH, Benedict CR, Fitzgerald C, et al: Serotonin as a mediator of cyclic flow variations in stenosed canine coronary arteries. Circulation 73:572, 1986.
145. Ashton JG, Schmitz JM, Campbell WB, et al: Inhibition of cyclic flow variations in stenosed canine coronary arteries by thromboxane A_2/prostaglandin H_2 receptor antagonists. Circ Res 59:568, 1986.

146. Eichhorn EJ, Grayburn PA, Willard JE, et al: Spontaneous alterations in coronary blood flow velocity before and after coronary angioplasty in patients with severe angina. J Am Coll Cardiol 17:43–52, 1991.
147. Folts JD, Crowell EB, Rowe GG: Platelet aggregation in partially obstructed vessels and its elimination with aspirin. Circulation 54:365–370, 1976.
148. Pozzati A, Bugiardini R, Ottani F, et al: Coronary hemodynamic effects of systemic thrombolysis in patient with unstable angina. Clin Cardiol 15:88–92, 1992.
149. Hamberg M, Svensson J, Samuelsson B: A new group of biologically active compounds derived from prostaglandin endoperoxides. Proc Natl Acad Sci USA 72:2994–2998, 1975.
150. Ellis EF, Oelz O, Roberts CJII, et al: Coronary arterial smooth muscle contraction by a substance released from platelets: Evidence that it is thromboxane A_2. Science 193:1135–1137,1976.
151. Golino P, Buja LM, Ashton JH, et al: Effect of thromboxane and serotonin receptor antagonists on intracoronary platelet deposition in dogs with experimentally stenosed coronary arteries. Circulation 78:701–711, 1988.
152. Golino P, Ashton JH, Buja LM, et al: Local platelet activation causes constriction of large epicardial canine coronary arteries in vivo: Thromboxane A_2 and serotonin are possible mediators. Circulation 78:154–166, 1989.
153. Rensing BJ, Hermans WRM, Beatt KJ, et al: Quantitative angiographic assessment of elastic recoil after percutaneous transluminal coronary angioplasty. Am J Cardiol 66:1033, 1990.
154. Anderson HV, Kirkeeide RL, Stuart Y, et al: Coronary flow monitoring following coronary interventions. Am J Cardiol 17:62D, 1993.
155. Sunamura M, Di Mario C, Piek JJ, et al: Cyclic flow variations after angioplasty: A rare phenomenon predictive of immediate complications. Am Heart J 131:843–848, 1996.
156. Kern MJ, Aguirre FV, Donohue TJ, et al: Continuous coronary flow monitoring during coronary interventions: Velocity trend patterns associated with adverse events. Am Heart J 128:426–434, 1994.
157. Isner JM, Kaufman J, Rosenfield K, et al: Combined physiologic and anatomic assessment of percutaneous revascularization using a Doppler guidewire and ultrasound catheter. Am J Cardiol 71:70D–86D, 1993.
158. Wilson RF, Johnson MR, Marcus ML, et al: The effect of coronary angioplasty on coronary flow reserve. Circulation 77:873–885, 1988.
159. Kern MJ, Deligonul U, Vandormael M, et al: Impaired coronary vasodilatory reserve in the immediate postcoronary angioplasty period: Analysis of coronary arterial velocity flow indexes and regional cardiac venous efflux. J Am Coll Cardiol 13:860–872, 1989.
160. Heller LI, Silver KH, Villegas BJ, et al: Blood flow velocity in the right coronary artery: Assessment before and after angioplasty. J Am Coll Cardiol 24:1012–1017, 1994.
161. Deychak YA, Segal J, Reiner JS, Nachnani S: Doppler guidewire-derived coronary flow reserve distal to intermediate stenoses used in clinical decision making regarding interventional therapy. Am Heart J 128:178–181, 1994.
162. Moses JW, Shanovich A, Kreps EM, et al: Clinical follow-up of intermediate coronary lesions not hemodynamically significant by Doppler flow wire criteria. Circulation 89(abst suppl):P1216, 1994.
163. Ferrari N, Werner GS, Schmitt HA, et al: Safety of deferring angioplasty in patients with normal coronary flow reserve. Eur Heart J 18(abst suppl):238, 1997.
164. Bech GJW, De Bruyne B, Bartunek J, et al: Long-term follow-up after deferral of PTCA based on coronary pressure measurements. Eur Heart J 18(abst suppl):238, 1997.
165. Serruys PW, Emanuelsson H, van der Giessen W, et al: Heparin-coated Palmaz-Schatz stents in human coronary arteries: Early outcome of the Benestent-II pilot study. Circulation 93:412–422, 1996.
166. Di Mario C, Muramatsu T, Moses J, et al: Aggressive dilatation strategy to optimize the angiographic and functional PTCA results: Preliminary results of the DESTINI study. Eur Heart J 18(abst suppl):238, 1997.
167. Bach RG, Kern MJ, Bell C, et al: Clinical application of coronary flow velocity for stent placement during coronary angioplasty. Am Heart J 125:873–877, 1993.
168. Fischman DL, Leon MB, Baim D, et al: A randomized comparison of coronary stent placement and balloon angioplasty in the treatment of coronary artery disease. N Engl J Med 331:496–501, 1994.
169. Serruys PW, de Jaegere P, Kiemeneij F, Group BS: A comparison of balloon-expandable stent implantation with balloon angioplasty in patients with coronary artery disease. N Engl J Med 331:489–495, 1994.
170. Liu MW, Roubin GS, King SB: Restenosis after coronary angioplasty: Potential biologic determinants and role of intimal hyperplasia. Circulation 79:1374–1387, 1989.
171. Zarins CK, Zatina MA, Giddens DP, et al: Shear stress regulation of artery lumen diameter in experimental atherogenesis. J Vasc Surg 5:413–420, 1987.
172. Kern MJ, Aguirre FV, Bach RG, et al: Alterations of coronary flow velocity distal to coronary dissections before and after intracoronary stent placement. Cathet Cardiovasc Diagn 31:309–315, 1994.
173. Ge J, Erbel R, Zamorano J, et al: Improvement of coronary morphology and blood flow after stenting: Assessment by intravascular ultrasound and intracoronary Doppler. Int J Cardiac Imaging 11:81–87, 1995.
174. Haude M, Baumgart D, Caspari G, Erbel R: Does adjunct coronary stenting in comparison to balloon angioplasty have an impact on Doppler flow velocity parameters? Circulation 92:I-547, 1995.
175. Verna E, Gil R, Di Mario C, et al: Does coronary stenting following balloon angioplasty improve distal coronary flow reserve? Circulation 92:I-536, 1995.
176. Pijls NHJ, Herzfeld I, De Bruyne B, et al: Evaluation of adequate stent deployment by measuring myocardial fractional flow reserve. Circulation 92:I-536, 1995.
177. Deychak YA, Thompson MA, Rohrbeck SC, et al: A Doppler guidewire used to assess coronary flow during directional coronary atherectomy. Circulation 86:I-122, 1992.
178. Khoury AF, Aguirre FV, Bach RG, et al: Influence of percutaneous transluminal coronary rotational atherectomy with adjunctive percutaneous transluminal coronary angioplasty on coronary blood flow. Am Heart J 131:631–638, 1996.
179. Bowers TR, Stewart RE, O'Neill WW, et al: Effect of Rotablator atherectomy and adjunctive balloon angioplasty on coronary blood flow. Circulation 95:1157–1164, 1997.
180. Friedman HZ, Elliott MA, Gottlieb G, O'Neill WW: Mechanical rotary atherectomy: The effects of microparticle embolization on myocardial blood flow and function. J Intervent Cardiol 2:77–83, 1989.
181. Van Leenen TG, van Erven L, Meertens JH, et al: Origin of arterial wall dissections induced by pulsed Excimer and mid-infrared laser ablation in the pig. J Am Coll Cardiol 19:1610, 1992.
182. Isner JM, Pickering JG, Mosseri M: Laser-induced dissections: Pathogenesis and implications for therapy. J Am Coll Cardiol 19:1619, 1992.
183. Isner JM, Kaufman J, Rosenfield K, et al: Combined physiologic and anatomic assessment of percutaneous revascularization using a Doppler guidewire and ultrasound catheter. Am J Cardiol 17:70D, 1993.
184. Kern MJ, Moore JA, Aguirre FV, et al: Determination of angiographic (TIMI grade) blood flow by intracoronary Doppler flow velocity during acute myocardial infarction. Circulation 94:1545–1552, 1996.
185. Claeys MJ, Vrintz CJ, Bosmans J, et al: Coronary flow reserve during coronary angioplasty in patients with a recent myocardial infarction: Relation to stenosis and myocardial viability. J Am Coll Cardiol 28:1712–1719, 1996.
186. Miller DD, Nallamothu RB, Shaw LJ, et al: Does intracoronary Doppler assessment of post-stenotic reperfusion flow enhance cardiac event prediction as compared to other post-myocardial infarction risk markers? J Am Coll Cardiol 29(Supp A):71A, 1997.
187. Eng C, Patterson RE, Horowitz SF, et al: Coronary collateral function during exercise. Circulation 66:309–316, 1982.
188. Mautz FR, Gregg DE: Dynamics of collateral circulation following chronic occlusion of coronary arteries. Proc Soc Exp Biol Med 36:797–801, 1973.
189. Chansky M, Levy MN: Collateral circulation to myocardial regions supplied by anterior descending and right coronary arteries in the dog. Circ Res 11:414–417, 1962.
190. Levy MN, Imperial ES, Zieske H Jr: Collateral blood flow to the myocardium as determined by the clearance of rubidium 86 chloride. Circ Res 9:1035–1043, 1961.

191. Bloor CM, Roberts LE: Effect of intravascular isotope content on the isotopic determination of coronary collateral blood flow. Circ Res 16:537-544, 1965.
192. Gensini GG, DaCosta BC: The coronary collateral circulation in living man. Am J Cardiol 24:394-400, 1969.
193. Helfant RH, Vokonas PS, Gorlin R: Functional importance of the human coronary collateral circulation. N Engl J Med 284:1277-1281, 1971.
194. Cohen M, Rentrop KP: Limitation of myocardial ischemia by collateral circulation during sudden controlled coronary artery occlusion in human subjects: A prospective study. Circulation 74:469-476, 1986.
195. Khaja F, Sabbah HN, Brymer JF, Stein PD: Influence of coronary collaterals on left ventricular function in patients undergoing angioplasty. Am Heart J 116:1174-1180, 1988.
196. Rentrop KP, Thornton JC, Feit F, Van Buskirk M: Determinants and protective potential of coronary arterial collaterals as assessed by an angioplasty model. Am J Cardiol 61:677-684, 1988.
197. Rentrop KP, Cohen M, Blanke H, Phillips RA: Changes in collateral channel filling immediately after controlled coronary artery occlusion by an angioplasty balloon in human subjects. J Am Coll Cardiol 5:587-592, 1985.
198. Donohue TJ, Kern MJ, Aguirre FV, et al: Comparison of hemodynamic and pharmacologic perturbations of coronary collateral flow velocity in patients during angioplasty. J Am Coll Cardiol 19:393A, 1992.
199. Probst P, Zangl W, Pachinger O: Relation of coronary arterial occlusion pressure during percutaneous transluminal coronary angioplasty to presence of collaterals. Am J Cardiol 55:1264-1269, 1985.
200. Dervan JP, McKay RG, Baim DS: Assessment of the relationship between distal occluded pressure and angiographically evident collateral flow during coronary angioplasty. Am Heart J 114:491-497, 1987.
201. Kern MJ, Donohue TJ, Bach RG, et al: Quantitating coronary collateral flow velocity in patients during coronary angioplasty using a Doppler guidewire. Am J Cardiol 17:34D, 1993.
202. Donohue T, Kern MJ, Bach R, et al: Examination of the effects of hemodynamic and pharmacologic interventions on coronary collateral flow in a patient during cardiac catheterization. Cathet Cardiovasc Diagn 28:155, 1992.
203. Fujita M, McKown DP, McKown MD, Franklin D: Electrocardiographic evaluation of collateral development in conscious dogs. J Electrocardiogr 21:55, 1988.
204. Feldman RL, Pepine CJ: Evaluation of coronary collateral circulation in conscious humans. Am J Cardiol 53:1233, 1984.
205. Scheel KW, Eisenstein BL, Ingram LA: Coronary, collateral, and perfusion territory responses to aortic banding. Am J Physiol 246:H768, 1984.
206. Yamada T, Okamoto M, Sueda T, et al: Relation between collateral flow assessed by Doppler guidewire and angiographic collateral grades. Am Heart J 130:32-37, 1995.
207. Bach RG, Donohue TJ, Caracciolo EA, et al: Quantification of collateral blood flow during PCA by intravascular Doppler. Eur Heart J 16:74-77, 1995.
208. Piek JJ, van Liebergen RA, Koch KT, et al: Clinical, angiographic, and hemodynamic predictors of recruitable collateral flow assessed during balloon angioplasty coronary occlusion. J Am Coll Cardiol 29:275-282, 1997.
209. Tron C, Donohue TJ, Bach RG, et al: Differential characterization of human coronary collateral blood flow velocity. Am Heart J 132:508-515, 1996.
210. Piek JJ, van Liebergen RA, Koch KT, et al: Comparison of collateral vascular response in the donor and recipient coronary artery during transient coronary occlusion assessed by intracoronary blood flow velocity analysis in patients. J Am Coll Cardiol 29:1528-1535, 1997.
211. Piek JJ, van Liebergen RAM, Koch KT, et al: Pharmacological modulation of the human collateral vascular resistance in acute and chronic coronary occlusion assessed by intracoronary blood flow velocity analysis in an angioplasty model. Circulation 96:106-115, 1997.
212. Kern MJ, Aguirre F, Penick D, et al: Enhanced intracoronary flow velocity during intraaortic balloon counterpulsation in critically ill patients. J Am Coll Cardiol 21:359, 1993.
213. Kern MJ, Aguirre F, Bach R, et al: Augmentation of coronary blood flow by intraaortic balloon pumping in patients after coronary angioplasty. Circulation 87:500, 1991.
214. Ishihara M, Sato H, Tateishi H, et al: Intraaortic balloon pumping as the post-angioplasty strategy in acute myocardial infarction. Am Heart J 122:385-389, 1991.
215. Ohman EM, Califf RM, George BS, et al: The use of intra-aortic balloon pumping as an adjunct to reperfusion therapy in acute myocardial infarction. Am Heart J 121:895-901, 1991.
216. Bach RG, Donahue TJ, Caracciolo EA, et al: Intraaortic balloon pumping augments distal coronary blood flow provided through perfusion balloon catheters during high-risk PTCA. J Am Coll Cardiol 25(abst suppl):150A, 1995.
217. Furchgott RF, Zawadzki JV: The obligatory role of endothelial cells in the relaxation of smooth muscle by acetylcholine. Nature 288:373-376, 1980.
218. Palmer RM, Ashton DS, Moncada S: Vascular endothelial cells synthesize nitric oxide from L-arginine. Nature 333:664-666, 1988.
219. Vallance P, Collier J, Moncada S: Effects of endothelium-derived nitric oxide on peripheral arteriolar tone in man. Lancet 2:997-1000, 1989.
220. Panza JA, Quyyumi AA, Brush JEJR, et al: Abnormal endothelium-dependent vascular relaxation in patients with essential hypertension. N Engl J Med 323:22-27, 1990.
221. Johnstone MT, Gallagher SJ, Scales KM, et al: Endothelium-dependent vasodilatation is impaired in patients with insulin-dependent diabetes mellitus. Circulation 68:I-618, 1992.
222. Fostermann U, Mugge A, Alheid U, et al: Selective attenuation of endothelium-mediated vasodilation in atherosclerotic human coronary arteries Circ Res 62:185-190, 1988.
223. Ludmer PL, Selwyn AP, Shook TL, et al: Paradoxical vasoconstriction induced by acetylcholine in atherosclerotic coronary arteries. N Engl J Med 315:1046, 1986.
224. Werns SD, Walton JA, Hsia HH, et al: Evidence of endothelial dysfunction in angiographically normal coronary arteries of patients with coronary artery disease. Circulation 79:287, 1989.
225. Vita JA, Treasure CB, Nabel EG, et al: Coronary vasomotor response to acetylcholine relates to risk factors in coronary artery disease. Circulation 81:491, 1990.
226. Yasue H, Matsuyama K, Okumura K, et al: Responses of angiographically normal human coronary arteries to intracoronary injection of acetylcholine by age and segment. Circulation 81:482-490, 1990.
227. Okumura K, Yasue H, Matsuyama T, et al: A study of coronary hemodynamics during acetylcholine-induced coronary spasm in patients with variant angina: Endothelium-dependent dilation in the resistance vessels. J Am Coll Cardiol 19:1426-1434, 1992.
228. Vrints CJM, Bult H, Hitter E, et al: Impaired endothelium-mediated/cholinergic coronary vasodilatation in patients with angina and normal coronary arteriograms. J Am Coll Cardiol 19:21-31, 1992.
229. Cox DA, Vita JA, Treasure CB, et al: Atherosclerosis impairs flow-mediated dilation of coronary arteries in humans. Circulation 80:458-465, 1989.
230. Nabel EG, Selwyn AP, Ganz P: Large arteries in humans are responsive to changing blood flow: An endothelium-dependent mechanism that fails in patients with atherosclerosis. J Am Coll Cardiol 16:349-356, 1990.
231. Drexler H, Zeiher AM, Wollschlager H, et al: Flow-dependent coronary artery dilatation in humans. Circulation 80:466-474, 1989.
232. Zeiher AM, Drexler H, Wollschlager H, et al: Coronary vasomotion in response to sympathetic stimulation in humans: Importance of the functional integrity of the endothelium. J Am Coll Cardiol 14:1181-1190, 1989.
233. McFadden EP, Clarke JG, Davies GJ, et al: Effect of intracoronary serotonin on coronary vessels in patients with stable angina and in patients with variant angina. N Engl J Med 342:648-654, 1991.
234. Zeiher AM, Schachinger V, Weitzel SH, et al: Intracoronary thrombus formation causes focal vasoconstriction of epicardial arteries in patients with coronary artery disease. Circulation 83:1519-1525, 1991.
235. Yao SK, Ober JC, Willerson JT, et al: Endogenous nitric oxide protects against platelet aggregation and cyclic flow variations in stenosed and endothelium injured arteries. Circulation 86:1302-1309, 1992.

236. Garg UC, Hassid A: Nitric oxide-generating vasodilators and 8-bromocyclic guanosine monophosphate inhibit mitogenesis and proliferation of cultured rat vascular smooth muscle cells. J Clin Invest 83:1774-1777, 1989.
237. Zeiher AM, Drexler H, Wollschläger H, Just H: Modulation of coronary vasomotor tone in humans: Progressive endothelial dysfunction with different early stages of coronary atherosclerosis. Circulation 83:391-401, 1991.
238. Hodgson J, Nair R, Sheehan HM, Reddy KG: Endothelial dysfunction in coronary arteries precedes ultrasonic evidence of atherosclerosis in patients with risk factors. J Am Coll Cardiol 19:323A, 1992.
239. Hodgson JB, Marshall JJ: Direct vasoconstriction and endothelium-dependent vasodilation. Circulation 79:1043-1051, 1989.
240. Zeiher AM, Drexler H, Wollschläger H, Just H: Endothelial dysfunction of the coronary microvasculature is associated with impaired coronary blood flow regulation in patients with early atherosclerosis. Circulation 84:1984-1992, 1991.
241. Selke FW, Armstrong ML, Harrison DG: Endothelium-dependent vascular relaxation is abnormal in the coronary microcirculation of atherosclerotic primates. Circulation 81:1586-1593, 1990.
242. Chilian WM, Dellsperger KC, Layne SM, et al: Effects of atherosclerosis on the coronary microcirculation. Am J Physiol 258:H529-H539, 1990.
243. Yamamoto H, Bossalier C, Cartwright J, Henry PD: Videomicroscopic demonstration of defective cholinergic arteriolar vasodilation in atherosclerotic rabbit. J Clin Invest 81:1752-1758, 1988.
244. Di Mario C, Strikwerda S, Gil R, et al: Response of conductance and resistance coronary vessels to scalar concentrations of acetylcholine: Assessment with quantitative angiography and intracoronary Doppler echocardiography in 29 patients with coronary artery disease. Am Heart J 127:514-531, 1994.
245. Bassenger E, Busse R: Endothelial modulation of coronary tone. Progr Cardiovasc Dis 30:349-380, 1988.
246. Newman CM, Maseri A, Hackett DR, et al: Response of angiographically normal and atherosclerotic left anterior descending coronary artery to acetylcholine. Am J Cardiol 66:1070, 1990
247. Busse R, Trogisch G, Bassenge E: The role of endothelium in the control of vascular tone. Basic Res Cardiol 80:475, 1990.
248. Angus JA, Campbell GR, Cocks TM, et al: Vasodilatation by acetylcholine is endothelium dependent: A study by sonomicrometry in canine femoral artery in vivo. J Physiol 344:209-244, 1983.
249. Vrints C, Bosmans J, Bult H, et al: Loose parallelism between the coronary vasomotor responses to acetylcholine and to serotonin. J Am Coll Cardiol 19:323A, 1992.
250. Golino P, Piscione F, Willerson JT, et al: Divergent effects of serotonin on coronary artery dimensions and blood flow in patients with coronary atherosclerosis and coronary patients. N Engl J Med 324:641-648, 1991.
251. Hillis DL, Lange RA: Serotonin and acute ischemic heart disease. N Engl J Med 342:688-689, 1991.
252. Verbeuren TJ, Jordaens FH, Zonnekyn LL, et al: Effect of hypercholesterolemia on vascular reactivity in the rabbit. Circ Res 58:552-564, 1986.
253. Takahishi M, Yui Y, Yasumoto H, et al: Lipoproteins are inhibitors of endothelium-dependent relaxation of rabbit aorta. Am J Physiol 258:H1-H8, 1990.
254. Drexler H, Zeiher AM, Doster W, et al: Endothelial dysfunction in the coronary circulation in hypercholesterolemia: Protective effect of high HDL cholesterol. Circulation 86:I117, 1992.
255. Chillian WM, Easthman CL, Marcus ML: Microvascular distribution of coronary vascular resistance in beating left ventricle. Am J Physiol 20:H779-H788, 1986.
256. Harrison DG, Armstrong ML, Freiman PC, Heistad DD: Restoration of endothelium-dependent relaxation by dietary treatment of atherosclerosis. J Clin Invest 80:1801-1811, 1987.
257. Cooke JP, Andon NA, Girerd XJ, et al: Arginine restores cholinergic relaxation of hypercholesterolemic rabbit thoracic aorta. Circulation 83:1057-1062, 1991.
258. Drexler H, Zeiher AM, Meinzer K, Just H: Correction of endothelial dysfunction in coronary microcirculation of hypercholesterolemic patients by L-arginine. Lancet 338:1546, 1991.
259. Auch-Swelk W, Bossaler C, Claus M, et al: ACE inhibitors potentiate endothelium-dependent relaxations to threshold concentrations of bradykinin in coronary arteries. J Am Coll Cardiol 19:190A. 1992.
260. Dohi Y, Criscione L, Pfeiffer K, Luscher TF: Normalization of endothelial dysfunction of hypertensive mesenteric resistance arteries by chronic therapy with benazepril or nifedipine. J Am Coll Cardiol 19:226A, 1992.
261. Williams JK, Adams MR, Herrington DM, Clarkson TB: Short-term administration of estrogen and vascular responses of atherosclerotic coronary arteries. J Am Coll Cardiol 20:452-457, 1992.
262. Egashira K, Hirooka Y, Kai H, et al: Reduction in serum cholesterol with pravastatin improves endothelium-dependent coronary vasomotion in patients with hypercholesterolemia. Circulation 89:2519-2524, 1994.
263. Anderson TJ, Meredith IT, Yeung AC, et al: The effect of cholesterol lowering and antioxidant therapy on endothelium-dependent coronary vasomotion. N Engl J Med 332:488-493, 1995.
264. Treasure CB, Klein JL, Weintraub WS, et al: Beneficial effects of cholesterol-lowering therapy on the coronary endothelium in patients with coronary artery disease. N Engl J Med 332:481-487, 1995.
265. Mancini GB, Henry GC, Macaya C, et al: Angiotensin-converting enzyme inhibition with quinalapril improves endothelial vasomotor dysfunction in patients with coronary artery disease: The TREND (Trial on Reversing ENdothelial Dysfunction) Study. Circulation 94:258-265, 1996.
266. Li W, van der Steen AFW, Lancee CT: Temporal correlation of bloodscattering signals in vivo from radiofrequency intravascular ultrasound. Ultrasound Med Biol 22:583-590, 1996.
267. Li W, Lancee CT, Cespedes I, et al: Decorrelation properties of intravascular echo signals. J Acoust Soc Am 1997 (in press).
268. Li W, van der Steen AFW, Lancee CT, et al: Potentials of volumetric blood-flow measurement. Semin Intervent Cardiol 2:49-54, 1997.
269. Carlier S, Li W: In vivo validation of a new intracoronary volumetric blood flow measurement method with intravascular ultrasound. Circulation (abst) (in press).
270. Kern MJ, De Bruyne B, Pijls NHJ: From research to clinical practice: Current role of intracoronary physiologically based decision making in the cardiac catheterization laboratory. J Am Coll Cardiol 30:613-620, 1997.

Chapter 2

Decreased coronary flow reserve in hypertrophic cardiomyopathy is related to remodeling of the coronary microcirculation.

R Krams, MJM Kofflard, DJ Duncker, C Von Birgelen, **S Carlier**, M Kliffen, FJ ten Cate, PW Serruys.

Circulation 1998;97:230-233.

Decreased Coronary Flow Reserve in Hypertrophic Cardiomyopathy Is Related to Remodeling of the Coronary Microcirculation

R. Krams, MD, PhD; M.J.M. Kofflard, MD; D.J. Duncker, MD, PhD; C. Von Birgelen, MD; S. Carlier, MD; M. Kliffen, MD, PhD; F.J. ten Cate, MD, PhD; P.W. Serruys, MD, PhD

Background—Ischemia occurs frequently in hypertrophic cardiomyopathy (HCM) without evidence of epicardial stenosis. This study evaluates the hypothesis that the occurrence of ischemia in HCM is related to remodeling of the coronary microcirculation.

Methods and Results—End-diastolic septal wall thickness was significantly increased in patients with HCM (25.8±2.9 mm) in comparison with cardiac transplant recipients (control subjects: 11.4±3.0 mm; $P<0.05$). Although the diameter of the left anterior descending coronary artery was similar in both groups (3.0±0.8 versus 3.0±0.5 mm, P=NS), the coronary resistance reserve ($CRR=CRR_{basal}/CRR_{hyperemic}$), corrected for extravascular compression (end-diastolic left ventricular pressure), was reduced to 1.5±0.6 in HCM ($P<.05$; control, 2.6±0.8). Arteriolar lumen (AL) divided by wall area was lower in HCM (21±5% versus 30±4%; $P<.05$), and capillary density tended to decrease (from 1824±424 to 1445±513 per mm^2, $P=.11$) in HCM. CRR was linearly related to normalized AL according to the formula $CRR=0.1\ AL-0.45$ ($r=.57$; $P<.05$). Further analysis revealed that CRR, AL, and capillary density were all linearly related to the degree of hypertrophy.

Conclusions—Decrements in CRR were related to changes of the coronary microcirculation. Both the decrease in CRR and these changes in the coronary microcirculation were related to the degree of hypertrophy. All these factors might contribute to the well-known occurrence of ischemia in this patient group. (*Circulation*. 1998;97:230-233.)

Key Words: cardiomyopathy ■ arteries ■ capillaries ■ ischemia

Anginal symptoms and signs of ischemia occur frequently in patients with HCM without detectable lesions of the major epicardial arteries,[1-5] suggesting that the presence of ischemia is the result of abnormalities of the coronary microcirculation. Indeed, postmortem analysis of HCM hearts showed the existence of arterioles with abnormally thick walls.[6,7] Furthermore, in experimentally induced hypertrophy, it has been shown that the hypertrophic process is accompanied not only by decrements in CFR but also by structural changes in the coronary microcirculation (coronary remodeling), including a decreased capillary density.[8-10] The resulting increased diffusion distances for oxygen and the disturbed perfusion of the capillary bed have been forwarded as an explanation for ischemia.[8-10]

Although the CFR is decreased in HCM, in accordance with the findings of experimentally induced hypertrophy,[9,10] it is unknown at present whether the decreased CFR is related to the abnormal arterioles and whether a decrease in capillary density accompanies this decrease in AL. To that end, we measured CFR in combination with a quantitative analysis of AL, wall area and capillary density in myocardial tissue obtained during surgery (HCM) and obtained from endomyocardial biopsies (HTx).

Methods

Subjects and Protocol

Studies were performed in a group of patients with hypertrophic obstructive cardiomyopathy (HCM; n=10) who were referred for cardiac catheterization. The control group consisted of asymptomatic cardiac transplant recipients (HTx group; n=8) undergoing follow-up coronary angiography after transplantation. Informed consent was obtained from all patients. Patients in the HCM group were symptomatic (NYHA class II or III) despite β-blockade therapy (n=5) or therapy with calcium antagonists (n=5). These patients were considered candidates for surgery (myotomy/myectomy). Medical therapy was continued in both groups. Right heart catheterization was performed with a 7F balloon-tipped flow-directed thermodilution catheter. A 7F temporary pacemaker was positioned into the right atrium. Left heart catheterization was carried out, after which left ventricular angiography and coronary arteriography were performed with standard techniques. A 0.014-in Doppler guidewire with a floppy distal end (Cardiometrics, Inc) was introduced through an 8F guiding catheter and positioned at the midsegment of the LAD to measure Doppler flow velocity at rest and after hyperemia. In both groups, hearts were paced at a constant heart rate of 100 bpm to avoid metabolic vasodilatation during determination of the CFR. After optimization of the settings of the velocity signal and 3 to 5 minutes after intracoronary injection of a bolus of 2 to 3 mg isosorbide dinitrate, baseline recordings of flow velocity and perfusion pressure were collected and digitized at a sample rate of 125 Hz for off-line

Received August 22, 1997; revision received October 30, 1997; accepted October 31, 1997.

From the Department of Cardiology of the Thoraxcenter and Department of Pathology (M.K.), Erasmus University Rotterdam, Netherlands.

Correspondence to Rob Krams, MD, PhD, Laboratory for Hemodynamics, Room Ee2322, Erasmus University Rotterdam, PO Box 1738, Dr Molewaterplein 30, 3000 DR Rotterdam, The Netherlands.

Selected Abbreviations and Acronyms

AL = normalized arteriolar lumen
CFR = coronary flow reserve
CRR = coronary resistance reserve
HCM = hypertrophic cardiomyopathy
HTx = cardiac transplant
LAD = left anterior descending coronary artery

analysis. Maximal hyperemia was induced by an intracoronary bolus injection of 18 μg adenosine.[10]

Doppler Measurements

The sample volume of the Doppler wire was positioned at a distance of 5.2 mm from the transducer and was ≈2.25 mm wide. After power spectral analysis based on a fast Fourier transform algorithm, the maximal Doppler shift (kHz) was automatically tracked and converted to the instantaneous velocity values (cm/s). CFR was defined as hyperemic divided by basal velocity (V_{cor}). Coronary resistance was defined as $(P_{ao}-P_{ed})/V_{cor}$, where P_{ao} is aortic pressure and P_{ed} is end diastolic pressure. P_{ed} was subtracted to account for increments in extravascular compression. CRR was defined as the ratio of basal divided by hyperemic resistance.

Quantitative Angiographic Measurements

A validated on-line analysis system operating on digital images (ACA-DCI, Philips[11]) was used during the catheterization procedure. With this system, the end-diastolic diameter of the LAD was determined in the segment of the LAD in which the sample volume of the Doppler wire was located.

Echocardiographic Measurements

Two-dimensional echocardiographic studies were performed (HP Sonos 1500) with the heart being visualized from standard cross-sectional planes while images were recorded on videotape (VHS) for off-line analysis. Septal wall thickness was measured in diastole from both the parasternal short-axis and long-axis views. From the recordings on videotape, representative stop-frames from the various cross-sectional planes were acquired to determine septal wall thickness with the aid of a computer and a dedicated software program. To obtain an average for septal wall thickness, the various cross-sectional planes were pooled. One patient from the control group was not analyzed because of insufficient image quality. Thickness of the septal wall for the HCM and the control groups was defined as the degree of hypertrophy.

Histological Measurements

The myocardial tissues from the HCM group (n=9) and from the control group (n=8) were obtained from surgical myectomy (left ventricular septal tissue; weight, 0.3 to 1 g) and myocardial biopsies (left ventricular septal tissue; weight, 0.5 to 1 mg), respectively. During catheterization, one HCM patient presented without a subvalvular pressure gradient and was not operated on. The tissue was fixed with paraldehyde and immersed in 10% buffered formalin. van Gieson staining was used for identification and analysis of intramyocardial small arteries. Arterioles were identified on the basis of the appearance of a layer of media and diameter <100 μm. Only arterioles with round cross sections and without side branches were analyzed. Capillaries were identified with specific antibodies (CD34) against endothelium. Quantitative morphometric analysis of the histological sections occurred with an in-house–developed software program applied to a morphometric system (Clemex Technology Inc) that calculated density of capillaries (capillaries per square millimeter), taking tissue shrinkage into account. Five cross sections per patient (≈1000 capillaries) were analyzed. In addition, software was available that allowed us to trace the arteriolar lumen-intima and adventitia-media borders, which defined the lumen and wall thickness regions. The areas of these regions were obtained from the number of pixels in the two regions. Normalized wall area is given by circular wall area/(lumen area+wall area). This value was calculated for 10 arterioles per patient. Data are presented as mean±SD. Regression analysis, ANOVA, and *t* tests were performed with standard statistical software (SPSS). A value of $P<.05$ was considered significant.

Results

The HTx recipients, who served as control subjects, had no cardiac complaints, and all of them had normal coronary arteriograms. The time interval of catheterization after transplantation was 4±2 years. Medication of HTx patients at the time of catheterization was immunosuppression (n=8) Ca^{2+} antagonists (n=8), aspirin (n=5), and dipyridamole (n=4). No member of the control group had signs of rejection on the basis of the biopsies. Age distributions between the HCM (45.5±14.6 years) and control (48.7±6.0 years) groups were similar. HCM patients were symptomatic (NYHA class II or III), whereas all members of the control group were symptom free (NYHA class I). HCM patients had a subvalvular gradient of 88±31 mm Hg and a lower aortic pressure (103±14 versus 120±15 mm Hg, $P<.05$), a higher end-diastolic left ventricular pressure (22±1 versus 12±6 mm Hg, $P<.05$), a lower cardiac index (2.7±0.5 versus 3.5±0.7 L/m^2, $P<.05$), and a lower heart rate during baseline conditions (70±13 versus 97±13 bpm, $P<.05$) than the control group.

End-diastolic septal wall thickness was significantly increased in patients with HCM (25.8±2.9 mm) compared with members of the control group (11.4±3.0 mm; $P<.05$). All HCM patients had normal angiograms. The diameter of the LAD was similar in both groups (3.0±0.8 versus 3.0±0.5 mm). Coronary velocity during baseline conditions was higher for HCM patients (34±11 versus 20±11 cm/s, $P<.05$), whereas velocities during hyperemia were similar (49±20 versus 53±22 cm/s). As a consequence, the CFR was reduced from 2.6±0.8 in the control group to 1.8±0.9 in the HCM group ($P<.05$). Coronary resistance values, corrected for extravascular compression (see above), were lower (3.7±2.1 versus 6.5±2.2 mm Hg · s · cm^{-1}, $P<.05$) during baseline conditions and were similar during hyperemia (2.6±1.5 versus 2.6±1.0, P=NS) in HCM. Consequently, the CRR was lower (1.5±0.6 versus 2.6±0.8, $P<.05$) in HCM than in the control group. Arteriolar wall area was similar (5720±2130 versus 7107±3544 μm^2; P=NS), but lumen area (1273±688 versus 2260±1165 μm^2; $P<.05$) and diameters were significantly lower (19.6±4.5 versus 25.9±4.3 μm; $P<.05$) in HCM compared with control values. Consequently, AL was lower in the HCM (21±5%) than in the control group (30±4%; $P<.05$), and capillary density tended to decrease from 1824±424 to 1445±513 per square millimeter in HCM ($P=.11$). In addition, both the CFR and the CRR were linearly related to AL according to the formula CFR=0.1 AL−0.45 ($r=.57$; $P<.05$) and CRR=0.07 AL+0.35 ($r=.50$; $P<.05$; Fig 1A). Further analysis revealed that the degree of AL (AL=−0.85 Hyp+43.7; $r=.71$; $P<.05$; Fig 1B), the CFR (CFR=−0.17 Hyp+5.9; $r=.80$; $P<.05$), the CRR (CRR=−1.2 Hyp+4.7; $r=.7$; $P<.05$; Fig 1C), and the capillary density (CD=−51 Hyp+2750; $r=.53$; $P<.05$; Fig 1D) were all inversely related to the degree of hypertrophy (Hyp). In addition, a linear relationship between AL and

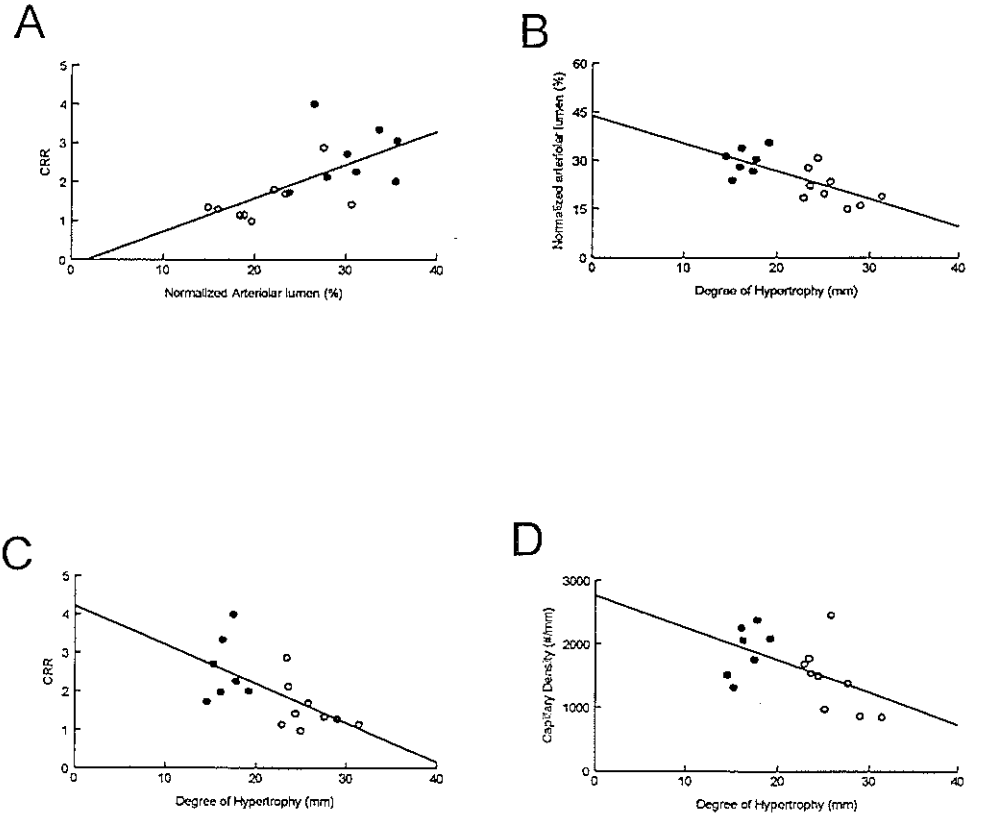

Relationship of CRR with AL (A), AL and degree of hypertrophy (B), CRR and degree of hypertrophy (C), and capillary density and degree of hypertrophy (D).

capillary density was measured (AL=42 CD+577; r=.54; P<.05).

Discussion

In symptomatic patients with HCM without evidence of a functional stenosis of the epicardial vessels, decrements in CFR were detected, confirming earlier studies.[1-5] Similar decrements in CRR were measured, implying that these findings could not be explained by increments in extravascular compression.[9,10] Abnormal arterioles with decreased lumen were detected in HCM patients, suggesting that a structural change in the coronary arterial vascular tree might be related to this finding. Indeed, a positive relationship between both CFR and CRR and AL, corrected for tissue shrinkage by normalization to the wall area,[7] was detected. Furthermore, an inverse relationship was noted between AL and the degree of hypertrophy, confirming earlier postmortem studies.[7] Because of this relationship, an inverse relationship between CFR and the degree of hypertrophy could be measured. Again, a similar relationship was found between CRR and degree of hypertrophy, implying that extravascular compressive forces were not essential for these findings. In large-animal models of pressure overload–induced left ventricular hypertrophy, vascular medial hypertrophy has been observed only when the coronary circulation was exposed to high perfusion pressures. The present arteriolar abnormalities were obtained at normal to low aortic pressures and might imply that hypertrophy of the arterioles, in parallel to the hypertrophy of the myocardium, is an independent process.[7]

A decreased capillary density has been measured in several animal studies with experimentally induced secondary hypertrophy and recently in humans with secondary hypertrophy.[12,13] Although differences between the groups in capillary density did not reach levels of statistical significance, there clearly was an inverse relationship between capillary density and degree of hypertrophy. Furthermore, the decrements in capillary density and decrements of AL are related in HCM. These findings may imply that the decreased AL induces periods of ischemia, which results in increased angiogenesis. This angiogenesis normalizes the decrements in capillary density. However, because we did not analyze HCM myocardial tissue without hypertrophy, we cannot exclude the possibility that the occurrence of changes in the coronary microcirculation in HCM is a more independent phenomenon and not directly related to the degree of hypertrophy.[6,7]

In conclusion, septal hypertrophy is associated with decrements in CFR and CRR in HCM patients. Arterioles of HCM patients exhibited a smaller lumen at similar wall thickness, which correlated well with decrements in CFR and CRR. These findings suggest that abnormal arterioles might contribute to the perfusion abnormalities found in these patients, resulting in recurrent myocardial ischemia.

References

1. O'Cannon RO, Schenke WH, Maron BJ, Tracy CM, Leon MB, Brush JE, Rosing DR, Epstein SE. Differences in coronary flow and myocardial metabolism at rest and during pacing between patients with obstructive and patients with non-obstructive hypertrophic cardiomyopathy. *J Am Coll Cardiol.* 1987;10:53–62.
2. Camici P, Chiriatti G, Lorenzoni R, Bellina RC, Gistri R, Italiani G, Parodi O, Salvadori PA, Nista N, Papi L, L'Abbati A. Coronary vasodilatation is impaired in both hypertrophied and non-hypertrophied myocardium of patients with hypertrophic cardiomyopathy: a study with nitrogen-13 ammonia and positron emission tomography. *J Am Coll Cardiol.* 1991;17:879–886.
3. Pasternac A, Noble J, Streulens Y, Elie R, Henschke C, Bourassa M. Pathophysiology of chest pain in patients with cardiomyopathies and normal coronary arteries. *Circulation.* 1982;65:778–788.
4. Nienaber CA, Gambhir SS, Vaghaiwalla F, Ratib O, Huang S-G, Phelps ME, Schelbert HR. Regional myocardial blood flow and glucose utilization in symptomatic patients with hypertrophic cardiomyopathy. *Circulation.* 1993;87:1580–1590.
5. Toshima H, Maron BJ, eds. *Hypertrophic Cardiomyopathy.* Cardiomyopathy Update, 2. Tokyo, Japan: Tokyo Press; 1988.
6. Maron BJ, Wolfson JK, Epstein SE, Robert WC. Intramural ('small vessel') coronary artery disease in hypertrophic cardiomyopathy. *J Am Coll Cardiol.* 1986;8:545–557.
7. Tanaka M, Fujiwara H, Onodera T, Wu DJ, Matsuda M, Hamashima Y, Kawai C. Quantitative analysis of narrowing of intramyocardial small arteries in normal heart, hypertensive hearts, and hearts with hypertrophic cardiomyopathy. *Circulation.* 1987;75:1130–1139.
8. O'Gara PT, Bonow RO, Maron BJ, Damske BA, van Lingen A, Bacharach SL, Larson SM, Epstein SE. Myocardial perfusion abnormalities in patients with hypertrophic cardiomyopathy: assessment with thallium-201 emission computed tomography. *Circulation.* 1987;76:1214–1223.
9. Spaan JAE, ed. *Coronary Blood Flow; Mechanics, Distribution, and Control.* Developments in Cardiovascular Medicine. Boston, Mass; Kluwer Academic Publishers; 124; 1991.
10. Marcus ML. *The Coronary Circulation in Health and Disease.* New York, NY: McGraw-Hill Publishing Co; 1983.
11. Serruys PW, di Mario C, Meneveau N, de Jaegere P, Strikwerda S, de Feyter PJ, Emanuelsson H. Intracoronary pressure and flow velocity with sensor-tip guidewires: a new methodological approach for assessment of coronary hemodynamics before and after coronary interventions. *Am J Cardiol.* 1993;71:41D–53D.
12. Schwartzkopff B, Motz W, Frenzel H, Vogt M, Knauer S, Strauer B. Structural and functional alterations of the intramyocardial coronary arterioles in patients with arterial hypertension. *Circulation.* 1993;88:993–1003.
13. Rakusan K, Flanagan MF, Geva T, Southern J, Van Praagh R. Morphometry of human coronary capillaries during normal growth and the effect of age in left ventricular pressure-overload hypertrophy. *Circulation.* 1992;86:38–46.

Chapter 3

Acquisition of raw intracoronary Doppler signal for better characterization of flows.

SG Carlier, E Gordov, E Gailly, G Van Camp, B Cosyns, H Geschwind, JL Vandenbossche.

Computers in Cardiology, IEEE Computer Society Press, 1996; p 205-208.

Acquisition of Raw Intracoronary Doppler Signal for Better Characterization of Flows

S Carlier, E Gordov[1], E Gailly[2], G Van Camp, B Cosyns, H Geschwind[1], JL Vandenbossche

CHU Saint Pierre, Free University of Brussels, Belgium
[1] CHU Henri Mondor, Université Paris XII, Créteil, France
[2] von Karman Institute for Fluids Dynamics, Brussels , Belgium

Abstract

Intracoronary investigations using Doppler-tipped guidewires are now performed routinely to assess severity of stenosis. Maximal peak velocity and average peak velocity computed on-line are used to this end, but when the quality of the Doppler signal is poor, the contour recognition fails to follow maximal velocity.

We describe a system allowing the acquisition of intracoronary raw Doppler signals (I and Q components) with pressures, ecg,... for recording and postprocessing. The technique of multiple beats averaging allowed for obtaining improvement of signal to noise ratio.

In-vitro experiments on steady and pulsatile flows in small tubes were performed. Influencing factors such as depth of measurements, rotations, quality of the signal have been investigated.

Our system may help collect high quality Doppler signals along with pressures which is useful for coronary blood flow assessment.

1. Introduction

Coronary angiography was thought to allow precise anatomic evaluation of the extent of coronary artery disease. Moreover, quantitative angiography has been proved to allow repeat measurements to analyze evolution of coronary atherosclerosis [1]. But an anatomical approach, even based on computed geometrical indexes, fails to give a reliable functional assessment of coronary stenosis in unselected patients with diffuse lesions [2,3]. Technological advances have allowed the development and the availability in catherization laboratories of very small Doppler and pressure devices mounted on guidewires in order to measure coronary velocities and pressures without hemodynamic perturbation. This has allowed functional assessment of the severity of coronary stenosis which could be well correlated with clinical evaluation of myocardial ischemia [3,4]. These approaches have been proved to even allow deferring safely angioplasty of stenosis which were not hemodynamically significant [5].

By definition, coronary flow reserve is the ratio between coronary flow during maximal vasodilatation and baseline values. It is estimated with the Doppler guidewire by the ratio of the velocities during pharmacological hyperemia and baseline state. It has limitations because of its dependency on hemodynamic conditions [6]. Recent developments integrating simultaneous measurements of aortic pressure and intracoronary velocities have tried to overcome these problems [7]. Such relation should be further investigated, with assessment of the pressure-flow relation distal to a coronary stenosis, in order to fully describe its hemodynamic influence compared to a more diffuse alteration of the distal vascular bed [8].

2. Aim of the study

Our aim was to develop a system allowing acquisition of intracoronary raw Doppler signals along with pressure, ECG and other signals. With raw Doppler signals, all the information of the complete spectrum is still available and can be stored for postprocessing. We wanted to be able to investigate alternative maximal frequency detection, power spectrum estimation (autoregressive modeling e.g.) and also to improve Doppler measurements by multibeats averaging in order to improve the signal to noise ratio. This should allow finally more precise determination of functional severity of stenosis then those achievable with conventional technique.

3. Material and methods

The Doppler system unit investigated is used everyday for clinical cath-lab investigations and has been validated in-vitro and in-vivo [9]. It is based on a 0.014 inch angioplasty guidewire, 175-cm-long flexible,

0276-6547/96 $5.00 © 1996 IEEE

steerable guidewire with a floppy distal end with a 15 MHz piezoelectric transducer mounted at the tip (Cardiometrics Inc). It is basically a pulsed Doppler system with a pulsed repetition frequency (PRF) ranging from 15 to 120 kHz, allowing to measure velocities up to ± 2.4m/s. The depth of the sampling volume can be adjusted. The clinical usual setup uses a depth of 5 mm, which gives a width of 2.2 mm for the sample, due to the diverging shape of the ultrasound beam. We have compared two depths: 5 and 10 mm. A real time fast-Fourier transform (FFT) computes the power spectrum, plotted on the screen with a conventional gray-scale. A maximal frequency estimation is performed also on-line for each spectral line to give the instantaneous peak velocity (IPV). With IPV, the maximal peak velocity (MPV) and the average peak velocity (APV) over the last 2 cardiac cycles are computed.

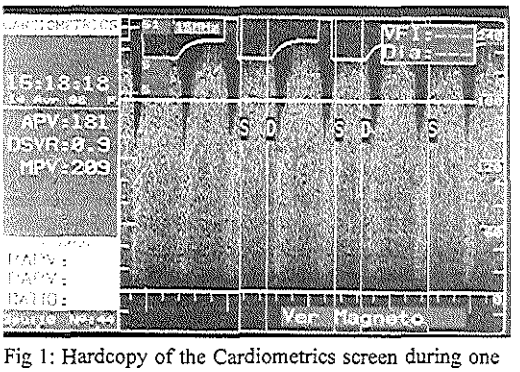

Fig 1: Hardcopy of the Cardiometrics screen during one in-vitro experiment. The instantaneous peak velocity plotted in white dots presents jittering and does not follow the maximal contour of the spectrum in this case.

For the acquisition of the raw I and Q Doppler signals coming after conventional quadrature demodulation in the Cardiometrics system, we used a system previously described [10] but improved by using a high speed (1 MHz) A/D acquisition board (Wavebook 512, IOTech Inc). I and Q are sampled at the PRF, but with only a period of 1 µs between them, minimizing mirror artifacts (between forward and reverse flow occurring during computation of the power spectrum, unless one uses expensive sample and hold on the A/D board) [10]. Up to six other channels were free to record ECG, pressures,... Power spectrum is computed off-line, after the acquisition, by FFT. The maximal frequency of each spectral line is estimated with an improved method proposed by Mo [11] and the maximal contour recognized can be filtered, using information from adjacent points to smooth it. For pulsatile flow, the variance of the power spectrum can be reduced by averaging multiple cycles (up to 20), in order to improve the contour recognition [12,13].

For preliminary tests, we have developed a simplified in-vitro model of a coronary artery, with tubes ranging from 2 to 5 mm in diameter. Steady or pulsatile flows, obtained with a roller pump from which a synchronization signal was available, were used. The fluid was a 4 % by volume of hardened red blood cells in physiological saline, which gives roughly the same Doppler power as that obtained with 45 % hematocrit [14]. To estimate the flow, we have used a simple collecting bag suspended to a weighting system with an analogic output which could be digitized simultaneously with the synchronization signal and the I and Q Doppler signals, up to 60 kHz, directly to the hard disk, allowing thus to record continuously seconds of signals, which could be then easily archived, reviewed, zoomed on screen and processed on a PC.

4. Results

Although the use of depth of 10 mm should allow to increase the width of the sample volume in straight tube (because of the diverging angle of the ultrasound beam) in order to detect more easily the maximal velocity in the insonified profile, the quality of the Doppler spectra was lower and the system failed to detect correctly the maximal contour. This gave a statistically significant difference (paired t-test) between APV (91±47 vs 81±36 cm/s) and MPV (109±51 vs 100±41) recorded respectively for a depth of 5 and 10 mm in a set of 12 flows.

Figure 2 shows a pulsatile flow recorded with its synchronization signal and the flow measurement.

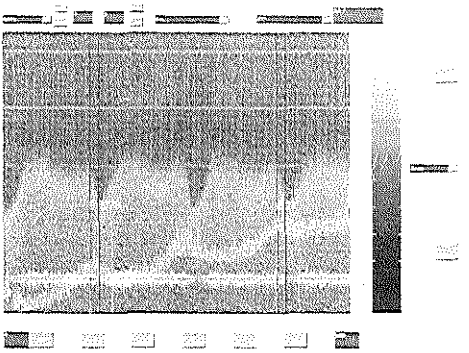

Fig 2: Presentation of the raw Doppler spectrum recorded along with pseudo-ecg and the weight of the collecting bag, with possibilities to zoom, to select, to detect ecg.

We could verify in this in-vitro system with transparent tubes that the alignment of the guidewire with the flow is a major problem. MPV could change up to 50% during a 360 degrees wire rotation, sometimes abruptly, just because the wire was looking towards the edge of the tube. This might lead to significant underestimation of flow, and stenosis, under study

Figures 3 and 4 compare one selected pulsatile cycle and the improvement in the signal to noise ratio, with a decrease of the variance of the Doppler spectrum with an averaging of 10 cycles. The contour detection was dramatically improved. On a subset of flows where the Cardiometrics system failed to recognize correctly the maximal contour (because there was not a sharp, well defined spectrum like in figure 1 where underestimation and jittering is present in the IPV recognized), this postprocessing allowed with our system to improve the contour detection (figure 4 compared to 1).

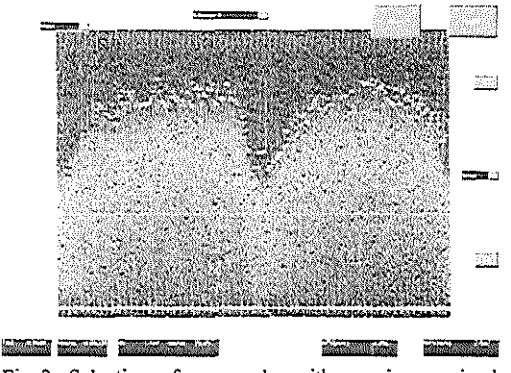

Fig 3: Selection of one cycle, with a noisy maximal contour detected because poor quality of Doppler signal.

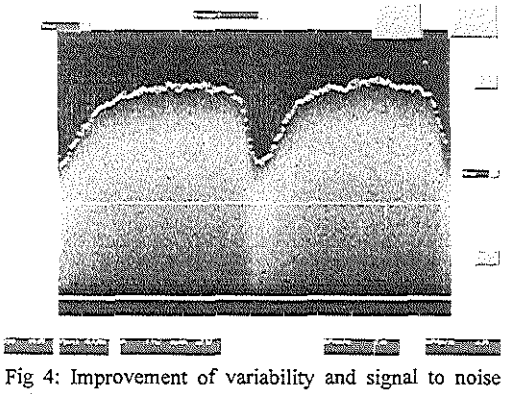

Fig 4: Improvement of variability and signal to noise ratio allowing a better contour detection thanks to an averaging of ten consecutive cycles.

5. Conclusions

This system seems a valuable tool to study coronary blood flow. It offers viewing, archiving and postprocessing utilities for Doppler intracoronary studies. It can improve direct on-line measurements. It should allow extensive studies of intracoronary fluid dynamics for physiological assessment of stenosis for example, thanks to the possibilities of simultaneous recordings of pressures.

Acknowledgments

This research was funded by « La Fondation Vésale » et la « Ligue Cardiologique Belge ».

We express our thanks to R Vanherle for his expert technical assistance.

References

[1] de Feyter PJ, Serruys PW, Davies MJ, Richardson P, Lubsen J, Oliver MF. Quantitative coronary angiography to measure progression and regression of coronary atherosclerosis. Value, limitations and implications for clinical trials. Circulation 1991;84:412-23.

[2] White CW, Wright CB, Doty DB, Hiratza LF, Eastham CL et all. Does visual interpretation of the coronary arteriogram predict the physiologic importance of a coronary stenosis ? N Engl J Med 1984; 310:819-24.

[3] Miller DD, Donohue TJ, Younis LT, Bach RG, Aguirre FV et all. Correlation of pharmocological ^{99m}Tc-sestamibi myocardial perfusion imaging with poststenotic coronary flow reserve in patients. Circulation 1994;89:2150-60.

[4] De Bruyne B, Bartunek J, Sys S, Heyndrickx R. Relation between myocardial fractional flow reserve calculated from coronary pressure measurements and exercice-induced myocardial ischemia. Circulation 1995;92:39-46.

[5] Kern MJ, Donohue TJ, Aguirre FV, Bach RG, Caracciolo EA et all. Clinical outcome of deferring angioplasty in patients with normal translesional pressure-flow velocity measurements. J Am Coll Cardiol 1995;25:178-87.

[6] McGinn AL, White CW, Wilson RF. Interstudy variability of coronary flow reserve. Influence of heart rate, arterial pressure and ventricular preload. Circulation 1990;81:1319-30.

[7] Di Mario C, Krams R, Gil R, Serruys PW. Slope of the instantaneous hyperemic diastolic coronary flow velocity-pressure relation. A new index for assessment of the physiological significance of coronary stenosis in humans. Circulation 1994;90:1215-24.

[8] Demer L, Gould KL, Kirkeeide R. Assessing stenosis severity: coronary flow reserve, collateral function, quantitative coronary arteriography, PET and digital substraction angiography. A review and analysis. Progress in Cardiovascular Diseases 1988;30:5, 307-322.

[9] Doucette JW, Corl DP, Payne HP, Flyn AE, Goto M et all. Validation of a Doppler guide wire for intravascular measurement of coronary artery flow velocity. Circulation 1992;85:1899-1911.

[10] Carlier S, Vandenbossche JL, Englert M. A PC based system for the acquisition and the analysis of Doppler ultrasound signal. Computers in Cardiology 1990. IEEE Computer Society Press 1990;385-7.

[11] Mo L. Comparison of four digital maximum frequency estimators for Doppler ultrasound. Ultrasound in Med & Biol 1988; 14:5, 355-63.

[12] Cloutier G, Allard L, Guo Z, Durand LG. The effect of averaging cardiac Doppler spectrograms on the reduction of their amplitude variability. Med & Biol Eng Comput 1992, 30:177-86.

[13] Carlier S, Verdonck P, Dimmer C, Vandenbossche JL. Assessment of an automatic determination of left ventricular dP/dt from Doppler Spectra of Mitral regurgitation. Computers in Cardiology 1995. IEEE Computer Society Press 1995, 321-4.

[14] Law YF, Johnston KW, Routh HF, Cobbold RSC. On the design and evaluation of a steady flow model for Doppler ultrasound studies. Ultrasound in Med & Biol 1989;15:5, 505-16.

Address for correspondence:
Stephane Carlier
CHU Saint Pierre - Cardiologie
322 rue Haute - 1000 Bruxelles - Belgium
e-mail :SCARLIER@ULB.AC.BE

Chapter 4

Randomized comparison of primary stenting and provisional balloon angioplasty guided by flow velocity measurement.

PW Serruys, B de Bruyne, **SG Carlier**, JE Sousa, J Piek, T Muramatsu, C Vrints, P Probst, R Seabra-Gomes, I Simpson, V Voudris, O Gurne, N Pijls, J Belardi, GA van Es, E Boersma, MA Morel, B van Hout, B

Circulation 2000;102:2930-2937.

With the editorial "Provisional versus routine stenting. Routine stenting is here to stay" by HV Vernon and BA Carabello.

Randomized Comparison of Primary Stenting and Provisional Balloon Angioplasty Guided by Flow Velocity Measurement

Patrick W. Serruys, MD; Bernard de Bruyne, MD; Stéphane Carlier, MD; José Eduardo Sousa, MD; Jan Piek, MD; Toshiya Muramatsu, MD; Chris Vrints, MD; Peter Probst, MD; Ricardo Seabra-Gomes, MD; Ian Simpson, MD; Vasilis Voudris, MD; Olivier Gurné, MD; Nico Pijls, MD; Jorge Belardi, MD; Gerrit-Anne van Es, PhD; Eric Boersma, PhD; Marie-Angèle Morel, MS; Ben van Hout, PhD; on behalf of the Doppler Endpoints Balloon Angioplasty Trial Europe (DEBATE) II Study Group

Background—Coronary stenting improves outcomes compared with balloon angioplasty, but it is costly and may have other disadvantages. Limiting stent use to patients with a suboptimal result after angioplasty (provisional angioplasty) may be as effective and less expensive.

Methods and Results—To analyze the cost-effectiveness of provisional angioplasty, patients scheduled for single-vessel angioplasty were first randomized to receive primary stenting (97 patients) or balloon angioplasty guided by Doppler flow velocity and angiography (523 patients). Patients in the latter group were further randomized after optimization to either additional stenting or termination of the procedure to further investigate what is "optimal." An optimal result was defined as a flow reserve >2.5 and a diameter stenosis <36%. Bailout stenting was needed in 129 patients (25%) who were randomized to balloon angioplasty, and an optimal result was obtained in 184 of the 523 patients (35%). There was no significant difference in event-free survival at 1 year between primary stenting (86.6%) and provisional angioplasty (85.6%). Costs after 1 year were significantly higher for provisional angioplasty (EUR 6573 versus EUR 5885; $P=0.014$). Results after the second randomization showed that stenting was also more effective after optimal balloon angioplasty (1-year event free survival, 93.5% versus 84.1%; $P=0.066$).

Conclusions—After 1 year of follow-up, provisional angioplasty was more expensive and without clinical benefit. The beneficial value of stenting is not limited to patients with a suboptimal result after balloon angioplasty. (***Circulation.* 2000;102:2930-2937.**)

Key Words: stents ■ angioplasty ■ balloon ■ random allocation ■ cost-benefit analysis

Over the last 2 decades, percutaneous transluminal coronary angioplasty has proven to be a safe and effective option for treating patients with coronary artery disease.[1] However, treatment results may be transient because of recoil, restenosis, and reocclusion. Although these disadvantages are partly overcome by coronary stenting,[2–6] the costs of coronary stenting are high compared with balloon angioplasty, and the long-term outcome remains a matter of concern.[7,8]

It has been suggested that optimal balloon angioplasty could yield a clinical outcome similar to stenting.[9–12] The Doppler Endpoints Balloon Angioplasty Trial Europe (DEBATE) I results support this hypothesis in that the outcome for patients with both a diameter stenosis (DS) ≤35% and a coronary flow reserve (CFR) >2.5 was comparable to that achieved with stenting in the Belgian Netherlands Stent (BENESTENT) trials.[3,13] Thus, the following provisional approach emerges: stent only those patients likely to reap an additional benefit. Such an approach challenges the intervener who must decide on overall patient care. "Provisional

See p 2910

Received May 31, 2000; revision received September 8, 2000; accepted September 19, 2000.

From the Thoraxcenter, Rotterdam, the Netherlands (P.W.S., S.C.); the Cardiovascular Center, OLV Hospital, Aalst, Belgium (B.d.B.); Instituto Dante Pazzanese, Sao Paulo, Brazil (J.E.S.); Academisch Medisch Centrum, Amsterdam, the Netherlands (J.P.); Kawasaki Central Hospital, Kawaka-Shi Kanagawa, Japan (T.M.); University Hospital Antwerp, Edegem-Antwerp, Belgium (C.V.); Allgemeines Krankenhaus der Stadt Wien, Vienna, Austria (P.P.); Hospital Santa Cruz, Linda-A-Velha, Portugal (R.S.-G.); Wessex Cardiology Center, Southampton, United Kingdom (I.S.); Onassis Cardiac Surgery Center, Athens, Greece (V.V.); Hôpital Universitaire de Mont-Godinne, Yvoir, Belgium (O.G.); Catharina Hospital, Eindhoven, the Netherlands (N.P.); Instituto Cardiovascular de Buenos Aires, Buenos Aires, Argentina (J.B.); Cardialysis, Rotterdam, the Netherlands (G.-A.v.E., M.-A.M.); Erasmus University, Rotterdam, the Netherlands (E.B.); and the Institute for Medical Technology Assessment, Rotterdam, the Netherlands (B.v.H.).

A complete list of the DEBATE II study group investigators can be found in the Appendix.

Reprint requests to Patrick W. Serruys, Department of Interventional Cardiology, Thoraxcenter Bd-418, University Hospital Dijkzigt, Dr Molewaterplein 40, 3015GD Rotterdam, The Netherlands. E-mail serruys@card.azr.nl

Circulation is available at http://www.circulationaha.org

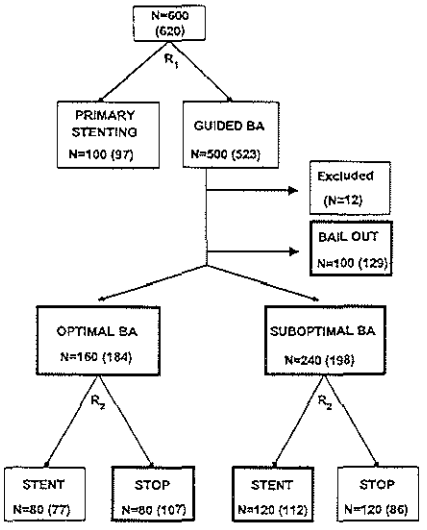

Figure 1. Study flowchart. R_1 indicates first randomization; R_2, second randomization; and BA, balloon angioplasty. Patient groups with provisional stenting are framed in bold. Actual number of patients in clinical subsets lie between parentheses; theoretical assumptions are denoted by n. Twelve patients were excluded from study between randomizations 1 and 2 (10 due to inconsistencies between randomization service and investigators, and 2 due to missing CFR values).

angioplasty" refers to a status of angioplasty that satisfies predefined criteria of optimal results based on pressure gradients,[11] early loss of minimal lumen diameter,[10] or intravascular ultrasound measurements.[12] A failure to meet the criteria would change the intended treatment and results in stent implantation.

DEBATE II was a prospective, randomized study that used criteria identified in DEBATE I. It addressed the following questions. (1) Should elective treatment be by stenting or balloon angioplasty (provisional angioplasty being guided by the stated criteria)? (2) What is the relative cost/benefit ratio of these strategies? (3) Do patients with optimal balloon angioplasty obtain an additional benefit from stenting?

Methods

Patient Selection

Patients were eligible for the study if they were scheduled to undergo angioplasty for stable or unstable angina pectoris (excluding Braunwald classification III),[14] documented myocardial ischemia due to a single de novo coronary stenosis potentially amenable to stent implantation, or both. The target lesion was to supply viable myocardium and be <25 mm long. Excluded patients manifested total coronary occlusion; lesions that were ostial or at a bifurcation; lesions in vessels that were previously bypassed, tortuous, or contained thrombus; or previous Q-wave infarction (in the target vessel territory or from an evolving myocardial infarction of the previous week). The study was performed according to the principles in the Declaration of Helsinki. Every patient provided written, informed consent.

Study Objectives and Trial Design

The primary trial objective was to compare the cost-effectiveness of elective stent implantation (primary stenting) with provisional bal-

TABLE 1. Baseline Clinical and Angiographic Characteristics

	First Randomization	
	Primary Stenting	Guided Balloon Angioplasty
n	97	523
Male sex	72	73
Age, y	60±10	59±11
Previous conditions		
Q-wave myocardial infarction	6	10
Non Q-wave myocardial infarction	18	17
Coronary artery bypass grafting	1	1
Angioplasty	9	11
Diabetes mellitus	10	10
Insulin-dependent	2	2
Hypertension	46	39
Hypercholesterolemia	48	53
Family history	43	38
History of stroke	2	2
Peripheral vascular disease	7	5
Smoking history		
Never smoked	35	36
Previous smoker	38	37
Current smoker	27	27
Stable angina	59	58
Canadian Cardiovascular Society classification		
1	5	5
2	32	31
3	19	20
4	3	2
Unstable angina	39	34
Braunwald classification[14]		
IB	8	12
IIB	24	17
IC	4	2
IIC	3	3
Silent ischemia	2	8
No. of diseased vessels		
1	91	90
2	9	8
3	0	2
Target vessel		
Right coronary	26	30
Left anterior descending	61	53
Left circumflex	13	18
Lesion type[27]		
A	12	18
B1	23	26
B2	59	51
C	6	6
DS,* %	70±12	70±11

Values are mean±SD or % of patients, unless otherwise indicated.
*Assessed by the investigator during the procedure.

TABLE 2. Angiography and CFR During the Procedure

	First Randomization			GBA: Second Randomization			
	PS	GBA	GBA Ballout	Stent: Optimal	Stent: Suboptimal	Balloon: Optimal	Balloon: Suboptimal
n	97	523	129	77	112	107	86
Initial DS, %	70±12	70±11	72±11	67±11	70±11	69±12	69±11
Initial CFR	...	1.6±0.6	1.6±0.6	1.7±0.6	1.5±0.6	1.7±0.6	1.4±0.4
DS before second randomization, %	...	...	...	22±8	22±9	23±8	24±11
CFR before second randomization	...	...	...	3.1±0.5	2.0±0.4	3.1±0.6	2.0±0.4
Lesion length, mm				9±4	9±4	9±3	9±4
Reference diameter, mm				2.78±0.42	2.73±0.44	2.71±0.47	2.62±0.45
Final DS, %	9±8	...	...	8±8	7±8	...	...
Stent length, mm				15±4	16±4	...	...
Balloon length, mm				...	...	20±2	20±4
Final CFR	...	...	...	3.3±0.7	2.4±0.7	...	...

Values are mean±SD. PS indicates primary stenting; GBA, guided balloon angioplasty.

Twelve patients were excluded from the study after the first randomization; 10 patients due to inconsistencies between randomization service and investigators, and 2 patients due to missing CFR values.

loon angioplasty guided by quantitative angiography and Doppler flow velocity measurements. The strategy after provisional angioplasty was to limit stent implantation to bailout situations and cases in which an "optimal result" (DS ≤35% and CFR >2.5)[13] was not achievable. The secondary objective was to evaluate the benefit differences from additional stenting in patients with and without an optimal result. Therefore, double randomization was required (Figure 1).

It would be incorrect to estimate the costs and benefits of provisional angioplasty using average costs and benefits combining (1) patients with bailout stents, (2) patients with optimal balloon angioplasty, and (3) patients with stenting after a suboptimal result. Patients left after bailout stenting would then receive too much weight, because the bailout decision was made before the second randomization, leading to 4 groups instead of the 2 created by the provisional angioplasty strategy. Therefore, a weighted average was used that weighted bailout stenting by the probability of bailout stenting and stenting in patients who did not require bailout stenting by the probabilities of belonging to either the optimal balloon angioplasty or suboptimal angioplasty groups. Thus, the provisional angioplasty group is a constructed or virtual group.

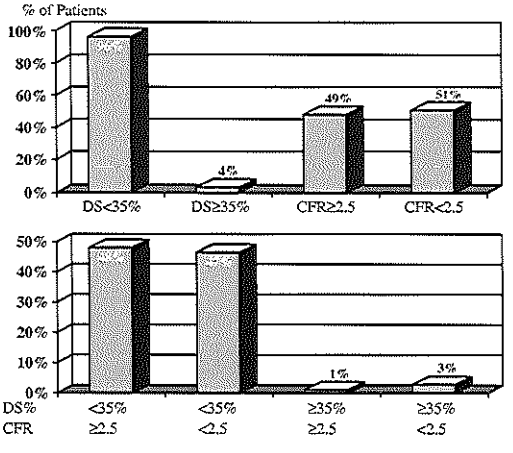

Figure 2. Relative role of DS and CFR in classifying patients in balloon angioplasty group (bailout patients not included).

Primary Stenting

A conventional guidewire was used in patients randomized to primary stenting, and predilatation was performed in all patients before stent implantation.

Guided Balloon Angioplasty

During guided balloon angioplasty, quantitative angiography and CFR measurements were made using standardized protocols[13,15] to achieve an optimal result (criteria defined earlier in article).

A 0.014-inch Doppler guidewire (Cardiometrics FloWire, EndoSonics) was advanced distal to the lesion, and velocity recordings were obtained under basal and hyperemic conditions. Maximal hyperemia was induced by adenosine, which was administered as an intracoronary bolus (right coronary artery, 12 μg; left coronary artery, 18 μg) or as an intravenous infusion (140 $\mu g \cdot kg^{-1} \cdot min^{-1}$).[16,17] These 2 methods were proven to be equivalent.

If an optimal result was not achieved, the operator was urged to perform iterative dilatations by upsizing the balloon, increasing the inflation pressure, or both. Bailout stenting was allowed in the presence of residual stenosis >50%; dissection types D, E, or F; persistent myocardial ischemia with dissection type C; reduction of TIMI flow[18] by ≥1 grade; or the existence of TIMI grades 0 or 1. The final DS and CFR were assessed after an optimal result was achieved or when the operator considered further improvement attempts unsafe. A second randomization was then performed that disregarded the measurements.

Efficacy End Points

The efficacy end point compiled major adverse cardiac events within 12 months of the procedure; these included death from any cause, nonfatal myocardial infarction, and percutaneous or surgical target lesion revascularization. Myocardial infarction was defined as the development of a new Q-wave or a rise of serum creatinine kinases with an abnormal plasma concentration of myocardial isoenzymes. Enzymes were sampled twice in the first 24 hours. Patients visited the outpatient clinic 1, 6, and 12 months after hospital discharge. At each visit, records were kept of anginal status, cardiac medication, 12-lead ECG, and complete physical examination. No follow-up angiogram was performed unless clinically indicated.

TABLE 3. Frequency of Primary Clinical End Points at 12 Months in Descending Order of Severity

	First Randomization			GBA: Second Randomization			
	PS	GBA	GBA Ballout	Stent: Optimal	Stent: Suboptimal	Balloon: Optimal	Balloon: Suboptimal
n	97	523	129	77	112	107	86
Death	2.1	1.3	0.8	2.6	0.9	0.9	2.3
MI	4.1	3.6	7.0	0.0	3.6	1.9	3.5
Q-wave	2.1	1.9	3.1	0.0	1.8	1.9	1.2
Non–Q-wave	2.1	1.7	3.9	0.0	1.8	0.0	2.3
CABG	0.0	1.1	2.3	0.0	0.9	0.9	0.0
TLPR	7.2	9.8	7.8	3.9	5.4	12.1	20.9
MACE-free	86.6	84.1	82.2	93.5	89.3	84.1	73.3
Any MACE	13.4	15.9	17.8	6.5	10.7	15.9	26.7

All values except n are percent. MI indicates myocardial infarction; CABG, coronary artery bypass grafting; TLPR, target lesion percutaneous revascularisation; MACE, major adverse clinical events; PS, primary stenting; and GBA, guided balloon angioplasty.

Twelve patients were excluded from the study after the first randomization: 10 patients due to inconsistencies between the randomization service and investigators, and 2 patients due to missing CFR values.

Costs

Cost analysis was limited to direct medical costs, which were calculated as resource utilization volume × unit costs in 1999 at the University Hospital Rotterdam-Dijkzigt, the Netherlands.[19] Resources included the materials used in the initial procedure (eg, stents, balloons, and Doppler wires); length of stay in the intensive care unit, coronary care unit, or general ward; major curative and diagnostic procedures; and rehospitalization within 12 months of the initial procedure. Although it could be expected that a guided strategy would lengthen procedures, we decided not to estimate the cost consequences of such an action. We hypothesized that the increased duration would not reduce the number of procedures possible per day; thus, the "fixed costs" would remain fixed. Also, the data may be biased by the time taken for a second randomization, thus breaking the continuity of procedures.

Cost Effectiveness

The balance between costs and benefits was addressed by calculating incremental cost-effectiveness ratios (ie, additional costs per additional event-free survivor after 1 year) and by estimating the probabilities that the provisional angioplasty was (1) more effective and more costly, (2) more effective and more costly, (3) less effective and cost saving, or (4) less effective and more costly.

Sample Size

Assumptions for sample size calculation were based on BENESTENT-1, BENESTENT-2 pilot, and DEBATE I experiences.[2,3,13] All additional benefits of stenting were attributed to patients with suboptimal results. With these assumptions, it was calculated that for the randomization scheme in Figure 1, 600 patients were needed to detect, with 80% power, a difference (α=0.05) of EUR 680 between provisional angioplasty and primary stenting in cost-effectiveness per survivor (no major adverse cardiac event) after 1 year.[20]

Statistical Analysis

Continuous variables are expressed as means±SD. Differences between patient groups were studied using Student's unpaired t test or 1-way ANOVA, whichever was appropriate. Categorical variables are presented as percentages, and differences between groups were evaluated using Fisher's exact test. Kaplan-Meier event-free survival curves were calculated, and differences between patient groups were compared by a log-rank test.

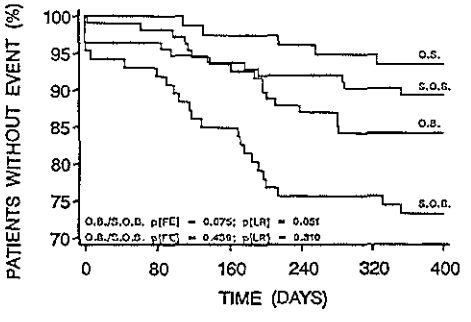

Figure 3. Event-free survival (Kaplan-Meier curves) at 12 months. Patients with suboptimal and optimal balloon angioplasty were randomized to additional stenting or no further treatment. OS indicates optimal stenting (n=77); SOS, suboptimal stenting (n=112); OB, optimal balloon angioplasty (n=107); SOB, suboptimal balloon angioplasty (n=86); FE, Fisher's exact test; and LR, log-rank test. For definitions of optimal and suboptimal, see text.

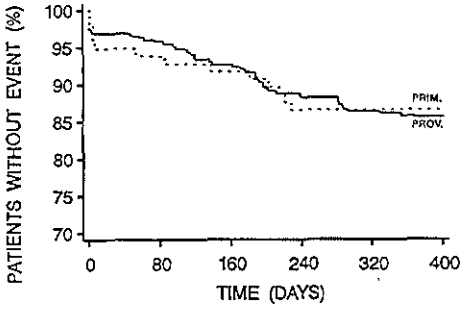

Figure 4. Event-free survival (Kaplan-Meier curves) at 12 months in patients who had primary stenting (PRIM; n=97) or provisional angioplasty (PROV; n=523).

TABLE 4. Costs and Event-Free Survival After 12 Months

	Unit Cost per Patient, €	PS	PA*	Optimal Stenting	Optimal Balloon	Suboptimal Stenting	Suboptimal Balloon	Bailout
No. of patients		97	523	77	107	112	86	129
Procedure and initial hospitalization								
Fixed procedure costs, €		1167	1167	1167	1167	1167	1167	1167
Resource use, Unit per patient								
Guiding catheter	82	1.20	1.20	1.19	1.24	1.21	1.14	1.13
Guidewire	95	1.03	0.55	0.40	0.42	0.56	0.44	0.70
FloWire	483	0.26	1.09	1.12	1.11	1.07	1.07	1.07
Balloon	368	1.52	1.55	1.52	1.27	1.67	1.31	1.78
Mounted stent	817	0.58	0.41	0.57	0.04	0.49	0.07	0.82
Nonmounted stent	454	0.56	0.37	0.49	0.04	0.60	0.05	0.49
Reoperation	1021	0.02	0.03	0.04	0.01	0.04	0.03	0.05
IVUS catheter	545	0.05	0.04	0.03	0.02	0.06	0.09	0.05
Contrast medium, mL	0	249	284	333	253	301	307	307
CCU days	856	0.58	0.62	0.53	0.49	0.58	0.84	0.86
ICU days	941	0.00	0.01	0.00	0.00	0.00	0.03	0.05
Non–CCU/ICU days	305	3.36	2.76	2.43	2.27	3.06	2.40	3.00
Follow-up, Unit per patient								
Second interventions	2800	0.16	0.16	0.12	0.19	0.15	0.22	0.15
CABG	8622	0.00	0.02	0.00	0.01	0.01	0.01	0.05
Recatheterization	1934	0.20	0.23	0.27	0.21	0.27	0.31	0.22
Vascular surgery	1157	0.00	0.01	0.00	0.00	0.00	0.00	0.02
CCU days	856	0.22	0.21	0.09	0.18	0.15	0.40	0.35
ICU days	941	0.00	0.03	0.00	0.03	0.02	0.01	0.05
Non–CCU/ICU days	305	1.38	2.62	0.82	2.55	2.72	2.11	2.56
Costs of initial hospitalization, €		4456	4486	4493	3606	4769	4084	5305
Costs of follow-up, €		1420	2055	1139	1927	1995	2352	2330
Total cost, €		5885	6573	5632	5533	6764	6519	7763
Event-free survival, %		86.6	85.6	93.5	84.1	89.3	73.3	82.2

CCU indicates coronary care unit; ICU, intensive care unit; CABG, coronary artery bypass grafting; PS, primary stenting; and PA, provisional angioplasty.
*Costs and effects of the provisional angioplasty group were assessed by calculating a weighted average.

Because the costs and benefits of provisional angioplasty were calculated as weighted averages, bootstrapping techniques were used to evaluate differences in the balance between costs and benefits after primary stenting and provisional angioplasty.[21,22] A total of 3000 bootstrap samples were drawn iteratively, with replacement when sample sizes equalled the total number of patients studied. Odds ratios and 95% confidence intervals are presented; a Breslow-Day test for homogeneity of odds ratios between subgroups and χ^2 tests were also applied.

Statistical tests were 2-tailed, with significance stated at the 0.05 level. Uncertainties surrounding cost, benefits, and cost-effectiveness were addressed by probability ellipses in the "cost-effectiveness plane."[21]

Results

Patient Characteristics

Baseline characteristics of the patients in this trial are presented in Table 1. There were no significant differences between patients allocated to primary stenting and to guided balloon angioplasty. Of the 523 patients randomized to guided balloon angioplasty, 129 (25%) underwent bailout stenting at the time of initial dilatation (n=103) or during the optimization process (n= 26). Of the remaining 394 patients, 382 underwent the second randomization. Twelve were not subrandomized for technical and logistical reasons.

Procedural Results

Table 2 summarizes the procedural results, and Figure 2 shows the relative roles of DS and CFR in classifying patients. Optimal results, with an average DS of 22±8% and a CFR of 3.1±0.6, were achieved in 35% of patients. In the suboptimal group, DS was 23±10% and CFR was 2.0±0.4. Additional stenting in patients with optimal balloon angioplasty resulted in a DS of 8±8% and a CFR of 3.3±0.7; in patients with suboptimal balloon angioplasty, additional stenting resulted in a DS of 7±8% but a CFR of 2.4±0.7.

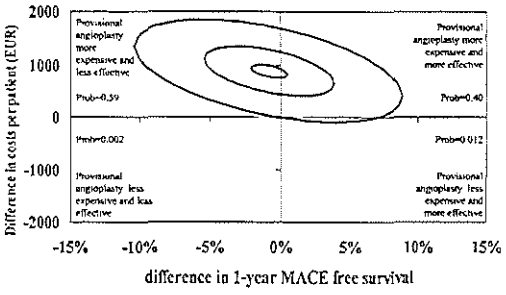

Figure 5. Incremental cost-effectiveness of provisional angioplasty vs primary stenting. Outer ellipse defines smallest area (95% probability) containing incremental costs and effectiveness of provisional angioplasty compared with primary stenting. Middle and inner ellipses define smallest areas (50% and 5% probabilities, respectively). Center of ellipse represents point estimate of incremental costs and effects. Prob indicates estimated probability that cost and effect are in respective quadrant; MACE, major adverse cardiac events.

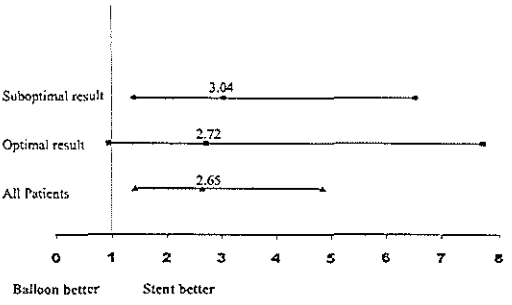

Figure 6. Relative risk ratios at 12 months for patients with suboptimal or optimal balloon angioplasty who survived event-free and were randomized to additional stenting or no further treatment. Bars indicate 95% confidence intervals.

Primary Stenting Versus Provisional Angioplasty

Table 3 shows the incidence of major adverse cardiac events in both the initial groups and the 4 subgroups, ranked in hierarchical order. In general, patients with optimal results experienced fewer major adverse cardiac events than patients with suboptimal results, and stented patients fared better than those undergoing balloon angioplasty alone (Figure 3).

Freedom from these events, which were calculated as weighted averages, was similar for patients undergoing primary stenting (86.6%) and provisional angioplasty (85.6%) (Figure 4). The weight for patients needing bailout stenting was 129/(129+107+112+86+77) or 25.2%; the weight for patients stented after a suboptimal result was 38.7% (calculated as the probability of not needing a bailout stent [100.0%–25.2%=74.8%] multiplied by the probability of a suboptimal result {[112+86]/[77+107+112+86]=51.8%}); and the weight for patients with a stent after an optimal result was 36.0% (calculated as the probability of not needing a bailout stent [74.8%] multiplied by the probability of an optimal result [100%–51.8%=48.2%]).

Table 4 presents cost estimates for the 2 initial groups and 4 subgroups. The cost of FloWire in the initial procedure was only partially covered by the lower stent use. Costs for the provisional angioplasty group during follow-up were higher due to longer hospitalizations and surgical revascularization. After 1 year, the costs of provisional angioplasty outweighed those of direct stenting by EUR 688. Figure 5 presents the estimates of costs, benefits, and cost effectiveness. The point estimate of the incremental cost-effectiveness ratio suggests that provisional angioplasty is less effective and more expensive.

Stenting Versus Balloon Angioplasty After the Second Randomization

The analysis of subrandomized patients in the balloon angioplasty group (Figure 6) indicates that stenting was associated with fewer major adverse cardiac events than balloon angioplasty alone in both patients with suboptimal (10.7% versus 26.7%; odds ratio, 3.0; $P=0.005$) and optimal results (6.5% versus 15.9%; odds ratio, 2.7; $P=0.066$). The Breslow-Day test for homogeneity of odds ratios was not significant ($P=0.865$). The higher cumulative costs of balloon angioplasty alone during the follow-up period almost matched the high initial costs of balloon angioplasty followed by stenting.

Discussion

The main result of this study was a lack of significant difference between clinical outcomes when comparing primary stenting and provisional balloon angioplasty. However, with the current unit costs of FloWire and stents, a strategy of provisional angioplasty is more costly than primary stenting.

Relevance and Critical Appraisal of Cost-Effectiveness Analysis

Cost considerations dominate many decisions about therapeutic interventions and are very relevant from a societal viewpoint. As emphasized in the literature, an independent person without commercial affiliations must analyze cost-effectiveness in such studies to avoid financial bias.[23] However, cost-effectiveness analyses are limited by multiple factors. First, cost data are transient and are affected by product acceptance, market dynamics, and reimbursement systems. Second, changing patterns of practice affect the selection of treatment devices, how they are used, and overall procedure time. Thus, the costs used here represent only a snapshot in time. For example, direct stenting without predilatation (an increasingly used technique) will undoubtedly affect cost-effectiveness in the future, but this method of treatment was not applied here.

Two crucial factors in the present study exerted a major influence on overall costs: the costs of FloWire and those of stenting. When the study was designed, its power calculation was based on market prices in 1996 and the cost estimates related to bleeding complications and the longer hospital stays associated with stenting. The reported cost estimates were based on unit costs in 1999 (costs of primary stenting versus provisional angioplasty, EUR 5916 versus EUR 6724;

$P=0.029$). However, an application of 1996 unit costs does not change the conclusion. The absence of expected differences is mainly because in the year 2000, stenting is no longer associated with bleeding complications and longer hospital stays, whereas the bailout rate with the balloon angioplasty group has increased from 15% to 25%.

Moreover, we did not take into account differences in procedure time. The time for guided angioplasty in the present study was 26 minutes longer (mean) than that of stenting, which further tipped the cost-effectiveness balance in favor of primary stenting.

The Additional Value of Stenting After Optimal Angioplasty: A Flow-Mediated Phenomenon?

An unexpected observation in this study was a further reduction in the rate of major adverse cardiac events in patients stented after optimal balloon angioplasty. This observation was made possible by the trial's double randomization design. On the basis of stent-like angioplasty results in other trials,[9,13,24] we had hypothesized no such additional benefits. However, the perceived benefits of additional stenting may have resulted from a selection process that ignored the outcome of patients with unsatisfactory or complicated balloon angioplasty (ie, bailout and suboptimal groups).

Although a similar DS was achieved in all patients stented after angioplasty (7%), a diminished CFR persisted after stenting in the suboptimal group (2.4) compared with the optimal group (3.3). Fewer major cardiac events were observed in the latter group (10.7% versus 6.5%). Further investigations are needed to fully understand the underlying mechanisms.

Clinical Relevance of the Findings of This Study

The present study failed to demonstrate a favorable economic profile for provisional angioplasty (guided by quantitative angiography and Doppler flow velocity measurements) compared with primary stenting. Indeed, although there was no significant difference in clinical effectiveness, the data pointed to higher costs with provisional angioplasty. Thus, the current data do not provide economic arguments to switch from primary stenting, even though clinical benefits result when stenting follows optimal balloon angioplasty. A limitation of our study was the inclusion of patients with only a single, relatively short lesion. However, it would seem from a literature survey that the patients studied represented possibly up to 70% of patients presently treated by percutaneous techniques worldwide.[25,26]

Appendix

Study Investigators, Their Location, and Number of Patients Treated

The Netherlands: P.W. Serruys, M.v.d. Brand, S.G. Carlier, P. de Feyter, D. Foley, W.v.d. Giessen, J. Hamburger (n=67); J.J. Piek, F.v.d. Wal (n=36); N.H.J. Pijls, J.P.M. van Asseldonk (n=20); V.A.W.M. Umans (n=13); G.J. Laarman, F. Kiemeneij (n=13); Belgium: B. de Bruyne, W. Wijns, G.R. Heyndrickx (n=60); C. Vrints (n=29); O. Gurné (n=24); C. Hanet, N. Debbas, D. Huyberechts (n=13); Brazil: J.E. Sousa, I. Pinto, L. Mattos, A. Chaves, A. Abizaid, A. Sousa (n=43); Japan: T. Muramatu (n=32); K. Kurogane (n=5); S. Mizuno (n=3); Austria: P. Probst, G. Porenta (n=28); Portugal: R. Seabra-Gomes, J. Baptista, J.L. Palos, F.P. Machado (n=28); United Kingdom: I.A. Simpson, K.D. Dawkins, H.H. Gray (n=28); P.M. Schofield (n=14); C. Ilsley, M. Mason, M. Bustami (n=13); K.G. Oldroyd (n=4); Greece: V. Voudris, J. Malakos, D.Y. Cokkinos (n=27); Argentina: J. Belardi, L. Guzmán, Rubén Piraino, F. Cura (n=17); France: J.-L.Guermonprez, F. Ledru (n=15); P. Dupouy (n=7); M. Bory (n=4); J. Puel (n=3); F. Tarragano (n=2); Italy: E. Verna (n=13); Germany: A.W. Frey, A. Grove, A. Henning, V. Bassignana (n=12); E. Fleck, E. Wellnhofer (n=11); R. Simon, M. Lins, P. Papechrysanthou (n=10); Israel: R. Beyar, M. Kapeliovich (n=10); M.S. Gotsman, M. Mosseri (n=4); Denmark: P. Thayssen (n=7); Czech Republic: P. Widimsky (n=5).

Acknowledgments

We are indebted to Cordis, a Johnson & Johnson company, Warren, NY, that provided the stents free of charge. This study was supported by EndoSonics, Rancho Cordova, Calif, which makes the Doppler guidewire used in the study.

References

1. Lehmann KG, Maas AC, van Domburg R, et al. Repeat interventions as a long-term treatment strategy in the management of progressive coronary artery disease. *J Am Coll Cardiol*. 1996;27:1398–1405.
2. Serruys PW, de Jaegere P, Kiemeneij F, et al. A comparison of balloon expandable stent implantation with balloon angioplasty in patients with coronary artery disease. *N Engl J Med*. 1994;331:489–495.
3. Serruys PW, van Hout B, Bonnier H, et al. Randomised comparison of implantation of heparin-coated stents with balloon angioplasty in selected patients with coronary artery disease (BENESTENT II). *Lancet*. 1998; 352:673–681.
4. Erbel R, Haude M, Hopp HW, et al. Coronary-artery stenting compared with balloon angioplasty for restenosis after initial balloon angioplasty: Restenosis Stent Study Group. *N Engl J Med*. 1998;339:1672–1678.
5. Simes PA, Golf S, Myreng Y, et al. Sustained benefit of stenting chronic coronary occlusion: long-term clinical follow-up of the Stenting in Chronic Coronary Occlusion (SICCO) study. *J Am Coll Cardiol*. 1998; 32:305–310.
6. Rubartelli P, Niccoli L, Verna E, et al. Stent implantation versus balloon angioplasty in chronic coronary occlusions: results from the GISSOC trial: Gruppo Italiano di Studio sullo Stent nelle Occlusioni Coronariche. *J Am Coll Cardiol*. 1998;32:90–96.
7. Mintz GS, Mehran R, Waksman R, et al. Treatment of in-stent restenosis. *Semin Interv Cardiol*. 1998;3:117–121.
8. Cohen DJ, Krumholz HM, Sukin CA, et al. In-hospital and 1-year economic outcomes after coronary stenting or balloon angioplasty: results from a randomized clinical trial: Stent Restenosis Study Investigators *Circulation*. 1995;92:2480–2487.
9. Foley DP, Serruys PW. Provisional stenting–stent-like balloon angioplasty: evidence to define the continuing role of balloon angioplasty for percutaneous coronary revascularization. *Semin Interv Cardiol*. 1996;1: 269–273.
10. Rodriguez A, Ayala F, Bernardi V, et al. Optimal coronary balloon angioplasty with provisional stenting versus primary stent (OCBAS): immediate and long-term follow-up results. *J Am Coll Cardiol*. 1998;32: 1351–1357.
11. Bech GJ, Pijls NH, De Bruyne B, et al. Usefulness of Fractional flow reserve to predict clinical outcome after balloon angioplasty. *Circulation*. 1999;99:883–888.
12. Haase KK, Athanasiadis A, Mahrholdt H, et al. Acute and 1-year follow-up results after vessel size adapted PTCA using intracoronary ultrasound. *Eur Heart J*. 1998;19:263–272.
13. Serruys P, Di Mario C, Piek J, et al. Prognostic value of intracoronary flow velocity and diameter stenosis in assessing the short- and long-term outcome of coronary balloon angioplasty: the DEBATE study. *Circulation*. 1997;96:3369-3377.
14. Braunwald E. Unstable angina: a classification. *Circulation*. 1989;80: 410–414.
15. Serruys P, Foley D, de Feyter P. *Quantitative Coronary Angiography in Clinical Practice*. Dordrecht, the Netherlands: Kluwer Academic Publishers; 1993.

16. Kern MJ, Deligonul U, Aguirre F, et al. Intravenous adenosine: continuous infusion and low dose bolus administration for determination of coronary vasodilator reserve in patients with and without coronary artery disease. *J Am Coll Cardiol*. 1991;18:718–729.
17. Wilson RF, Wyche K, Christensen BV, et al. Effects of adenosine on human coronary circulation. *Circulation*. 1990;82:1595–1606.
18. The Thrombolysis in Myocardial Infarction (TIMI) trial. Phase I findings: TIMI study group. *N Engl J Med*. 1985;312:932–936.
19. van Hout BA, Al MJ, Gordon GS, et al. Costs, effects, and C/E-ratios alongside a clinical trial. *Health Econ*. 1994;3:309–319.
20. Al MJ, van Hout BA, Michel BC, et al. Sample size calculation in economic evaluations. *Health Econ*. 1998;7:327–336.
21. Briggs A, Fenn P. Confidence intervals or surfaces? Uncertainty on the cost-effectiveness plane *Health Econ*. 1998;7:723–740.
22. Effron B. An introduction to the bootstrap. In: Tibshirani, ed. *Monograph on Statistics and Applied Probability*. New York: Chapman and Hall; 1993.
23. Kassirer JP, Angell M. The journal's policy on cost-effectiveness analyses. *N Engl J Med*. 1994;331:669–670.
24. Holmes DR Jr, Kip KE, Yeh W, et al. Long-term analysis of conventional coronary balloon angioplasty and an initial "stent-like" result: the NHLBI PTCA registry *J Am Coll Cardiol*. 1998;32:590–595.
25. Maier W, Enderlin MF, Bonzel T, et al. Audit and quality control in angioplasty in Europe: procedural results of the AQUA Study 1997: assessment of 250 randomly selected coronary interventions performed in 25 centres of five European countries: AQUA Study Group, Nucleus Clinical Issues, Working Group Coronary Circulation, of the European Society of Cardiology. *Eur Heart J*. 1999;20:1261–1270.
26. Kastrati A, Elezi S, Dirschinger J, et al. Influence of lesion length on restenosis after coronary stent placement. *Am J Cardiol*. 1999;83:1617–1622.
27. Ellis SG, Roubin GS, King SB, et al. Importance of stenosis morphology in the estimation of restenosis risk after elective percutaneous transluminal coronary angioplasty. *Am J Cardiol*. 1989;63:30–34.

Editorial

Provisional Versus Routine Stenting

Routine Stenting Is Here To Stay

H. Vernon Anderson, MD; Blase A. Carabello, MD

The introduction of coronary artery stents into widespread clinical use in the mid-1990s was a significant advance that almost rivals the introduction of balloon angioplasty itself 15 years earlier. It is noteworthy that the success of stents required several paradigm shifts. For example, higher-pressure balloon inflations and slight oversizing were needed to achieve full stent expansion (anathema in balloon angioplasty), and antiplatelet therapies were required rather than anticoagulation, including a reduction and now almost elimination of heparin. Yet, these changes were quickly accomplished. Technical advances in equipment also occurred, and now stenting, quite literally, has become the standard in clinical practice when it can be performed (which is most of the time).

See p 2930, 2938, and 2945

One curious and intriguing question that arises with any new device, and stents are no exception, is whether they are needed in all situations where they are being used. Is it possible that balloon angioplasty alone might be sufficient for excellent immediate and long-term benefit, provided the final procedural result is good enough? If one could determine this to be true, then such a strategy would avoid the additional cost of a stent and the problem (or pseudo-problem) of in-stent restenosis. However, a provisional stent strategy raises the further and not inconsiderable question of how to decide when balloon angioplasty results are "good enough." The limitations of standard angiography notwithstanding, is there anything better than the eyes and minds of experienced angiographers? Additional "objective" measures to assess procedural results have long been sought. A number of investigators have championed intracoronary ultrasound as one approach, whereas others suggest alternative methods.

In this issue of *Circulation*, 2 separate groups report their findings using combined anatomic and functional coronary measures to assess balloon angioplasty results for the purpose of provisional stenting.[1,2] These measures are on-line quantitative coronary arteriography (QCA) and coronary flow reserve (CFR) measured with a Doppler wire. In addition, as a worthy companion to these 2 reports on provisional stenting, this issue also contains a report from a large-scale clinical registry, the National Heart, Lung, and Blood Institute (NHLBI) Registry,[3] detailing the substantial improvements in the outcomes of coronary interventions in the years 1985/1986 through 1997/1998, during which time coronary stents were introduced. We offer some analysis, interpretation, and opinions on these reports.

The NHLBI Dynamic Registry

First established in 1979 at the dawn of coronary angioplasty, the NHLBI Registry has been a continuing source of valuable information through the years. The data reported by Williams et al[3] compare the in-hospital and 1-year outcomes in patients treated in 1997/1998, which include those treated with stents, with the outcomes of patients treated in 1985/1986, before stents were used. Let us begin with the in-hospital outcomes. The Registry report documents dramatic reductions in the frequencies of adverse events occurring during index hospitalization for coronary intervention. The frequency of the combined triple end point of death, myocardial infarction, or coronary bypass surgery (CABG) fell from 9.8% in 1985/1986 to 5.9% in 1997/1998. This decline was due entirely to reductions in myocardial infarction (from 4.9% to 2.8%) and especially CABG (from 6% to 1.5%), because in-hospital mortality was unchanged (1.4% versus 1.9%). The frequency of stent usage in the 1997/1998 Dynamic Registry was 70%; no stents were used in 1985/1986.

These findings are consistent with other recent, large-scale reports and deserve brief elaboration here. Using Medicare data from 1994 and 1996, Ritchie et al[4] found in patients without acute myocardial infarction that the frequency of same-admission CABG was cut in half after the introduction of coronary stents. In patients with acute myocardial infarction, the difference was even greater. Similarly, Hannan et al,[5] using the New York State Coronary Angioplasty Registry, found that stents reduced the frequency of same-admission CABG at hospitals in New York by more than one-third but did not change in-hospital mortality.

If the data from these 3 large reports,[3-5] representing 293 000 patients, are combined, the introduction of stents reduced the already low CABG rates of the mid-1990s by 50% (from 2.55% to 1.26%) and the in-hospital mortality rates by 15% (from 1.28% to 1.08%). These are impressive numbers. Practicing interventionalists and clinicians have many anecdotes that reinforce these statistics. Clearly, the widespread use of stents has favorably influenced early outcomes. The mechanisms for this benefit relate to the stent's ability to prevent or treat threatening dissections and abrupt closures. These are the most common causes of failed balloon angioplasty leading to urgent bypass operations and

The opinions expressed in this editorial are not necessarily those of the editors or of the American Heart Association.

From the University of Texas Health Science Center–Houston (H.V.A.) and Baylor College of Medicine and the Veterans Administration Medical Center (B.A.C.), Houston, Tex.

Correspondence to H. Vernon Anderson, MD, Cardiology Division, University of Texas Health Science Center–Houston, 6431 Fannin, Suite 1246, Houston, TX 77030. E-mail h.v.anderson@uth.tmc.edu

(*Circulation*. 2000;102:2910-2914.)

Circulation is available at http://www.circulationaha.org

TABLE 1. Routine and Provisional Stenting in 4 Trials

	Routine Stenting				Provisional Stenting			
	FROST	DESTINI	DEBATE-II	OPUS-1	FROST	DESTINI	DEBATE-II	OPUS-1
No. of patients	125	370	97	230	126	365	523	249
Women, %	17	25	28	25	19	27	27	28
Diabetics, %	18	18	10	18	13	19	10	18
Unstable angina, %	67	46	39	72	62	52	34	69
LAD lesion, %	56	41	61	32	43	38	53	33
Type C lesion, %	66*	56†	65†	...	68*	60†	57†	...
Lesion length, mm, mean	9.7	12.7	9	10	10.0	12.7	...	10
Reference diameter, mm, mean	3.07	3.09	2.6–2.8	3.32	3.09	3.03	...	3.34
Final MLD, mm, mean	2.64	2.92	...	...	2.50	2.29/2.87‡	...	...
Final stenosis, %, mean	13.8	9.3	9	1	18.8	24.8/10.2‡	...	9
End points								
Interval, mo	6	12	12	6	6	12	12	6
Event (frequency)	Angiographic restenosis (21.4%)	TLR (14.9%)	TLR (7.2%)#	TLR (5.2%)#	Angiographic restenosis (27.1%)	TLR (15.6%)	TLR (10.9%)#	TLR (14.9%)#
	...	MACE (17.8%)	MACE (13.4%)	MACE (6.1%)	...	MACE (18.9%)	MACE (15.9%)	MACE (14.9%)

LAD indicates left anterior descending coronary artery; MLD, minimum lumen diameter.
*B or C.
†B2 or C.
‡Values for nonstented group/stented group.
#Percutaneous coronary intervention and CABG.

deaths. In addition to these immediate benefits, the initial reports of 6-month and 1-year outcomes with coronary stents were favorable, and these also contributed to the eagerness of stent adoption. However, keen observers during these years noted that when balloon angioplasty results were good ("stent-like"), then both short- and long-term outcomes were favorable. Provisionalists used this to urge a cautious approach to stenting: if balloon angioplasty results were good enough, then stop; if they were not good enough, then stent.

Provisional Stenting

DiMario et al,[1] for the Doppler End Point Stenting International Investigation (DESTINI) study group, report no benefit at 1 year with a provisional compared with a routine stenting approach. Serruys et al,[2] for the second Doppler End Points Balloon Angioplasty Trial Europe (DEBATE-II) investigators, report that provisional stenting has less favorable 1-year outcomes and is more expensive than routine stenting. These 2 new reports closely parallel another recent report on provisional stenting by LaFont et al[6] for the French Randomized Optimal Stenting Trial (FROST) study group. Taken together, these 3 studies constitute a uniform approach to provisional stenting: they use similar technologies (on-line QCA and Doppler CFR) and nearly identical definitions. In FROST, optimal balloon angioplasty that would not require a stent was defined as a final diameter stenosis <35% by QCA and a CFR >2.2. In DESTINI, the definition of an optimal result was a final diameter stenosis <35% and a CFR >2.0, and in DEBATE-II, it was a final diameter stenosis <35% and a CFR >2.5. Table 1 lists some of the important clinical features of patients enrolled in these 3 provisional stenting studies and the reported outcomes. For additional comparison, we also included data from another recent provisional stenting trial, the Optimum Percutaneous Transluminal Coronary Angioplasty Compared With Routine Stent Strategy Trial (OPUS-1).[7]

In FROST, the study end point was angiographic restenosis at 6 months. This occurred in 21.4% of the routinely stented group and in 27.1% of the provisionally stented group (P=0.37). Importantly, 48.4% (61 of 126) of the provisional patients required stents. In DESTINI and DEBATE-II, the end points were 12-month clinical outcomes, as determined by a combination of major adverse cardiovascular events (MACE). Target lesion revascularization (TLR) was also important. Overall in both DESTINI and DEBATE-II, the frequencies of TLR ranged from 7% to 16%, and the frequencies of MACE ranged from 13% to 19%. In OPUS-1, clinical outcomes were obtained at a shorter, 6-month follow-up, and both TLR and MACE were significantly less frequent in the routine stent group compared with the provisional stent group (5.2% versus 14.9% for TLR and 6.1% versus 14.9% for MACE; both P<0.01). The clinical event rates, as expected, are somewhat lower than the angiographic restenosis rates found in FROST. Of interest, all event rates in the 4 studies are uniformly lower in the routine compared with the provisional stent groups. Furthermore, a quick calculation reveals that the primary end points of either angiographic restenosis or MACE occurred in 14.5% (118 of 813) of routinely stented patients in these 4 studies and was more frequent (17.6%; 221 of 1254) in provisionally stented patients (2-sided P=0.062).

TABLE 2. Use of Stents in Provisional Arms of 3 Trials

Trial	Lesions Randomized to Provisional Arm, n	Lesions Receiving Stents, n	Criteria Justifying Provisional Stent, % of Stents Received			
			Bailout	Diameter Stenosis	Doppler CFR	Both Diameter and Doppler
FROST	126	61	28	18	33	21
DESTINI	384	218	11	10	35	44
DEBATE-II	511	241*	25	4.5	51†	52†
Total	1021	520				

*Includes only stents deployed for bailout purposes or suboptimal results.
†Not mutually exclusive.

The small differences in angiographic and clinical outcomes between these 4 studies might easily be explained both by the slightly different criteria for success (in terms of CFR, where it was used) and the slightly different clinical characteristics of the patients. Overall, there is a sense of harmony in almost all respects in these 4 studies. The randomized lesions were short (≈9 to 12 mm) and were located in medium-to-large arteries (≈2.6 to 3.3 mm). The left anterior descending coronary artery may have been somewhat underrepresented in the provisionally stented groups. The OPUS-1 and DEBATE-II trials are the only 2 with economic analyses, and both conclude that a provisional stenting strategy is more expensive than routine stenting.

Frequency of Stenting in Provisional Arms

The important point about these provisional stent trials is this: stenting was exceedingly common, even in these large and sophisticated centers seeking to avoid it. Table 2 lists the frequency of stent deployment in the provisional arms of FROST, DESTINI, and DEBATE-II, which used similar methodologies for decision-making. Overall, stents were needed for 520 of 1021 lesions (51%), which is more than half of the provisional lesions treated. In OPUS-1, stents were used in 37% of the 249 lesions randomly assigned to a provisional strategy. The proportions of stents deployed according to the specific provisional criteria are also listed in Table 2. Often (11% to 28% of lesions), a stent was used for a "bailout" condition, which was defined as either threatening dissection or abrupt closure. Furthermore, it is apparent that a failure to meet angiographic diameter stenosis criteria alone was not that frequent (only ≈5% to 18% of lesions stented); CFR criteria accounted for most of the provisionally stented lesions. In other words, in these situations, the operators were happy with the angiographic results and no threatening dissections were seen, but the CFR criteria were less than desired. *The physiological and clinical meaning of this is presently unknown.*

An evaluation of the immediate results of balloon angioplasty and stenting by anything other than standard angiography (meaning the eyes and minds of experienced operators) is not yet fully understood and accepted. The only technique that comes close is intravascular ultrasound, and its role has mainly been to confirm full stent expansion. Only recently have studies comparing various methodologies, including on-line QCA, fractional flow reserve using a pressure wire, intravascular ultrasound, and CFR using a Doppler wire, begun to appear.[8–13] Very importantly, these technologies are not widely available, and there is as yet little agreement, even among the cognoscenti (like us) who use them occasionally. The desire to avoid stenting even an acceptable balloon angioplasty result on the basis of its having a good CFR result seems unwarranted at this time. Whether or not a stent can actually be placed technically is another matter.

Optimal and Suboptimal Results

The DEBATE-II investigators included a second randomization in their trial; it yielded some new insights on the meaning of good results and raised new questions. After excluding the 129 patients that required stents for bailout situations, they were left with 382 patients that either met the criteria for optimal balloon angioplasty or had suboptimal results but no threatening dissections or closures. These 382 patients were then randomly assigned either to required stenting or to no further treatments. This created 4 subgroups, 2 of which are very interesting: a group with "optimal" balloon angioplasty that was stented anyway and a group with "suboptimal" balloon angioplasty (but no threatening dissections) that received no further treatment. This last group would have received a mandated stent in the FROST or DESTINI trials.

Table 3 lists the clinical outcomes of these 2 interesting groups from DEBATE-II along with the outcomes of the bailout stent group from DEBATE-II and parallel groups from DESTINI. For the patients in DESTINI and DEBATE-II with optimal balloon angioplasty and no stents (ie, acceptable results with balloon angioplasty alone), the rates of TLR (17.6% and 13%, respectively) and MACE (20.1% and 15.9%, respectively) were similarly good. However, for the 77 patients in DEBATE-II with optimal balloon angioplasty that were stented anyway (achieving a final mean diameter stenosis of 8%), the rates were significantly better: only 3.9% underwent TLR and only 6.5% experienced MACE. Unacceptable results with balloon angioplasty alone are also revealing. In DESTINI, the provisional stent arm had a TLR rate of 14.1% and a MACE rate of 18.0%. The equivalent groups in DEBATE-II would be the suboptimal balloon angioplasty group that was stented and the bailout group. Interestingly, both had TLR and MACE rates lower than the rates in DESTINI. Finally, there were 86 patients in DEBATE-II with suboptimal results after balloon angioplasty (again, mostly on the basis of CFR criteria, because the final diameter stenosis was no different from that of the optimal balloon angioplasty group). These patients received no fur-

TABLE 3. Treatment of Patients With Optimal and Suboptimal Results and 1-Year Outcomes

	Acceptable Results With BA			Unacceptable Results With BA			
	DESTINI, Optimal BA	DEBATE-II, Optimal BA and No Stent	DEBATE-II, Optimal BA With Stent	DEBATE-II, Suboptimal BA With Stent	DESTINI, Provisional Stent	DEBATE-II, Ballout Stent	DEBATE-II, Suboptimal BA and No Stent
No. of patients	159	107	77	112	206	129	86
Final DS, %, mean	24.8	23	8	7	10.2	...	24
TLR, %	17.6	13.0	3.9	6.3	14.1	10.1	20.9
MACE, %	20.1	15.9	6.5	10.7	18.0	17.8	26.7

BA indicates balloon angioplasty; DS, diameter stenosis.

ther treatments, and they had the highest event rates of all: 20.9% required TLR and 26.7% experienced MACE.

Re-examining these numbers leads to the conclusion that stenting after optimal balloon angioplasty is best (MACE rate of 6.5%), optimal balloon angioplasty without a stent or suboptimal balloon angioplasty with a stent is next best (MACE rate of 11% to 20%), and suboptimal balloon angioplasty with no stent is the worst (MACE rate of 27%). This clearly means that when a stent cannot be used (for whatever reason), achieving an optimal balloon angioplasty result is the next best thing. We all know and accept this. But why should stenting a patient who has an optimal balloon angioplasty result produce a more favorable long-term outcome than leaving well enough alone? The answer to this goes right to the core of whatever it is that stents do, whether that means mechanically supporting small and invisible dissections, preventing late elastic recoil, or somehow altering the biological course of restenosis. Using a stent to obtain a large, smooth (some would say "cosmetically pleasing") lumen visualized by standard angiography to the satisfaction of the operator seems to provide the best results yet achieved.

Long-Term Outcomes

A final perspective on the long-term benefits of stenting in the real world comes from a reconsideration of the NHLBI Dynamic Registry that we started with, along with the previously mentioned New York State Registry[5] and a recent study from the British Columbia Cardiac Registries in Canada.[14] Table 4 lists the odds ratios for the long-term benefits of stenting compared with balloon angioplasty for each of these 3 reports. Both the Canadian and New York State Registries noted significant long-term benefits with stenting. In the Dynamic Registry, the 1-year outcomes of the 1997/1998 collection (stent era) were significantly better than those in the 1985/1986 collection. Admittedly, these are retrospective data. However, the studies are methodologically sound, and the results are consistent. The routine use of coronary stents is associated with improved clinical outcomes at 1 to 2 years compared with performing conventional balloon angioplasty.

TABLE 4. Long-Term Outcomes of Stenting and Balloon Angioplasty in 3 Studies

	Canadian Registry	New York State Registry	NHLBI Dynamic Registry
No. of patients	9594	19 792	3990
Follow-up interval	1 year	2 years	1 year
Odds ratio for			
Death	1.14	0.78	0.9
TLR	0.72	0.65	0.6
Favors	Stent	Stent	Stent era

Limits of Technology

The reasons why provisional stenting has not become common, and likely never will, are 4-fold. First, the proven results of routine stenting are excellent. Second, a large number (≈50%) of the lesions where stents might wish to be avoided under a provisional strategy must be stented anyway. Third, the technology required to undertake provisional stenting is uncommon, and its applicability is unclear. This does not mean that intravascular ultrasound, QCA, and Doppler are not useful. They clearly can be valuable on an individualized basis. However, for the purpose of deciding whether to stent, at the present time and for the foreseeable future, they have not yet been proven to add anything of value to the eyes of experienced angiographers. Finally, 2 current studies indicate that routine stenting is less costly than provisional stenting. The increased procedure time required to use the additional technology and the greater numbers of repeat procedures in the provisional strategy probably account for this. Given the dramatic reductions in adverse clinical events that stents have brought about, the indications that long-term stent results are more favorable than balloon angioplasty, the high percentage of provisional strategy patients that ultimately receive stents, and the reportedly favorable economics of routine compared with provisional stenting, it is fair to say that routine stenting wins.

References

1. DiMario C, Moses JW, Anderson TJ, et al. Randomized comparison of elective stent implantation and coronary balloon angioplasty guided by online quantitative angiography and intracoronary doppler. *Circulation*. 2000;102:2930–2937.
2. Serruys PW, de Bruyne B, Carlier S, et al. Randomized comparison of primary stenting and provisional balloon angioplasty guided by flow velocity measurement. *Circulation*. 2000;102:2938–2944.
3. Williams DO, Holubkov R, Yeh W, et al. Percutaneous coronary intervention in the current era compared with 1985–1986: the National Heart, Lung, and Blood Institute registries. *Circulation*. 2000;102:2945–2951.
4. Ritchie JL, Maynard C, Every NR, et al. Coronary artery stent outcomes in a Medicare population: less emergency bypass surgery and lower mortality rates in patients with stents. *Am Heart J*. 1999;138:437–440.

5. Hannan EL, Racz MJ, Arani DT, et al. A comparison of short- and long-term outcomes for balloon angioplasty and coronary artery stent placement. *J Am Coll Cardiol*. 2000;36:395–403.
6. LaFont A, Dubois-Rande JL, Steg PG, et al. The French randomized optimal stenting trial: a prospective evaluation of provisional stenting guided by coronary velocity reserve and quantitative coronary angiography. *J Am Coll Cardiol*. 2000;36:404–409.
7. Weaver WD, Reisman MA, Griffin JJ, et al. Optimum percutaneous transluminal coronary angioplasty compared with routine stent strategy trial (OPUS-1): a randomised trial. *Lancet*. 2000;355:2199–2203.
8. Kern MJ, Dupuoy P, Drury JH, et al. Role of coronary artery lumen enlargement in improving coronary blood flow after balloon angioplasty and stenting: a combined intravascular ultrasound doppler flow and imaging study. *J Am Coll Cardiol*. 1997;29:1520–1527.
9. Serruys PW, di Mario C, Piek J, et al. Prognostic value of intracoronary flow velocity and diameter stenosis in assessing the short- and long-term outcomes of coronary balloon angioplasty. *Circulation*. 1997;96: 3369–3377.
10. Abizaid A, Mintz GS, Pichard AD, et al. Clinical, intravascular ultrasound, and quantitative angiographic determinants of the coronary flow reserve before and after percutaneous transluminal coronary angioplasty. *Am J Cardiol*. 1998;82:423–428.
11. van Liebergen RAM, Piek JJ, Koch KT, et al. Immediate and long-term effect of balloon angioplasty or stent implantation on the absolute and relative coronary blood flow velocity reserve. *Circulation*. 1998;98: 2133–2140.
12. Hanekamp CEE, Koolen JJ, Piljs NHJ, et al. Comparison of quantitative coronary angiography, intravascular ultrasound, and coronary pressure measurement to assess optimum stent deployment. *Circulation*. 1999;99: 1015–1021.
13. Kern MJ, Puri S, Bach RG, et al. Abnormal coronary flow velocity reserve after coronary artery stenting in patients: role of relative coronary reserve to assess potential mechanisms. *Circulation*. 1999;100: 2491–2498.
14. Rankin JM, Spinelli JJ, Carere RG, et al. Improved clinical outcome after widespread use of coronary-artery stenting in Canada. *N Engl J Med*. 1999;341:1957–1965.

KEY WORDS: Editorials ■ stents ■ angioplasty

Chapter 5

In vitro study of FFR, QCA and IVUS for the assessment of optimal stent deployment.

K Matthys, **SG Carlier**, P Segers, J Ligthart, G Sianos, P Serrano, P Verdonck, PW Serruys.

Catheterization and Cardiovascular Interventions 2001; (in press).

Editorial comment not yet available.

In Vitro Study of FFR, QCA, and IVUS for the Assessment of Optimal Stent Deployment

K. Matthys, MSc,[1]* S. Carlier, MD,[2] P. Segers, MSc, PhD,[1] J. Ligthart, BSc,[2] G. Sianos, MD,[2] P. Serrano, MD,[2] P. Verdonck, MSc, PhD,[1] and P.W. Serruys, MD, PhD[2]

We tested whether fractional flow reserve (FFR) discriminates between suboptimally and optimally deployed stents. Latex tubes (4 mm in diameter) with stenosis 40% (n=3), 50% (n = 3) and 60% (n = 3) were tested in a pulsatile flow system, using water. Measurements were done at baseline (n = 9; FFR/QCA) and after suboptimal (SOD; 3-mm balloon at 8 atm) and optimal (OD; 4 mm balloon at 16 atm) deployment of a 35-mm stent (n = 6; FFR/QCA/IVUS). Varying Q from 150 to 50 ml/min increased FFR by 2–7%. Conversely, at 100 ml/min, FFR increased by only 0.8% from SOD to OD ($P < 0.05$). Extrapolating data to blood flow, the gain in FFR from SOD to OD is less than 5% for Q = 100 ml/min, while FFR may increase by 15–20% by changes in blood flow from 50 to 150 ml/min. We conclude that IVUS and QCA are more appropriate for the assessment of optimal stent deployment. *Cathet Cardiovasc Intervent 2001;54:000–000.*

Key words: flow reserve; intravascular ultrasound; angiography; suboptimal stent deployment

INTRODUCTION

Fractional flow reserve (FFR) is defined as the ratio of myocardial flow in a stenosed coronary segment during hyperemia (Q) to hyperemic flow through the same segment in the hypothetical case that there is no stenosis present (Q^N) [1,2]. Pijls et al. [3] and De Bruyne et al. [4] have shown that FFR can be obtained from pressure measurements proximal and distal to the stenosis only and that it assesses the physiologic significance of a coronary stenosis [5]. The pressure-based FFR is easily measured during transluminal interventions and normal and cutoff values have unequivocally been determined [6,7].

The availability of ultrathin pressure wires, permitting accurate pre- and poststenotic pressure measurements, has increased the use of FFR in clinical practice. Nevertheless, FFR has some important limitations, as FFR is determined by the pressure drop over the lesion. First, this pressure drop is function of flow. FFR is thus by definition sensitive to the flow level in the coronary artery. Myocardial infarction may have a large impact on maximally recruitable flow during hyperemia and, consequently, on the calculated values of FFR. Second, FFR has been proposed as a valuable tool to assess optimal stent deployment during intervention [8]. This implies that the difference in pressure drop over a sub- and optimally deployed stent is large enough to allow discrimination between both situations.

In this study, we use an in vitro setup to address both raised concerns regarding FFR, (1) testing the flow dependency of FFR, and (2) investigating whether FFR is able to discriminate between suboptimally and optimally deployed stents.

METHODS

Concept of FFR

The simplified model of the coronary circulation as proposed by Pijls and De Bruyne and their coworkers consists of a resistance representing the stenosis (R_s) placed in series with the myocardial resistance R (Fig. 1, top). Pressure drops along these resistances are defined as:

$$\Delta P_{\text{stenosis}} = P_a - P_d$$

[1]Institute Biomedical Technology IBITECH, Hydraulics Laboratory, Ghent University, Belgium.
[2]Thorax Centre, Rotterdam, The Netherlands.

Grant sponsor: Institute for the Promotion of Innovation by Science and Technology (Flanders); Grant number: IWT-991175; Grant sponsor: Special Research Fund of Ghent University;

*Correspondence to: Koen Matthys, Institute Biomedical Technology IBITECH, Hydraulics Laboratory, Ghent University, Sint-Pietersnieuwstraat 41, B-9000 Ghent, Belgium.
E-mail: koen.matthys@rug.ac.be

Received 18 September 2001; Revision accepted 17 May 2001

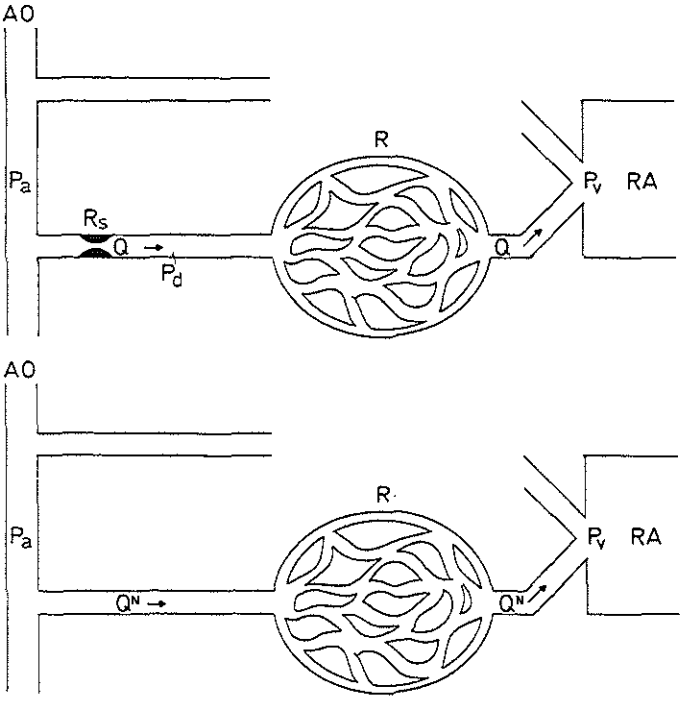

Fig. 1. Simplified model of the coronary circulation as proposed by Pijls and De Bruyne, consisting of a resistance representing the stenosis (R_s) in series with the myocardial resistance (R). AO: aorta; P_a: aortic pressure; P_d: pressure distal to the stenosis; P_v: venous pressure; Q: flow (Q^N = Q when R_s = 0); RA: right atrium. (Modified from Pijls and De Bruyne [6].)

$$\Delta P_{\text{myocard}} = P_d - P_v$$

where P_a stands for mean aortic pressure, P_d for mean distal coronary pressure, and P_v for mean central venous pressure. P_a, P_d, and P_v need to be measured during maximal coronary hyperemia when myocardial resistance is minimal and assumed to be constant [6]. This condition is imperative for the calculation of flow in the model of Pijls–De Bruyne, as, in the case of constant myocardial resistance, flow is directly proportional to the pressure drop causing the flow movement. Maximal myocardial flow (Q) can then be written as:

$$Q = \frac{\Delta P_{\text{myocardium}}}{R} = \frac{P_d - P_v}{R}$$

In the absence of a stenosis, P_d would approximate P_a (Fig. 1, bottom). In this hypothetical case, flow (Q^N) is given as

$$Q^N = \frac{P_a - P_v}{R}$$

and FFR can be expressed as

$$\text{FFR} = \frac{Q}{Q^N} = \frac{(P_d - P_v) \cdot R}{R \cdot (P_a - P_v)} = \frac{(P_d - P_v)}{(P_a - P_v)} \approx \frac{P_d}{P_a}$$

In Vitro Setup

The experimental setup comprises a cardiovascular simulator to generate physiologic aortic pressures in a closed hydraulic circuit, using water as the test fluid. Water viscosity is roughly three times lower than blood viscosity. In order to fulfil the requirements of fluid-dynamic similarity between the experimental model (water) and the real (blood) flow in the coronary circulation, experiments are performed at low water flows (range: 50–200 ml/min), corresponding to blood flows of 150–600 ml/min, largely covering the normal physiological range of hyperemic coronary blood flow. The conversion is further addressed in detail in the discussion and in the Appendix. Stenosed Latex tubes, representing diseased epicardial coronary segments with different degree of stenosis severity, were inserted in this circuit. We tested nine Latex tubes (∅ = 4 mm) with stenosis length of 15 mm and a target diameter stenosis (DS) of 40% (n = 3), 50% (n = 3), and 60% (n = 3).

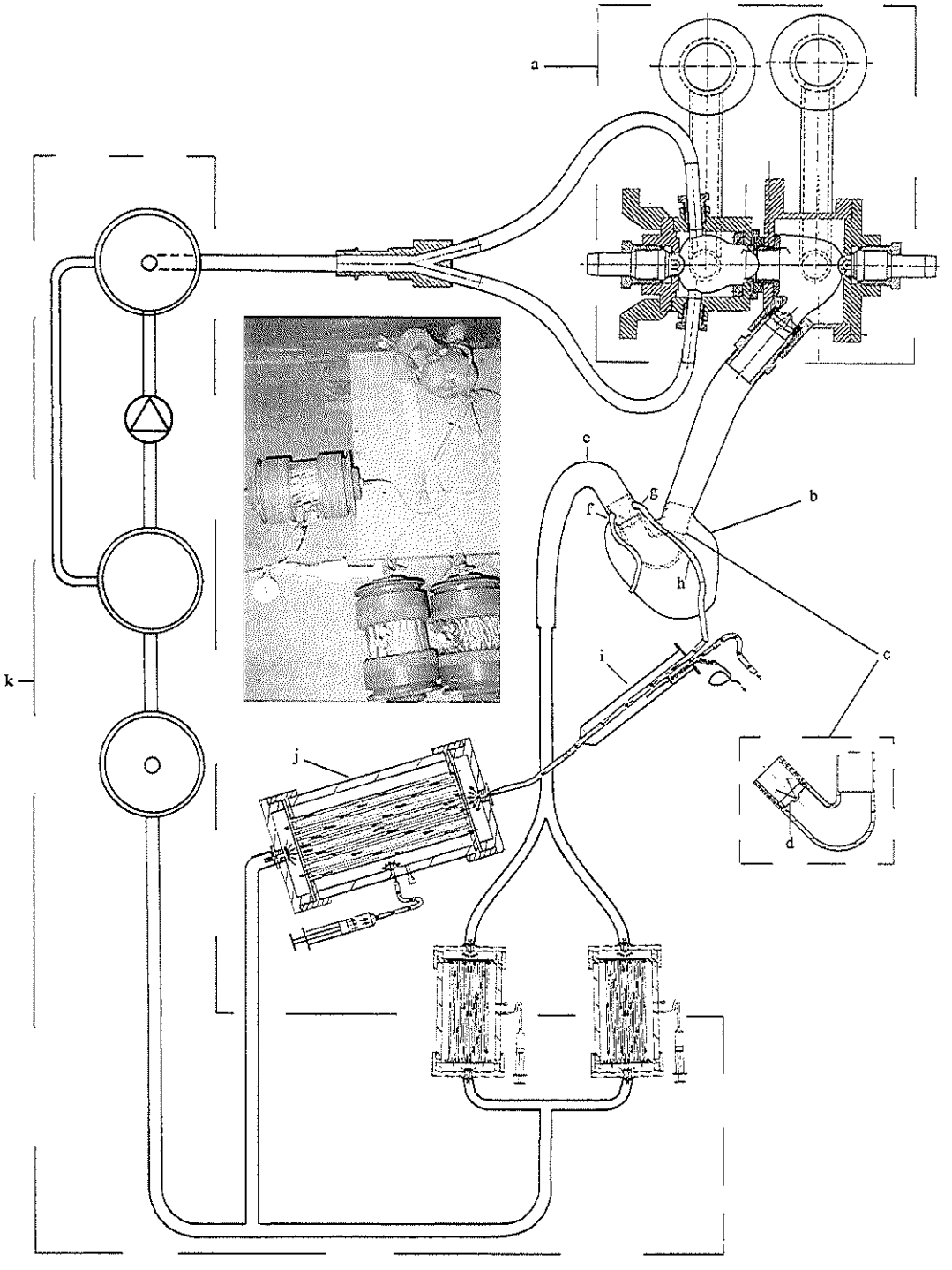

Fig. 2. Schematic drawing of the in vitro setup. Top right: the cardiovascular simulator generating physiologic aortic pressures. Middle: coronary artery phantom (h) mounted on a 3D shape of a human heart (b), together with active (i) and passive (j) resistance models. Left: afterload circuit (k).

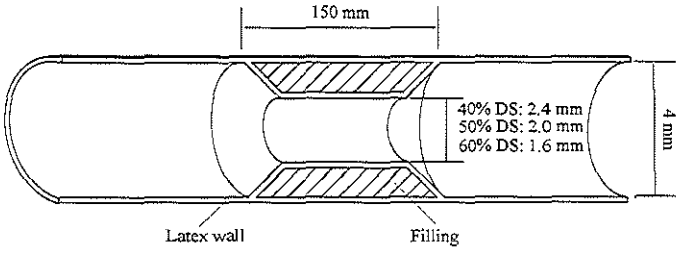

Fig. 3. Drawing of the coronary artery phantom. A plastic substance is introduced at the site of the narrowing (filling). The elastic Latex compound is used solely for the healthy part of the coronary segment. Depending on the degree of diameter stenosis (40%, 50%, and 60% DS, respectively), different inner diameters (2.4, 2.0, 1.6 mm, respectively) had to be accounted for.

The cardiovascular simulator. The cardiovascular simulator was described in earlier work [9–11] and is not discussed in detail. Figure 2 shows a schematic drawing of the setup of the heart (a) and coronaries. To simulate the tortuous pattern of the coronary tree in an anatomically correct way, the Latex coronary artery phantoms were mounted on a three-dimensional (3D) shape of a human heart, a thin-walled Latex "epicardial surface" (b). We connected the aortic outlet of the original simulated heart, to the inlet of this Latex epicardium. The normal flow path of blood within the heart was bypassed by a V-shaped PVC-tube (c). To have coronary inflow immediately distal to the aortic valve, a bileaflet aortic prosthetic valve (d) (St. Jude Medical, St. Paul, MN) was placed at the V-tube outlet. Intra-arterial pressure measurements show realistic aortic pressure wave contours distal to the aortic valve at the outlet (see Fig. 5, bottom), which justifies this intervention in the afterload of the simulator.

At the aortic outlet, a Latex aorta model (e) and two epicardial coronary vessels can be connected (f,g). In this study, we only used the connection in the LAD position (g) to mount one of nine Latex coronary artery phantoms (h). The epicardial segment is connected downstream to a computer-controlled time-varying resistance (i), which impedes coronary flow in systole, representing the myocardial resistance vessels. This myocardial resistance is then, in turn, connected to a passive resistance element (j), modeling the capillaries of the myocardium.

Coronary artery phantoms. The stenotic epicardial coronary segments were modeled as Latex tubes molded in several layers on three tubular molds (∅ = 4 mm), with different narrowing sizes in the middle according to the desired stenosis severity (DS = 40%, 50%, and 60%). In previous attempts to dilate 100% Latex tubes by means of a balloon catheter, the stenosed segment returned completely to its original dimensions due to elastic recoil. Therefore, we introduced a plastic substance at the site of the narrowing, and used the elastic Latex compound solely for the healthy part of the coronary segment (Fig. 3). The elastic–plastic model thus obtained suited the purpose of the tests of which the results are commented below. We also refer to the discussion for further details on the coronary artery phantoms.

Passive and active myocardial resistance. The passive resistance element is composed of 29 capillaries captured in a water-filled reservoir [10] (Fig. 4, right). The resistance can be changed by increasing the pressure in the water reservoir and thus occluding the capillaries. Coronary flow, however, is inhibited during systole due to the mechanical contraction of the heart muscle, and myocardial blood delivery is maximal during relaxation [6,12]. We therefore connected the passive resistance in series with a time-varying resistance, which impedes the flow during systole, and is minimal during diastole. A 10-ml syringe is used as an air-filled reservoir, with one Latex tube (representing a myocardial resistance vessel) on the inside (Fig. 4, left). The air-filled reservoir of the resistance is connected via an electromagnetic on/off valve to a buffer reservoir in the pneumatic circuit of the cardiovascular simulator. This way, the Latex tube is collapsed—and myocardial flow impeded—in phase with myocardial contraction. Figure 5 (top left) clearly shows that without the myocardial resistance, maximal flow is delivered during systole, which is not physiologically correct. Maximal blood delivery shifts to diastole when the resistance is activated (Fig. 5, top right).

Measurement Protocol

Intra-arterial pressure was measured proximal (P_p) and distal (P_d) to the stenosis at a sampling rate of 200 Hz, using epidural catheters connected directly to piezoelectric pressure transducers (Becton Dickinson, Franklin Lakes, NJ). The pressure catheters do not cross the stenosis. Flow was measured proximal to the stenosis by means of a two-channel ultrasonic flowmeter (Transonic Systems, Ithaca, NY). A second flow probe was mounted distal to the capillary resistance as control. Heart rate was set to 60 bpm and initial mean aortic blood pressure to 100 mmHg. Throughout a single experiment, flow was varied stepwise from 50 ml/min to about 200 ml/min by changing the capillary resistance value.

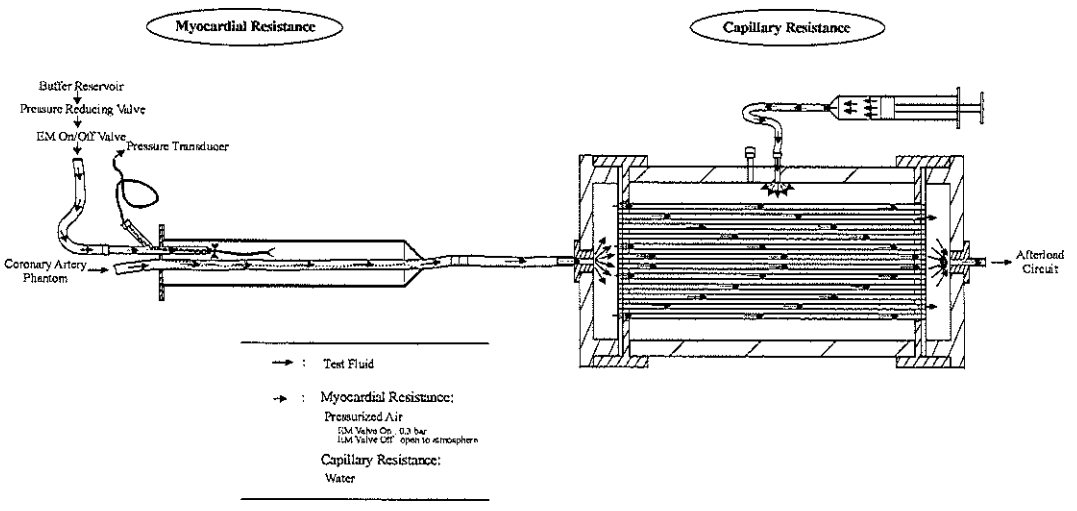

Fig. 4. The capillaries of skeletal muscles, tissue, and organs are modeled as a passive resistance element (right side). The contraction of the myocardial muscle is simulated by a time-varying resistance (left side). When an electromagnetic (EM) on/off valve closes, the time-varying resistance becomes inactive, and flow passes through the Latex tube, enclosed in the syringe (full line contour). When the time-varying resistance is activated, pressure is delivered from a buffer reservoir through the opened on/off valve into the syringe and the Latex tube collapses (dotted line contour).

First, baseline (BL) measurements were done in all nine stenotic Latex tubes (∅ = 4 mm). A 35-mm ACS Multilink stent (Guidant/ACS, Santa Clara, CA) was deployed in 6 tubes, with a 3-mm balloon at 8 atm. This allowed us to simulate conditions of suboptimal stent deployment (SOD). After hydraulic tests in the hydraulic bench, the tubes were taken to the catheter laboratory for intravascular ultrasound (IVUS) and biplane QCA with the tubes tested under static pressure conditions at 100 mmHg. Stents were then further optimally deployed (OD) under angiographic guidance using a 4-mm balloon at 16 atm. QCA and IVUS were repeated, and the OD tubes were taken to the hydraulic bench for flow measurement and assessment of FFR.

Data Analysis

Fractional flow reserve. Intra-arterial pressure measurements P_a and P_d were averaged over five heart cycles. Fractional flow reserve (FFR) was calculated for each tube as P_d/P_a. Values were averaged over three tubes per target stenosis severity and are given as mean ±SD.

QCA. The reference diameter (RD) measured in the frontal and lateral view with the biplane QCA was averaged, as well as the frontal and lateral minimal lumen diameter (MLD). Diameter stenosis (DS) percentages were then calculated with:

$$DS = 100 \cdot \frac{RD_{avg} - MLD_{avg}}{RD_{avg}}$$

Intravascular ultrasound The IVUS images were used in a qualitative way to verify whether or not the coronary stent was well opposed to the vessel wall. IVUS procedures were done following clinical guidelines as published by Di Mario et al. [13]. The data were analyzed using two-way repeat-measurement analysis of variance (ANOVA) to study the effect of flow and stenosis level on pressure–flow relations and FFR. QCA data were analyzed using one-way repeat-measurement ANOVA. The Bonferroni t-test was used as a post hoc test if significance was reached ($P < 0.05$). FFR data were analyzed at 100 ml/min, pooling data from all nine tubes. Differences between BL, SOD, and OD were assessed using paired t-tests.

RESULTS

Baseline QCA yielded effective DS values of 40%, 54%, and 59%, respectively (Table I). There was significant residual stenosis after SOD as confirmed by IVUS and QCA (DS = 35 ± 3%, 32 ± 1% and 39 ± 2%, respectively). OD reduced DS values down to 13 ± 4%, 10 ± 2%, and 10 ± 2%, respectively, and IVUS images confirmed overall contact of the stent with the vessel wall

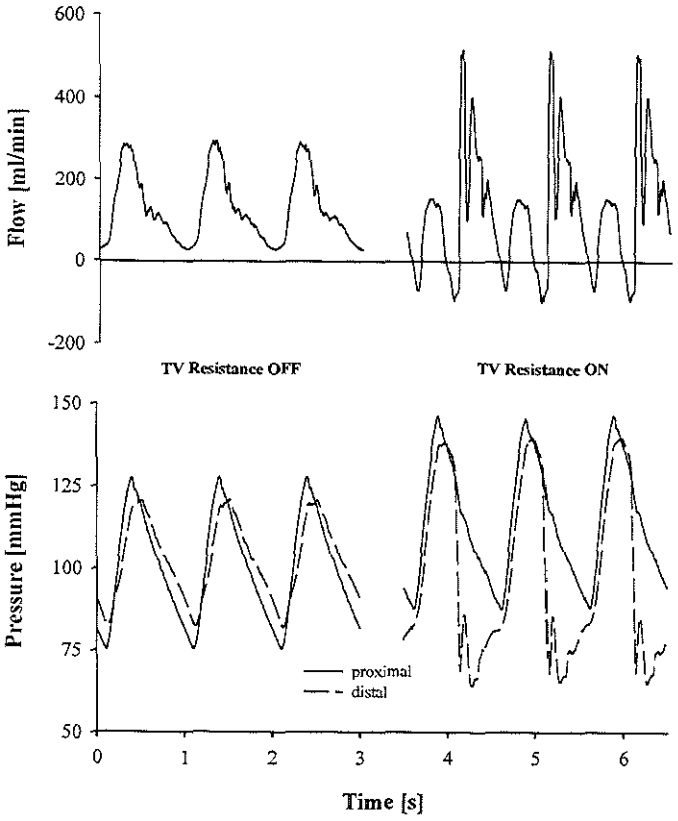

Fig. 5. Intra-arterial pressure and flow waves, measured distal to the aortic valve (see Fig. 2d). Without the time-varying (TV) resistance (on/off valve closed), maximal flow is delivered during systole (top left). Maximal blood supply shifts to diastole when the TV resistance is active (top right).

TABLE I. QCA Analysis Results

		BL			SOD			OD		
Target DS [%]	Tube #	RD [mm]	MLD [mm]	DS [%]	RD [mm]	MLD [mm]	DS [%]	RD [mm]	MLD [mm]	DS [%]
	1				3.9	2.6	33	4.2	3.5	15
40	2	3.2	1.9	40						
	3				4.2	2.6	37	4.3	3.9	10
	4				3.9	2.6	33	4.1	3.6	11
50	5	3.3	1.5	54						
	6				4.2	2.9	31	4.1	3.8	9
	7				4.1	2.5	38	4.2	3.8	9
60	8	4.0	1.6	59						
	9				4.2	2.5	41	4.2	3.7	11

Reference diameter (RD), minimal lumen diameter (MLD) and diameter stenosis percentages (DS) are shown for baseline conditions (BL), suboptimally deployed (SOD) and optimally deployed (OD) stents.

(Fig. 6). The differences between BL, SOD, and OD were significant (one-way ANOVA) when assessed by means of QCA and IVUS, except for 40% DS (no difference between BL and SOD).

At BL, for Q = 100 ml/min, FFR was 0.964 ± 0.005, 0.947 ± 0.004 and 0.923 ± 0.012 for 40%, 50% and 60% DS, respectively. FFR varied inversely with Q ($P < 0.001$, 2-way RM ANOVA) at BL, SOD and OD (Fig. 7). At BL, varying Q from 150 to 50 ml/min increased FFR by 2–7%. For OD, variation is less than 5%. Pooling all data at 100 ml/min, FFR increased from 0.955 ± 0.009 after SOD to 0.963 ± 0.005 after OD (+ 0.8%; $P < 0.05$; paired t-test).

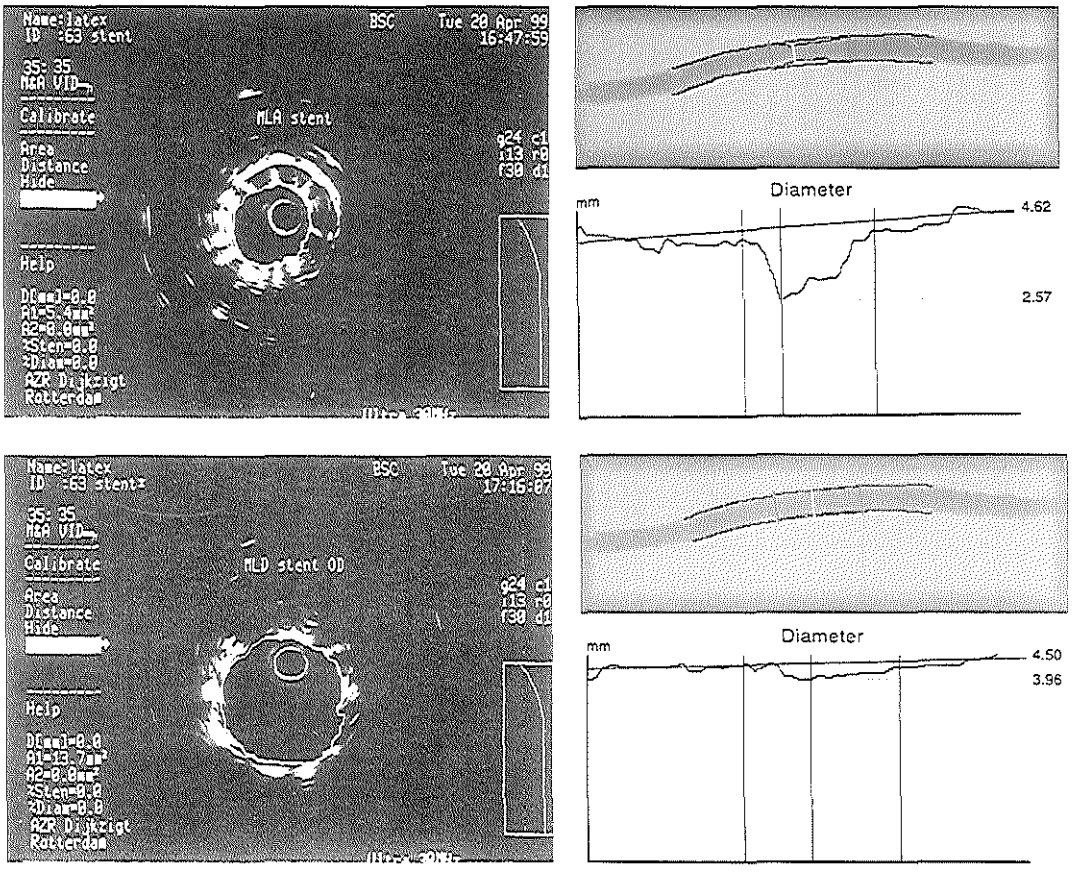

Fig. 6. Top: IVUS and QCA images for a suboptimally deployed (SOD) stent. The minimal lumen diameter is clearly detected via the QCA analysis; IVUS shows the loose struts of the malapposed stent. Bottom: IVUS and QCA for the same stent after optimal deployment (OD). There is a minor residual stenosis; IVUS shows stent struts, well apposed against the coronary artery wall.

DISCUSSION

In this study, we have used a hydraulic coronary artery model to address some limitations of FFR in clinical practice. We have demonstrated its flow dependency, and assessed its (in)sensitivity to optimal stent deployment.

From a hydraulic point of view, the flow dependency of FFR is easily demonstrated if P_d is replaced in the formula for FFR by its equivalent, $P_d = P_a - \Delta P$, where ΔP is the pressure drop over the stenosis. FFR then becomes

$$\mathrm{FFR} = \frac{P_d}{P_a} = \frac{P_a - \Delta P(Q)}{P_a} = 1 - \frac{\Delta P(Q)}{P_a} = \mathrm{FFR}(Q)$$

ΔP is always function of flow. In the case of laminar Poiseuille flow, there is a linear relation between Q and ΔP. Over a stenosis, this relation is quadratic [14]. P_a is often taken the (mean) central aortic pressure; it is relatively insensitive to the flow level in the investigated coronary artery. Note that ΔP is also function of blood viscosity. For the same flow, ΔP is higher if viscosity is higher; the hematocrit or fibrinogen concentration may therefore modulate FFR. A solution to enhance the flow independence of FFR might be to measure pressure proximal to the stenosis and not in the aorta (FFR = P_d/P_p instead of P_d/P_a). One should also realize that in clinical practice, catheters cross the stenosis, disturbing the flow

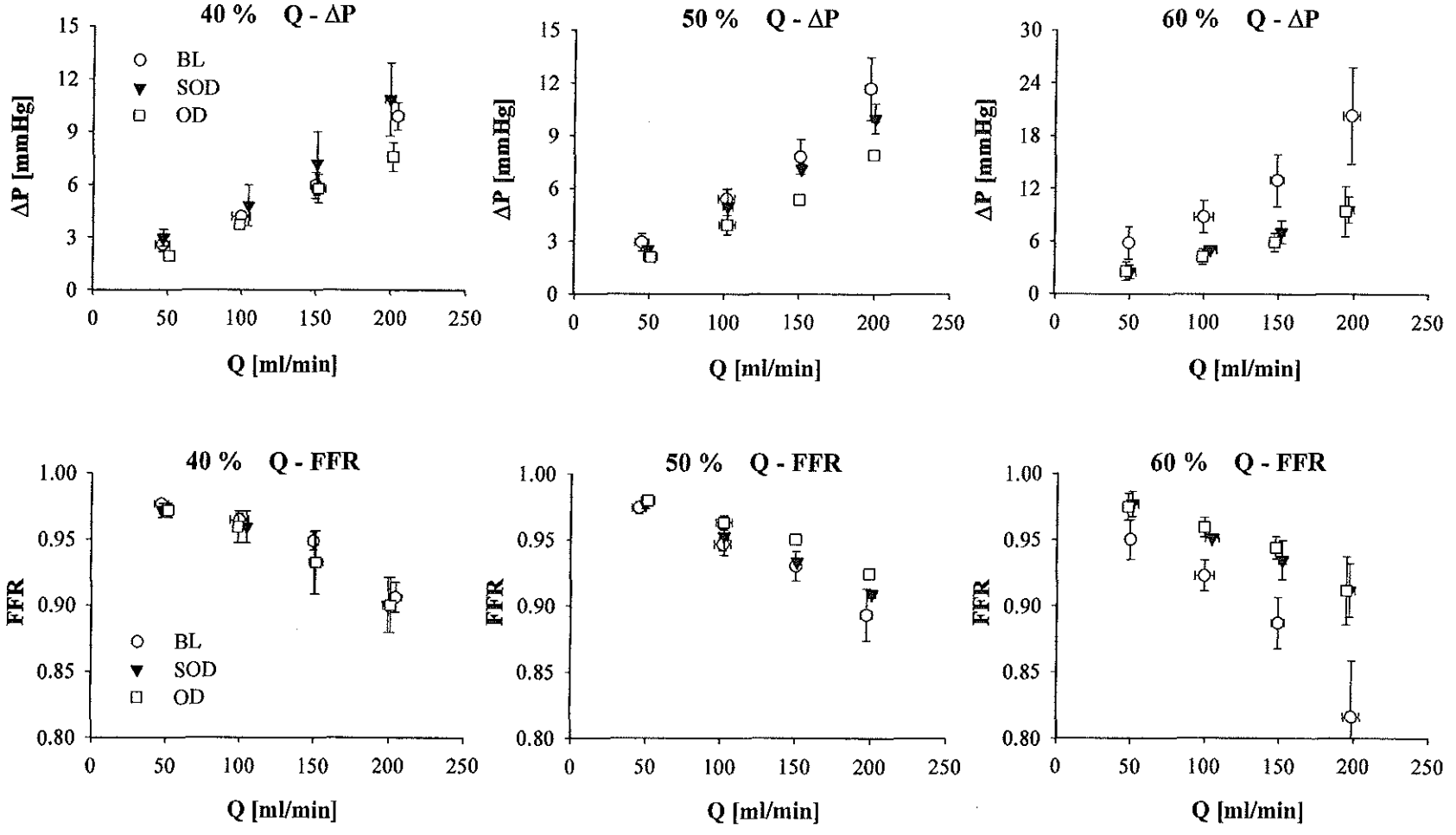

Fig. 7. Top: measured flow values (Q) and pressure drops (ΔP) for baseline (BL), suboptimal (SOD), and optimal (OD) deployment conditions. Values are shown for each of the target diameter stenosis percentages separately (40%, 50%, and 60%, respectively). From these data, we derived the Q-FFR relationships (bottom). These data clearly demonstrate the flow dependency of FFR.

pattern and contributing to ΔP. Even for ultrathin wires commonly used, their influence is not always negligible [15,16].

In clinical practice, FFR is useful to assess the severity of a coronary stenosis and to decide whether to perform an intervention. A threshold value of 0.75 is used. This value was assessed in patients with stable angina [5,17]. In patients with postmyocardial reperfusion or unstable angina, maximal hyperemic flow could be lower than in stable angina patients. As FFR is function of flow, the 0.75 threshold might not hold in these patients. This was recently shown by Jeremias et al. [18], who demonstrated that the FFR measured post balloon occlusion was lower than post-adenosine hyperemia (0.58 ± 0.2 vs. 0.63 ± 0.23, $P < 0.001$). This difference was related to a higher hyperemic flow obtained after balloon occlusion than after intracoronary administration of adenosine [18].

Our study shows little discriminating power of FFR between suboptimally (SOD) and optimally deployed (OD) stent. Given the definition of FFR, this means that the pressure drop over the tested stenosed Latex tube does not differ significantly between SOD and OD (at the same flow level). In hydraulic terms, the pressure drop over an SOD stent may arise from (1) pressure losses due to the higher residual stenosis, or (2) pressure losses due to flow turbulence around the loose struts in the flow. We found little effect of the difference in residual DS (11 ± 2% for OD, 35 ± 4% for SOD) on the pressure drop and FFR. This is not surprising, and confirms other studies showing effects of stenosis on pressure drops only for high stenosis values [14]. More remarkable is the observation that the pressure losses attributable to loose stent struts are not significant either. Some interesting studies on flow turbulence due to the positioning of the stent struts were performed by Peacock et al. [19] and Berry et al. [20]. Unfortunately, these studies emphasized mainly flow visualization and characterization, rather than the quantification of pressure losses.

In recent work, Hanekamp et al. [8] tested the feasibility of FFR for the assessment of optimal stent deployment. A cutoff value of 0.94 was proposed, with FFR ≥0.94 indicating optimal deployment. The agreement between optimal stent expansion by IVUS, with (1) complete apposition of all struts, (2) symmetry index >0.7, and (3) in-stent minimal cross-sectional area >90% of reference area, and an FFR of >0.94 was 91%. Hanekamp et al. concluded that IVUS and FFR were of similar value to assess optimal stent deployment and that, for this purpose, coronary pressure measurement can be used as a cheap and rapid alternative for IVUS. Although the mean reference diameter (RD) in the study by Hanekamp and colleagues is not given, it is expected that it was ~3.0 mm, the most common size of a stented coronary vessel [21,22]. In these conditions, a suboptimal stent expansion with a suboptimal residual diameter stenosis (DS) of 30% gives a minimal lumen diameter (MLD) of 2 mm, whereas an optimally expanded stent with a residual DS of 10% is associated to aMLD of 2.7 mm. In our in vitro experiments performed with Latex tubes presenting a mean RD of 4 mm, SOD stents, with a mean residual DS of 36%, had a MLD of 2.6 mm, and the OD with a mean DS of 11% had a MLD of 3.6 mm. This may explain the discrepancy between our results, demonstrating minimal change of the FFR between SOD and OD stent expansion and the clinical data of Hanekamp et al. However, our IVUS pullbacks demonstrated that although a sufficient MLD was restored to give an FFR value of >0.9, large segments of stents were still malapposed and were not detected by abnormal FFR values. These extensive segments would have surely had clinical implications such as (sub)acute thrombosis in a clinical setting.

In previous configurations of the cardiovascular simulator, the arteries were mounted in a horizontal plane, neglecting the 3D component of the peripheral vascular bed. The coronary arteries, however, are particularly tortuous. In order to respect their 3D anatomical shape, we had to mount them on a Latex epicardial surface, as shown in Figure 2. This setup more closely resembles coronary anatomy but is still a merely static supporting structure. A dynamically moving structure would further decrease model limitations.

For the Latex coronary artery phantoms, we performed a feasibility study comparing phantom fills of 100% Latex with various types of plastic substances. We simulated a PTCA procedure, as well as the deployment of (home made) stents [23]. As a criterion, we used the residual stenosis percentage of the stenosed segment and compared it to that what is usually observed in clinical practice immediately after PTCA or (optimal) stent deployment. Experiments led to the currently used configuration. Nevertheless, optimal stent deployment still yielded average residual DS of ≥10%, which, in clinical practice, is an upper limit for OD deployment [24]. Thus, further and more elaborate investigation of an appropriate stenosed coronary artery phantom may be required.

With the time-varying resistance, we obtained more realistic flow patterns, realizing flow impediment during systole. However, there are still some limitations leading to perturbations during activation of the myocardial resistance (Fig. 5). Replacing the simple on/off valve with a regulating actuator would probably smooth out the flow wave. Furthermore, we only simulated one coronary artery with no side branches. In vivo, the heart is irrigated by a dense network of arteries, arterioles, and capillaries. Extending our Latex model in greater detail, i.e., more epicardial branches and more myocardial resistance ves-

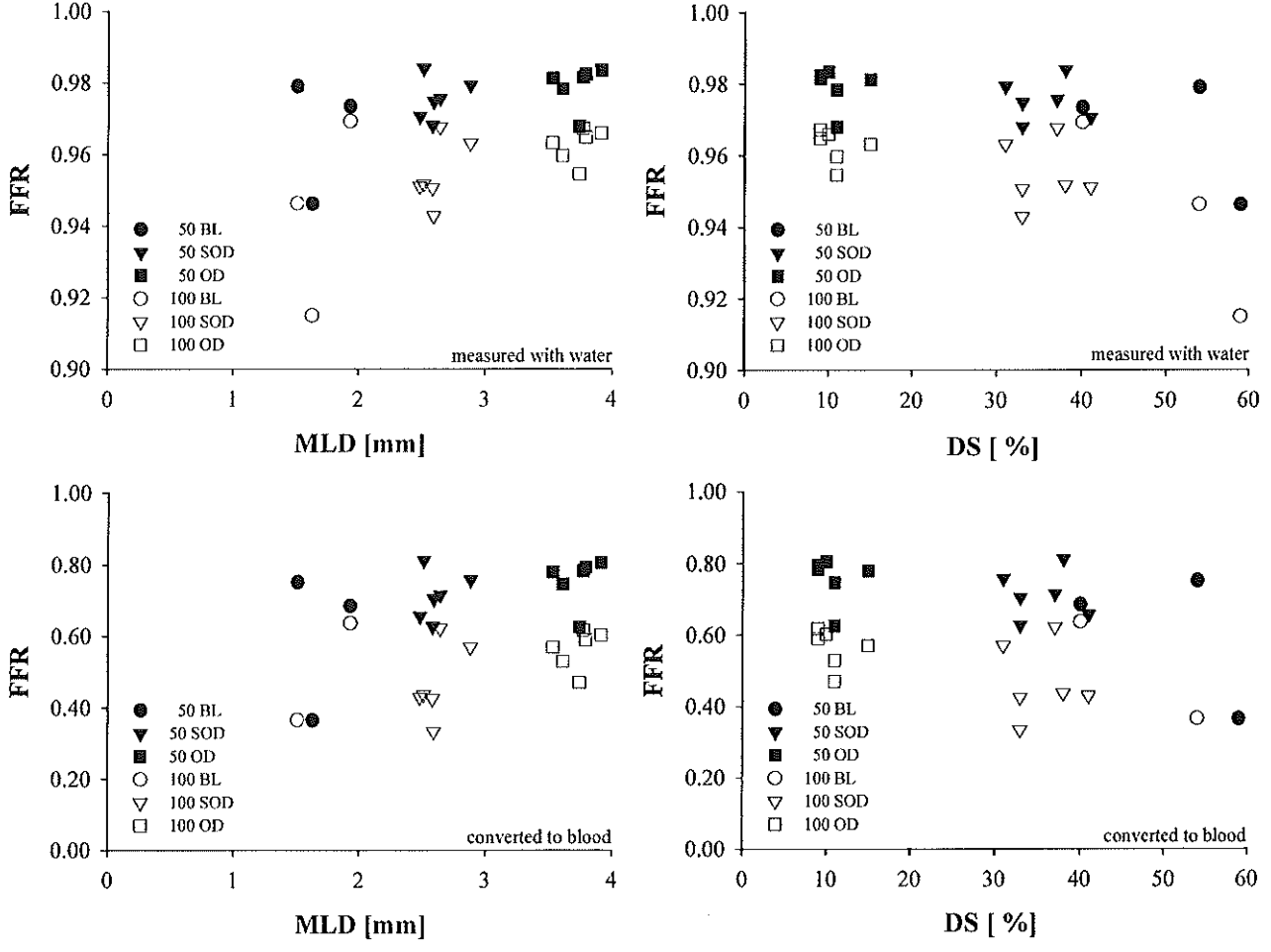

Fig. 8. Relationship between fractional flow reserve (FFR) and minimal lumen diameter (MLD) (left) and between FFR and diameter stenosis percentage (DS) (right). Data shown for baseline (BL), suboptimal (SOD), and optimal (OD) deployment conditions at two different flow (Q) levels (50 and 100 ml/min). Top: measured values with water. Bottom: same data, but with values converted to blood.

sels, would also improve the physiological relevancy of the simulated coronary flow pattern.

QCA and IVUS tests were done in the catheter laboratory, while the hydraulic tests were performed in the hydraulic laboratory. For practical and technical reasons, it was impossible to use the cardiovascular simulator in the catheter laboratory. We therefore used a 2D static setup in the catheter laboratory, in which the coronary phantom was inserted after previous testing in the hydraulic bench. There was no 3D supporting structure, nor was there a pulsatile flow regime during QCA and IVUS. The coronary artery phantoms were however filled with water and contrast agent and then pressurized to 100 mmHg, similar to mean aortic pressure (P_a) in the hydraulic tests with the cardiovascular simulator.

Another limitation of our work is the use of water for test fluid. Being Newtonian, water has no shear-thinning effects, but this aspect is less important as the dimensions of the coronary phantoms largely exceed those of blood particles, and velocity and shear rate are high enough to neglect non-Newtonian effects. More important is the fact that the viscosity of water is 3 to 4 times lower than blood. Consequently, pressure drops are 3 to 4 times lower as well, and calculated FFR values are higher than the values for blood at the same flow level. Nevertheless, our results can be converted to blood flow using dimensionless numbers and the theory of dynamic similarity [25]. For each FFR value at a certain flow level with water experiments, there is a corresponding lower FFR value for blood at a (higher) blood flow level. A detailed outline of such a conversion is given in the Appendix. As an example, for a coronary artery phantom with target diameter stenosis of 60%, we found that after optimal stent deployment (OD), $FFR_{water} = 0.98$ for $Q_{water} = 50.54$ ml/min. These values correspond to a blood flow (Q_{blood}) of 168.47 ml/min, and $FFR_{blood} = 0.81$ (see Appendix). The water experiments, covering a range of 50–200 ml/min, cover a blood range of 150–600 ml/min. Figure 8 illustrates FFR values for water (upper panels) and the converted values for blood (lower panels) for BL, SOD, and OD as a function of MLD and DS. Note that changes in flow have a much larger effect on FFR than going from SOD to OD.

In conclusion, we demonstrated that FFR is confounded by the blood flow level and the blood viscosity. Further, we found only small differences in FFR between a suboptimally and an optimally deployed stent assessed by IVUS (complete stent apposition). Anatomical parameters postpercutaneous coronary intervention remain strong predictors of restenosis, for example, and assessing optimal stent deployment is more dependent on anatomical measures than measures of functional perfusion. Thus, we believe that IVUS and QCA are more appropriate for the assessment of optimal stent deployment than FFR when a minimal lumen diameter has been reached, normalizing the FFR to >0.9. In clinical conditions such as unstable angina/postmyocardial infarction reperfusion, cautious interpretation of FFR measurements should be based on potential low-flow conditions.

ACKNOWLEDGMENTS

The authors thank Ivo Vanderick from Guidant for supplying the stents.

From the calculations done in apppendix,we conclude that $FFR_{water} = 0.98$, at a flow level of $Q_{water} = 50.54$ ml/min, corresponds to $FFR_{blood} = 0.81$ for $Q_{blood} = 168.47$ ml/min.

REFERENCES

1. Carlier SG, Van Langenhove G, Lupotti F, Albertal M, Mastik F, Bom K, Serruys PW. Coronary flow reserve versus geometric measurements of coronary dimensions: advantages and limitations of the functional stenosis assessment. J Intervent Cardiol 1999; 12:411–424.
2. Kern MJ. Coronary physiology revisited: practical insights from the cardiac catheterization laboratory. Circulation 2000;101:1344–1351.
3. Pijls NHJ, van Son JAM, Kirkeeide RL, De Bruyne B, Gould KL. Experimental basis of determining maximum coronary, myocardial and collateral blood flow by pressure measurements for assessing functional stenosis severity before and after percutaneous transluminal coronary angioplasty. Circulation 1993;87:1354–1367.
4. De Bruyne B, Baudhuin T, Melin JA, Pijls NHJ, Heyndrickx GR, Wijns W. Coronary flow reserve calculated from pressure measurements in man: validation with positron emission tomography. Circulation 1994;89:1013–1022.
5. Pijls NHJ, De Bruyne B, Peels K, Van der Voort P, Bonnier HJRM, Bartunek J, Koolen JJ. Measurement of fractional flow reserve to assess the functional severity of coronary artery stenoses. N Engl J Med 1996;334:1703–1708.
6. Pijls NHJ, De Bruyne B. 1997. Coronary pressure. Dordrecht: Kluwer Academic; 344 p.
7. Pijls NHJ, Kern MJ, Yock PG, De Bruyne B. Practice and potential pitfalls of coronary pressure measurement. Cathet Cardiovasc Intervent 2000;49:1–16.
8. Hanekamp CEE, Koolen JJ, Pijls NHJ, Michels HR, Bonnier HJRM. Comparison of quantitative coronary angiography, intravascular ultrasound, and coronary pressure measurement to assess optimum stent deployment. Circulation 1999;99:1015–1021.
9. Segers P, Dubois F, De Wachter D, Verdonck P. Role and relevancy of a cardiovascular simulator. J Cardiovasc Eng 1998;3: 48–56.
10. Segers P, Fostier G, Neckebroeck J, Verdonck P. Assessing coronary artery stenosis severity: in vitro validation of the concept of fractional flow reserve. Cathet Cardiovasc Intervent 1999;46:375–379.
11. Verdonck P, Kleven A, Verhoeven R, Angelsen B, Vandenbogaerde J. Computer-controlled in vitro model of the human left heart. Med Biol Eng Comput 1992;30:656–659.

12. Mates RE, Gupta RL, Bell AC, Klocke FJ. Fluid dynamics of coronary artery stenosis. Circ Res 1978;42:152–162.
13. Di Mario C, Görge G, Peters R, Kearney P, Pinto F, Hausmann D, von Birgelen C, Colombo A, Mudra H, Roelandt J, Erbel R. Clinical application and image interpretation in intracoronary ultrasound. Study group on intracoronary imaging of the working group of coronary circulation and of the subgroup on intravascular ultrasound of the working group of echocardiography of the European Society of Cardiology. Eur Heart J 1998;19:207–229.
14. Young DF, Tsai F. Flow characteristics in models of arterial stenoses. II. Unsteady flow. J Biomech 1973;6:547–559.
15. De Bruyne B, Pijls NHJ, Paulus WJ, Vantrimpont PJ, Sys SU, Heyndrickx GR. Transstenotic coronary pressure gradient measurement in humans: in vitro and in vivo evaluation of a new pressure monitoring angioplasty guide wire. J Am Coll Cardiol 1993;22:119–126.
16. Krams R, Wentzel JJ, Céspedes I, Carlier SG, van der Steen AFW, Lancée CT, Slager CJ. Effect of catheter placement on 3-D velocity profiles in curved tubes resembling the human coronary system. Ultrasound Med Biol 1999;25:803–810.
17. Pijls NHJ, De Bruyne B. Coronary pressure measurement and fractional flow reserve. Heart 1998;80:539–542.
18. Jeremias A, Filardo SD, Whitbourn RJ, Kernoff RS, Yeung AC, Fitzgerald PJ, Yock PG. Effects of intravenous and intracoronary adenosine 5'-triphosphate as compared with adenosine on coronary flow and pressure dynamics. Circulation 2000;101:318–323.
19. Peacock J, Hankins S, Jones T, Lutz R. Flow instabilities induced by coronary artery stents: assessment with an in vitro pulse duplicator. J Biomech 1995;28:17–26.
20. Berry JL, Moore JE Jr, Newman VS, Routh WD. In vitro flow visualization in stented arterial segments. J Vasc Invest 1997;3:63–68.
21. Serruys PW, de Jaegere P, Kiemeneij F, Macaya C, Rutsch W, Heyndrickx G, Emanuelsson H, Marco J, Legrand V, Materne P, Belardi J, Sigwart U, Colombo A, Goy JJ, van den Heuvel P, Delcan J, Morel MA. A comparison of balloon expandable stent implantation with balloon angioplasty in patients with coronary artery disease. N Engl J Med 1994;331:489–495.
22. Serruys PW, Foley DP, Kirkeeide RL, King SR. Restenosis revisited: insights provided by quantitative coronary angiography. Am Heart J 1993;126:1243–1267.
23. De Scheerder IK, Wang K, Kerdsinchai P, Desmet W, Dens J, Supanantaroek C, Piessens JH. Clinical and angiographic outcome after implantation of a homemade stent for complicated coronary angioplasty. Cathet Cardiovasc Diagn 1997;42:339–347.
24. de Jaegere P, Mudra H, Figulla H, Almagor Y, Doucet S, Penn I, Colombo A, Hamm C, Bartorelli A, Rothman M, Nobuyoshi M, Yamaguchi T, Voudris V, Di Mario C, Makovski S, Hausmann D, Rowe S, Rubinovich S, Sunamura M, van Es GA. Intravascular ultrasound-guided optimized stent deployment. Immediate and 6 months clinical and angiographic results from the Multicenter Ultrasound Stenting in Coronaries Study (MUSIC Study). Eur Heart J 1998;19:1214–1223.
25. Streeter VL. 1961. Handbook of fluid dynamics. New York: McGraw-Hill.

APPENDIX

Converting flow and pressure measurements for water to results for blood requires two steps. First, extra parameters have to be calculated for water in order to derive two nondimensional numbers: Reynolds (Re_{water}) and Euler (ζ_{water}). Second, applying the theory of dynamic similarity, we express that Re_{water} equals Re_{blood} and ζ_{water} equals ζ_{blood}. From these two equations, it is then possible to obtain flow and pressure values for blood, as demonstrated below.

Step 1: Re_{water} and ζ_{water}

Internal diameter of the coronary artery phantom, as well as the physical properties of water is given in Table A1. Cross-sectional area $A_{phantom}$ is calculated with:

$$A = \pi \cdot D^2/4$$

TABLE A1. Measured and Derived Parameters for Water

Parameter	Symbol [units]	Formula	Value
Internal diameter	$D_{phantom}$ [m]		0.004
Cross-sectional area	$A_{phantom}$ [mm^2]	$A = \pi \cdot D^2/4$	12.6
Water density	ρ_{water} [kg/m^3]		1000
Water viscosity	μ_{water} [Pa s]		0.001
Water velocity	U_{water} [m/s]	$U = \frac{Q}{A}$	0.067
Water flow	Q_{water} [ml/min]		50.54
Proximal stenosis pressure	$P_{p\ water}$ [mmHg]		106.55
Distal stenosis pressure	$P_{d\ water}$ [mmHg]		104.79
Pressure drop	ΔP_{water} [mmHg]	$\Delta P = P_p - P_d$	1.76
FFR_{water} (OD)	FFR_{water}	$FFR = \frac{P_d}{P_p}$	0.98
$Reynolds_{water}$	Re_{water}	$Re = \frac{U \cdot D \cdot \rho}{\mu}$	268
$Euler_{water}$	ξ_{water}	$\xi = \frac{\Delta P}{\rho \cdot U^2}$	52

TABLE AII. Corresponding Parameters for Blood

Parameter	Symbol [units]	Formula	Value
$Reynolds_{blood}$	Re_{blood}	$Re_{blood} = Re_{water}$	268
Internal Diameter	$D_{phantom}$ [m]		0.004
Blood Density	ρ_{blood} [kg/m^3]		1050
Blood Viscosity	μ_{blood} [Pa s]		0.0035
Blood Velocity	U_{blood} [m/s]	$U_{blood} = Re_{blood} \cdot \frac{\mu_{blood}}{D \cdot \rho_{blood}}$	0.22
Cross-sectional area	$A_{phantom}$ [mm^2]	$A = \pi \cdot D^2/4$	12.6
Blood Flow	Q_{blood} [ml/min]	$Q = U \cdot A$	168.47
$Euler_{blood}$	ξ_{blood}	$\xi_{blood} = \xi_{water}$	52
Pressure drop	ΔP_{blood} [mmHg]	$\Delta P_{blood} = \xi_{blood} \cdot \rho_{blood} \cdot U^2_{blood}$	20.58
Proximal stenosis pressure	$P_{p\,blood}$ [mmHg]	$P_{p\,blood} = P_{p\,water}$	106.55
Distal stenosis pressure	$P_{d\,blood}$ [mmHg]	$P_d = P_p - \Delta P$	85.97
FFR_{blood} (OD)	FFR_{blood}	$FFR = \frac{P_d}{P_p}$	0.81

while water velocity U_{water} is derived from the measured flow Q_{water} (= 50.54 ml/min) with

$$U = \frac{Q}{A}$$

Pressure drop ΔP_{water} and FFR_{water} are derived from the measured proximal and distal stenosis pressures with

$$\Delta P = P_p - P_d$$

and

$$FFR = \frac{P_d}{P_p}$$

resulting in ΔP_{water} = 1.76 mmHg and FFR_{water} = 0.98. Finally, the Reynolds and Euler number (Re_{water}, ζ_{water}) are calculated using

$$Re = \frac{U \cdot D \cdot \rho}{\mu} \quad \text{and} \quad \xi = \frac{\Delta P}{\rho \cdot U^2}$$

giving Re_{water} = 268. and ζ_{water} = 52 (Table AI).

Step 2: Q_{blood} and FFR_{blood}

Calculations are to be done in an 'inverse' way, starting from Re and ζ. Necessary physical properties for blood are given in Table AII. Blood velocity (U_{blood}) is calculated using

$$U_{blood} = Re_{blood} \cdot \frac{\mu_{blood}}{D \cdot \rho_{blood}}$$

with $Re_{blood} = Re_{water}$ = 268. Blood flow (Q_{blood}) is then obtained via

$$Q = U \cdot A$$

resulting in Q_{blood} = 168.47 ml/min.

As ζ_{water} equals ζ_{blood}, it is possible to derive ΔP_{blood} with

$$\Delta P_{blood} = \xi_{blood} \cdot \rho_{blood} \cdot U^2_{blood}$$

giving 20.58 mmHg. Finally, stating that $P_{p\,blood}$ equals $P_{p\,water}$, $P_{d\,blood}$ can be found

$$P_d = P_p - \Delta P$$

and also FFR_{blood}

$$FFR_{blood} = \frac{P_d}{P_p}$$

yielding a value of 0.81.

PART 2

Intracoronary Flow Measurements with IVUS catheters

Chapter 6

Flow estimation using an intravascular imaging catheter.

AFW van der Steen, EI Cespedes, **SG Carlier**, F Mastik, F Lupotti,
JMG Borsboom, W Li, PW Serruys, N Bom.

Ultrasonics 2000; 38:363-368.

ELSEVIER

Ultrasonics 38 (2000) 363–368

Ultrasonics

www.elsevier.nl/locate/ultras

Flow estimation using an intravascular imaging catheter

A.F.W. van der Steen [a,b,*], E.I. Céspedes [c], S.G. Carlier [a], F. Mastik [a], F. Lupotti [a,b], J.M.G. Borsboom [a,d], W. Li [a,b], P.W. Serruys [a,b], N. Bom [a,b]

[a] *Thorax Centre, Erasmus University, Rotterdam, Netherlands*
[b] *Interuniversity Cardiology Institute of the Netherlands, Netherlands*
[c] *Endosonics Corporation, Rancho Cordova, CA, USA*
[d] *Department of Electrotechnical Engineering, Technical University Delft, Delft, Netherlands*

Abstract

Coronary flow assessment can be useful for determining the hemodynamic severity of a stenosis and to evaluate the outcome of interventional therapy. We developed a method for measuring the transverse flow through the imaging plane of an intravascular ultrasound (IVUS) catheter. This possibility has raised great clinical interest since it permits simultaneous assessment of vessel geometry and function with the same device. Furthermore, it should give more accurate information than combination devices because lumen diameter and velocity are determined at the same location.

Flow velocity is estimated based on decorrelation estimation from sequences of radiofrequency (RF) traces acquired at nearly the same position. Signal gating yields a local estimate of the velocity. Integrating the local velocity over the lumen gives the quantitative flow.

This principle has been calibrated and tested through computer modeling, in vitro experiments using a flow phantom and in vivo experiments in a porcine animal model, and validated against a Doppler element containing guide wire (Flowire®) in humans.

Originally the method was developed and tested for a rotating single element device. Currently the method is being developed for an array system.

The great advantage of an array over the single element approach would be that the transducer has no intrinsic motion. This intrinsic motion sets a minimal threshold in the detectable velocity components. Although the principle is the same, the method needs some adaptation through the inherent different beamforming of the transducer. In this paper various aspects of the development of IVUS flow are reviewed.

Keywords: Blood flow; Decorrelation; Intravascular ultrasound; RF data processing

1. Introduction

Currently, intravascular ultrasound (IVUS) is the only clinically available technique capable of providing real-time cross-sectional images of coronaries at high resolution in vivo. It delivers information that is not available from X-ray angiography. As the number of available interventional techniques for treatment of atherosclerotic luminal narrowing increases, specific diagnostic information that can aid in the selection becomes increasingly important. For this reason, IVUS is more and more routinely used for guiding interventional procedures [1] and for studying the mechanisms for restenosis [2].

In the last couple of years the possibilities of accessing a sufficient amount of RF data at adequate speed have improved significantly. This has allowed us to study IVUS data in a totally different way [3,4]. Traditionally, the emphasis was on imaging itself, while RF analysis also allows tissue characterization [5,6], elasticity imaging [7–10], flow estimation and enhanced boundary detection.

Assessment of blood flow has long been recognized as an important approach to evaluate the functional status of a diseased artery. Intracoronary Doppler is a conventional ultrasonic method for measurement of blood velocities, and has been applied for coronary flow reserve assessment and to evaluate the severity of coro-

* Corresponding author. Address for correspondence: Thorax Centre, Ee 2302, Erasmus University, Rotterdam, PO Box 1738, 3000 DR Rotterdam, The Netherlands. Tel.: +31-10-408-8036; fax: +31-10-408-9445.
E-mail address: vandersteen@tch.fgg.eur.nl (A. der Steen)

0041-624X/00/$ - see front matter
PII: S0041-624X(99)00213-9

nary lesions [11]. The use of Doppler velocimetry alone, however, does not allow direct measurement of flow volume. For quantitative measurement of flow volume, the vessel cross-sectional area and the blood velocity must be assessed coincidentally in time and space. IVUS is a tomographic imaging technique that allows accurate measurement of the vessel cross-sectional area, irrespective of vessel geometry [12]. The feasibility of simultaneous use of intracoronary Doppler for velocity measurement and IVUS imaging for area measurement to estimate blood flow has been demonstrated [13]. One potential limitation of this approach is that the flow volume is estimated from the mean Doppler velocity with an assumed velocity profile. Additionally, the simultaneous use of multiple ultrasound transducers could cause cross-talk between the Doppler and IVUS transducer [14].

A unique feature of IVUS techniques is that the direction of blood flow is almost normal to the imaging plane. As blood particles move across the imaging plane, the received echo signals decorrelate at a rate proportional to flow velocities. In this paper, we review a method that allows a direct measure of local velocity as well as volume flow by means of analysis of the intravascular RF echo signals. The flow measurements obtained with the decorrelation method (IVUS-flow) are compared with the data of an electromagnetic flow meter (EM-flow) in vivo under various flow conditions in an animal model. Furthermore, clinical data are presented.

Since a rotating single element transducer suffers from some inherent motion artifacts, we are currently developing the method for an array transducer system. These transducers get their inherent resolution and image quality by synthetic aperture focussing techniques. Since this is based on reconstruction of the image from multiple pulses from different directions towards the same 'static' object, this technique is not directly suited for flow estimation, because the blood particles are moving in the time course of the acquisition. The scanning protocol of the array had to be changed. In this paper another scanning protocol is described, based on a computer model of the array and included in an intravascular ultrasound system. Preliminary patient data using this catheter are presented.

Finally possibilities to use this method for automatic boundary detection in IVUS are discussed.

2. Methods

2.1. Decorrelation of blood echoes

The displacement of an ultrasound-scattering material such as blood moving through the beam of an ultrasound transducer results in decorrelation in the received echo signal. The decorrelation phenomenon can be clearly observed in the intravascular environment in which the ultrasound beam is transmitted perpendicularly to the arterial tissue and blood flow (Fig. 1). In IVUS, it is commonly observed from real-time display that the scattering pattern of flowing blood varies rapidly over time. This is due to the fact that the flow stream drives the randomly distributed blood particles constantly in/out of the image plane, causing the received echo signals to decorrelate with time.

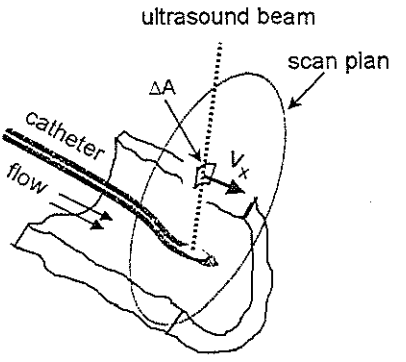

Fig. 1. The coordinates of the IVUS imaging set-up. The scanning plane is perpendicular to the direction of blood flow.

Correlation has been found to decrease approximately linearly with increasing flow velocity. This result suggests that if the velocity–correlation relation is prequantified for the type of transducers used, the measured decorrelation value from blood scattering signals can be converted into flow velocity.

2.2. Decorrelation-to-flow quantification

The method is based on decorrelation processing of a series of RF signals (time RF sequence) acquired at approximately the same transmission angle.

2.2.1. Spatial decorrelation model

Unlike most other medical imaging techniques, the majority of IVUS signals are acquired in the near field of the ultrasound beam (0.1–4 mm). The relationship between the correlation of echo signals and the scatterer motion across the ultrasound beam (lateral decorrelation) can be approximated with a linear model in the near field [15,16]. The slope, termed the displacement decorrelation slope (mm^{-1}), is characterized by the beam pattern. The linear dependence of signal correlation upon the scatterer lateral displacement has been validated in both computer simulation and in vitro with a flow phantom. Our results show that, because the beam pattern may change significantly in the near field, the displacement correlation slope must be calibrated for the type of transducer used [15,16].

2.2.2. Time decorrelation measurement

At each transmission angle, a sequence of RF traces separated by a fixed time interval is acquired at a high pulse repetition rate. The decorrelation rate of the range-gated echo is evaluated in two steps.

1. Align the RF traces across the sequence, using axial cross-correlation. This procedure removes the decorrelation due to the axial displacement (along the ultrasound beam) of blood scatterers.
2. Compute the correlation coefficient between aligned RF pairs. A slope is obtained by fitting a linear model through the correlation versus displacement. The slope $\alpha_t^{\perp}$, termed the time decorrelation slope (s^{-1}), is related to the transverse blood velocity (normal to the ultrasound beam) for a given beam position.

2.2.3. Velocity estimation

Thus, the transverse velocity can be estimated at each window position from the ratio between the *calibrated* decorrelation function and the *measured* decorrelation slope from a time RF sequence. Note that the calibration procedure needs to be carried out only once for a specific type of transducer.

2.2.4. Volume flow integration

Local velocities in small range windows can be obtained throughout the lumen cross-section to provide two-dimensional flow mapping. As illustrated in Fig. 1, the volume flow is calculated by integrating the local transverse velocity with its corresponding area element over the complete imaging plane. Because wall tissues move more slowly than blood, the contribution of tissue velocities can be automatically removed by setting a threshold. Thus, no contour tracing of the arterial lumen is needed.

3. Results

The methods described above have been implemented on a rotating single element IVUS system (DuMed/Endosonics Inc.) and validated in a number of ways. In vitro data showed good agreement with a calibrated electromagnetic flow meter [16]. In the carotid artery of a pig the IVUS flow showed good agreement with electromagnetic flow estimation (Fig. 2) [17,18].

The relation, under a variety of flow conditions, approached unity. In patient studies the IVUS flow is compared with the values obtained by a Doppler flow wire [19]. Again a good agreement was found. This method has been evaluated extensively in the catheterization laboratory [17,20] (Fig. 3).

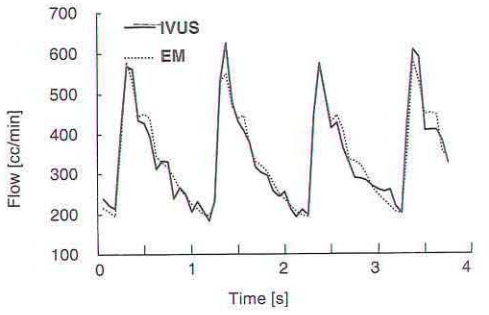

Fig. 2. Flow curves of phasic EM-flow (dotted line) and IVUS-flow (solid line) in a pig carotid artery, showing an almost identical beat-to-beat change in blood volume flow [17,18].

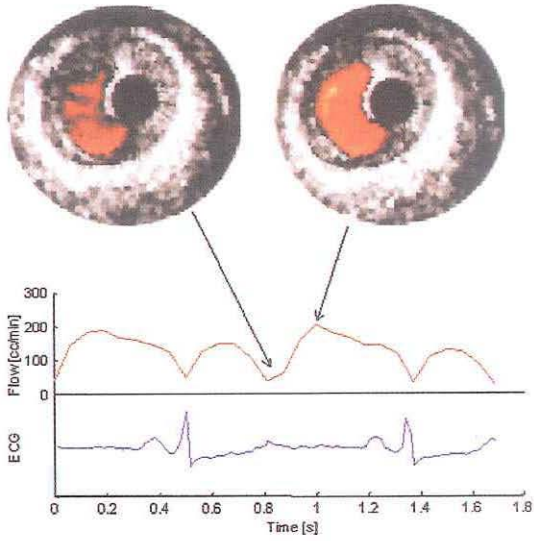

Fig. 3. Upper panel: coronary flow mapping obtained in patient for low (left) and high (right) flow rates during the cardiac cycle. Lower panel: IVUS flow curve showing a typical two-phasic diastolic flow pattern of a coronary artery.

3.1. Influence of catheter

One important issue in this flow measurement is the question of whether the catheter itself influences the flow measurement. There are three important aspects that should be addressed.

1. Is the flow profile changed by the catheter?
2. Does the catheter cause secondary flow?
3. Does the catheter impede the flow?

(1) This is indeed the case, but it does not affect the flow estimation, since the values of the transverse veloc-

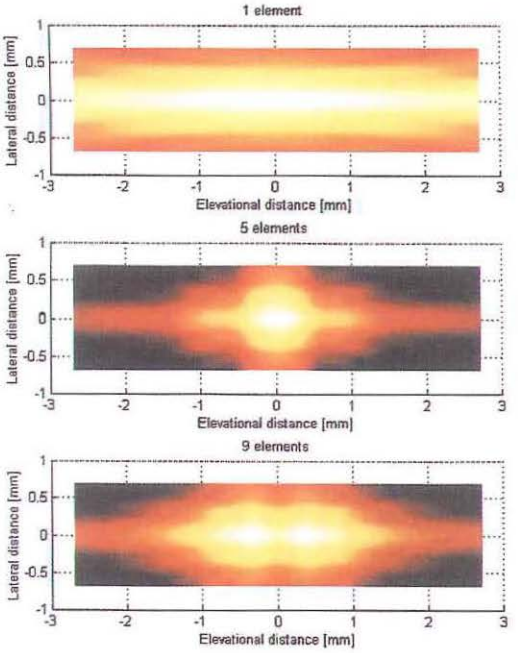

Fig. 4. Intensity plots at a distance of 2 mm from an array transducer that is operated in linear array mode using one, five or nine elements [24].

ity profile are integrated over the full cross-section and the exact profile is not important.

(2) The method is able to discriminate between axial and transverse flow, but incapable of discriminating transverse motion through the plane from in-plane transverse motion. The latter is referred to as secondary flow and a significant presence of this could cause a bias in the flow estimation. This secondary flow has been studied using finite element modeling [21]. The flow through a curved vessel with a catheter inside at a variety of positions is compared with the flow without a catheter present. The main conclusion of the study was that the secondary flow with a catheter inside has only a minor influence on the flow estimation [22]. A peculiar fact is that secondary flow with a catheter inside is even less than without a catheter. The catheter seems to have a regulating effect on the secondary flow.

(3) The impediment of the catheter on the flow is also under study. This is done in an in vitro set-up where tubes with several stenoses are studied. The pressure drop over the stenosis is established without a catheter, with a guide wire and with a catheter.

This pressure drop is a direct measure of the impedance of the flow. Preliminary results show that if the stenosis is severe enough, there is an influence of the catheter on the flow. The exact influence still has to be determined.

3.2. Flow estimation using an array transducer

Although the flow estimation seems to work well on a rotating single element catheter there are certain disadvantages. One is the fact that motion of the catheter with respect to the blood cannot be separated from motion of the blood with respect to the catheter. In principle, the decorrelation due to element rotation can be corrected for, but two problems remain.

1. If the flow becomes very slow the relative decorrelation due to rotation becomes significant. Therefore only velocity components above a certain threshold can be used.
2. The correction is based on a uniform rotation of the

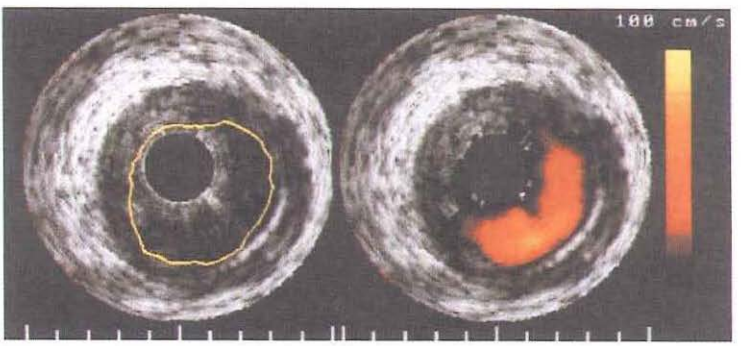

Fig. 5. IVUS flow image (right) and automated detected boundary from flow (left) obtained with an array catheter. Note that the resolution of the image is limited because no SAFT was used [18].

element. If this is not the case the results may be biased.

For these reasons the methods are currently evaluated on a phased array system. The tip of the catheter consists of 64 static elements. The image is constructed using synthetic aperture focusing techniques (SAFT) [23]. This is based on sequential excitation and receiving of individual elements. For the reconstruction it is essential that the imaged object does not move during the acquisition time. For blood flow estimation this mode is not suitable. The array needs to be operated in linear array mode. This means that a number of elements are excited simultaneously and the same elements are used for receiving. The influence of the number of elements that need to be used for this has been studied extensively [24] (Fig. 4). If the number is too low, the resolution is poor and the ultrasound energy will be concentrated close to the transducer. If the number is too high the ultrasound beam will split. This is because, due to the curvature of the surface, the far field of the transducer can never be reached. For the 64-element catheter, an optimal number would be four or five elements. Another aspect is the shape of the decorrelation curve of the array system in linear array mode. For the near field of the single element transducer it had proven to be close to linear [15], but for the array transducer this is not necessarily the case. Computer modeling has shown that for four elements the decorrelation at varying distance is fairly linear, although a different calibration has to be performed at different distances to the transducer [25,26]. It seems that, in principle, the array is suited for flow estimation. Currently it is evaluated in the catheterization laboratory (Fig. 5) [20].

3.3. Automated boundary detection

Because the flow usually has a higher velocity than wall motion, blood echo signals decorrelate significantly faster than those of tissues. The different correlation time in the received RF signals between blood and tissue has been documented in vivo in our earlier studies [27]. The time in which the blood RF signals maintain a correlation above 0.2 is less than 1 ms, which is significantly shorter than that measured in wall echoes ($\gg$6 ms). In this way the regions that are potentially identified as blood are distinguished from those that are potentially identified as vascular wall. After this, additional image filtering is applied [4]. The result of this automated detection of the arterial lumen boundary based on RF processing techniques is illustrated in Fig. 5.

Other methods of assessing the flow area have recently been described [28–30]. Although not capable of quantitative flow measurement, these are very capable of detecting areas with or without flow, making them well suited for guidance of stent placement [31].

4. Conclusions

A method has been developed and tested for quantitative flow estimation using an IVUS imaging catheter. This method is currently under development for a phased array system. A useful spin-off is the possibility for automated boundary detection.

Acknowledgements

This project was financially supported by The Dutch Technology Foundation (STW), NWO, Bekales and Vesale Foundation. The support of J.J. Wentzel, R. Krams, J. Honkoop and P. Segers, University of Gent is highly appreciated.

References

[1] J. Baptista, C. Di Mario, Y. Ozaki, J. Escaned, R. Gil, P.J. de Feyter, J.R.T.C. Roelandt, P.W. Serruys, Impact of plaque morphology and composition on the mechanisms of lumen enlargement using intracoronary ultrasound and quantitative angiography after balloon angioplasty, Am. J. Cardiol. 77 (1996) 115–121.

[2] G.S. Mintz, J.J. Popma, K.M. Kent, L.F. Satler, S.C. Wong, M.K. Hong, J.A. Kovach, M.B. Leon, Arterial remodeling after coronary angioplasty. A serial intravascular ultrasound study, Circulation 94 (1996) 35–43.

[3] N. Bom, W. Li, A.F.W. van der Steen, C.T. Lancée, E.I. Céspedes, C.J. Slager, C.L. de Korte, Novel developments in intravascular imaging, Euro. J. Ultrasound 7 (1998) 9–14.

[4] A.F.W. van der Steen, E. Céspedes, C. de Korte, S.G. Carlier, W. Li, F. Mastik, C. Lancée, J. Borsboom, F. Lupotti, R. Krams, P. Serruys, N. Bom, Novel developments in intravascular imaging, In: IEEE Ultrasonics Symposium (1998) 1733–1742.

[5] T. Spencer, M.P. Ramo, D.M. Salter, T. Anderson, P.P. Kearney, G.R. Sutherland, K.A.A. Fox, W.N. McDicken, Assessment of regional vascular distensibility in deceased iliofemoral arteries by intravascular ultrasound, Ultrasound Med. Biol. 20 (1997) 529–542.

[6] S.L. Bridal, P. Fornes, P. Bruneval, G. Berger, Parametric (integrated backscatter and attenuation) images constructed using backscattered radio frequency signals (25–56 MHz) from human aortae in vitro, Ultrasound Med. Biol. 23 (1997) 215–229.

[7] C.L. de Korte, A.F.W. van der Steen, E.I. Céspedes, G. Pasterkamp, Intravascular ultrasound elastography of human arteries: initial experience in vitro, Ultrasound Med. Biol. 24 (1998) 401–408.

[8] C.L. de Korte, Intravascular ultrasound elastography, PhD Thesis, Erasmus University, Rotterdam, 1999.

[9] E.I. Céspedes, C.L. de Korte, A.F.W. van der Steen, Intravascular ultrasonic palpation: assessment of local wall compliance, in: IEEE Ultrasonics Symposium (1997) 1079–1082.

[10] A.F.W. van der Steen, C.L. de Korte, E.I. Céspedes, Intravascular ultrasound elastography, Ultraschal Med. 19 (1998) 196–201.

[11] J.W. Doucette, P.D. Corl, H.M. Payne, A.E. Flynn, M. Goto, M. Nassi, J. Segal, Validation of a Doppler guide wire for intravascular measurements of coronary artery flow velocity, Circulation 85 (1992) 1899–1911.

[12] C. Di Mario, S.H.K. The, S. Madrestma, R.J.v. Suylen, R.A. Wilson, N. Bom, P.W. Serruys, E.J. Gussenhoven, J.R.T.C. Roe-

landt, Detection and characterization of vascular lesions by intravascular ultrasound: and in vitro study correlated with histology, J. Am. Soc. Echocardiogr. 5 (1992) 135–146.
[13] T.M. Chou, K. Sudhir, S. Iwanaga, K. Chatterjee, P.G. Yock, Measurement of volumetric coronary blood flow by simultaneous intravascular two-dimensional and Doppler ultrasound: validation in an animal model, Am. Heart J. 128 (1994) 237–243.
[14] J.M. Isner, J. Kaufman, K. Rosenfield, A. Pieczek, R. Schainfeld, K. Ramaswamy, B.D. Kosowsky, Combined physiologic and anatomic assessment of percutaneous revascularization using a Doppler guidewire and ultrasound catheter, Am. J. Cardiol. 71 (1993) 70D–86D.
[15] W. Li, C.T. Lancée, E.I. Céspedes, A.F.W. van der Steen, N. Bom, Decorrelation properties of intravascular echo signals, J. Acoust. Soc. Am. 102 (1998) 3785–3794.
[16] W. Li, A.F.W. van der Steen, C.T. Lancée, E.I. Céspedes, N. Bom, Blood flow imaging and volume flow quantitation with intravascular ultrasound, Ultrasound Med. Biol. 24 (1998) 203–214.
[17] E.I. Céspedes, S.G. Carlier, W. Li, F. Mastik, A.F.W. van der Steen, N. Bom, P.D. Verdouw, P.W. Serruys, Blood flow assessment using a mechanical intravascular ultrasound catheter: initial evaluation in vivo, J. Vasc. Invest. 4 (1998) 39–44.
[18] A.F.W. van der Steen, W. Li, E.I. Céspedes, S. Carlier, M. Eberle, P.D. Verdouw, P.W. Serruys, N. Bom, In vivo validation of blood flow estimation using the decorrelation of radiofrequency intravascular echo signals, in: IEEE Ultrasonics Symposium (1997) 1247–1250.
[19] S.G. Carlier, W. Li, I. Céspedes, A.F. van der Steen, J.N. Hamburger, N. Bom, P.W. Serruys, Images in cardiovascular medicine. Simultaneous morphological and functional assessment of a renal artery stent intervention with intravascular ultrasound, Circulation 97 (1998) 2575–2576.
[20] S.G. Carlier, E.I. Céspedes, W. Li, F. Mastik, A.F.W. van der Steen, N. Bom, P.W. Serruys, Blood flow assessment using IVUS, Cardiovasc. Intervent. Online 2 (1998) 22–24.
[21] J.J. Wentzel, R. Krams, A.F.W. van der Steen, W. Li, E.I. Céspedes, N. Bom, C.J. Slager, Disturbance of 3D velocity profiles induced by an IVUS catheter: evaluation with computational fluid dynamics, Comput. Cardiol. 24 (1997) 597–600.
[22] R. Krams, J. Wentzel, E.I. Céspedes, R. Vinke, S.G. Carleir, A.F.W. van der Steen, C.T. Lancée, C.J. Slager, Effect of catheter placement on 3D velocity profiles in curved tubes, Ultrasound Med. Biol. 25 (1999) 803–810.
[23] M. O'Donnell, M.J. Eberle, D.N. Stephens, J.L. Litzza, K. San Vicente, B.M. Shapo, Synthetic phased arrays for intraluminal imaging of coronary arteries, IEEE Trans. Ultrason., Ferroelect., Freq. Control 44 (1997) 714–721.
[24] J.M.G. Borsboom, E.I. Céspedes, A.F.W. van der Steen, C.T. Lancée, E. Deprettere, Simulation of circular array ultrasound transducers for intravascular applications, J. Acoust. Soc. Am. (1999) in press.
[25] F. Lupotti, E.I. Céspedes, A.F.W. van der Steen, Decorrelation characteristics of transverse blood flow along an intravascular array catheter, IEEE Trans. Ultrason. Ferroelect. Freq. Control, in press.
[26] F. Lupotti, E.I. Céspedes, A.F.W. van der Steen, Influence of red blood cell aggregation on decorrelation characteristics of transverse blood flow, in preparation.
[27] W. Li, A.F.W. van der Steen, C.T. Lancée, Temporal correlation of blood scattering signals in vivo from radio frequency intravascular ultrasound, Ultrasound Med. Biol. 22 (1996) 583–590.
[28] E.I. Céspedes, W. Li, F. Mastik, A.F.W. van der Steen, S. Carlier, R.H. van Bremen, M. Eberle, N. Bom, Intravascular power flow imaging: theory and potentials for planimetry, in: IEEE Ultrasonics Symposium (1997) 1273–1276.
[29] J.R. Crowe, B.M. Shapo, D.N. Stephens, D. Bleam, M.J. Eberle, C.C. Wu, D.W.M. Muller, J.A. Kovatch, R.J. Lederman, M. O'Donnell, Coronary artery flow imaging with an intraluminal array. In: IEEE Ultrasonics Symposium (1996) 1481–1484.
[30] M. O'Donnell, M.J. Eberle, D.N. Stephens et al., Catheter arrays: can intravascular ultrasound make a difference in managing coronary artery disease, In: IEEE Ultrasonics Symposium (1997) 1447–1456.
[31] E.I. Céspedes, S. Carlier, M. Sabate, J. Ligthart, P.W. Serruys, N. Bom, Angiographically undetected stent mal-apposition resolved by intravascular ultrasound and flow imaging, J. Vasc. Invest. 4 (1998) 81–84.

Chapter 7a

Preliminary clinical experience:

Blood flow assessment with intravascular ultrasound catheters: the ideal tool for simultaneous assessment of the coronary haemodynamics and vessel wall?

SG **Carlier**, EI Cespedes, W Li, F Mastik, AFW van der Steen, N Bom, PW Serruys.

Seminars in Interventional Cardiology 1998; 3:21-9.

Semin Intervent Cardiol 1998; 3: 21–29

Blood flow assessment with intravascular ultrasound catheters: the ideal tool for simultaneous assessment of the coronary haemodynamics and vessel wall?

S. G Carlier*, E. I. Cespedes†, W Li*,‡, F. Mastik*, A. F. W. Van Der Steen*,‡, N. Bom*,‡ & P. W. Serruys*,‡

**Erasmus University Rotterdam, Thoraxcentre, The Netherlands; †EndoSonics Corp., Rancho Cordova, CA, USA; ‡Interuniversity Cardiology Institute of The Netherlands*

We present the potentials of a novel method of intracoronary flow visualization and quantification that is based on conventional intravascular ultrasound (IVUS) imaging catheters. The quantification of flow is obtained from analysis of the rate of decorrelation of digitized radiofrequency ultrasound echo signals. Flow information is superimposed on the IVUS image using a colour scale. Integration of the blood velocity components normal to the scan plane permits calculation of the volume flow. Validation using IVUS and electromagnetic (EM) flowmeter recordings were obtained *in vivo* from instrumented pigs. IVUS flow ($IVUS_f$) compared favourably to EM flow (EM_f): $IVUS_f=1.0\ EM_f+5.72$ cc/min, $r^2=0.98$. Clinical results for the first five patients investigated are reported. A Doppler wire was used to measure the flow in four coronary arteries and one renal artery in baseline and hyperaemia conditions. IVUS flow and derived coronary flow reserve (CFR) demonstrated a very good agreement with the data derived from the combination of quantitative angiography and velocity when measured with the Doppler wire (DOP_f): $IVUS_f=1.01\ DOP_f-20$ cc/min, $r^2=0.90$ and $IVUS_{cfr}=1.03\ DOP_{cfr}-0.03$, $r^2=0.93$. This demonstrates that simultaneous morphological and physiological assessment of coronary or peripheral arteries with one IVUS catheter is feasible. This method should be very useful for the evaluation of intermediate coronary stenoses or the results of revascularization procedures.

Key words: coronary flow, intravascular ultrasound, radiofrequency signal

Introduction

The limitations of quantitative coronary arteriography (QCA) for the physiological assessment of intermediate coronary lesions in unselected patients with extensive coronary atherosclerosis have been recognized [1, 2]. The haziness of the borders of the vessel after PTCA also limits the use of QCA for the assessment of the acute results of an intervention. Intravascular ultrasound (IVUS) assessment allows for a better characterization of the vessel wall morphology and of the atherosclerotic plaque and for a direct assessment of the arterial remodelling process, which cannot be seen on the luminograms obtained with conventional angiography [3–5]. Although IVUS has already revolutionized the visualization of atherosclerotic disease and of the restenotic process, the benefit in clinical outcome remains under evaluation in ongoing trials. However, IVUS is simply another, albeit improved, tool to assess a lesion morphology, and does not permit a precise evaluation of the physiological importance of a coronary stenosis [6]. Conversely, intracoronary velocity and pressure measurements, derived from miniaturized Doppler or pressure sensors mounted on 0.014-inch wires, permit the evaluation of physiological parameters like the coronary flow reserve (CFR). The agreement of these measurements with non-invasive scintigraphic or echocardiographic stress tests is very good, and has been extensively reported [7–10]. It has recently been demonstrated that the association of a CFR>2.5 and a residual diameter stenosis <35% after PTCA is a prognostic factor for the recurrence of symptoms and for the restenosis rate [11]. The safety of not performing

Correspondence: S. G. Carlier, Thoraxcentre, Experimental Echocardiography Ee2302, Erasmus University, PO Box 1730, 3000 DR, Rotterdam, The Netherlands.

1084-2764/98/010021+09 $12.00/0

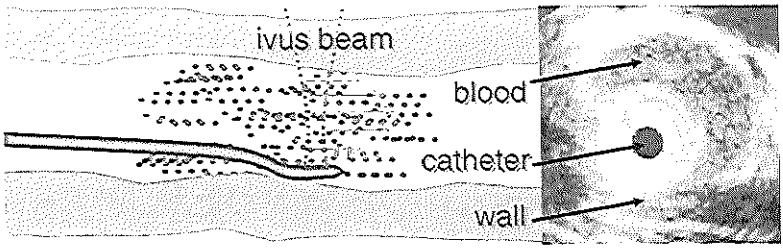

Figure 1. Schematic representation of the IVUS catheter in a coronary artery showing the flowing red blood cells crossing the ultrasound imaging plane, together with a representative IVUS image.

an angioplasty for intermediate stenosis without a functional significant severity assessed by flow or pressure measurements has also been demonstrated [12, 13]. Intracoronary physiologic assessments of coronary lesions and interventions appear more and more to complement coronary lumenology and morphology assessments obtained with angiography and IVUS [14].

The possibility to obtain quantitative flow information using an IVUS catheter has recently been investigated in our laboratory. This approach could be the ideal one allowing simultaneous morphological and physiological assessments of coronary arteries in the catheterization laboratory. Blood flow quantification is based on the measurement of changes in the received radiofrequency (rf) IVUS signal as red blood cells transverse the ultrasound scan plane [15–17].

Principle of flow estimation based on the decorrelation approach

In essence, this approach quantifies changes in the rf echo signals that result from flow of red blood cells, the predominant scatterers in blood, through the ultrasound beam (Fig. 1). This approach is totally different from velocity estimation based on the Doppler effect, where the ultrasound beam and the flowing red blood cells must be optimally aligned. The details of the technique have been previously reported [17–19]. The underlying hypothesis is that the rate of rf signal decorrelation is related to flow velocity: for a given ultrasound beam, the faster blood particles move across the imaging plane, the higher the decorrelation rate of the received rf signals. This hypothesis was tested by computer simulation and in an *in vitro* experimental set-up where the echo correlation of a blood mimicking phantom was measured at various flow velocities. The relationship between echo decorrelation and flow velocity observed was approximately linear, suggesting that if the velocity–correlation relation is pre-quantified for the type of transducers used, the measured decorrelation value from blood scattering signals can be converted into flow velocity. Since blood moves relative to the stationary vessel wall, automatic discrimination of the area of flow and quantification of flow velocity is feasible based on echo signal analysis.

We modified the triggering mode of an available IVUS scanner in order to obtain images comparable to those of conventional echographic M-mode scanning, the same position in space being sampled successively by consecutive ultrasound bursts. We obtained the velocity measurements for the corresponding angular position of the beam. The calculation of flow involves the estimation of echo decorrelation after removal of echo shifts along the direction of the ultrasound beam. This separation procedure isolates axial (along the beam axis) and transverse (across the scan plane) velocity components. The procedure is performed in small rf signal windows and repeated for all angular positions of the beam. Velocity estimates are superimposed on the conventional IVUS image using a colour scale. The resulting colour flow images can be displayed by video animation.

A representative IVUS image with the corresponding M-mode acquired at one angular position are shown in Fig. 2. Note in the M-mode that the echo signal undergoes little change in the arterial wall (W), since tissue is relatively static. However, the echoes from blood change within the M-mode and particularly toward the centre of the lumen, between the catheter (C) and the wall. Quantification of these changes in small regions of interest is used to estimate local blood velocity. Integration of the spatial blood velocity distribution over the entire lumen yields the volume flow; that is, the volume of blood crossing the image plane per unit of time. Because the lateral motion of wall tissues has a much lower velocity than blood, this contribution can be automatically removed by setting a threshold. Thus, no contour tracing of the arterial lumen is needed.

The RF acquisition set-up

Radiofrequency echo signals were obtained in each experiment using 4.1 French (1.36 mm diameter), 30 MHz center frequency Princeps™ IVUS catheters (EndoSonics/Du-Med, Rijswijk, The Netherlands)

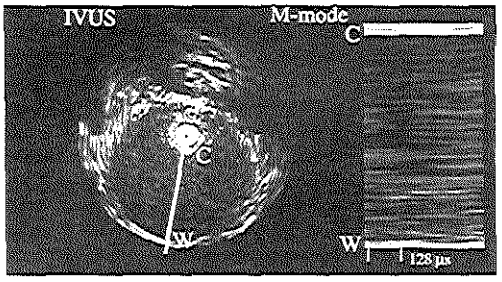

Figure 2. At one angular position, successive radiofrequency (rf) signals are acquired for correlation analysis. On the calculated M-mode, the decorrelation rate can be estimated: nearly constant echoes are found in the vessel wall (W). The calculated correlation values between rf pairs will be high in this region, with a corresponding slow decorrelation rate along time. On the contrary, rapid changes are observed in the lumen, mainly in its centre, corresponding to the rapidly flowing red blood cells. At that level, there will be a low correlation between successive rf traces, and an high decorrelation rate along time. The position of the catheter is marked by C.

driven by a modified EndoSonics/Du-Med scanner. We obtained 1000 rf echo lines per revolution, at a frame rate of 16 s^{-1} and M-mode pulse repetition frequency of 15.6 kHz, with a corresponding pulse repetition interval of 64 µs. The rf signals were digitized at 200 MHz and 8 bits, using a Signatec PC board (Signatec, Corona, CA, USA), and stored in computer memory for off-line processing of flow with subsequent animation of the flow image frames. The memory capacity of the acquisition system permits recording of a total of 3.75 s of rf data at 100 angles per revolution. The system is also capable of simultaneous digitization of the signal from an electromagnetic flowmeter or other low-frequency signal sources (ECG, blood pressure, etc).

Flow velocity was measured using the described principle. The axial velocity component was removed by aligning the rf traces before calculation of decorrelation as well as the decorrelation component due to beam rotation related to the mechanical transducer, giving only a pseudo-M mode. Decorrelation estimation was performed on data windows (40 samples long) with 50% overlap corresponding to an axial resolution of 0.19 mm. A temporal median filter was used to reduce the number of spurious flow estimates.

Animal validation experiment

Mean and phasic measurements of carotid flow were measured *in vivo* in two 30–35 kg Yorkshire pigs [20]. The experimental procedure was approved by the Committee on Animal Experiments of the Erasmus University Rotterdam. Following overnight fasting, the pigs were sedated and subsequently intubated and mechanically ventilated. Under sterile conditions, the left femoral artery and vein were cannulated for infusion of drugs and blood pressure monitoring. A pacemaker lead was advanced to the right atrium via a jugular vein. An electromagnetic (EM) flow probe was fitted on the contralateral, exposed common carotid artery and adequately calibrated. A 9-F guiding catheter was advanced under fluoroscopy up to this carotid artery. A sterile IVUS catheter was advanced into it to the common carotid artery under fluoroscopic guidance and positioned 5 cm proximal to the EM probe. The distance corresponds approximately to 11 radii of the artery, allowing near laminar flow at the location of the EM probe. Data from the EM flowmeter was digitized synchronously with the RF echo signals. Zatebradine (UL-FS 49) 0.5 mg/kg was given to produce complete AV block, and the pacemaker was set to approximately 60 bpm. In order to induce high-(hyperaemic) and low-flow conditions, adenosine (0.5 mg.kg/min, i.v.) and ergotamine (20 µg/kg) were infused, respectively.

Preliminary clinical experience

We studied five patients referred for percutaneous coronary intervention with stable angina pectoris related to a single vessel lesion ($n=4$) or with medically-uncontrolled hypertension related to an ostial lesion of the right renal artery ($n=1$). All the patients signed an informed consent.

After intravenous administration of 10 000 IU heparin and 250 mg acetylsalicylic acid, an 8-F guiding catheter was advanced up to the ostium of the artery to be studied. After the intervention, a Doppler guidewire (Flowire™, Cardiometrics Inc.) was positioned into the mid-segment of the vessel. After coronary injection of a bolus of 3 mg isosorbide dinitrate, the Princeps™ IVUS catheter was advanced on this wire. The imaging transducer was positioned approximately 5 cm proximal to the tip of the Doppler wire, to allow recovery of a fully developed velocity profile at the site of the Doppler measurement. Simultaneous Doppler and IVUS flow measurements were performed in baseline condition and during hyperaemia produced by an intravenous infusion of adenosine (140 µg/kg/min) to evaluate the coronary flow reserve (CFR).

A cineangiogram was performed in two orthogonal views, in order to estimate the lumen cross-sectional area at the measurement site of the Doppler. The guiding catheter, filmed devoid of contrast medium, was used as a scaling device. A previously validated analysis system (CAAS II, Pie Medical) was used for the quantitative coronary analysis (QCA). The two measured diameters, 5 mm down the Doppler tip, were averaged to compute a mean cross-sectional area at the level of the velocity measurements. The Doppler derived flow was computed as the product of the cross-sectional area and the average peak Doppler velocity (APV).

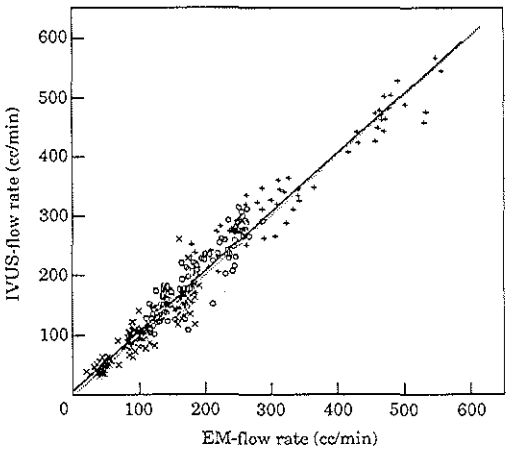

Figure 3. Scatter plot of IVUS and EM flow measurements in the validation study realized in the porcine carotid model, for the low (x), normal (o) and high flow (+) conditions. $IVUS_f = 1.0\ EM_f + 5.7$; SEE = 25.2 cc/min; $r^2 = 0.98$.

Results

Figure 3 shows a scatter plot of EM vs IVUS phasic flow measurements for five recordings in the pig model. One hyperaemic response was discarded because the EM probe lost contact with the artery due to vasospasm. Overall, the instantaneous volume flow ranged from 20 to 557 cc/min. Each recording corresponded to 3–4 heart cycles. The overall mean values of the EM and IVUS measurements were 175.8 and 181.7 cc/min, respectively. The mean cross-sectional velocities ranged from 3 to 79 cm/s. The mean vessel diameter was 4.3 mm with IVUS. As shown in the scatter plot, IVUS and EM flow measurements were in good agreement for low-, basal- and high-flow conditions. The linear regression equation relating IVUS to EM flow was $IVUS_f = 1.0\ EM_f + 5.72$ cc/min, $r^2 = 0.98$ ($p < 0.0001$) and the standard error of the estimate (SEE) was 25.2 cc/min.

No complications related to the IVUS flow measurement were seen in our patients. Figure 4 illustrates the recording after a stent implantation at the ostium of a renal artery [21]. Three IVUS frames (1, end systole; 2, diastole; and 3, peak systole) demonstrate the change in the colour velocity mapping corresponding to the change in the measured flow, with a maximum flow at peak systole. The corresponding flow measured for all the successive IVUS frames is plotted below, together with the derived area, and the simultaneously-recorded blood pressure, ECG and Doppler instantaneous peak velocity. A very good phasic response of the IVUS flow can be appreciated. The mean flow in this recording was 214 cc/min. The recording obtained with the Doppler wire appears at the bottom right of Figure 4, with an average peak velocity (APV) of 28 cm/s. The area at the level of the Doppler recording was 11.2 mm^2 (derived from the diameters measured in two orthogonal angiographic views by QCA). The Doppler derived flow was 28 cm/s $\times$ 0.112 $cm^2 \times 60 = 188\ cm^3$/min.

Figure 5 illustrates the assessment of the coronary flow reserve in a right coronary artery. The difference between the lower flow at end-diastole (on the left) and the mid-diastole (on the right) is well appreciated with the mapping of the velocities in the arterial lumen. This recording was obtained during hyperaemia (adenosine 140 μg/kg/min). The IVUS derived flow was 148 cc/min. In baseline condition, the IVUS flow (not illustrated) was 48 cc/min, giving a coronary flow reserve of 3.1. The corresponding Doppler recording is on the bottom right of the figure, baseline APV was 11 cm.s and during hyperaemia APV reached 30 cm/s. The Doppler derived coronary flow reserve was 2.8.

For the first five patients investigated, there was a linear correlation between the IVUS derived and Doppler derived flow (average of two measurements of each whenever possible): $IVUS_f = 1.01\ Dop_f - 20$, $r^2 = 0.90$. The mean difference between the two flow estimations following Bland-Altman was 19 ± 29 cc/min, for a mean flow of 113 cc/min, ranging from 30–305 cc/min (in one patient, the IVUS flow was assessed in two positions, once in the left main artery). There was also a linear correlation between IVUS and Doppler-derived coronary flow reserve: $IVUS_{cfr} = 1.03\ Dop_{cfr} - 0.03$, $r^2 = 0.93$. The agreement between the two methods was very good, with a mean difference between the CFR estimations of -0.01 ± 0.21, for a mean CFR of 1.9, ranging from 1.3–3.2. The mean vessel diameter measured by QCA at the level of the Doppler tip was 3.3 ± 0.7 mm.

Discussion

We have evaluated a technique for velocity imaging and volume flow quantification and demonstrated applicability in the catheterization laboratory. The quantification capabilities of the decorrelation approach were validated *in vivo* by comparison of the results to simultaneous readings from an electromagnetic flowmeter, the gold standard in flow assessment. Preliminary clinical data demonstrated the feasibility of this method and a good agreement with flow estimated by the combination of intracoronary Doppler and quantitative angiography.

In the current implementation, rotation of the ultrasound beam during acquisition of the M-mode introduces an undesired source of motion and gives only a pseudo-M mode recording. Additionally, the variability of this rotation exacerbates the problems, further limiting the ability to reliably measure low-flow velocities. In mechanical IVUS, such unavoidable velocity non-uniformity in the rotation of the driving shaft is a result of the typically tortuous path followed by the catheter inside the arterial tree [22]. An improved

implementation of our flow measurement technique, based on array-catheter technology that permits electronically scanned M-mode operation, is currently being implemented [23]. Electronically-steered array transducers for IVUS offer the ideal scanning configuration for flow measurements, since the ultrasound beam is static during acquisition of a rf true M-mode.

A number of limitations of the technique are currently being addressed. One is the influence of the catheter itself on the flow: the Princeps catheter used is a 4.1-F device. This corresponds to a diameter of 1.36 mm and a cross-sectional area of 1.45 mm^2. In a proximal coronary artery with a diameter of 3.5 mm, the catheter occupies approximately 10% of the lumen area, and should not increase the resistance of this epicardial segment. On the contrary, once advanced more distally, e.g. across a 50% diameter stenosis, two potential problems arise: (i) the friction of blood along a longer portion of the catheter; and (ii) in the stenosis, the catheter occupies 55% of the free lumen area. There will be limitation of the flow, mainly in hyperaemia. However, this problem could be overcome in the future with the development of a smaller catheter. This trend is observed with the newly developed IVUS devices. The smallest systems available today are imaging core wires which can even be advanced in the free lumen of balloons [24].

The presence of the catheter in a curved artery creates secondary flow components that are in the imaging plane. This contributes to the decorrelation rate among successively-recorded rf traces, but does not participate in any net flow across the imaging plane in the artery. Preliminary simulations by finite element modelling in our laboratory have shown that the relative proportion of theses recirculating flows is in the order of 1% [25]. The presence of turbulence is another limiting factor, because it also induces a significant decorrelation rate of the rf signals. In proximal coronary segments, no significant turbulence has been observed in an idealized set-up [26]. Depending on the flow and the shear rate, the effect of red blood cell aggregation could also potentially modify the backscattering properties and the decorrelation rate as a function of flow [27, 28]. This issue is currently under evaluation in our laboratory by numerical simulation.

In the catheterization laboratory, there is no true gold standard for the invasive assessment of coronary blood flow. Doppler velocimetry with miniaturized wires has emerged, but there are two crucial steps required to accurately calculate absolute volume: (1) the calculation of the mean blood flow velocity in a given vascular cross-section; (2) the accurate measurement of this cross-sectional area [29].

(1) The ultrasound beam must be optimally aligned parallel with the centerline of flow, and the entire flow profile or at least a significant proportion that includes the maximal velocity must be insonified. Moreover, the physical presence of the Doppler probe should not modify the velocity profile at the site of the Doppler sample volume. During our recordings, care was taken to have a distance of approximately 5 cm between the tip of the IVUS catheter and the Doppler crystal. The Doppler sample was 5 mm beyond the tip of the Doppler wire. This permits recovery of the velocity profile [30]. According to the Poiseuille equation, when considering a parabolic flow profile, the mean velocity is the maximal velocity (V_{max}) divided by two [29]. But the non-Newtonian characteristics of blood and the pulsatility of the flow induce a blunted velocity profile, so that the mean blood flow velocity may be underestimated by $V_{max}/2$ [26, 31, 32]. Nevertheless, validation studies have shown a high correlation both *in vitro* and *in vivo* between volumetric flow measured with an electromagnetic flowmeter [33] or with a transit-time ultrasound flowmeter [34] and flow derived from Doppler measurements using $V_{max}/2$. Conversely, other *in vitro* and *in vivo* data using a 3-F Doppler system (Millar) or the Doppler Flowire also demonstrated a very good correlation between the flow calculated as cross-sectional area $\times$ V_{max} and the measured reference [35–38]. Since, in most of the recordings in human coronary arteries, the assumption of a parabolic velocity profile is rarely encountered, no definitive value can be defined and we used simply V_{max}. In most clinical situations, it is the ratio of the hyperaemic flow over the baseline flow that is clinically relevant to estimate the coronary flow reserve. In that case, CFR assessment could be considered insensitive to a velocity profile that may be assumed constant.

(2) A high-quality angiogram, suitable for measurements of the cross-section at the site of the Doppler sample volume, must be performed. It must be noted, however, that more accurate measurements are obtained when the probe is positioned in an arterial segment of uniform caliber, so that a mean cross-sectional area over a short arterial segment immediately distal to the Doppler probe can be obtained. However, any error in the diameter measurement will be squared in the cross-sectional area estimate. Moreover, QCA is performed on an end-diastolic frame and the variation of the coronary diameter during cardiac contraction is ignored. An alternative method is the combination of intracoronary Doppler and IVUS. The approach was first described by the sequential use of a 3-F Doppler catheter followed by an IVUS catheter [37, 39]. The introduction of the Doppler guidewire permitted easier simultaneous assessments with the IVUS catheter advanced over the Doppler wire [34]. We did not use the IVUS cross-sectional area, because a long distance between the IVUS plane and the Doppler measurement is present with the Princeps catheter we used. Indeed, there is a rather long distal monorail system separating the imaging crystal from the tip of the catheter ($\sim$35 mm) and

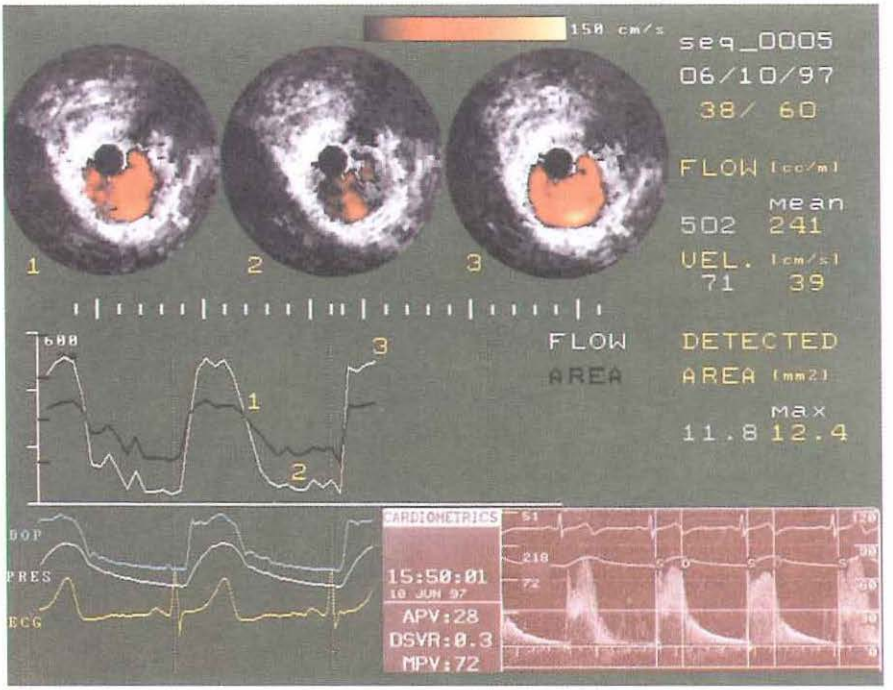

Figure 4

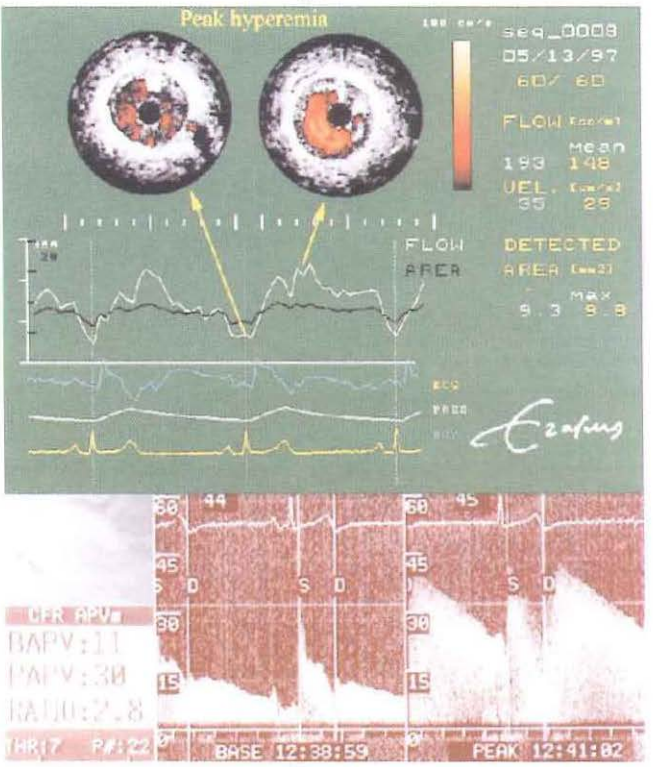

Figure 5

an additional distance was required to avoid turbulence downstream of the IVUS catheter in the Doppler sampling region (5–6 × the catheter diameter [40]). For the same reason, it was crucial to perform our recordings in long segments without major side branches. An alternative, when flow in the left main artery was evaluated, was to first perform Doppler and QCA measurements, and then advance the IVUS and record the rf signals.

As reflected by our data, the Doppler measurements were perhaps not the most robust gold standard for the clinical evaluation of our method, in comparison to the measurements obtained in the porcine validation experiments. Nevertheless, the limitations related to the unknown velocity profile and the exact cross-sectional area at the Doppler tip are simplified when computing the coronary flow reserve. We observed a good correlation (close to identity) and a very good agreement between the IVUS and Doppler derived CFR.

One of the advantages of our IVUS flow method is the reduction in the number of intracoronary devices introduced. The results of coronary interventions could be ideally monitored, and this approach could be more cost-effective, offering simultaneous information on both the selection of balloon or stent size pre-intervention, and concerning optimization of the morphological and functional results. Evaluation of the significance of intermediate lesions may also be possible, as well as the assessment of endothelial function and arterial distensibility. Presently, most of these studies have used QCA and/or intracoronary Doppler during administration of acetylcholine (AcCh) [41–43]. As a consequence of its higher resolution, IVUS has been used to measure changes in cross-sectional area during similar pharmacologic challenges [44]. At the same time, the visualization of atherosclerotic lesions not visible on angiography allows for a better understanding of the response to the AcCh infusion [45]. The assessment of the contribution of different mediators, such as nitric oxide or endothelin, have been studied in complex protocols with simultaneous intracoronary IVUS and Doppler recordings during specific infusion of inhibitors and/or precursors [46, 47]. We believe that our simultaneous capabilities to assess flow and lumen area would constitute the ideal tool for such studies of coronary haemodynamics and vessel wall.

Presently, IVUS flow is not obtained on-line: 3.75 s of acquisition represents 128 Mbytes of data in the computer memory that are first stored on the hard disk in ~90 s and then processed in ~3 min, thanks to a newly implemented algorithm [48]. It is expected that with the increasing speed and power of new computers, processing time will go down. Implementation of a digital signal processing board for on-line performance is currently under study.

Finally, even in the cases in which the true flow is being impeded with the IVUS catheter in a narrow artery, a semi-quantitative assessment associated to colour-flow imaging could improve visualization of plaque dissections, false lumens, automated lumen area quantification or detection of improperly expanded stents, as recently reported [49, 50]. With conventional IVUS, detection of plaque fractures and dissections remains challenging: frequent saline flushes are often required.

Conclusion

Auxiliary use of echo signals available from conventional imaging IVUS catheters can provide blood flow information in addition to the structural information depicted by the echo image. Morphological and physiological information may be simultaneously obtained with a single ultrasound catheter. Notwithstanding the preliminary nature of these developments, we have demonstrated the potential of IVUS flowmetry for sufficient accuracy and reproducibility to warrant clinical applicability. Preliminary clinical data have demonstrated the feasibility of the technique in the catheterization laboratory.

Acknowledgements

The authors wish to thank the patient assistance of Rob van Bremen, Jan van Meegen and the personnel of the animal and catheterization laboratories of the Thoraxcenter. We gratefully acknowledge the fundamental technical assistance of Jan Honkoop and the careful review assistance of Dr M. J. B. Kutryk. This project was supported by the Dutch Technology Foundation (RGN44.3462), the Vésale Foundation, and the Bekales Foundation.

Figure 4. Recording performed in a renal artery after ostial stent implantation. Three representative IVUS frames (1–3) during one cardiac cycle are depicted with a colour mapping of the intraluminal blood velocity. High velocities (yellow) at peak systole (3) are clearly seen in the centre of the lumen. The IVUS flow calculated on all the consecutive frames (16/s) is plotted in white, together with the simultaneously acquired ECG, blood pressure and instantaneous peak velocity measured with a Doppler wire. The mean IVUS flow was 241 cc/min. The recorded Doppler signal is shown in the bottom right. The average peak Doppler velocity (APV) was 28 cm/s. By quantitative angiography, the cross-sectional lumen area at the Doppler tip was 11.2 mm^2. Doppler derived flow was 188 cm^3/min.

Figure 5. Volumetric blood flow measurement in a right coronary artery. Top right frame shows, during hyperaemia, mid-diastole high flow. On the top left, the decrease of coronary flow at end diastole is well visualized. The calculated IVUS flow on the 60 consecutively-acquired IVUS frames is plotted together with ECG, pressure and Doppler data as in Figure 4. The corresponding Doppler spectrum is shown at the bottom right. The Doppler average peak velocity was 30 cm/s. The coronary cross-sectional area measured with quantitative coronary angiography at the level of the tip of the Doppler wire was 7.42 mm^2. The Doppler derived mean coronary blood flow (134 cc/min) is in agreement with the mean flow measured with the IVUS RF processing (148 cc/min). The coronary flow reserve derived from the IVUS method was 3 (baseline flow, not illustrated, was 48 cc/min), close to the Doppler estimation: 2.8 (lower left corner).

References

1 Legrand V, Mancini G, Bates E, Hodgson J, Gross M, Vogel R. Comparative study of coronary flow reserve, coronary anatomy and results of radionuclide exercise tests in patients with coronary artery disease. *J Am Coll Cardiol* 1986; **8**: 1022–1032.

2 Miller D, Donohue T, Younis L, Bach R, Aguirre F, Wittry M, Goodgold H, Chaitman B, Kern M. Correlation of pharmacological 99mTc-sestamibi myocardial perfusion imaging with poststenotic coronary flow reserve in patients with angiographically intermediate coronary artery stenoses. *Circulation* 1994; **89**: 2150–2160.

3 Di Mario C, Gorge G, Peters R, Kearney P, Pinto F, Hausmann D, von Birgelen C, Colombo A, Mudra H, Roelandt J, Erbel R. Clinical application and image interpretation in intracoronary ultrasound. Study Group on Intracoronary Imaging of the Working Group of Coronary Circulation and the Subgroup on Intravascular Ultrasound of the Working of Echocardiography of the European Society of Cardiology. *Eur Heart J* 1998; **19**: 207–209.

4 Kimura T, Kaburagi S, Tamura T, Yokoi H, Nakagawa Y, Hamasaki N, Nosaka H, Nobuyoshi M, Mintz GS, Popma JJ, Leon MB. Remodelling of human coronary arteries undergoing coronary angioplasty or atherectomy. *Circulation* 1997; **96**: 475–483.

5 Topol EJ, Nissen SE. Our preoccupation with coronary luminology. The dissociation between clinical and angiographic findings in ischemic heart disease. *Circulation* 1995; **92**: 2333–2342.

6 Moses JW, Undermir C, Strain JE, Kreps EM, Higgins JE, Gleim GW, Kern MJ. Relation between single tomographic intravascular ultrasound image parameters and intracoronary Doppler flow velocity in patients with intermediately severe coronary stenoses. *Am Heart J* 1998; **135**: 988–994.

7 Heller LI, Cates C, Popma J, Deckelbaum LI, Joye JD, Dahlberg ST, Villegas BJ, Arnold A, Kipperman R, Grinstead WC, Balcom S, Ma Y, Cleman M, Steingart RM, Leppo JA. Intracoronary Doppler assessment of moderate coronary artery disease: comparison with 201Tl imaging and coronary angiography. FACTS Study Group. *Circulation* 1997; **96**: 484–490.

8 Miller DD, Donohue TJ, Wolford TL, Kern MJ, Bergmann SR, Cauley MB, Mechem CM, Hartman JJ. Assessment of blood flow distal to coronary artery stenoses. Correlations between myocardial positron emission tomography and poststenotic intracoronary Doppler flow reserve. *Circulation* 1996; **94**: 2447–2454.

9 Pijls NHJ, de Bruyne B, Peels K, van der Voort P, Bonnier HJRM, Bartunek J, Koolen J. Measurement of fractional flow reserve to assess the functional severity of coronary-artery stenoses. *N Engl J Med* 1996; **334**: 1703–1708.

10 Bartunek J, Marwick TH, Rodrigues ACT, Vincent M, Van Schuerbeeck E, Sys SU, De Bruyne B. Dobutamine-induced wall motion abnormalities: correlations with myocardial fractional flow reserve and quantitative coronary angiography. *J Am Coll Cardiol* 1996; **27**: 1429–1436.

11 Serruys P, Di Mario C, Piek J, Schroeder E, *et al.* Prognostic value of intracoronary flow velocity and diameter stenosis in assessing the short and long term outcome of coronary balloon angioplasty: the D.E.B.A.T.E. study. *Circulation* 1997; **96**: 3369–3377.

12 Kern MJ, Donohue TJ, Aguirre FV, Bach RG, Caracciolo EA, Wolford T, Flynn MCJMS, Chaitman B. Clinical outcome of deferring angioplasty in patients with normal translesional pressure-flow velocity measurements. *J Am Coll Cardiol* 1995; **25**: 178–187.

13 Bech GJ, De Bruyne B, Bonnier HJ, Bartunek J, Wijns W, Peels K, Heyndrickjx GR, Koolen JJ, Pijls NH. Long-term follow-up after deferral of percutaneous transluminal coronary angioplasty of intermediate stenosis on the basis of coronary pressure measurement. *J Am Coll Cardiol* 1998; **31**: 841–847.

14 Kern MJ, De Bruyne B, Pijls NHJ. From research to clinical practice: current role of intracoronary physiologically based decision making in the cardiac catheterization laboratory. *J Am Coll Cardiol* 1997; **30**: 613–620.

15 Li W, van der Steen AFW, Lancee CT. Temporal correlation of blood scattering signals *in vivo* from radio frequency intravascular ultrasound. *Ultrasound Med Biol* 1996; **22**: 583–590.

16 Li W, van der Steen AFW, Lancee CT, Céspedes EI, Carlier S, Gussenhoven EJ, Bom N. Potentials of volumetric blood-flow measurement. *Semin Intervent Cardiol* 1997; **2** 49–54.

17 Li W, van der Steen AFW, Lancee CT, Céspedes EI, Bom N. Blood flow imaging and volume flow quantitation with intravascular ultrasound. *Ultrasound Med Biol* 1998; **24**: 203–214./s18

18 Li W. Image and signal processing in intravascular ultrasound [Ph.D. thesis]. Erasmus University Rotterdam, 1997.

19 Li W, Lancée CT, Céspedes EI, van der Steen AFW, Bom N. Decorrelation of intravascular echo signals: potential for blood velocity estimation. *J Acoust Soc Am* 1998; **102**: 3785–3794.

20 Céspedes EI, Carlier SG, Li W, Mastik F, van der Steen AFW, Bom N, Verdouw PD, Serruys PW. Blood flow assessment using a mechanical intravascular ultrasound catheter: initial evaluation *in vivo*. *J Vasc Invest* 1998; **4**: 39–44.

21 Carlier SG, Li W, Cespedes I, van der Steen AF, Hamburger JN, Bom N, Serruys PW. Images in cardiovascular medicine. Simultaneous morphological and functional assessment of a renal artery stent intervention with intravascular ultrasound. *Circulation* 1998; **97**: 2575–275e.

22 ten Hoff H, Korbijn A, Smit TH, Klinkhamer JFF, Bom N. Imaging artifacts in mechanically driven ultrasound catheters. *Int J Card Imag* 1989; **4**: 195–199.

23 O'Donnell M, Shapo BM, Eberle MJ, Stephens DN. Experimental studies on an efficient catheter array imaging system. *Ultrasound Imag* 1995; **17**: 83–94.

24 Di Mario C, Akiyama T, Moussa I, Reimers B, Jang YT, Tobis J, Colombo A. First experience with imaging core wires. *Semin Intervent Cardiol* 1997; **2**: 69–73.

25 Wentzel JJ, Krams R, van der Steen AFW, Li W, Céspedes EI, Bom N, Slager CJ. Disturbance of 3D velocity profiles induced by an IVUS catheter: evaluation with computational fluid dynamics. *Comp Cardiol* 1997; **24**: 597–600.

26 Asakura T, Karino T. Flow patterns and spatial distribution of atherosclerotic lesions in human coronary arteries. *Circ Res* 1990; **66**: 1045–1066.

27 van der Heiden M, de Kroon MGM, Bom N, Borst C. Ultrasound backscatter at 30 MHz from human blood: influence of rouleau size affected by blood modification and shear rate. *Ultrasound Med Biol* 1995; **21**: 817–826.

28 Cloutier G, Qin Z, Durand LG, Teh BG. Power Doppler ultrasound evaluation of the shear rate and shear stress dependences of red blood cell aggregation. *IEEE Trans Biomed Eng* 1996; **43**: 441–450.

29 Carlier SG, Di Mario C, Kern M, Serruys PW. Intracoronary Doppler and pressure monitoring. In: Topol EJ (ed.). *Textbook of Interventional Cardiology (3rd edn.)*. Philadelphia: W. B. Saunders Company, 1998; 748–781.

30 Tadaoka S, Kigiyama M, Hiramatsu O, *et al.* Accuracy of 20 MHz Doppler catheter coronary artery velocimetry for measurement of coronary blood flow velocity. *Cathet Cardiovasc Diagn* 1990; **19**: 205.

31 Ling SC, Atabek HB, Fry DL, Patel DJ, Janicki JS. Application of heated-film velocity and shear probes to hemodynamic studies. *Circ Res* 1968; **23**: 789.

32 Ritter M, Vassalli G, Kiowski W, Vieli A, Schuiki E, Amann FW, Hess OM, Jenni R. How does the velocity profile affect the assessment of coronary reserve? In vitro evaluation by Doppler catheter. *Eur Heart J* 1995; **16**(Suppl:), P1190 (abstract).

33 Doucette JW, Corl PD, Payne HM, Flynn AE, Goto M, Nassi M, Segal J. Validation of a Doppler guide wire for intravascular measurements of coronary artery flow velocity. *Circulation* 1992; **85**: 1899–1911.

34 Chou TM, Sudhir S, Iwanaga S, Chatterjee K, Yock PG. Measurement of volumetric coronary blood flow by simultaneous intravascular two-dimensional and Doppler ultrasound: validation in an animal model. *Am Heart J* 1994; **128**: 237–243.

35 Labovitz AJ, Anthonis DM, Cravens TL, Kern MJ. Validation of volumetric flow measurements by means of a Doppler-tipped coronary angioplasty guide wire. *Am Heart J* 1993; **126**: 1456–1461.

36 Sudhir K, Hargrave VK, Johnson EL, Aldea G, Mori H, Ports TA, Yock PG. Measurement of volumetric coronary blood flow with a Doppler catheter: validation in an animal model. *Am Heart J* 1992; **124**: 870–875.

37 Eichhorn EJ, Alvarez LG, Jessen ME, Fass SM, Chao RY, Haagen D, Grayburn PA. Measurement of coronary and peripheral artery flow by intravascular ultrasound and pulsed Doppler velocimetry. *Am J Cardiol* 1992; **70**: 542–545.

38 Grayburn PA, Willard JE, Haagen DR, Brickner ME, Alvarez LG, Eichhorn EJ. Measurement of coronary flow using high-frequency intravascular ultrasound imaging and pulsed Doppler velocimetry: *in-vitro* feasibility studies. *J Am Soc Ech* 1992; **5**: 5–12.

39 Linker DT, Torp H, Groenningsaether A, *et al.* Instantaneous arterial flow estimated with an ultrasound imaging and Doppler catheter. *Circulation* 1989; **80**: II-580.

40 Caro CG, Pedley TJ, Schroter RC, Seed WA. Flow in pipes and around objects. In: Caro CG, Schroter RC, Seed WA (eds). *The Mechanics of the Circulation*. New York: Oxford University Press, 1978; 44–73.

41 Hodgson JB, Marshall JJ. Direct vasoconstriction and endothelium dependent vasodilation. *Circulation* 1989; **79:** 1043–1051.
42 Quyyumi AA, Cannon RO III, Panza JA, Diodati JG, Epstein SE. Endothelial dysfunction in patients with chest pain and normal coronary arteries. *Circulation* 1992; **86:** 1864–1871.
43 Houghton JL, Davison CA, Kuhner PA, Torossov MT, Strogatz DS, Carr AA. Heterogeneous vasomotor responses of coronary conduit and resistance vessels in hypertension. *J Am Coll Cardiol* 1998; **31:** 374–382.
44 Reddy KG, Nair RN, Sheehan HM, Hodgson JM. Evidence that selective endothelial dysfunction may occur in the absence of angiographic or ultrasound atherosclerosis in patients with risk factors for atherosclerosis. *J Am Coll Cardiol* 1994; **24:** 833–843.
45 Manginas A, Voudris V, Pavlides G, Karatasakis G, Athanassopoulos G, Cokkinos DV. Effect of plaque burden on coronary vasoreactivity in early atherosclerosis. *Am J Cardiol* 1998; **81:** 402–406.
46 Sudhir K, Mullen WL, Hausmann D, Fitzgerald PJ, Chou TM, Yock PG, Chatterjee K. Contribution of endothelium-derived nitric oxide to coronary arterial distensibility: an in vivo two-dimensional intravascular ultrasound study. *Am Heart J* 1995; **129:** 726–732.
47 Sudhir K, Ko E, Zellner C, Wong HE, Hutchison SJ, Chou TM, Chatterjee K. Physiological concentrations of estradiol attenuate endothelin 1-induced coronary vasoconstriction *in vivo*. *Circulation* 1997; **96:** 3626–3632.
48 Li W, Mastik F, Céspedes EI, Carlier SG, van der Steen AFW. Echo decorrelation estimated from signal powers. *Ultrasound Med Biol* 1998; (in press).
49 Céspedes EI, Li W, Mastik F, van der Steen AFW, Carlier S, van Bremen RH, Eberle M, Bom N. Intravascular power flow imaging: theory and potentials for planimetry. *IEEE Ultrasound Symp* 1997; 1273–1276.
50 Céspedes EI, Carlier SG, Sabate M, Ligthart J, Serruys PW. Angiographically undetected stent mal-apposition resolved by intravascular ultrasound and flow imaging. *J Vasc Invest* 1998; **4:** 81–84.

Chapter 7b

Preliminary clinical experience:

Simultaneous morphological and functional assessment of a renal artery stent intervention with intravascular ultrasound.

SG Carlier, W Li, EI Cespedes, AFW van der Steen, JN Hamburger, N Bom, PW Serruys.

Circulation 1998;97:2575-2576.

Simultaneous Morphological and Functional Assessment of a Renal Artery Stent Intervention With Intravascular Ultrasound

Stéphane G. Carlier, MD; Wenguang Li, PhD; E. Ignacio Céspedes, PhD; Antonius F.W. van der Steen, PhD; Jaap N. Hamburger, MD; Nicolaas Bom, PhD; Patrick W. Serruys, MD, PhD

A 73-year-old woman with a history of high blood pressure and hypercholesterolemia developed medically uncontrolled hypertension (200/100 mm Hg). Serum creatinine level was 145 μmol/L, and creatinine clearance was 34 mL/min. Renal ultrasound demonstrated a small right kidney (80 mm long) compared with the left one (92 mm long). Left ventricular hypertrophy was present on the ECG and was confirmed by echocardiography. On isotope radiography with ^{99m}Tc-mercaptoacetyltriglycine after oral intake of 25 mg captopril, the right kidney was small, with delayed excretion and impaired function (36%). Renal arteriography showed subocclusive ostial stenosis of the right renal artery.

The lesion was related to a calcified plaque extending from the aortic wall into the renal artery ostium (angiogram I in Figure 1, arrow). After an unsuccessful angioplasty attempt in the interventional radiology department (failure to cross the stenosis), the patient was investigated in the cardiac catheterization laboratory. The lesion was crossed with a hydrophilic guidewire and predilated. A short (9-mm) stent was then implanted by use of a 4.5-mm balloon inflated up to 18 atm for postdilatation (angiogram II).

The immediate result of the intervention was assessed by both biplane angiography (angiogram III, anteroposterior projection) and intravascular ultrasound (IVUS). Distal to the stent, IVUS shows a normal arterial wall (panel 1 in Figure 1). A cross section within the stent (panel 2) demonstrates good expansion and apposition of the struts (arrows). The lumen area measured at this level was 18.9 mm^2. The arrows in panel 3 demonstrate the highly calcified plaque at the junction with the aorta.

The top of Figure 2 shows images obtained with a newly developed method to quantify the blood flow with an IVUS imaging catheter. They were recorded distally to the stent at different times (a through e) during the cardiac cycle. This blood flow measurement method has recently been validated and calibrated in vitro against electromagnetic flowmeter data and in vivo in porcine carotid arteries.[1] The principle is based on the analysis of decorrelation of the IVUS radiofrequency (RF) signals. Red blood cells flowing in the ultrasound beam result in a decorrelation of successively received RF signals. The rate of decorrelation is proportional to the local blood flow velocity.[2,3] These are then converted into color maps representing local instantaneous blood flow velocity in the arterial cross section. The color scheme used goes from dark red (10 cm/s) to yellow (100 cm/s). Flow velocities are measured at 100 angular positions, with a depth resolution of 160 μm. Cross sections with color flow data can be recorded during a 4-second period at 16 frames per second.

The moment of each IVUS image with flow information in the cardiac cycle is indicated at the bottom right of Figure 2, showing flow traces recorded simultaneously with the ECG. The instantaneous flow calculated with the IVUS method is

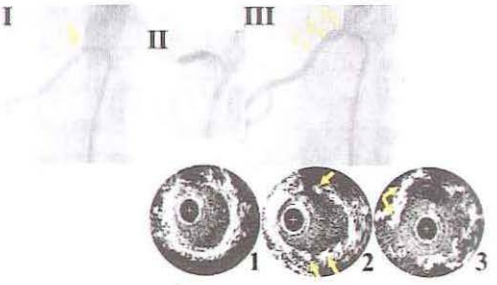

Figure 1. Angiograms before (I), during (II), and after (III) stent implantation in right renal artery. Tight stenosis is indicated by arrow in angiogram I. Intravascular ultrasound (IVUS) images (1 through 3) obtained after stenting at corresponding levels indicated by arrows in angiogram III. Arrows in IVUS panel 2 show well-apposed struts of stent, and in panel 3, calcified plaque at junction with aorta (Ao).

From Thoraxcentre Erasmus University Rotterdam, Netherlands (all authors); Interuniversity Cardiology Institute of the Netherlands (W.L., A.F.W.v.d.S., N.B., P.W.S.); and Endosonics Corp, Rancho Cordova, Calif (E.I.C.).

Correspondence to Stéphane G. Carlier, MD, Thoraxcentre Ee2302, Erasmus University Rotterdam, PO Box 1738, NL-3000 DR Rotterdam, Netherlands.

E-mail carlier@tch.fgg.eur.nl

The editor of Images in Cardiovascular Medicine is Hugh A. McAllister, Jr, MD, Chief, Department of Pathology, St Luke's Episcopal Hospital and Texas Heart Institute, and Clinical Professor of Pathology, University of Texas Medical School and Baylor College of Medicine.

Circulation encourages readers to submit cardiovascular images to Dr Hugh A. McAllister, Jr, St Luke's Episcopal Hospital and Texas Heart Institute, 6720 Bertner Ave, MC1-267, Houston, TX 77030.

(*Circulation*. 1998;97:2575-2576.)

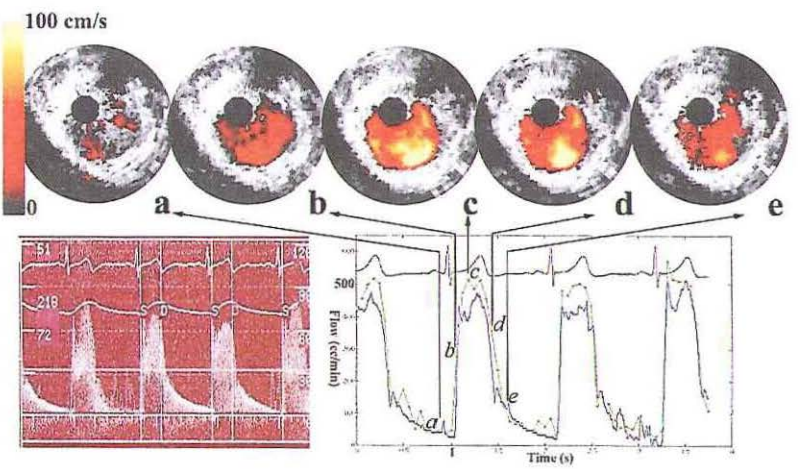

Figure 2. Color mapping of blood flow velocity inside arterial lumen after procedure, at different phases of cardiac cycle (a through e), calculated from intravascular ultrasound (IVUS) radiofrequency signal analysis. IVUS volume flow (green trace) and Doppler-based volume flow (blue trace) with corresponding ECG (black trace). Doppler-based volume flow is calculated from depicted Doppler sonogram (range, 0 to 120 cm/s) and diameter measured by quantitative coronary angiography on angiogram III at level of tip of Doppler wire. IVUS volume flow is calculated by integrating velocity components over arterial lumen area. The two flow estimations are in good agreement.

represented in green and the flow derived from an intravascular Doppler wire in blue. In panel a, very low blood flow velocities at end diastole are not encoded, because they fall below the sensitivity threshold level, which is ≈10 cm/s. With increasing flow in early systole (b), the color map shows homogeneous blood flow velocities encoded in red. Maximal velocities are reached at peak systole (c). The decrease in blood flow in diastole is seen in panels d and e. Integration of the velocities over the lumen area allows the computation of instantaneous volumetric blood flow (green curve) during a 4-second period. The measurements are in agreement with the blood flow simultaneously measured with the Doppler wire (in blue: Doppler instantaneous peak velocity times the cross-sectional vessel area at Doppler wire tip). The mean IVUS flow was 238 mL/min, whereas the flow derived from the Doppler wire measurements was 208 mL/min. This demonstrates the feasibility of simultaneous assessment of morphological and physiological parameters during interventional procedures with an intravascular imaging catheter. The method is presently being evaluated in coronary arteries.

This patient was discharged 2 days after the procedure and is doing well. Good early and long-term results of stenting ostial renal lesions have been reported recently,[4] with a restenosis rate of 10%, making this procedure the best current therapy for renovascular disease related to critical ostial stenoses.

Acknowledgments

The excellent technical support of J. Honkoop and F. Mastik was of paramount importance for the realization of this work.

References

1. Carlier S, Li W, Mastik F, Honkoop J, van der Steen AFW, Lancée CT, de Zeeuw S, van Bremen R, Céspedes EI, Serruys PW, Bom K. New intracoronary volumetric blood flow measurement method with intravascular ultrasound: in-vitro assessment and first in vivo results. *Eur Heart J*. 1997;18:376. Abstract.
2. Li W, van der Steen AFW, Lancée CT, Céspedes EI, Gussenhoven EJ, Bom N. Estimation of local blood velocity and volume flow with intravascular ultrasound. *Ultrasound Med Biol*. In press.
3. Li W. Image and Signal Processing in Intravascular Ultrasound [PhD thesis]. Rotterdam, Netherlands: Erasmus University; 1997.
4. Blum U, Krumme B, Flügel P, Gabelmann A, Lehnert T, Buitrago-Tellez C, Schollmeyer P, Langer M. Treatment of ostial renal-artery stenoses with vascular endoprotheses after unsuccessful balloon angioplasty. *N Engl J Med*. 1997;336:459–465.

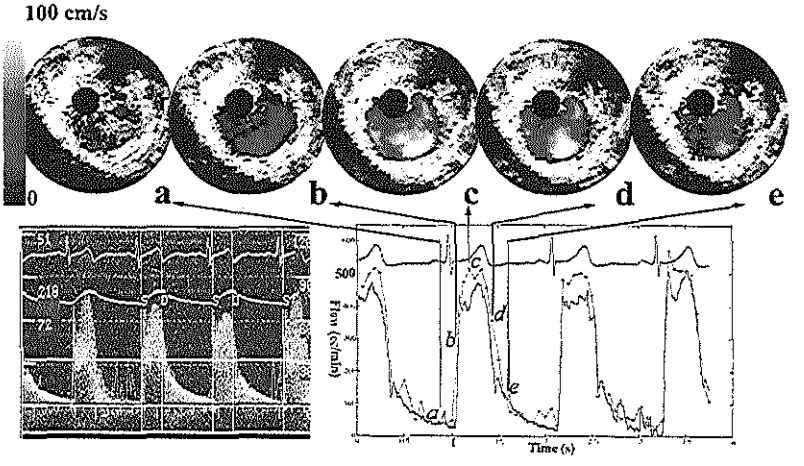

Figure 2. Color mapping of blood flow velocity inside arterial lumen after procedure, at different phases of cardiac cycle (a through e), calculated from intravascular ultrasound (IVUS) radiofrequency signal analysis. IVUS volume flow (green trace) and Doppler-based volume flow (blue trace) with corresponding ECG (black trace). Doppler-based volume flow is calculated from depicted Doppler sonogram (range, 0 to 120 cm/s) and diameter measured by quantitative coronary angiography on angiogram III at level of tip of Doppler wire. IVUS volume flow is calculated by integrating velocity components over arterial lumen area. The two flow estimations are in good agreement.

represented in green and the flow derived from an intravascular Doppler wire in blue. In panel a, very low blood flow velocities at end diastole are not encoded, because they fall below the sensitivity threshold level, which is ≈10 cm/s. With increasing flow in early systole (b), the color map shows homogeneous blood flow velocities encoded in red. Maximal velocities are reached at peak systole (c). The decrease in blood flow in diastole is seen in panels d and e. Integration of the velocities over the lumen area allows the computation of instantaneous volumetric blood flow (green curve) during a 4-second period. The measurements are in agreement with the blood flow simultaneously measured with the Doppler wire (in blue: Doppler instantaneous peak velocity times the cross-sectional vessel area at Doppler wire tip). The mean IVUS flow was 238 mL/min, whereas the flow derived from the Doppler wire measurements was 208 mL/min. This demonstrates the feasibility of simultaneous assessment of morphological and physiological parameters during interventional procedures with an intravascular imaging catheter. The method is presently being evaluated in coronary arteries.

This patient was discharged 2 days after the procedure and is doing well. Good early and long-term results of stenting ostial renal lesions have been reported recently,[4] with a restenosis rate of 10%, making this procedure the best current therapy for renovascular disease related to critical ostial stenoses.

Acknowledgments

The excellent technical support of J. Honkoop and F. Mastik was of paramount importance for the realization of this work.

References

1. Carlier S, Li W, Mastik F, Honkoop J, van der Steen AFW, Lancée CT, de Zeeuw S, van Bremen R, Céspedes EI, Serruys PW, Born K. New intracoronary volumetric blood flow measurement method with intravascular ultrasound: in-vitro assessment and first in vivo results. *Eur Heart J.* 1997;18:376. Abstract.
2. Li W, van der Steen AFW, Lancée CT, Céspedes EI, Gussenhoven EJ, Born N. Estimation of local blood velocity and volume flow with intravascular ultrasound. *Ultrasound Med Biol.* In press.
3. Li W. Image and Signal Processing in Intravascular Ultrasound [PhD thesis]. Rotterdam, Netherlands: Erasmus University; 1997.
4. Blum U, Krumme B, Flügel P, Gabelmann A, Lehnert T, Buitrago-Tellez C, Schollmeyer P, Langer M. Treatment of ostial renal-artery stenoses with vascular endoprotheses after unsuccessful balloon angioplasty. *N Engl J Med.* 1997;336:459–465.

Chapter 8

Effect of catheter placement on 3D-velocity profiles in curved tubes resembling the human coronary system.

R Krams, JJ Wentzel, EI Cespedes, R Vinke,
S Carlier, AFW van der Steen, CT Lancée, CJ Slager.

Ultrasound in Medicine & Biology, 1999; 25:803-810.

ELSEVIER

Ultrasound in Med. & Biol., Vol. 25, No. 5, pp. 803–810, 1999

0301-5629/99/$–see front matter

PII S0301-5629(99)00018-6

● *Original Contribution*

EFFECT OF CATHETER PLACEMENT ON 3-D VELOCITY PROFILES IN CURVED TUBES RESEMBLING THE HUMAN CORONARY SYSTEM

R. KRAMS,[†] J. J. WENTZEL,[†]* I. CESPEDES,[‡§] R. VINKE,[†] S. CARLIER,[‡]
A. F. W. VAN DER STEEN,[‡]* C. T. LANCEE[‡] and C. J. SLAGER[†]

[†]Laboratory Hemodynamics and [‡]Experimental Echocardiography, Thoraxcenter, Erasmus University Rotterdam, Rotterdam, The Netherlands; *ICIN, Utrecht, The Netherlands; and [§]Endosonics Corporation, Rancho Cordova, CA, USA

(*Received* 11 *November* 1998; *in final form* 28 *January* 1999)

Abstract—Novel measurement techniques based on intravenous ultrasound (IVUS) technology ('IVUS-Flowmetry') require the location of a catheter inside the coronary bed. The present study quantifies disturbances in the 3-D velocity profile induced by catheter placement inside a tube, applying computational fluid dynamics. Two curved, circular meshes (radius K = 0.025 m and K = 0.035 m) with and without a catheter inside the lumen were applied. The catheter was located at the inner curve, the outer curve and at the top position. Boundary conditions were: no slip on the wall, zero stress at the outlet, uniform inflow with entrance velocities of 0.1, 0.2 and 0.4 m/s. Curvature-associated centrifugal forces shifted the maximal velocity to the outer curve and introduced two symmetrical vortices. Additional catheter placement redistributed the 3-D axial velocity field away from the catheter, which was accompanied by the appearance of multiple low-strength vortices. In addition, peak axial velocity increased, peak secondary velocities decreased, axial pressure drop increased and shear stress increased. Flow calculations simulated to resemble IVUS-based flowmetry changed by only 1% after considering secondary velocity. In conclusion, placement of a catheter inside a curved tube resembling the human coronary system changes the velocity field and reduces secondary patterns. The present study supports the usefulness of catheter-based flowmetry during resting flow conditions. During hyperemic flow conditions, flow measurements might be accompanied by large axial pressure drops because the catheter, itself, might act as a significant stenosis. © 1999 World Federation for Ultrasound in Medicine & Biology.

Key Words: **CFD, Catheter placement, Coronary artery, Shear stress.**

INTRODUCTION

Steady flow in cylindrical tubes distant from curved segments and side branches may be considered parabolic ("Poiseuille flow"). The velocity field, during these conditions, is described by a velocity vector, oriented parallel to the axes of the artery (Milnor 1982). The human arterial system, however, is a complex three dimensional (3-D) structure consisting of straight and curved segments with multiple side branches (Milnor 1982). During these circumstances, nonaxially directed velocity components ('secondary velocity') have been identified (Kilner et al. 1993; Moore et al. 1992). These secondary velocities might be implicated in the progression of atherosclerosis, and might affect the ultrasonic measurement of blood flow (Tortoli et al. 1995; Li et al. 1998, 1997; Carlier et al. 1998).

In general, ultrasound blood flow measurement techniques measure blood velocity in the direction of the ultrasound beam and assume Poiseuille blood flow to evaluate flow (Tortoli et al. 1995). Recently, a novel technique for intravascular applications has been developed that applies a modification of the transit-time method to estimate local blood velocity (Li et al. 1997, 1998). Due to its high in-plane resolution, this method not only enables calculation of complete 2-D velocity profiles but, due to its combination with intravascular ultrasound, one can also measure cross-sectional area, which allows the calculation of blood flow (Li et al. 1998).

Early results are very promising (Li et al. 1997, 1998), but limitations of the method are still under investigation. One of these limitations might be that velocity in only two directions is estimated (*i.e.* along and

Address correspondence to: R. Krams, M.D., Ph.D., Dept.Hemodynamics, Room 2322, P.O. Box 1738, Erasmus University Rotterdam, Rotterdam, The Netherlands. E-mail: krams@tch.fgg.eur.nl

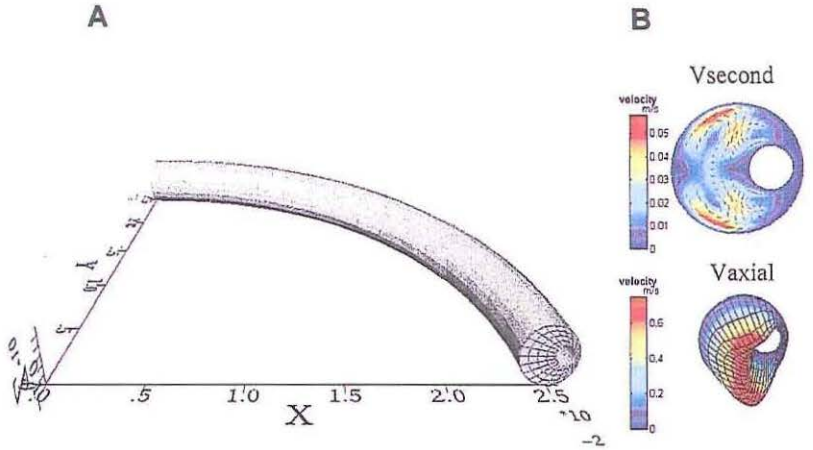

Fig. 2. (A) Example of the curved mesh with a catheter located in the outer curve. (B) The calculated 3-D velocity profiles in the axial direction (V_{axial}) and secondary velocities (V_{second}).

evaluated at the inner and outer curve of the curved tube. For each location, shear stress was normalized to the shear stress values obtained before catheter placement. In addition, a shear stress ratio is defined as the shear stress at the inner curve divided by the shear stress at the outer curve.

The pressure gradient was obtained directly from the output of the FEM package. Pressure difference was the total pressure drop and is reported in mmHg (1 kPa = 7.5 mmHg). To compare different tubes with different lengths, we normalized the pressure difference per length unit (mmHg/10 cm).

Reynolds number ($Re = (v*d*\rho)/\eta$) was calculated during fully developed conditions. In these formulas, v signifies the average velocity (m/s), d the tube diameter (m), ρ density (kg/m^3) and η viscosity (Pa.s).

RESULTS

Fully developed flow conditions and adequacy of mesh

The relative difference between the 3-D velocity fields at subsequent cross-sections in curved tubes without catheter placement decreased from 7.5% at Cross-section 2 to less than 1% at Cross-sections 11 to 14. In addition, increasing the mesh resolution by a factor of 1.5 did not change the 3-D velocity field by more than 1% at Cross-sections 11 to 14. A similar analysis after catheter placement revealed fully development of the velocity field at Cross-sections 5 to 15 and accurate solutions at Cross-sections 9 to 14. Hence, Cross-section 12, which corresponds to an axial distance of 0.0295 m (± 10 times the diameter), was used throughout the present analysis.

Axial velocity

In the absence of a catheter, the interplay of viscous, inertial and centrifugal forces in the curved tube redistributes the 3-D velocity field so that maximal axial velocity ($V_{max,ax}$) is shifted outward (Fig. 1 and Fig. 2, upper row and Table 1). The outward shift increases linearly with entrance velocity, but is unaffected by the radii of curvature as applied in the present study (Table 1). Insertion of a catheter modulates the distribution of the axial velocity field (Fig. 2 and Fig. 3, first column) in such a way that maximal axial velocity is shifted more outward when the catheter is in the inner and top position. When the catheter is in the outer curve, the velocity field is shifted toward the inner curve, introducing high gradients on the tube wall (Figs. 2 and 3, first column and Table 1). The location (% shift) of the maximal axial velocity is hardly affected by entrance velocity after the insertion of a catheter (Table 1).

$V_{max,ax}$ increased in parallel with entrance velocity and after catheter placement (Table 1). The largest increase of $V_{max,ax}$, at a constant entrance velocity, was calculated when the catheter was located in the inner curve (22%, Table 1); smaller increments were calculated when the catheter was in the top (18%, Table 1) and outer position (12%, Table 1).

Secondary velocity

In the absence of a catheter, two symmetrical vortices appeared at Cross-section 12 for both curvatures (Figs. 1 and 3, first row and second column). The distribution of these secondary velocity patterns and the maximum of the secondary velocity field were affected both

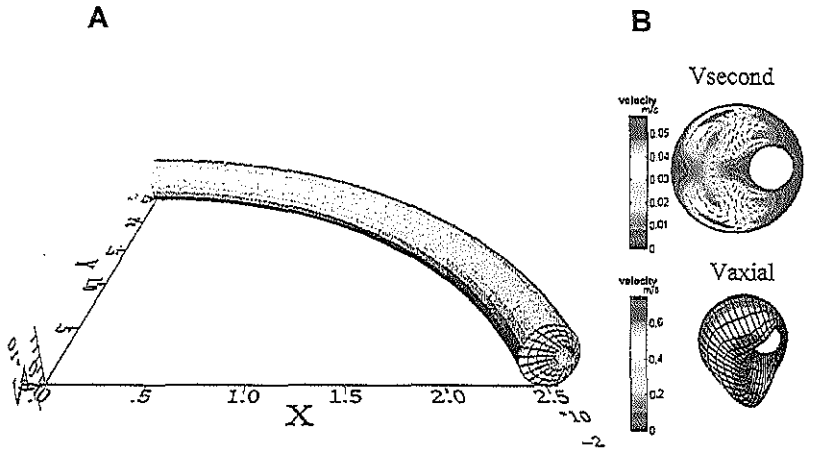

Fig. 2. (A) Example of the curved mesh with a catheter located in the outer curve. (B) The calculated 3-D velocity profiles in the axial direction (V_{axial}) and secondary velocities (V_{second}).

evaluated at the inner and outer curve of the curved tube. For each location, shear stress was normalized to the shear stress values obtained before catheter placement. In addition, a shear stress ratio is defined as the shear stress at the inner curve divided by the shear stress at the outer curve.

The pressure gradient was obtained directly from the output of the FEM package. Pressure difference was the total pressure drop and is reported in mmHg (1 kPa = 7.5 mmHg). To compare different tubes with different lengths, we normalized the pressure difference per length unit (mmHg/10 cm).

Reynolds number ($Re = (v*d*\rho)/\eta$) was calculated during fully developed conditions. In these formulas, v signifies the average velocity (m/s), d the tube diameter (m), ρ density (kg/m^3) and η viscosity (Pa.s).

RESULTS

Fully developed flow conditions and adequacy of mesh

The relative difference between the 3-D velocity fields at subsequent cross-sections in curved tubes without catheter placement decreased from 7.5% at Cross-section 2 to less than 1% at Cross-sections 11 to 14. In addition, increasing the mesh resolution by a factor of 1.5 did not change the 3-D velocity field by more than 1% at Cross-sections 11 to 14. A similar analysis after catheter placement revealed fully development of the velocity field at Cross-sections 5 to 15 and accurate solutions at Cross-sections 9 to 14. Hence, Cross-section 12, which corresponds to an axial distance of 0.0295 m (± 10 times the diameter), was used throughout the present analysis.

Axial velocity

In the absence of a catheter, the interplay of viscous, inertial and centrifugal forces in the curved tube redistributes the 3-D velocity field so that maximal axial velocity ($V_{max,ax}$) is shifted outward (Fig. 1 and Fig. 2, upper row and Table 1). The outward shift increases linearly with entrance velocity, but is unaffected by the radii of curvature as applied in the present study (Table 1). Insertion of a catheter modulates the distribution of the axial velocity field (Fig. 2 and Fig. 3, first column) in such a way that maximal axial velocity is shifted more outward when the catheter is in the inner and top position. When the catheter is in the outer curve, the velocity field is shifted toward the inner curve, introducing high gradients on the tube wall (Figs. 2 and 3, first column and Table 1). The location (% shift) of the maximal axial velocity is hardly affected by entrance velocity after the insertion of a catheter (Table 1).

$V_{max,ax}$ increased in parallel with entrance velocity and after catheter placement (Table 1). The largest increase of $V_{max,ax}$, at a constant entrance velocity, was calculated when the catheter was located in the inner curve (22%, Table 1); smaller increments were calculated when the catheter was in the top (18%, Table 1) and outer position (12%, Table 1).

Secondary velocity

In the absence of a catheter, two symmetrical vortices appeared at Cross-section 12 for both curvatures (Figs. 1 and 3, first row and second column). The distribution of these secondary velocity patterns and the maximum of the secondary velocity field were affected both

equations are solved with a standard, finite element method, implemented in the finite element package Sepran (Sepra, Leiden, Netherlands). The non-linear convective term in the Navier–Stokes equations is linearized with a Newton–Raphson approach and solved with a cut-off error of 10^{-4} (m/s). To obtain the pressure unknowns from the discrete Navier–Stokes equations, a penalty function approach was used. Eliminating the pressure unknowns with the penalty method and linearizing of the convective term results in a set of linear equations with velocity unknowns. A numerical solver, applying a direct profile method, of the well-validated (Bovendeerd et al. 1987), commercially available finite element package, which was implemented on a workstation (HP 715/80), solved the resulting matrices.

The following boundary conditions were imposed: uniform steady inflow at the entrance of the vessel; constant zero stress at the outlet;and no-slip conditions at the tube wall (Bovendeerd et al. 1987). We further assumed that blood behaved as a Newtonian fluid with a density of 1050 kg/m^3 and a viscosity of $3*10^{-3}$ (Pa.s) (Bovendeerd et al. 1987).

Protocols

Adequacy of mesh resolution and fully developed flow conditions. To determine the cross-section where flow was fully developed, we calculated the relative velocity difference, defined as $(v_i-v_{i-1}/v_{i-1})*100\%$. V_i signifies the points of the 3-D velocity profile at cross-section i and V_{i-1} the velocity profile at the previous cross-section. A root means squared difference smaller than 1% between successive 3-D velocity profiles was defined as fully developed.

Second, subsequent increments in mesh resolution by 50% were applied to evaluate if the lowest mesh resolution was adequate to obtain accurate solutions. A solution (3-D velocity field) in a given cross-section, was defined as accurate when the 3-D velocity field did not change more than 1% after increasing the mesh resolution. The difference between the 3-D velocity fields of both meshes was defined as $(v_l-v_h/v_l)*100$, where l and h refer to the low and high-resolution mesh.

Absence of catheter. 3-D velocity vector fields were calculated in curved tubes with radii of curvature of 0.035 m and 0.025 m, and a tube diameter of 0.003 m.. To cover a wide range of Reynolds values, three different entrance velocities (0.1 m/s, 0.2 m/s and 0.4 m/s) were applied to each radius of curvature, adding up to six different conditions.

Presence of catheter. We also evaluated to what extent placement of a catheter inside the lumen of a curved tube affected the 3-D-velocity field. As idealizations for the real situation, we positioned the catheter at the inner curve (9 o'clock), the outer curve (3 o'clock) and at the top (12 o'clock) position of the curved tube. These catheter positions were studied at two different curvatures (0.025 m and 0.035 m) and at three different entrance velocities (0.1, 0.2 and 0.4 m/s). This adds up to 18 different conditions.

Effect of tube size. To study the effect of tube size, we used tubes with diameters of 0.003 m and of 0.002 m, but catheter diameter was kept constant at 0.001 m.. The catheter was located at the outer wall and the radius of curvature was 0.025 m.. Entrance velocities were 0.1 m/s, 0.2 m/s and 0.4 m/s.

Analysis

The three components of the velocity field (u, v and w) were calculated. U and v are the cross-sectional in-plane velocity components and w the axial velocity component (*i.e.* along the tube). The in-plane velocity vectors u and v were added (vector addition) and are presented as secondary velocity components. Maximal axial ($V_{max,ax}$) and maximal secondary velocity ($V_{max,sec}$) were calculated for each condition and normalized to mean entrance velocity. In addition, the location of the maximal axial velocity component with respect to the center of mass of each cross-section was calculated. This location was subsequently normalized to the radius of the tube, and presented as percentage shift (%shift).

Comparison between meshes of different size and resolution was accomplished by interpolating the data points of the mesh with the lowest resolution to the resolution of the mesh with the highest resolution, applying a linear interpolation method (MATLAB, Mathworks Inc., Natick, MA, USA).

To simulate conditions resembling IVUS flowmetry, we calculated flow in two ways: Total flow was defined as the magnitude of the velocity vector multiplied with the cross-sectional area. Axial flow was the product of axial flow and cross-sectional area, in which axial velocity was defined as the magnitude of the velocity vector multiplied with normal on the cross-section. Due to the discretization of the mesh, we defined both parameters locally and summarized over the elements of the mesh. Regional area was calculated as $0.5(|\text{cross}(a,b)| + |\text{cross}(c,d)|)$, where a, b, c and d are the sides of a quadrangle in the cross-section of interest (cross signifies the vector cross product). Local velocity was calculated from the average of magnitudes of the four velocity vectors located at the vertices of the local area. The error in flow estimation was defined as ((totalflow − axialflow)/totalflow)*100.

Shear stress, calculated from the product of viscosity and the local gradient of the velocity field, was

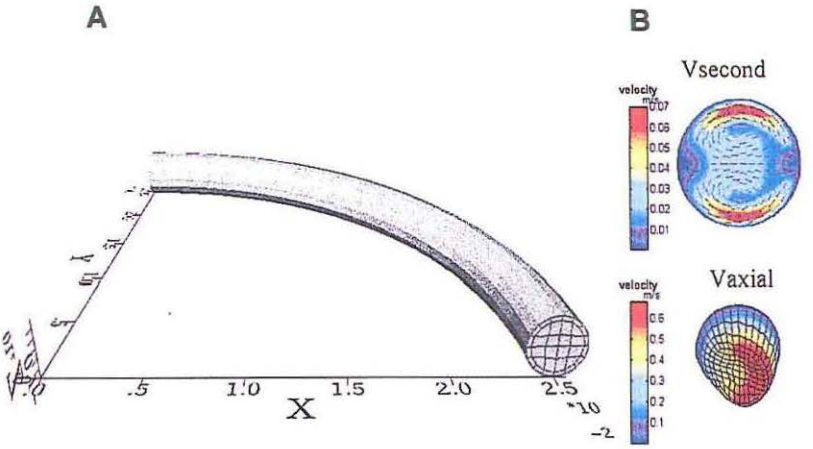

Fig. 1. (A) Example of the curved mesh with the catheter absent. (B) The calculated velocity profiles (V_{axial}) and secondary velocities (V_{second}).

across the ultrasound beam), thereby missing the circumferential component in the plane of imaging (Li et al. 1997). Hence, velocity components in the axial and in-plane direction cannot be completely separated. Consequently, significant secondary velocities could lead to an overestimation of the true blood flow. One other inherent limitation of the technique is introduced by the presence of the catheter, which might increase the pressure difference or disturb the velocity patterns and preclude the possibility of obtaining physiological velocity profiles *in vivo* (Wentzel et al. 1997).

The aim of the present study was multiple. First, the relative contribution of the secondary velocity components to blood flow was evaluated in curved tubes resembling the curvature of the human coronary arteries (Krams et al. 1997), before and after placement of a catheter. Second, the axial pressure difference is reported and, because the axial pressure difference is affected by flow, vascular resistance was evaluated. Third, due to the reported effect of shear stress on atherosclerosis, we also evaluated how shear stress is affected by the introduction of a catheter inside the lumen. Finally, to understand the nature of these disturbances in more detail, the modulating effect of the degree of curvature, tube diameter to catheter radius and Reynolds number are evaluated on these parameters.

MATERIAL AND METHODS

Simulated fluid flow can be studied in detail if the equations of motion are solved. Analytical solutions of these equations are only possible under certain simplified conditions (Bovendeerd 1987). For the present study, these simplified conditions are not met and the full non-linear partial differential ('Navier-Stokes') equations have to be solved numerically (Bovendeerd et al. 1987). The numerical technique is based on the discretization of the region of interest with finite elements ('3-D mesh').

3-D mesh formulation

To resemble the human coronary arteries (Krams et al. 1997), we generated a 3-D geometry consisting of a curved, circular tube with a radius of curvature of either 0.025 or 0.035 m and a diameter of 0.003 m (Fig. 1). The resulting vessel segments, which occupied a quarter of a circle, were represented by 16 cross-sections along the tube. This resulted in an axial resolution of $2.45*10^{-3}$ m and $3.45*10^{-3}$ m for radii of curvatures of 0.025 and 0.035 m. In the absence of a catheter, 32 elements were placed in each cross-section. When a catheter was located inside the tube, 80 elements were located in each cross-section to account for the increased geometrical complexities. The cross-sectional in-plane resolution was $2.2*10^{-7}$ m^2 for the 3-D-mesh without a catheter and $8.9*10^{-8}$ m^2 for a 3-D-mesh with a catheter.

Computational fluid dynamics

Each 3-D element of the mesh consists of an isoparametric hexahedral element with 27 nodes per element. At each nodal point, the nonlinear partial differential equations ('Navier-Stokes equations') for incompressible, isothermal fluids are implemented. These

Table 1. Characteristic parameters obtained from the 3-D velocity field obtained from the solutions of the Navier–Stokes equations.

	Curvature 0.025 m			Curvature 0.035 m		
	$Shift_{ax}$ (%)	$V_{max,ax}$ (m/s)	$V_{max,sec}$ (m/s)	$Shift_{ax}$ (%)	$V_{max,ax}$ (m/s)	$V_{max,sec}$ (m/s)
No catheter						
10 cm/s	8	0.19	0.0115	8	0.19	0.0088
20 cm/s	11	0.36	0.0334	11	0.37	0.0260
40 cm/s	15	0.68	0.0730	15	0.69	0.0586
Catheter out						
.1 m/s	14	0.22	0.0092	14	0.22	0.0070
.2 m/s	14	0.40	0.0254	14	0.41	0.0197
.4 m/s	17	0.74	0.0578	17	0.76	0.0451
Catheter in						
.1 m/s	16	0.23	0.0094	16	0.23	0.0074
.2 m/s	20	0.44	0.0274	20	0.44	0.0226
.4 m/s	20	0.83	0.0677	20	0.83	0.0571
Catheter top						
.1 m/s	17	0.22	0.0097	16	0.22	0.0075
.2 m/s	20	0.43	0.0311	17	0.44	0.0232
.4 m/s	17	0.81	0.0710	17	0.83	0.0572

% shift = relative position of maximal axial velocity with respect to the center of the tube (%); $V_{max,ax}$ = magnitude of maximal axial velocity (m/s); $V_{max,sec}$ = magnitude of maximal secondary velocity (m/s).

by entrance velocity ($V_{max,s}$, Table 1) and by curvature (Fig. 3, second column). Placement of a catheter either at the inner wall or at the top position shifted the vortices further outward; placement at the inner curve moved the vortices toward the inner curve (Fig. 3, second column).

Relative secondary velocities (*i.e.*, normalized to mean axial velocity) varied between 11 to 19% in the absence of a catheter and between 9 and 18% after introduction of a catheter (Table 1). Hence, the catheter reduced secondary velocities.

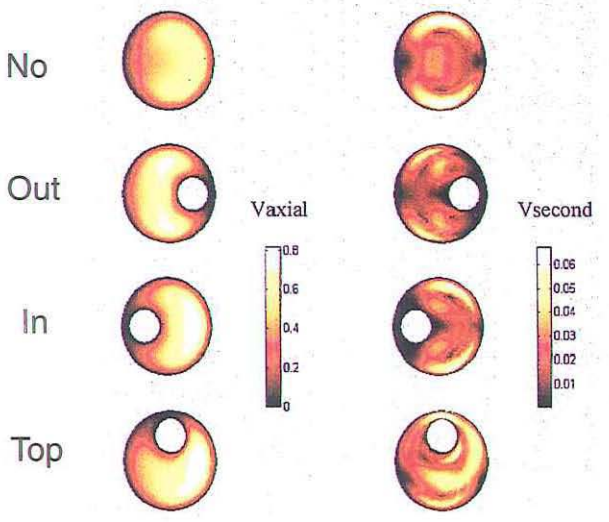

Fig. 3. Color map and isocontour lines of the 3-D axial velocity field (first column) and 3-D secondary velocity field (second column) at a curvature of 25 mm. The upper row is in the absence of a catheter (NO), a catheter in the outer position (OUT), the third row in the inner position (IN) and the bottom row for a catheter in the top position (TOP). V_{axial} is the axial velocity (m/s); V_{second} signifies the secondary velocities (m/s).

Table 2. Shear stress and axial pressure difference calculated from the solutions of the Navier–Stokes equations

	Curvature 0.025 m^{-1}			Curvature 0.035 m^{-1}			
	SS_{in} (N/m^2)	SS_{out} (N/m^2)	Δp_3 (mmHg)	Δp_2 (mmHg)	SS_{in} (N/m^2)	SS_{out} (N/m^2)	Δp_3 (mmHg)
No catheter							
.1 m/s	0.727	1.049	0.40	NA	0.727	0.996	0.53
.2 m/s	1.383	2.766	0.95	NA	1.380	2.635	1.22
.4 m/s	2.679	6.411	2.35	NA	2.700	8.199	2.97
Catheter out							
.1 m/s	1.117	0.225	0.72	3.55	1.200	0.231	0.96
.2 m/s	2.052	0.482	2.02	7.27	2.098	0.491	2.11
.4 m/s	3.818	1.107	3.86	15.28	3.890	1.094	4.91
Catheter in							
.1 m/s	0.240	1.564	0.68	NA	0.2057	1.517	1.01
.2 m/s	0.513	4.057	1.73	NA	0.441	3.863	2.36
.4 m/s	1.167	10.010	4.14	NA	1.051	10.010	5.27
Catheter top							
.1 m/s	1.119	1.271	0.75	NA	1.111	1.243	0.98
.2 m/s	2.116	3.484	1.70	NA	2.100	3.291	2.20
.4 m/s	4.024	8.595	4.23	NA	4.124	8.393	5.33

SS_{in} = shear stress at inner curve (N/m^2); SS_{out} = shear stress at outer curve (N/m^2); Δp_3 and Δp_2 = denote the axial pressure differences (mmHg) for tubes of 0.003 m and 0.002 m diameter, respectively; NA = not available.

Flow calculations

The ratio of axial regional flow over flow varied between 0.5 and 1% and remained in this range after catheter placement. Neither the different entrance velocity nor the placement of a catheter affected these values.

Shear stress

In the absence of a catheter, shear stress was higher in the outer curve as compared to the inner curve, leading to shear stress ratios of 1.44 for 0.025-m and 1.37 for 0.025-m curvatures for entrance velocities of 0.1 m/s. In addition, the shear stress ratio increased to 2.00 and 2.39 with entrance velocity to 0.2 m/s and to 0.4 m/s for 0.025-m curvatures and to 1.90 and to 2.30 for 0.035-m. curvatures. Catheter placement decreases shear stress in its own vicinity and increases shear stress at the opposite free wall (Table 2). Consequently, the shear stress ratio increases to values of 6.67, 7.87 and 8.55 for a catheter located at the inner wall of a 0.025-m curved tube at 0.1, 0.2 and 0.4 m/s entrance velocity. Changes to 1.14, 1.65 and 2.14 for a catheter located in the top position for a 0.025-m curved tube was calculated at 0.1, 0.2 and 0.4 m/s. For a catheter in the outer position, inner curve shear stress values increased over outer curve shear stress values, leading to shear stress ratios of 0.19, 0.23 and 0.29 (Table 2). Minimal additional differences in the effects were noted for 0.035-m curved vessels.

Pressure difference and tube resistance

The pressure difference calculated along the entire tube varies linearly with entrance velocity from 0.4 to 4.2 mmHg (Table 2). For comparison, between 0.025-m and 0.035-m curved tubes, we corrected the pressure difference for the different length of the tubes (Fig. 4). Catheter placement approximately doubles the normalized pressure difference at each entrance velocity for tubes of 0.003 m. For tubes of 0.002 m in diameter, a 7-fold increase in normalized pressure difference was noted (Fig. 4). Note that tube resistance, which is the ratio of pressure difference over flow, increases with entrance flow: 6.8, 8.7 and 10.4 mmHg.s/m^2 (*i.e.* 267%, 271% and 259% at 0.1, 0.2 and 0.4 m/s entrance velocity for tubes

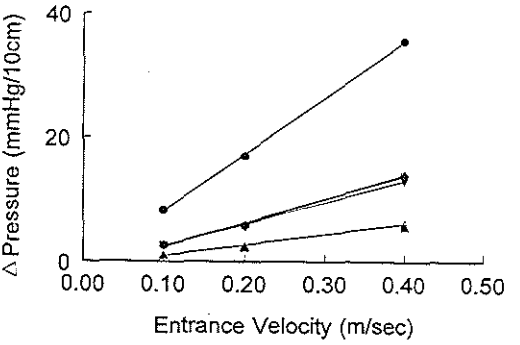

Fig. 4. Normalized pressure difference vs. entrance velocity for different conditions. △ and ▲ denote absence of catheter; ▽ and ▼ denote catheter in outer curve; ◇ and ◆ denote catheter in the inner curve; ○ denotes catheter in the upper position. ● Catheter in outer position in 0.002-m tube. Open enclosed symbols signify 0.025- and 0.035-m curvatures, respectively.

of 0.003 m, independently of catheter location). For the 0.002-m tube, resistance increases up to 38.2 mmHg.s/m^2.

DISCUSSION

The complex velocity patterns that have been identified in the arterial bed of humans (Milnor 1982; Kilner et al. 1993; Moore et al. 1992) are of significance because specific characteristics of those velocity patterns have been associated with the progression and regression of atherosclerosis (Kilner et al. 1993; Moore et al. 1992). At present, the Doppler-based methods assume Poiseuille flow conditions to calculate particle velocity from the Doppler shift. Recently, a novel technique, based on IVUS technology, has been developed that overcomes the simplifications induced by the Doppler methods (Li et al. 1998).

Some potential limitations of this novel method are currently under investigation. In this paper, we consider the fact that secondary velocity is not fully taken into account (Li et al. 1998) and, second, that the catheter itself disturbs the velocity profile. We applied a computational fluid dynamic (CFD) technique to quantify these effects. We will first discuss disturbances induced in the 3-D velocity field, followed by the effect on shear stress, flow and the pressure difference.

3-D velocity field

With laminar flow in a long straight tube with a Newtonian fluid, the velocity profiles are parabolic without secondary velocity components. In curved vessels, the 3-D velocity profile is distributed toward the outer curve, a phenomenon that is accompanied by secondary velocities. These secondary velocities arise as a consequence of the curvature-related centrifugal forces acting on the fluid elements in combination with viscous and inertial forces (Bovendeerd et al. 1987; Chang and Tarbell 1988; Nosovitsky et al. 1997). These forces induce pressure differences perpendicular to the axial direction of the tube, which induces the in-plane velocity ('secondary velocity'). In the present study, secondary velocities in the order of 10–15% were calculated, which is large compared to the values reported by Perktold et al. (1991). However, these authors used smaller curvatures than we did to simulate the coronary epicardial bed. We derived representative curvature values from 3-D reconstructions obtained directly from the coronary system of humans (Krams et al. 1997).

Secondary velocities decreased after inserting a catheter in the curved tubes. Insertion of a catheter also induces a shorter entrance length for flow development. These observations might be due to the existence of an additional boundary layer surrounding the catheter, which reduces the "freedom" to induce in-plane pressure differences. Support for this explanation is found in the fact that the effect of the catheter is the smallest where the boundary layer is minimal (*i.e.* when the catheter is located at the outer curve).

The observation that maximal axial velocity increases after catheter placement, even when normalized for mean velocity, might be explained by similar arguments. Due to the additional boundary layer of the catheter, the 'effective' flow region decreases more than is expected on basis of decrements in cross-sectional area caused by the insertion of the catheter. Hence, a similar flow has to pass through a smaller region and the fluid elements need a higher velocity.

Because the secondary velocities do not add to the forward flow, we also evaluated their effect on potential errors in volume flow measurements based on transit-time velocity measurement technique ("IVUS-Flowmetry"). We calculated that, under the present conditions, the secondary velocity components were in the order of 5–15% of total velocity. We calculated a deviation in the flow smaller than 1% when flow calculations based exclusively on axial velocity were compared to flow calculations based on the magnitude of the entire velocity vector. The small error arises because the magnitude of axial velocity is a projection (cosine) of total velocity vector. The estimated angle of the cosine was approximately 8°, which leads to an error of below 1%.

Shear stress and pressure difference

The catheter acts as a long stenosis and, consequently, it affects the pressure difference in our flow-driven system. We calculated an increase in pressure difference of 2 mmHg for an area stenosis of 11% (0.001-m catheter in a 0.003-m tube) and of 15 mmHg for an area stenosis of 25% (0.001-m catheter in a 0.002-m diameter tube). This highly nonlinear effect can be reconciled by the nonlinear relationship between pressure difference and area stenosis, which is due to the fourth order relationship between resistance and diameter (Milnor 1982).

Shear stress at the wall decreases near the catheter, but an increase in shear stress opposite to the catheter position was noted. The latter finding may be explained again by the existence of an additional boundary layer. Therefore, velocity and shear rate decrease near the catheter and increase distant from the catheter. At constant viscosity, shear stress changes in parallel with shear rate.

Limitations of the method

Entrance and outlet conditions and the grid resolution may affect computational fluid dynamics. We tested if the flow was fully developed to evaluate if restrictions imposed by the boundary conditions were of importance.

It could be shown that the flow field at Cross-section 12 (60° of the bend) was fully developed and, hence, independent of axial location in the tube. This finding is in accordance with theoretical estimates of 6 times the radius of the tube for full flow development, which is equivalent to 0.018 m of arc length (Olsen and Snyder 1985; Bovendeerd et al. 1987). The cross-section of analysis (*i.e.*, Cross-section 12) was positioned at approximately 0.032 m of arc length. Hence, the present analysis is independent of in- and outlet conditions and pertains to steady-state conditions. Increasing the resolution of the mesh did not affect the 3-D velocity vector field at Cross-section 12 under our conditions; hence, the axial velocity component is accurately calculated by this approach.

Although blood is a shear thinning viscoelastic fluid (Bovendeerd et al. 1987), as a first approach we assumed the fluid applied in the present calculations to be Newtonian. This assumption is not very restrictive, because the velocity gradients of the present calculations are high, especially after catheter placement. Blood can be considered Newtonian for shear rates higher than 100 s^{-1}. Consequently, nonNewtonian effects are expected to be minimal under the present conditions.

Coronary flow and not coronary velocity is kept relatively constant by the impedance of the microcirculation, due to autoregulation. However, the pressure differences calculated in the present conditions were so high that autoregulation would not be able to keep flow constant. Furthermore, the same autoregulation would induce a shear-dependent diameter expansion in the vessel segment under study. Hence, to avoid these complexities, we have assumed constant entrance velocity. Consequently, our data should be interpreted with caution because, in practice, both above-mentioned factors (*i.e.*, velocity and shear stress) may change after catheter placement.

We did not include side branches and elasticity of the walls to make the problem easy to solve analytically and numerically (Bovendeerd et al. 1987; Olsen and Snyder 1985; Berger and Talbot 1983). In addition, out of plane curvature has been measured in the human coronary system (Asakura and Karino 1990). The present analysis should, therefore, be considered as a first order analysis.

In summary, placement of a catheter inside a curved tube resembling the human coronary system affects the distribution of the velocity field, and appears to have a secondary velocity-reducing effect. Because the effect of secondary velocity on flow calculations is already small in the absence of a catheter, the present study supports the usefulness of catheter-based flowmetry during resting flow conditions. During hyperemic flow conditions, flow calculations might be accompanied by large axial pressure drops because the catheter, itself, might act as a significant stenosis. This effect is particularly pronounced in small tubes and in the presence of a stenosis. Consequently, hyperemic flow might be reduced despite accurate measurement of flow.

Acknowledgements—Financial support from the Intercardiology Institute of the Netherlands for J. J. Wentzel (Project 18) is greatly acknowledged.

REFERENCES

Asakura T, Karino T. Flow patterns and spatial distribution of atherosclerotic lesions in human coronary arteries. Circ Res 1990;66: 1045–1066.

Berger SA, Talbot L. Flow in curved pipes. Ann Rev Fluid Mech 1983;15:461–512.

Bovendeerd PHM, van Steenhoven AA, van de Vosse FN, Vossers G. Steady entry flow in a curved pipe. J Fluid Mech 1987;177:233–246.

Carlier SG, Li W, Cespedes EI, van der Steen AFW, Hamburger JN, Bom N, Serruys PW. Simultaneous morphological and functional assesment of a renal artery stent intervention with intravascular ultrasound. Circulation 1998;97:2575–2576.

Chang LJ, Tarbell JM. A numerical study of flow in curved tubes simulating coronary arteries J Biomechanics 1988;21:927–937.

Kilner PJ, Yang GZ, Mohiaddin RH, Firmin DN, Longmore DB. Helical and retrograde secondary flow patterns in the aortic arch studied by three directional magnetic velocity mapping. Circulation 1993;88:2235–2247.

Krams R, Wentzel JJ, Oomen JAF, Vinke R, Schuurbiers JCH, De Feyter PJ, Serruys PW, Slager CJ. Evaluation of endothelial shear stress and 3-D geometry as factors determining the development of atherosclerosis and remodeling in human coronary arteries. Arterioscler Thromb Vasc Biol 1997;17:2061–2066.

Li W, van der Steen AF, Lancee CT, Cespedes I, Bom N. Blood flow imaging and volume flow quantitation with intravascular ultrasound. Ultrasound Med Biol 1998;24:203–214.

Li W, van der Steen AF, Lancee CT, Cespedes EL, Carlier S, Gussenhoven EJ, Bom N. Potential of volumetric blood flow measurements. Semin Interv Cardiol 1997;2:49–54.

Milnor WR. Hemodynamics. Baltimore, MD: Williams and Wilkins, 1982.

Moore JF, Ku DN, Zarins CU, Glagov S. Pulsatile flow visualization in the abdominal aorta under differing physiological conditions: implications for increased susceptibility to atherosclerosis. J Biomed Eng 1992;114:391–397.

Nosovitsky VA, Ilegbusl OJ, Jiang J, Stone PH, Feldman CL. Effects of curvature and stenosis-like narrowing on wall shear stress in a coronary artery model with phasic flow. Comp Biomed Res 1997; 30:61–82.

Olsen DE, Snyder B. The upstream scale development in curved circular pipes. J Fluid Mech 1985;150:139–158.

Perktold K, Nerem RM, Peter PO. A numerical calculation of flow in a curved tube model of the left main coronary artery. J Biomech 1991;24:175–189.

Tortoli P, Guidi G, Newhouse VL. Improved blood velocity estimation using the maximum Doppler frequency. Ultrasound Med Biol 1995;21(4):527–532.

Wentzel JJ, Krams R, Vinke R, Oomen JAF, Schuurbiers JCH, Slager CJ. Disturbance of 3-D velocity profiles induced by IVUS catheter, evaluation with computational fluid dynamics. Comput Cardiol IEEE 1997;24:597–599.

Chapter 9

Quantitative volume blood flow using an intravascular array catheter: Influence of catheter ring-down, vessel diameter and noise

F Lupotti, **SG Carlier**, F Mastik, EI Cespedes, N Bom, PW Serruys, AFW van der Steen

To be submitted to Ultrasound in Medicine & Biology

Quantitative volume blood flow using an intravascular array catheter: Influence of catheter ring-down, vessel diameter and noise

Fermín A. Lupotti[1,2], Stephane G. Carlier[2,4], Frits Mastik[2], E. Ignacio Céspedes[3], Nicolas Bom[1,2], Patrick W. Serruys[3] and Antonius F. W. van der Steen[1,2]

[1]*Interuniversity Cardiology Institute of the Netherlands (I.C.I.N.), Utrecht, The Netherlands.*
[2]*Experimental Echocardiography, Thoraxcentre, Erasmus University Rotterdam, Rotterdam, The Netherlands.*
[3]*Department of Interventional Cardiology, Thoraxcentre, Rotterdam, The Netherlands*
[4] *JoMed Imaging, Rancho Cordova,*

All correspondence to:
Fermín A. Lupotti
Erasmus University Rotterdam
Room Ee 23.02, PO Box 1738
3000 DR Rotterdam, The Netherlands
E-mail: lupotti@tch.fgg.eur.nl

Abstract

In recent years, we introduced a new method to measure transverse blood flow based on the decorrelation of the Radio Frequency (RF) signals of Intravascular Ultrasound (IVUS) scanners. We report here in vitro testing to evaluate this decorrelation-based method using an intravascular array catheter. First, a calibration file was produced using a line-target moved transversally across the ultrasound beam. The autoconvolution of the measured acoustical beam was used as the calibration of the decorrelation-based method. Second, blood flow experiments were carried out with different catheters in tube with a diameter ranging from 3 to 5 mm. Flow was measured with a calibrated Transonic flowmeter (range: 0 to 341 cc/min). Excellent linear relationships were found between the IVUS derived flow and the calibrated flowmeter (all r>0.99). The catheter position within the tube and the size of the ring-down were experimentally and theoretically analyzed. These elements have an important influence on the IVUS blood flow measurements reflected by the offset and the slope of the linear relationships. Experimentally, the offset ranged from 6 to 182 cc/min and the slope from 0.13 to 0.39. However, by correcting the offset -that can be measured by processing the IVUS RF signals when the flow is interrupted- an excellent agreement between the estimation of the coronary flow reserve (CFR= flow / baseline flow) derived from the Transonic and the IVUS measurements could be found: the mean ± standard deviation of the differences between the two methods was 0±0.19, for a mean CFR of 2.
In conclusion, the results of this in-vitro validation of the decorrelation method of RF signals of an array IVUS scanner to derive quantitative volume blood flow and coronary flow reserve are very encouraging and warrant further in vivo investigations.

Introduction

Intravascular ultrasound (IVUS) has been used for many purposes as it provides real-time cross-sectional images of blood vessels at a high-resolution (Roelandt et al., 1993; Erbel et al., 1998; Nissen and Yock, 2001). As an imaging tool, IVUS allows to measure the lumen and vessel wall (von Birgelen et al., 1998) and the progression of atherosclerosis and restenosis (Di Mario et al., 1998). Furthermore, important applications of IVUS are the guidance of therapeutic interventions such as coronary stents implantation (Schatz, 1989; Colombo et al., 1995; de Jaegere et al., 1998; Schiele et al., 1998) and the evaluation of intravascular intervention (Di Mario et al., 1995; Blasini et al., 1997; Schwarzacher et al., 1997). Current research in IVUS has focused on obtaining information concerning the acoustic and elastic properties of the vessel wall and plaque for the purpose of vascular tissue characterization (Bridal et al., 1997; Spencer et al., 1997; Komiyama et al., 2000). RF-data processing has significantly enhanced the potential of IVUS (van der Steen et al., 1998) and aims now at obtaining information concerning vessel wall and mechanical plaque properties (Bridal et al., 1997; Céspedes et al., 1997; de Korte et al., 1998; de Korte et al., 2000). In addition, IVUS has been applied to measure blood flow velocity and volumetric flow (Li et al., 1996; Carlier et al., 1998; Li et al., 1998).

Methods to assess blood flow include Doppler processing and time-domain correlation techniques (Isner et al., 1993; Chou et al., 1994; Carlier et al., 1998). Intravascular volumetric blood flow can be assessed with configurations such as combined Doppler Flowire and IVUS or Doppler Flowire and Quantitative Coronary Angiography (QCA) (Serruys et al., 1993; Sudhir et al., 1993; Doriot et al., 2000). A Doppler Flowire is a guide wire with a Doppler transducer in the tip (Doucette et al., 1992). However, these configurations do not easily allow the operator to assess blood flow velocity and lumen area simultaneously and at the same location. Moreover, the mean blood flow velocity is derived from the assumption of a parabolic flow profile that is rarely encountered in human coronary arteries (Carlier et al., 1999).

Recent research have rendered the measurement of blood flow velocity and the quantification of volume blood flow using a decorrelation-based method with a rotating single-element catheter (Li et al., 1998; Li et al., 1998). The correlation of the received IVUS RF signals could be evaluated as a function of time using a sequence of RF signals acquired at a fixed pulse interval from the same angular position. After gating the RF signals with a fixed window length, the sequence of RF signal windows is phase-matched to remove the axial motion of the scatterers and then the correlation coefficients is calculated as a function of time. Next, in a controlled experimental environment, the correlation coefficients have been obtained as a function of transverse displacements of the scatterers to calibrate the

method. Thus, after the time and displacement correlation functions have been established, the correlation coefficients can be converted into velocity. Assuming that the only cause of decorrelation is the transverse displacement of the scatterers (i.e. noise-less RF signals), the velocity can be obtained from the ratio of the correlation coefficient as a function of displacement (calibration) and the correlation coefficient as a function of time (measured). First initial *in vivo* evaluations of volumetric blood flow assessment based on this method using a rotating single-element catheter have been presented (Carlier et al., 1998; Céspedes et al., 1998; Carlier et al., 1999).

The use of mechanically rotated transducer to measure flow requires compensation for the intrinsic decorrelation due to rotation. This could be cumbersome if the rotation is not uniform. IVUS array catheters are not hampered by rotational problems. The array transducer is capable of transmitting and receiving many echoes at a fixed angle. The array is scanned electronically (Eberle, 1997). The decorrelation properties of the IVUS array catheter during transverse blood flow have been simulated and recently reported (Lupotti et al., 2000; Lupotti et al., 2001). The mean decorrelation pattern for scattering media containing only point scatterers, as red blood cells (RBCs), corresponded to the autoconvolution of the acoustical beam.

During this study, *in vitro* recordings were performed to evaluate the decorrelation-based estimation of quantitative volume blood flow using the autoconvolution of the measured acoustical beam as a calibration file. The experiments were carried out for different lumen diameters, for several catheters, and for different catheter positions within the lumen. Coronary flow reserve was measured from the data; using a computer program, the influence of the catheter position and the ring-down size on the blood flow measurements was also studied.

Methods

IVUS transducer

The IVUS array catheter is formed by 64 elements mounted on a circular surface of a catheter tip with a diameter of 1.2 mm. The array transducer operates at a central frequency of 20 MHz and with a -20 dB bandwidth of 7.5 MHz (Eberle, 1997; O'Donnell et al., 1997). The element size of the array under study is 0.7 mm in length and 28 μm in width; the pitch of the elements was 59 μm. The array transducer operates in synthetic aperture focusing mode for imaging and linear mode for flow imaging. Synthetic aperture focusing mode is not suitable for flow assessment since the acoustical beam is formed over a time frame on the order of milliseconds, during which, the red blood cells will move through the beam and will influence flow assessment based on correlation. Therefore, in flow imaging, four elements are electronically tied together and produce a burst of ultrasound pulses in linear array mode. Then, the selected elements are electronically shifted by one and the next burst is generated. The circular array is linearly scanned and pulsed 64 times to produce a frame.

Experimental setup for measuring the Acoustical Beam

The measurement system was formed by a water tank that held the motion system, the echosystem (JoMed Imaging, Rancho Cordova, California 95670) with the IVUS array catheter (20 MHz Vision 64F/X™, JoMed Imaging), and the A/D-converter PC (Figure 1). The A/D-converter PC contained a Pentium computer with an acquisition board (Signatec, Corona, CA, USA) with 128 Mbytes to store the RF data at a sampling frequency of 200 MHz in 8 bits. The water tank was filled with degassed water at room temperature (≈ 22° C). An ultrasound absorber was placed on the bottom and on both sides of the tank to reduce ultrasound reflections. The motion system, with a precision in the order of microns, was a manual micrometer fixed to the water tank; the micrometer was capable of moving a target in x (transverse across the ultrasound beam) and z (along the ultrasound beam) directions. The target was a line reflector consisting of a fiber of 8 μm in diameter (Kevlar, Du Pont de Nemours Int. S.A., Geneva, Switzerland). The line-target was held in a ring fixed to the motion system placed under the water level and positioned orthogonal to the axes of the array transducer. Supported by a fixing system, the IVUS array catheter was placed under the water level between the ultrasound absorber and the line-target (Figure 1). The distance between the line-target and the array transducer surface was set by the motion system and depended on the acoustical-beam depth of interest.

Measurement of the Acoustical Beam

The line-target was moved across the ultrasound beam in

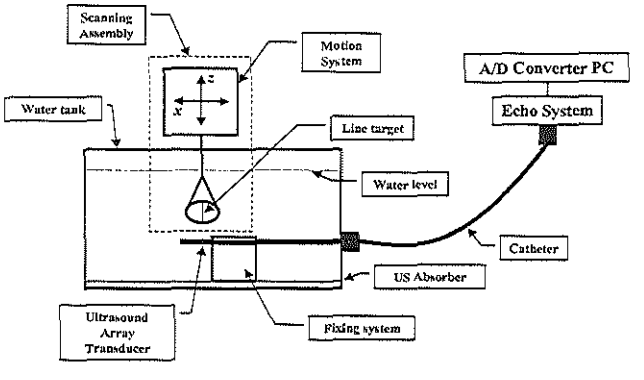

Lupotti *et al.*

Figure 1: Block diagram of the used set-up for measuring the ultrasound beam; the echosystem, the A/D-converter PC and the water tank with the motion system; the IVUS array catheter connected to the echosystem and placed into the water tank.

the transverse direction using the micrometer (Δx= 20 μm). At each displacement, three frames containing the backscattered RF signals (15 RF signals per angle for 64 angles) were acquired by the A/D-converter PC and then saved to hard disk. After the line-target was completely moved across the ultrasound beam, the 15 RF signals from the angle containing the ultrasound reflection from the line-target with maximum amplitude were averaged to reduce the electronic noise. This was performed over the three frames and then an average of the three frames was calculated. The averaged RF signals were used to calculate the autoconvolution of the acoustical beam. The experimental setup allowed the rotation of the array catheter so different elements of the array transducer -angles- could look towards the line-target. For the near field, the experiment was performed for 8 different catheters for 2 angles per catheter; and for the far field, the experiment was performed for 5 different catheters and for 2 different angles per catheter. A higher number of experiments was performed in the near field due to the observed irregularity of the acoustical beam close to the array transducer.

Calibration Method

As it was explained in the introduction, the decorrelation-based method needs to be calibrated in order to convert the measured correlation coefficients as a function of time into transverse velocity. Obtaining the correlation coefficients as a function of transverse displacements does this. The process to obtain such a calibration is time consuming since many experimental realizations have to be performed. A previous study (Lupotti et al., 2000) showed good agreement between RF correlation coefficients as a function of transverse displacements and the autoconvolution of the acoustical beam. Thus, the calibration of an ultrasound beam for measuring quantitative volume blood flow using decorrelation-based method could be assessed by only a theoretical evaluation of the acoustical beam such as the autoconvolution of the acoustical beam. The acoustical beam was experimentally measured for depths ranging from 0.5 mm to 6 mm with steps of 0.5 mm and then by performing the autoconvolution of the measured acoustical beam the calibration file was produced.

Experimental Setup for Blood Flow measurements

The experimental setup was formed by a water tank, the echosystem and the IVUS array catheter, the A/D-converter PC and a transonic flowmeter (30 MHz transducer, Transonic System Inc., Ithaca, NY, USA) (Figure 2).

The water tank (40 cm long) was filled with degassed water at room temperature (≈ 22° C) and an ultrasound absorber was placed on the bottom and at both sides of the tank to reduce ultrasound reflections. The IVUS array catheter was placed inside four different 40-cm long straight tubes with inner diameters of 3.0, 3.5, 4.0 and 5.0 mm. The location of the catheter inside the tubes was chosen to be preferably eccentric with respect to the lumen of the tube (i.e. against the tube wall). Laminar flow conditions were not required during the experiments since in coronary arteries this condition is hardly reached and thus flow in- and outcome effects were not taken into account. A valve was placed just after the upper bicker to regulate the blood flow. The transonic flowmeter was connected to the tubing system just after the exit of the water tank. Fifteen full frames for each flow condition were saved to hard disk and then used to calculate quantitative volume blood flow using the decorrelation-based method. The transonic flowmeter was previously calibrated using the same human blood sample, for a range of volumetric blood flow from 0 to 250 cc/min, using the conventional time-volume approach.

Blood preparation

Outdated packs of concentrated red blood cells (RBC) from the blood bank of our hospital were used during the experiments. The blood sample was diluted with Haemacel solution to reach normal hematocrit and preserved normal blood viscosity. During the experiments, blood manipulation was performed in such way to avoid cellular damage and changes in the hematocrit and in the mean corpuscular volume (MCV). The blood temperature was kept low, around 25° C, to avoid red blood cell destruction. A blood test for the RBC counts, hematocrit and MCV was performed just before and after the experiments and the results showed almost no change in both parameters. The hematocrit was 0.249 L/L and 0.278 L/L and the MCV was 62.4 fL and 62.2 fL, pre and post-experiments, respectively.

Simulation of zero flow RF signals plus noise

A computer simulation program (Borsboom et al., 2000; Lupotti et al., 2000), that simulates backscattered RF signals for the IVUS array catheter, was used during this study. In the computer simulation program, four elements were considered as one curved (convex) single element; its area

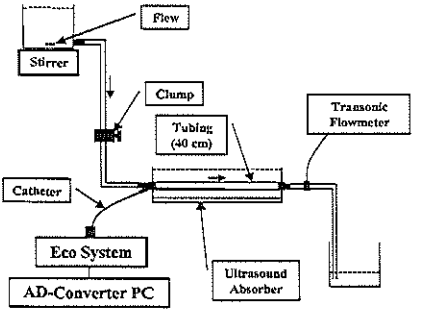

Lupotti *et al.*

Figure 2: Block diagram of the blood flow setup used during the experiments; the echosystem, the A/D converter PC and the water tank; the IVUS array catheter connected to the echosystem and placed into the water tank.

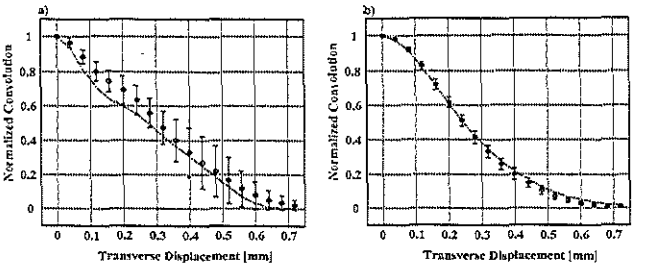

Lupotti *et al.*

Figure 3: Comparison between the simulated (solid line) and the mean autoconvolution of the measured acoustical beam (circles ± std). a) Near field and b) Far field.

was divided into a grid of small areas with dimensions less than a quarter of a wavelength. Thus, each small area transmits an echo and the entire transducer receives the backscattered response. The simulation program was used to generate RF signals in order to produce frames with zero transverse blood flow (i.e. all identical RF signals per angle and per frame). Then, independent noise was added at each RF signal at a given signal-to-noise ratio (SNR). The SNR is defined as the ratio of the average signal power to the average noise power. Next, the data was used to obtain the mean flow over 10 frames for different region of interests -circular regions of 3.0, 3.5, 4.0 and 5.0 mm in diameter- in order to compare the results with the zero-flow offset obtained from the experimental measurements.

Calculation of the coronary flow reserve

Coronary flow reserve in patients is measured as the ratio of the hyperemic flow measured during e.g. an infusion of adenosine over the baseline flow. This parameter evaluates the physiological significance of a coronary stenosis (Gould et al., 1990). In our *in vitro* set up, with flow ranging from 0 to more than 250 cc/min, we have arbitrarily computed the baseline flow for each catheter position and tube combinations as half the average of all the non-zero measured flows. The "simulated" coronary flow reserve for each recording was then computed as the measured flow over this defined baseline flow.

Calculation of ring-down obscuring

Through a computer program, we studied the effect of the ring-down size and catheter eccentricity on the obscuring of the vessel lumen. The radius of the IVUS catheter was 0.6 mm and the ring-down sizes were assumed to be 0.3 and 0.6 mm in depth. These ring-down sizes are representative of the limits in ring-down size from an IVUS array catheter. The vessel lumen was considered circular with radius ranging from 3.0 mm to 5.0 mm. The eccentricity of the catheter, in %, is defined as the distance between the center of the lumen of the tube and the center of the IVUS catheter divided by the radius of the lumen. Eccentricity 0 means a catheter placed in the center of the vessel lumen and thus maximum obscuring of the vessel lumen will occur.

Results

The mean autoconvolution of the experimentally measured acoustical beam is shown in Figure 3 compared to the simulated one (Lupotti et al., 2000), for the near field and for the far field, respectively. In the near field, the autoconvolution of the measured acoustical beam is wider than the theoretical one, which may correspond to the effect of the ring-down of the transducers. However, good agreement is clearly observed between curves in the far field.

Figure 4 shows quantitative volumetric blood flow measurements for different tube diameters versus calibrated Transonic flowmeter. Good linear relationships (all r > 0.99) are observed between the calibrated Transonic flowmeter and the volume blood flow measurement for all tube diameters (see also Table 1). However, the slope and the offset increase with increasing tube diameter. The slope

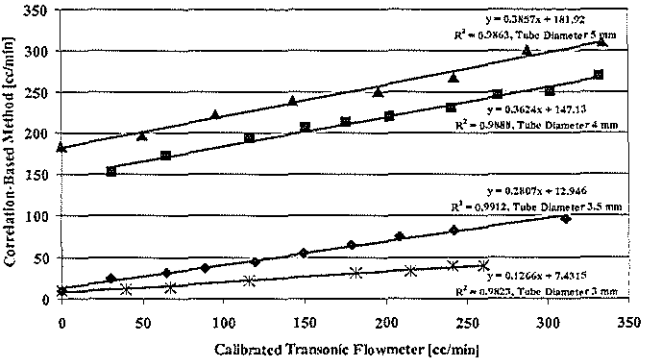

Lupotti *et al.*

Figure 4: Decorrelation-based method versus calibrated transonic flowmeter, results for different tube diameters (3.0, 3.5, 4.0 and 5.0 mm). Linear polynomial approximates to the points with a high R^2. The catheter was placed inside the lumen with maximum eccentricity.

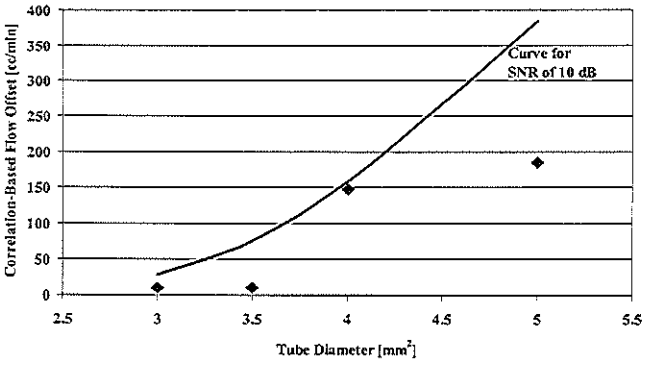

Lupotti *et al.*

Figure 5: Offset in [cc/min] from the experimental measurements plotted as a function of tube diameter. The offset values are shown below the 10 dB signal-to-noise ratio curve.

Table 1

Tube diameter (mm)	Catheter position	Eccentricity %	Catheter #	a	b (cc/min)	r
3	1	45	a	0.24	6.25	0.997
3	2	45	a	0.18	8.99	0.995
3	1	19	b	0.13	7.43	0.991
3.5	1	45	a	0.26	51.36	0.997
3.5	2	58	a	0.27	45.06	0.998
3.5	1	60	b	0.28	12.95	0.996
3.5	2	64	b	0.28	20.35	0.996
4	1	65	a	0.36	147.14	0.994
4	2	59	a	0.34	96.81	0.999
4	1	37	b	0.19	50.06	0.99
5	1	67	b	0.39	181.92	0.993

is in all the cases lower than 1 and the offset can reach up to 182 cc/min for a 5 mm tube diameter. Table 1 summarizes all flow measurements for the different catheters, catheter positions and tubes (see also figure 6 for eccentricity). There is a clear increase of the offset b (in cc/min, corresponding to linear regression: IVUS-flow = a x Transonic-flow + b) as a function of tube diameter. In Figure 5, the offset in cc/min is plotted as a function of tube diameter, which clearly shows the increment of the offset as the tube diameter increases. The curve for simulated data -no flow- with a SNR of 10 dB is presented here. The offset values from the experimental measurements are located below the 10 dB curve, meaning that the RF signals from the experiments were acquired with a SNR higher than 10 dB.

Figure 6 illustrates the effect of the transducer ring-down in masking blood near the surface of the catheter. Two IVUS echograms are presented in the top of the figure. The ring-down is less pronounced in the left one (estimated thickness: 0.2 mm) than in the right one (thickness ~0.4 mm). One RF signal per echogram is shown below each echogram, where at the beginning of the RF signals the ring-down is manifested by an increase on the amplitude, which shows amplitude saturation.

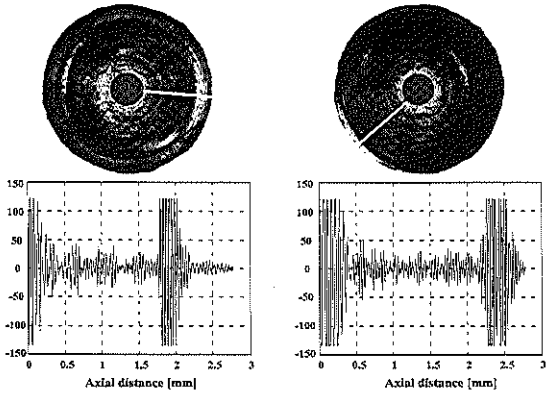

Lupotti *et al.*

Figure 6: top) Echograms of different catheters that show the ring-down size; the RF signals are plotted showing the signals saturation. **bottom)** Curves from two different catheters where the ring-down produces a decrease in the offset; the catheters, low ring-down (dashed and dotted line) and high ring-down (solid line), were placed in the tube lumen with a maximum eccentricity.

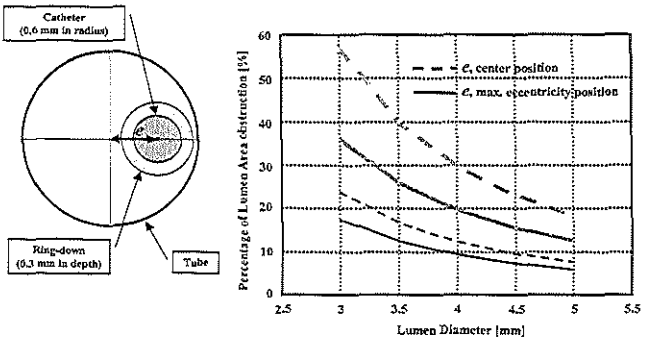

Lupotti *et al.*

Figure 7: Percentage of obscured area due to catheter eccentricity for different tube diameters when the eccentricity ranged from 0 (center of the lumen) to 60 %. Catheter radius of 0.6 mm with a ring-down size of 0.3 (thin black lines) and 0.6 (thick gray lines) mm in depth.

The results of percentage of the lumen area obscured by ring-down as a function of tube diameter are presented in Figure 7 for five different tube diameters (3.0, 3.5, 4.0, 4.5 and 5.0 mm) and for two ring-down sizes (0.3 and 0.6 mm in depth). In an artery of 3.5 mm in diameter, and for a catheter ring-down of 0.6 mm, the obstructed area goes from 25 up to 40 % of the lumen when moving the catheter from the centric (solid line) to the most eccentric position (dashed line).

Processing of the IVUS RF signals when the flow is interrupted (zero flow condition) gave values close to the offset of the linear regression in each case between the IVUS and Transonic flow values (e.g. as illustrated on figure 4 for the tube with diameter 5 or 3.5). These zero-flow recordings (IVUS0) were not performed in all the configuration tube/position/catheters. When they were available, the IVUS flow was corrected with this measured offset, and figure 8 shows (left, open diamonds) the excellent agreement existing then between the IVUS derived and the Transonic coronary flow reserve (CFR). The mean ± standard deviation of the differences between the two methods was 0±0.19, for a mean CFR of 2. For all the recordings, we also approximated the offset to use to correct the IVUS flow by computing the linear regression between the IVUS and Transonic flows. Figure 8, right part (filled diamonds) demonstrates that there was also then an excellent agreement between the IVUS and Transonic CFR.

Discussion

The mean experimental and simulated autoconvolution of the acoustical beam were shown in close agreement, in both near and far field (Fig. 3a and 3b). In the near field, a wider mean autoconvolution was observed, which could be explained by the presence of a ring-down (ultrasound reverberations from the array transducer) at the distance of interest (≈ 1 mm). The ring-down acts as a DC offset, widening the autoconvolution curve. If not compensated, this widening will introduce an underestimation of the blood flow velocity and the volumetric blood flow. In general, the acoustic field along the axis of an ultrasound transducer exhibits rapid fluctuations in the near field and gradually decays in the far

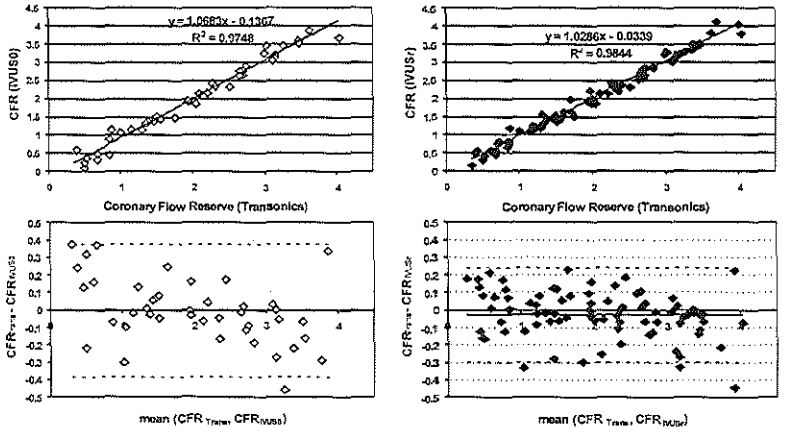

Lupotti *et al.*

Figure 8: Comparison between the coronary flow reserve (CFR) derived from the flow estimated with the IVUS decorrelation method and the true CFR computed on the measured Transonic flows. For each series of tube and catheter position, the baseline Transonic flow used to compute CFR was half the average of all flow measurements. On the left, the regression between both CFR is plotted (upper corner) as well as the Bland-Altman graph (difference versus mean). The baseline IVUS flow was half the average of all flows from which the zero-flow measurement (when available) was subtracted. On the right, similar relationships are shown using all tubes and catheter positions combinations and where the IVUS flow was corrected by the zero-flow estimated from the linear regression between the Transonic and the IVUS derived flows (y-intercepts on figure 4).

field (Christensen, 1988). The standard deviations showed an increase that corresponds to this irregularity of the ultrasound beam in the near field (Fig. 3a). However, in the far field (Fig. 3b), a full agreement was shown between curves and smaller standard deviations were also shown.

Results from experiments showed a good linear relationship for all tube diameters (Fig. 4 and Table 1) meaning that the decorrelation-based system is not being influenced by the volume flow ranging from 0 to 250 cc/min. The relationship between offset and tube diameter could not be clearly established. However, one could suggest that the reason for this is noise integrated over the lumen area. As the SNR is depth dependent, the blood flow offset will increase as a function of tube diameter. Simulated data were computed: frames with velocity zero were used in which noise at a given level was added to the RF signals. The measured data points at zero-flow condition were under the curve determined by the zero-flow simulated data with a noise level of 10 dB.

From the results, one could think that the ring-down is the reason of a slope lower than 1 (Fig. 4 and 7). The ring-down, formed by the interaction of the ultrasound beam and the packing material, obscures part of the lumen vessel area where blood is flowing, which will produce an under estimation of the measurements if the system is not compensated for it. When the amplitude of the RF signals is saturated (Fig. 6), no change due to blood flow can be detected by the decorrelation-based method. Flow estimated in that region is then null. The catheter with a smaller ring down will give a higher offset and a higher slope for the relationship between IVUS and Transonic flow values. The eccentricity of the catheter was shown to have an important effect on the blood flow measurements when ring-down is present. From Fig. 7, the ring-down is shown to obscure up to 45 % of the vessel lumen. Therefore, a maximum eccentricity of the catheter is important during *in vivo* recordings.

Absolute coronary blood flow would be the optimal parameter for intracoronary physiological studies. However, intracoronary flow measurements have been simplified for clini-cal practice. The most useful clinical index at the end of an intervention such as a stent implantation is the coronary flow reserve estimated from the ratio of the maximum flow velocity measured with a Doppler Flowire during hyperemia to the baseline velocity (Di Mario et al., 2000; Serruys et al., 2000). The results of our study suggest that the coronary flow reserve could be estimated in patients with an IVUS catheter. A limitation will be that the catheter must occupy a relatively stable position in the coronary lumen, ideally, at the most eccentric location, which can be achieved. With combined catheters including a balloon distal to the imaging transducer (Mudra et al., 1994), it is foreseen that the recording of the zero flow condition, while the balloon is inflated, will permit the estimation of the offset of the IVUS flow method during *in vivo* application. It would also be very interesting to assess the reduction of the maximal flow through moderate coronary stenosis, beside their conventional morphological IVUS assessment. However, presently, the relatively large diameter of the IVUS catheter (> 1 mm) would cause a significant increase of the pressure gradient across the stenosis, since most of these lesions have a minimal lumen diameter ranging between 1.5 and 2.5 mm. Further miniaturization of the IVUS device will be necessary for this application.

A factor, which was not considered here, is blood flow pulsatility highly present in coronary arteries that produces changes in the shear rates across the vessel lumen. In pulsatile flow, the velocity profile changes significantly as a function of the cardiac cycle (Milnor, 1989). The velocity profile is nearly flat during early systole, becomes almost parabolic at peak systole, depending on the hematocrit, and then flattens again during diastole. In the case of transverse blood-flow, the change in blood velocity profile produces significant velocity gradients, which in the present situation seem to not affect the blood-flow measurements using a decorrelation-based method. Aggregation of Red Blood Cells was also not considered here since previous results suggested that aggregation of RBCs, at random lengths and angles, does not affect the rate of decorrelation (Lupotti et al., 2001). Results from Cloutier (Cloutier and Shung, 1993) suggested that prolonged diastole is necessary to observe an aggregate size enlargement in systole because no cyclic variation on the Doppler power was found during pulsatile flow at 70 beats/min and using whole porcine blood. Rouleaux formation, during systole and at 70 beats/min, was not observed probably because the red cells do not have enough time in diastole to be brought into contact and to align themselves. As flow accelerates with a flat and more parabolic profile in late systole, the aligned red cells then probably form rouleaux until the shear rate within the Doppler-sample volume becomes sufficient to break them totally or partly.

Conclusions

We have characterized experimentally some of the limitations of the IVUS quantitative blood flow assessment. The results clearly indicate dependence of the measure flow on the magnitude of the inevitable ring-down artifact. Additionally, the severity of this effect is dependent on the position of the IVUS catheter within the lumen. In-place noise is also construed as flow and thus the noise characteristics of the entire system (IVUS instrument, catheter, catheterization laboratory environment) have to be measured. Despite the deleterious effect of the ring-down artifact, a practical solution is proposed for the calculation of flow reserve. Since the position of the catheter is constant during CFR measurement, the slope bias can be considered constant. This practical solution presents an intermediate and immediate solution to the limitation described in this paper. However, further advancement in IVUS transducer technology would be required to maximize the value of quantitative IVUS-based flow measurements. In conclusion, the results of this in-vitro validation of the decorrelation-based method to derive quantitative volume blood flow and coronary flow reserve using IVUS RF signals are very encouraging and warrant further *in vivo* investigations.

References:

Blasini, R., Neumann, F. J., Schmitt, C., Bokenkamp, J. and Schomig, A. Comparison of angiography and intravascular ultrasound for the assessment of lumen size after stent placement: impact of dilation pressures. Catheter Cardiovasc Diag 42(2): 113-119; 1997.

Borsboom, J. M. G., Céspedes, E. I., van der Steen, A. F. W. and Lancée,

C. T. Simulation of Cylindrical Intravascular Ultrasound Transducer. J Acoust Soc Am 108(2): 827-835; 2000.
Bridal, S. L., Fornes, P., Bruneval, P. and Berger, G. Correlation of ultrasonic attenuation (30 to 50 MHz) and constituents of atherosclerotic plaque. Ultrasound in Medicine and Biology 23(5): 691-703; 1997.
Carlier, S. G., Céspedes, E. I., Li, W., Mastik, F., van der Steen, A. F. W., Bom, N. and Serruys, P. W. Blood flow assessment with intravascular ultrasound catheters; the ideal tool for simultaneous assessment of the coronary haemodynamics and vessel wall? Semin Intervent Cardiol 3: 21-29; 1998.
Carlier, S. G., Di Mario, C., Kern, M. and Serruys, P. W. Intracoronary Doppler and pressure monitoring. Textbook of Interventional Cardiology (3rd ed). E. J. Topol. Philadelphia, W.B.Saunders Company: 748-781; 1998.
Carlier, S. G., Li, W., Céspedes, E. I., van der Steen, A. F. W., Hamburger, J. N., Bom, K. and Serruys, P. W. Simultaneous morphological and functional assessment of a renal artery stent intervention with intravascular ultrasound. Circulation 97: 2575-2576; 1998.
Carlier, S. G., van Langenhove, G., Lupotti, F. A., Albertal, M., Mastik, F., Bom, N. and Serruys, P. S. Coronary Flow Reserve versus Geometric Measurements of Coronary Dimensions: Advantages and Limitations of the Functional Stenosis Assessment. J Interv Cardiology 12(6): 411-424; 1999.
Céspedes, E. I., Carlier, S. G., Li, W., Mastik, F., van der Steen, A. F. W., Bom, N., Verdouw, P. D. and Serruys, P. W. Blood flow assessment using a mechanical intravascular ultrasound catheter: initial evaluation in vivo. J Vascular Investigation 4(1): 39-44; 1998.
Céspedes, E. I., de Korte, C. L., van der Steen, A. F. W., von Birgelen, C. and Lancée, C. T. Intravascular elastography: principles and potentials. Seminars in Interventional Cardiology 2(1): 55-62; 1997.
Chou, T. M., Sudhir, K., Iwanaga, S., Chatterjee, K. and Yock, P. G. Measurement of volumetric coronary blood flow by simultaneous intravascular two-dimensional and Doppler ultrasound: Validation in an animal model. American Heart Journal 128(2): 237-243; 1994.
Christensen, D. A. Ultrasonic Bioinstrumentation. J. W. Sons, New York: Chap. 8; 1988.
Cloutier, G. and Shung, K. K. Study of red cell aggregation in pulsatile flow from ultrasonic doppler power measurements. Biorheology 30: 443-461; 1993.
Colombo, A., Hall, P., Nakamura, S. and al., e. Intracoronary stenting without anticoagulation accomplished with intravascular ultrasound guidance. Circulation 91: 1676-1688; 1995.
de Jaegere, P., et al. Intravascular ultrasound-guided optimized stent deployment. Eur Heart J 19(8): 1214-1223; 1998.
de Korte, C. L., Pasterkamp, G., van der Steen, A. F. W., Woutman, H. A. and Bom, N. Characterization of Plaque Components using Intravascular Ultrasound Elastography in Human Femoral and Coronary Arteries in vitro. Circulation 102: 617-623; 2000.
de Korte, C. L., van der Steen, A. F. W., Céspedes, E. I. and Pasterkamp, G. Intravascular ultrasound elastography in human arteries: initial experience in vitro. Ultrasound in Medicine and Biology 24(3): 401-408; 1998.
Di Mario, C., Gil, R., Camenzind, E., Ozaki, Y., von Birgelen, C., Umans, V., de Jaegere, P., de Feyter, P. J., Roelandt, J. R. and Serruys, P. W. Quantitative assessment with intracoronary ultrasound of the mechanisms of restenosis after percutaneous transluminal coronary angioplasty and directional coronary atherectomy. Am J Cardiol 75(12): 772-777; 1995.
Di Mario, C., Gorge, G., Peters, R., Kearney, P., Pinto, F., Hausmann, D., Birgelen, C. v., Colombo, A., Mudra, H., Roelandt, J. R. T. C. and Erbel, R. Clinical application and image interpretation in intracoronary ultrasound. European Heart Journal 19(2): 207-209; 1998.
Di Mario, C., Moses, J. W., Anderson, T. J., Bonan, R., Muramatsu, T., Jain, A. C., Suarez de Lezo, J., Cho, S. Y., Kern, M., Meredith, I. T., Cohen, D., Moussa, I. and Colombo, A. Randomized comparison of elective stent implantation and coronary balloon angioplasty guided by online quantitative angiography and intracoronary Doppler. DESTINI Study Group (Doppler Endpoint STenting INternational Investigation). Circulation 102(24): 2938-2944; 2000.
Doriot, P., Dorsaz, P., Dorsaz, L. and Chatelain, P. Accuracy of coronary flow measurements performed by means of Doppler wires. Ultrasound Med Biol 26(2): 221-228; 2000.
Doucette, J. W., Corl, P. D., Payne, H. M., Flynn, A. E., Goto, M., Nassi, M. and Segal, J. Validation of a Doppler guide wire for intravascular measurement of coronary artery flow velocity. Circulation 85: 1899-1911; 1992.
Eberle, M. J. The latest in electronic imaging. Seminars in Interventional Cardiology 2(1): 19-23; 1997.
Erbel, R., Roelandt, J. R. T. C., Ge, J. and Gorge, G., Eds. Intravascular Ultrasound. London, Martin Dunitz; 1998.
Gould, K. L., Kirkeeide, R. L. and Buchi, M. Coronary flow reserve as a physiologic measure of stenosis severity. J Am Coll Cardiol 15: 459; 1990.
Isner, J. M., Kaufman, J., Rosenfield, K., Pieczek, A., Schainfeld, R., Ramaswamy, K. and Kosowsky, B. D. Combined physiologic and anatomic assessment of percutaneous revascularization using a Doppler guidewire and ultrasound catheter. American Journal Cardiology 71(14): 70D-86D; 1993.
Komiyama, N., Berry, G. J., Kolz, M. L., Oshima, A., Metz, J. A., Preuss, P., Brisken, A. F., Pauliina Moore, M., Yock, P. G. and Fitzgerald, P. J. Tissue characterization of atherosclerotic plaques by intravascular ultrasound radiofrequency signal analysis: An in vitro study of human coronary arteries. Am Heart J 140(4): 565-574; 2000.
Li, W., Lancée, C. T., Céspedes, E. I., van der Steen, A. F. W. and Bom, N. Decorrelation properties of intravascular echo signals: Potentials for blood velocity estimation. Journal of the Acoustical Society of America 102(6): 3785-3794; 1998.
Li, W., Lancée, C. T., van der Steen, A. F. W., Gussenhoven, E. J. and Bom, N. Blood velocity estimation with high frequency intravascular ultrasound. IEEE Ultrasonics Symposium, San Antonio, Texas: 1485-1488; 1996.
Li, W., van der Steen, A. F. W., Lancée, C. T., Céspedes, E. I. and Bom, N. Blood flow imaging and volume flow quantitation with intravascular ultrasound. Ultrasound in Medicine and Biology 24(2): 203-214; 1998.
Lupotti, F. A., Céspedes, E. I. and van der Steen, A. F. W. Decorrelation Characteristics of Transverse Blood Flow along an Intravascular Array Catheter. IEEE Transactions on Ultrasonics, Ferroelectrics, and Frequency Control 47(6): 1582-1592; 2000.
Lupotti, F. A., Céspedes, E. I. and van der Steen, A. F. W. Decorrelation Characteristics of Transverse Blood Flow along an Intravascular Array Catheter: Aggregates of Red Blood Cells. Ultrasound in Medicine and Biology in press; 2001.
Milnor, W. R. Hemodynamics. Baltimore, Hong Kong, London, Sydney, Williams & Wilkins; 1989.
Mudra, H., Klauss, V., Blasini, R., Kroetz, M., Rieber, J., Regar, E. and Theisen, K. Ultrasound guidance of Palmaz-Schatz intracoronary stenting with a combined intravascular ultrasound balloon catheter. Circulation 90(3): 1252-1261; 1994.
Nissen, S. and Yock, P. Intravascular Ultrasound. Novel pathophysiological insights and current clinical applications. Circulation 103: 604-616; 2001.
O'Donnell, M., Eberle, M. J., Stephens, D. N., Litzza, J. L., San Vicente, K. and Shapo, B. M. Synthetic phased arrays for intraluminal imaging of coronary arteries. IEEE Transactions on Ultrasonics, Ferroelectrics, and Frequency Control 44(3): 714-721; 1997.
Roelandt, J. R. T. C., Gussenhoven, E. J. and Bom, N., Eds. Intravascular Ultrasound. The Netherlands, Kluwer Academic Publishers; 1993.
Schatz, R. A. A view of vascular stents. Circulation 79(2): 445-457; 1989.
Schiele, F., Meneveau, N. and Vuillemont, A. Impact of Intravascular ultrasound guidance in stent deployment on 6-month restenosis rate: a multicenter, randomized study comparing two strategies - with and without intravascular ultrasound guidance. Journal of American College in Cardiology 32: 320-328; 1998.
Schwarzacher, S. P., Metz, J. A., Yock, P. G. and Fitzgerald, P. J. Vessel tearing at the edge of intracoronary stents detected with intravascular ultrasound imaging. Cardiovasc Diag 40(2): 152-155; 1997.
Serruys, P. W., de Bruyne, B., Carlier, S., Sousa, J. E., Piek, J., Muramatsu, T., Vrints, C., Probst, P., Seabra-Gomes, R., Simpson, I., Voudris, V., Gurne, O., Pijls, N., Belardi, J., van Es, G. A., Boersma, E., Morel, M. A. and van Hout, B. Randomized comparison of primary stenting and provisional balloon angioplasty guided by flow velocity measurement. Doppler Endpoints Balloon Angioplasty Trial Europe (DEBATE) II Study Group. Circulation 102(24): 2930-2937; 2000.
Serruys, P. W., Di Mario, C., Meneveau, N., de Jaegere, P., Strikwerda, S., de Feijter, P. J. and Emanuelsson, H. Intracoronary pressure and flow velocity with sensor-tip guidewires. A new methodological comprehensive approach for the assessment of coronary hemodynamics before and after coronary interventions. Am J Cardiol 71: 41D; 1993.
Spencer, T., Ramo, M. P., Slater, D. M., Anderson, T., Kearney, P. P., Sutherland, G. R., Fox, K. A. and McDicken, W. N. Characterization of atherosclerotic plaque by spectral analysis of intravascular ultrasound: an in vitro study with histological and radiological validation. Ultrasound in Medicine and Biology 23(2): 191-203; 1997.
Sudhir, K., MacGregor, J. S., Barbant, S. D., Foster, E., Fitzgerald, P. J., Chatterjee, K. and Yock, P. G. Assessment of coronary conductance and resistance vessel reactivity in response to nitroglycerin, ergonovine and adenosine: in vivo studies with simultaneous intravascular two-dimensional and Doppler ultrasound. J Am Coll Cardiol 21(5): 1261-1268; 1993.
van der Steen, A. F. W., Céspedes, E. I., de Korte, C. L., Carlier, S. G., Li, W., Mastik, F., Lancée, C. T., Borsboom, J. M. G., Lupotti, F. A., Krams, R., Serruys, P. W. and Bom, N. Novel developments in intravascular imaging. IEEE Ultrasonics Symposium 2: 1733-1742; 1998.
von Birgelen, C., Kutryk, M. J. B. and Serruys, P. W. Three-dimensional Intravascular Ultrasound Analysis of Coronary Stent Deployment and In-Stent Neointimal Volume: Current Clinical Practice and the Concepts of TRAPIST, ERASER, and ITALICS. J Invas Cardiol 10(1): 17-26; 1998.

PART 3

Characterization of Arterial Wall Mechanics by IVUS RF Processing

Chapter 10

Review in depth: intravascular ultrasound elastography.

SG Carlier, CL de Korte, E Brusseau, PW Serruys, AFW van der Steen.

Journal of Cardiovascular Risk 2001; (in press).

This review is an update of the work previously published by de Korte et al., "Characterization of plaque components and vulnerability with intravascular ultrasound elastography" in *Physics in Medicine & Biology 2000; 45:1465-1475.*

Submitted to *Journal of Cardiovascular Risk*

Imaging of Atherosclerosis: Review in Depth: Elastography

Stéphane G Carlier[1,2], Chris L de Korte[2], Elisabeth Brusseau[2], Patrick W Serruys[1], Anton FW van der Steen[2,3]

From:
[1] Thoraxcenter, Department of Interventional Cardiology, Erasmus Medical Center Rotterdam, Rotterdam, The Netherlands;
[2] Experimental Echocardiography Laboratory, Erasmus Medical Center Rotterdam, Rotterdam, The Netherlands;
[3] Interuniversity Cardiology Institute of The Netherlands (ICIN)

This review is an update of the work previously published by de Korte et al., "Characterization of plaque components and vulnerability with intravascular ultrasound elastography" in Physics in Medicine & Biology (2000)

Correspondence address:
S.G. Carlier, MD, Experimental Echo Laboratory, Erasmus University – Ee2302, Dr Molewaterplein 50, 3015 GE Rotterdam, The Netherlands
Phone: 31-10-408 74 74, Fax: 31-10-408 94 45, E-mail: CARLIER@TCH.FGG.EUR.NL

Summary

Intravascular ultrasound elastography is a method for measuring the local elastic properties of coronary atherosclerotic plaques using intravascular ultrasound (IVUS).
Mechanical properties of the different tissues within a plaque are measured through strain. In the last decade, several groups have applied elastography intravascularly with various levels of success. In this paper, the approaches of the different research groups will be discussed and the focus will be on our approach to the application of intravascular elastography.

1. Introduction

Sudden death is the leading symptom of coronary heart diseases in early middle age and stands at the most dreadful end of the spectrum of acute coronary syndromes. More than 50% of sudden deaths are related to an atherosclerotic plaque rupture or ulceration triggering thrombus formation and coronary occlusion.[1,2] Acute myocardial infarction and unstable angina are also related to a similar mechanism. A coronary atherosclerotic lesion can evolve during years without any clinical symptom and flow limitation.[3,4] Acute coronary syndromes frequently develop in arterial segments demonstrating only a mild stenosis on available prior angiograms.[5,6] The plaque morphology, its composition and the importance of the infiltration of macrophages and lymphocytes, more than the degree of stenosis, are the determinants of acute clinical events.[7-9] One of the major limitations of coronary angiography, the gold standard for the evaluation of symptomatic patients with coronary artery disease, is the inability to visualize the arterial wall.[10] Several techniques have been developed and are under development to characterize coronary atherosclerotic plaques.[11] The life-threatening plaques, prone to rupture, have been characterized by three major characteristics: i) the size and structure of the atheromatous lipid core, ii) the thickness of the fibrous cap (< 65 μm) and iii) the inflammation within or adjacent to the fibrous cap.
Catheter-based IntraVascular UltraSound (IVUS) is the only clinically available technique capable of providing real-time cross-sectional images of arteries in vivo.[12,13] IVUS provides quantitative information on the plaque burden and the lumen, as well as qualitative information on the plaque composition that has been compared with histology.[14,15] However, identification of the different plaque components is still limited: hard fibrous and soft plaques can show similar echo texture.[16,17] Especially, the sensitivity to identify lipid pools remains low.[15] Several IVUS-based methodologies have been proposed to improve tissue characterization[18-20] and detect plaque vulnerability.[21,22] However, IVUS, as well as other methodologies developed[11] to detect rupture-prone plaques are limited since they are based on the measurement of indirect vulnerability parameters such as plaque geometry, content, color or temperature. Plaque vulnerability is mainly a mechanical phenomenon: using computer simulations, concentrations of circumferential tensile stress were more frequently found in unstable plaques than in stable plaques.[23,24] For example, a thin fibrous cap shielding a lipid core from the blood may rupture since it is unable to bear the high circumferential stress due to the pulsating blood pressure (mechanical fatigue). These high stress regions can be caused by the geometry of the plaque[25] or by local weakening of the plaque due to macrophage infiltration.[26]
In 1991, a new technique was proposed to directly measure mechanical properties of tissue by ultrasound called elastography.[27] This technique has emerged to improve tissue characterization since a close correlation has been observed between the modification of the elastic properties of a tissue and the development of pathological processes. For example, it has been shown that the Young's modulus[28] (the ratio of a given force applied (stress) and the resulting deformation (strain)) of normal breast tissue is 20-40 kPa, but raises up to >500 kPa in breast carcinoma.[29] Elastography was developed using phantom studies[30] and evaluated in vivo.[31] The underlying principle is that a force (stress) is applied on the tissue and that the resulting strain is a function of the local mechanical properties.[28] The local strain of the material is obtained by means of comparing several ultrasound images acquired at different stress levels. Currently, this technique is developed in our laboratory for intravascular purposes. The objective of this paper is to give

a short overview of different implementations of elastography. Next, the methods and results of our intravascular elastography work will be presented and discussed.

2. Previous related work

Several techniques have been proposed to study the mechanical properties of soft tissues using ultrasound. The main differences are in the type of mechanical solicitation of the tissue (vibration at low or high frequency, or quasi static compression) and in the signal processing methods used for estimating the local elastic properties.

2.1. Sonoelasticity: vibration amplitude imaging

Lerner and Parker presented preliminary work on vibration amplitude 'sonoelasticity imaging'.[32] With this method, a low-frequency vibration (20–500 Hz) is applied externally to excite internal vibrations within the tissue under study. A stiff inhomogeneity surrounded by soft tissue produces a disturbance in the normal vibration eigenmode patterns. Doppler detection techniques are employed to make a real-time vibration image. In some organs, modal patterns can be created, revealing additional information to the shear wave speed of sound of tissue.[33] Two real-time methods, static strain imaging and vibrography (using 0.1-20 Hz compressions) have been recently tested in phantom experiments. Real-time performance with a PC is achieved thanks to an original algorithm (phased root seeking technique) to estimate the strain, faster than the cross-correlation methods.[34]

Recently, Sandrin et al. have reported the results obtained in phantoms of a new method based on such a low-frequency shear wave (200 Hz) visualized by means of an ultrafast imaging system (up to 10,000 frames/s) composed of a linear array of transducers at 3.5 MHz.[35] Sonoelasticity has not been evaluated for vascular tissue, but given the large wavelengths and the level of inhomogeneity in a diseased vessel, it seems not to be the technique of first choice. Ongoing research investigates the feasibility to use magne-tic resonance elastography using propagating acoustic shear waves.[36,37]

2.2. kHz dynamics: vibration amplitude imaging

In this technique, the tissue is excited using a 15–25 kHz sound field and the amplitude of vibration is measured with a 30 MHz transducer.[38] The amplitude of compression waves is related to the mechanical properties of the tissue but also on the size of the tissue inhomogeneities and resonance phenomena. Because of the potential problems related to the in vivo intravascular application of a 20 kHz sound field, this approach has been abandoned for intravascular elasticity imaging.

2.3. Ultrasound-stimulated vibro-acoustic spectrography

Fatemi and Greenleaf have proposed an alternative method based on the acoustic energy emitted from solids and tissue in response to an oscillatory radiation force produced by interfering focused beams of ultrasound. Interference in the intersection region of the two beams produces sinusoidal modulation of the ultrasound energy density that creates an oscillatory force vibrating the object at the selected region that can be measured some distance away. Using two coaxial, confocal transducer elements of a spherically focused annular array, they could image excised human iliac arteries and clearly detect calcified regions.[39]

2.4 Elastography: compression strain imaging

Elastography is an imaging technique based on the static deformation of a linear isotropic elastic material. The tissue under inspection is externally compressed and the displacement between pairs of A-lines with and without compression is determined using cross-correlation analysis.[27,30] From these data, the strain profile in the tissue under study can be determined. Whereas Ophir et al did not explore intravascular application, our group has demonstrated the feasibility to perform in vivo coronary elastography. The compression can be obtained from the systemic pressure difference or by using a compliant intravascular balloon.[40] The following techniques are all more or less based on this excitation principle, but use a variety of detection methods.

2.4.1. Envelope based intravascular elastography

Ryan and Foster developed a technique based on comparison of pre- and post-compression of vessel mimicking phantoms.[41] The displacement in these phantoms was based on speckle tracking in the video signals. The strain is calculated from this displacement. It was shown that phantom components of different hardness had different displacement magnitude. For use under physiological circumstances, the method still needs quite some adaptation. A big advantage of using the envelope is the fact that the correlation function is smoother than the RF-based correlation function and that the video signal is commonly available from any commercial echosystem. The disadvantage is the limited resolution. For intravascular applications, small tissue strains must be measured and therefore the use of RF data dramatically improves the resolution.

2.4.2. Spectral tissue strain

Talhami et al. introduced a technique that is capable of estimating the global radial strain in a vessel.[42] The technique is based on the Fourier scaling property of the signals and uses the chirp Z-transform. The envelope data are used for this analysis. The result is displayed as a color-coded ring around the image of the vessel. Initial results on vascular tissue in vitro and in vivo have been described, however without a validation of the technique.

2.4.3. Phase sensitive speckle tracking multicompression elasticity imaging

Shapo et al. developed another technique that is based on cross-correlation of A-lines.[43,44] This group proposed a large deformation to maximize the signal-to-noise ratio of the displacement and strain estimation. However, a large displacement will decorrelate the ultrasound signals to such an extent that correlation detection is unreliable. For this reason, the cross-correlation is calculated in several intermediate steps of intraluminal pressure. For detection, they use a phase-sensitive speckle tracking technique. The technique uses an IVUS catheter that is inserted in a compliant balloon. The balloon is used to strain the tissue up to 40%. The feasibility of this technique was demonstrated in simulations and tissue mimicking phantoms. Currently the technique is validated in vitro.

2.4.4. Broad-band radiofrequency-based elastography

Radiofrequency data are acquired at two levels of intraluminal pressure. The estimation of the deformation remains, in general, a study of the correlation between signals acquired before and after the application of a stress. The most common signal-processing technique used in elastography considers the local displacements within soft biological tissues as simple translations. Within the RF signal, these displacements will be translated by a delay of the acoustical signatures of the respective tissue regions. This results in a modeling of the post-compression signal as a locally delayed replica of the pre-deformation signal. The local tissue displacement is, in this case, a simple shift. It is computed as the location of the maximum of the cross-correlation function of gated pre- and post-compression echo signals (***time-delay estimation***). The strain is then computed as the displacement derivative.[45,46] In the case of small deformations [0-2 %], these techniques have proved to be efficient and accurate. However, they fail rapidly with increasing strains since then the signal is subjected to a variation in shape that has not been taken into account.

Another approach taking into account the change in shape of the signals has been recently described (***local scaling factor estimation***).[47-49] The signal after compression is processed as a delayed and scaled replica of the signal before deformation. These methods have been shown to be more robust to large deformation, but the performance for small strain values (<2%) remains low. An adaptative strain estimation method based on the computation of local scaling factors has been successfully applied to compute elastograms of cryogel phantoms mimicking vessels and of a freshly excised human carotid artery using a 30 MHz mechanical rotating single element ultrasound scanner (ClearView, CVIS, Boston Scientific Corp.).[50]

We will focus the rest of this review on the intravascular elastography methods that have been developed in our laboratory. Data are acquired at two levels of intraluminal pressure. Displacement and strain are calculated from broad-band RF traces. The strain information is presented as an independent complementary two-dimensional image of the echogram when it has been computed across the complete vessel wall (**elastogram**) or as one dimensional color-coded line congruent with the lumen perimeter when the strain is computed only for the inner layer of the arterial wall (**palpogram**).[51]

3. Materials and methods

3.1. Materials

3.1.1. Phantom.

Vessel phantoms with the morphology of atherosclerotic vessels were constructed from solutions of agar and gelatin with carborundum (SiC) particles used for scattering. A hard vessel containing a soft lesion with no echogenicity contrast between the wall and plaque was measured with intraluminal pressures of 50 and 55 mmHg.[52]

3.1.2. Femoral and coronary arteries in vitro.

Atherosclerotic human femoral (n=10) and coronary (n=4) arteries obtained post mortem were measured in vitro. Two IVUS scans were acquired at 80 mmHg and 100 mmHg. The vessel specimens were then fixed in a buffered formaldehyde solution (3.6%) and processed for routine paraffin embedding. For each segment, cross sections were stained for collagen (picro-Sirius red stain), for smooth muscle cells (anti-α-actin stain) and for macrophages (anti-CD68 stain).[53]

3.1.3. Coronary arteries in vivo.

Data were obtained from patients (n=12) referred for percutaneous coronary intervention. After intravenous administration of heparin and acetylsalicylic acid, a 6 Fr guiding catheter was advanced up to the ostium of the involved artery. After coronary injection of a bolus of 3 mg isosorbide dinitrate, pre-intervention IVUS assessment of the lesion was performed.[54]

The acquisition and signal processing have been explained in detail elsewhere[55] and are beyond the scope of this review. In summary, in vitro experiments on human femoral arteries were performed with a 4.3F Princeps® 30 MHz catheter (Dumed) connected to a stepper motor. The in vitro and in vivo coronary recordings were performed using a 64 F/X array IVUS transducer (EndoSonics/JoMed). In vivo, lesions were crossed and imaged without complication. The pressure was measured at the level of the coronary ostium via the guiding catheter connected to a standard fluid-line system. Ten microseconds (~7.5 mm) of the 64 angles (in Chromaflow mode) analog RF data output of the InVision system were digitized at high frequency (200 MHz, in 8 bits). Ten frames per second were acquired at cross sections where the IVUS echogram revealed diseased vessel wall and plaque. Due to the contraction of the heart, the catheter is moving in the lumen. For large motions, the frames acquired at the different intraluminal pressures may be misaligned thus hindering adequate displacement estimates. An algorithm to determine the similarity between sequential echo frames has been used as a figure of merit for the motion of the catheter in the lumen. Sequential frames with a high likelihood and a pressure differential large enough to result in strain levels of the order of 1% were processed to derive the elastograms.

4. Results

The principle of intravascular elastography is visualized in figures 1 and 2: the echo signal of the soft region (light gray) shows minute changes once the applied force has compressed this tissue, whereas the signal from the hard region (dark gray) remains nearly identical since the tissue thickness in that region did not change. Figure 2 shows the echogram of the phantom acquired at low pressure in the upper left corner. The echogram acquired at high pressure is shown in the lower left corner. The soft plaque area is not visible in the echograms. The local strain determined using the cross-correlation based time delay estimation algorithm is shown on the right. The soft plaque region is clearly visible in the elastogram from 7 to 11 o'clock.

An echogram, elastogram and histology of a human femoral artery segment are shown in figure 2. The echogram of this artery shows a slightly eccentric plaque with different echogenecities. Although the echogram perfectly reveals the geometry of this plaque, its composition remains uncertain. The elastogram reveals that the plaque can be divided into

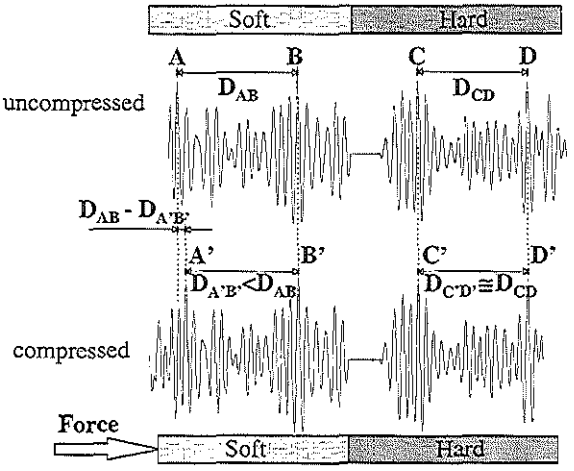

Carlier et al., J of Cardiovascular Risk

Figure 1: Principle of elastography: the echo signals of a soft material (left panel) show minute deformation once the material is compressed by the applied force. The distance D^{AB}, which can be measured by estimation of temporal shifts in the radiofrequency signal, is decreased to $D_{A'B'}$. On the contrary, with the absence of compression of the hard material (right panel), there is no change in the radiofrequency signal and $D_{CD}=D_{C'D'}$.

four quadrants: (a) and (c) demonstrating a low-compressibility, (b) and (d) with a higher compressibility. The strain in the low-compressing parts (0.2%) indicates that this may be fibrous tissue, which was confirmed by histology. The histology of the regions with a higher strain values (0.8–1%) reveals fatty material with macrophage accumulation. At each location investigated (n=45), 2 IVUS images were acquired at different intraluminal pressures (80 and 100 mm Hg). Elastographic data and histology were matched using the IVUS echogram. The cross sections were segmented in regions (n=125) that were based on the strain values on the elastogram. The dominant plaque types in these regions (fibrous, fibro-fatty, or fatty) were obtained from histology and correlated with the average strain and echo intensity. The strain for the 3 plaque types as determined by histology differed significantly (P=0.0002). This difference was mainly evident between fibrous and fatty tissue (P=0.0004). The plaque types did not reveal echo-intensity differences in the IVUS echogram (P=0.882).[5]

In all in vivo experiments, elastograms were determined from two echograms acquired near end-diastole. Analysis of the likelihood curves revealed that the minimal motion of the catheter was present in this part of the heart cycle for all patients. There was on average a pressure differential of approximately 5 mmHg between sequential frames in this part of the heart cycle. Figure 4 demonstrates an echogram, an elastogram and a palpogram of a human coronary artery. The echogram reveals a large calcified area (from noon to 3 o'clock). The elastogram and the palpogram identify this area as being composed of hard material since low strain values are found in this region. Among the 12 patients investigated, 3 demonstrated similar calcified regions (104±70°). The corresponding average strain was 0.20±0.07. Conversely, the average strain in all non-calcified regions was 0.51±0.20 (p<0.001).

5. Discussion

Imaging tissue elastic parameters is rapidly drawing attention for its ability to provide new information on biological tissue. Intravascular elastography has been developed to assess the local mechanical properties of the vascular wall. Knowledge of the mechanical properties may help the clinician in choosing the proper interventional

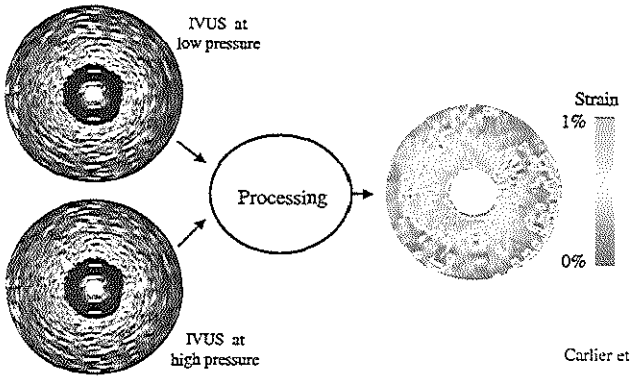

Carlier et al., J of Cardiovascular Risk

Figure 2: Schematic representation of deriving elastograms. From 2 IVUS images acquired at low (upper panel) and high pressure (lower panel), no detection of the soft inclusion in this phantom is possible. However, using cross-correlation techniques, the local strain can be measured and plotted as an additional image on the right, showing the softer region between 7 and 11 o'clock demonstrating a higher strain.

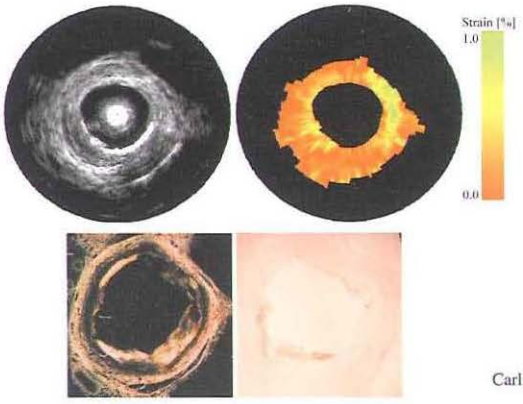

Carlier et al., J of Cardiovascular Risk

Figure 3: Intravascular echogram (top left) and elastogram (top right) of a diseased human femoral artery with corresponding histology: bottom left, picro-Sirius red with polarized light microscopy (for collagen staining), bottom right, anti-CD68 antibody (for macrophage staining). Echogram shows a slightly eccentric plaque with different echogenecities. Elastogram reveals two soft regions (b and d) and two harder regions (a and c). Histology reveals that the soft regions b and d contain mainly fatty material and shows macrophage accumulation in d.

technique and in detecting rupture prone plaques.

The phantom experiments demonstrate that hard and soft material can be identified by IVUS elastography, independently of the echogenicity contrast of the materials.

The results of the in vitro experiments on human femoral arteries support these findings. Fibrous material was identified by the low strain values as observed from the elastogram. In the specimen containing two plaque types, the elastogram clearly revealed the fibrous and the fatty plaque regions. This identification was not possible using the echogram since both regions demonstrated the same echogenicity.

These findings make the technique promising for the identification of rupture-prone plaques characterized by a necrotic core and a thin, fibrous cap.[2] The rupture of a plaque often occurs at places with a high stress concentration.[56] The elastogram does not provide information on the source of this high strain region that can be caused by soft material present in this region or by a stress concentration caused by the geometry. Figure 3 shows that in this particular case, the high radial strain was related to the accumulation of fatty material. Additionally, an increased macrophage concentration has been observed in regions with high strain values. The sensitivity and specificity of the technique remain to be investigated to identify different plaque components and vulnerable regions.

For in vivo elastograms of diseased human coronary arteries, a dynamic instead of static pressure differential is used to strain the tissue. The advantage is that this excitation source is naturally present in the arterial system. Using gated acquisition, different levels of intravascular pressure are obtained. Our preliminary results indicate that reproducible elastograms and palpograms can be obtained with this acquisition set-up scheme. The elastographic findings could not be validated using histology during the in vivo experiments. Therefore, only a partial validation has been performed using the low resolution echogram (64 angles of the Chromaflo imaging mode) to differentiate between calcified and non-calcified material. Since echography gives no information regarding the presence of lipid or fibrous material, further validation has not been possible at this point. A dramatic improvement in the RF signal acquisition scheme has been obtained recently with a direct digital interface incorporated in the Endosonics In-Vision console that communicates directly with a PC in which long sequences of RF echo frames at full rate can be stored in random access memory. High-resolution IVUS images (12 bits resolution, 512 phased-array angles) are now available for comparison with the elastograms.

Compared with the in vitro experiments on human femoral arteries, the pressure differential between the two frames is smaller: 3–5 mmHg instead of 20 mmHg. A smaller pressure differential will immediately result in lower strain values. However, the strain values found during the in vivo experiments are in the same range as the ones found in the in vitro experiments indicating that the tissue during in vivo examination is softer. A possible explanation is that the elastic moduli of tissue will be elevated after excision of the

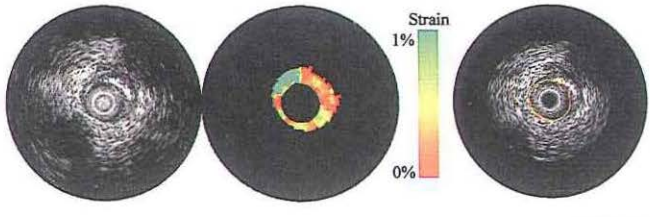

Carlier et al., J of Cardiovascular Risk

Figure 4: *In vivo* echogram (left panel), elastogram (center) and palpogram (right panel) of a cross section in the left anterior descending artery of a patient. The echogram reveals calcified material between noon and 3 o'clock. In this region, a very low strain value was assessed on both the elastogram and the palpogram (color-coded in red).

tissue[57] and may even further increase after cold storage. Additionally, since the in vitro study was performed at room temperature, fatty tissues will be harder at room temperature than at body temperature resulting in decreased strain values.

One of the limitations of intravascular elastography presently is the computing time required and the use of only one-dimensional echo-tracking. Elastographic methods to compute both lateral and axial strains have recently been reported.[58] The palpograms have been developed in order to improve the clinical applicability and the robustness in presence of catheter movements in vivo as well as to advance coronary elasticity to real-time imaging.[51] This technique produces compound images of the strain obtained of the first part of the arterial wall (user defined, typical 600 μm) and conventional sonographic information. Palpograms are computed by applying a two-dimensional echo tracking technique, an outlier rejection filter and a finite difference strain estimator. A composite palpogram, as illustrated in figure 4 (right panel), reconstructed for each cardiac cycle of a 6-second acquisition can presently be computed in less than one minute.[59]

A final limitation of intravascular elastography to stress in is that so far we have computed maps of the strain inside the arterial wall, but not of the Young's modulus. Theoretically, the reconstruction of the Young's modulus would improve the accuracy of tissue characterization and would be independent of the local stress magnitude and its inhomogenous distribution. This final step in elasticity imaging has been described for non-vascular applications[58,60] but is still under preliminary investigation in our laboratory.

6. Conclusion

Intravascular elastography encompasses techniques based on conventional IVUS providing a means for remote palpation and elasticity quantitation of the vessel wall. We have obtained the first elastograms of diseased arteries *in vitro* and *in vivo*. The results show that tissue characterization based on elasticity information from regions with various pathologies may be feasible. This method could potentially improve the detection of rupture-prone plaque based on the assessment of locally increased strain. This information, which is useful for diagnosis and for guiding interventional procedures, is frequently inconclusive or unavailable from IVUS echograms or x-ray angiograms.

7. References

1. Davies MJ, Thomas AC. Plaque fissuring--the cause of acute myocardial infarction, sudden ischaemic death, and crescendo angina. *Br Heart J.* 1985;53:363-73.

2. Virmani R, Kolodgie FD, Burke AP, Farb A, Schwartz SM. Lessons from sudden coronary death: a comprehensive morphological classification scheme for atherosclerotic lesions. *Arterioscler Thromb Vasc Biol.* 2000;20:1262-75.

3. Glagov S, Weisenberg E, Zarins CK. Compensatory enlargement of human atherosclerotic coronary arteries. *N Engl J Med.* 1987;316:1371-1375.

4. Ge J, Erbel R, Gerber T, Gorge G, Koch L, Haude M, Meyer J. Intravascular ultrasound imaging of angiographically normal coronary arteries: a prospective study in vivo. *Br Heart J.* 1994;71:572-8.

5. Ambrose JA, Tannenbaum MA, Alexopoulos D, Hjemdahl-Monsen CE, Leavy J, Weiss M, Borrico S, Gorlin R, Fuster V. Angiographic progression of coronary artery disease and the development of myocardial infarction. *J Am Coll Cardiol.* 1988;12:56-62.

6. Little WC, Constantinescu M, Applegate RJ, Kutcher MA, Burrows MT, Kahl FR, Santamore WP. Can coronary angiography predict the site of a subsequent myocardial infarction in patients with mild-to-moderate coronary artery disease? *Circulation.* 1988;78:1157-66.

7. Stary HC, Chandler AB, Dinsmore RE, Fuster V, Glagov S, Insull W, Jr., Rosenfeld ME, Schwartz CJ, Wagner WD, Wissler RW. A definition of advanced types of atherosclerotic lesions and a histological classification of atherosclerosis. A report from the Committee on Vascular Lesions of the Council on Arteriosclerosis, American Heart Association. *Circulation.* 1995;92:1355-74.

8. Falk E, Shah PK, Fuster V. Coronary plaque disruption. *Circulation.* 1995;92:657-71.

9. van der Wal AC, Becker AE, van der Loos CM, Das PK. Site of intimal rupture or erosion of thrombosed coronary atherosclerotic plaques is characterized by an inflammatory process irrespective of the dominant plaque morphology. *Circulation.* 1994;89:36-44.

10. Topol EJ, Nissen SE. Our preoccupation with coronary luminology. The dissociation between clinical and angiographic findings in ischemic heart disease. *Circulation.* 1995;92:2333-2342.

11. Pasterkamp G, Falk E, Woutman H, Borst C. Techniques characterizing the coronary atherosclerotic plaque: influence on clinical decision making? *J Am Coll Cardiol.* 2000;36:13-21.

12. Di Mario C, Görge G, Peters R, Kearney P, et al. Clinical application and image interpretation in intracoronary ultrasound. Study Group on Intracoronary Imaging of the Working Group of Coronary Circulation and of the Subgroup on Intravascular Ultrasound of the Working Group of Echocardiography of the European Society of Cardiology. *European Heart Journal.* 1998;19:207-29.

13. Nissen S, Yock P. Intravascular Ultrasound. Novel pathophysiological insights and current clinical applications. *Circulation.* 2001;103:604-616.

14. di Mario C, The SHK, Madrestma S, van Suylen RJ, Wilson RA, Born N, Serruys PW, Gussenhoven EJ, Roelandt JRTC. Detection and characterization of vascular lesions by intravascular ultrasound: an in vitro study correlated with histology. *Journal of American Society Echocardiography.* 1992;5:135-146.

15. Prati F, Arbustini E, Labellarte A, Dal Bello B, Sommariva L, Mallus MT, Pagano A, Boccanelli A. Correlation between high frequency intravascular ultrasound and histomorphology in human coronary arteries. *Heart.* 2001;85:567-70.

16. Kimura BJ, Bhargava V, DeMaria AN. Value and limitations of intravascular ultrasound imaging in characterizing coronary atherosclerotic plaque. *Am Heart J.* 1995;130:386-96.

17. Hiro T, Leung CY, De Guzman S, Caiozzo VJ, Favid AR, Karimi H, Helfant RH, Tobis JM. Are soft echoes really soft? Intravascular ultrasound assessment of mechanical properties in human atherosclerotic tissue. *American Heart Journal.* 1997;133:1-7.

18. Wilson LS, Neale ML, Talhami HE, Appleberg M. Preliminary results from attenuation-slope mapping of plaque using intravascular ultrasound. *Ultrasound in Medicine and Biology.* 1994;20:529-542.

19. Komiyama N, Berry GJ, Kolz ML, Oshima A, Metz JA, Preuss P, Brisken AF, Pauliina Moore M, Yock PG, Fitzgerald PJ. Tissue characterization of atherosclerotic plaques by intravascular ultrasound radiofrequency signal analysis: An in vitro study of human coronary arteries. *Am Heart J.* 2000;140:565-74.

20. Vince DG, Dixon KJ, Cothren RM, Cornhill JF. Comparison of texture analysis methods for the characterization of coronary plaques in intravascular ultrasound images. *Comput Med Imaging Graph.* 2000;24:221-9.

21. Yamagishi M, Terashima M, Awano K, Kijima M, Nakatani S, Daikoku S, Ito K, Yasumura Y, Miyatake K. Morphology of vulnerable coronary plaque: insights from follow-up of patients examined by intravascular ultrasound before an acute coronary syndrome. *J Am Coll Cardiol.* 2000;35:106-11.

22. Hiro T, Fujii T, Yasumoto K, Murata T, Murashige A, Matsuzaki M. Detection of fibrous cap in atherosclerotic plaque by intravascular ultrasound by use of color mapping of angle-dependent echo-intensity variation. *Circulation.* 2001;103:1206-11.

23. Cheng GC, Loree HM, Kamm RD, Fishbein MC, Lee RT. Distribution of circumferential stress in ruptured and stable atherosclerotic lesions. A structural analysis with histopathological correlation. *Circulation.* 1993;87:1179-1187.

24. Richardson PD, Davies MJ, Born GVR. Influence of plaque configuration and stress distribution on fissuring of coronary atherosclerotic plaques. *Lancet.* 1989;21:941-944.

25. Loree HM, Kamm RD, Stringfellow RG, Lee RT. Effects of fibrous

cap thickness on peak circumferential stress in model atherosclerotic vessels. *Circulation Research.* 1992;71:850-858.
26.Lendon CL, Davies MJ, Born GVR, Richardson PD. Atherosclerotic plaque caps are locally weakened when macrophage density is increased. *Atherosclerosis.* 1991;87:87-90.
27.Ophir J, Céspedes EI, Ponnekanti H, Yazdi Y, Li X. Elastography: a method for imaging the elasticity in biological tissues. *Ultrasonic Imaging.* 1991;13:111-134.
28.Lee RT, Kamm RD. Vascular mechanics for the cardiologist. *Journal of the American College of Cardiology.* 1994;23:1289-1295.
29.Krouskop TA, Wheeler TM, Kallel F, Garra BS, Hall T. Elastic moduli of breast and prostate tissues under compression. *Ultrason Imaging.* 1998;20:260-74.
30.Céspedes EI. Elastography: imaging of biological tissue elasticity. In. Houston, Texas, CA, USA: University of Houston; 1993.
31.Céspedes EI, Ophir J, Ponnekanti H, Maklad N. Elastography: elasticity imaging using ultrasound with application to muscle and breast in vivo. *Ultrasonic Imaging.* 1993;17:73-88.
32.Lerner RM, Parker KJ. Sonoelasticity images, ultrasonic tissue characterization and echographic imaging. In: Thijssen J, ed. *7th European Communities Workshop.* Nijmegen, The Netherlands; 1987.
33.Parker KJ, Lerner RM. Sonoelasticity of organs, shear waves ring a bell. *Journal of Ultrasound in Medicine.* 1992;11:387-392.
34.Pesavento A, Lorenz A, Siebers S, Ermert H. New real-time strain imaging concepts using diagnostic ultrasound. *Phys Med Biol.* 2000;45:1423-1435.
35.Sandrin L, Catheline S, Tanter M, Hennequin X, Fink M. Time-resolved pulsed elastography with ultrafast ultrasonic imaging. *Ultrason Imaging.* 1999;21:259-72.
36.Muthupillai R, Lomas DJ, Rossman PJ, Greenleaf JF, Manduca A, Ehman RL. Magnetic resonance elastography by direct visulazation of acoustic strain waves. *Science.* 1995;269:1854-1857.
37.Kruse SA, Smith JA, Lawrence AJ, Dresner MA, Manduca A, Greenleaf JF, Ehman RL. Tissue characterization using magnetic resonance elastography: preliminary results. *Phys Med Biol.* 2000;45:1579-90.
38.de Korte CL, Céspedes EI, van der Steen AFW, Lancée CT. Local compressibility assessment using 20kHz sound excitation. *Ultrasonic Imaging.* 1996;18:67-68.
39.Fatemi M, Greenleaf JF. Ultrasound-stimulated vibro-acoustic spectrography. *Science.* 1998;280:82-85.
40.Sarvazyan AP, Emelianov SY, Skovorada AR. Intracavity device for elasticity imaging. In. US: 1993.
41.Ryan LK, Foster FS. Ultrasonic measurement of differential displacement and strain in a vascular model. *Ultrasonic Imaging.* 1997;19:19-38.
42.Talhami HE, Wilson LS, Neale ML. Spectral tissue strain: a new technique for imaging tissue strain using intravascular ultrasound. *Ultrasound in Medicine and Biology.* 1994;20:759-772.
43.Shapo BM, Crowe JR, Skovoroda AR, Eberle M, Cohn NA, O'Donnell M. Displacement and strain imaging of coronary arteries with intraluminal ultrasound. *IEEE Transactions on Ultrasonics, Ferro-electrics, and Frequency Control.* 1996;43:234-246.
44.Shapo BM, Crowe JR, Erkamp R, Emelianov SY, Eberle M, O'Donnell M. Strain imaging of coronary arteries with intraluminal ultrasound: experiments on an inhomogeneous phantom. *Ultrasonic Imaging.* 1996;18:173-191.
45.Céspedes EI, de Korte CL, van der Steen AFW, von Birgelen C, Lancée CT. Intravascular elastography: principle and potentials. *Seminars in Interventional Cardiology.* 1997;2:55-62.
46.de Korte CL, van der Steen AF, Cespedes EI, Pasterkamp G. Intravascular ultrasound elastography in human arteries: initial experience in vitro. *Ultrasound Med Biol.* 1998;24:401-8.
47.Alam KS, Ophir J, Konofagou E. An adaptative strain estimator for elastography. *IEEE Transactions on Ultrasonics, Ferroelectrics, and Frequency Control.* 1998;45:461-472.
48.Bilgen M. Wavelet-based strain estimator for elastography. *IEEE Transactions on Ultrasonics, Ferroelectrics, and Frequency Control.* 1999;46:1407-1415.
49.Brusseau E, Perrey C, Delachartre P, Vogt M, Vray D, Ermert H. Axial strain imaging using a local estimation of the scaling factor from RF ultrasound signals. *Ultrasonic Imaging.* 2000;22:95-107.
50.Brusseau E, Fromageau J, Finet G, Delachartre P, Vray D. Axial strain imaging of intravascular data: results on plyvinyl alcohol cryogel phantoms and carotid artery. *Ultrasound in Medicine and Biology.* 2001:(submitted).
51.Cespedes EI, de Korte CL, van der Steen AF. Intraluminal ultrasonic palpation: assessment of local and cross- sectional tissue stiffness. *Ultrasound Med Biol.* 2000;26:385-96.
52.de Korte CL, Céspedes EI, van der Steen AFW, Lancée CT. Intravascular elasticity imaging using ultrasound: feasibility studies in phantoms. *Ultrasound in Medicine and Biology.* 1997;23:735-746.
53.de Korte CL, Pasterkamp G, van Der Steen AF, Woutman HA, Born N. Characterization of Plaque Components With Intravascular Ultrasound Elastography in Human Femoral and Coronary Arteries In Vitro. *Circulation.* 2000;102:617-623.
54.de Korte CL, Carlier SG, Mastik F, Doyley MM, van der Steen AFW, Serruys PW, Born N. Morphologic and mechanic information of coronary arteries obtained with intravascular elastography: feasibility study in vivo. *Eur Heart J.* 2001:(in press).
55.de Korte CL, van der Steen AF, Cepedes EI, Pasterkamp G, Carlier SG, Mastik F, Schoneveld AH, Serruys PW, Born N. Characterization of plaque components and vulnerability with intravascular ultrasound elastography. *Phys Med Biol.* 2000;45:1465-75.
56.Lee RT, Loree HM, Cheng GC, Lieberman EH, Jaramillo N, Schoen FJ. Computational structural analysis based on intravascular ultrasound imaging before in vitro angioplasty: prediction of plaque fracture locations. *Journal of American College of Cardiology.* 1993;21:777-782.
57.Gow BS, Hadfield CD. The elasticity of canine and human coronary arteries with reference to post-mortem changes. *Circulation Research.* 1979;45:588-594.
58.Konofagou E, Ophir J. A new elastographic method for estimation and imaging of lateral displacements, lateral strains, corrected axial strains and Poisson's ratios in tissues. *Ultrasound Med Biol.* 1998;24:1183-99.
59.Doyley MM, de Korte CL, Mastik F, Carlier SG, Cespedes E, van der Steen AFW, Serruys PW, Born N. Clinical intravascular elasticity imaging: methods and performance evaluation. *Ultrasound in Medicine and Biology.* 2001:(submitted).
60.Emelianov SY, Lubinski MA, Skovoroda AR, Erkamp RQ, Leavey SF, Wiggins RC, O'Donnell M. Reconstructive ultrasound elasticity imaging for renal transplant diagnosis: kidney ex vivo results. *Ultrason Imaging.* 2000;22:178-94.

Chapter 11

Morphological and mechanical information of coronary arteries obtained with intravascular elastography: feasibility study in vivo.

CL de Korte, **SG Carlier**, F Mastik, MM Doyley, AFW van der Steen, PW Serruys, K Bom.

European Heart Journal 2001; (in press).

Editorial comment not yet available.

European Heart Journal
doi:10.1053/euhj.2001.2806, available online at http://www.idealibrary.com on IDEAL®

Morphological and mechanical information of coronary arteries obtained with intravascular elastography

Feasibility study in vivo

C. L. de Korte[1], S. G. Carlier[1], F. Mastik[1], M. M. Doyley[1,2], A. F. W. van der Steen[1,2], P. W. Serruys[1] and N. Bom[1,2]

[1]*Experimental Echocardiography, Thoraxcentre, Erasmus University Rotterdam, The Netherlands;* [2]*Interuniversity Cardiology Institute of the Netherlands, Utrecht, The Netherlands*

Aims Plaque composition is a major determinant of coronary related clinical syndromes. In vitro experiments on human coronary and femoral arteries have demonstrated that different plaque types were detectable with intravascular ultrasound elastography. The aim of this study was to investigate the feasibility of applying intravascular elastography during interventional catheterization procedures.

Methods and Results Data were acquired in patients (n=12) during PTCA procedures with an EndoSonics InVision echoapparatus equipped with radiofrequency output. The systemic pressure was used to strain the tissue, and the strain was determined using cross-correlation analysis of sequential frames. A likelihood function was determined to obtain the frames with minimal motion of the catheter in the lumen, since motion of the catheter prevents reliable strain estimation. Minimal motion was observed near end-diastole. Reproducible strain estimates were obtained within one pressure cycle and over several pressure cycles. Validation of the results was limited to the information provided by the echogram. Strain in calcified material (0·20±0.07 %) was lower (P<0·001) than in non-calcified tissue (0·51±0.20 %).

Conclusion In vivo intravascular elastography is feasible. Significantly higher strain values were found in non-calcified plaques than in calcified plaques.

Key Words: IVUS elastography, atherosclerosis, coronary artery disease, ultrasound.

See doi: 10.1056/euhj.0000.0000 for the Editorial comment on this article

Introduction

There is a great variation in the stability of coronary atherosclerotic plaques. When coronary flow is limited by plaque, patients develop angina, which can be stable for years. However, disruption of coronary plaques with superimposed thrombosis is the main cause of acute coronary events, such as unstable angina pectoris, sudden coronary death and acute myocardial infarction[1–3]. There are two major mechanisms underlying plaque disruption[4,5]: rupture of a fibrous cap of a lipid-rich plaque[6] and denudation and erosion of the endothelial surface[7].

It is now widely accepted that the propensity of a lesion to rupture is poorly predicted by coronary angiography[6,8]. A major problem is that vulnerability of plaque is not directly related to plaque size[7,9] but that the plaque composition is a major determinant[8]. Using intravascular ultrasound, the geometry of lumen, plaque and vessel wall can be obtained and is closely correlated to clinical angina[10]. However, identification of the different plaque components is still limited[11,12] although some promising ultrasound based techniques are currently being developed[13–15].

A wide range of techniques have the potential to visualize or characterize the plaque. Using scintigraphy, detection of plaque instability remained confined[16–18].

Revision submitted 11 May 2001, and accepted 16 May 2001

Correspondence: Chris L. de Korte, Exp.Echo. Ee23.02, PO Box 1738, 3000 DR Rotterdam, The Netherlands

Other potential techniques may be magnetic resonance imaging[19,20] or optical coherence tomography[21]. With spectroscopy,[22] as well as with angioscopy[23] and Raman spectroscopy certain plaque components may be detectable [24,25]. Promising new techniques are electrical impedance imaging[26] and thermal examination[27,28] of plaque surfaces, since a positive correlation between plaque vulnerability and parameters obtained using these techniques were found.

The main disadvantage of the techniques described above is that plaque vulnerability is associated with indirect parameters, such as plaque geometry, content, colour or temperature, although plaque vulnerability is mainly a mechanical phenomenon: using computer simulations, concentrations of circumferential tensile stress were more frequently found in unstable than in stable plaques[29,30]. For example, a thin brous cap shielding a lipid core from the blood may rupture since it is unable to bear the high circumferential stress due to the pulsating blood pressure. These high stress regions can be caused by the geometry of the plaque[30,31] or by local weakening of the plaque due to macrophage in ltration[32].

In 1991, a new technique was proposed, called elastography, which directly measures mechanical properties of tissue by ultrasound[33]. This technique was developed using phantom studies[34] and evaluated in vivo[35]. The underlying principle is that tissue is strained and that the strain rate is related to the local mechanical properties. The local strain of the material is obtained by comparing several ultrasound images. Currently, this technique is developed for intravascular purposes[36-38] and was recently applied in human coronary and femoral arteries in vitro[39,40]. These experiments revealed that the local strain, as measured with intravascular elastography is signi cantly different for brous and fatty plaque components. Furthermore, this technique had the potential to identify plaque vulnerability. Since the radial strain can be obtained, the technique may detect regions with elevated stress: increased circumferential stress is associated with an increased radial strain of the material.

In this study, the feasibility of obtaining elastographic images in vivo has been investigated. Elastograms were determined, using data obtained from arteries, where a PTCA procedure was planned. The pulsatile intracoronary pressure was used to obtain different levels of strain in the arterial wall. Since the catheter was moving in the lumen due to the contraction of the heart, an algorithm to determine the echo frames with minimal motion artefacts was applied on the data. The elastographic results were compared with echographic results.

Patient description and intravascular ultrasound examination

Intravascular ultrasound data was obtained in patients (n=12) referred for percutaneous intervention (Table 1).

Table 1 Baseline clinical and intravascular ultrasound characteristics

Patients, n	12
Age, years	56 ± 12 [36-75]
Male, %	7 (58%)
Systolic blood pressure (mmHg)	132 ± 18 [98-156]
Diastolic blood pressure (mmHg)	79 ± 14 [57-107]
Stable angina, %	5 (42%)
Unstable angina, %	7 (58%)
Prior MI, %	4 (33%)
Risk factors, %	
Diabetes mellitus	1 (8%)
Hypercholesterolaemia	7 (58%)
Hypertension	4 (33%)
Smoking history	4 (33%)
Artery, %	
Left main	1 (8%)
Left anterior descending	3 (25%)
Circum ex	3 (25%)
Right coronary	4 (33%)
Renal artery	1 (8%)
Lesion characteristics, %	
De novo	10 (83%)
Restenotic	2 (17%)
Concentric	7 (58%)
Eccentric	5 (42%)

All the patients signed an informed consent. The culprit lesion to be treated was situated in the left anterior descending artery (n=3), the circum ex (n=3) and the right coronary artery (n=4). The left main coronary artery was investigated in another patient and the renal artery in the nal patient. After intravenous administration of 10 000 IU heparin and 250 mg acetylsalicylic acid, a 6 Fr guiding catheter was advanced up to the ostium of the involved artery. After injection of a bolus of 3 mg isosorbide dinitrate, pre-intervention intravascular ultrasound assessment of the lesion was performed with a 3 5 Fr 64F/X intravascular ultrasound catheter (n=5) or a MegaSonics© (EndoSonics, Rijswijk, The Netherlands), a combination device consisting of an angioplasty balloon (3-3 5 mm diameter, length 20 0 mm) and a 64 F/X array intravascular ultrasound transducer proximal to the balloon (n=7). Lesions were crossed and imaged without complication. With the catheter crossing the lesions without inducing symptomatic ischaemia, a stable position was sought for the transducer in the centre of the lumen, offering visualization of signi cant plaque. The radiofrequency data were acquired as described below. The pressure was measured at the level of the extremity of the guiding catheter connected to a standard uid-line system (Ohmeda, Bilthoven, The Netherlands).

Methods

The 64-element phased array catheter was connected to an EndoSonics InVision system. The system is equipped with analog radiofrequency data output. This output

provides the data for a ChromaFlo© ow mode image[41]. In this mode, the catheter operates in linear instead of phase array mode, thus providing low-resolution images[42]. Each frame contains 64 angles, including a radiofrequency signal of 10 μs (corresponding to 7 5 mm). These data were digitized in a custom-made acquisition system, containing a Pentium computer with an acquisition board (Signatec, Corona, CA, U.S.A.) with 128 Mbyte to store the radiofrequency data at a sampling rate of 200 MHz in 8 bits.

Ten frames per second were acquired at cross-sections where the intravascular ultrasound echogram revealed diseased vessel wall and plaque. For determination of the strain, cross-correlation techniques were applied to the data[39]. First the movement of the tissue along the ultrasound beam was determined. The local strain was obtained from this displacement. Due to the contraction of the heart, the catheter was moving in the lumen[43]. For in-plane motion (catheter moving in the imaging plane), correction algorithms were developed[44]. For large longitudinal motion (i.e. motion along the catheter), the frames acquired at the different intraluminal pressures may image different tissue. In this case, the echo signals are not correlated, thus hindering adequate displacement estimates.

An algorithm to determine the similarity between sequential echo frames was used as a gure of merit for the motion of the catheter in the lumen. The normalized absolute difference between two sequential echo frames was determined using the likelihood between the frames: 0% corresponding to no similarity between the frames and 100% was obtained when both frames were exactly the same. Sequential frames with a high likelihood and a pressure differential large enough (5 mmHg on average) to result in strain levels between 0 and 1% were taken to calculate the elastograms.The determined strain values were tested on validity, using the relation between strain and peak-value of the cross-correlation function[39,45]. Erroneous strain estimates were replaced by the median value of the surrounding strain estimates. The typical number of erroneous strain estimates was 10%. Elastograms with more than 35% erroneous strain estimates were considered unreliable.

Since validation of the experimental results using histology was not available, the elastographic experiments could only be partially validated using the echogram. Strain values for calci ed material, accurately and speci cally identi ed using the echogram by the bright echo and the distal shadowing, were compared to the values corresponding to plaque accumulation and normal coronary segments. Low strain values were expected in the calci ed segments.

Statistical analysis

Values are reported as means ± SD. Analyses were accomplished using a standard software package (SPSS 9.0, SPSS Inc. Chicago, IL, U.S.A.). Differences in strain between calci ed and non-calci ed regions were evaluated by an unpaired Student s t-test. Comparison between groups of patients was evaluated by one way analysis of variance.

Results

Intra-cardiac cycle reproducibility

The acquisition of intravascular elastograms in vivo is illustrated in Fig. 1. The pressure curve (in blue) shows a diastolic pressure of 105 mmHg and a systolic pressure of 135 mmHg. The curve representing the resemblance between the sequential echo frames is in green. Relating this likelihood curve to the pressure curve reveals that the sequential frames have the best match near end-diastole. The maximum likelihood is present just before the P wave of the ECG (in red). The minimal motion of the catheter in this phase corresponds well to the absence of movement and contraction in this phase of the heart cycle. As can be appreciated, the pressure differential between frames at this point in the pressure curve is in the order of 4 mmHg.

The intravascular ultrasound echogram (upper right corner) reveals a concentric plaque in this artery. The echogenicity of the plaque is lower than the echogenicity of the wall. A strong re ection of the lumen- plaque boundary is observed between 4 and 8 o clock. Between 11 and 1 o clock the echogenicity is low and the thickness of the plaque is small.

Three frames near end-diastole were taken to determine two elastograms. The pressure differential of 4 mmHg is large enough to strain the vessel wall and plaque between 0 and 1% (colour coded from red to green). Both images indicate that the region between 11 and 2 o clock has high strain values indicating soft tissue. The region at 3 o clock is relatively hard. The region between 3 and 6 o clock has intermediate strain values at the lumen vessel wall boundary and high strain levels distal to this region. The region between 6 and 11 o clock has low strain values. The similarity between the two frames is high, indicating that the determination of the strain values in one pressure cycle is reproducible.

Inter-cardiac cycles reproducibility

Data from another patient is presented in Fig. 2. Blood pressure was between 100 and 150 mmHg. The likelihood curve (in green) again demonstrates that during systole the resemblance between the frames is small but that near end-diastole the similarity between frames is high. The pressure differential between sequential frames near end-diastole is approximately 5 mmHg.

The echogram of this cross-section shows an eccentric plaque between 3 and 9 o clock. At 8 o clock, a calci ed deposit is visible in the plaque. In all the elastograms, low strain values are observed in the corresponding region. The arterial wall between 9 and 3 o clock has moderate to high strain levels. The plaque area between 3 and 7 o clock has low strain estimates. It can be

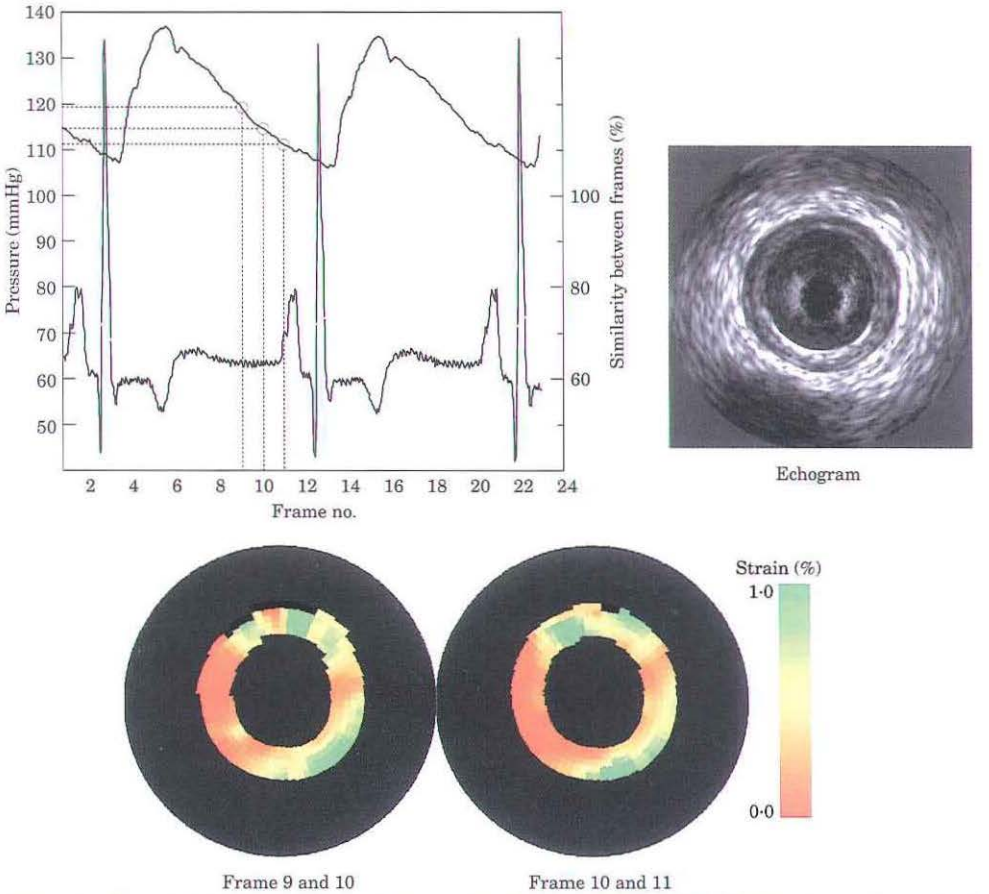

Figure 1 **The principle of acquiring an intravascular elastogram in vivo. The likelihood curve (green line) reveals a maximum near end-diastole. Three echoframes (9, 10 and 11) were taken to determine two elastograms. Both reveal soft material between 10 and 2 o'clock, hard material between 7 and 10 o'clock and mixed (soft material distal to hard material) between 2 and 7 o'clock.**

appreciated that the elastograms have a similar appearance over the sequential pressure cycles. At 3 o clock, erroneous strain estimates can be observed caused by not properly working transducer elements. This artefact was also visible when the ChromaFlo™ mode was activated.

The mean strain pro le with error bars is shown in Fig. 3. Errorbars increase with increasing mean strain value. For low strain values (<0 4%), a standard deviation of 0 08% is present. The standard deviation increases to 0 25% for strain values of 1%.

Strain estimates in function of plaque morphology

In Fig. 4, two echograms and an elastogram are presented. The data for determining the elastogram were acquired near end-diastole. The left echogram is the original echogram as produced using the EndoSonics InVision system. The echogram reveals a highly calci ed wall between 1 and 9 o clock with distal shadowing. The region between 9 and 1 o clock contains no calci ed material. The low-resolution echogram in the middle is the echogram determined directly from the radiofrequency data. Since the radiofrequency data is acquired in ChromaFlo™ mode, only 64 angles are available at low resolution. The elastogram (Fig. 4left) shows very low strain values (average=0 15%) between 2 and 9 o clock corresponding to the calci ed area. The region between 9 and 2 o clock has high strain levels (average = 0.76%), indicating soft material in this region.

Among the 12 IVUS cross-sections acquired in the 12 patients investigated, three demonstrated similar calci- ed regions (104 ± 70°). The corresponding average strain values was 0 20 ± 0 07. Conversely, the average

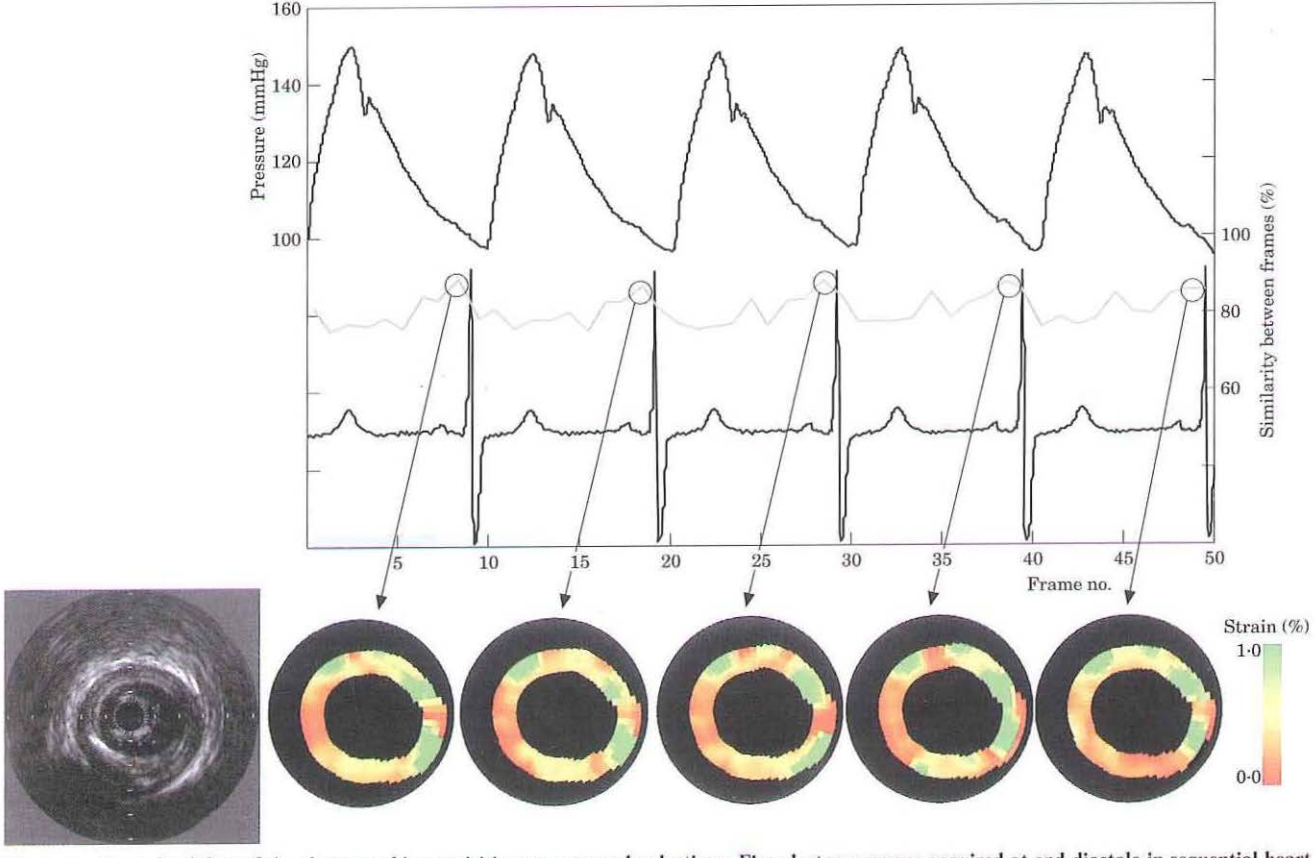

Figure 2 **Reproducibility of the elastographic acquisition over several pulsations. Five elastograms are acquired at end-diastole in sequential heart cycles. The elastograms show similar features in all the elastograms.**

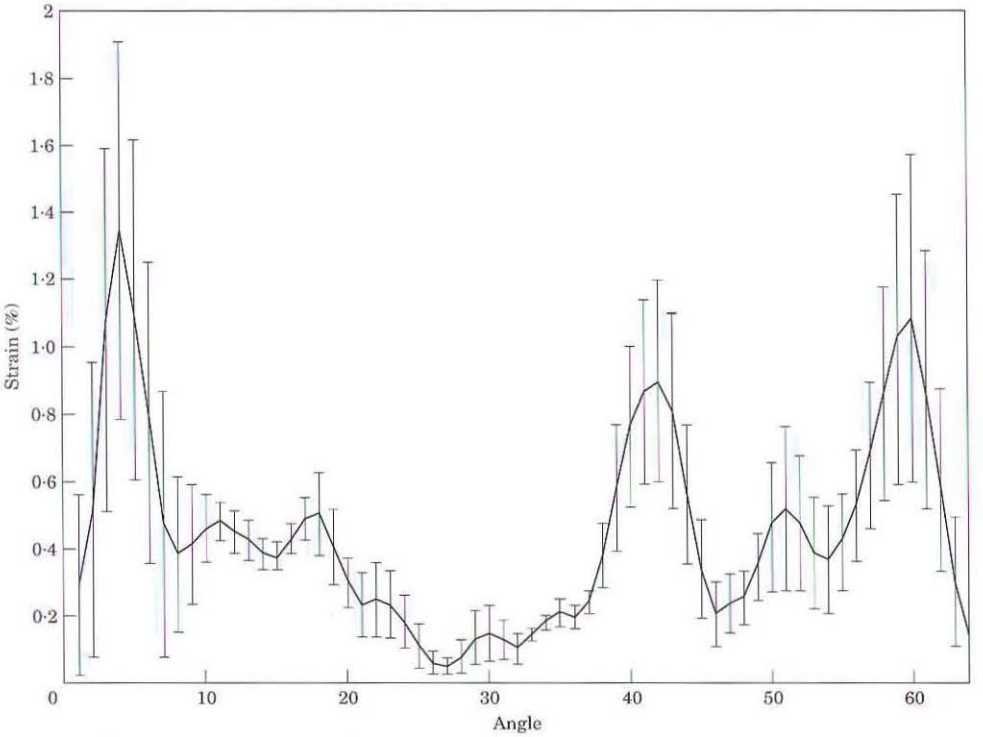

Figure 3 **Mean strain and standard deviation of five elastograms acquired over five sequential pulsations (Fig. 2). The standard deviation increases for higher mean strain values. The high standard deviation near elements 1 and 64 can be explained by the poor sensitivity of the elements at this side of the catheter.**

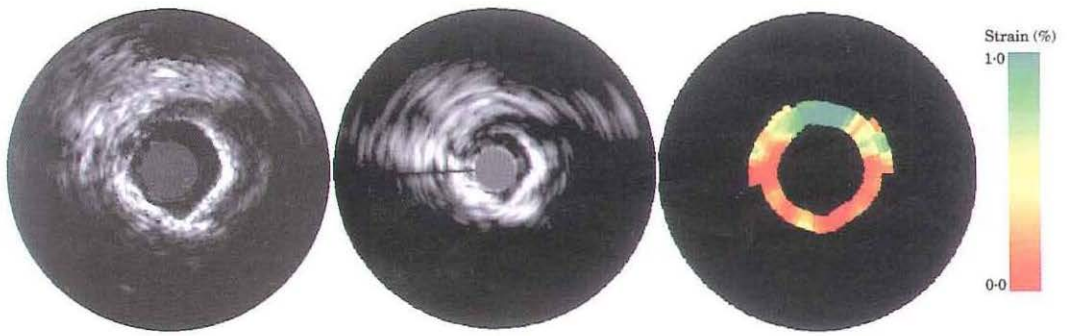

Figure 4 **Echogram (acquired in image and ChromaFlo mode) and elastogram of a cross-section in the LAD. The echogram (left) reveals calcified material between 12 and 9 oclock. The echogram acquired in ChromaFlo™ (middle) reveals the decreased resolution of this acquisition mode. The elastogram shows low compression in this area and high compression in the remaining region (between 9 and 12 oclock).**

strain value in all non-calci ed regions was 0 51 ± 0 20 (P<0 001).

Patients characteristics are given in Table 1. No statistical differences in average strain value over each cross-section were found in function of these characteristics (concentric/eccentric, stable/unstable angina, etc.).

Discussion

Identi cation of plaque vulnerability is crucial. Currently, there is no clinically available tool for reliably detecting vulnerable plaque. Elastography is a promising technique, capable of assessing the local mechanical

properties of the vessel wall and plaque[40]: in vitro experiments demonstrated that strain values obtained with intravascular elastography differ signi cantly for brous and fatty plaque components. It was also shown that fatty regions with an increased macrophage content were co-localized with high strain values.

In this study, in vivo elastograms of diseased human coronary arteries are presented. Contrary to a previous in vitro study[40], a dynamic instead of static pressure differential is used to strain the tissue. The advantage is that this excitation source is already present in the arterial system. Using gated acquisition, different levels of intravascular pressure were obtained. These preliminary results indicate that reproducible elastograms can be obtained using this acquisition scheme.

Compared to the in vitro study, the pressure differential between the two frames is smaller: 4- 5 mmHg instead of 20 mmHg. A smaller pressure differential will immediately result in lower strain values. However, the strain values found in this in vivo study were in the same range as the strain values found in the in vitro study indicating that the tissue in this study is softer. A possible explanation is that the elastic moduli of tissue will be elevated after the tissue is excised[46] and may even further increase after cold storage. Additionally, since the in vitro study was performed at room temperature, fatty tissues will be harder than at body temperature[47] resulting in decreased strain values.

Another way to strain the tissue is to use a compliant angioplasty type of balloon with the transducer in the balloon, as proposed by Shapo *et al.*[38]. Although the motion artefacts due to the contraction of the heart are minimized, this technique has several disadvantages (interruption of the blood ow, non-radial expansion of the artery when the lumen is not circular, movement of the transducer in the balloon due to in ation of the balloon, balloon dilatation in an artery segment which may not require an angioplasty).

Contrary to the in vitro validation study, a phased array transducer, used every day in our catheterization laboratory for clinical purposes, was used for the data acquisition. This monorail catheter presents better trackability and pushability than single element catheters and there is no artefact from the guidewire. Moreover, the use of an array catheter removes the artefacts due to non-uniform rotation. Therefore, two-dimensional instead of one-dimensional cross-correlation techniques might be applied to determine the strain values. These techniques are currently being implemented. In principle, two-dimensional cross-correlation techniques are more robust and should lead to more reliable strain estimates[48].

Limitations

A major problem of advancing intravascular elastography to cardiac in vivo applications is the acquisition of data in a pulsating artery located in a contracting heart. The catheter will move in the lumen and this will result in a mismatch of the data acquired at the low and high pressure. Correct strain estimates are only obtained when the two echoframes (at low and high pressure) image the same cross-section. This study revealed that the motion of the catheter is minimal near end-diastole in the relaxed phase of the cardiac cycle. Figure 3 shows that the standard deviation of the strain estimate increases with increasing mean strain. This increased standard deviation is caused by decorrelation effects at higher strain rates[45]. The use of the high resolution beam-formed data will improve the signal to noise ratio and thus decrease the standard deviation.

Useful data were not obtained during all measurements. In four other patients, the motion was still too large even near end-diastole. This large motion resulted in an increased number of erroneous strain estimates (more than 35%). Currently, improved signal processing tools are being developed to increase the robustness of the method[48]. Another possible solution to this problem is to obtain data during in ation of the angioplasty balloon of the Megasonics catheter: by in ating the balloon, the position of the transducer is xed in the artery.

In this study, the pressure is measured in the ostium using a uid lled line. Therefore, the pressure at the cross-section of interest may have a delay and may deviate from this pressure. For reconstruction of Young s modulus images and to investigate the in uence of a severe stenosis between the measured cross-section and the ostium, the pressure would have to be measured using a high delity pressure wire.

The elastograms presented in this study could not be validated using histology. Therefore, the elastographic ndings were compared with the echographic ndings. Intravascular ultrasound echograms have proven to be a useful tool for the detection of calci ed regions and assessment of the morphology of the plaque and vessel wall[49- 51]. However recent intravascular ultrasound studies revealed that the correlation between echogenicity and brous, bro-fatty or fatty plaque components is low[11,12,40]. Additionally, intravascular ultrasound echograms present limited information for the detection of microcalci cation accumulation[52]. Therefore, no validation of the high strain regions in the elastograms was performed. Currently, the technique is validated using an atherosclerotic yucatan minipig animal model. Validation of the elastographic ndings in humans could be performed using a directional atherectomy device. However, the correlation of the excised plaque with the intravascular ultrasound image in a radial and longitudinal direction will be extremely difficult. Validation of small spots would need a system that is able to determine the tissue type with a higher resolution. The current developments in optical coherence tomography[21] and Raman spectroscopy[53] may allow performing such validation of intravascular elastography in vivo in the near future[54]. Plaque unstability detected by elastography will be compared in the future with thermographic recordings, recently demonstrated as a potential useful method[28].

The resolution of the described system is 200 μm in a radial direction. This resolution is above the thickness of caps of rupture prone plaques that are typically thinner than 100 μm. Therefore, the thickness of the brous cap will be over-estimated. However, a cap that is rupture prone will have increased circumferential stress values[55]. The resulting increased radial strain is obtained using elastography. The power of elastography is that the actual strain is measured and is not based on assumptions[55,56].

We could demonstrate a signi cantly lower strain value in the calci ed regions of the cross-sections recorded among these 12 patients than in the rest of the vessel wall, as expected. However, no further differentiation among these segmented regions in function of the plaque composition (normal/neointimal thickening, soft/brous plaque)[11] could be performed because of the poor resolution of the acquired cross-sections in the 64 angles ChromaFlo® mode, as illustrated on Fig. 4. This is being currently improved on the new high-speed digital interface available for the EndoSonics In-Vision platform. It was also not possible to demonstrate strain differences in function of the clinical presentation. This will be investigated in the future among a more important study population.

Conclusions

It is feasible to apply intravascular elastography in vivo. Using the pulsatile pressure as a mechanical stimulus, different strain levels were measured for different tissue components. The strain in non-calci ed material is signi cantly higher than in calci ed material.

We thank M. B. van der Brand, P. J. de Feyter, D. P. Foley, W. J. van de Giessen and B. Rensing for their co-operation during the interventional procedures. We thank J. Thulis and J. Ligthart for their experienced ultrasound assistance. This work is supported by the Dutch Technology Foundation (STW). C. L. de Korte is a NWO fellow.

References

[1] Falk E. Coronary thrombosis: pathogenesis and clinical manifestations. Am J Cardiol 1991; 68: 28B-35B.
[2] Fuster V, Badimon L, Badimon JJ, Chesebro JH. The pathogenesis of coronary artery disease and the acute coronary syndromes. N Engl J Med 1992; 326: 242-50.
[3] Kragel AH, Gertz SD, Roberts WC. Morphologic comparison of frequency and types of acute lesions in the major epicardial coronary arteries in unstable angina pectoris, sudden coronary death and acute myocardial infarction. J Am Coll Cardiol 1991; 18: 801-8.
[4] Burke AP, Farb A, Malcolm GT, Liang Y, Smialek J, Virmani R. Coronary risk factors and plaque morphology in men with coronary disease who died suddenly. N Engl J Med 1997; 336: 1276-82.
[5] Davies MJ. Stability and instability: two faces of coronary atherosclerosis. Circulation 1996; 94: 2013-20.
[6] Falk E, Shah P, Fuster V. Coronary plaque disruption. Circulation 1995; 92: 657-71.
[7] Fishbein MC, Sighel RJ. How big are coronary atherosclerotic plaques that rupture. Circulation 1996; 94: 2662-6.
[8] Lee RT, Libby P. The unstable atheroma. Arterioscler Thromb Vasc Biol 1997; 17: 1859-67.
[9] Topol EJ, Nissen SE. Our preoccupation with coronary luminology: the dissociation between clinical and angiographic ndings in ischemic heart disease. Circulation 1995; 92: 2333-442.
[10] Hodgson JMB, Reddy KR, Suneja R, Nair RN, Lesnefsky EJ, Sheehan HM. Intracoronary ultrasound imaging: correlation of plaque morphology with angiography, clinical syndrome and procedural results in patients undergoing angioplasty. J Am Coll Cardiol 1993; 21: 35-44.
[11] di Mario C, Gorge G, Peters R *et al.* Clinical application and image interpretation in intracoronary ultrasound. Study Group on Intracoronary Imaging of the Working Group of Coronary Circulation and of the Subgroup on Intravascular Ultrasound of the Working Group of Echocardiography of the European Society of Cardiology. Eur Heart J 1998; 19: 207-29.
[12] Prati F, Arbustini E, Labellarte A *et al.* Correlation between high frequency intravascular ultrasound and histomorphology in human coronary arteries. Heart 2001; 85: 567-70.
[13] Bridal SL, Fornes P, Bruneval P, Berger G. Correlation of ultrasonic attenuation (30 to 50 MHz) and constituents of atherosclerotic plaque. Ultras Med Biol 1997; 23: 691-703.
[14] Spencer T, Ramo MP, Salter DM *et al.* Assessment of regional vascular distensibility in deceased iliofemoral arteries by intravascular ultrasound. Ultras Med Biol 1997; 20: 529-42.
[15] Hiro T, Fujii T, Yasumoto K, Murata T, Murashige A, Matsuzaki M. Detection of brous cap in atherosclerotic plaque by intravascular ultrasound by use of color mapping of angle-dependent echo-intensity variation. Circulation 2001; 103: 1206-11.
[16] Vallabhajosula S, Paidi M, Badimon JJ *et al.* Radiotracers for low density lipoprotein biodistribution studies in vivo: technetium-99m low density lipoprotein versus radiolodinated low density lipoprotein preparations. J Nucl Med 1988; 29: 1237-45.
[17] Lees AM, Lees RS, Scoen F *et al.* Imaging human atherosclerosis with 99mTc-labeled low density lipoproteins. Arteriosclerosis 1988; 8: 461-70.
[18] Miller DD, Rivera FJ, Garcia OJ, Palmaz JC, Berger HJ, Weisman HF. Imaging of vascular injury with 99m Tc-labeled monoclonal antiplatelet antibody S12: Preliminary experience in human percutaneous transluminal angioplasty. Circulation 1991; 85: 1354-63.
[19] Fayad Z, Fuster V, Fallon J *et al.* Nonivasive in vivo human coronary artery lumen and wall imaging using black-blood magnetic resonance imaging. Circulation 2000; 102: 506-10.
[20] Botnar R, Stuber M, Kissinger K, Kim W, Spuentrup E, Manning W. Nonivasive coronary vessel wall and plaque imaging with magnetic resonance imaging. Circulation 2000; 102: 2582-7.
[21] Brezinski ME, Tearney GJ, Weissman NJ *et al.* Assessing atherosclerotic plaque morphology: comparison of optical coherence tomography and high frequency ultrasound. Heart 1997; 77: 397-403.
[22] Toussaint JF, Southern JM, Fuster V, Kantor HL. 13 C-NMR spectroscopy of human atherosclerotic lesions: relation between fatty acid saturation, cholesteryl ester content and luminal obstruction. Circulation 1994; 14: 1951-7.
[23] Feld S, Ganim M, Carell ES *et al.* Comparison of angioscopy, intravascular ultrasound imaging and quantitative coronary angiography in predicting clinical outcome after coronary intervention in high risk patients. J Am Coll Cardiol 1996; 28: 97-105.
[24] Brennan JF, Römer TJ, Lees RS, Tercyak AM, Kramer JR, Feld MS. Determination of human coronary artery composition by Raman spectroscopy. Circulation 1997; 96: 99-105.
[25] Römer TJ, Brennan JF, 3rd, Puppels GJ *et al.* Intravascular ultrasound combined with Raman spectroscopy to localize and quantify cholesterol and calcium salts in atherosclerotic

coronary arteries. Arterioscler Thromb Vasc Biol 2000; 20: 478-83.

[26] Bouma C. Lipid detection in atherosclerotic lesions by intravascular impedance imaging [PhD Thesis]. Utrecht University: Utrecht, The Netherlands: 1998.

[27] Casscells W, Hathorn B, David M *et al.* Thermal detection of cellular in ltrates in living atherosclerotic plaques:possible implications for plaque rupture and thrombosis. Lancet 1996; 347: 1447-9.

[28] Stefanidis C, Diamantopoulos L, Vlachopoulos C *et al.* Thermal heterogeneity within human atherosclerotic coronary arteries detected in vivo: A new method of detection by application of a special thermography catheter. Circulation 1999; 99: 1965-71.

[29] Cheng GC, Loree HM, Kamm RD, Fishbein MC, Lee RT. Distribution of circumferential stress in ruptured and stable atherosclerotic lesions. A structural analysis with histopathological correlation. Circulation 1993; 87: 1179-87.

[30] Richardson PD, Davies MJ, Born GVR. In uence of plaque con guration and stress distribution on ssuring of coronary atherosclerotic plaques. Lancet 1989; 21: 941-4.

[31] Loree HM, Kamm RD, Stringfellow RG, Lee RT. Effects of brous cap thickness on peak circumferential stress in model atherosclerotic vessels. Circ Res 1992; 71: 850-8.

[32] Lendon CL, Davies MJ, Born GVR, Richardson PD. Atherosclerotic plaque caps are locally weakened when macrophage density is increased. Atherosclerosis 1991; 87: 87-90.

[33] Ophir J, Céspedes EI, Ponnekanti H, Yazdi Y, Li X. Elastography: a method for imaging the elasticity in biological tissues. Ultras Imag 1991; 13: 111-34.

[34] Céspedes EI. Elastography: imaging of biological tissue elasticity (PhD Thesis). University of Houston; Houston, Texas, CA, USA: 1993.

[35] Céspedes EI, Ophir J, Ponnekanti H, Maklad N. Elastography: elasticity imaging using ultrasound with application to muscle and breast in vivo. Ultras Imag 1993; 17: 73-88.

[36] de Korte CL, Céspedes EI, van der Steen AFW, Lancée CT. Intravascular elasticity imaging using ultrasound: feasibility studies in phantoms. Ultras Med Biol 1997; 23: 735-46.

[37] Ryan LK, Foster FS. Ultrasonic measurement of differential displacement and strain in a vascular model. Ultras Imag 1997; 19: 19-38.

[38] Shapo BM, Crowe JR, Erkamp R, Emelianov SY, Eberle M, O Donnell M. Strain imaging of coronary arteries with intraluminal ultrasound: experiments on an inhomogeneous phantom. Ultras Imag 1996; 18: 173-91.

[39] de Korte CL, van der Steen AFW, Céspedes EI, Pasterkamp G. Intravascular ultrasound elastography of human arteries: initial experience in vitro. Ultras Med Biol 1998; 24: 401-8.

[40] de Korte CL, Pasterkamp G, van der Steen AFW, Woutman HA, Bom N. Characterization of plaque components using intravascular ultrasound elastography in human femoral and coronary arteries in vitro. Circulation 2000; 102: 617-23.

[41] Crowe JR, Shapo BM, Stephens DN *et al.* Blood Speed Imaging with an Intraluminal Array. IEEE Trans UFFC 2000; 47: 672-81.

[42] Borsboom JM, Céspedes EI, van der Steen AFW, Lancée CT. Simulation of phased array ultrasound transducers for intravascular applications. J Ac Soc Am 2000; 108: 827-35.

[43] Arbab-Zadeh A, DeMaria AN, Penny WF, Russo RJ, Kimura BJ, Bhargava V. Axial movement of the intravascular ultrasound probe during the cardiac cycle: Implications for three-dimensional reconstruction and measurements of coronary dimensions. Am Heart J 1999; 138: 865-72.

[44] Janssen C, de Korte CL, van der Heiden M, Wapenaar C, van der Steen A. Angle matching in intravascular elastography. Ultrasonics 2000; 38: 417-23.

[45] Céspedes EI, de Korte CL, van der Steen AFW. Echo decorrelation from displacement gradients in elasticity and velocity estimation. IEEE trans UFFC 1999; 46: 791-801.

[46] Cow BS, Had eld CD. The elasticity of canine and human coronary arteries with reference to post-mortem changes. Circ Res 1979; 45: 588-94.

[47] Lundberg B. Chemical composition and physical state of lipid deposits in atherosclerosis. Atherosclerosis 1985; 56: 93-110.

[48] Doyley MM, de Korte CL, Mastik F, Carlier SG et al. Advancing intravascular palpography towards clinical applications. In: Wells PNT, Halliwell M, eds. Acoustical Imaging; 2000; Bristol: Plenum Press, 2000: 493-500.

[49] Nishimura RA, Edwards WD, Warnes CA *et al.* Intravascular ultrasound imaging: In vitro validation and pathologic correlation. J Am Coll Cardiol 1990; 16: 145-54.

[50] Potkin BN, Bartorelli AL, Gessert JM *et al.* Coronary artery imaging with intravascular high-frequency ultrasound. Circulation 1990; 81: 1575-85.

[51] van der Lugt A, Gussenhoven E, Stijnen T *et al.* Comparison of intravascular ultrasonic ndings after coronary balloon angioplasty evaluated in vitro with histology. J Am Coll Cardiol 1995; 76: 661-6.

[52] Friedrich GJ, Moes NY, Muhlberger VA *et al.* Detection of intralesional calcium by intracoronary ultrasound depends on the histologic pattern. Am Heart J 1994; 128: 435-41.

[53] Römer TJ, Brennan JF, 3rd, Schut TC *et al.* Raman spectroscopy for quantifying cholesterol in intact coronary artery wall. Atherosclerosis 1998; 141: 117-24.

[54] de Korte CL, Buschman HPJ, van der Poll SWE, van der Steen AFW, Puppels GJ, van der Laarse A. Vascular plaque characterization using intravascular ultrasound elastography and NIR Raman spectroscopy in vitro. In: Shung KK, Insana MF, eds. SPIE Medical Imaging; 2000; San Diego, CA, USA: 2000. 180-6.

[55] Lee RT, Loree HM, Cheng GC, Lieberman EH, Jaramillo N, Schoen FJ. Computational structural analysis based on intravascular ultrasound imaging before in vitro angioplasty: prediction of plaque fracture locations. J Am Coll Card 1993; 21: 777-82.

[56] Huang H, Virmani R, Younis H, Burke A, Kamm R, Lee R. The impact of calcl cation on the biomechanical stability of atherosclerotic plaques. Circulation 2001; 103: 1051-6.

Chapter 12

Advancing intravascular ultrasonic palpation towards clinical applications

MM Doyley, F Mastik, CL de Korte, **SG Carlier**, EI Céspedes, P.W. Serruys, N. Bom, AFW van der Steen.

Submitted to Ultrasound in Medicine and Biology.

Advancing intravascular ultrasonic palpation towards clinical applications

M. M. Doyley[1,2], F. Mastik[1], C. L. de Korte[1], S.G. Carlier[1], E. I. Céspedes[3], P.W. Serruys[1], N. Bom[1,2], and A. F. W. van der Steen[1,2]

[1]Thoraxcentre, Erasmus University, PO Box 1738, 3000DR Rotterdam, The Netherlands
[2]Inter-university Cardiology Institute of the Netherlands
[3]JOMED imaging, Rancho Cordova, CA, USA

Running title: Intravascular ultrasonic palpation

Address for correspondence
Chris L. de Korte, Ph.D., Erasmus University Rotterdam, Department of Echocardiography, Room 2302, P.O. Box 1738, Rotterdam 3000 DR
Tel. +31(01) 408-8033, Fax: +31(01) 408-9445, Email dekorte@tch.fgg.eur.nl

Abstract

This paper describes the first reported attempt to develop a real-time intravascular ultrasonic palpation system. We also report on our first experience in the catherization laboratory with this new elastographic imaging technique. The prototype system was based on commercially available intravascular ultrasound scanner that was equipped with a 20 MHz array catheter. Digital beam-formed radio-frequency (RF) echo data (i.e. 12 bits, 100 Hz) was captured at full frame rate from the scanner and transferred to PC memory using a fast data acquisition system. Composite palpograms were created by applying a one-dimensional echo tracking technique in combination with global motion compensation and multi-frame averaging to several pairs of RF echo frames that were obtained in the diastolic phase of the cardiac cycle. The quality of palpograms was assessed by conducting experiments on vessel phantoms and on patients. The results demonstrated that robust and consistent palpograms could be generated in almost real-time using the proposed system. Good correlation was observed between low strain values and regions of calcification as identified from the IVUS sonograms. Although the clinical results are clearly preliminary, it was concluded that the prototype system performed sufficiently well to warrant further and more in depth clinical investigation.

Key words: Atherosclerosis, elastography, elasticity imaging, intravascular ultrasound, multi-frame averaging, palpation, palpogram, and tissue characterization.

Introduction

Catheter based interventional techniques that are used for treating atherosclerotic lesions such as angioplasty, stenting, and atherectomy are predominantly mechanical in nature. Therefore the morphology and composition of atherosclerotic lesion could influence their outcome. Additionally, circumferential stress is known to concentrate in the fibrous cap overlying the lipid pool making it prone to rupture (Richardson et al., 1989; Cheng et al., 1993). Additionally, it should be possible to identify vulnerable plaques by imaging the elastic properties of vascular tissues.

Currently, intravascular ultrasound (IVUS) is the only medical imaging modality that is able to produce real-time cross-sectional images of the arterial wall *in vivo* at high resolution. Consequently, attempts have been made to classify the composition of different plaque types based on their backscatter signal strength (i.e. their echogenicity) (Di Mario et al., 1998). The problem with this approach is that the echogenicity of soft tissues is highly dependent on scanner settings. A problem that is circumvented by normalising the echogenicity of the intima to the echogenicity of the adventia (Hodgson et al., 1993). Thus, an intimal thickening with less echogenicity than the adventitia is considered as soft plaque, whereas those with equal or higher echogenicity is perceived as hard plaques. However, it has been demonstrated that many plaques, which are classified as being soft, are often resistant to dilation (Hiro et al., 1997), thus indicating that there is no direct relation between tissue stiffness and echogenicity. The presence of acoustic shadowing and reverberations are specific landmarks that indicate the presence of calcification. However, densely fibrotic plaques often produce bright echoes, and a high attenuation of the echo-signal can easily be misinterpreted as acoustic shadowing (Di Mario et al., 1998). Furthermore, de Korte et al. (2000) have recently demonstrated that no correlation exists between mean echogenicity and tissue elasticity for non-calcified plaques. In addition to these problems large operator variability is generally associated with such qualitative tissue characterisation approaches.

It is envisaged that these limitations can be overcome using a system that is capable of imaging tissue elasticity. Unfortunately, none of the established medical imaging modality such as Magnetic Resonance Imaging (MRI), IVUS and X-ray angiography can provide a direct measure of vascular elasticity. However, most can provide information regarding induced mechanical response (i.e. strain or displacement) that is related to tissue elasticity. Several groups (Talhami et al., 1994; Shapo et al., 1996; Ryan and Foster, 1997) including ours (Céspedes et al., 1997; de Korte et al., 1997b; de Korte *et al.*, 1998; Céspedes et al., 2000) have proposed various IVUS based elasticity-imaging techniques for characterising the composition of different plaque types, and potentially for detecting vulnerable plaques. The elasticity images of the intra-coronary artery produced using these techniques generally possess better contrast compared to standard IVUS images. This occurs because the ultrasonic properties of soft tissues are related to bulk elastic properties, which generally does not vary widely between different plaque types; Whereas, the elastic property (i.e. Shear or Young's modulus) of different tissue types generally spans several orders of magnitude.

In spite of this, more widespread clinical utilisation is currently limited by lack of a real-time intravascular elasticity imaging system.

The long-term objective of this work is to develop a real-time clinical intravascular elasticity imaging system. Currently, we are investigating the possibility of developing such a system based on the intravascular ultrasonic palpation approach proposed by Céspedes et al. (2000). This is basically a low axial resolution intravascular elastography technique. In IVUS palpation radial strain is estimated using large non-overlapping* kernels and processing is restricted to tissues within the inner layer of the arterial wall. Furthermore, the radial strain information is colour coded and superimposed on the IVUS echogram at the lumen-vessel interface to produce a compound image that is known as a strain palpogram. The primary advantage of this technique is that it is simple enough to be implemented in real-time using relatively inexpensive hardware and in exchange for reducing axial resolution we expect it to be more robust compared to IVUS elastography.

Despite these desirable features catheter motion presents problems in clinical utilisation of IVUS palpation. Decorrelation noise due to catheter motion will either degrade image quality or may even result in failure to estimate radial strain. One of the primary objectives of this work was to develop an elasticity imaging system that is able to cope with this problem.

In addition to catheter motion there is also structural decorrelation noise (Varghese and Ophir, 1997), which occurs because the underlying tissue structure displaces in all coordinate directions when soft tissues are deformed. Structural decorrelation noise will corrupt the signature of the post-deformed echo signal, and thus will limit our ability to accurately track tissue motion in the presence of large internal strain (i.e. internal tissue strain exceeding 2 %). The following techniques have been proposed to cope with this problem: (a) temporal stretching (Céspedes and Ophir, 1993; Varghese et al., 1996), (b) adaptive stretching (Alam et al., 1998), (c) global and local companding (Chaturvedi et al., 1998a; Chaturvedi et al., 1998b), (d) envelope tracking (Doyley et al., 1996; Shiina et al., 1996), and (e) multi-compression processing (Varghese and Ophir, 1996).

Finally, there is random noise, which dominates in the presence of low internal strain. The main contributors of this source of measurement noise are: a) quantisation noise, which occurs during digitisation, b) electronic noise, which is associated with the ultrasonic imaging system, and c) bias errors that are introduced by the curve-fitting interpolation methods that are used for estimating sub-sample time-delays (Céspedes et al., 1995). Quantisation errors can be minimised by digitising RF echo signals to large number of significant bits, whilst electronic noise can be minimised using either a band-pass filter (Haykin, 1989) or by performing signal averaging. Sampling noise associated with the curve fitting interpolation methods that are used to improve the resolution of time-delay estimation can be reduced using a reconstructive interpolation filter proposed by Céspedes et al. (1995).

* Non-overlapping kernels are used because this generally produced more robust (i.e. smaller variance) strain estimates but at the expense of resolution (Céspedes et al., 1995b)

This paper described the first reported attempt to investigate the feasibility of developing a real-time clinical intravascular elasticity imaging system. We also report on our first clinical experience intravascular ultrasonic palpation.

Materials

Phantom

A 15 cm long vessel phantom, which had inner and outer diameters of 3 mm and 20 mm, respectively was fabricated from 8 % by weight porcine skin gelatine (Type A, approximately 175 bloom, Sigma chemical St. Louis, MO) and 1 % by weight Agar (Boom BC, Meppel, The Netherlands) as described by de Korte *et al.*, (1997a). Carborundum particles (1 % by weight, 3-10 μm mean diameter) were added to create acoustic scattering centres.

Patients

Elasticity measurements were performed with the informed consent on patients whom were referred for percutaneous coronary intervention.

Methods

Data acquisition system

A schematic diagram of the equipment used for acquiring data is shown in Fig. 1. Echo imaging was performed using an InVision intravascular ultrasound scanner (JOMED, Imaging, Rancho Cordova, CA, USA), which was equipped with a 20 MHz 64 F/X Visions catheter (JOMED, Imaging, Rancho Cordova, CA, USA). This scanner was equipped with a RF interface to provide direct access to the high resolution digital beam formed RF echo frames, and three synchronisation signals: start of frame (SOF), start of line (SOL) and pixel clock. A fast data acquisition system was developed based on a modified PCI bus Coreco Viper digital frame grabber (Coreco Inc. Quebec, Canada) and interfaced to the IVUS imaging system. Sequences of beam-formed radio frequency (RF) echo frames were transferred at 30 frames per second (fps) from the scanner directly in random access memory using this system. All RF echo frames were digitised to 12 bits at a sampling rate of 100 MHz. Each digitised echo frame contained a total of 512 RF A-lines, each consisting of 1024 sample points (corresponding to scan depth of 7.5 mm). The pressure within the lumen was measured using a pressure sensor, which was connected to a standard fluid line system (Ohmeda, Bilthoven, The Netherlands). The resulting physiological signals (i.e. electrocardiogram and pressure signals) were digitised to 12 bits at a sampling frequency of 5 kHz per channel using a multi-channel input-output (I/O) PCI card (National instruments). Both sets of data (i.e. low frequency physiological signals and RF echo frames) were stored on a 450 MHz Xeon based PC.

Phantom study

The aim of this part of the study was to evaluate the performance of the motion compensation and multi-frame averaging procedures, which we have developed to minimise the primary noise sources incurred during IVUS assessment. All measurements were performed in an 18 cm (long) by 8 cm (high) by 10 cm (wide) water tank, which was equipped with two sheaths (8 F), one was located at each side of tank. The phantom was connected between both sheaths.

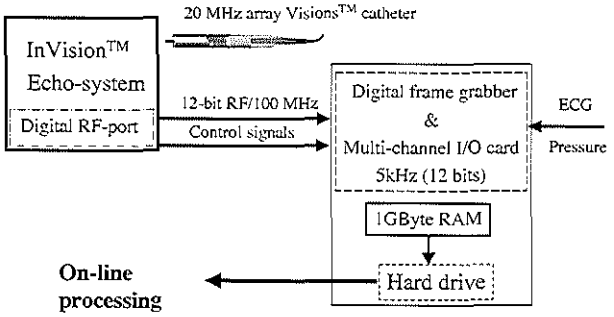

Doyley et al.

Figure 1: Schematic diagram of the equipment used, for clinical elasticity imaging.

Evaluation of motion compensation

Data acquisition

The catheter was inserted in the proximal sheath and positioned approximately in the centre of the lumen, before pressurising the vessel to 50 mmHg (i.e. reference pressure), with a column-based system (de Korte et al., 1997a). The pressure within the phantom was further increased to produce applied strain of 0.2 %, 0.5 %, and 1.5 %. Eight sets of RF images were obtained at the reference and all subsequent pressure increments. Rotational catheter motion was simulated in software by rotating the echo frames obtained at each strain increment clockwise between 0 and 6° in steps of 0.7°. The backscatter signal strength is rotational invariant for a phase array catheter; therefore the simulated RF echo-frames were representative of that incurred if the actual experiment was performed.

Pre-processing (motion compensation)

A localised motion compensation technique was applied to pairs of RF echo frames prior to strain estimation. The aim was to determine the in-plane translation T(r) and rotation R (α) vector, which maximises the similarity between a series of kernels that were defined in pairs of IVUS sonograms, which were acquired at different pressures. The similarity between a given pair of kernels was evaluated using the sum-of absolute difference (SAD) method (Bohs, 1994). This method has proven to be effective for intravascular elasticity imaging (Janssen et al., 2000). Furthermore, the accuracy of the SAD approach is similar to that of the cross-correlation approach when performing 2D displacement estimation (Bohs, 1994). However, the SAD approach has the distinct advantage over the normalised cross correlation approach of being relatively easily implemented in hardware and computationally less demanding.

To illustrate our motion compensation method lets consider a pair of IVUS images, **X** and **Y** that were obtained at different intra-coronary pressures. First, a small region of data was selected from image **X**, which is generally called the reference kernel. The degree of similarity between the reference kernel and similar size kernels within a predefined search kernel that was defined in Y (i.e. the test image) was calculated as follows:

$$\varepsilon_{r\alpha} = \sum_{i=1}^{L}\sum_{j=1}^{M}\left|X_{i,j} - Y_{i+r,j+\alpha}\right| \qquad (1)$$

where **L** and **M** represents the dimension of the kernel in polar co-ordinates, and r and represents the offsets in the radial and angular direction, respectively. Finally, the co-ordinate in **Y** was adjusted so as to minimise the SAD function. This procedure was repeated for several kernels to produce a vector of radial and angular offsets, which were subsequently used to correctly position the observation sight in the post-deformed RF echo frame (i.e. that corresponding to a high intra-coronary pressure) during strain estimation. All echo tracking was performed in the polar co-ordinate system, since this allowed us to define rectangular kernels.

Processing (strain estimation)

The technique that was used to create palpograms can be summarised into the following steps.

a) Detect the lumen-vessel interface automatically by applying a simple threshold algorithm to the digitised RF echo frames.
b) Estimate induced radial displacements of tissue within the inner layer of the artery by performing one-dimensional cross-correlation analysis on RF echo frames that are obtained at different intracoronary pressure.
c) Compute induced radial tissue strains by applying a finite difference strain estimator (Ophir et al., 1991) to the measured displacements. The least squares strain estimate approach proposed by Kallel and Ophir (1997) generally produced better strain estimates (i.e. it doesn't amplify displacement errors). However, it is not meaningful to apply it for only two displacements estimates.
d) Reject erroneous strain estimates by applying an outlier rejection filter to the strain estimates (see below).
e) Colour code valid strain estimates using a traffic light notation (where red, amber and green represents low, medium and high strain, respectively), and erroneous strain estimates as purple.
f) Super-impose the colour coded elasticity information on the IVUS sonogram at the lumen vessel interface.

The outlier rejection filter was based on decorrelation model proposed by (Céspedes et al., 1999). The general idea was to compute a theoretical estimate of the peak cross-correlation coefficient using the following expression

$$\hat{\rho}_{th} = \mathrm{sinc}(\varepsilon f_c T) \qquad (2)$$

where ε represents the measured strain, T represents the

length of the kernel used during cross-correlation analysis, and f_c represent the center-frequency of the ultrasound transducer. A strain estimate was considered erroneous when the difference between the peak value of correlation coefficients measured at two locations within the arterial wall (i.e. $\hat{\rho}_1$ and $\hat{\rho}_2$) was greater than 20 % of the computed peak value of cross-correlation function for the measured strain. This threshold represents the 95% confidence interval that was determined by conducting experiments on phantoms (Céspedes et al., 1995) for the range of strain that are generally incurred in intravascular applications (≤ 2 %). All cross-correlation analysis performed in both studies was conducted using non-overlapping kernels that had an optimum kernel size of 0.5 mm, which was determined empirically.

Evaluation of multi-frame averaging procedure

Data acquisition

Pulsatile pressure (1Hz) was generated in the vessel using a programmable peristaltic pump (Watson and Marlow 5000), that was connected to the proximal sheath. One hundred and twenty-five subsequent RF echo frames were captured from the scanner at 30 fps.

Frame selection

Processing was restricted to RF echo frames that were acquired in the diastolic phase of the cardiac cycle using the negative derivative of the intra-coronary pressure signal as the primary frame selection criterion. The decision to limit the processing to these frames was based on observation that the contraction of the heart and therefore catheter motion is relatively small in this phase of the cardiac cycle. Additionally, in this phase of the cardiac cycle the intra-coronary pressure decays relatively slowly and approximately constant compared to other regions (i.e. systole), which should enable us to cope with structural decorrelation noise.

Processing (multi-frame averaging)

A series of radial strain profiles were measured by applying the single-step strain estimation produced described in the previous part of the study to the selected RF echo frames. All cross-correlation analysis was conducted using 1 mm long kernels.

Composite strain profiles were measured at each cardiac cycle by computing the arithmetic mean of the valid strain estimates at each angular position. The composite strain profiles were colour coded as before and super-imposed on the IVUS sonogram at the lumen vessel interface to produce a compound image.

Data analysis

Performance was assessed using two different criteria: a) qualitatively by viewing the palpograms and b) quantitatively by assessing the elastographic signal to noise ratio, which was defined as follows:

$$SNR = \frac{\mu_s}{\sigma_s} \qquad (3)$$

where μ_S and σ_S represents the mean and standard deviation of the radial strain estimated within an elastically homogeneous tissue region.

Patient study

The aim of this preliminary clinical study was to gain insight into the performance of the strain estimation approach before conducting large-scale clinical trial.

Data acquisition

A 6 Fr. guiding catheter was advanced up to the coronary ostium of each patient after 10,000 IU heparin and 250-mg acetylsali-cyclic acid was administrated intravenously. A bolus injection of 3 mg of isosorbide dinitrate was administered prior to IVUS assessment. RF echo frames were captured for 4 s from the scanner at a frame rate of 30 fps. The arterial pressure was measured at the level of coronary ostium via the guiding catheter, which was connected, to a standard fluid line system (Ohmeda, Bilthoven, The Netherlands).

Frame selection

RF echo frames corresponding to the diastolic phase of the cardiac cycle were selected using the negative derivative of the intra-coronary pressure signal.

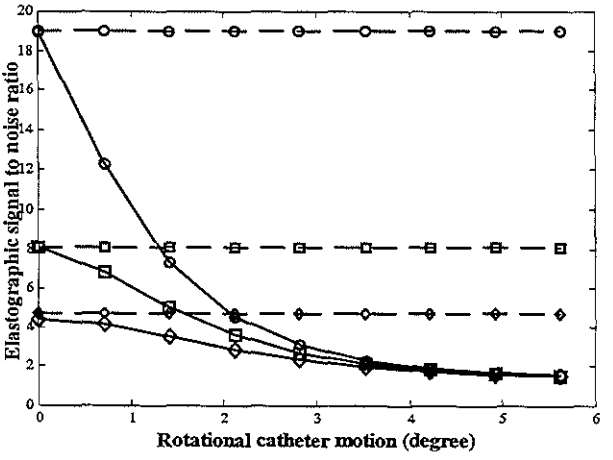

Doyley et al.

Figure 2: Mean elastographic signal to noise ratio computed from palpograms that were created using a simple strain estimation approach when the catheter was rotated, and the vessel phantom was deformed using applied strain of 0.2 % (circle), 0.5 % (square), and 1.5 % (diamond), respectively. The dotted lines denote the elastographic signal to noise ratio measured when palpograms were computed using a motion compensated strain estimation approach.

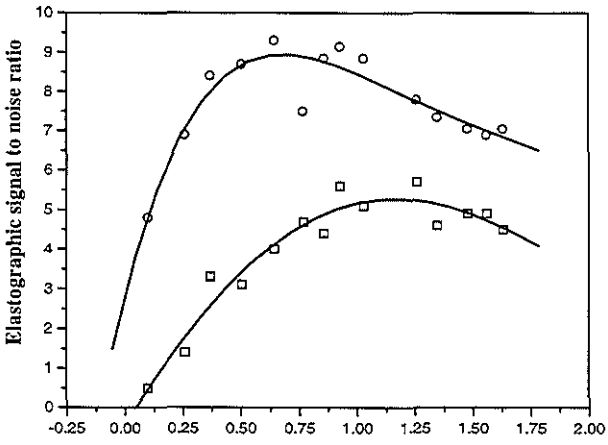

Doyley et al.

Figure 3: Strain filters measured from palpograms computed using multi-frame averaging (circle) and single-step (square) strain estimation approach.

Processing

Composite palpograms were computed by applying the multi-frame averaging strain estimation procedure described in the phantom study to different combination of RF echo frames before and after compensating for rotational catheter motion. Cross-correlation analysis was performed using kernel size of 0.6 mm (long) and 0.7 mm (long) for case 1 and 2, respectively. The size of the kernel was chosen based on the plaque thickness, which was evaluated by visual inspection of the IVUS sonogram.

Results

Phantom study

Evaluation of motion compensation procedure

Figure 2 shows the effect of rotational catheter motion on the elastographic signal-to-noise ratio (SNR) for different tissue strain values, which were computed before and after the motion compensation procedure were applied. The mean and standard deviation was computed from 512 independent strain estimates, which were equally distributed between 0 and 2Π.Note the rapid decrease in SNR that occurred in cases where the motion compensation procedure was not applied prior to strain estimation. This rapid degradation in image quality represents the change in the beam pattern (i.e. decorrelation) that occurs as one moves across the beam in the angular direction. It is also apparent that increasing the tissue strain compromised the quality of both sets of images (i.e. those computed before and after global motion compensation). This behaviour represents the effect of structural decorrelation noise, which increases in the presence of large internal tissue strain.

Evaluation of multi-frame averaging procedure

Figure 3 shows examples of strain filters that were derived experimentally from palpograms, which were created using the multi-frame averaging approach, and single-step approach (i.e. without frame averaging). The characteristic trade off that exists between structural decorrelation and electronic noise can clearly be seen in both cases. At low strain the quality of the palpograms is limited predominantly by random errors, and thus increasing the magnitude of the internal tissue strain (i.e. the differential pressure) results in a rapid increase in elastographic SNR. However, because structural decorrelation noise also increases with increasing

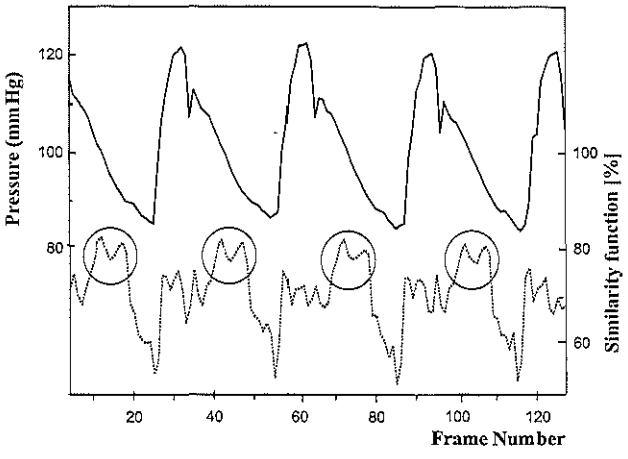

Doyley et al.

Figure 4: The pressure signal (__) with the corresponding similarity function (.....) of patient 1. The similarity function shows that catheter motion is small near end-diastole.

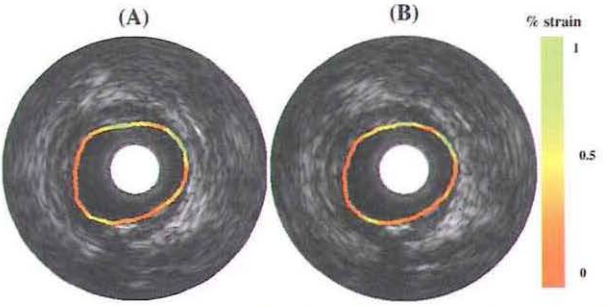

Doyley et al.

Figure 5: Examples of composite palpograms computed for patient 1. These palpograms were performed by applying the multi-frame strain estimation approach before (A) and after (B) correcting images for catheter motion to consecutive pairs of RF echo frames (with an average pressure difference of 2 mmHg) obtained near end-diastole. Showing a calcified spot at 6 o'clock.

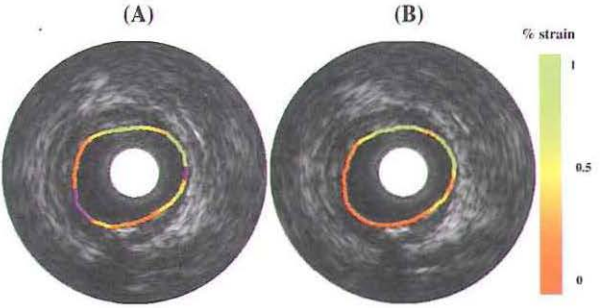

Doyley et al.

Figure 6: Example of composite palpograms computed for patient 1. These palpograms were produced by processing RF echo frames using an inter-frame strain of 4 and pressure difference of 8 mmHg with the multi-frame strain estimation approach before (A) and after (B) correcting images for catheter motion. Regions where it was not possible to compute valid strain estimates are denoted in purple.

applied strain there is an upper limit on the maximum SNR that can be achieved by increasing tissue strain. Further increase in tissue strain beyond the upper limit results in a rapid degradation in the elastographic SNR (Varghese and Ophir, 1997). Nevertheless, it is apparent that better images were produced at all strain increments when palpograms were computed using the multi-frame averaging approach.

Preliminary in vivo assessment

Patient 1

Figure 4 shows the pressure signal and the similarity curve that was obtained in patient 1. Figure 5 (A-B) shows typical examples of composite palpograms, which were computed by processing pairs of RF echo frames using a pressure difference of 2 mmHg and an inter-frame interval of two. It is clear from the IVUS sonogram that the catheter was eccentric. Consequently, since we didn't correct for catheter eccentricity the palpograms also appeared eccentric. Nevertheless, it is interesting to note that we were able to produce complete palpograms that possess good contrast resolution in both cases (i.e. before and after correcting for in-plane rotational catheter motion) using this inter-frame increment and pressure difference. Additionally, no significant difference was observed in the visual appearance of palpograms that were created using both approaches.

A calcium spot can clearly be seen at 6 o'clock in the IVUS

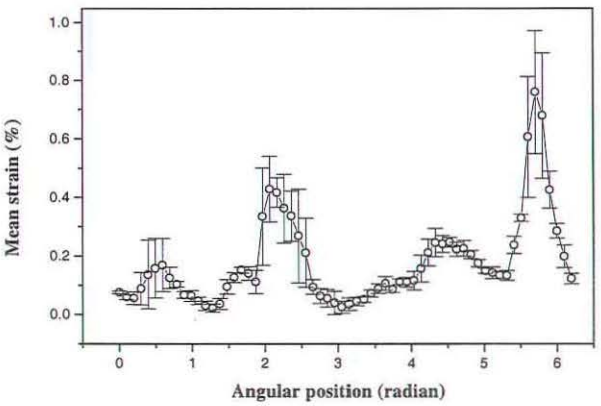

Doyley et al.

Figure 7: Mean radial strain profile corresponding to Fig. 6. The error bar represents ± one standard deviation computed over four cardiac cycles.

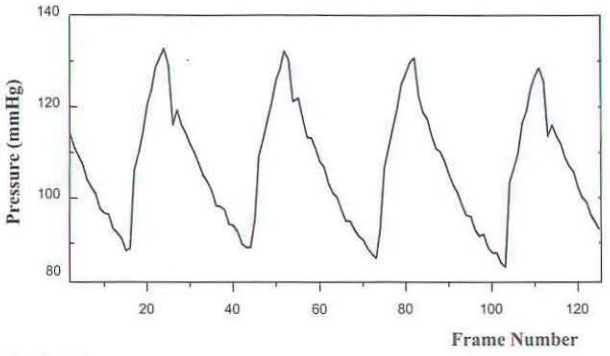

Doyley et al.

Figure 8: Pressure curve of patient 2.

sonograms, which appears as a localised region of low strain (the mean strain computed in this region was 0.13% ± 0.07) in the palpograms. Regions of high strain can clearly be seen on the palpograms between 11 and 2 o'clock, which could represent fatty material. An increased strain is also found at 7 o'clock that corresponds to a transition area between calcified and non-calcified material. It is known that increased circumferential stress and thus increased radial strain is present at these junctions. Furthermore, from the global appearance of palpogram this plaque would appear to be composed predominantly of a harder material such as fibrous tissue.

Figure 6 (A-B) shows examples of palpograms produced using both strain estimation approaches using a differential pressure of 8 mmHg and an inter-frame increment of four. Note that in this case it wasn't possible to produce a complete palpograms (as indicated by purple area) without first correcting for in-plane rotational catheter motion. Figure 7 shows the mean radial strain profile computed from four palpograms (i.e. one palpogram was computed at each cardiac cycle) that were produced using the motion compensated strain estimation technique.

There is a region of elevated strain next to the calcified spot (also visible in Fig 5A-B and Fig. 6A) but is not visible in Fig 6B. Note that at each angular position the mean and standard deviation was computed from four independent strain estimates. Increased error bars are observed for increasing strain values. From Figure 3 it is known that for strain values between 0.25 % and 1.5 %, the elastographic signal to noise ratio is similar. Therefore, larger error bars are expected for increased strain values.

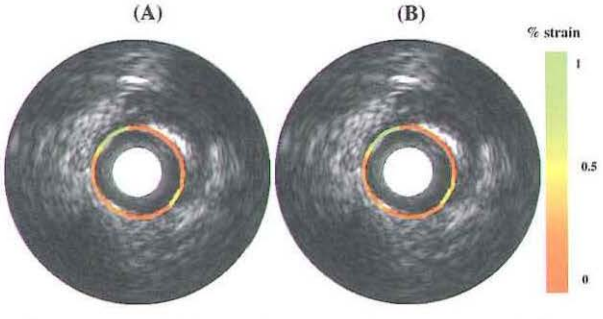

Doyley et al.

Figure 9: Examples of composite palpograms computed for patient 2. These palpograms were produced by processing consecutive pairs of RF echo frames (i.e. using an inter-frame increment of 1 and a pressure difference of 3 mmHg) using the multi-frame strain estimation approach, before (A) and after (B) correcting images for in-plane catheter motion. A large region of calcified material can clearly be seen between 12 and 2 o'clock.

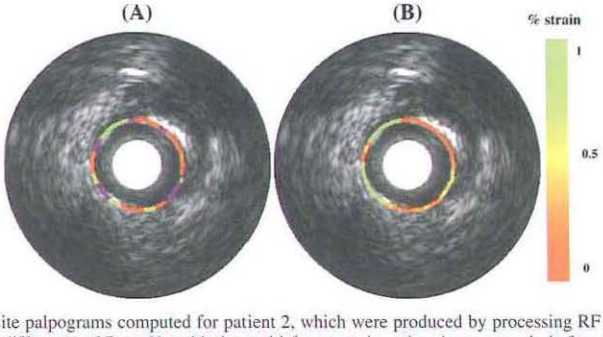

Doyley et al.

Figure 10: Examples of composite palpograms computed for patient 2, which were produced by processing RF echo frames using an inter-frame strain of 3 and a pressure difference of 7 mmHg with the multi-frame strain estimation approach, before (A) and after (B) correcting images for catheter motion. Regions where it wasn't possible to compute valid strain estimates are denoted in purple.

Patient 2

The pressure curve of this patient is shown in Figure 8. Figure 9 (A-B) shows examples of composite palpogram computed using a pressure difference of 4 mmHg and inter-frame interval of one within diastole, before and after correcting for in-plane catheter motion. Compared to the previous case this patient had a concentric plaque, and thus the palpogram appeared concentric. In addition, no significant difference can be observed in the quality of the palpograms produced using the two strain estimation approaches. A large region of calcification can clearly be seen in the IVUS sonograms between 12 and 3 o'clock, which corresponds to a region of low strain (mean strain of 0.15% ± 0.06) in the palpograms.

Figure 10 (A-B) shows examples of palpograms that were created using an inter-frame increment of three and a pressure difference was 7 mmHg. As in the previous case (i.e. patient 1) it wasn't possible to produce a complete palpogram without applying the motion compensation procedure. Increased strain values were found between 7 and 9 o'clock. This corresponds to a hypoechoic area that can be observed between 7 and 9 o'clock. It was apparent from a visual assessment of the IVUS cine-loop that this was due to the presence of a side branch. This side branch may result in increased strain values and thus an artefactual representation of the mechanical properties. Figure 11 shows the mean radial strain profile computed over four cardiac cycles from palpograms that were produced using a pressure difference of 4mmHg and an inter-frame increment of one with the motion compensated strain estimation technique. Catheter motion was quite severe in this case, since we were unable to correct for out-off plane catheter motion. It is reasonable to assume that the apparent degradation in the repeatability of the palpograms represents the effect of out-off-plane catheter motion.

Discussion

In this paper we describe a prototype elasticity imaging system, which was developed based on the intravascular ultrasonic palpation approach that was proposed by Céspedes et. al., (2000). The system was based on a commercially available Endosonics InVision IVUS scanner that was equipped with a 20 MHz array catheter. A fast data acquisition system was used to capture sequences of RF echo frames from the scanner directly into PC memory at full frame rate.

A novel strain estimation strategy was developed and incorporated on the system to minimise the primary noise sources, incurred during clinical application. Decorrelation noise incurred as a result of in-plane rotational catheter motion was minimised using a motion compensation procedure, which was developed based on the SAD approach. Despite the effectiveness of this technique, which is demonstrated in Fig. 2, compensating for catheter motion using this technique significantly increases the computational load. For instance, it took 8 s to compute a compo-site palpogram when the motion compensation procedure was not employed. This is assuming all consecutive pairs of RF echo frames in diastolic cycle are processed (i.e. 15 frames processed, assuming a heart rate of 60 beats/min). Although this is not real-time the presentation speed is reasonable for most clinical applications. However, the computational load was found to increase tenfold when the motion compensation procedure was allowed to compensate for rotational motion up to ± 6°. Note that computational load of the motion compensation procedure is highly dependent on size of the reference and search kernels.

It was apparent from Fig. 2 that quality of the image degraded significantly in the presence of large internal tissue strain. Incorporating either a local and/or a global distortion compensation procedure (i.e. either temporal stretching or companding) prior to strain estimation should circumvent this problem. However, we envisage that it will be very difficult to implement such complex signal processing methods in hardware. To cope with this problem processing was restricted to RF echo frames that were obtained in the diastolic phase of the cardiac cycle. In this phase of the cardiac cycle the intra-coronary pressure decays slowly and approximately constant compared to systole. Therefore, by choosing appropriate pairs of frames for processing (i.e. those corresponding to small pressure difference) we were able to minimise structural decorrelation effects.

A multi-frame averaging procedure was also developed and incorporated on the system since it has been demonstrated in elastography (O'Donnell et al., 1994; Varghese et al., 1996)

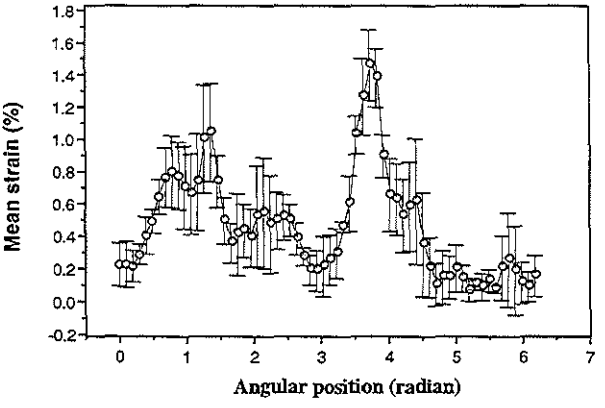

Figure 11: Mean radial strain profile corresponding to Fig. 10. The error bar represents ± one standard deviation, which was computed over four cardiac cycles.

that this signal processing method has the distinct advantage of improving the elastographic signal to noise ratio by factor of N^2, where N is the number of elastograms (or palpograms in our case) that are averaged. Figure 3 demonstrates that the quality of palpograms produced using the multi-frame averaging procedure is superior compared to those produced using a single-step approach. The quality of both sets of palpograms was limited predominately by random errors when the internal tissue strain was small, and thus increasing the magnitude of the applied strain results a rapid improvement in image quality. However, there is limit on the amount of improvement in image quality that can be achieved by increasing tissue strain since this also increases structural decorrelation noise. It was also apparent from Fig. 3 that palpograms should be created using larger interframe interval (i.e. using strains on the order of 1 %) in order to maximise the elastographic signal to noise ratio. Incorporating an optimisation procedure in strain estimation technique should result in further improvement in image quality. This could be accomplished by computing a composite palpogram from a series of partial palpograms that are created using all possible image combinations, but at the expense of further increasing the computation load.

It is apparent from our preliminary clinical investigation that the proposed system is able to produce consistent palpograms, which possess good contrast resolution and elastographic signal to noise ratio under physiological conditions. We also demonstrated that because of structural decorrelation, large variance will be incurred in region of high tissue strain.

If this system is to be clinically useful, methods must be developed to reduce strain projection artefacts that occur when the radial strains and the sound beam are poorly aligned (de Korte et al., 1999). This is important since the catheter is generally eccentric in most clinical cases. A crude global measure of the degree of catheter motion incurred during pre-interventional IVUS assessment can be obtained by constructing a similarity function by computing normalised sum of absolute difference between consecutive pairs of IVUS sonograms. We have observed that this function generally has a relatively broad peak near-end diastole (Fig. 4), where the catheter is believed to be more stable (i.e. small catheter motion) compared to other regions of the cardiac cycle. Therefore, the computational efficiency of the technique could be improved by incorporating the similarity function as part of the frame selection criterion. We estimate that it would take less than 4 s to compute a composite palpogram if additional constrains is imposed on the frame selection criterion using the similarity function. Finally, it is important to realise that the signal processing methods described in this paper can be applied to intravascular elastography, but currently at a prohibitive computational cost.

Study limitation

A limitation of the study is the absence of histologic validation, which was not possible since directional coronary atherectomy was not performed. Therefore, with the exception of calcified plaques, we could only speculate on the composition of the plaque based on the palpogram. For instance, regions of high strain can clearly be seen in the palpograms corresponding to patient 1 (Fig. 5(A-B)) at 11 and 12 o'clock and 1-2 o'clock. Based on the magnitude of the strain it is reasonable to assume that this represents fatty tissue since the strain incurred in fatty tissues are higher compared to other tissue types. Similarly, two regions of high strain can clearly been in the palpograms corresponding to patient 2 (Fig. 9 (A-B)) at 4-6 o'clock and 10-12 o'clock, which is consistent with fatty material. Further work is currently planned to validate our system in vivo using an atherosclerotic animal-model, and to improve our automatic contour detection algorithm.

Conclusion

We have demonstrated for the first time that intravascular ultrasonic palpation can produce clinicaly useful and reliable information in almost real-time, under typical physiological conditions in the catherization laboratory.

References

Alam, S.K., Ophir, J. and Konofagou, E. E. An adaptive strain estimator for elastography. IEEE Transactions on Ultrasonics Ferroelectrics and Frequency Control 45: 461-472; 1998.

Bohs, L.H., Friemel., B.H., McDermott, B.A., Trahey, G.E. A real-time system for quantifying and displaying two-dimensional velocities using ultrasound. Ultrasound in medicine and Biology 19: 751-761; 1994.

Céspedes, E.I., de Korte, C.L. and van der Steen, A.F.W. Intraluminal ultrasonic palpation: assessment of local and cross-sectional tissue stiffness. Ultrasound Medicine and Biology 26: 385-96; 2000.

Céspedes, E. I., de Korte, C. L. and van der Steen, A. F. W. Echo decorrelation from displacement gradients in elasticity and velocity estimation. IEEE transactions on Ultrasound, Ferroelectrics and Frequency Control: 46: 761-801; 1999.

Céspedes, E. I., de Korte, C. L. and van der Steen, A. F. W. Intravascular ultrasonic palpation: assessment of local wall compliance. IEEE Ultrasonics Symposium, (Toronto) (Piscataway, NJ: IEEE) 1079-1082; 1997.

Céspedes, E. I., Huang, Y., Ophir, J. and Spratt, S. Methods for estimation of sub-sample time delays of digitized echo signals. Ultrasonic Imaging 17: 142-171; 1995a.

Céspedes, E. I., Insana, M. F. and Ophir, J. Theoretical bounds on strain estimation in elastography. IEEE Transactions on Ultrasonics, Ferroelectrics, and Frequency Control 42: 969-972; 1995b.

Céspedes, I. and Ophir, J. Reduction of image noise in elastography. Ultrasonic Imaging 15: 89-102; 1993.

Chaturvedi, P., Insana, M. F. and Hall, T. J. 2-D companding for noise reduction in strain imaging. IEEE Transactions on Ultrasonics Ferroelectrics and Frequency Control 45: 179-191; 1998a.

Chaturvedi, P., Insana, M. F. and Hall, T. J. Testing the limitations of 2-D companding for strain imaging using phantoms. IEEE Transactions on Ultrasonics Ferroelectrics and Frequency Control 45: 1022-1031; 1998b.

Cheng, G. C., Loree, H. M., Kamm, R. D., Fishbein, M. C. and Lee, R. T. Distribution of circumferential stress in ruptured and stable atherosclerotic lesions. A structural analysis with histopathological correlation. Circulation 87: 1179-1187; 1993.

de Korte, C. L., Pasterkamp, G., van der Steen, A.F.W., Woutman, H. A. and Bom, N. Characterization of plaque components with intravascular ultrasound elastography in human femoral and coronary arteries in vitro. Circulation 102: 617-23; 2000.

de Korte, C. L., Céspedes, E. I. and van der Steen, A.F.W. Influence of catheter position on Estimated Strain in Intravascular Elastography. IEEE Transactions on Ultrasound, Ferroelectrics and Frequency Control: 46: 616-625; 1999.

de Korte, C.L., Céspedes, E. I. and van der Steen, A.F.W; Norder, B.; and Nijenhuis, K.T., Elastic and acoustic properties of vessel mimicking material for elasticity imaging. Ultrasonic Imaging,19: 112-126, 1997a.

de Korte, C. L., Céspedes, E. I., van der Steen, A. F. W. and Lancée, C. T. Intravascular elasticity imaging using ultrasound: feasibility studies in phantoms. Ultrasound in Medicine and Biology 23(5): 735-746; 1997b.

de Korte, C.L., van der Steen, A.F.W., Céspedes, E. I. and Pasterkamp, G. Intravascular elastography in human arteries: initial experience in vitro. Ultrasound in Medicine and Biology 24: 401-408; 1998.

Di Mario, C., Gorge, G., Peters, R., Kearney, F., Pinto, D., Hausmann, D., von Birgelen, C., Colombo, A., Mudra, H., Roelandt, J. and Erbel, R.

Clinical application and image interpretation in intracoronary ultrasound. European Heart Journal 19: 207-229; 1998.
Doyley, M. M., Bamber, J. C., Shiina, T. and Leach, M. O. Reconstruction of elasticity modulus distribution from envelope detected B-mode data. IEEE Ultrasonics Symposium, (San Antonio, Texas), (Piscataway, NJ: IEEE) 1611-1614; 1996.
Hiro, T., Leung, C. Y., De Guzman, S., Caiozzo, V. J., Farvid, A. R., Karimi, H., Helfant, R. H. and Tobis, J. M. Are soft echoes really soft? Intravascular ultrasound assessment of mechanical properties in human atherosclerotic tissue. American Heart Journal 133: 1-7; 1997.
Hodgson, J. M. B., Reddy, K. R., Suneja, R., Nair, R. N., Lesnefsky, E. J. and Sheehan, H. M. Intracoronary ultrasound imaging: coorelation of plaque morphology with angiograph, clinical syndrome and procedural results in patients undergoing angioplasty. Journal of American College of cardiology 21(1): 35-44; 1993.
Janssen, C. R. M., de Korte, C. L., van der Heiden, M. S., Wapenaar, C. P. A. and van der Steen, A. F. W. Angle matching in intravascular elastography. Ultrasonics 38: 417-423; 2000.
O'Donnell, M., Skovoroda, A. R., Shapo, B. M. and Emelianov, S. Y. Internal Displacement and Strain Imaging Using Ultrasonic Speckle Tracking. IEEE Transactions on Ultrasonics, Ferroelectronics and Frequency Control 41: 314-325; 1994.
Ophir, J., Céspedes, E.I., Ponnekanti, H., Yazdi, Y., Li, X. Elastography - a quantitative method for imaging the elasticity of biological tissues. Ultrasonic Imaging, 1991. 13: 111-134.
Richardson, P. D., Davies, M. J. and Born, G. V. R. Influence of plaque configuration and stress distribution on fissuring of coronary atherosclerotic plaques. The Lancet 21: 941-944; 1989.
Ryan, L. K. and Foster, F. S. Ultrasonic measurement of differential displacement strain in a vascular model. Ultrasonic Imaging 19: 19-38; 1997.
Shapo, B. M., Crowe, J. R., Erkamp, R., Emelianov, S. Y., Eberle, M. and O'Donnell, M. Strain imaging of coronary arteries with intraluminal ultrasound: experiments on an inhomogeneous phantom. Ultrasonic Imaging 18: 173-191; 1996.
Shiina, T., Doyley, M. M. and Bamber, J. C. Strain imaging using combined RF and autocorrelation processing. IEEE Ultrasonics Symposium, (San Antonio, Texas), (Piscataway, NJ: IEEE) 1331-1336; 1996.
Talhami, H. E., Wilson, L. S. and Neale, M. L. Spectral tissue strain: a new technique for imaging tissue strain using intravascular ultrasound. Ultrasound in Medicine and Biology 20: 759-772; 1994.
Varghese, T. and Ophir, J. Performance optimization in elastography: multicompression with temporal stretching. Ultrasonic Imaging 18: 193-214; 1996.
Varghese, T. and Ophir, J. A theoretical framework for performance characterization of elastography: the strain filter. IEEE Transactions On Ultrasonics Ferroelectrics And Frequency Control 44: 164-172; 1997.
Varghese, T., Ophir, J. and Céspedes, E.I. Noise reduction in elastograms using temporal stretching with multicompression averaging. Ultrasound In Medicine And Biology 22: 1043-1052; 1996.

PART 4

Intravascular ultrasound and intracoronary brachytherapy

Chapter 13

The role of intravascular ultrasound imaging in vascular brachytherapy.

SG Carlier, VLMA Coen, M Sabate, IP Kay,
JMR Ligthart, WJ van der Giessen, PC Levendag,
K Bom, PW Serruys.

International Journal of Cardiovascular Intervententions 2000;3:3-12.

The role of intravascular ultrasound imaging in vascular brachytherapy

Stéphane G Carlier[1], Véronique LMA Coen[2], Manel Sabaté[1], I Patrick Kay[1], Jurgen MR Ligthart[2], Willem J van der Giessen[1], Peter C Levendag[2], K Bom[3] and Patrick W Serruys[1]

[1]The Thoraxcenter, Heart Center, Department of Interventional Cardiology, Academisch Ziekenhuis Rotterdam-Dijkzigt and the Experimental Echocardiography Laboratory, Erasmus University, Rotterdam, The Netherlands
[2]The Daniel den Hoed Cancer Center, Rotterdam, The Netherlands
[3]Interuniversity Cardiology Institute of The Netherlands (ICIN)

Correspondence:
SG Carlier MD
Experimental Echo Laboratory
Erasmus University - Ee2302
Dr Molewaterplein 50
3015 GE Rotterdam
The Netherlands
Tel: (+31) 10 408 7474
Fax: (+31) 10 408 9445
E-mail: CARLIER@TCH.FGG.EUR.NL

Received 27 October 1999
Accepted 21 January 2000

Intracoronary brachytherapy has recently emerged as a new therapy to prevent restenosis. Initial experimental work was achieved in animal models and the results were assessed by histomorphometry. Initial clinical trials used angiography to guide dosimetry and to assess efficacy. Intravascular ultrasound (IVUS) permits tomographic examination of the vessel wall, elucidating the true morphology of the lumen and transmural components, which cannot be investigated on the lumenogram obtained by angiography.

This paper reviews the use of IVUS in the clinical studies of brachytherapy conducted to date. IVUS allows clinicians to make a thorough assessment of the remodeling of the vessel and appears to have a major role to play in facilitating understanding of the underlying mechanisms of action in this emerging field. The authors propose that state-of-the-art IVUS techniques should be employed to further knowledge of the mechanisms of action of brachytherapy in atherosclerotic human coronary arteries. (Int J Cardiovasc Intervent 2000; 3: 3–12)

Keywords: brachytherapy – intravascular ultrasound – restenosis

Introduction

On the verge of an exponential increase of the use of brachytherapy in interventional cardiology, it is appropriate to keep in mind that this new therapeutic modality is still in its infancy. The first case of brachytherapy was initiated in Europe as recently as 1992 by Liermann et al, in patients who had undergone a femoral percutaneous angioplasty.[1] Since radiotherapy has proven to be effective in treating the exuberant fibroblastic activity of keloid scar formation and other nonmalignant benign processes such as ocular pterygia,[2,3] it has been assumed that this adjunctive treatment could inhibit restenosis. Mechanisms involved in the restenosis process are elastic recoil of the artery, local thrombus formation, vascular remodeling with shrinkage of the vessel and an exuberant healing process with neointimal cellular proliferation and matrix synthesis.[4–6] Stent implantation minimizes elastic recoil and remodeling of vessels, but exacerbates the normal proliferative reaction in response to the traumatizing intervention.[7,8] Depending on the type of lesions treated, a significant restenosis rate of 15–50% remains the major hindrance to the success of stent therapy and is mainly caused by this exacerbated proliferative reaction.

Clinical coronary applications of brachytherapy were carried out after the experimental work achieved mainly in the United States by Wiedermann et al in New York,[9] Waksman et al in Atlanta[10] and Mazur et al in Houston.[11] They demonstrated a reduction of intimal hyperplasia in swine models of restenosis, initially using γ-radiation (^{192}Ir) and thereafter ß-sources.[12] In parallel, Verin et al in Geneva conducted experimental studies with the pure ß-emitter ^{90}Y in carotid and iliac arteries of rabbits.[13] Concomitantly, Hehrlein et al demonstrated a marked reduction of neointima formation in rabbits with low-dose radioactive stents,[14] while Carter showed that the dose response of a ß-particle-emitting radioactive stent in a porcine coronary restenosis model was actually complex, presenting a bell-shape.[15] These groups provided compelling experimental evidence of efficacy of brachytherapy in the prevention of restenosis. In these studies, the short- and long-term results were evaluated by histomorphometry,

measuring the amount of neointima formation after balloon overstretch injury.

The objective of this review is to emphasize the potential of intravascular ultrasound (IVUS) imaging in guiding dose prescription, in assessing the results of brachytherapy in clinical trials as a surrogate of histomorphometry and in reviewing the different modalities which have been implemented so far.

Intravascular ultrasound

An update on its value in predicting restenosis

Coronary interventions depend mainly on imaging techniques as the source of guidance. Angiography alone provides a good representation of the complete coronary anatomy but a relatively poor image of the diseased vessel wall. Angiograms that are difficult to interpret are frequently encountered. These include images of ostial lesions, tortuous vessel segments, vessel overlap, intermediate lesions, dissections and thrombus. Although the value of angiography remains unquestioned, radiographic imaging depicts a two-dimensional silhouette of the arterial lumen. This 'lumenogram' is a limited standard on which to base therapeutic decisions.[16] Angiography demonstrates only lumen narrowing well, but is inherently limited in defining the distribution and extent of wall disease. Furthermore, angiography is insensitive to early atheromatous thickening of the arterial wall, partly owing to vascular remodeling that allows plaque to grow to occupy an average of 40% of the vessel cross-section before luminal encroachment occurs.[17] Plaque burden in reference segments that are considered angiographically normal can reach on average 35-40%.[18]

In the late Eighties, IVUS emerged as a promising imaging modality with which to assess vascular disease.[19] IVUS provides real-time tomographic images of vessel wall cross-sections, elucidating the true morphology of the lumen and transmural components of atherosclerotic arteries. The field of intravascular ultrasound imaging has led to improvements in the understanding of atherosclerotic disease and its response to various therapeutic interventions. However, a main thrust of this technique is the guidance of therapeutic interventions, and controversial data exist in the literature on the value of postintervention IVUS parameters to predict the restenosis rate. For percutaneous transluminal coronary angioplasty (PTCA), no criteria were found in the PICTURE study including 200 patients,[20] whereas Mintz et al found that the residual plaque burden measured with IVUS was an independent predictor of restenosis.[6] The final report of the GUIDE trial that showed the predictive value of IVUS plaque area and minimal lumen cross-section is still pending.[21] On the other hand, it has been demonstrated that, based on IVUS, it was safe to increase the nominal balloon-to-artery ratio.[22] A low rate (14 %) of clinical events at one year has been reported in a single-center nonrandomized study of 252 patients where the balloon sizes were based on the external elastic membrane diameters.[23] For stenting, a very recent combined analysis from three registries (MUSIC, WEST-II, ESSEX) and two randomized stent restenosis trials (ERASER and TRAPIST) (n = 800 patients) has demonstrated that the IVUS criteria minimum lumen cross-sectional area (MLCSA), mean in-stent lumen area, stent length and lumen diameter were predictors of six-month in-stent restenosis, defined as luminal diameter stenosis >50% by quantitative angiography (QCA),[24] in agreement with other reports which demonstrated also the predictive value of an ostial lesion location and the preinterventional and residual lesion site plaque burden.[25-28] Finally, it remains also controversial whether IVUS guidance may decrease in-stent restenosis and improve event-free survival after an intervention.[29] In a study matching patients between two centers, one performing IVUS guidance, the other using only angiography, there was a significant decrease of the restenosis rate (9.2% versus 22.3%) at an early stage where the IVUS criteria implied aggressive dilatation using oversized balloons.[30] However, this led to a high incidence of vessel ruptures. IVUS criteria were modified, the balloon-artery ratio used was decreased to achieve a stent cross-sectional area (CSA) equal to or greater than the distal lumen CSA, and no further difference in the outcome of the patients was found between the angiographic and IVUS guidance groups.

IVUS guidance improved the minimal CSA in the stent at the end of the intervention in the MUSIC trial, and comparison of angiographic data with earlier studies demonstrated that the improvement of this minimal lumen diameter (MLD) (2.9 mm versus 2.5 mm) was associated with a lower restenosis rate (9.7% versus 20% respectively for the MUSIC and Benestent I).[31,32] When the IVUS criteria for optimal stent expansion are met, the restenosis rate is lower.[33] However, these criteria cannot be met in all patients, and the results of two randomized trials (RESIST and OPTICUS) comparing IVUS with angiographic guidance today show no difference in clinical and angiographic outcome at six-month follow-up.[34,35]

On the other hand, it has been demonstrated that the rate of target vessel revascularization in the randomized CRUISE trial was reduced from 15.3% to 8.5% ($P < 0.05$) in the arm with IVUS-guided stent implantation. The results of AVID, a large multicentre and randomized study including 800 patients, were recently revealed by Dr Russo at the TCT'99 meeting. IVUS was used in one arm to document the results of a stent implantation, and in the other arm to guide optimal stent implantation using the following criteria: (i) full apposition of stent struts; (ii) MLCSA >90% of the distal vessel CSA; and (iii) absence of major dissection. In the IVUS-guided arm, 42% of the patients required additional treatment. This led to a mean increase of the MLD of 0.3 mm and of the MLCSA of 1.27 mm^2 (+20.3%). At 12-month follow-up, the primary end-point (target lesion revascularization, TLR) was 12.4% in the IVUS-documented arm, and 8.4% in the IVUS-guided arm. This difference did not reach statistical significance (P = 0.08). However, in subgroups, a strong benefit of IVUS guidance could be demonstrated, for example when treat-

ing saphenous bypass lesions (TLR 20.8 versus 5.1%; $P < 0.01$).

A major limitation of these studies is that there is no comparison between quantitative IVUS and quantitative angiographic guidance: only visual assessment of the angiographic results was carried out. Recently, the concordance between physiological (fractional myocardial flow reserve: FFRmyo), IVUS and QCA data has been reported. The best agreement was found between IVUS and FFRmyo, with a concordance rate of 91%. The concordance rate between QCA and IVUS was only 48%.[36]

Brachytherapy might be the ideal field in which to apply the unique characteristics of IVUS.[37] Indeed, with its potential for tomographic imaging of the complete arterial wall and quantification of different structures such as the volume of plaque or in-stent hyperplasia, IVUS might fill the gap between the experimental knowledge acquired from histology and the results of ongoing clinical studies.

IVUS imaging

IVUS imaging is usually performed before an intervention, or after the placement of a stent, and the interpretation is based on the successive cross-sections obtained when moving the transducer manually. A comprehensive review of the clinical use of IVUS has recently been published by the study group of intracoronary imaging of the European Society of Cardiology.[38] A natural extension to cross-sectional ultrasound imaging is three-dimensional (3D) imaging. To obtain a 3D survey of the vessel, ultrasound images are acquired during the 'pull back' of the imaging catheter (20–30 frames per second). Typical velocity of the pull-back ranges from 0.5 to 1 mm/s. The sequence of images contains 3D information that can be presented in various ways. A common form of presentation is the longitudinal or sagital view, which shows one of the image planes perpendicular to the set of cross-sectional images. Since during the pull-back there is motion because of the movement of the heart, longitudinal scans may have a jagged appearance. Although this artifact does not impede the understanding of the vessel structure, the use of ECG-triggered pull-backs improves the reconstruction.[39] Recently, the fusion of biplane angiography and IVUS images has been described for true 3-D reconstruction of coronary segments for computation of parameters such as wall shear stress.[40]

Dosimetry evaluation from IVUS

Assuming that the catheter containing the radioactive source is lying in the same position as the IVUS catheter, it is possible to measure the distance from the source to any vascular structure in one cross-sectional image, and to construct isodose plots when the activity and physical characteristics (dose fall-off with distance) of the source are known.[41] This is illustrated in Figure 1. Isodoses may also be superimposed on the sagital view of the pull-back. However, the evaluation of the overall dosimetry in the arterial wall from successive cross-sectional images is difficult. Dose–volume histograms (DVH) have been introduced in radiotherapy to condense the large body of information of the complete 3-D dose distribution data into a plot summarizing graphically the radiation distribution throughout the target volume and the anatomical structures of interest.[42,43] The present authors recently described the methodology for computing DVH for coronary brachytherapy from 3-D IVUS data[44] and the clinical applications will be illustrated in the review of the clinical trials which follows.

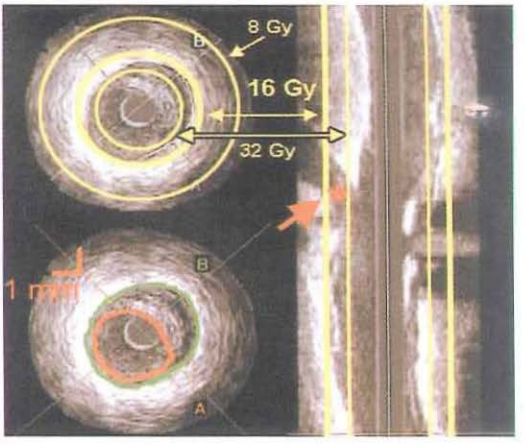

Figure 1
Lower left panel: a typical intravascular ultrasound (IVUS) cross-section demonstrating a mixed plaque from 11 to 5 o' clock, and highlighted luminal (in red) and external elastic lamina (EEL) (in green) contours. Upper left panel: isodoses of 8, 16 and 32 Gy corresponding to a ^{90}Sr ß-source are superimposed on the IVUS ^{90}Sr/Y. Right panel: longitudinal reconstruction of a 30 mm segment of a patient included in the BERT trial, acquired with an ECG-triggered pull-back device. The position of a side-branch is indicated by the arrow. The 32 and 16 Gy isodoses permit a quick evaluation of the dose delivered to the target, the adventitia, limited by the EEL.

Overview of the use of IVUS in clinical brachytherapy trials

The Venezuelan experience

Condado and colleagues in Venezuela introduced brachytherapy in human coronary arteries using a hand-delivered ^{192}Ir wire into a non-centered closed-end lumen catheter.[45] They explored the feasibility and safety of this approach in 22 lesions in 21 patients. The doses were prescribed at 1.5 mm from the source (single doses of 18 Gy, $n = 1$; 20 Gy, $n = 11$; 25 Gy, $n = 9$) using angiographic assessment. Although reported as positive, an unexplained early reduction of the minimal lumen diameter of 0.45 mm on average after only 24 hours might have blurred the real efficacy of the applied radiotherapy in these patients[37]

who presented no additional loss in MLD between 24 hours and six-month follow-up. However, doses of up to 92.5 Gy could have been delivered to the lumen wall because of the non-centered device.[37] This may well be over the vascular tolerance limits. Such a high dose could explain the observation that two patients experienced early total vessel occlusion, and four others developed an aneurysm at two-year follow-up. IVUS guidance could have stressed cases with over-dosage administration.

The Geneva trial

In Geneva, Verin et al employed ß-irradiation in human coronary arteries using a radioactive wire (^{90}Y) in a centering balloon device.[46] The dose prescribed was 18 Gy at the surface of the balloon corresponding to the vessel luminal surface. No IVUS assessment was performed. The findings were disappointing, with a restenosis rate of 40% among the 15 studied patients. A retrospective analysis of the dose prescribed revealed that at a depth of 2 mm in the vessel wall, the dose was only ~2.7 Gy, probably below the nominal effective dose against the proliferating cells involved in the post-angioplasty restenosis process.[47]

The SCRIPPS study

Shortly after Condado, Teirstein et al started to treat restenosis lesions with γ-therapy in a randomized placebo-controlled study. They demonstrated a substantial reduction of the angiographic restenosis rate (17% versus 54%) among 55 patients presenting with in-stent restenosis.[48] The recently published two-year follow-up data demonstrate the long-term efficacy of this new therapeutic modality: the target-lesion revascularization was significantly lower in the ^{192}Ir group (15.4% versus 44.8%; $P < 0.01$). Non-target-lesion revascularization was similar in the two groups (19.2% versus 20.7%). The composite end-point of death, myocardial infarction or target-lesion revascularization was significantly lower in ^{192}Ir-treated versus placebo-treated patients (23.1% versus 51.7%; $P = 0.03$).[49]

A sealed ^{192}Ir γ-source in a non-centered catheter was used (Best Medical/Cordis Corp, Warren, NJ, USA). This study was the first where the dosimetry was based on IVUS measurements. A series of tomographic IVUS images were obtained with a motorized pull-back apparatus. The distance between the center of the ultrasound catheter (supposed equivalent to the source position) and the adventitial border (the target) was measured every 1 mm along the stented segment. As illustrated in Figure 2, the aim was to adjust the dwell time to administer 8 Gy to the target farthest from the source (A), provided that no more than 30 Gy was delivered to the closest target (B). The importance of IVUS has been clearly demonstrated in a retrospective subgroup analysis.[50] Late luminal loss and loss index were calculated for patients with diabetes, in-stent restenosis or minimum dose exposure of the target of 8.00 Gy. Two-factor analysis of variance was used to test for an interaction between patient characteristics and treatment effect. In the treated group (^{192}Ir), late loss was particularly low in patients with diabetes (0.19 versus 0.46 mm), in-stent restenosis (0.17 versus 1.02 mm) and also in patients who received a minimum radiation dose to the entire adventitial border of at least 8.00 Gy (0.06 versus 0.92). The loss index in this subgroup was 0.03. The two-factor analysis of variance demonstrated a significant interaction between treatment effect (late loss) and the subgroup characteristic of receiving a minimum dose of 8.00 Gy to the adventitial border ($P = 0.009$). This illustrates the usefulness of IVUS in clarifying results of a brachytherapy trial.

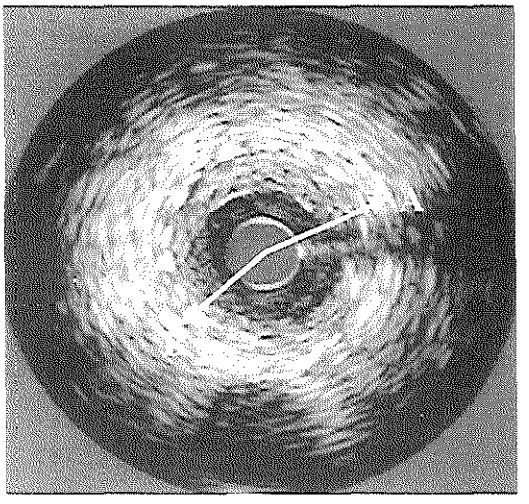

Figure 2
In the SCRIPPS study, IVUS was used in order to administer at least 8 Gy to the target (external elastic lamina) farthest from the source (A), provided that no more than 30 Gy was delivered to the closest target (B).

The WRIST trials

The series of WRIST (Washington Radiation for In-Stent Restenosis) trials addressed different issues: native or saphenous (SVG) bypass in-stent restenosis, long lesions, ß- or γ-sources. They were initiated with a gamma ribbon source (^{192}Ir) or placebo ribbon. Dosage prescribed was 15 Gy at 2 mm from the source in vessels of 2.0–4.0 mm in diameter and at 2.4 mm for vessels >4.0 mm in diameter. The data recently presented for 130 patients (100 native, 30 SVG) have confirmed the efficacy of brachytherapy: the angiographic restenosis rate was significantly lower (19% versus 58%; $P < 0.001$) as were mortality, myocardial infarction and repeat target lesion revascularization combined end-points (29% versus 68%).[51]

In this series, IVUS was not used for dosage prescription, but was performed systematically after irradiation and at six-month follow-up for off-line analysis. From

these measurements, it could be demonstrated that the volume of intimal hyperplasia increased by 60 mm^3 in the placebo group, but that in the treated group it was only 2 mm^3, with patients even demonstrating a melting of the residual intimal hyperplasia left at the time of the procedure. IVUS was also useful for estimating the minimum and maximum dose administered to the lumen border (7.3 Gy and 45 Gy, respectively).

Initially performed with a γ-source, the expanding WRIST series has recently investigated ß-radiation (with the ^{90}Y source of the Boston Scientific brachytherapy system) for in-stent restenosis (beta-WRIST). With this system, which incorporates a balloon to center the source in the artery, 20.6 Gy was prescribed at 1 mm from the surface of the balloon. The preliminary results recently presented of the first 49 patients with six-month follow-up demonstrated a similar efficacy of ß-radiotherapy for in-stent restenotic lesions, with a 50% reduction in major adverse cardiac events, compared with historical controls from the γ-WRIST.[52]

The BERT trial

The Beta Energy Restenosis Trial (BERT) was initially conducted in the United States. This study was designed to evaluate the feasibility and safety of the delivery of 12–16 Gy with a $^{90}Sr/Y$ source after balloon angioplasty of de novo lesions. A special device (Beta-Cath, Novoste Corp, Norcross, GA, USA) consisting of a hand-held hydraulic delivery system was used to send 12 encapsulated sources in a 5.4 F. catheter lying across the target lesion (total irradiated length: 30 mm). The results of the American arm in which delivery of ß-radiation was attempted in 23 patients were obtained with neither IVUS guidance nor IVUS documentation. A late loss of 0.05 mm, a late loss index of 4% and a restenosis rate of 15% were lower than in previous restenosis trials using similar angiographic methods.[53] In the Canadian arm initiated later, the 30 patients included were systematically documented by IVUS. QCA data were similar, and the IVUS findings after six-month follow-up were very recently reported[54]: there was no significant change in lumen area (5.7 ± 1.7 mm^2 post-treatment, 6.0 ± 2.6 mm^2 at follow-up), nor in external elastic lamina (EEL) area (13.7 ± 4.5 mm^2 post-treatment to 14.2 ± 4.7 mm^2). With these IVUS findings, it was suggested that ß-radiation inhibit neointima formation with no reduction of total vessel area at six-month follow-up. The authors' findings discussed in the following section, and based on 3-D ECG-triggered IVUS assessment of the treated area, are more in favor of an adaptative remodeling with an increase of the vessel size (EEL) and plaque.

The Thoraxcenter experience

One of the first IVUS scanners was developed in the authors' institution.[55] IVUS is performed routinely and systematically in studies evaluating new antirestenotic strategies, even when it is not mandatory for the trial.

Three-dimensional image reconstruction and analysis systems have been introduced that can be used for complete quantitative analysis of IVUS images.[56–59] However, image artifacts that result from cyclic changes in coronary dimensions and from the movement of the IVUS catheter in the arterial lumen limit the accuracy of the 3-D boundary detection systems.[60] This led to the development of a new approach. In order to limit cyclic movement artifacts, an ECG-gated image acquisition workstation is employed which controls a dedicated pullback device. The complete 3-D dataset of the coordinates of the automatically detected lumen (corresponding to the highly echogenic blood–vessel interface) and of the echogenic media–adventitia interface (EEL) over the complete length of the treated area can be used to study the change between baseline and six-month follow-up of lumen, plaque and vessel volumes. Dosimetry evaluation at the time of the iradiation is then feasible, when considering the source in the same position as the IVUS catheter.[44]

Analyzing 21 patients consecutively included in the European arm of BERT in the authors' institution, Sabate et al have recently demonstrated that over the 30 mm of the irradiated segments with the Beta-Cath delivery system, mean EEL and plaque volumes increased significantly (from 451 ± 128 mm^3 to 490 ± 159 mm^3 and from 201 ± 59 mm^3 to 242 ± 74 mm^3; $P = 0.01$ and $P = 0.001$, respectively), whereas luminal volume remained unchanged.[61] On the other hand, edges of the treated segments presented an increase in mean plaque volume with no net change in EEL, resulting in a decrease in mean luminal volume. This very meticulously conducted 3-D analysis could assess subtle changes in the remodeling of human irradiated coronary arteries. This would otherwise have only been possible in an animal study with serial histomorphometric assessment. Analyzing a total of 206 coronary subsegments of 2 mm lying in the treated area, it was possible to demonstrate that the independent predictors of the plaque volume at follow-up were the plaque volume post-treatment, the type of plaque and the minimal dose absorbed by 90% of the adventitial volume (DV90adv).[62]

From the 3-D IVUS dataset, it has been also possible to compute DVH to describe the cumulative distribution of dose over three specific volumes: at the level of the luminal surface, the EEL, and in the volume encompassed between the luminal surface and the EEL (plaque + media). On average, DVH derived from the authors' BERT cases demonstrate that the minimal dose in 90% of the adventitial volume (defined with a thickness of 0.5 mm from the EEL) was 37 ± 16 % of the prescribed dose; the minimal dose in 90% of the plaque + media volume was 58 ± 24% and of the luminal surface volume was 67 ± 31%. The minimal dose in the 10% most exposed luminal surface volume was 296 ± 42%.[63] Simulations of the use of a γ-emitter and/or a radioactive source train centered in the lumen have also been evaluated, with a comparison of the homogeneity of the dose distribution. A typical DVH is illustrated in Figure 3.

10.9% of targets would receive <7 Gy, believed to be subtherapeutic. With the angiographic model, the mean minimal dose would be 7.51 ± 1.44 Gy, but 38.7% of patients would receive a minimal adventitial dose <7 Gy. With a fixed-dose strategy of 15 Gy delivered at 2 mm from the source, the mean minimal dose would be 8.59 ± 1.64 Gy, with 17.9% of patients receiving <7 Gy at the adventitia. However, with this strategy, 41.5% of targets would receive >30 Gy. This demonstrates that probably only IVUS permits the optimal dosimetry, adapted to the remodeling of the specific lesion of a patient.

Limitations of IVUS for dosimetry

A major assumption made when using IVUS to assess the dosimetry is to consider that both the imaging catheter and the brachytherapy delivery system are following the same course in the treated coronary segment. Compared with a 5 F. (~ 1.7 mm) device such as the Beta-Cath, the IVUS catheter, which is smaller (2.9 F. ~ 1 mm), will be in a more eccentric position in the coronary lumen. However, no easy correction can be applied since the channel source in the delivery device is not in the center of the catheter. When using a centering balloon for the source such as in PREVENT or the Schneider Dose Finding Study, it is easy to calculate the center of gravity of the lumen of each slice from the 3-D IVUS dataset. However, even with the use of radiotherapy and IVUS catheters of the same size, or centered, it is not certain that when advanced sequentially in the arterial lumen, they will occupy the same position. Although both catheters should be on the shortest 3-D path in the lumen, coronary arteries have a complex curved geometry in space, and are partially deformed by the catheter lying in their lumen. Thus, catheters with differing rigidity will occupy different positions. These methodological limitations could be partially overcome with existing imaging wires which could be introduced in the lumen of the irradiation delivery catheter itself.[66] Another very interesting device, illustrated in Figure 5, has recently been developed. The unique characteristic of this catheter, designed for directional radiation (BRIGADE™, EndoSonics Corp, Rancho Cordova, CA, USA) is the combination of a solid-state IVUS imaging array proximal to the site in the delivery system where the source lies.[67] A second unique feature of this device is a gold attenuator surrounding the radioactive source asymmetrically, in order to direct preferentially radiation in eccentric plaques. The incorporation of the imaging possibilities allows for rotation of the system towards the most eccentric plaque. Clinical trials will soon be launched, after the demonstration of the feasibility of this new approach in an animal model.

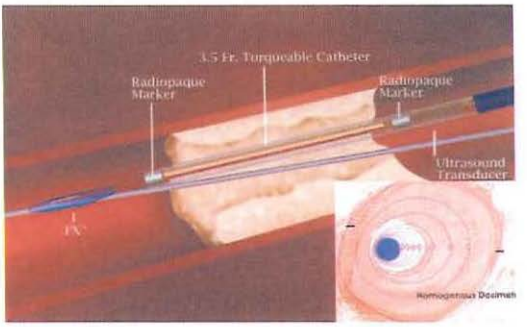

Figure 5
Illustration of a directional radiation catheter, including an asymmetric gold attenuator encompassing only the top half of the area where the source is positioned for coronary brachytherapy (between the two radiopaque markers). This configuration offers an asymmetric dose distribution which optimizes the dosimetry of eccentric lesions (panel). Optimal orientation of such a device can only be performed thanks to the incorporated intravascular ultrasound transducer attached proximally in this combined device.

Conclusion

Radiation therapy bears some resemblance to antibacterial therapy, which requires the right dosage to achieve its therapeutic goal, without excessive toxicity related to overdose or incorrect targeting (classically called by the radiotherapist a 'geographical miss'). At the present stage, IVUS appears to be an indispensable tool for understanding the mechanisms of action of radiotherapy in the prevention of restenosis and in finding the target volume. The confounding and negative results of the early clinical studies, performed without IVUS guidance, support the need to at least document by IVUS the ongoing clinical trials, even when there is no direct guidance of dosage administration. To treat coronary arteries effectively, it seems necessary to evaluate the dose absorbed in different arterial structures since there is still controversy about the target volume to be irradiated. This cannot be appreciated with angiography, which gives only a lumenogram of the artery. Methods based on the determination of specific dose–volume histograms might be useful. Only the future will tell us whether angiography is a sufficient guideline to establish and apply the correct dose. The desire to simplify the methodological approach of brachytherapy in this early phase might be fatal for this technique in its infancy.

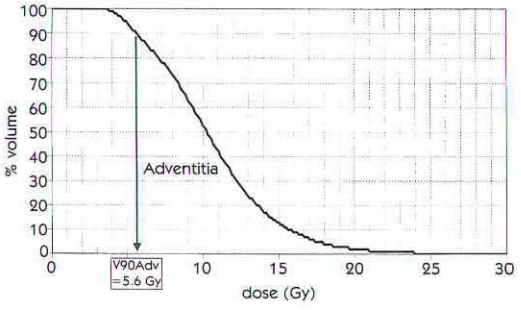

Figure 3
Example of the integral dose–volume histogram at the adventitia level of the patient illustrated in Figure 1, representing the fraction of volume (*y*-axis: % volume) receiving greater than or equal to a specific dose (*x*-axis: dose (Gy)). For this patient, 90% of the target volume for coronary brachytherapy, believed to be the adventitia, receives a dose of at least 5.6 Gy.

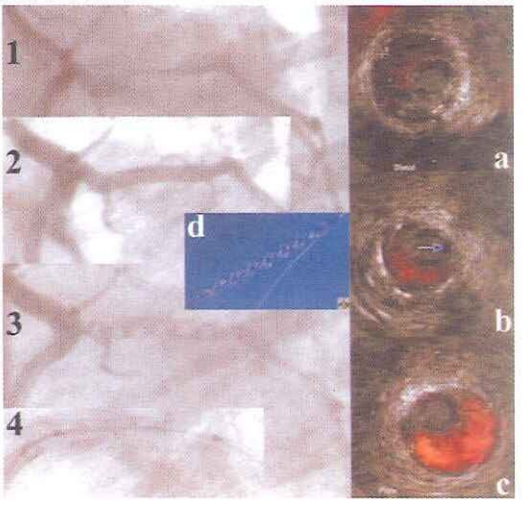

Figure 4
Panel 1 shows the lesion in the circumflex artery of a patient included in the PREVENT trial in the authors' institution. After stent implantation (panel 2), the helical balloon (panel d) used to maintain the ^{32}P wire in the center of the lumen permits the preservation of distal perfusion (panel 3). Its size was chosen using the IVUS stent diameter measured in panel b (3 mm). The dwelling time of the source (seen in panel 4) is calculated in order to give 16, 20 or 24 Gy at 2 mm in the vessel wall. The size of the vessel is calculated as the average of the distal (panel a) and proximal (panel c) intravascular ultrasound vessel size dimensions.

Ongoing trials

There is a series of ongoing trials, recently reviewed by Waksman,[64] that is soon expected to shed light on the utility of brachytherapy for prevention of restenosis. Modalities of IVUS as used in these trials are very different. In PREVENT, conducted with a ^{32}P ß-source delivered with an automatic afterloader (Galileo™, Guidant Corp, Houston, TX, USA), the radioactive wire is centered in the target lesion (de novo or in-stent restenosis) in a helical balloon which preserves distal perfusion (Figure 4). The size of this balloon is based on the coronary dimensions derived from IVUS measurements at the minimal cross-sectional area in the lesion. Proximal and distal reference segments are measured to estimate the mean vessel diameter. This measurement is used to prescribe a dose of 16, 20 or 24 Gy at 2 mm in the vessel wall.

In GAMMA-I, a ^{192}Ir source or a placebo was manually delivered following successful treatment for in-stent restenosis in 252 patients. A dose greater than 8 Gy but less than 30 Gy was administered to the EEL, with a similar IVUS guidance to that used in the SCRIPPS trial. The angiographic outcome recently reported was a reduction at six-month follow-up of the angiographic restenosis rate from 52% for the placebo group to 21.6% for the irradiated group.

In the ARREST trial investigating the restenosis rate after PTCA and provisional stenting, a mechanical delivery of a ^{192}Ir source in a partially centering balloon (3.2 F.) is used. A dose greater than 8 Gy but less than 30 Gy is also prescribed to the adventitia based on IVUS measurements.

There are also studies in which the dose is administered at a given distance from the source, without the use of IVUS. In the BETA-CATH trial (ß- $^{90}Sr/Y$ source), it is 14 Gy in vessels >2.7 mm and <3.35 mm, and 18 Gy in vessels >3.35 mm and <4.0 mm; in the SMARTS trial, which is designed for small vessels (<2.75 mm), it is 12 Gy to a distance of 2 mm from a γ-^{192}Ir source. In the ARTISTIC trial investigating patients with in-stent restenosis, the same mechanical delivery system of a ^{192}Ir source as in ARREST is used, but a dose of 12, 15 or 18 Gy is prescribed at 2 mm from the source. In the CURE study conducted with a balloon filled with ^{188}Re, a dose of 13 Gy at 0.5 mm from the surface of the balloon is prescribed.

Positive results are not obtained only when using IVUS. The data of the Schneider/Boston Scientific ß-intracoronary irradiation dose-finding study very recently presented by Verin at the European Congress of Cardiology (Barcelona, August 1999) demonstrate that with 9–18 Gy at 1 mm tissue depth, there was a significant dose-related inhibitory effect on restenosis after PTCA and a beneficial effect on remodeling. The delivery of 18 Gy at 1 mm tissue depth resulted in a low overall restenosis rate of 8.3% and an even lower rate of 4.3% in those patients treated with balloon angioplasty and radiation alone. Measurements were based on QCA. However, Russo et al have compared the method of dosage using IVUS during the SCRIPPS trial to a method based on an angiographic model and a fixed-dose strategy.[65] From 119 IVUS pull-backs, the IVUS method would give mean minimal and maximal adventitial doses of 7.73 ± 0.69 Gy and 25.81 ± 5.26 Gy, and

References

1. Liermann D, Böttcher HD, Kollath J et al. Prophylactic endovascular radiotherapy to prevent intimal hyperplasia after stent implantation in femoropopliteal arteries. Cardiovasc Intervent Radiol 1994; 17: 12–16.
2. Enhamre A, Hammar H. Treatment of keloids with excision and post-operative x-ray irradiation. Dermatologica 1983; 167: 90–93.
3. Bahrassa F, Datta R. Postoperative beta radiation treatment of pterygium. Int J Radiat Oncol Biol Phys 1983; 9: 679–684.
4. Serruys PW, Luijten HE, Beatt KJ et al. Incidence of restenosis after succesful coronary angioplasty: a time-related phenomenon: a quantitative angiography study in 342 consecutive patients at 1, 2, 3 and 4 months. Circulation 1988; 77: 361–371.
5. Schwartz RS, Holmes DR, Topol EJ. The restenosis paradigm revisited: an alternative proposal for cellular mechanism. J Am J Cardiol 1992; 20: 1284–1293.
6. Mintz GS, Popma JJ, Pichard AD et al. Arterial remodeling after coronary angioplasty. A serial intravascular ultrasound study. Circulation 1996; 94: 35–43.
7. Hanke H, Kamenz J, Hassenstein S et al. Prolonged proliferative response of smooth muscle cells after experimental intravascular stenting. Eur Heart J 1995; 16: 785–793.
8. van Beusekom HM, Whelan DM, Hofma SH et al. Long-term endothelial dysfunction is more pronounced after stenting than after balloon angioplasty in porcine coronary arteries. J Am Coll Cardiol 1998; 32: 1109–1117.
9. Wiedermann JG, Leavy JA, Amols H et al. Effects of high-dose intracoronary irradiation on vasomotor function and smooth muscle histopathology. Am J Physiol 1994; 267: H125–132.
10. Waksman R, Robinson KA, Crocker IR, Gravanis MB, Cipolla GD, King SB. Endovascular low dose irradiation inhibits neointimal formation after coronary artery balloon injury in swine: a possible role for radiation therapy in restenosis prevention. Circulation 1995; 91: 1533–1539.
11. Mazur W, Ali MN, Khan MM. High dose rate intracoronary radiation for inhibition of neointimal formation in the stented and balloon-injured porcine models of restenosis: angiographic, morphometric, and histopathologic analyses. Int J Radiat Oncol Biol Phys 1996; 36: 777–788.
12. Waksman R, Robinson KA, Crocker IR et al. Intracoronary low-dose beta-irradiation inhibits neointima formation after coronary artery balloon injury in the swine restenosis model. Circulation 1995; 92: 3025–3031.
13. Verin V, Popowski Y, Urban P et al. Intra-arterial beta-irradiation prevents neointimal hyperplasia in a hypercholesterolemic rabbit restenosis model. Circulation 1995; 92: 2284–2290.
14. Hehrlein C, Gollan C, Donges K et al. Low-dose radioactive endovascular stents prevent smooth muscle cell proliferation and neointimal hyperplasia in rabbits. Circulation 1995; 92: 1570–1575.
15. Carter AJ, Laird JR, Bailey LR et al. Effects of endovascular radiation from a beta particle emitting stent in a porcine coronary restenosis model. Circulation 1996; 94: 2364–2368.
16. Topol EJ, Nissen SE. Our preocupation with coronary luminology. The dissociation between clinical and angiographic findings in ischemic heart disease. Circulation 1995; 92: 2333–2342.
17. Glagov S, Weisenberg E, Zarins CK. Compensatory enlargement of human atherosclerotic coronary arteries. N Engl J Med 1987; 316: 1371–1375.
18. Hodgson J, Reddy D, Suneja R, Nair R, Lesnefsky E, Sheehan H. Intracoronary ultrasound imaging: correlation of plaque morphology with angiography, clinical syndrome and procedural results in patients undergoing coronary angioplasty. J Am Coll Cardiol 1993; 21: 35–44.
19. Yock PG, Linker DT. Intravascular ultrasound. Looking below the surface of vascular disease. Circulation 1990; 81: 1715–1718.
20. Peters RJG, Kok WEM, Di Mario C et al. Prediction of restenosis after coronary balloon angioplasty. Results of PICTURE (Post-Intracoronary Treatment Ultrasound Result Evaluation), a prospective multicenter intracoronary ultrasound imaging study. Circulation 1997; 95: 2254–2261.
21. The GUIDE Trial Investigators. IVUS-determined predictors of restenosis in PTCA and DCA: final report from the GUIDE trial, phase II. J Am Coll Cardiol 1996; 27 (suppl A):156A.
22. Stone GW, Hodgson JM, St Goar FG et al. Improved procedural results of coronary angioplasty with intravascular ultrasound-guided balloon sizing: the CLOUT Pilot Trial. Circulation 1997; 95: 2044–2052.
23. Schroeder S, Baumbach A, Haase KK et al. Reduction of restenosis by vessel size adapted percutaneous transluminal coronary angioplasty using intravascular ultrasound. Am J Cardiol 1999; 83: 875–879.
24. de Feyter PJ, Disco C, Serruys P et al. A reference chart derived from post stent implantation IVUS predictors for 6-month expected QCA restenosis. Circulation 1999; 100: 1777–1783.
25. Hoffman R, Mintz GS, Mehran R et al. Intravascular ultrasound predictors of angiographic restenosis in lesions treated with Palmaz–Schatz stents. J Am Coll Cardiol 1998; 31: 43–49.
26. Kasaoka S, Tobis JM, Akiyama T et al. Angiographic and intravascular ultrasound predictors of in-stent restenosis. J Am Coll Cardiol 1998; 32: 1630–1635.
27. Prati F, Di Mario C, Moussa I et al. In-stent neointimal proliferation correlates with the amount of residual plaque burden outside the stent: an intravascular ultrasound study. Circulation 1999; 99: 1011–1014.
28. Hong MK, Mintz GS, Pichard AD et al. Intravascular ultrasound predictors of target lesion revascularization after stenting of protected left main coronary artery stenoses. Am J Cardiol 1999; 83: 175–179.
29. Moussa I, Moses J, Di Mario C et al. Does the specific intravascular ultrasound criterion used to optimize stent expansion have an impact on the probability of stent restenosis? Am J Cardiol 1999; 83: 1012–1017.
30. Albiero R, Rau T, Schluter M et al. Comparison of immediate and intermediate-term results of intravascular ultrasound versus angiography-guided Palmaz–Schatz stent implantation in matched lesions. Circulation 1997; 96: 2997–3005.
31. de Jaegere P, Mudra H, Figulla H et al. Intravascular ultrasound-guided optimized stent deployment. Immediate and 6 months clinical and angiographic results from the Multicenter Ultrasound Stenting in Coronaries Study (MUSIC Study). Eur Heart J 1998; 19: 1214–1223.

32. Serruys PW, Deshpande NV. Is there MUSIC in IVUS guided stenting? Is this MUSIC going to be a MUST? Multicenter Ultrasound Stenting in Coronaries study. Eur Heart J 1998; 19: 1122–1124.
33. Blasini R, Neumann FJ, Schmitt C, Walter H, Schomig A. Restenosis rate after intravascular ultrasound-guided coronary stent implantation. Cathet Cardiovasc Diagn 1998; 44: 380–386.
34. Schiele F, Meneveau N, Vuillemenot A. Impact of intravascular ultrasound guidance in stent deployment on 6-month restenosis rate: a multicenter, randomized study comparing two strategies, with and without intravascular ultrasound guidance. RESIST Study Group. REStenosis after Ivus guided STenting. J Am Coll Cardiol 1998; 32: 320–328.
35. Mudra H, Macaya C, Zahn R et al. Interim analysis of the 'OPTimization with ICUS to reduce stent restenosis' (OPTICUS) trial. Circulation 1998; 98: I–363.
36. Hanekamp CE, Koolen JJ, Pijls NH, Michels HR, Bonnier HJ. Comparison of quantitative coronary angiography, intravascular ultrasound, and coronary pressure measurement to assess optimum stent deployment. Circulation 1999; 99: 1015–1021.
37. Serruys P, Levendag PC. Intracoronary brachytherapy: the death knell of restenosis or just another episode of a never-ending story ? Circulation 1997; 96: 709–712.
38. Di Mario C, Görge G, Peters R et al. Clinical application and image interpretation in intracoronary ultrasound. Study Group on Intracoronary Imaging of the Working Group of Coronary Circulation and of the Subgroup on Intravascular Ultrasound of the Working Group of Echocardiography of the European Society of Cardiology. Eur Heart J 1998; 19: 207–229.
39. von Birgelen C, de Vrey EA, Mintz GS et al. ECG-gated three-dimensional intravascular ultrasound: feasibility and reproducibility of an automated analysis of coronary lumen and atherosclerotic plaque dimensions in humans. Circulation 1998; 96: 2944–2952.
40. Krams R, Wentzel JJ, Oomen JA et al. Evaluation of endothelial shear stress and 3D geometry as factors determining the development of atherosclerosis and remodeling in human coronary arteries in vivo. Combining 3D reconstruction from angiography and IVUS (ANGUS) with computational fluid dynamics. Arterioscler Thromb Vasc Biol 1997; 17: 2061–2065.
41. Amols HI, Zaider M, Weinberger J, Ennis R, Schiff PB, Reinstein LE. Dosimetric considerations for catheter-based beta and gamma emitters in the therapy of neointimal hyperplasia in human coronary arteries. Int J Radiat Oncol Biol Phys 1996; 36: 913–921.
42. Drzymala RE, Mohan R, Brewster L et al. Dose-volume histograms. Int J Radiat Oncol Biol Phys 1991; 21: 71–78.
43. Fox T, Crocker I. Dosing in vascular radiotherapy. Vasc Radiother Monitor 1998; 1: 45–53.
44. Carlier SG, Marijnissen JPA, Coen VLMA et al. Guidance of intracoronary radiation therapy based on dose-volume histogram derived from quantitative intravascular ultrasound. IEEE Trans Med Imaging 1998; 17: 772–778.
45. Condado JA, Waksman R, Gurdiel O et al. Long-term angiographic and clinical outcome after percutaneous transluminal coronary angioplasty and intracoronary radiation therapy in humans. Circulation 1997; 96: 727–732.
46. Verin V, Urban P, Popowski Y et al. Feasibility of intracoronary beta-irradiation to reduce restenosis after balloon angioplasty. Circulation 1997; 95: 1138–1144.
47. Teirstein P. Beta-radiation to reduce restenosis. Too little, too soon ? Circulation 1997; 95: 1095–1097.
48. Teirstein PS, Massullo V, Jani S et al. Catheter based radiotherapy to inhibit restenosis after coronary stenting. N Engl J Med 1997; 336: 1697–1703.
49. Teirstein PS, Massullo V, Jani S et al. Two-year follow-up after catheter-based radiotherapy to inhibit coronary restenosis. Circulation 1999; 99: 243–247.
50. Teirstein PS, Massullo V, Jani S et al. A subgroup analysis of the Scripps Coronary Radiation to Inhibit Proliferation Post-stenting Trial. Int J Radiat Oncol Biol Phys 1998; 42: 1097–1104.
51. Waksman R, White LR, Chan RC et al. Intracoronary radiation therapy for patients with in-stent restenosis: 6 month follow-up of a randomized clinical study. Circulation 1998; 98: I-651.
52. Waksman R, White RL, Chan RC et al. Intracoronary beta radiation therapy for in-stent restenosis: preliminary report from a single center clinical study. J Am Coll Cardiol 1999; 33: 19A.
53. King SB, Williams DO, Chougule P et al. Endovascular beta-radiation to reduce restenosis after coronary balloon angioplasty. Results of the Beta Energy Restenosis Trial (BERT). Circulation 1998; 97: 2025–2030.
54. Meerkin D, Tardif JC, Crocker IR et al. Effects of intracoronary beta-radiation therapy after coronary angioplasty : an intravascular ultrasound study. Circulation 1999; 99: 1660–1665.
55. Bom N, Lancée CT, Van Egmond FC. An ultrasonic intracardiac scanner. Ultrasonics 1972; 72–76.
56. Rosenfield K, Losordo DW, Ramaswamy K et al. Three-dimensional reconstruction of human coronary and peripheral arteries from images recorded during two-dimensional intravascular ultrasound examination. Circulation 1991; 84: 1938–1956.
57. Coy KM, Park JC, Fishbein MC et al. In vitro validation of three-dimensional intravascular ultrasound for the evaluation of arterial injury after balloon angioplasty. J Am Coll Cardiol 1992; 20: 692–700.
58. Matar FA, Mintz GS, Douek P et al. Coronary artery lumen volume measurement using three-dimensional intravascular ultrasound: validation of a new technique. Cathet Cardiovasc Diagn 1994; 33: 214–220.
59. von Birgelen C, di Mario C, Li W et al. Morphometric analysis in three-dimensional intracoronary ultrasound: an in-vitro and in-vivo study performed with a novel system for the contour detection of lumen and plaque. Am Heart J 1996; 132: 516–527.
60. Roelandt JRTC, di Mario C, Pandian NG et al. Three-dimensional reconstruction of intracoronary ultrasound images: rationale, approaches, problems and directions. Circulation 1994; 90: 1044–1055.
61. Sabate M, Serruys PW, van der Giessen WJ et al. Geometric vascular remodeling after balloon angioplasty and beta-radiation therapy: a three-dimensional intravascular ultrasound study. Circulation 1999; 100: 1182–1188.
62. Sabate M, Marijnissen JPA, Carlier SG et al. Regional analysis of dosimetry and volumetric morphological changes in coronary segments treated with beta-radiation following successful balloon angioplasty. Circulation 2000 (in press).
63. Carlier SG, Marijnissen JPA, Coen VLMA et al. Comparison of brachytherapy strategies based on dose-volume histograms derived from quantitative intravascular ultrasound. Cardiovasc Radiat Med 1999; 1: 115–124.

64. Waksman R. Intracoronary radiation therapy for restenosis prevention: status of the clinical trials. Cardiovasc Radiat Med 1999; 1: 3–7.
65. Russo R, Massullo V, Tripuraneni P, Jani S, Silva PD, Teirstein PS. Is intravascular ultrasound necessary for dose prescription during intracoronary radiation therapy? J Am Coll Cardiol 1999; 33: 20A.
66. Di Mario C, Akiyama T, Moussa I et al. First experience with imaging core wires. Semin Intervent Cardiol 1997; 2: 69–73.
67. Ciezki JP. Brachytherapy guided by ultrasound. In: Waksman R, Serruys P, eds. Handbook of Vascular Brachytherapy 2nd ed. London: Martin Dunitz Ltd, 2000: 152–162.

Chapter 14

Comparison of brachytherapy strategies based on dose-volume histograms derived from quantitative intravascular ultrasound.

SG Carlier, JPA Marijnissen, VLMA Coen, M Sabate, WJ van der Giessen, J Ligthart, A den Boer, PC Levendag, PW Serruys.

Cardiovascular Radiation Medicine 1999; 1:115-124.

With the editorial "Circumventing the learning curve of dose and volume in intravascular brachytherapy" by Y Yu, MC Schell and P Rubin.

ELSEVIER

Cardiovascular Radiation Medicine 1:2 (1999) 170–171

CARDIOVASCULAR RADIATION MEDICINE

EDITORIAL

CIRCUMVENTING THE LEARNING CURVE OF DOSE AND VOLUME IN INTRAVASCULAR BRACHYTHERAPY

Yan Yu, Ph.D.,* M. C. Schell, Ph.D., and P. Rubin, M.D.

Department of Radiation Oncology, University of Rochester, Rochester, New York, USA

Received 29 April 1999; accepted 30 April 1999

In 1976, Anderson published the spacing nomograph for ^{125}I, which was a rapid dose planning method to facilitate interstitial brachytherapy of the prostate [1]. Under this "dimension averaging" technique [2], the three orthogonal lengths of the prostate were measured operatively and averaged, from which the total radioactive strength of the implant was determined by a lookup table. The therapeutic dose was characterized by the matched peripheral dose (MPD) concept—a dose cloud having the same volume as that of an ellipsoid constructed from the three measured dimensions The lack of technological sophistication, of course, reflected the overall limitation of that era. However, the simplicity of the method found ready acceptance in this largely interventional procedure, even up to today.

During the course of the past 23 years, our understanding of clinical dosimetry for prostate brachytherapy has undergone fundamental changes. Suboptimal dose distribution due to technical limitations was identified as the possible cause of unfavorable outcomes from the early series of open surgical implants [3]. Transrectal ultrasound (TRUS) was used to provide real-time visualization of the target volume in three dimensions [4], and was used to develop quantitative dosimetric planning customized to each patient [5]. Computed tomography was used postoperatively to assess organ-specific dose-volume histograms (DVH), which revealed that the MPD was an unreliable indicator of dosimetric quality [6]. Later, it was shown that the minimum peripheral dose was also an illusive parameter given the inaccuracies in radiation source placement, and that a dose to 90% of the target volume from the DVH, D_{90}, would be a more consistent parameter for dose specification [7]. This conclusion was supported by a recent clinical study, which demonstrated a clear dose response at 140 Gy for D_{90} [8]. Based on ongoing studies such as these, both the American Association of Physicists in Medicine and the American Brachytherapy Society recommended reporting a handful of parameters obtainable from the DVH as potentially significant indicators of therapeutic effectiveness [9, 10].

As a case study in interventional radiotherapy, this body of literature demonstrates the interesting interplay between technological advancement and clinical needs. It is the nature of brachytherapy to accept rapid dose fall-off in the vicinity of the radioactive source. The actual dose delivered to a radiation target is therefore not a single number, but a range of values for different percentages of the target volume. A dosimetric parameter based on idealized geometries, such as the MPD, may not correlate with any therapeutic outcome. On the other hand, more complex characterization of the dose distribution, such as the DVH, requires serial image acquisition, target identification, and computerized dosimetry calculation, all customized to each given patient. Wide availability of these tools in turn is expected to promote greater understanding of dose response and radiation toxicity in a multi-institutional setting. In prostate brachytherapy, it may be said that we have finally negotiated the learning curve and are ready to scale new heights.

In this context, it is particularly exciting to see the paper by Carlier *et al.* [11] in this second issue

*Correspondence to: Yan Yu, Ph.D., Department of Radiation Oncology, University of Rochester Medical Center, 601 Elmwood Avenue, Rochester, NY 14642, USA.

1522-1865/99/$–see front matter.
PII S1522-1865(99)00009-8

of *Cardiovascular Radiation Medicine*. The authors applied an electrocardiogram (ECG)-gated image acquisition technique developed previously for intravascular ultrasound (IVUS) to control cardiac cycle artifacts. Serial cross-sectional images were registered by means of constant-step pullback of IVUS as controlled by the ECG trigger algorithm, which also rejected premature beats. Analysis of the irradiated segment was achieved using automated identification of the lumen–intima and the media–adventitia boundaries. Based on this target-specific information, the DVH was generated for the actual radioactive source used in the study, and for simulation of centered vs. noncentered irradiation from both β and γ sources. This pioneering study demonstrates the feasibility of IVUS-guided target-specific dosimetry in intravascular brachytherapy at a time when reliable, detailed dosimetry information is urgently needed to supplement the design and analysis of clinical trials.

The current spectacular revival of prostate brachytherapy is due in large part to real-time TRUS guidance. The growing emphasis on target-specific dosimetry also motivated optimized inverse planning of radiation delivery [12]. This technology enables the clinician-user to define the dosimetric intent, from which an optimized irradiation strategy is generated automatically. The feasibility of using this technology intraoperatively to perform real-time planning has been demonstrated [13]. Whereas Carlier *et al.* [11] recognized the lack of real-time generation of dosimetry based on IVUS due to processing speed, the challenge is likely to be met soon. This era of accelerated growth of technology has helped us shape the field of interventional radiotherapy in many important ways.

As a case study in interventional radiotherapy, intravascular brachytherapy and prostate brachytherapy have striking similarities: Both are amenable to real-time ultrasound imaging. Uncertainty exists in target movement and irregularity, and in radiation source placement. The radiation dosimetry is modified by the presence of calcification and other tissue heterogeneities. There is a lack of consensus understanding regarding the extent of the target volume for irradiation. Finally, as in prostate brachytherapy, there is some indication that a dose–response exists, below which the effect of radiation to prevent restenosis is diminished significantly [14, 15]. All these similarities point to the importance of quantitative, volumetric dosimetry analysis and reporting in the present context.

The DVH study reported by Carlier *et al.* [11] is likely to be the first of a body of literature that, as in prostate brachytherapy, deepens our understanding of this therapeutic modality. However, we are now in a position to circumvent the learning curve and proceed to new grounds.

References

[1] Anderson LL. Spacing nomograph for interstitial implants of ^{125}I seeds. Med. Phys. 1976;3:48–51.

[2] Henschke UK, Ceve P. Dimension averaging a simple method for dosimetry of interstitial implants. Radiobiol. Radiother. (Berl) 1968;9:287–298.

[3] Zelefsky MJ, Whitmore WF Jr. Long-term results of retropubic permanent ^{125}iodine implantation of the prostate for clinically localized prostatic cancer. J. Urol. 1997;158: 23–29.

[4] Holm HH, Juul N, Pedersen JF, Hansen H, Stroyer I. Transperineal ^{125}iodine seed implantation in prostatic cancer guided by transrectal ultrasonography. J. Urol. 1983;130: 283–286.

[5] Grimm PD, Blasko JC, Radge H. Ultrasound-guided transperineal implantation of iodine-125 and palladium-103 for the treatment of early stage prostate cancer; Technical concepts in planning, operative technique and evaluation. Atlas Urol. Clin. North Am. 1994;2:113–125.

[6] Roy JN, Wallner KE, Harrington PJ, Ling CC, Anderson LL. A CT-based evaluation method for permanent implants: application to prostate. Int. J. Radiat. Oncol. Biol. Phys. 1993; 26:163–169.

[7] Yu Y, Waterman FM, Suntharalingam N, Schulsinger A. Limitations of the minimum peripheral dose as a parameter for dose specification in permanent ^{125}I prostate implants. Int. J. Radiat. Oncol. Biol. Phys. 1996;34:717–725.

[8] Stock RG, Stone NN, Tabert A, Iannuzzi C, DeWyngaert JK. A dose–response study for I-125 prostate implants. Int. J. Radiat. Oncol. Biol. Phys. 1998;41:101–108.

[9] Yu Y, Anderson LL, Li Z, *et al.* Permanent prostate seed implant brachytherapy: report of the American Association of Physicists in Medicine Task Group No. 64. Med. Phys. 1999; Submitted.

[10] Nag S, Bice W, DeWyngaert K, Prestidge B, Stock R, Yu Y. The American Brachytherapy Society recommendations for permanent prostate brachytherapy post-implant dosimetric analysis. Int. J. Radiat. Oncol. Biol. Phys. 1998; Submitted.

[11] Carlier SG, Marijnissen JPA, Coen VLMA, *et al.* Comparison of brachytherapy strategies based on dose-volume histograms derived from quantitative intravascular ultrasound. Cardiovasc. Radiat. Med. 1999;1:115–124.

[12] Yu Y, Zhang JBY, Brasacchio RA, *et al.* Automated treatment planning engine for prostate seed implant brachytherapy. Int. J. Radiat. Oncol. Biol. Phys. 1999;43:647–652.

[13] Messing EM, Zhang JB, Rubens DJ, *et al.* Intraoperative optimized inverse planning for prostate brachytherapy: early experience. Int. J. Radiat. Oncol. Biol. Phys. In press.

[14] Taylor AJ, Gorman PD, Farb A, Hoopes TG, Sweet B, Virmani R. Different effects of ^{32}P β-emitting stents on the intima and adventitia in the dog model. Circulation 1998;98: 4085.

[15] Waksman R, Robinson KA, Crocker IR, Gravanix MB, Cipolla GD, King SB III. Endovascular irradiation inhibits a restenosis-like response after balloon angioplasty of pig coronaries: dose–response relationship. Circulation 1994;90:142.

ELSEVIER

Cardiovascular Radiation Medicine 1:2 (1999) 115–124

CARDIOVASCULAR RADIATION MEDICINE

CLINICAL ORIGINAL ARTICLE

COMPARISON OF BRACHYTHERAPY STRATEGIES BASED ON DOSE-VOLUME HISTOGRAMS DERIVED FROM QUANTITATIVE INTRAVASCULAR ULTRASOUND

Stéphane G. Carlier, M.D.,[a] Johannes P. A. Marijnissen,[b] Veronique L. M. A. Coen,[b] Manel Sabate,[a] Willem J. van der Giessen,[a] Jurgen Ligthart,[a] Ad den Boer,[a] Peter C. Levendag,[b] and Patrick W. Serruys[a]

[a]*Department of Interventional Cardiology, Thoraxcenter, Erasmus University Rotterdam, Rotterdam, The Netherlands*
[b]*Daniel den Hoed Cancer Center, Erasmus University Rotterdam, Rotterdam, The Netherlands*

Received 23 February 1999; accepted 1 April 1999

Purpose. We present in this paper the comparison, by simulation, of different treatment strategies based either on β- or γ-sources, both with and without a centering device. Ionizing radiation to prevent restenosis is an emerging modality in interventional cardiology. Numerous clinical studies are presently being performed or planned, but there is variability in dose prescription, and both γ- and β-emitters are used, leading to a wide range of possible dose distributions over the arterial vessel wall. This paper discusses the potential merits of dose-volume histograms (DVH) based on three-dimensional (3-D) reconstruction of electrocardiogram (ECG)-gated intravascular ultrasound (IVUS) to compare brachytherapy treatment strategies.

Materials and Methods. DVH describe the cumulative distribution of dose over three specific volumes: (1) at the level of the luminal surface, a volume was defined with a thickness of 0.1 mm from the automatically detected contour of the highly echogenic blood-vessel interface; (2) at the level of the IVUS echogenic media-adventitia interface (external elastic lamina [EEL]), an adventitial volume was computed considering a 0.5-mm thickness from EEL; and (3) the volume encompassed between the luminal surface and the EEL (plaque + media). The IVUS data used were recorded in 23 of 31 patients during the Beta Energy Restenosis Trial (BERT) conducted in our institution.

Results. On average, the minimal dose in 90% of the adventitial volume was 37 ± 16% of the prescribed dose; the minimal dose in 90% of the plaque + media volume was 58 ± 24% and of the luminal surface volume was 67 ± 31%. The minimal dose in the 10% most exposed luminal surface volume was 296 ± 42%. Simulations of the use of a γ-emitter and/or a radioactive source train centered in the lumen are reported, with a comparison of the homogeneity of the dose distribution.

Conclusions. It is possible to derive DVH from IVUS, to evaluate the dose delivered to different parts of the coronary wall. This process should improve our understanding of the mechanisms of action of brachytherapy. © 1999 Elsevier Science Inc.

Keywords: Brachytherapy; Restenosis; Vascular; Intravascular ultrasound (IVUS); Dosimetry.

Correspondence to: S.G. Carlier, M.D., Experimental Echo Laboratory, Erasmus University—Ee2302, Dr Molewaterplein 50, 3015 GE Rotterdam, The Netherlands; E-mail: CARLIER@TCH.FGG.EUR.NL

1522-1865/99/$–see front matter.
PII S1522-1865(99)00003-7

Introduction

Coronary artery diseases remain the major cause of death and disabilities in industrialized countries. The

only revascularization procedure available up to 1977 was bypass surgery. Percutaneous transluminal coronary angioplasty (PTCA) introduced by Andreas Grüntzig [1] profoundly modified our therapeutic arsenal with a minimally invasive alternative. Presently, interventional cardiology consists of several techniques to cut, drill, scrape, burn, and otherwise remove atherosclerotic plaque [2]. With more than one million interventions undertaken per year worldwide, angioplasty is now a cornerstone therapy for coronary artery diseases. However, despite a high acute procedural success rate, the long-term benefit is hindered by the phenomenon of restenosis. Mechanisms involved in the restenosis process are the elastic recoil of the artery, local thrombus formation, vascular remodeling with shrinkage of the vessel, and exuberant healing process with neointimal cellular proliferation and matrix synthesis [3–5]. Stent implantation minimizes elastic recoil and remodeling of vessels, and carefully controlled and randomized clinical trials have demonstrated a significant decrease in the rate of restenosis [6–8]. However, stents increase the proliferative response of tissue to the intervention and, depending on the type of lesions treated, a significant restenosis rate of 15–50% remains the key limitation of transcatheter procedures. Restenosis is the subject of numerous investigations to further improve applicability and cost-effectiveness of angioplasty and to reduce the need of reinterventions. Virtually all attempts to limit restenosis with systemic drugs have failed, with the recent exceptions of abciximab, probucol, and cilostazol [9–11].

Some investigators have considered restenosis as an accentuation of the wound healing process associated with the trauma of angioplasty, and because radiotherapy had proved effective for the treatment of keloid formation and other nonmalignant diseases, radiation therapy for intravascular application was attempted. The therapy was introduced by Friedman *et al.* [12] early in 1964, for the prevention of atherosclerosis, and subsequent animal experiments demonstrated a reduction of intimal hyperplasia following endovascular irradiation. Waksman [13] has recently reviewed these early studies. Three clinical studies have been reported that confirmed a significant reduction in the restenosis rate using additional brachytherapy [14–16].

Currently, the vascular brachytherapy devices available for clinical trials are radioactive stents and catheter-based systems using a radioactive wire advanced with an afterloader, or radioactive seeds delivered with a hydraulic delivery system. Other systems based on radioactive balloons are in development. There is variability in the dose prescription, and both γ- and β-emitters are used. These variations lead to a wide range of dose distributions over the arterial vessel wall requiring a careful interpretation and comparison of the results of the ongoing studies. The typical dose prescription distance in the coronary arteries is in the range of 2 mm from the source axis. Because of the steep dose fall-off, particularly for β-emitters, accurate dosimetry requires precise knowledge of geometry.

In this paper, we describe a dosimetry evaluation tool for coronary brachytherapy based on three-dimensional (3-D) reconstruction of electrocardiogram (ECG)-gated intravascular ultrasound (IVUS) images. IVUS was developed to overcome the limitations of x-ray angiography. Its methodology and clinical applications have been reviewed extensively [17]. IVUS, by its tomographic approach, provides a mean for the evaluation of both lumen and vessel wall morphology. Assuming that the catheter containing the radioactive source is lying in the same position as the IVUS catheter, it is possible to measure the distance from the source to any vascular structure in one cross-sectional image, and to construct isodose plots. IVUS recordings can be performed with a constant speed motorized pull-back device (*e.g.*, 0.5 mm/s), which permits the evaluation of the length of a stenosis. Recently, 3-D image reconstruction and analysis systems have been introduced that can be used for complete quantitative analysis of IVUS images [18–21]. However, image artifacts that result from cyclic changes in coronary dimensions and from the movement of the IVUS catheter in the arterial lumen limit the accuracy of the 3-D boundary detection systems [22]. This problem led to the development of a new approach in our institution. To limit cyclic movement artifacts, we use an ECG-gated image acquisition workstation that controls a dedicated pull-back device. Feasibility, reproducibility, and improvement in the quantitative parameters analyzed have been reported recently [23, 24]. The complete 3-D data set of the coordinates of the automatically detected lumen corresponding to the highly echogenic blood–vessel interface, and of the echogenic media–adventitia interface can be used for dosimetry evaluation.

Dose-volume histograms (DVH) are used everyday in radiotherapy to condense the large body of information of the complete 3-D dose distribution data into a plot graphically summarizing the radiation distribution throughout the target volume and the anatomical structures of interest [25, 26]. We have recently reported preliminary data on the methodology to compute DVH for coronary brachytherapy from 3-D IVUS data [27].

Material and Methods

Study population

We used the IVUS data acquired during the Beta Energy Restenosis Trial conducted in our institu-

tion (BERT 1.5 arm). Thirty-one patients were enrolled. We report the data of the 23 patients who had an ECG-triggered pull-back available before a stent implantation (18 men, 5 women, mean age: 58 ± 9 years). All were in sinus rhythm. The Medical Ethics Committee of our institution approved the study and all patients signed a written informed consent form. Before catheterization, the patients received 250 mg aspirin and 10,000 IU heparine parenterally. If the duration of the intervention exceeded 1 h, the activated clotting time was measured and intravenous heparin was used to maintain an activated clotting time >300 s. The coronary segments examined were the right (n = 7) and left (n = 10) anterior descending coronary arteries, and the left circumflex coronary artery (n = 6).

Interventional procedure and BERT 1.5 trial

The BERT 1.5 trial was the European arm of a feasibility study of coronary radiation therapy with a $^{90}Sr/Y$ source delivered by a hydraulic system (Beta-Cath™ System, Novoste Corp., Norcross, GA) [16]. All patients had a single *de novo* coronary stenotic lesion >60% with a maximal length of 15 mm and a reference vessel diameter of 2.5–3.5 mm. After successful PTCA, irradiation using a 5 Fr (~1.6 mm) over-the-wire triple-lumen delivery catheter was performed. The catheter has one open lumen and two closed lumens. The open lumen allows for advancement of the device over a 0.014-inch guide wire, and positioning at the site of the PTCA (Fig. 1). One of the closed lumens permits the hydraulic advancement of the radiation source train (12 independent cylindrical sealed $^{90}Sr/Y$ sources, total length 30 mm) to the lesion site. This advancement is performed manually, with a saline-filled syringe connected to the delivery system. The other closed lumen, in communication with the first one at the tip of the delivery catheter, permits the opposite fluid flow direction at the end of the irradiation time (~3 min) for the retrieval of the sources into the back in the shielded transfer device. A randomized dose of either 12, 14, or 16 Gy was prescribed at a distance of 2 mm from the source axis.

IVUS image acquisition

IVUS was performed prior to the insertion of the radiation delivery catheter. Intracoronary nitrates were administered before the coronary segments were examined. The ClearView™ (CardioVascular Imaging System [CVIS], Sunnyvale, CA) was used with IVUS catheter incorporating a 30-MHz single-element rotating transducer in a 2.9 Fr sheath (~1 mm). The ECG-gated image digitization system (EchoScan, TomTec, Munich, Germany) received the video signal input from the IVUS console, and the ECG signal from the patient. This system steered the ECG-gated stepping pull-back device by increments of 0.2 mm. Images were acquired at end-diastole for heart cycles falling within a predetermined range (0.125 s) around the heart rate of the patient. Premature beats and RR-intervals outside this range were excluded and the IVUS catheter remained at the same site. By experience, we have noticed that with these settings, on average 10–15% of the RR intervals are rejected, and that for a heart rate of 60 beats/min, on average, the pull-back speed is 1 cm/min.

Image analysis system

A contour detection program developed in our laboratory [28] was used for the automated 3-D analysis of the IVUS images corresponding to the irradiated segment. Two longitudinal sections (corresponding to the A and B lines on the IVUS cross-section in Fig. 2) were constructed from the data set. The contours of the lumen–intima (internal contour on Fig. 2, lower left panel) and the media–adventitia (ex-

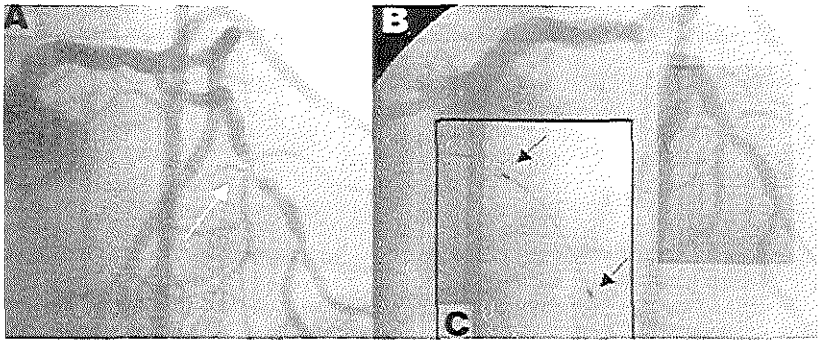

Figure 1. Angiograms of one patient included in the Beta Energy Restenosis Trial (BERT). (A) The initial lesion in the mid-portion of the left anterior descending artery at a bifurcation point with a diagonal and a septal side-branches is indicated by an arrow. (B) The angiogram after successful percutaneous transluminal coronary angioplasty (PTCA). (C) The triple-lumen delivery catheter advanced to the angioplasty site. The sealed radioactive cylinders (total length 30 mm) will be between the two gold markers (small arrows).

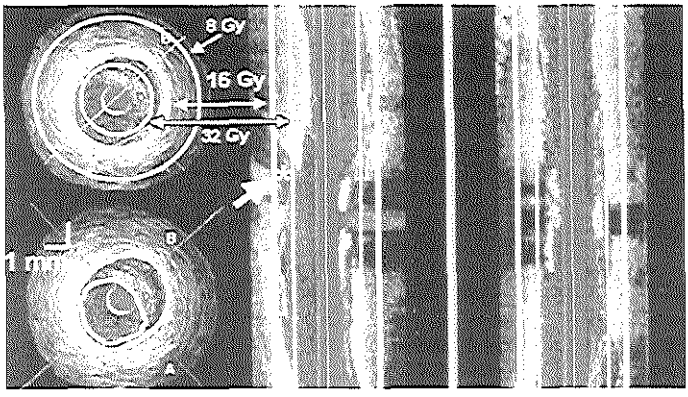

Figure 2. The three-dimensional intravascular ultrasound (IVUS) data set: the bottom left panel demonstrates an IVUS cross-section image, with the catheter in the center, surrounded by blood. The catheter is against the lumen wall at 2 o'clock. The first detected contour that corresponds to the blood–vessel wall interface is highlighted. The second highlighted contour, more externally, corresponds to the media-adventitia interface, which encompasses the residual plaque lying between 11 and 4 o'clock. Lines A and B correspond to the cutting planes of the corresponding longitudinal views on the right panel. The isodoses of 32 and 16 Gy are superimposed on the longitudinal views and on the IVUS cross-section of the upper left panel.

ternal contour on Fig. 2) boundaries were identified using a minimum-cost-based analysis algorithm. These longitudinal contours were used to guide automated contour detection in every planar cross-sectional image. Scrolling through the entire data set is possible in this Windows™-based program, for manual corrections of the contours. From these tracings, the total vessel area (encompassing the media–adventitia border) and the lumen area were determined for each cross-section. The residual plaque burden (%) on each cross-section was calculated as total vessel area minus lumen area divided by the total vessel area.

DVH

Selection of the IVUS segment matching the irradiated site was based on anatomical landmarks lying next to the treated segment (side branches, bifurcations, *etc.*). For example, the diagonal artery seen on the angiogram of Fig. 1 is marked with an arrow on the longitudinal IVUS pull-back of Fig. 2 (right panel). The coordinate of the center of the IVUS catheter was used as a reference, and was considered at the same location as the center of the radiation train. This assumption is probably violated when looking at the differences in size of the IVUS and delivery catheters (2.9 vs 5 Fr), but it has to be kept in mind that the source does not occupy the center of the delivery catheter, and that no easy correction might be applied. The radii of the lumen and the media–adventitia contours were calculated in 24 pie-slices (15°), in all the cross-sections corresponding to the irradiated site (30-mm length of the train source). The number of required slices was a function of their thickness, which was on average 0.2 mm.

DVH describe the cumulative distribution of dose over a specific volume, and summarize the dosimetry that would otherwise have to be interpreted from numerous IVUS cross-sections with superimposed isodoses plotted (Fig. 2, upper left panel). Three volumes have been studied: the first one at the level of the luminal surface is arbitrarily defined with a thickness of 0.1 mm from the automatically detected lumen contour. The second volume, defining the adventitia volume, is computed considering a thickness of 0.5 mm from the second contour detected, corresponding to the echogenic media–adventitia interface. The third volume, corresponding to the plaque and media structures, is encompassed between the two detected contours. The dose distribution over the total vessel wall was calculated with 0.1 mm spatial resolution. The DVH provided a tool for reporting the actual delivered dose in different arterial structures, or to detect excessive radiation at the luminal level. From the complete 3-D IVUS data set, simulations of DVH of alternative brachytherapy strategies such as the use of a γ-emitter or a centered radioactive source were tested. To compute the isodoses and the DVH for the Novoste system, we used the dose distribution and dose rate around the source train as provided by the manufacturer in the user manual. Calibration was performed at the National Institute of Standards Technology, using both an extrapolation chamber and GafChromic Dosimetry media. For the γ-source, data were derived from Amols *et al.* [29].

Results

No complications related to the brachytherapy and IVUS procedures were seen. Figure 1 demonstrates a typical procedure on a lesion situated in the mid-portion of the left anterior descending coronary artery, at the level of the emergence of a septal and a diagonal side branch. These anatomical landmarks observed on the angiograms were used for positioning both the IVUS catheter and the irradiation device at the site of the lesion. The angiogram after PTCA is shown in Fig. 1B. The corresponding ECG-triggered IVUS pull-back performed at that time is illustrated in Fig. 2. The position of the side-branch is clearly seen on the mid-portion of the longitudinal view (* and arrow in right panel of Fig. 2). After withdrawal of the IVUS catheter, the brachytherapy delivery catheter was positioned at the PTCA site, using its two radio-opaque gold markers as landmark (Fig. 1C).

Of the 31 patients included in the BERT 1.5, a total of 7 required stent implantation. In 3 of these patients, the IVUS was performed before stenting. Absence of an ECG-triggered pull-back or technical problems limited the total number of analyzable patients without a stent to 23. Quantitative IVUS data analysis of these 23 patients demonstrated a mean lumen area of 7.7 ± 3.0 mm^2 (~150 cross-sections per patient). The mean vessel area was 14.8 ± 3.9 mm^2 and the residual plaque area was 7.1 ± 1.6 mm^2, corresponding to a residual plaque burden of 49 ± 8%. For each patient, the minimal, mean and maximal distance (~radius *r*) between the center of the IVUS catheter and the lumen or the media–adventitia interface were computed along the complete pull-back. The minimal *r* was 0.51 ± 0.02 mm, the mean *r* was 1.42 ± 0.25 mm, and the maximal *r* was 3.36 ± 0.70 mm. For the vessel (media–adventitia interface) minimal *r* was 0.88 ± 0.17 mm, mean *r* was 2.07 ± 0.25 mm, and maximal *r* was 3.80 ± 0.63 mm. Computer simulation of the placement of the IVUS catheter in the center of the lumen in each cross-section of the pull-back demonstrated a significant increase of minimal *r* ($p < 0.0001$): 0.67 ± 0.17 mm and 1.23 ± 0.25 mm, respectively, for the lumen and the vessel. In parallel, there was a significant decrease of maximal *r* ($p < 0.0001$): 2.46 ± 0.42 mm and 3.41 ± 0.41 mm, respectively, for the lumen and the vessel.

On the longitudinal view (right panel) of the IVUS pull-back in Fig. 2, and on one cross-section (upper left panel), the isodoses corresponding to 8, 16, and 32 Gy are superimposed. The derived DVH for this patient for the luminal surface and adventitial volumes are plotted on Fig. 3. The minimal dose in 90% (DV90*adv*) of the predefined adventitial volume was 47% (this corresponds to the *x*-axis value of the DVH plot with the *y*-axis value = 90%). Among the 23 patients, the average DV90*adv* was 37 ± 16% of the prescribed dose and the minimal dose in 90% (DV90*lum*) of the luminal surface volume was 67 ± 31% of the prescribed dose, and was 58 ± 24% in 90% of the plaque + media volume. The average minimal dose in the upper 10% (DV10*adv*) of the adventitial volume exposed to the highest dose (the *x*-axis value of the *y*-axis value 10%) was 133 ± 19% of the prescribed dose. For the luminal surface volume, DV10*lum* was 296 ± 42%. Figure 3 summarizes these data with a plot of the mean ± SD of DV95, DV90, DV75, DV50, DV25, DV10, and DV05 for the luminal surface and the

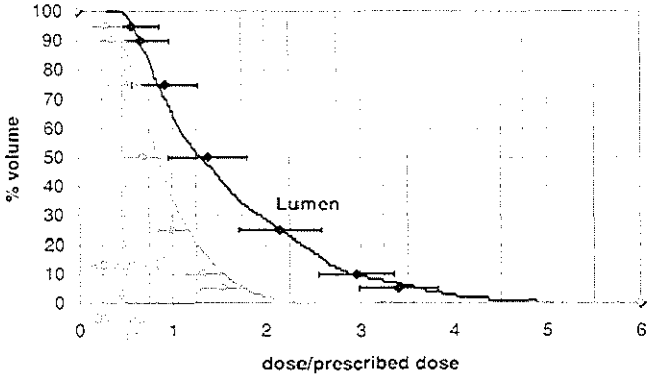

Figure 3. Example of integral dose-volume histograms (DVH) at the level of the luminal surface and adventitial volumes of the patient illustrated in Figures 1 and 2, representing the fraction of volume (*y*-axis, % volume) receiving greater than or equal to a specific relative dose (*x*-axis, dose/dose prescribed). For this patient, the minimal dose in 90% of the adventitial volume (DV90*adv*) was 47% of the prescribed dose. The superimposed plots with the error bars correspond to the average among the 23 investigated patients of the DV95, DV90, DV75, DV50, DV25, DV10, and DV05 of the predefined luminal surface and adventitial volumes.

Table 1. Summary of the computer simulations of the use of a β- or a γ-source (with the same dose prescribed at 2 mm from the center of the catheter) or a centering device

	Noncentered		Centered	
	DV90	DV10	DV90	DV10
β				
Lum.	0.67 ± 0.31*†	2.96 ± 0.42*†	1.06 ± 0.31	2.03 ± 0.49†
P + M.	0.58 ± 0.24*†	2.16 ± 0.32*†	0.73 ± 0.20†	1.66 ± 0.35†
Adv.	0.37 ± 0.16*†	1.33 ± 0.19*†	0.49 ± 0.14†	1.05 ± 0.20
γ				
Lum.	0.79 ± 0.21*	2.34 ± 0.31*	1.05 ± 0.21	1.70 ± 0.32
P + M.	0.72 ± 0.17*	1.78 ± 0.21*	0.83 ± 0.13	1.45 ± 0.23
Adv.	0.58 ± 0.12*	1.24 ± 0.13*	0.67 ± 0.09	1.05 ± 0.13

DV90 = relative minimal dose (dose/dose prescribed) of 90% of the predefined luminal surface (lum. thickness = 0.1 mm), adventitial (adv. thickness = 0.5 mm), and plaque + media (P + M = between luminal and external elastic lamina contours) volumes. Means ± SD for the 23 available electrocardiogram-triggered pull-backs performed during the Beta Energy Restenosis Trial (BERT) 1.5. Means were compared by paired *t*-test.

*$p < 0.0001$, centered vs. noncentered radiation catheter; †$p < 0.0001$, β- vs γ-source.

adventitial volumes. By randomization, the actual doses administered were 12 Gy in 8 patients, 14 Gy in 6 patients, and 16 Gy in 9 patients. Plots of relative dose (dose/dose prescribed) allow the pooling of data from patients who received different randomized doses.

The simulations (assuming that the source was centered in the lumen and/or the use of a γ-source [^{192}Ir]), with the same dose prescribed at 2 mm from the catheter as in the BERT protocol, are summarized in Table 1. A direct comparison of the homogeneity of the absorbed dose or of the high dose absorbed by the upper 10% of the luminal surface and adventitial volumes is possible. Figure 4 illustrates the improvement of the homogeneity of the dose distribution for the case of Figs. 1–3 when simulating a source situated in the center of the lumen. Figure 5 illustrates similar improvement of the homogeneity when considering a γ-source. Optimally, DVH should demonstrate a right step at the dose prescribed (x-axis = 1).

Discussion and Conclusion

Restenosis rates of 15–50% after percutaneous angioplasty procedures are the major hindrance to the success of transcatheter therapies. Supported by encouraging results obtained in animal models of coronary restenosis [13], several clinical trials of vascular brachytherapy have been designed, but with different systems and isotopes [30]. The discussion below focuses on the catheter-based device like the one used in this work. Dosimetry for radioactive stents has been described recently by Janicki *et al.* [31].

In the ongoing clinical trials, there is variability in the dose prescribed; the target site for the dose prescription, and both γ- and β-emitters are used.

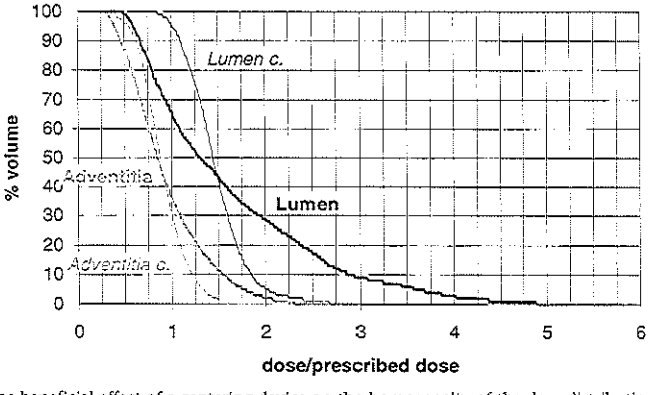

Figure 4. Illustration of the beneficial effect of a centering device on the homogeneity of the dose distribution for the same patient as in Figures 1–3. The dose-volume histograms (DVH) were recalculated simulating the irradiation source (^{90}Sr/Y) lying in the center of the lumen. The DVH curves for the centered position (Lumen c. and Adventitia c.) are steeper, with a DV10 for the lumen decreasing from 2.9 to 1.8.

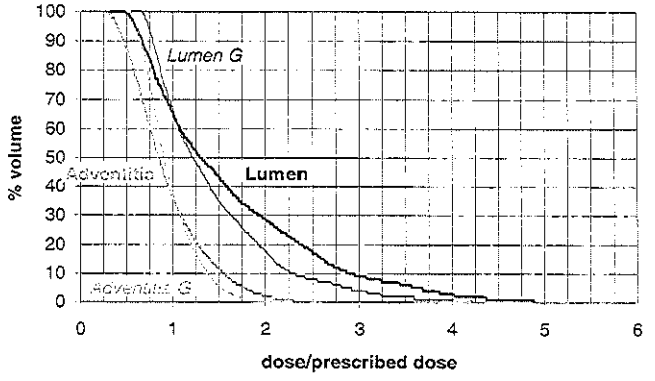

Figure 5. Illustration of the improvement of the dose homogeneity for the same patient as in Figures 1–3, simulating the use of a γ-source for which the same dose would have been prescribed at 2 mm from the center of the catheter (noncentered situation). The DVH curves for the γ-source (Lumen G and Adventitia G) are steeper, with a DV10 for the lumen decreasing from 2.9 to 2.3.

The consequence is a wide range of possible dose distributions over the arterial vessel wall requiring a careful interpretation and comparison of the results of these studies. The typical dose prescription distance in the coronary arteries is in the range of 2 mm. As the dose fall-off at this close vicinity is steep, particularly for β-emitters, accurate dosimetry requires knowledge of the exact geometry, which can be only partly assessed by coronary angiography.

Among the four published clinical brachytherapy studies today, Condado *et al.* [14] used a manual afterloader, noncentered, in 22 lesions, with a ^{192}Ir γ-source. The doses were prescribed at 1.5 mm (single doses of 18 Gy, n = 1; 20 Gy, n = 11; 25 Gy, n = 9) and only angiographic assessment was used. Although reported as positive, an unexplained early reduction of the minimal lumen diameter of 0.45 mm on average after only 24 h might have blurred the real efficacy of the applied radiotherapy in these patients [32] who presented no additional loss in minimal lumen diameter at the 6 months follow-up. However, doses of up to 92.5 Gy could have been delivered to the lumen wall because of the noncentered device. This maximum dose may well be over the vascular tolerance limits [32]. This finding could partly explain the observation that two patients experienced early total vessel occlusion, and four others developed a pseudoaneurysm at 2 years follow-up. In Geneva, Verin *et al.* [33] developed a mean for β-irradiation in human coronary arteries using a radioactive wire (^{90}Y) in a centering balloon device. The dose prescribed was 18 Gy at the surface of the balloon corresponding to the vessel luminal surface. No IVUS was performed. The findings were disappointing, with a restenosis rate of 40% among the 15 patients studied. A retrospective analysis of the dose prescribed in the vessel wall revealed that at a depth of 2 mm, the dose was only ~2.7 Gy, probably below the nominal effective dose against the proliferating cells involved in the post-angioplasty restenosis process [34]. The only placebo-controlled study of coronary brachytherapy published to date demonstrated a substantial reduction of the restenosis rate (17% vs 54%) among 55 patients presenting with in-stent restenosis [15]. A sealed ^{192}Ir γ-source in a noncentered catheter was used. The dosimetry was calculated, based on IVUS measurements, to be in the range of 8–30 Gy. Finally, King *et al.* [16] recently reported a restenosis rate of 15% and a late loss index of 4% for the American arm of the BERT, using the same hydraulic delivery system as the one we used in this study.

IVUS was developed to overcome the limitations of x-ray angiography, which portrays only overlapping shadows of the lumen of the coronary arteries (luminogram) [35]. In the field of vascular radiation therapy it is important to characterize precisely the dose prescribed in the vessel wall. IVUS imaging, by its angiotomographic nature, can be used to evaluate both lumen and vessel wall morphology. The results of our preliminary investigation, using the complete 3-D information available from carefully recorded ECG-triggered IVUS pull-back, demonstrate the potential applications for dosimetry and the possibilities for the evaluation of doses in specific target volumes of the vessel wall. DVH appear to be a valuable tool and summarize, in a graphic form, the large amount of information included in the dose distribution of the complete 3-D IVUS data sets. DVH cannot be used alone because of the lack

of information regarding the spatiality of the dose distribution [25]. For the spatiality, two-dimensional isodose displays, such as in Fig. 2, superimposed on IVUS images will still be required for the guidance of a vascular irradiation plan. In our study, there was no direct guidance of the brachytherapy with IVUS because of the nature of this trial, which was a feasibility study in which the prescribed dose was predetermined. However, the data set constitutes a preliminary database for the assessment of several radiation strategies, as illustrated in Table 1. The homogeneity of the dose distribution might be estimated by the difference between the DV10 and the DV90. Ideally, a DVH should demonstrate a steep curve around the desired prescribed dose. Flattening reflects that some regions are underexposed, whereas others are overexposed. Potential advantages of a centering device for a β-source, as illustrated in Table 1 and Figs. 4 and 5, are that the DV90 increases for the luminal (1.06 ± 0.31 vs 0.67 ± 0.31, $p < 0.0001$ by paired *t*- test), the adventitial (0.49 ± 0.14 vs 0.37 ± 0.16, $p < 0.0001$) and the plaque + media (0.73 ± 0.20 vs 0.58 ± 0.24, $p < 0.0001$) volumes. In parallel, DV10 decreases for the luminal (2.03 ± 0.49 vs 2.96 ± 0.42, $p < 0.0001$), the adventitial (1.05 ± 0.20 vs 1.33 ± 0.19, $p < 0.0001$) and the plaque + media (1.66 ± 0.35 vs 2.16 ± 0.32, $p < 0.0001$) volumes. As a consequence, the homogeneity, which can be expressed as DV10 − DV90, is improved for the lumen (0.97 vs 2.29), the adventitia (0.56 vs 0.96), and the plaque + media (0.93 vs 1.58, respectively, for a centered and a noncentered delivery system). However, only one number, such as DV10 − DV90, cannot summarize a complete DVH curve. The complete shape of the curve, as presented in the figures, is important. Several other parameters have been proposed [36, 37], but no definitive one has emerged as a gold-standard to assess the dose homogeneity. Looking at the slope of the DVH, for example, is a proposed alternative, but the slope will vary with the interval chosen to compute it. The DVH presented in this study are cumulative plots: this integral format shows the fraction of volume receiving greater than or equal to a specific dose. Another format is the differential DVH constructed by dividing the range of dose values into equal intervals and accumulating partial volumes in those bins according to their dose values. Plots of dose–volume distributions have also been proposed [38]. Our definition of the thickness of the luminal and adventitial volumes is arbitrary. The intima is formed only by a superficial layer of endothelial cells and a thin subendothelial layer of connective tissue. Its thickness increases with age and reaches 250 μm at 40 years. Diffuse thickening is common in older patients, even without atherosclerosis. The adventitia is composed of loose collagen and elastic tissue, which merge with the periadventitial tissue. The normal thickness of the adventitia is 300–500 μm [17]. However, we evaluated these DVH for another thickness (0.2 mm) and the results are in close agreement with the data presented in Table 1 (J.P.A. Marijnissen *et al.*, personal communication). The differences found with the simulations of the use of a γ-emitter or a radioactive source train centered in the lumen are also present for the plaque + media volume for which no arbitrary choice has been made.

On average, in the conditions of our study, whereas only 10% of the advential volume were exposed to a minimal dose 1.33 times the prescribed dose, 10% of the luminal surface volume absorbed at least 2.96 times the prescribed dose. For a prescribed dose of 16 Gy, this corresponds to an actual dose of 47.2 Gy, which may well be above the recognized vascular tolerance limit. The simulations in Table 1 demonstrate that the use of a device to maintain the source in the center of the arterial lumen would decrease this overexposure, which has potential deleterious effect such as the development of an aneurysm. With centering, the upper 10% of the luminal surface volume is exposed to a reduced minimal relative dose of 2. Following our results, the best strategy could be the use of a centered γ-source: the minimal relative dose would then be reduced to 1.7 for the upper 10% of the luminal surface volume. No clinical data presently support these potential advantages, and to our knowledge, no trial is planned to address this issue. Nevertheless, γ-sources have other drawbacks, at the radioprotection level, for example, because these more penetrating radiations require stringent shielding precautions [39]. These radiation safety issues may be improved if lower energy gamma sources can be manufactured.

There is an interindividual variability related to the geometry of the lesion and the morphology of different coronary arteries, as demonstrated by the rather large standard deviations in Table 1. The choice of the brachytherapy modality (centering device or not, β- vs γ-) cannot be only guided from DVH, but must integrate all the information available from the angiogram and the 3-D IVUS pullback (such as morphology of the lesion, length, eccentricity of the plaque). Potentially, catheters combining IVUS and asymmetric sources might be helpful in the guidance of a radiation treatment for eccentric lesions. Such a device with a C-shape shielding screen around a radioactive wire has been described recently [40].

Another limitation of our approach is that we reconstructed an artificially straight coronary segment. However, this limitation might be overcome

by image fusion of biplane angiography and IVUS, as developed in our center, to assess the true 3-D geometry of coronary vessels [41]. Presently, we also do not implement different dose fall-off characteristics in function of the type of plaque seen (fibro-fatty, calcified, *etc.*). Although there are probably differences, no data are available.

One major assumption made in this work was to consider that the IVUS and delivery catheters were lying in the same position in the treated coronary segment. It is important to realize first that because the size of the IVUS catheter is smaller (2.9 Fr ~ = 1 mm in diameter) than the brachytherapy device we used (5 Fr ~ = 1.6 mm), it lies in a more eccentric position in the coronary lumen. However, no easy correction can be applied because the channel source in the delivery device is not in the center of the catheter. The real average DV10*lum* in our patients is thus in the range 2.03–2.96 given in Table 1. Moreover, even with the use of radiotherapy and IVUS catheters of the same size, it is not certain that when advanced sequentially in the arterial lumen, they will occupy the same position. Although they should be on the shortest 3-D path in the lumen, coronary arteries have a complex curved geometry in space, and are partially deformed by the catheter lying in their lumen. Thus, catheters with differing rigidity will occupy different positions. Finally, it is important to understand that the position of a catheter inside the arterial lumen is not fixed and varies along the cardiac cycle because of ventricular contractions. These methodological limitations could be partially overcome with existing imaging wires, which could be introduced in the lumen of the irradiation delivery catheter itself. Presently, another limitation we face in our catheterization laboratory is that DVH are not obtained on-line. Further implementations with faster processing of the 3-D IVUS data set for optimal automatic contour detection are under study.

In conclusion, we think that the body of additional information available from IVUS and derived dosimetry parameters such as DVH should improve our understanding of the mechanisms of action of brachytherapy and be helpful for the comparison of trials based on different dosimetry strategies. In our center, we systematically assess the lesions treated by vascular radiation therapy by IVUS.

Acknowledgments

The authors thank all the team of the Department of Interventional Cardiology of the Thoraxcenter, and Jan Oomen and Wenguang Li for software support. This work was supported by the Wenckebach prize, awarded to P. W. Serruys. S. G. Carlier is a recipient of a grant of the Vésale and Békales Foundations.

References

[1] Grüntzig AR, Senning A, Siegenthaler WE. Nonoperative dilatation of coronary artery stenosis. N. Engl. J. Med. 1979; 301:61–68.

[2] Waller BF. Crackers, breakers, stretchers, drillers, scrapers, shavers, burners, welders and melters. The future treatment of atherosclerotic coronary artery disease. J. Am. Coll. Cardiol. 1989;13:969–987.

[3] Serruys PW, Luijten HE, Beatt KJ, *et al.* Incidence of restenosis after succesful coronary angioplasty: a time-related phenomenon: a quantitative angiography study in 342 consecutive patients at 1, 2, 3 and 4 months. Circulation 1988;77:361–371.

[4] Schwartz RS, Holmes DR, Topol EJ. The restenosis pradigm revisited: an alternative proposal for cellular mechanism. J. Am. Coll. Cardiol. 1992;1992:1284–1293.

[5] Mintz GS, Popma JJ, Pichard AD, *et al.* Arterial remodeling after coronary angioplasty. A serial intravascular ultrasound study. Circulation 1996;94:35–43.

[6] Serruys PW, de Jaegere PPT, Kiemeneij F, *et al.* A comparison of balloon expandable stent implantation with balloon angioplasty in patients with coronary artery disease. N. Engl. J. Med. 1994;331:489–495.

[7] Fischman DL, Leon MB, Baim D, *et al.* A randomized comparison of coronary stent placement and balloon angioplasty in the treatment of coronary artery disease. N. Engl. J. Med. 1994;331:496–501.

[8] Serruys PW, van Hout B, Bonnier H, *et al.* Randomised comparison of implantation of heparin-coated stents with balloon angioplasty in selected patients with coronary artery disease (Benestent II). Lancet 1998;352:673–681.

[9] Topol EJ, Califf RM, Weisman HF, Ellis SG, *et al.* Randomised trial of coronary intervention with antibody against platelet IIb/IIIa integrin for reduction of clinical restenosis: results at six months. Lancet 1998;343:881–886.

[10] Tardif JC, Cote G, Lesperance J, *et al.* Probucol and multivitamins in the prevention of restenosis after coronary angioplasty. Multivitamins and Probucol Study Group. N. Engl. J. Med. 1997;337:365–372.

[11] Sekiya M, Funada J, Watanabe K, Miyagawa M, Akutsu H. Effects of probucol and cilostazol alone and in combination on frequency of poststenting restenosis. Am. J. Cardiol. 1998;82:144–147.

[12] Friedman M, Felton L, Byers S. The antiatherogenic effect of ^{192}Ir upon the cholesterol-fed rabbit. J. Clin. Invest. 1964; 43:185–192.

[13] Waksman R. Response to radiation therapy in animal restenosis models. Semin. Intervent. Cardiol. 1997;2:95–101.

[14] Condado JA, Waksman R, Gurdiel O, *et al.* Long-term angiographic and clinical outcome after percutaneous transluminal coronary angioplasty and intracoronary radiation therapy in humans. Circulation 1997;96:727–732.

[15] Teirstein PS, Massullo V, Jani S, *et al.* Catheter based radiotherapy to inhibit restenosis after coronary stenting. N. Engl. J. Med. 1997;336:1697–1703.

[16] King SB, Williams DO, Chougule P, *et al.* Endovascular beta-radiation to reduce restenosis after coronary balloon angioplasty. Results of the Beta Energy Restenosis Trial (BERT). Circulation 1998;97:2025–2030.

[17] Di Mario C, Görge G, Peters R, Kearney P, *et al.* Clinical application and image interpretation in intracoronary ultrasound. Study Group on Intracoronary Imaging of the Working Group of Coronary Circulation and of the Subgroup on Intravascular Ultrasound of the Working Group of Echocardiography of the European Society of Cardiology. Eur. Heart J. 1998;19:207–229.

[18] Rosenfield K, Losordo DW, Ramaswamy K, *et al.* Three-dimensional reconstruction of human coronary and peripheral arteries from images recorded during two-dimensional

intravascular ultrasound examination. Circulation 1991;84: 1938–1956.
[19] Coy KM, Park JC, Fishbein MC, *et al.* In vitro validation of three-dimensional intravascular for the evaluation of arterial injury after balloon angioplasty. J. Am. Coll. Cardiol. 1992;20:692–700.
[20] Matar FA, Mintz GS, Douek P, *et al.* Coronary artery lumen volume measurement using three-dimensional intravascular ultrasound: validation of a new technique. Cathet. Cardiovasc. Diagn. 1994;33:214–220.
[21] von Birgelen C, di Mario C, Li W, *et al.* Morphometric analysis in three-dimensional intracoronary ultrasound: an in-vitro and in-vivo study performed with a novel system for the contour detection of lumen and plaque. Am. Heart J. 1996;132:516–527.
[22] Roelandt JRTC, di Mario C, Pandian NG, *et al.* Three-dimensional reconstruction of intracoronary ultrasound images: rationale, approaches, problems and directions. Circulation 1994;90:1044–1055.
[23] von Birgelen C, Mintz GS, Nicosia A, *et al.* Electrocardiogram-gated intravascular ultrasound image acquisition after coronary stent deployement facilitates on-line three-dimensional reconstruction and automated lumen quantification. J. Am. Coll. Cardiol. 1997;30:436–443.
[24] von Birgelen C, de Vrey EA, Mintz GS, *et al.* ECG-gated three-dimensional intravascular ultrasound: feasibility and reproducibility of an automated analysis of coronary lumen and atherosclerotic plaque dimensions in humans. Circulation 1998;96:2944–2952.
[25] Drzymala RE, Mohan R, Brewster L, *et al.* Dose-volume histograms. Int. J. Radiat. Oncol. Biol. Phys. 1991;21:71–78.
[26] Fox T, Crocker I. Dosing in vascular radiotherapy. Vasc. Radiother. Monitor 1998;1:45–53.
[27] Carlier SG, Marijnissen JPA, Coen VLMA, *et al.* Guidance of intracoronary radiation therapy based on dose-volume histogram derived from quantitative intravascular ultrasound. IEEE Trans. Med. Imaging 1998;17:772–778.
[28] Li W, von Birgelen C, di Mario M, *et al.* Semi-automatic contour detection for volumetric quantification of intracoronary ultrasound. In: Computers in cardiology 1994. Los Alamitos, CA: IEEE Computer Society Press, 1994, pp. 277–280.
[29] Amols HI, Zaider M, Weinberger J, Ennis R, Schiff PB, Reinstein LE. Dosimetric considerations for catheter-based beta and gamma emitters in the therapy of neointimal hyperplasia in human coronary arteries. Int. J. Radiat. Oncol. Biol. Phys. 1996;36:913–921.
[30] Waksman R. Clinical trials in radiation therapy for restenosis: past, present and future. Vasc. Radiother. Monitor 1998; 1:10–18.
[31] Janicki C, Duggan DM, Coffey CW, Fischell DR, Fischell TA. Radiation dose from a phosphorous-32 impregnated wire mesh vascular stent. Med. Phys. 1997;24:437–445.
[32] Serruys P, Levendag PC. Intracoronary brachytherapy: the death knell of restenosis or just another episode of a never-ending story? Circulation 1997;96:709–712.
[33] Verin V, Urban P, Popowski Y, *et al.* Feasibility of intracoronary β-irradiation to reduce restenosis after balloon angioplasty. Circulation 1997;95:1138–1144.
[34] Teirstein P. Beta-radiation to reduce restenosis. Too little, too soon? Circulation 1997;95:1095–1097.
[35] Topol EJ, Nissen SE. Our preoupation with coronary luminology. The dissociation between clinical and angiographic findings in ischemic heart disease. Circulation 1995;92: 2333–2342.
[36] Viggars DA, Shalev S, Stewart M, Hahn P. The objective evaluation of alternative treatment plans III: the quantitative analysis of dose volume histograms. Int. J. Radiat. Oncol. Biol. Phys. 1992;23:419–427.
[37] Panitsa E, Rosenwald JC, Kappas C. Developing a dose-volume histogram computation program for brachytherapy. Phys. Med. Biol. 1998;43:2109–2121.
[38] Niemierko A, Goitein M. Dose-volume distributions: a new approach to dose-volume histograms in three-dimensional treatment planning. Med. Phys. 1994;21:3–11.
[39] Jani SK, Massullo V, Steuterman S, Tripuraneni P, Teirstein P. Physics and safety aspects of a coronary irradiation pilot study to inhibit restenosis using manually loaded ^{192}Ir ribbons. Semin. Intervent. Cardiol. 1997;2:119–123.
[40] Ciezki JP, Tuzcu EM, Lee EJ, Hafeli O. IVUS-directed conformal intravascular brachytherapy: the Navius system. Adv. Cardiovasc. Radiat. Ther. II, Proc. 1998:226.
[41] Krams R, Wentzel JJ, Oomen JA, *et al.* Evaluation of endothelial shear stress and 3D geometry as factors determining the development of atherosclerosis and remodeling in human coronary arteries *in vivo*. Combining 3D reconstruction from angiography and IVUS (ANGUS) with computational fluid dynamics. Arterioscler. Thromb. Vasc. Biol. 1997;17:2061–2065.

Chapter 15

Residual plaque burden, delivered dose, and tissue composition predict 6-month outcome after balloon angioplasty and β-radiation therapy.

M Sabate, JPA Marijnissen, **SG Carlier**, IP Kay, WJ van der Giessen, VLMA Coen, JLMR Ligthart, E Boersma, MA Costa, PC Levendag, PW Serruys.

Circulation 2000:101:2472-2477.

Residual Plaque Burden, Delivered Dose, and Tissue Composition Predict 6-Month Outcome After Balloon Angioplasty and β-Radiation Therapy

Manel Sabaté, MD; Johannes P.A. Marijnissen, PhD; Stéphane G. Carlier, MD; I. Patrick Kay, MBChB; Willem J. van der Giessen, MD, PhD; Veronique L.M.A. Coen, MD; Jurgen M.R. Ligthart, BSc; Eric Boersma, PhD; Marco A. Costa, MD; Peter C. Levendag, MD, PhD; Patrick W. Serruys, MD, PhD

Background—Inhomogeneity of dose distribution and anatomic aspects of the atherosclerotic plaque may influence the outcome of irradiated lesions after balloon angioplasty (BA). We evaluated the influence of delivered dose and morphological characteristics of coronary stenoses treated with β-radiation after BA.

Methods and Results—Eighteen consecutive patients treated according to the Beta Energy Restenosis Trial 1.5 were included in the study. The site of angioplasty was irradiated with the use of a β-emitting $^{90}Sr/^{90}Y$ source. With the side branches used as anatomic landmarks, the irradiated area was identified and volumetric assessment was performed by 3D intracoronary ultrasound imaging after treatment and at 6 months. The type of tissue, the presence of dissection, and the vessel volumes were assessed every 2 mm within the irradiated area. The minimal dose absorbed by 90% of the adventitial volume ($D_{v90}Adv$) was calculated in each 2-mm segment. Diffuse calcified subsegments and those containing side branches were excluded. Two hundred six coronary subsegments were studied. Of those, 55 were defined as soft, 129 as hard, and 22 as normal/intimal thickening. Plaque volume showed less increase in hard segments as compared with soft and normal/intimal thickening segments ($P<0.0001$). $D_{v90}Adv$ was associated with plaque volume at follow-up after a polynomial equation with linear and nonlinear components ($r=0.71$; $P=0.0001$). The multivariate regression analysis identified the independent predictors of the plaque volume at follow-up: plaque volume after treatment, $D_{v90}Adv$, and type of plaque.

Conclusions—Residual plaque burden, delivered dose, and tissue composition play a fundamental role in the volumetric outcome at 6-month follow-up after β-radiation therapy and BA. (***Circulation.*** **2000;101:2472-2477.**)

Key Words: balloon ■ angioplasty ■ radioisotopes ■ ultrasonics ■ restenosis

Endovascular radiation therapy is a promising new technique aimed at preventing restenosis after percutaneous coronary intervention.[1-3] Although its effectiveness has been proven in the treatment of in-stent restenosis,[4] the value of intracoronary irradiation in de novo coronary lesions remains to be established. Radiation delivered to the coronary artery by means of catheter-based systems can use both γ- and β-emitters.[5] Long-term results after treatment may be influenced by absolute dose and by the homogeneity in dose distribution. β-Emitters demonstrate a more rapid dose fall-off than γ-emitters because of the short range of electrons.[6] This feature may lead to a less homogeneous dose distribution when treating coronary segments with variable degrees of curvature, tapering, remodeling, and plaque extent. The use of dose-volume histograms allows one to evaluate the cumulative dose received by a certain specified tissue volume[7] and has been recently implemented in the field of intracoronary brachytherapy as a tool for dosimetry.[8] Aims of the study were (1) to determine, by the use of dose-volume histograms, the dose distribution of the β-emitter $^{90}Sr/^{90}Y$ along the coronary irradiated segment when delivered by a noncentered device, (2) to establish the dose that could be predictive of efficacy in intracoronary brachytherapy, and (3) to determine the intravascular ultrasound (IVUS) predictors of the plaque volume at 6-month follow-up of coronary segments treated with balloon angioplasty (BA) followed by β-radiation therapy.

Methods

Patient Selection

Eighteen consecutive patients with single de novo coronary stenosis successfully treated with BA followed by intracoronary β-radiation

Received September 22, 1999; revision received November 23, 1999; accepted December 22, 1999.

From the Thoraxcenter, Heartcenter, Rotterdam, Dijkzigt Academisch Ziekenhuis Rotterdam, The Netherlands (M.S., S.G.C., I.P.K., W.J.v.d.G., J.M.R.L., E.B., M.A.C., P.W.S.), and Daniel den Hoed Cancer Center, Rotterdam, The Netherlands (J.P.A.M., V.L.M.A.C., P.C.L.).

Correspondence to Prof P.W. Serruys, MD, PhD, Heartcenter, Academisch Ziekenhuis Rotterdam, Erasmus University, Bd 418, PO Box 2040, Dr Molewaterplein 40, 3015 GD Rotterdam, The Netherlands. E-mail serruys@card.azr.nl

Circulation is available at http://www.circulationaha.org

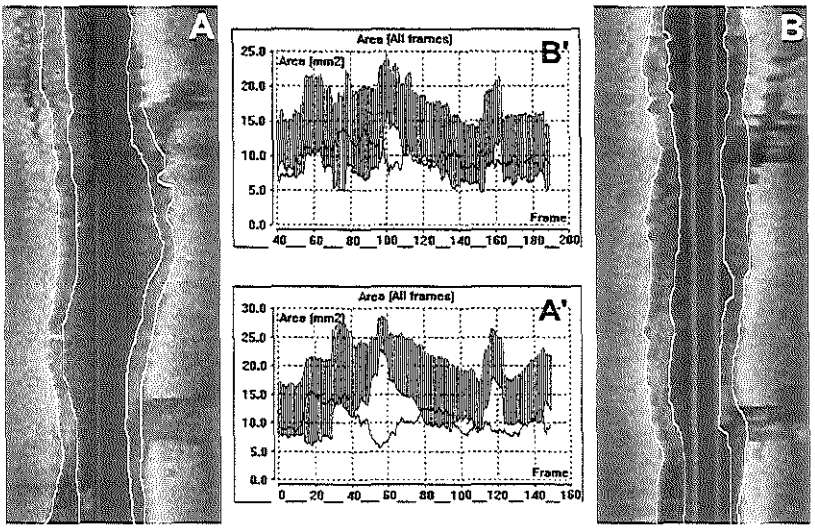

Figure 1. Longitudinal reconstruction and volumetric calculations (charts) of irradiated coronary segments after treatment (A and A') and at 6-month follow-up (B and B').

therapy were included in the study. Patients receiving a stent were excluded from the analysis. β-Radiation was delivered according to the Beta Energy Restenosis Trial 1.5. The isotope selected was the pure β-emitting $^{90}Sr/^{90}Y$, and patients were randomly assigned to receive 12, 14, or 16 Gy at 2 mm from the source axis. The inclusion and exclusion criteria of this trial have been previously reported.[9] The delivery of the radiation was performed by the use of the Beta-Cath System (Novoste Corp).[10] The radiation source train of this system consists of a series of 12 independent 2.5-mm-long cylindrical seeds that contain the $^{90}Sr/^{90}Y$ sources and is bordered by 2 gold radiopaque markers at distal and proximal parts separated by 30 mm.[10]

IVUS Analysis

The treated coronary segment was evaluated by means of 3D IVUS imaging, which allowed volumetric calculations of the irradiated area. The selection of the area of interest has been reported elsewhere.[11] In brief, a few steps were followed: First, an angiogram was performed after positioning the delivery catheter and the relation between anatomic landmarks and the 2 gold markers were documented. The anatomic landmark closest to either of the gold markers was used as a reference point. This angiographic reference point was identified during a contrast injection with the IVUS imaging element at the same position as the gold marker of the source. The image from the IVUS imaging element was recorded and the reference point identified. During the subsequent pullback, this reference point was recognized and used for selecting the area subject to the analysis: 30 mm for the irradiated segment.[12] The system used for imaging was a mechanical IVUS system (ClearView, CVIS, Boston Scientific Corp) with a sheath-based IVUS catheter incorporating a 30-MHz, single-element transducer rotating at 1800 rpm (Ultracross, CVIS). The transducer is placed inside a 2.9F, 15-cm-long sonolucent distal sheath that alternatively houses the guide wire (during the catheter introduction) or the transducer (during imaging). The IVUS transducer was withdrawn through the stationary imaging sheath by an ECG-triggered pullback device with a stepping motor.[12] The ECG-gated image acquisition and digitization was performed by a workstation designed for the 3D reconstruction of echocardiographic images[12] (EchoScan, Tomtec). Description of this system has been previously reported in detail.[12–14] In brief, the steering logic of the workstation considered the heart rate variability and only acquired images from cycles meeting a predetermined range and coinciding with the peak of the R wave. If an R-R interval failed to meet the preset range, the IVUS catheter remained at the same site until a cardiac cycle met the predetermined R-R range. The IVUS transducer then was withdrawn 0.2 mm to acquire the next image.[12–14] This system ensures the segment-to-segment independence by avoiding taking images during the axial movement of the IVUS catheter that occurs during the cardiac cycle. Given the slice thickness of 0.2 mm and the length subject to the analysis of 30 mm (distance between the 2 gold markers of the radiation source), 150 cross-sectional images per segment were digitized and analyzed. A semiautomatic contour detection program was used for the 3D analysis.[15] This program constructs 2 longitudinal sections from the data set and identifies the contours corresponding to the lumen-intima and media-adventitia boundaries. Corrections could be performed interactively by "forcing" the contour through visually identified points; the entire data set then was updated.[15] Careful checking and editing of the contours of the 150 planar images was performed with an average of 45 minutes for complete evaluation. The area encompassed by the lumen-intima and media-adventitia boundaries defined the luminal and the total vessel volumes, respectively. The difference between total vessel and luminal volumes defined the plaque volume. Because media thickness cannot be measured accurately, we assumed that the plaque volume included the atherosclerotic plaque and the media.[16] Volumetric data were calculated by the formula $V=\Sigma^{n}_{i=1}A_i \cdot H$, where V=volume, A=area of total vessel or lumen or plaque in a given cross-sectional ultrasound image, H=thickness of the coronary artery slice that is reported by this digitized cross-sectional IVUS image, and n=the number of digitized cross-sectional images encompassing the volume to be measured.[15] At follow-up, meticulous matching of the region of interest was performed by comparing the longitudinal reconstruction with that after treatment as previously described[11] (Figure 1). The feasibility and intraobserver and interobserver variability of this system have been previously reported.[11,13,17,18] For the purposes of the study, the computed volume of the irradiated segment was divided into 2-mm-long subsegments. Since the irradiated segment measured 30 mm, 15 subsegments were defined per patient, each of them with 10 IVUS cross sections (0.2 mm per cross section). All individual cross sections were studied by 2 investigators, blinded to the dosimetry results. Type of plaque and the

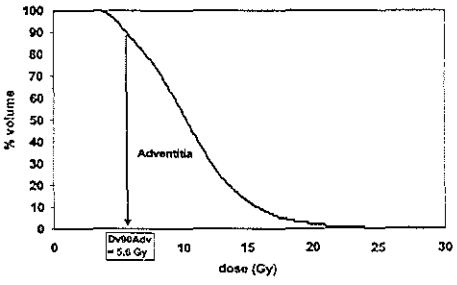

Figure 2. Dose-volume histogram showing cumulative dose received at level of adventitial layer. Minimal dose received by 90% of adventitial volume (D_{v90}Adv) is calculated.

presence of dissection were qualitatively assessed. Type of plaque was defined in every cross section as intimal thickening, soft, fibrous, mixed, and diffuse calcified according to the guidelines previously reported.[19] Intimal thickening was defined when the thickness of the intima-media complex was <0.3 mm.[19] Soft tissue was defined when ≥80% of the cross-sectional area was constituted by material showing less echoreflectivity than the adventitia, with an arc of calcium <10°, fibrous plaque when the echoreflectivity of ≥80% of the material was as bright as or brighter than the adventitia without acoustic shadowing, diffuse calcified plaque when it contained material brighter than the adventitia showing acoustic shadowing in >90°, and mixed when the plaque did not match the 80% criterion.[19] We categorized the 2-mm-long subsegments as normal/intimal thickening, soft, hard (fibrous and mixed), and diffuse calcified when ≥80% of the cross sections within the subsegment were of the same type. In those cross sections containing up to 90° of calcium arc, the contour of the external elastic membrane was imputed from noncalcified slices. Dissection of the vessel was defined as a tear parallel to the vessel wall.[19] Changes in luminal, plaque, and total vessel volume between immediately after treatment and at follow-up were also computed per subsegment. Those subsegments in which the origin of side branches involved >90° of the circumferential arc in >50% of the cross sections or were defined as diffuse calcified were excluded from the analysis.

Dose Calculation

The actual dose received by the vessel was retrospectively calculated by means of dose-volume histograms[7] in every 2-mm-long subsegment. This method is based on quantitative IVUS under the assumption that the radiation source is positioned at the same place as the IVUS catheter.[8] The distance between the center of the catheter and media-adventitia interface was calculated in 24 pie slices (15°) in all cross sections corresponding to the irradiated area.[9] Considering the prescribed dose and the accurate geometric data obtained from the IVUS, the cumulative curve of the dose-volume histogram for a predefined volume (ie, adventitia as calculated at 0.5 mm outside the external elastic membrane) can be obtained (Figure 2). From this curve, the minimum dose received by 90% of the adventitial volume (D_{v90}Adv) was calculated. The methodology and feasibility of this dosimetry approach in vascular brachytherapy has been previously reported.[8]

Statistical Analysis

Data are presented as mean±SD or proportions. Differences in quantitative IVUS data between the types of tissue were assessed by means of 1-way ANOVA. Differences in quantitative IVUS data between subsegments with and without dissection and with and without calcium were evaluated by the use of an unpaired Student's *t* test. To determine the relation between the dose received by the adventitia and the plaque volume at follow-up, linear regression analysis was performed first. Then, nonlinear components were added to the equation (x^{-1} and x^{-2} were added to describe the steep

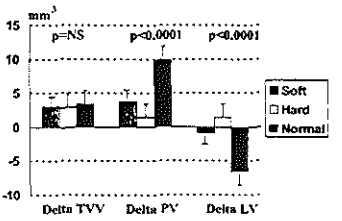

Figure 3. Changes between postprocedure and 6-month measurements in total vessel, plaque, and luminal volumes regarding different types of tissue. TVV indicates total vessel volume; PV, plaque volume; and LV, luminal volume.

increase of plaque volume at low dose). These components were included in the model if they described the relation significantly better. Finally, the model was corrected for the plaque volume after treatment. Multivariable regression analyses were performed to identify independent predictors of plaque volume at follow-up among IVUS-derived (types of tissue, dissection, and plaque volume after treatment) and dosimetric variables (D_{v90}Adv). All tests were 2-tailed, and a value of $P<0.05$ was considered statistically significant.

Results

Baseline Characteristics

Two hundred seventy subsegments were defined in 18 patients successfully treated with BA followed by intracoronary brachytherapy. Sixty-four subsegments were excluded from the final analysis because of either diffuse calcified plaque that precluded the quantification of the total vessel volume (n=30) or side branches that involved >90° of the circumferential arc in >50% of the cross sections (n=34). Therefore, 206 irradiated subsegments were the subject of the study. Fifty-five (27%) subsegments were defined as soft, 129 (62%) as hard, and 22 (11%) as normal/intimal thickening. Dissection was observed in 34 (16.5%) subsegments.

Volumetric Changes and Dosimetry

On average, total vessel volume increased at follow-up (32.5±9 mm³ after treatment to 35.5±11 mm³ at follow-up; $P<0.0001$), accommodating a parallel increase in plaque volume (15.3±6 to 18.3±7 mm³; $P<0.0001$). As a result, mean luminal volume remained unchanged (17.1±7 to 17.0±7 mm³; P=NS). Subsegments with hard tissue demonstrated less increase in plaque, resulting in an increase in luminal volume as compared with soft and normal/intimal thickening subsegments (Figure 3). The behavior of those hard subsegments containing

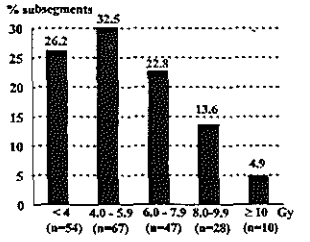

Figure 4. Range of dose distribution in irradiated coronary subsegments as calculated by dose-volume histograms.

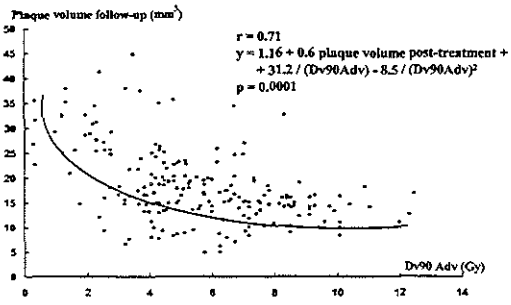

Figure 5. Relation between plaque volume at follow-up and D_{v90}Adv.

mixed calcified tissue (up to 90°; n=104) was compared with those containing mixed noncalcified tissue (n=25). Mean changes in plaque and total vessel volumes were comparable (Δplaque [mm³]: +1.3±4.2 in mixed calcified vs +1.8±5.2 in mixed noncalcified; P=NS; Δtotal vessel volume [mm³]: +2.6±6.2 in mixed calcified vs +4.2±5.8 in mixed noncalcified; P=NS), resulting in a comparable mean increase in luminal volume at follow-up (+1.3±5.2 mm³ in mixed calcified vs +1.9±5.7 mm³ in mixed noncalcified; P=NS). Dissected subsegments demonstrated a trend toward a smaller increase in plaque as compared with nondissected subsegments (+1.2±3 vs +3.3±6 mm³; P=0.08). The mean of all 3 prescribed doses at 2 mm from the source was 14±1.8 Gy. The calculated D_{v90}Adv was 5.5±2.5 Gy (range 0.2 to 12.4). A wide range of dose distribution was observed in the irradiated coronary subsegments (Figure 4). The association between D_{v90}Adv with the plaque volume at follow-up is depicted in Figure 5. The model appeared

Parameters Associated With Plaque Volume at Follow-Up

	Parameter Estimate	95% CI	P
Plaque volume after treatment, mm³	0.6	0.8/0.5	0.0001
D_{v90}Adv, Gy	−4.4	−5.6/−2.9	0.0001
Type of plaque (hard vs other)	−1.6	−3.4/0.1	0.06

to follow a polynomial equation with linear and nonlinear components. Nonlinear components described the increase in plaque volume at lower doses, whereas the residual plaque volume after treatment accounted for the linear relation of the curve. Changes in plaque volume appeared to decrease with dose (Figure 6). Four Gray was the minimum effective dose to be delivered to 90% of the adventitia because subsegments receiving at least this dose demonstrated a significantly smaller increase in plaque volume as compared with those receiving <4 Gy (P<0.001). As a result, luminal volume decreased significantly less in those subsegments receiving ≥4 Gy and even increased when the minimal dose to the adventitia was >6 Gy. Multivariable regression analyses identified plaque volume after treatment as a positive predictor of plaque volume at follow-up, whereas D_{v90}Adv and type of plaque (hard) were negative predictors (Table).

Discussion

This study demonstrates for the first time the relation between plaque increase, as assessed by IVUS, and the dose received by the adventitia, as calculated by means of dose-volume histograms. A plot of dose-volume histogram is a standard method used in radiotherapy that condenses the large body of information available from conventional 3D distribution data

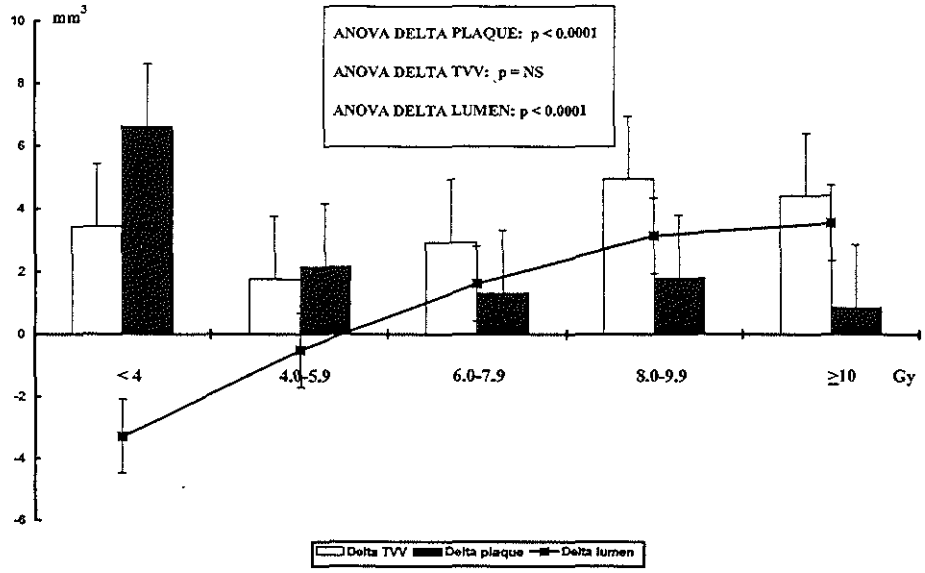

Figure 6. Changes in total vessel, plaque, and luminal volumes regarding 5 ranges of doses as calculated by dose-volume histograms. TVV indicates total vessel volume.

into a plot summarizing graphically the radiation distribution throughout the target volume.[7]

The assumption of the adventitia as the target tissue is supported by experimental studies.[20,21] Scott et al[20] localized the proliferating cells in the adventitia and their migration into the neointima after angioplasty by using bromodeoxyuridine immunohistochemistry. Similarly, Waksman et al[21] demonstrated a greater cell proliferation in control vessels 3 days after angioplasty in the adventitia at the site of the medial tear as compared with the medial wall in the same region. In this study, the proliferation was significantly reduced in irradiated vessels with either a source of $^{90}Sr/^{90}Y$ or ^{192}Ir that delivered 14 or 28 Gy at 2 mm into the artery wall.[21]

The actual dose received by the adventitia appeared to be rather low as compared with the prescribed dose at 2 mm from the source. Furthermore, the dose varied considerably between coronary subsegments, as demonstrated by the dose distribution depicted in the Figure 4. The use of β-radiation may account in part for this dose inhomogeneity. As compared with γ-radiation, β-sources have more fall-off because of the short range of electrons.[6] This feature may become crucial when treating vessels with a great degree of vessel tapering or, alternatively, lesions showing positive remodeling where the distance from the source to the surrounding adventitia may be smaller or greater than expected. In this regard, the use of IVUS as a tool for dosimetry in β-radiation therapy may become mandatory.

Dose uniformity also may be influenced by the source centering in the lumen.[22] By the use of dose-volume histograms, Carlier et al[8] demonstrated in 10 patients treated with balloon angioplasty followed by intracoronary β-radiation that the prescribed dose was administered in only 35% of the adventitia. After centering the source in the lumen, up to 60% of the adventitia may have received this dose.

The remnant plaque burden at the site of angioplasty becomes a powerful predictor of the outcome. This is in accordance with other studies that identified, either in nonstented or stented coronary segments, postintervention cross-sectional area as a predictor of restenosis.[23,24] In this regard, the usefulness of a debulking technique before radiation therapy should be addressed in further studies.

D_{90}Adv was also identified as an independent predictor of the plaque volume at follow-up. The relation between D_{90}Adv and plaque volume at follow-up appeared to be polynomial with linear and nonlinear components. This may model the survival curve of mammalian cells.[25] The minimal effective dose to be delivered to 90% of the adventitial volume appeared to be 4 Gy. Further increase in dose resulted in net increase in luminal volume at follow-up. Similarly, in a subgroup analysis of the SCRIPPS trial, late loss was significantly lower when the entire circumference of the adventitial border was exposed to $\geq$8 Gy.[26] Radiation doses >20 Gy have been suggested to be able to completely eliminate the smooth muscle cell population from the treated area.[27] However, because cells from normal tissue have a limited capacity to proliferate,[28] lower doses probably would be sufficient to permanently prevent restenosis.

Finally, subsegments containing hard tissue (fibrotic and calcified material up to 90° of the circumferential arc) demonstrated a trend to be a negative predictor of plaque volume at follow-up. Hard plaque on IVUS consists of a more mature tissue with low cellularity and high content of extracellular matrix.[29,30] These features may induce either a physical barrier for migration of smooth muscle cells from the surrounding layers or a reduced capacity to proliferate when injured as compared with that of the soft tissue with a high concentration of smooth muscle cells.[29-31] Further, it is hypothesized that tissue composition may potentially exert a different degree of shielding effect on radiation and thus become less effective. However, the degree of remodeling was similar between the different types of tissue, suggesting that the effects of attenuation of radiation induced by hard material (either containing calcium up to 90° of circumferential arc or mixed noncalcified tissue) may be negligible as compared with that of soft tissue.

Study Limitations

We assumed that the IVUS and the delivery catheters were lying in the same position in the treated coronary segment. The size of the IVUS catheter is smaller (2.9F) than the brachytherapy device (5F), which is thus to some extent more centered in the lumen. Although the catheters should be on the shortest 3D path in the lumen, coronary arteries have a complex curved geometry in space and can be partially deformed by the catheters. Thus, catheters with different rigidity may occupy different positions. The development of new systems incorporating the IVUS imaging element on the delivery catheter might resolve this drawback.

During irradiation, the position of the delivery catheter inside the lumen is not fixed and may vary along the cardiac cycle because of ventricular contractions, which may lead to some degree of inhomogeneity not assumed by data derived from the static end-diastolic IVUS images.

The behavior of diffuse calcified plaques after radiotherapy has not been evaluated because the acoustic shadowing would have impeded the reliable analysis of total vessel and plaque volumes.[19]

It has not been possible to differentiate those areas that have been traumatized and irradiated from those only irradiated. Thus, no conclusions regarding the effect on radiation in irradiated but noninjured segments can be drawn. Further studies will address this problem by defining meticulously the injured and the irradiated areas either on IVUS or quantitative coronary angiography.

Finally, the dose as presented by the use of dose-volume histograms is not a direct measurement. The theoretical value obtained at the level of the adventitia is derived from the fall-off of the isotope and the geometrical data obtained from the IVUS study. The influence of the attenuation of the radiation caused by different tissue characteristics has not been taken into consideration. Future investigations should address the implementation of a dosimetry program on-line to prescribe the radiation dose in a more refined fashion.

Acknowledgments

Dr Kay was supported by The National Heart Foundation of New Zealand. The Wenckebach prize was awarded to Dr Serruys by the

Dutch Heart Foundation for brachytherapy research in the catheterization laboratory.

References

1. Waksman R, Robinson KA, Crocker IR, et al. Endovascular low-dose irradiation inhibits neointima formation after coronary artery balloon injury in swine: a possible role for radiation therapy in restenosis prevention. *Circulation.* 1995;91:1553–1559.
2. Wiedeman JG, Marboe C, Amols H, et al. Intracoronary irradiation markedly reduces restenosis after balloon angioplasty in a porcine model. *J Am Coll Cardiol.* 1994;23:1491–1498.
3. Verin V, Popowski Y, Urban P, et al. Intra-arterial β-irradiation prevents neointimal hyperplasia in a hypercholesterolemic rabbit restenosis model. *Circulation.* 1995;92:2284–2290.
4. Teirstein PS, Massullo V, Jani S, et al. Catheter-based radiotherapy to inhibit restenosis after coronary stenting. *N Engl J Med.* 1997;336:1697–1703.
5. Waksman R, ed. *Vascular Brachytherapy.* Armonk, NY: Futura Publishing Inc; 1999.
6. Amols HI. Isotopes for use in vascular brachytherapy. In: Waksman R, Serruys PW, eds. *Handbook of Vascular Brachytherapy.* London, UK: Martin Dunitz Ltd; 1998:1–4.
7. Drzymala RE, Mohan R, Brewster MS, et al. Dose-volume histograms. *Int J Radiat Oncol Biol Phys.* 1991;21:71–78.
8. Carlier SG, Marijnissen JPA, Coen VLMA, et al. Guidance of intracoronary radiation therapy based on dose-volume histograms derived from quantitative intravascular ultrasound. *IEEE Trans Med Imaging.* 1998;17:772–778.
9. King SB III, Williams DO, Chogule P, et al. Endovascular β-radiation to reduce restenosis after coronary balloon angioplasty: results of the Beta Energy Restenosis Trial (BERT). *Circulation.* 1998;97:2025–2030.
10. Hillstead RA, Johnson CR, Weldon TD. The Beta-Cath system. In: Waksman R, Serruys PW, eds. *Handbook of Vascular Brachytherapy.* London, UK: Martin Dunitz Ltd; 1998:41–51.
11. Sabaté M, Serruys PW, van der Giessen WJ, et al. Geometric vascular remodeling after balloon angioplasty and β-radiation therapy: a 3-dimensional intravascular ultrasound study. *Circulation.* 1999;100:1181–1188.
12. Bruining N, von Birgelen C, Di Mario C, et al. Dynamic 3-dimensional reconstruction of IVUS images based on an ECG-gated pullback device. In: *Computers in Cardiology.* Los Alamitos, Calif: IEEE Computer Society Press; 1995:633–636.
13. von Birgelen C, de Vrey EA, Mintz GS, et al. ECG-gated 3-dimensional intravascular ultrasound: feasibility and reproducibility of the automated analysis of coronary lumen and atherosclerotic plaque dimensions in humans. *Circulation.* 1997;96:2944–2952.
14. Bruining N, von Birgelen C, de Feyter PJ, et al. ECG-gated versus non-gated 3-dimensional intracoronary ultrasound analysis: implications for volumetric measurements. *Cathet Cardiovasc Diagn.* 1998;43:254–260.
15. Li W, von Birgelen C, Di Mario C, et al. Semi-automated contour detection for volumetric quantification of intracoronary ultrasound. In: *Computers in Cardiology.* Washington, DC: IEEE Computer Society Press; 1994:277–280.
16. Mallery JA, Tobis JM, Griffith J, et al. Assessment of normal and atherosclerotic arterial wall thickness with an intravascular ultrasound imaging catheter. *Am Heart J.* 1990;119:1392–1400.
17. von Birgelen C, Di Mario C, Li W, et al. Morphometric analysis in 3-dimensional intracoronary ultrasound: an in vitro and in vivo study performed with a novel system for the contour detection of lumen and plaque. *Am Heart J.* 1996;132:516–527.
18. von Birgelen C, Mintz GS, Nicosia A, et al. Electrocardiogram-gated intravascular ultrasound image acquisition after coronary stent deployment facilitates on-line 3-dimensional reconstruction and automated lumen quantification. *J Am Coll Cardiol.* 1997;30:436–443.
19. DiMario C, Görge G, Peters R, et al. Clinical application and image interpretation in intracoronary ultrasound: study group on intracoronary imaging of the working group of coronary circulation and of the subgroup on intravascular ultrasound of the working group of echocardiography of the European Society of Cardiology. *Eur Heart J.* 1998;19:207–229.
20. Scott NA, Cipolla GD, Ross CE, et al. Identification of a potential role for the adventitia in the vascular lesion formation after balloon overstretch injury of porcine coronary arteries. *Circulation.* 1996;93:2178–2187.
21. Waksman R, Rodriguez JC, Robinson KA, et al. Effect of intravascular irradiation on cell proliferation, apoptosis and vascular remodeling after balloon overstretch injury of porcine coronary arteries. *Circulation.* 1997;96:1944–1952.
22. Amols HI, Zaider M, Weinberger J, et al. Dosimetric considerations for catheter-based beta and gamma emitters in the therapy of neointimal hyperplasia in human coronary arteries. *Int J Radiat Oncol Biol Phys.* 1996;36:913–921.
23. Mintz GS, Popma JJ, Pichard AD, et al. Intravascular predictors of restenosis after transcatheter coronary revascularization. *J Am Coll Cardiol.* 1996;27:1678–1687.
24. Prati F, Di Mario C, Moussa I, et al. In-stent neointimal proliferation correlates with the amount of residual plaque burden outside the stent: an intravascular ultrasound study. *Circulation.* 1999;99:1011–1014.
25. Hall EJ, Miller RC, Brenner DJ. The basic radiobiology of intravascular irradiation. In: Waksman R, ed. *Vascular Brachytherapy.* 2nd ed. Armonk, NY: Futura Publishing Co Inc; 1999:63–72.
26. Teirstein PS, Massullo V, Jani S, et al. A subgroup analysis of the Scripps Coronary Radiation to Inhibit Proliferation Poststenting Trial. *Int J Radiat Oncol Biol Phys.* 1998;42:1097–1104.
27. Brenner DJ, Miller RC, Hall EJ. The radiobiology of intravascular radiation. *Int J Radiat Oncol Biol Phys.* 1996;36:805–810.
28. Fowler JF. Dose response curves for organ function or cell survival. *Br J Radiol.* 1983;56:497–500.
29. Di Mario C, The SHK, Madretsma S, et al. Detection and characterization of vascular lesions by intravascular ultrasound: an in vitro study correlated with histology. *J Am Soc Echocardiogr.* 1992;5:135–146.
30. Rasheed Q, Dhawale PJ, Anderson J, et al. Intracoronary ultrasound-defined plaque composition: computer-aided plaque characterization and correlation with histologic samples obtained during directional coronary atherectomy. *Am Heart J.* 1995;129:631–637.
31. Stary HC, Chandler AB, Dinsmore RE, et al. A definition of advanced types of atherosclerotic lesions and a histological classification of atherosclerosis: a report from the Committee on Vascular Lesions of the Council on Arteriosclerosis, American Heart Association. *Arterioscler Thromb Vasc Biol.* 1995;15:1512–1531.

Chapter 16

Correlation between radiation dose delivered to the vessel wall and angiographic outcome of balloon angioplasty followed by β-intracoronary brachytherapy.

M Sabate, JPA Marijnissen, **SG Carlier**, IP Kay, WJ van der Giessen, VLMA Coen, JLMR Ligthart, E Boersma, MA Costa, PC Levendag, PW Serruys.

Submitted to the European Heart Journal.

Correlation between Radiation Dose Delivered to the Vessel Wall and Angiographic Outcome of Balloon Angioplasty Followed by β-Intracoronary Brachytherapy

Stéphane Carlier[1], Tim Fox[2], Ken Kozuma[1], Manel Sabate[1], Ian Crocker[2], Veronique Coen[3], Jurgen Ligthart[1], Wim van der Giessen[1], Peter Levendag[3], Patrick Serruys[1]

[1]Thoraxcenter, Erasmus Medical Center Rotterdam, Rotterdam, The Netherlands
[2]Department of Radiation Oncology, Emory University School of Medicine, Atlanta, GA 30322 USA
[3]Department of Radiotherapy, Daniel den Hoed Cancer Center, Erasmus Medical Center Rotterdam, NL

Running title: Dose delivered in arterial wall vs. restenosis
Keywords: brachytherapy, intravascular ultrasound, restenosis, coronary angioplasty

Correspondence address:
S.G. Carlier, MD, Experimental Echo Laboratory, Erasmus Medical Center Rotterdam – Ee2302, Dr Molewaterplein 50, 3015 GE Rotterdam, The Netherlands
Phone: 31-10-408 74 74, Fax: 31-10-408 94 45, E-mail: CARLIER@TCH.FGG.EUR.NL

Word count: 6022

Dr S.G. Carlier was supported by a grant from the Bekales and Vesale Foundations. The Wenckebach prize was awarded to P.W. Serruys by the Dutch Heart Foundation for brachytherapy research in the catheterization laboratory.

STRUCTURED ABSTRACT:

Aim: *b-radiation reduces late lumen loss after PTCA. However, this benefit is not observed in all patients. We hypothesized that this may be related to the dose delivered to the coronary wall. Therefore we investigated by 3-d IVUS the actual radiation energy deposited and correlated this to 6-month angiographic late loss.*

Methods and results: *β-radiation was administered using a $^{90}Sr/Y$ source. Twenty-seven consecutive patients with successful PTCA of de novo lesions without stenting underwent a retrospective analysis of the dose delivered to the treated segment using an IVUS-based treatment planning system. Dose surface histograms were calculated for the luminal surface (lum) and the external elastic lamina (eel). The minimum dose on 90% of lum (DS_{90}lum) and eel (DS_{90}eel) were 9.7±6.1 and 5.1±3.0 Gy, respectively. At 6-month follow-up, the patients with a DS90eel > 5.2 Gy (n=11) had a lower angiographic loss (-0.01±0.39 vs. 0.47±0.62 mm, p=0.03) and late loss index (-0.4±58 vs. 44±56 %, p=0.06). These arteries were smaller (reference diameter: 2.67±0.52 vs. 3.17±0.59 mm, p<0.001) but had a similar relative gain (0.35 vs. 0.36 mm) post-angioplasty. Conclusion: Angiographic loss after PTCA followed by b-brachytherapy is minimal when 90% of the eel receives a minimum dose estimated from our study to be 5.2 Gray.*

Abstract:

We have evaluated the dose delivered to the coronary wall of twenty-seven patients treated with β-brachytherapy after successful PTCA without stenting. The dose was measured with an IVUS-based treatment planning system. Dose surface histograms were calculated for the luminal surface and the external elastic lamina (eel). At 6-month follow-up, the patients with a minimum dose on 90% of the eel > 5.2 Gy (n=11) had a lower angiographic loss (-0.01±0.39 vs. 0.47±0.62 mm, p=0.03). We conclude from this study that the angiographic loss after PTCA followed by β-brachytherapy depends on the minimum dose delivered in the coronary wall.

INTRODUCTION

Intracoronary radiation therapy is a new therapeutic modality to prevent restenosis. Positive results observed in animal experiments(1-5) have supported the blossoming of numerous clinical trials. The strong reduction of the restenosis rate for the treatment of in-stent restenosis using γ-radiation(6-8) or more recently β-radiation(9) contrasts with more controversial data observed with the use of β-radiation as adjunctive therapy after percutaneous angioplasty (PTCA) of de novo lesions(10). However, three recent studies have demonstrated that a reduced late lumen loss could be achieved when treating de novo lesions by angioplasty followed by β-radiation.(11-13) The benefits were, however, not observed for all the patients and the reported late lumen loss demonstrates large standard deviation. We hypothesized that this phenomenon may be related to the dose of radiation delivered to the coronary vessel wall. Teirstein et al., for example, have already reported that γ-therapy was only effective when the minimum dose to the furthest point of the adventitia was at least 8 gray.(14)

The aim of this study is to demonstrate the relationship between the angiographic changes and actual dose in the setting of catheter-based β-radiation. To this purpose, we have correlated the dose delivered to different coronary structures such as the luminal surface or the external elastic lamina (eel) to the angiographic outcome assessed by quantitative coronary angiography (QCA). This dose was derived from dose-volume histograms (DVH) computed on the three-dimensional (3-d) intravascular ultrasound (IVUS) pullbacks using a method recently described.(15, 16)

METHOD

Population

Twenty-seven consecutive patients presenting with de novo coronary stenosis, successfully treated with balloon angioplasty followed by intracoronary β-radiation therapy were included in this study. Patient characteristics are given in table 1. Patients receiving a stent were excluded from the analysis. Radiation was delivered within the framework of brachytherapy trials conducted in our institution that were

Table 1: Baseline characteristics

Patients, n	27
Age, y	58.7 ± 9.6 [39 - 75]
Male, %	21 (78 %)
Prior MI, %	9 (33 %)
Diabetes mellitus	4 (15 %)
Hypercholesterolemia	9 (33 %)
Smoking history	16 (59 %)
Artery, %	
Left anterior descending	10 (37 %)
Circumflex	7 (26 %)
Right coronary	10 (37 %)
Lesion characteristics, %	
A	4 (15 %)
B	23 (85 %)
Dose prescribed at 2 mm off source axis	
12 Gy	9 (33 %)
14 Gy	9 (33 %)
16 Gy	7 (26 %)
18 Gy	2 (8%)

approved by our Investigational Review Board. All patients gave written informed consent. The isotope used was the pure β-emitting ^{90}Sr/Y. Patients were randomized to receive 12 to 18 Gray at 2 mm off source axis. Brachytherapy was performed with the BetaCath System™ (Novoste Corp., Norcross, GA). The radiation source train of this system consists of a series of twelve independent 2.5 mm-long cylindrical seeds that contain the ^{90}Sr/Y source (total length is 30 mm).(11)

Intravascular ultrasound image acquisition

The treated coronary segment was evaluated by means of three-dimensional (3-d) IVUS imaging for volumetric estimation of the irradiated area. The selection of the area of interest has been reported elsewhere.(17, 18) In brief, selection of the IVUS segment matching the irradiated site was based on anatomical landmarks such as side branches or ostial locations. An angiogram was performed after the placement of the delivery catheter to document the relationship between the anatomical landmarks and the source train. This angiographic reference point was again identified during a contrast injection with the IVUS imaging element at the same position. The system used for imaging was a mechanical IVUS system (ClearView, CVIS, Boston Scientific Corporation, Maple Grove, NW) with a sheath-based IVUS catheter incorporating a 30 MHz single-element transducer rotating at 1800 rpm (Ultracross™, CVIS). ECG-gated image acquisition and digitisation was performed by a workstation designed for the 3-d reconstruction of echocardiographic images (EchoScan, Tomtec, Munich, Germany) as described before.(19)

Intravascular ultrasound quantification

A Microsoft Windows™–based contour detection program, developed at the Thoraxcenter, was used for off-line volumetric quantification following a methodology detailed elsewhere.(17, 18) Briefly, this program identified the contours corresponding to the lumen and eel boundaries in

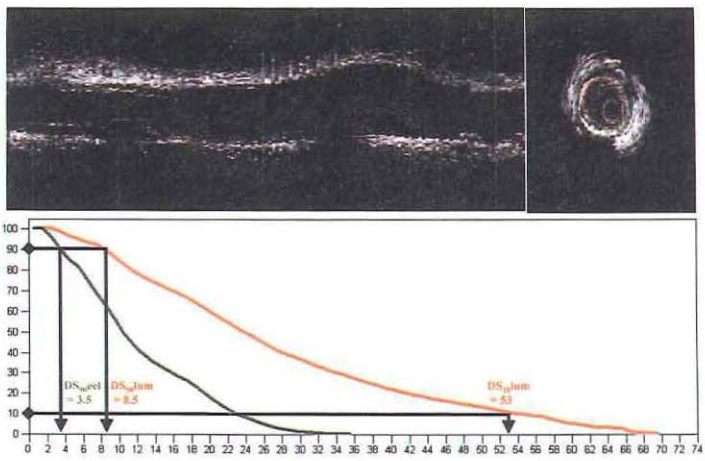

Carlier et al.

Figure 1: Top panels: typical IVUS cross-section and sagital reconstruction of an IVUS pull-back. The 24 points (+) of the luminal surface (*lum*, in red) and external elastic lamina (*eel*, in green) where the dose has been calculated, considering that the Sr/Y90 source was lying in the same position than the IVUS catheter, are superimposed on the cross-section. Bottom panel: the corresponding cumulative dose surface histogram for the lumen (in red) and the eel (in green) are shown in the bottom panel. The prescribed dose was 16 Gy at 2 mm from the source axis. DS_{90}lum (8.5 Gy) is the minimum dose (x-axis) received by at least 90% of the voxels (y-axis) corresponding to the luminal surface along the complete IVUS pullback illustrated. DS_{10}lum (53 Gy) is the highest dose received by at least 10% of these voxels. Similarly, DS90eel (3.5 Gy) is the minimum dose delivered on at least 90% of the eel.

successive cross-sectional images. Volumetric data of the vessel segment of interest were calculated as the sum of all cross-section areas multiplied by the slice thickness (on average 200 μm). Contours were checked and edited by experienced analysts.

Dose calculation

The dose delivered in the irradiated coronary segments was calculated by means of dose-volume histograms (DVH) and dose-surface histograms (DSH) derived from the 3-d IVUS pull-backs. DVH's summarize the dose distribution information for a region of interest and identify characteristics such as dose uniformity and hot or cold spots. To calculate a DVH, the dose distribution data must be available for the region of interest. The histogram is a plot of the accumulated volume of those elements receiving a dose in a specified dose interval versus a set of equal-spaced dose intervals (see figure 1). DSH's are computed for the surface area of various target regions.

The contours of the EchoScan program were processed with a software written in MatLab (The MathWorks, Inc., Natick, MA) to compute the distances between the centre of the source and both the lumen-intima and media-adventitia (eel) interfaces in 24 pie-slices (15°) in all cross-sections corresponding to the fully irradiated segment (25 mm), excluding the dose fall-off zone. Because media thickness cannot be measured accurately, we assumed that the plaque volume included the atherosclerotic plaque and the media.(20) The dose distribution over the luminal and eel surfaces and in the plaque+media volume was retrospectively computed using an intracoronary treatment planning system (*i*Plan™, Emory University, Atlanta, GA). This system incorporates a dose calculation engine based on the AAPM TG-60 formalism using catheter based delivery systems with the following radiation sources: ^{90}Sr/Y, ^{32}P, ^{125}I and ^{192}Ir. The dosimetry is based on the method discussed by Soares et al. for calibrating β-sources and includes anisotropy factors to account for the dose fall-off on the end of the seeds in the transverse axis.(21) The coordinate of the center of the IVUS catheter was used as a reference, and was considered at the same location as the center of the radiation train. Validation of *i*Plan™ dosimetry calculation has been previously reported.(22) The average voxel dose (D_{50}) was computed as well as the cumulative curve of the dose from which two measurements, D_{90} and D_{10} were derived. D_{90} is the minimum dose received by at least 90% of the voxels corresponding to the volume (or surface) of tissue considered. D_{10} is the highest dose received by at least 10% of these voxels. DS_{90}eel is thus the minimum dose deposited on 90% of the eel surface. DV_{90}p+m is the minimum dose deposited in 90% of the plaque plus media volume.

Quantitative angiography

Quantitative coronary angiography (QCA) was performed pre-, post-procedure and at 6-month follow-up in ≥ 2 orthogonal matched projections with the CAAS II analysis system (Pie Medical BV, Maastricht, The Netherlands) after intracoronary administration of nitrates. This method has been extensively validated(23, 24) and applied in numerous clinical trials. The following measurements were obtained: minimum lumen diameter (MLD), reference diameter, percent diameter stenosis (%DS). Acute gain was defined as MLD post-procedure minus MLD pre-intervention. Late lumen loss was defined as MLD post-procedure minus MLD at 6-month follow-up. The late loss index was computed as the ratio of the late loss over the acute gain.(25) Relative gain and loss were computed respectively as the gain and the loss divided by the reference diameter. Restenosis at 6 months was defined as a %DS>50 %. The fully irradiated segment of the vessel was analysed.

Statistical analysis

Data are presented as mean ± standard deviation. Sensitivity (percentage of patients with restenosis that does exceed a given dose threshold) and specificity (percentage of restenosis-free patients that does not exceed a dose threshold) were computed. Angiographic and IVUS variables were compared for the groups of patients with a DS_{90}eel lower or equal and a DS_{90}eel higher than the dose corresponding to the crossing of the sensitivity and specificity curves. Receiver operating curves were constructed and the area under the curve is reported.(26) Continuous variables were compared with the use of unpaired Student's t-test. Binary variables were compared with the use of the chi-square test with normal approximation or Fisher's exact test, when appropriate. All tests were two-tailed and a p value <0.05 was considered statistically significant.

Table 2: QCA and IVUS results

	preangioplasty	postirradiation	6-month follow up
Reference vessel diameter (mm)	2.96±0.54	2.96±0.61	2.78±0.55
Minimal lumen diameter (mm)	0.92±0.39	1.98±0.42	1.71±0.62
Diameter stenosis (%)	69±11	32±9	39±18
Acute gain (mm)		1.06±0.42	
Late luminal loss (mm)			0.27±0.58
Loss index (%)			26±60
Binary restenosis			7 (26 %)
Luminal volume (mm³)		225±97	
Vessel volume (mm³)		423±127	
Plaque volume (mm³)		197±49	
Minimal luminal cross section area (MLCSA, mm²)		4.5±1.7	
Vessel area at MLCSA (mm²)		11.4±3.9	
Plaque at MLCSA (mm²)		6.9±2.9	
Residual obstruction at MLCSA (%)		59±11	

Table 3: Minimum dose deposited on 90%, 50% and 10% of the luminal surface, of the external elastic lamina and in the plaque+media volume

	D 90 (Gy)	D 50 (Gy)	D 10 (Gy)
Lumen	9.7±6.1	23.3±8.6	49.0±7.8
Eel	5.1±3.0	11.6±4.5	28.1±6.0
Plaque+media	7.0±4.0	16.1±6.0	35.1±6.4

RESULTS

QCA and IVUS measurements

QCA and IVUS results are summarized in table 2. Patients were comparable to a Benestent-like population(27) with unremarkable risks factors and non-complex lesions. Angiographic acute gain and late loss were comparable to similar PTCA patients in historic trials. The mean IVUS lumen diameter, derived from the lumen volume divided by the 25 mm of the pullback length (see figure 1), was 3.3 mm and the mean vessel diameter was 4.6 mm.

Dosimetry

The minimum dose delivered on 90, 50 and 10 % of the luminal and eel surfaces and in the plaque+media volume are given in table 3. On average, DS_{90}eel was 5.1 Gy and DV_{90}p+m was 7.0 Gy, for an average dose of 14.1 Gy prescribed 2 mm off source axis.

Seven patients had a diameter stenosis larger than 50% at follow-up within the fully irradiated segment. The area under the ROC curves for DS_{90}eel, DS_{50}eel, DV_{90}p+m and DV_{50}p+m were respectively 0.56, 0.49, 0.54 and 0.51. As shown on figure 2, the sensitivity and specificity curves to predict a DS>50% at 6-month for DS_{90}eel crossed at 4.5 Gy. Sensitivity and specificity were then 0.58. No significant threshold could be found for DS_{90}lum and DS_{50}lum. The Beta-Cath source has been recently recalibrated by the NIST and the doses prescribed to our patients were actually 15% higher than believed (e.g. a dose of 16.1 Gy has actually been given to the patients randomised to 14 Gy). The threshold of 4.5 Gy that we have derived for DS_{90}eel corresponds to an actual dose of 5.2 Gy.

Late luminal loss in function of the dose delivered on the eel

A significantly lower loss (-0.01±0.39 vs. 0.47±0.62 mm, p=0.03), relative loss (-0.007±0.158 vs. 0.15±0.21 mm, p=0.04) and loss index (-0.4±58 vs 44±56 %, p=0.06) were found in the 11 patients with a DS_{90}eel > 5.2 Gy (see table 4).

Similar results were found for the patients with a DV_{90}p+m > 7.1 Gy. There was no difference in the clinical characteristics of the patients with a DS_{90}eel ≤ or > than 5.2 Gy. Figure 3 demonstrates that the vessels with a DS_{90}eel > 5.2 Gy were smaller, had less plaque accumulation, but that the gain (1.15±0.38 vs. 0.93±0.46 mm, p=ns) and the relative gain (0.36±0.10 vs. 0.35±0.15 mm, p=ns) were similar. None of the observed differences in the angiographic and IVUS parameters could predict a lower restenosis rate, loss and loss index at 6 month. Among the 11 patients with a DS_{90}eel > 5.2 Gy, the binary restenosis rate was 18% (2/11) compared to 31 % (5/16) when the dose delivered on 90 % of the eel was ≤ 5.2 Gy. This difference did not reach statistical significance. Figure 4 demonstrates the cumulative plots of the minimum lumen diameter (MLD) post-intervention and at 6-month follow-up. The median loss of the patients with a DS_{90}eel ≤ 5.2 Gy was 0.55 mm whereas it can be clearly appreciated that at 6-month follow-up, the majority of the patients with a DS_{90}eel > 5.2 Gy at least preserved their MLD, and that 40% demonstrated even a positive remodelling (larger MLD at follow-up than post-intervention).

DISCUSSION

The objective of this study was to evaluate the relationship between the quantitative angiographic changes and actual dose in the setting of catheter-based ß-radiation. The major finding is that the late angiographic outcome of patients treated for de novo coronary lesion by angioplasty followed by β-radiation therapy can be partially explained by the dose delivered in the vessel wall. This dose can be derived from dose volume histograms computed from 3-d IVUS pullbacks. A significantly lower loss (-0.01±0.39 vs. 0.47±0.62 mm, p=0.03) and relative loss (0.15±0.21 vs. -0.007±0.158 mm, p=0.04) were present at 6-month follow-up when the radiation energy deposited on the external elastic lamina was higher than 5.2 Gy (see table 4).

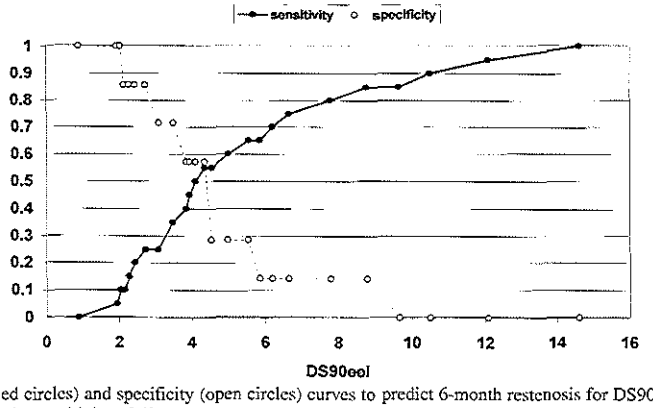

Carlier et al.

Figure 2: Sensitivity (filled circles) and specificity (open circles) curves to predict 6-month restenosis for DS90eel. The two curves cross at 4.5 Gy for a specificity and a sensitivity of 58%.

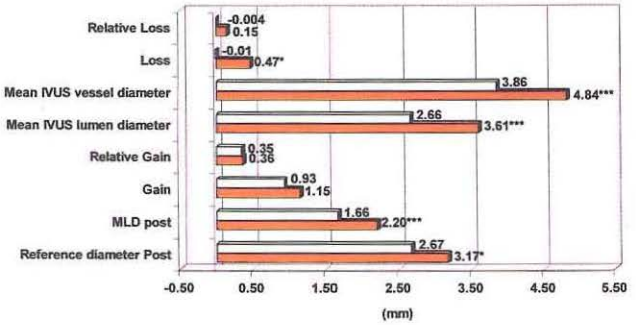

Carlier et al.

Figure 3: Comparison of the QCA and IVUS measurements of the 16 patients with a DS_{90}eel < 5.2 Gy (4.5 x 115%, corrected dose, see text) and the 11 patients with a DS_{90}eel > 5.2 Gy. The arteries with a dose delivered on 90% of the eel > 5.2 Gy were smaller, had less plaque accumulation, but had a similar gain and relative gain. None of the observed differences in the angiographic and IVUS parameters could predict the lower loss and loss index observed at 6 months.

Dose volume histograms to predict restenosis

We have investigated whether a given threshold of the minimum dose delivered on 90% of the external elastic lamina (DS_{90}eel) is a predictor of restenosis at 6-month. The threshold of 5.2 Gy for DS_{90}eel that we find is in agreement with a previous IVUS analysis in which we have analysed 2-mm sub-segments of coronary arteries treated with brachytherapy. We could demonstrate that there was an increase of the luminal volume, related to an increase of the vessel volume larger than the plaque growth, when the DS_{90}eel was greater or equal to 6 Gy.(17) Several brachytherapy trials have demonstrated that in a majority of patients the luminal diameter at the site of the treated lesion may increase during the follow-up.(13) This phenomenon is induced by the positive remodelling of the vessel wall as demonstrated by IVUS.(17) We do not report the 6-month IVUS data since an ECG-triggered pull-back was not systematically performed in our cohort.

The major determinant of clinical recurrence of symptoms is the minimum luminal diameter (MLD) at 6-month.(25, 28). We have compared the lumen late loss in the 11 patients with a DS_{90}eel > 5.2 Gy and the 16 patients with a DS_{90}eel ≤ 5.2 Gy. The arteries with a DS_{90}eel > 5.2 Gy demonstrated a statistically lower loss (table 4). These arteries were smaller (figure 3), which can be expected with the prescription method used with the Beta-Cath system, with a fixed dose prescribed at 2 mm off the source axis. However, the relative gain was identical in these arteries with a reference diameter on average 0.5 mm smaller. The observed lower loss and loss index could not have been predicted in these conditions(25, 29, 30) and must directly reflect the effect of radiation therapy which mainly leads to a remodelling of the vessel, with an enlargement of the eel with an adequate dose.(17)

The target volume of coronary brachytherapy

Animal studies showing the efficacy of intracoronary brachytherapy were followed immediately by human clinical trials. At the time that they were initiated there was little information available as to the mechanism of radiation in preventing restenosis. This situation continues today. Various opinions exist as to the target cell of radiation in preventing restenosis. Rubin has postulated the importance of the monocyte-macrophage in regulating the development

Table 4: QCA and IVUS data in function of the dose delivered on 90% of the external elastic lamina surface (DS90eel)

DS_{90}eel ≤ 5.2 Gy (n=16)	Preangioplasty	Postirradiation	6-month Follow up
Reference vessel d. (mm)	3.12±0.58	3.17±0.59*	2.91±0.63
Minimal lumen d. (mm)	1.05±0.40*	2.20±0.38***	1.73±0.73
Diameter stenosis (%)	66±11	30±5	41±21
Acute gain (mm)		1.15±0.38	
Late luminal loss (mm)			0.47±0.62*
Loss index (%)			44±56
Luminal volume (mm^3)		276±94***	
Vessel volume (mm^3)		496±112***	
Plaque volume (mm^3)		218±48**	
DS_{90}eel > 5.2 Gy (n=11)	**Preangioplasty**	**Postirradiation**	**6-month Follow up**
Reference vessel d. (mm)	2.72±0.39	2.67±0.52	2.59±0.37
Minimal lumen d. (mm)	0.74±0.32	1.66±0.25	1.68±0.45
Diameter stenosis (%)	73±11	36±12	36±14
Acute gain (mm)		0.93±0.46	
Late luminal loss (mm)			-0.01±0.39
Loss index (%)			-0.4±58
Luminal volume (mm^3)		150±31	
Vessel volume (mm^3)		316±44	
Plaque volume (mm^3)		166±33	

*: p<0.05, **: p<0.01; ***: p<0.001 – unpaired t-test, DS_{90}eel < 5.2 Gy vs. > 5.2 Gy

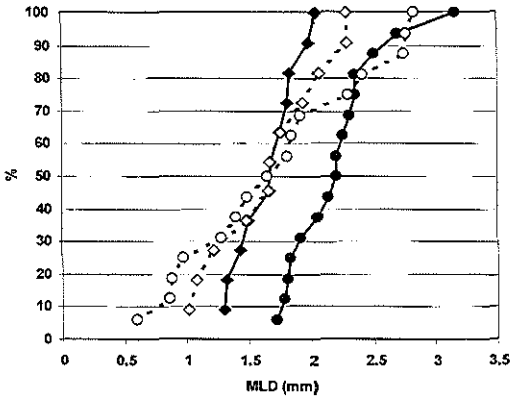

Carlier et al.

Figure 4: Cumulative plots of the minimum lumen diameter (MLD) post-intervention (filled markers) and at 6-month follow-up (open markers). The round markers represents the 16 patients with a DS_{90}eel < 5.2 Gy. The median loss of these patients was 0.55 mm. The square markers represents the 11 patients with a DS_{90}eel > 5.2 Gy. It can be clearly appreciated that at 6-month follow-up, the majority of these patients (open squares) at least preserved their MLD, and that 40% demonstrated even a positive remodelling (larger MLD at follow-up than post-intervention).

of the proliferative neointima.(31, 32) Robinson, Wilcox and others have stressed the importance of the modified smooth muscle cell in the development of the restenotic lesion without invoking the monocyte-macrophage in the process.(33-35) The site of origin of these modified smooth muscle cells is however in dispute. Robinson has proposed that these cells are most likely to originate in the torn edges of the media. Wilcox has shown suggestive evidence that the proliferative activity in the vessel wall is seen first in the adventitia and only later in the media, suggesting that the neointimal cells may have migrated there from the adventitia. Thus there remains debate as to how deep from the luminal surface the prescribed dose of radiation needs to be. There seems to be consensus that in animal models the proliferative cells forming the cellular neointima does not originate from the entire circumference of the vessel wall but primarily from the site of damaged tunica media. The proliferation following PTCA in human coronary arteries seems to occur similarly in a focal manner. Recently Mintz and others have shown that shrinkage of the vessel (negative remodelling) may play the major role in late lumen loss following coronary intervention (atherectomy, PTCA).(36) Waksman and Wilcox have shown that the adventitial myofibroblasts are responsible for this process as a result of the contractile nature of these cells and their capacity to participate in a form of scar contraction of the arterial wall after angioplasty. This may present an additional reason to target dose to the tissues beyond the eel.(37) Our data support that the target for brachytherapy lies at least at the level of the external elastic lamina and may be the adventitia since the angiographic outcome was best correlated with the DS_{90}eel, and not with the DS_{90}lum.

The minimum dose to prevent restenosis and to induce remodelling

One thing that is clear from the preclinical studies of restenosis is that a broad range of doses seems to be effective in preventing restenosis. Work carried out by the Emory group with β- and γ- sources has shown that doses of 3.5 to 56 Gy were all effective in reducing restenosis in comparison to controls.(2, 38) However, the data of the subanalysis of the SCRIPPS(14) and of the Dose Finding Study(13) cleared demonstrated a dose-effect relationship in a narrower range of dose delivered to the vessel wall. In SCRIPPS, there was no difference between the placebo group and the patients who received less than 8 Gy to the most distant part of the eel. In the Dose Finding Study, for the patients treated by balloon angioplasty alone, the late lumen loss was 0.31 mm in the group in which 9 Gy was prescribed 1 mm in the vessel wall, but -0.04 mm in the 18 Gy group. These data support our findings of a significant relationship between the dose deposited in the arterial wall and the QCA outcomes.

Limitations of the study

Dose volume histograms (DVH) describe the cumulative distribution of dose over a specific volume(39) and summarize the dosimetry that would otherwise have to be interpreted from numerous IVUS cross-sections with superimposed isodoses plotted. We have concentrated our analysis on the minimum dose delivered to 90 % of the eel (DS_{90}eel) but we show that similar results could be derived from the DV_{90}p+m. Several other parameters can be derived from DVHs.(40, 41) but no definitive one has emerged as a gold-standard.

The reported doses were not directly measured. The theoretical value obtained at the level of the adventitia is derived from the isotope dose distribution and the geometrical data obtained with IVUS. The influence of the attenuation of the radiation due to different tissue densities has not been taken into consideration so far. However, this is likely to be significant and warrants further investigation. It is expected that a plaque heavily calcified will decrease the dose reaching the eel.(42)

A recognized limitation of coronary brachytherapy is the development of a new stenosis at the edges of the irradiated area. This has been likened to the radiation oncology concept of geographic miss, where the radiation field does not fully cover the target.(43) We limited our analysis to the fully irradiated segment in order to draw unequivocal relationship between the angiographic loss and the dose, without the possibility of geographical miss. The clinical outcome

depends also on other complications such as late thrombosis.(44) Although it has been suggested that the higher the dose in the adventitia is, the higher the thrombosis rate is,(45) we did not include any patient presenting a late thrombosis, which would have blurred the interpretation of the loss and loss index. A larger group of patients would be necessary for an analysis of the rate of thrombosis in function of the dosimetry, as well as for a study of the influence of the clinical characteristics (e.g. diabetes) or the type of plaque. The analysis of the receiver operating curves demonstrated that the dose is not the only parameter influencing restenosis since the area under the curves were not statistically different from 0.5.

We assumed that the IVUS and the delivery catheters were lying in the same position in the treated coronary segment. The brachytherapy device (5 Fr) is larger than the IVUS catheter (2.9 Fr) and is to some extent self-centered in the lumen. The true dose delivered in different vessel wall regions could vary from the data calculated. When using a centering balloon for the source,(12, 13) the center of gravity of the lumen of each slice can be calculated from the 3-D IVUS to more correctly position the source.(46) For a non-centered device, even with the use of a brachytherapy and an IVUS catheters of the same size, there will always remain an uncertainty on the location of the source in the lumen. Moreover, the position of a catheter inside the arterial lumen is not fixed and varies during the cardiac cycle.(47) These methodological limitations could be partially overcome with imaging wires, which could be introduced into the lumen of the irradiation delivery catheter itself.(48)

CONCLUSION

Dose volume histogram analysis of 3-d IVUS pullback permits the evaluation of the radiation dose delivered to different parts of the coronary wall. We have demonstrated an inverse relationship between the minimum dose delivered to 90 % on the external elastic membrane and the angiographic loss and the restenosis rate.

REFERENCES

1. Wiedermann JG, Leavy JA, Amols H, Schwartz A, Homma S, Marboe C, et al. Effects of high-dose intracoronary irradiation on vasomotor function and smooth muscle histopathology. Am J Physiol 1994;267(1 Pt 2):H125-32.
2. Waksman R, Robinson KA, Crocker IR, Gravanis MB, Cipolla GD, King SB. Endovascular low dose irradiation inhibits neointimal formation after coronary artery balloon injury in swine: a possible role for radiation therapy in restenosis prevention. Circulation 1995;91:1533-9.
3. Mazur W, Ali MN, Khan MM, Dabaghi SF, DeFelice CA, Paradis P, Jr., et al. High dose rate intracoronary radiation for inhibition of neointimal formation in the stented and balloon-injured porcine models of restenosis: angiographic, morphometric, and histopathologic analyses. Int J Radiat Oncol Biol Phys 1996;36(4):777-88.
4. Waksman R, Robinson KA, Crocker IR, Wang C, Gravanis MB, Cipolla GD, et al. Intracoronary low-dose beta-irradiation inhibits neointima formation after coronary artery balloon injury in the swine restenosis model. Circulation 1995;92(10):3025-31.
5. Verin V, Popowski Y, Urban P, Belenger J, Redard M, Costa M, et al. Intra-arterial beta irradiation prevents neointimal hyperplasia in a hypercholesterolemic rabbit restenosis model. Circulation 1995;92(8):2284-90.
6. Teirstein PS, Massullo V, Jani S, Russo RJ, Cloutier DA, Schatz RA, et al. Two-year follow-up after catheter-based radiotherapy to inhibit coronary restenosis. Circulation 1999;99(2):243-7.
7. Waksman R, White RL, Chan RC, Bass BG, Geirlach L, Mintz GS, et al. Intracoronary gamma-radiation therapy after angioplasty inhibits recurrence in patients with in-stent restenosis. Circulation 2000;101(18):2165-71.
8. Leon MB, Teirstein PS, Moses JW, Tripuraneni P, Lansky AJ, Jani S, et al. Localized intracoronary gamma-radiation therapy to inhibit the recurrence of restenosis after stenting. N Engl J Med 2001;344(4):250-6.
9. Waksman R, Bhargava B, White L, Chan RC, Mehran R, Lansky AJ, et al. Intracoronary beta-radiation therapy inhibits recurrence of in-stent restenosis. Circulation 2000;101(16):1895-8.
10. Verin V, Urban P, Popowski Y, Schwager M, Nouet P, Dorsaz PA, et al. Feasibility of intracoronary beta-irradiation to reduce restenosis after balloon angioplasty. Circulation 1997;95:1138-44.
11. King SB, Williams DO, Chougule P, Klein L, Waksman R, Hilstead R, et al. Endovascular beta-radiation to reduce restenosis after coronary balloon angioplasty. Results of the Beta Energy Restenosis Trial (BERT). Circulation 1998;97:2025-30.
12. Raizner AE, Oesterle SN, Waksman R, Serruys PW, Colombo A, Lim YL, et al. Inhibition of restenosis with beta-emitting radiotherapy : report of the proliferation reduction with vascular energy trial (PREVENT). Circulation 2000;102(9):951-8.
13. Verin V, Popowski Y, de Bruyne B, Baumgart D, Sauerwein W, Lins M, et al. Endoluminal beta-radiation therapy for the prevention of coronary restenosis after balloon angioplasty. The Dose-Finding Study Group. N Engl J Med 2001;344(4):243-9.
14. Teirstein PS, Massullo V, Jani S, Popma JJ, Mintz GS, Russo RJ, et al. A subgroup analysis of the Scripps Coronary Radiation to Inhibit Proliferation Poststenting Trial. Int J Radiat Oncol Biol Phys 1998;42(5):1097-104.
15. Fox T, Crocker I. Dosing in vascular radiotherapy. Vascular Radiotherapy Monitor 1998;1(2):45-53.
16. Carlier SG, Marijnissen JP, Coen VL, van der Giessen WJ, Sabate M, Ligthart J, et al. Guidance of intracoronary radiation therapy based on dose-volume histograms derived from quantitative intravascular ultrasound. IEEE Trans Med Imaging 1998;17(5):772-8.
17. Sabate M, Serruys PW, van der Giessen WJ, Ligthart JMR, Coen VLMA, Kay IP, et al. Geometric vascular remodeling after balloon angioplasty and beta-radiation therapy: a three-dimensional intravascular ultrasound study. Circulation 1999;100:1182-1188.
18. Kozuma K, Costa MA, Sabate M, Slager CJ, Boersma E, Kay IP, et al. Relationship between tensile stress and plaque growth after balloon angioplasty treated with and without intracoronary beta-brachytherapy. Eur Heart J 2000;21(24):2063-70.
19. von Birgelen C, Mintz GS, Nicosia A, Foley DP, van der Giessen WJ, Bruining N, et al. Electrocardiogram-gated intravascular ultrasound image acquisition after coronary stent deployement facilitates on-line three-dimensional reconstruction and automated lumen quantification. J Am Coll Cardiol 1997;30:436-43.
20. Mallery JA, Tobis JM, Griffith J, Gessert J, McRae M, Moussabeck O, et al. Assessment of normal and atherosclerotic arterial wall thickness with an intravascular ultrasound imaging catheter. Am Heart J 1990;119(6):1392-400.
21. Soares CG, Halpern DG, Wang CK. Calibration and characterization of beta-particle sources for intravascular brachytherapy. Med Phys 1998;25(3):339-46.
22. Fox T, Soares C, Crocker I, Brooks K, Davis L. Calculated dose distributions of beta-particles sources used for intravascular brachytherapy. Int J Radiat Oncol Biology Physics 1997;39(2):334.
23. Haase J, Escaned J, van Swijndregt EM, Ozaki Y, Gronenschild E, Slager CJ, et al. Experimental validation of geometric and densitometric coronary measurements on the new generation Cardiovascular Angiography Analysis System (CAAS II). Cathet Cardiovasc Diagn 1993;30(2):104-14.
24. Di Mario C, Hermans WR, Rensing BJ, Serruys PW. Calibration using angiographic catheters as scaling devices--importance of filming the catheters not filled with contrast medium. Am J Cardiol 1992;69(16):1377-8.
25. Serruys PW, Foley DP, Kirkeeide RL, King SBd. Restenosis revisited: insights provided by quantitative coronary angiography. Am Heart J 1993;126(5):1243-67.
26. Erdreich LS, Lee ET. Use of relative operating characteristic analysis in epidemiology. A method for dealing with subjective judgement. Am J Epidemiol 1981;114(5):649-62.
27. Serruys PW, de Jaegere P, Kiemeneij F, Macaya C, Rutsch W, Heyndrickx G, et al. A comparison of balloon expandable stent implantation with balloon angioplasty in patients with coronary artery disease. N Engl J Med 1994;331:489-95.
28. Rensing BJ, Hermans WR, Deckers JW, de Feyter PJ, Serruys PW.

Which angiographic variable best describes functional status 6 months after successful single-vessel coronary balloon angioplasty? J Am Coll Cardiol 1993;21(2):317-24.
29. Foley DP, Melkert R, Serruys PW. Influence of coronary vessel size on renarrowing process and late angiographic outcome after successful balloon angioplasty. Circulation 1994;90(3):1239-51.
30. Kuntz RE, Gibson CM, Nobuyoshi M, Baim DS. Generalized model of restenosis after conventional balloon angioplasty, stenting and directional atherectomy. J Am Coll Cardiol 1993;21(1):15-25.
31. Rubin P, Williams JP, Riggs PN, Bartos S, Sarac T, Pomerantz R, et al. Cellular and molecular mechanisms of radiation inhibition of restenosis. Part I: role of the macrophage and platelet-derived growth factor. Int J Radiat Oncol Biol Phys 1998;40(4):929-41.
32. Rubin P, Soni A, Williams JP. The molecular and cellular biologic basis for the radiation treatment of benign proliferative diseases. Semin Radiat Oncol 1999;9(2):203-14.
33. Wilcox JN, Waksman R, King SB, Scott NA. The role of the adventitia in the arterial response to angioplasty: the effect of intravascular radiation. Int J Radiat Oncol Biol Phys 1996;36(4):789-96.
34. Scott NA, Cipolla GD, Ross CE, Dunn B, Martin FH, Simonet L, et al. Identification of a potential role for the adventitia in vascular lesion formation after balloon overstretch injury of porcine coronary arteries. Circulation 1996;93(12):2178-87.
35. Robinson KA. Animal models to study restenosis. In: Waksman R, editor. Vascular brachytherapy. Armonk: Futura Publishing Company, Inc.; 1999. p. 31-41.
36. Mintz GS, Popma JJ, Pichard AD, Kent KM, Satler LW, Wong SC, et al. Arterial remodeling after coronary angioplasty. A serial intravascular ultrasound study. Circulation 1996;94:35-43.
37. Waksman R, Rodríguez JC, Robinson KA, Cipolla GD, Crocker IR, Scott NA, et al. Effect of intravascular irradiation on cell proliferation, apoptosis, and vascular remodeling after balloon overstretch injury of porcine coronary arteries. Circulation 1997;96(6):1944-52.
38. Waksman R, Robinson KA, Crocker IR, Gravanis MB, Palmer SJ, Wang C, et al. Intracoronary radiation before stent implantation inhibits neointima formation in stented porcine coronary arteries. Circulation 1995;92(6):1383-6.
39. Drzymala RE, Mohan R, Brewster L, Chu J, Goitein M, Harms W, et al. Dose-volume histograms. International Journal of Radiation Oncology and Biological Physics 1991;21:71-78.
40. Viggars DA, Shalev S, Stewart M, Hahn P. The objective evaluation of alternative treatment plans III: the quantitative analysis of dose volume histograms. Int J Radiation Oncology Biol Phys 1992;23:419-27.
41. Panitsa E, Rosenwald JC, Kappas C. Developing a dose-volume histogram computation program for brachytherapy. Phys Med Biol 1998;43:2109-21.
42. Rahdert DA, Sweet WL, Tio FO, Janicki C, Duggan DM. Measurement of density and calcium in human atherosclerotic plaque and implications for arterial brachytherapy. Cardiovasc Radiat Med 1999;1(4):358-67.
43. Sabate M, Costa M, Kozuma K, Kay IP, van der Giessen WJ, Coen VLMA, et al. Geographical miss: a cause of treatment failure in radio-oncology applied to intracoronary radiation therapy. Circulation 2000;101(21):2467-71.
44. Costa MA, Sabate M, van der Giessen WJ, Kay IP, Cervinka P, Ligthart JM, et al. Late coronary occlusion after intracoronary brachytherapy. Circulation 1999;100(8):789-92.
45. Vodovotz Y, Waksman R, Kim WH, Bhargava B, Chan RC, Leon M. Effects of intracoronary radiation on thrombosis after balloon overstretch injury in the porcine model. Circulation 1999;100(25):2527-33.
46. Carlier SG, Marijnissen JPA, Coen VLMA, van der Giessen WJ, Sabate M, Ligthart J, et al. Comparison of brachytherapy strategies based on dose-volume histograms derived from quantitative intravascular ultrasound. Cardiovascular Radiation Medicine 1999;1(2):115-124.
47. Arbab-Zadeh A, DeMaria AN, Penny WF, Russo RJ, Kimura BJ, Bhargava V. Axial movement of the intravascular ultrasound probe during the cardiac cycle: implications for three-dimensional reconstruction and measurements of coronary dimensions. Am Heart J 1999;138 (5 Pt 1):865-72.
48. Di Mario C, Akiyama T, Moussa I, Reimers B, Jang YT, Tobis J, et al. First experience with imaging core wires. Semin Interv Cardiol 1997;2(1):69-73.

PART 5

Transthoracic Echocardiography for Biomechanical Assessment of the Left Ventricle and the Aorta

Chapter 17

Cardiovascular Echography.

N Bom, AFW van der Steen, CT Lancee, **SG Carlier**, N Bruining, CL de Korte, N de Jong, JRTC Roelandt.

Klinische Fysica 2000; 3:18-22.

Prof.dr.ir. N. Bom, Dr.ir. A.F.W. van der Steen, Dr.ir. C.T. Lancée, Drs. S.G. Carlier, Dr.ing. N. Bruining, Dr.ir. C.L. de Korte, Dr.ir. N. de Jong, Prof.dr. J.R.T.C. Roelandt.

Thoraxcentre, Erasmus University and University Hospital Rotterdam - Dijkzigt, and Interuniversity Cardiology Institute of the Netherlands

Cardiovascular Echography

Introduction

In 1953, Edler and Hertz [1] introduced the M-mode technique in Lund, Sweden allowing the recording of the motion pattern of cardiac structures along a single sound beam. They described many of the presently known echo patterns. Furthermore efforts were carried out to show two-dimensional sequential images of the heart. This was based on a mirror system with a yield of 7 frames per second (Åsberg et al. [2]). The phased array electronic sector scanner was first described by Somer in 1968 [3]. This system, originally introduced for neurology, has become the "working horse" of clinical cardiology today. The phased array transducer with its small "footprint" proved excellent for probe manoeuvrability between the ribs. First practical two-dimensional images of the moving heart, however, were obtained with an electronic scanner presented in 1971 in Rotterdam by Bom [4] and Kloster [5] and was based on the linear array technique. A survey on use of echo techniques in cardiology in 1980 in the Netherlands resulted in: a) application of M-mode with linear array by 32 % of the clinicians, b) exclusive M-mode by 32 %, c) M-mode with mechanical sector scan by 29 % and d) M-mode plus electronic sector scan by 7 % of the users. Thereafter the phased array technique became dominant in cardiology and linear arrays with the larger transducer footprint were increasingly used outside cardiology in for instance obstetrics, radiology and internal medicine.

An early invasive, catheter-based system for echo studies of the arteries and veins was described by Wells in 1966 [6]. This was based on mechanical rotation of the acoustic element. An electronic technique with 32 elements was described by Bom et al. in 1972 [7].

Only with the introduction of interventional cardiology and the balloon dilation methods in the mid-eighties, intravascular echography became important. A practical, mechanically rotated system was described around 1985 by Yock et al. and patented in 1989 [8].

The evolution of non-invasive echocardiography seems logical: from information along a single sound beam towards cross-sectional imaging. Thereafter, increase of the number of cross-sections (in the early years only two perpendicular cardiac planes were studied) to today's first applications of 3-dimensional echocardiography. Also intravascular and intracardiac echography started with a single beam in one direction only [9] and thereafter the imaging became 2D and recently 3D [10]. Overall there was improvement of image quality by better transducer characteristics and processing techniques.

Probe size, scan depth and resolution versus frequency.

In Figure 1, the frequency range of various cardiovascular applications is illustrated. Since attenuation increases with

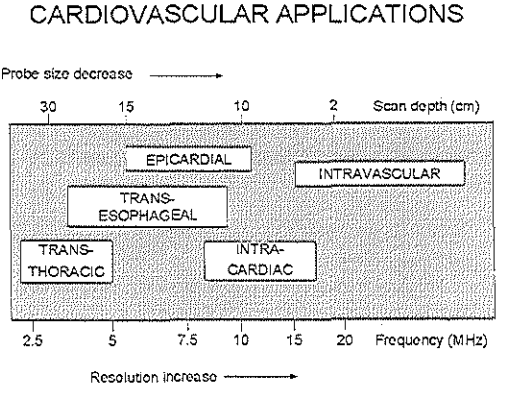

Fig. 1 Range of cardiovascular applications with optimal frequency.

frequency it becomes clear that for non-invasive echocardiography in adults (large depth range) low frequencies around 4 MHz must be used. The mid frequency range around 10 MHz is indicated for esophageal echo work in children or intracardiac imaging. At the high frequency, intravascular echography can be used since the distance from echo element to vascular wall to be investigated is very limited here. As can be observed from the figure, the used transducer size decreases with frequency. This is related with the acoustic active transducer surface, which for proper beam forming must encompass a given number of wavelengths. Echo transducers must have a broad frequency spectrum around the resonant frequency for proper depth resolution. With the introduction of contrast imaging in cardiology and based on the fact that in recent years the non linear properties of contrast as well as from tissue have been discovered, second harmonic imaging is becoming to be integrated in the echo instruments. This in turn requires very broadband transducers. A method described by de Jong et al [11] is based on integration of two phased array transducers with different resonant frequency into one. Apart from separation between contrast and tissue, harmonic imaging also decreases transducer near field reverberation and side lobe effects as illustrated in Figure 2.

Prof.dr.ir. N. Bom, Dr.ir. A.F.W. van der Steen, Dr.ir. C.T. Lancée, Dr.ing. N. Bruining, Dr.ir. C.L. de Korte and Dr.ir. N. de Jong *hold functions in the field of technology at the Cardiac Department of the Thoraxcentre.* **Drs. S.G. Carlier** *is a cardiologist as well as* **Prof.dr. J.R.T.C. Roelandt** *who is the Head of this department. Prof. Bom is also a Managing Director of the Interuniversity Cardiology Institute of the Netherlands (ICIN).*

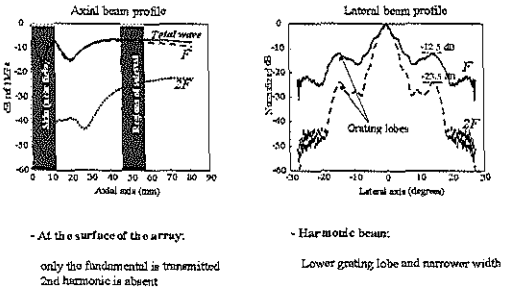

Fig. 2 Harmonic imaging decreases transducer near field reverberation as illustrated to the left. The harmonic beam pattern has a lower grating lobe and narrower main lobe thus reducing image artefacts (figure to the right).

Standard instruments versus small, battery-powered instruments.

In the cardiology department the standard- or laboratory instrument is rather bulky. It contains all the possible features and is mostly permanently located in either the echo- or function department, the operating theatre or the interventional laboratory. The following list indicates what type of parameters can be obtained or studies can be carried out with such machines:

- Measurement of cardiac anatomy, global function and regional wall motion.
- Valve pathology, severity and haemodynamic consequences (Doppler)
- Presence of pericardial fluid and mass lesions
- Doppler blood flow and tissue information (Tissue Doppler, backscatter analysis)
- Detection of ischemia or viability by stress echocardiography. Contrast agents can be injected to enhance the echo image. This technique is used to better visualise endocardial borders, enhance Doppler signals and to study myocardial perfusion. Exercise and pharmacological stress is used to induce ischaemic and regional motion abnormalities under stress conditions. Some applications require a transesophageal approach. On average an echocardiographic study in the echo lab would take approximately 25 minutes.

Handheld portable echo devices have been recently introduced on a large scale. An early system was the Minivisor. Roelandt [12,13] described first clinical experience in 1978 and 1980. However, for widespread use it was too early at the time. Now these systems are introduced for use in the ambulance, outpatient clinic, intensive care, post operative ward and at all other locations where in the hospital the cardiologists' advice is requested. Although the introduction is only beginning, it is foreseen that these devices will in particular be used for screening purposes and quick observations such as:

- Measurement of chamber/structure size.
- Detection of abnormal wall motion
- Diagnoses of valve pathology
- Observation of presence of pericardial fluid, mass lesions.

From two-dimensional (2D) to three-dimensional (3D) echocardiography.

Echocardiography is an interactive technique. The cardiologist or echo technician must aim the transducer at the diagnostic area of interest. For a proper echographic survey extensive experience in aiming at cardiac structures is needed. Since the heart is a complex three- dimensional organ there may be variability in the interpretation of difficult pathology amongst investigators. If the echo data were not limited to a number of selected cross-sectional imaging planes, but the full 3D data were available, then more accurate and reproducible data could become available obviating geometric assumptions. In 3D, the acquisition could become more standardised. In addition, observation may be carried out in reconstructed diagnostic cross-sections not available in standard 2D. Gradually all these advantages are becoming clear. So far the vast amount of data, complex transducer technology and display post processing time involved (all 3D results are not instantly available) have limited the advancement of 3D.

Free hand scanning.
In order to obtain spatially correct data, one of the approaches is to track the motion of an ultrasound 2D probe in space. This so-called "free-hand scanning" can be carried out with an acoustic (spark gap) locator as described by Moritz and Sherve in 1976 [14]. Electromagnetic location as described by Raab et al [15] and mechanical articulated arm reported by Dekker et al [16] are other methods.

Sequential triggered scanning.
With a stepper motor the acquisition plane is sequentially rotated by, for instance, steps of 2 degrees. When acquisition is time gated by triggering derived from the electrocardiogram and respiration, all data become available to reconstruct the moving heart in its proper geometry and time sequence. Obviously, the transducer should be held steady during the acquisition period otherwise motion artefacts are introduced.

Fast acquisition systems.
Presently two systems have been described where the acquisition is so fast that virtually no motion artefacts will occur. Firstly this is the electronic real time volumetric ultrasound imaging system developed at Duke University by Von Ramm and Smith [17]. They use a novel matrix phased array transducer in which the elements are arranged in a two dimensional grid. With insonification in a wide cone and parallel processing in reception fast 3D (or selected 2D) display becomes available. Lancée and Djoa described another approach [18]. They use a fast rotating phased array transducer enabling acquisition of 16 volumetric data sets of the beating heart per second. A photograph of this probe is shown in Figure 3.

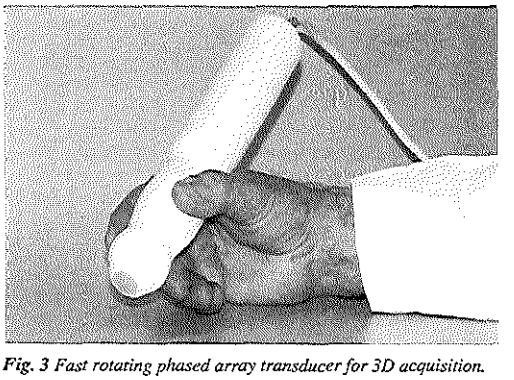

Fig. 3 Fast rotating phased array transducer for 3D acquisition.

Display methods.
The collected two-dimensional images are digitised and realigned according to their spatial and temporal sequences. Interpolation algorithms are applied and as a following step the display principle must be selected. Examples are:

- Mainplane (orthogonal)
- The anyplane method where arbitrarily diagnostic cross-sectional views of the heart which are difficult or physically impossible to obtain from conventional acoustic windows can be computed.
- Paraplane views
- A wire-frame display might be selected where 3D images of a specific structure are presented.
- A volume rendered display for depth perception with for instance gradient shading.

After surface detection reconstructions can be rotated in space to look at them from different perspectives.

An example of a 3D rendered image of the heart valves is illustrated in figure 4 [19]. With the introduction of real time acquisition of 3D and faster computers, the use of 3D will become much more practical. Today the method is particularly indicated for congenital diagnosis of heart disease and for correct calculation of volumetric parameters.

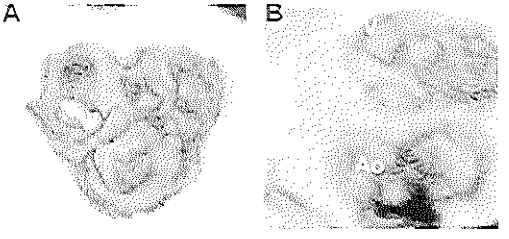

Fig. 4 3D rendered image of the heart valves. Attachment of small vegetation to the cusps of the aortic valve (panel A) and the pulmonary valve (panel B) are visualised. PV = pulmonary valve. Ao = aortic valve.

Intravascular ultrasound (IVUS)

The technique of intravascular ultrasound is based on the flex-shaft mechanically rotated single element or the electronically steered phased array method, with or without the use of a guide wire (figure 5). They produce cross-sectional vascular real-time images of the lumen, plaque and arterial wall [20]. An example of an intravascular image of an artery is shown in Figure 6. Mostly the intravascular procedure is applied for further decision-making when X-ray angiographic data are less conclusive. For obvious reasons there is a strong urge to combine "see and do" in interventional procedures. This leads to catheters in which, for instance, an angioplasty balloon is combined with ultrasonic imaging in or close to the balloon. Other combinations may provide guidance during stent implantation. Since intravascular imaging provides accurate geometrical information within the cross-section, combination with other interventional procedures is likely to expand in future. In this category falls the assessment of the dose deposited in the arterial wall during intracoronary brachytherapy or by radioactive stents as described by Carlier [21]

Additional parameters
Where present, intravascular scanners yield detailed cross-sectional geometric information of the arterial wall. For the evaluation of the arterial function the remaining blood flow

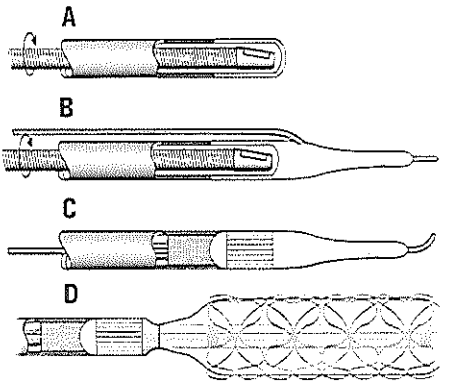

Fig. 5 Schematic drawing of present intravascular echo catheters. Flex-shaft mechanically rotated element method (A), with guide wire (B), electronical beam switching (C) and a combination of electronic switching with a the therapeutic stent placing technique (D).

through the obstruction is also an important parameter. Using a decorrelation technique with the Radio Frequency (RF) echo signal, sequentially obtained at the same location, it seems possible to combine imaging with measurement of instantaneous volume flow through the lumen. An example of this technique is illustrated in Figure 7, where blood velocity is colour-coded, and instantaneous flow estimated along several cardiac cycles is in agreement with flow derived from conventional intracoronary Doppler measurements [22, 23].
First attempts have shown that RF echo data also enable the assessment of mechanical properties of the arterial wall. In this approach, the echo data are compared in the same location, but at different pressures [24].

3D imaging and quantitative data
All organs have a three-dimensional configuration and therefore the concept of ultrasonic 3D imaging has become

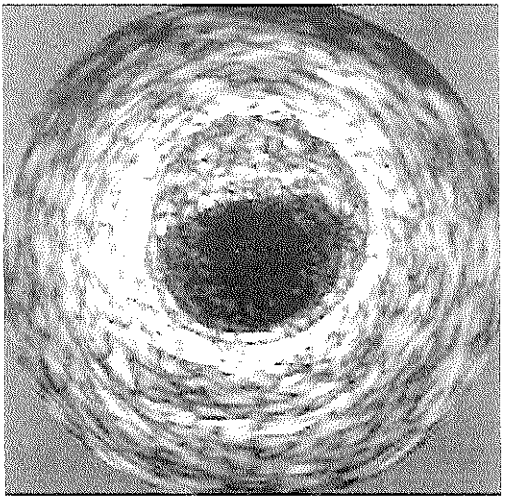

Fig. 6 Example of an intravascular image with a lesion between 10 and 2 o'clock.

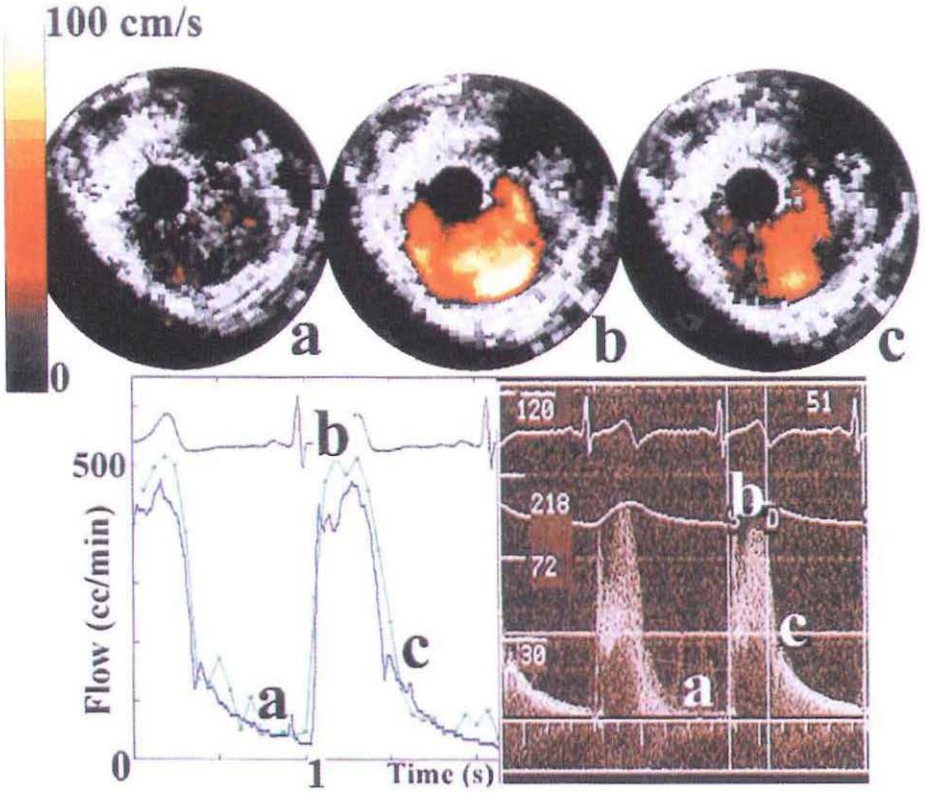

Fig. 7 Image and local colour-coded blood velocity yielding volume flow during various phases of the cardiac cycle (a, b and c) with corresponding Doppler recording (bottom).

increasingly important. In non-invasive echo imaging real-time volumetric echo data acquisition has been described. It is not expected that this will become possible in real-time intravascular methods since it will always require pullback of the catheter in order to accumulate all the necessary data. Such a device enables data acquisition for the construction of arterial 3D images, which are very informative as illustrated for control of stent deployment in Figure 8.
Based on 3D echo-data files, it has become possible, with interactive semi-automatic contour analyses, to obtain precise quantitative information on plaque volume and open lumen over the entire arterial segment studied.

Conclusion

Echocardiography has seen an enormous development from the first poor images up to now. It has (with integrated Doppler which is dealt with in another chapter in this issue) amongst the other imaging techniques such as CT or MRI taken the position of primary diagnostic method in cardiology. The 3D use is still in its infancy but undoubtedly it will break through in the coming years. We have noted the introduction of small rather cheap devices that will further expand diagnostic echocardiography.
The use of echo catheters for intravascular applications is much more recent, and it is limited by the expenditure due to single use of these devices. If these catheters become cheap, and combined with therapeutic devices, things will change.

Future intravascular scanners will provide improved image quality, have interventional therapeutic capabilities incorporated and possibly be combined with other diagnostic methods such as Raman spectroscopy. Furthermore, 3D display and quantitative data extraction will become more and more routine rather than research.

Acknowledgement

Authors would like to thank the Technology Foundation (STW) of the Netherlands for their support of our Thoraxcentre Rotterdam and Inter University Cardiology (ICIN) projects.

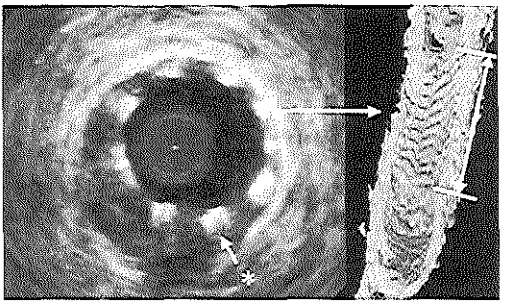

Fig. 8 Echo image of stent with struts(*) and corresponding 3D image.

References

1. Edler I, Hertz C (1954) The use of the ultrasonic reflectoscope for the continuous recording of movements of heart walls. Kungl Fysiogr Sällsk Lund Förhandl: 24(5): 40-58.
2. Åsberg A (1967) Ultrasonic cinematography of the living heart. Ultrasonics: April: 113-117.
3. omer JC (1968) Electronic sector scanning for ultrasonic diagnosis. Progress Report Institute of Medical Physics TNO: August: 37-43.
4. Born N, Lancée CT, Honkoop J, Hugenholtz PG (1971) Ultrasonic viewer for cross-sectional analysis of moving cardiac structures. Biomed-Engng 6: 500-503 and 508.
5. Kloster FE, Roelandt J, Ten Cate FJ, Born N (1973) Multiscan echo-cardiog--raphy Part II: Technique and initial clinical results. Circulation XLVII: 1075-1084.
6. Wells PNT (1966) Developments in Medical Electronics. World Med Electron 66(4): 272-277.
7. Born N, Lancée CT, Van Egmond FC (1972) An ultrasonic intracardiac scanner. Ultrasonics 10: 72-76.
8. Yock PG (inventor) Catheter apparatus, system and method for intravascular two-dimensional ultrasonography. US Patent 4,794,931 issued Jan. 3, 1989.
9. Cieszynski T (1960) Intracardiac method for the investigation of structure of the heart with the aid of ultrasonics. Arch Immun Ter Dow 8: 551-557.
10. Von Birgelen C, de Vrey EA, Mintz GS, Nicosia A, Bruining N, Li W, Slager CJ, Roelandt JRTC, Serruys PW, de Feyter PJ (1997) ECG-gated three-dimensional intravascular ultrasound: feasibility and reproducibility of an automated analysis of coronary lumen and atherosclerotic plaque dimensions in humans. Circulation 96: 2944-2952.
11. De Jong N, Bouakaz A, Frinking P (2000) Design of a phased array transducer for contrast imaging. In: Ten Cate FJ, De Jong N, Cosgrove D (eds) Abstracts of the Fifth Heart Centre Symposium on Ultrasound Contrast Imaging. Rotterdam, January 20-21: pp13-15.
12. Roelandt J, Wladimiroff JW, Baars AM (1978) Ultrasonic real time imaging with a hand-held scanner (Part II: Initial clinical ex-perience). Ultrasound Med Biol 4: 93-97.
13. Roelandt J, Born K, Hugenholtz PG (1980) The ultrasound cardioscope: A hand-held scanner for real-time cardiac imaging. J Clin Ultra-sound 8: 221-225.
14. Moritz WE, Shreve PL (1976) A microprocessor-based spatial locating system for use with diagnostic ultrasound. IEEE Trans Biomed Eng: 96-974.
15. Raab FH, Blood EB, Steiner TO, et al (1993) Three-dimensional colour Doppler imaging. Ultrasound Med Biol 19: 95-104.
16. Dekker DL, Piziali RL, Dong E, Jr (1974). A system for ultrasonically imaging the human heart in three dimensions. Comput Biomed Res 7: 544-553.
17. Von Ramm OT, Smith SW (1990). Real time volumetric ultrasound imaging system. J Digit Imaging 3: 261-266.
18. Djoa KK, de Jong N, van Egmond FC, Kasprzak JD, Vletter WB, Lancée CT, van der Steen AFW, Born N, Roelandt JRTC (2000) A fast rotating scanning unit for real-time three-dimensional echo data acquisition. Ultrasound Med Biol 26: 863-869.
19. Roelandt JRTC (ed.) (2000) Three-dimensional Echocardiography of the Heart and Coronary Arteries. Alphen aan de Rijn, Van Zuiden Publications: p. 171.
20. Ji-Bin Liu, Goldberg BB, eds. (1998) Endoluminal Ultrasound. London, Martin Dunitz.
21. Carlier SG, Marijnisson JPA, Coen VLMA, Sabaté M, Kay IP, van der Giessen WJ, Ligthart J, den Boer A, Levendag PC, Serruys PW (1999) Comparison of brachytherapy strategies based on dose-volume histograms derived from quantative intravascular ultrasound. Cardiovascular Radiation Medicine 1(2): 115-124.
22. Carlier SG, Céspedes EI, Li W, Mastik F, van der Steen AFW, Born N, Serruys PW (1998). Blood flow assessment with intravascular ultrasound catheters: the ideal tool for simultaneous assessment of the coronary haemodynamics and vessel wall?. Semin Intervent Cardiol 3: 21-29.
23. Born N, Carlier SG, van der Steen AFW, Lancée CT (2000). Intravascular Scanners. Ultrasound Med Biol 26 (Suppl. 1): S6-S9.
24. Korte C.L. de, Pasterkamp G, van der Steen AFW, Born N (2000) Characterization of Plaque Components using Intravascular Ultrasound Elastography in human femoral and coronary arteries in vitro. Circulation 102: 617-623.

Address for correspondence:
Prof. dr ir N. Born
Erasmus University Rotterdam
Thoraxcentre Ee 2302
P.O. Box 1738
3000 DR Rotterdam, the Netherlands
Tel. +31 10 408 8030 - Fax +31 10 408 9445
e-mail: born@tch.fgg.eur.nl

Chapter 18

Non-invasive characterization of total arterial compliance by simultaneous acquisition of pressure and flow: advantages of the pulse pressure method.

S Carlier, P Segers, A Pasquet, G Armstrong, NL Greenberg, N Stergiopulos, T Marwick, JD Thomas.

Computers in Cardiology.IEEE Computer Society Press, 1998; p 665-668.

Non-invasive Characterization of Total Arterial Compliance by Simultaneous Acquisition of Pressure and Flow: Advantages of the Pulse Pressure Method

S Carlier, P Segers*, A Pasquet, G Armstrong, N L Greenberg,
N Stergiopulos+, T Marwick, J D Thomas

Cleveland Clinic Foundation, Cleveland, Ohio
*Hydraulics Laboratory - Institute Biomedical Technology, University Gent, Belgium
+Biomedical Engineering Laboratory, Swiss Federal Institute of Technology, Lausanne, Switzerland

Abstract

We compare three proposed indices of total arterial compliance (Ctot) in normal volunteers (n=9) and patients with coronary artery disease (n=14) using a non-invasive approach (echo-Doppler and carotid tonometry): (1) the pulse pressure method (PPM), (2) the area method (AM) and (3) the stroke volume-to-pulse pressure ratio (SV/PP).

The best agreement was found between the PPM and SV/PP. Compliance estimates were lower in the patient group (PPM: 1.2±0.4 vs. 1.6±0.2; AM: 1.6±0.6 vs. 2.8±1.3; SV/PP: 1.8±0.6 vs. 2.4±0.4), being older (64±14 vs. 35±4 y) and with known atherosclerosis. The best correlation between compliance and age was found with PPM (r^2=0.52). AM varied with the chosen computation interval in diastole. These preliminary data describing the very first use of the PPM on non-invasive human recordings suggest that PPM could be a more robust estimator of Ctot than the widely used AM, and that SV/PP could be a reasonable simpler surrogate.

1. Introduction

Total arterial compliance (Ctot) is by definition the increment of volume of the systemic arterial bed (dV) for an increment in distending pressure (dP): Ctot= dV / dP.

Ctot is an important determinant of ventricular afterload and is directly related to the arterial stiffness of the large arteries. It expresses the ability to store blood in systole, mainly in the proximal aorta, without excessive pressure rise. This biomechanical property also allows optimal coronary flow in diastole.[1] Total peripheral resistance, easily measured as the ratio of mean blood pressure and cardiac output, reflects the non-pulsatile cardiac load. Conversely, Ctot allows estimation of the pulsatile load. Although very important to measure because of its changes with ageing[2] or with physiopathological conditions such as hypertension[3], direct Ctot evaluation can not be exactly performed in-vivo because of the difficulty to measure dV. Moreover the overall pressure-volume relationship of the arterial bed is nonlinear and varies with the absolute level of P.[4] Consequently, different indirect methods have been proposed, but none has been universally accepted.[5]

Almost all estimations of Ctot rely on the assumption that the vascular bed behaves like a windkessel (WK, =capacitance chamber), following Hales' original idea.[6] Early methods were based on the diastolic decay of the blood pressure, approximated by a monoexponential. An integral variation of this principle has been described by Liu[7] and has been extensively used in various physiopathological conditions.[8-10]

The ratio of stroke volume (SV) and pulse pressure (PP=systolic P– diastolic P) is a crude estimate of Ctot which was introduced by Remington et al.[11]. Although it might violate the fundamental concept of the WK, the interest of this readily obtained parameter, has been stressed recently.[12, 13]

The pulse pressure method (PPM) has been introduced by Stergiopulos et al.[14] PPM is based on a recursive evaluation of Ctot by comparing the measured PP and the one computed in a 2-element WK with the measured flow as input. Comparison with other methods has been described in a computerized distributed model of the arterial circulation.[5] The purpose of this study was (i) to evaluate the feasibility of the PPM on non-invasive human recordings, and (ii) to compare the three Ctot estimates.

2. Materials and methods

2.1. Patient data

In 9 normal subjects (34 ± 5 yrs) and 14 patients (62 ± 12 yrs) with known coronary artery disease, applanation

0276-6547/98 $10.00 © 1998 IEEE

tonometry was performed at the carotid level using a Millar SPT-301 pen-like transducer. Calibration was performed with the mean (calculated as [2x diastolic BP + systolic BP]/3) and the diastolic brachial blood pressure (BP – sphygmomanometer). Simultaneously, audio Doppler signals from an echocardiographic system (ATL HDI 3000) were acquired with an A/D board (Wavebook/512, IOTech Inc.) and a laptop. Customized software allowed spectral computation and automatic detection of the maximal velocity contour. Aortic (Ao) flow was computed as cross-sectional area of the left ventricular outflow tract times Ao velocity (Doppler echocardiography). The ECG was measured along the complete procedure. Post-processing by averaging multiple beats allowed reconstructing pressure (P_{car}) and flow data (Q_{ao}) for one representative heart cycle. The aortic PP was considered equal to the carotid PP.

2.2. Total arterial compliance

In the 2-element windkessel model, the whole arterial tree is modeled as an elastic chamber with a constant compliance (C) in parallel with the vascular resistance (R) calculated as mean pressure/ cardiac output (CO). The governing equation in the frequency domain is:

$$Z_{in} = \frac{R}{1 + j\omega RC}$$

where $\omega=2\pi f$, f is the frequency, Z_{in} is the input impedance, R is mean BP / mean Qao and C compliance.

In the area method (AM), compliance is calculated as:

$$RC = \int_{t_1}^{t_2} P dt / (P_1 - P_2)$$

where t_1 and t_2= time of start and end of the interval for Ctot evaluation, P_1 is pressure at t_1, P_2 at t_2

We compared the values of C derived for the intervals [t1 ;t2] corresponding (i) to the mid-third of diastole ($C_{AM2/3}$) and (ii) to the last third of the diastole ($C_{AM3/3}$).

The pulse pressure method (PPM) is based on the fact that the modulus of the input impedance of the arterial system is represented very well by the 2-element WK model for the low frequencies (1st to ~5th harmonics). A gross low frequency feature like the pulse pressure (PP) is thus similar in the true arterial tree and the 2-element WK. The method is based on an iterative scheme based that finds the value of C that gives the best fit between the measured PP and the PP predicted by the 2-element WK, using as input the measured flow (Q_{ao}) and R.

3. Results

3.1. Patient data

An overview of measured and computed hemodynamic data is given in Table 1. As expected, PP_{car}, $C_{AM2/3}$, C_{PPM}, $C_{SV/PP}$ were significantly different between the young normal controls and the older patients presenting known coronary artery disease, but $C_{AM3/3}$ was unable to differentiate the two groups.

	Controls (n=9)	Patients (n=14)
age (yrs)	35±4	64±14*
SBP (mmHg)	133±11	144±16
DBP (mmHg)	91±7	87±9
MBP (mmHg)	105±7	106±10
HR (/min)	71±8	70±9
CO (l/min)	5.0±1.1	5.2±1.4
PP_{car} (mmHg)	31±6	45±10*
$C_{AM2/3}$ (ml/mmHg)	2.8±1.3	1.6±0.6*
$C_{AM3/3}$ (ml/mmHg)	2.2±0.5	2.1±0.8
C_{PPM} (ml/mmHg)	1.6±0.2	1.2±0.4*
$C_{SV/PP}$ (ml/mmHg)	2.4±0.4	1.8±0.6*

Table 1. Mean value and standard deviation of hemodynamic data (SBP, DBP, MBP: systolic, diastolic and mean sphygmomanometric blood pressure; HR: heart rate; CO: cardiac output), PP_{car} carotid tonometric pulse pressure, $C_{AM2/3}$ compliance with AM computed on last 2 third of diastole, $C_{AM3/3}$ is computed on the last third of diastole, C_{PPM} compliance with the PPM and $C_{SV/PP}$ compliance calculated with the stroke volume-to-aortic pulse pressure ratio. *: P<0.001

3.2. Relationship between C_{PPM}, C_{AM}, $C_{SV/PP}$

Figure 1a demonstrates the best correlation which was found between C_{PPM} and $C_{SV/PP}$ ($C_{SV/PP}$=1.5xC_{PPM} – 0.04, r^2=0.94). $C_{AM3/3}$ was poorly correlated with C_{PPM} (figure 1b) and $C_{SV/PP}$ (r^2= 0.35 and 0.32, respectively). The correlations between $C_{AM2/3}$ and C_{PPM} or $C_{SV/PP}$ were even worse. There was a rather large difference between $C_{AM2/3}$ and $C_{AM3/3}$: the mean difference between individual values of $C_{AM2/3}$ and $C_{AM3/3}$ was –0.12±1.1, for an overall mean value of C of 2.1 ml/mmHg.

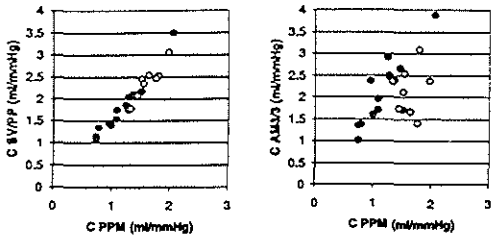

Figure 1: a) left: relationship between total arterial compliance estimated non-invasively by the pulse pressure method (C_{PPM}) and the stroke volume-to-aortic pulse ratio (Csv/PP); b) right: relationship between C_{PPM} and the Ctot estimation from the area method ($C_{AM3/3}$). (controls: open, patients filled circles)

3.3. Evolution of Ctot with age

The best correlation between Ctot and age, showing a statistically significant decrease, was found with C_{PPM}: C_{PPM} = 0.015 x Age + 2.145, r^2=0.52, p=0.0002). As illustrated on figure 2, the relationship between age and $C_{AM2/3}$ demonstrated more scattering of the data, with a r^2 of only 0.26 (p=0.01). The correlation with $C_{SV/PP}$ was intermediate (r^2=0.45, p=0.0006). There was no correlation between age and $C_{AM3/3}$.

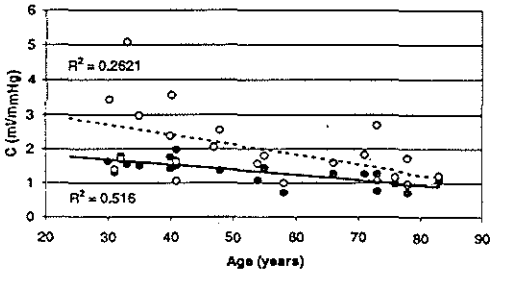

Figure 2: The correlation between age and C_{PPM} (filled circle) was significantly higher than with C_{AM} (open circles).

4. Discussion and conclusion

We describe the first non-invasive evaluation of total arterial compliance with the pulse pressure method in human subjects. We have compared the results with two previously reported methods: the area method and the stroke volume-to-aortic pulse pressure ratio.

The area method was calculated over two different intervals: the mid-third ($C_{AM2/3}$) and the last third ($C_{AM3/3}$) of the diastole. It is believed that the chosen interval is not important,[7] but our results demonstrated that the two derived estimations of Ctot are not interchangeable. The compliance derived from the area method is a value for the mean pressure in the chosen interval of integration. The compliance of the large arteries decreases non-linearly with an increasing pressure.[4] This was not reflected by the average difference between $C_{AM2/3}$ and $C_{AM3/3}$ that we found (-0.12 ml/mmHg). Moreover, there was a large interval of agreement between $C_{AM2/3}$ and $C_{AM3/3}$: the standard deviation of the differences was 1.1 ml/mmHg for an overall mean compliance value of 2.1 ml/mmHg. These discrepancies could be related to an inherent additional noise added on the pressure signals that we recorded non-invasively with a tonometer at the carotid level. We tried to reduce the artefacts by maintaining a constant holding pressure of the transducer and by using a representative pressure recording that was the average of at least 5 to7 good-looking cycles out of a continuous recording of minimum 30 seconds. The AM, which uses only the mean cardiac output to compute mean peripheral resistance, does not take into account the whole body of information included in the complete flow profile available with simultaneous Doppler echo-cardiography performed at the level of the aortic valve.

The pulse pressure method and the stroke volume-to-aortic pulse pressure ratio rely only on a gross feature of the pressure recording: the systolo-diastolic pulse. In a computer model of the arterial tree, Stergiopoulos et al. found that the PPM proved to be the most accurate of all the methods reported to evaluate total arterial compliance.[5] We demonstrated the feasibility to apply the PPM on non-invasive human recordings. We found a very close correlation between C_{PPM} and $C_{SV/PP}$ (r^2=0.94) which was recently demonstrated as a very good surrogate of Ctot (using invasive recordings of aortic pressure and thermodilution in 31 catheterized patients).[13] A limitation of our method is related to the assumption that the carotid tonometric pressure is similar to the aortic pressure, but invasive recordings have demonstrated a very close similitude between aortic and carotid recordings.[15] Moreover, possible other sources of errors are introduced into our measurements via the calibration of the tonometer to the mean and diastolic sphygmomanometer pressure: diastolic blood pressure presents probably a slow decrease along the arterial tree and the computation of MBP=(SBP+2.DBP)/3 may vary with age or cardiovascular disease. Nevertheless, the same limitations are present for the area method. The PPM demonstrated the best differentiation between the controls and the investigated patients being older, with known coronary artery disease and who were expected to present a lower compliance.

SV/PP estimates of compliance were higher than the PPM. This is expected because the SV/PP method assumes that the complete stroke volume is buffered in the large elastic arteries in systole, without any flow to the periphery. However, there is a continuous flow towards the capillaries and the volume increase (dV) during the ejection is only a fraction of SV.

With C_{PPM} and C_{AM}, Ctot is estimated at different pressures: C_{PPM} corresponds to the mean pressure whereas C_{AM} is the compliance at the mean pressure during the integration interval. This can explain why C_{AM} was higher than C_{PPM}.

With ageing and the development of atherosclerosis, stiffening of the arterial tree occurs, lowering Ctot. The reported amplitude of the decrease of compliance with age[8,12] was in good agreement with our findings. We found that the relationship between age and C_{PPM} was stronger (r^2=0.52, p=0.0006) than between age and C_{AM} or $C_{SV/PP}$.

In conclusion, we have demonstrated the feasibility to estimate total arterial compliance non-invasively in human subjects with the pulse pressure method. Our observations suggest that overall, the pulse pressure method appears to be a more robust estimator of Ctot for non-invasive applications. The stroke volume-to-pulse pressure could be a reasonable simpler surrogate.

Acknowledgements

Dr. Carlier was the recipient of a fellowship of the Belgian American Educational Foundation and of the NATO. This research was also funded by a research grant of the Flemish Institute for the Promotion of the Scientific-Technological Research in Industry, Brussels (IWT/OZM/960250).

References

[1] D. A. Kass, A. Saeki, R. S. Tunin, and F. A. Recchia, "Adverse influence of systemic vascular stiffening on cardiac dysfunction and adaptation to acute coronary occlusion," *Circulation*, vol. 93, pp. 1533-1541, 1996.

[2] A. Avolio, D. F. Quan, W. Q. Li, and e. al., "Effects of ageing on arterial distensibility in populations with high and low prevalence of hypertension: comparison between urban and rural communities," *Circulation*, vol. 71, pp. 202-210, 1985.

[3] M. Weber, D. Smith, J. Neutel, and W. Graettinger, "Arterial properties of early hypertension," *Journal of Human Hypertension*, vol. 5, pp. 417-423, 1991.

[4] G. J. Langewouters, K. H. Wesseling, and W. J. A. Goedhard, "The static elastic properties of 45 human thoracic and 20 abdominal aortas in vitro and the parameters of a new model," *Journal of Biomechanics*, vol. 17, pp. 425-435, 1984.

[5] N. Stergiopulos, J. J. Meister, and N. Westerhof, "Evaluation of methods for estimation of total arterial compliance," *American Journal of Physiology*, vol. 268, pp. H1540-H1548, 1995.

[6] S. Hales, "Statistical Essays: Containing Haemastaticks, vol 2. London: Innys and Manby, 1733. Reprint, n. 22, History of Medicine Series, Library of New York Academy of Medicine, New York: Hafner Publishing, 1964.

[7] Z. Liu, K. P. Brin, and F. C. P. Yin, "Estimation of total arterial compliance: an improved method and evaluation of current methods," *American Journal of Physiology*, vol. 251 (Heart Circ. Physiol. 20), pp. H588-H600, 1986.

[8] R. H. Marcus, C. Korcarz, G. McCray, A. Neumann et al., "Noninvasive method for determination of arterial compliance using Doppler Echocardiography and subclavian pulse tracings. Validation and clinical application of a physiological model of the circulation," *Circulation*, vol. 89, pp. 2688-2699, 1994.

[9] A. Poppas, S. G. Shroff, C. E. Korcarz, J. U. Hibbard, D. S. Berger, M. D. Lindheimer, and R. M. Lang, "Serial assessment of the cardiovascular system in normal pregnancy. Role of arterial compliance and pulsatile arterial load," *Circulation*, vol. 95, pp. 2407-2415, 1997.

[10] B. A. Kingwell, K. L. Berry, J. D. Cameron, G. L. Jennings, and A. M. Dart, "Arterial compliance increases after moderate-intensity cycling," *American Journal of Physiology*, vol. 273 (Heart Circ. Physiol. 42), pp. H2186-H2191, 1997.

[11] J. W. Remington, C. B. Nobach, W. F. Hamilton, and J. J. Gold, "Volume elasticity characteristics of the human aorta and the prediction of stroke volume from the pressure pulse," *American Journal of Physiology*, vol. 153, pp. 198-308, 1948.

[12] G. de Simone, M. J. Roman, S. R. Daniels, G. Mureddu, T. R. Kimball, R. Greco, and R. B. Devereux, "Age-related changes in total arteral capacitance from birth to maturity in a normotensive population," *Hypertension*, vol. 29, pp. 1213-1217, 1997.

[13] D. Chemla, J.-L. Hebert, C. Coirault, K. Zamani, I. Suard, P. Colin, and Y. Lecarpentier, "Total arterial compliance estimated by stroke volume-to-aortic pulse pressure ratio in humans," *American Journal of Physiology*, vol. Heart Circ. Physiol. 43, pp. H500-H505, 1998.

[14] N. Stergiopulos, J. J. Meister, and N. Westerhof, "Simple and accurate way for estimating total and segmental arterial compliance: the pulse presure method," *Annals of Biomedical Engineering*, vol. 22, pp. 392-397, 1994.

[15] C. H. Chen, C. T. Ting, A. Nussbacher, E. Nevo, D. Kass et al., "Validation of carotid artery tonometry as a means of estimating augmentation index of ascending aortic pressure," *Circulation*, vol. 27, pp. 168-175, 1996.

Address for correspondence:
Dr. J D Thomas
Cardiovascular Imaging/F15 -The Cleveland Clinic Foundation
9500 Euclid Avenue
Cleveland OH 44195

or e-mail: SGCARLIER@HOTMAIL.COM

Chapter 19

Individualizing the aorta-radial pressure transfer function: feasibility of a model-based approach.

P Segers, S Carlier, A Pasquet, SI Rabben, LR Hellevik, E Remme, T De Backer, J De Sutter, JD Thomas, P Verdonck.

American Journal of Physiology (Heart Circ Physiol) 2000, 279:H542-H549.

Am J Physiol Heart Circ Physiol
279: H542–H549, 2000.

Individualizing the aorto-radial pressure transfer function: feasibility of a model-based approach

P. SEGERS,[1] S. CARLIER,[2] A. PASQUET,[2] S. I. RABBEN,[3] L. R. HELLEVIK,[3] E. REMME,[3] T. DE BACKER,[4] J. DE SUTTER,[4] J. D. THOMAS,[2] AND P. VERDONCK[1]
[1]*Hydraulics Laboratory, Institute of Biomedical Technology, University of Gent, 9000 Gent, Belgium;* [2]*The Cleveland Clinic Foundation, Cleveland, Ohio 44195;* [3]*Norwegian University of Science and Technology, Trondheim, Norway; and* [4]*Cardiology Department, University Hospital, University of Gent, Belgium*

Received 11 March 1999; accepted in final form 4 February 2000

Segers, P., S. Carlier, A. Pasquet, S. I. Rabben, L. R. Hellevik, E. Remme, T. De Backer, J. De Sutter, J. D. Thomas, and P. Verdonck. Individualizing the aorto-radial pressure transfer function: feasibility of a model-based approach. *Am J Physiol Heart Circ Physiol* 279: H542–H549, 2000.—We fitted a three-segment transmission line model for the radial-carotid/aorta pressure transfer function (TFF) in 31 controls and 30 patients with coronary artery disease using noninvasively measured (tonometry) radial and carotid artery pressures (P_{car}). Except for the distal reflection coefficient (0.85 ± 0.21 in patients vs. 0.71 ± 0.25 in controls; $P < 0.05$), model parameters were not different between patients or controls. Parameters were not related to blood pressure, age, or heart rate. We further assessed a point-to-point averaged TFF (TFF_{avg}) as well as upper (TFF_{max}) and lower (TFF_{min}) enveloping TFF. Pulse pressure (PP) and augmentation index (AIx) were derived on original and reconstructed P_{car} ($P_{car,r}$). TFF_{avg} yielded closest morphological agreement between P_{car} and $P_{car,r}$ (root mean square = 4.3 ± 2.3 mmHg), and TFF_{avg} best predicted PP (41.5 ± 11.8 vs. 41.1 ± 10.0 mmHg measured) and AIx (−0.02 ± 0.19 vs. 0.01 ± 0.19). PP and AIx, calculated from P_{car} or $P_{car,r}$, were higher in patients than in controls, irrespectively of the TFF used. We conclude that *1*) averaged TFF yield significant discrepancies between reconstructed and measured pressure waveforms and subsequent derived AIx; and *2*) different TFFs seem to preserve the information in the pressure wave that discriminates between controls and patients.

blood pressure; model; applanation tonometry

KNOWLEDGE OF CENTRAL AORTA PRESSURE is clinically important because it permits, together with aortic flow, one to compute arterial input impedance and hemodynamic parameters characterizing ventricular-arterial interaction (wave reflection indexes, hydraulic power) of diagnostic value in cardiology (1, 5, 14, 19). Using tonometry, one can estimate, noninvasively, the central aortic pressure wave by measuring the arterial pulse *1*) at a superficial artery close enough to the heart (subclavian, carotid artery) so that the effects of wave distortion can be neglected (1, 5, 6, 14, 16), or *2*) at a peripheral superficial artery (radial or carotid artery) with use of a pressure transfer function (TFF) to compute the pressure wave at the central aorta (4, 7–9, 12).

Averaging transfer functions, measured directly in (relatively) large human populations, yielded generalized TFF for the radial-aorta (7, 12) and the carotid-aorta (11) pathway. Such generalized TFF have been integrated into commercially available systems, predicting central aorta pressure and derived indexes, such as the augmentation index (AIx), from the carotid or radial artery pressure wave (4, 23). However, there is large scatter in measured transfer functions, and the morphology of reconstructed central pressure, using such a generalized TFF, may differ considerably from the directly measured pressure.

The aim of this work was to provide a method to individualize TFF, based on a transmission line model for the radial-aortic/carotid pathway (9). If model parameters characterizing the pressure transfer function are related to easily measured patient characteristics (age, blood pressure, etc.), then TFF can be predicted on a patient-to-patient basis, enabling a better estimate of the central aorta pressure wave morphology. First, we fitted the model to a published radial-aorta pressure transfer function that was derived from invasively recorded pressures (7). This way, we obtained reference values for all model parameters. Second, we fitted the model to (noninvasively) measured radial-carotid transfer functions in controls and in patients using a selected number of model parameters, and we studied the correlation between these model parameters and easily measured hemodynamic indexes. Because we were unable to assess any relation, we further studied the impact of using upper and lower limit transfer functions, enveloping measured data, on estimated central blood pressure and on derived indexes such as pulse pressure (PP) and the AIx.

Address for reprint requests and other correspondence: P. Segers, Hydraulics Laboratory, Institute Biomedical Technology, Univ. of Gent, Sint-Pietersnieuwstraat 41, B-9000 Gent, Belgium (E-mail: patrick.segers@navier.rug.ac.be).

The costs of publication of this article were defrayed in part by the payment of page charges. The article must therefore be hereby marked "*advertisement*" in accordance with 18 U.S.C. Section 1734 solely to indicate this fact.

MATERIALS AND METHODS

Transmission Line Model For Radial-Aortic/Carotid Pathway

The model simulating the aorta-radial pathway is analoguous to the model used by Karamanoglu and Fenely (9) for the finger carotid pathway and consists of a stepwise tapered transmission line with three segments (proximal, middle, and distal) terminated by a lumped parameter model (Fig. 1). For each segment, the transmission line equations describing the propagation of pressure (P) and flow (Q) harmonics waves apply

$$\begin{cases} P(x) = P_f e^{-\gamma x} + P_b e^{\gamma x} \\ Q(x) = Q_f e^{-\gamma x} + Q_b e^{\gamma x} \end{cases}$$

with x as the longitudinal coordinate and f and b indicating forward and backward waves, respectively. The wave propagation coefficient (γ), accounting for wave propagation and damping, is given as

$$\gamma = \frac{i\omega/c}{\sqrt{1 - F_{10}}}$$

with F_{10} as the Bessel function as given by Womersley (24) and c as the wave propagation velocity given as

$$c = c_0 e^{i\theta/2}$$

with c_0 as the inviscid Moens-Korteweg wave velocity. Wall viscosity is taken into account by the viscoelastic phase angle θ as a function of frequency (ω) (2, 9, 10)

$$\theta = \theta_0(1 - e^{-2\omega})$$

The relation between pressure and flow harmonics is given by the characteristic impedance (Z_0)

$$Z_0 = \frac{P_f}{Q_f} = -\frac{P_b}{Q_b} = \frac{\rho c/A}{\sqrt{1 - F_{10}}}$$

with A as the cross-section of the segments and blood density ρ = 1,050 kg/m^3. Values for vessel dimensions and θ_0 are given in Table 1. The impedance mismatch between the terminating windkessel model and the distal segment results in wave reflection. Instead of explicitly modeling the terminating lumped parameter model, the distal reflection coefficient ($\Gamma = P_b/P_f = -Q_b/Q_f$) is modeled as (9)

$$\Gamma = \Gamma_0 e^{-\omega\tau}$$

where Γ_0 and τ are the modulus and phase of the distal reflection coefficient, respectively.

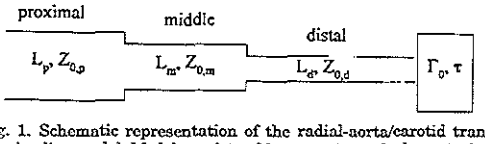

Fig. 1. Schematic representation of the radial-aorta/carotid transmission line model. Model consists of 3 segments, each characterized by its length (L) and characteristic impedance (Z_0). The transmission line termination is modeled as a reflection site determined by the modulus of distal reflection coefficient (Γ_0) and phase of the distal reflection coefficient (τ).

Table 1. *Geometrical and mechanical characteristics of the transmission line model segments fitting the radial-aorta transfer function of Chen et al.*

	Proximal	Middle	Distal	Terminal Model
D, mm	12.5	8	4	
θ_0, °	5	7	9	
L, cm	24	27	15	
c_0, m/s	6.88	8.46	6.51	
Z_0, mmHg· ml^{-1}· s^{-1}	0.44	1.33	4.08	
Γ_0, –				0.86
τ, s				0.00

D, Segment diameter; L, segment length; θ_0, viscoelastic phase angle at high frequencies; c_0, inviscid wave velocity; Z_0, segment characteristic impedance; Γ_0 and τ are modulus and phase of the distal reflection coefficient, respectively. The values corresponding to D, θ_0, and L were assumed; the others were the result of the fitting procedure. See also Fig. 2 for more information concerning the transfer function of Chen et al. (7).

Assessing Reference Model Parameters: Fitting the Model to the Transfer Function of Chen et al.

The modulus and phase angle data for the steady-state radial-aorta transfer function of Chen et al. (7) were digitized, and the complex form of the measured transfer function (TFF_{Chen}) was calculated. We then derived the transfer function for the transmission line model (TFF_{model}), which depends on the eight model parameters: length L and wave propagation speed c_0 for each of the three line segments, and two distal model parameters (Γ_0 and τ). Reference values for these parameters were estimated by fitting TFF_{model} to TFF_{Chen}, hereby minimizing the (complex) sum of squared differences between TFF_{Chen} and TFF_{model} (Matlab, The Mathworks, Natic, MA). To reduce the number of parameters in the minimization procedure, L was set to fixed values between 10 and 30 cm for the proximal and between 15 and 45 cm for the middle and distal segments. For each set of segment lengths, the remaining five parameters were determined using a least square fitting algorithm. The goodness of fit, expressed as the modulus of the root mean square (RMS) value of the difference between TFF_{Chen} and TFF_{model}, was stored for all combinations of segment lengths. The final set of parameters, further considered as a reference, was the one yielding the lowest |RMS|.

After assessing reference model parameters, we studied the effect of changes in characteristic impedance (half and twice the parameter values following from fitting Chen's function) of the proximal segment and of all segments together, changes in vascular tone , i.e, the distal wave reflection coefficient (Γ_0 = 0 − 1), and the effect of a 20% variation in segment length.

Fitting Measured Radial-Carotid Pressure Transfer Functions

In vivo measurements. Applanation tonometry was performed successively at the carotid (P_{car}) and radial (P_{rad}) artery with a Millar SPT-301 penlike transducer (5) in 31 controls and 30 patients, in three different centers, and by three different operators. Patients were subjects with known coronary artery disease confirmed by wall motion abnormalities (rest and/or during dobutamine infusion) on a recent echocardiographic examination and/or a positive treadmill stress test. No patients with uncontrolled hypertension were included. The measured sequence of heartbeats was pro-

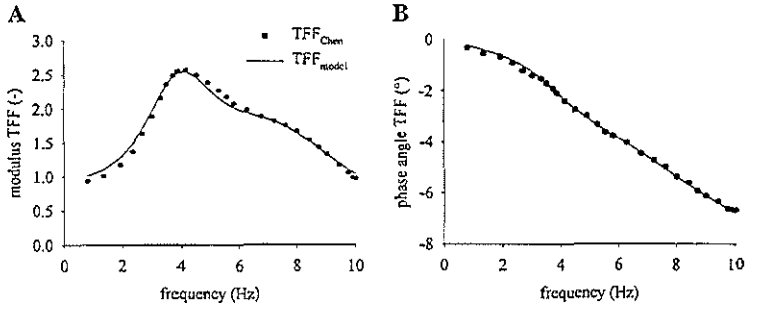

Fig. 2. With the use of the transmission line model from Fig. 1 and with the model parameters of Table 1, the transfer function (TFF) of Chen et al. (TFF_{Chen}) (7) is well predicted. *A*: transfer function modulus; *B*: transfer function phase angle.

cessed off-line. Using the measured electrocardiogram signal, we identified individual heart cycles, and an average pressure wave was calculated from at least five heartbeats. This signal was then calibrated by setting its mean and diastolic value equal to diastolic and mean brachial blood pressure measured with a cuff sphygmomanometer. Fourier analysis was applied on both pressure waves, and the ratio of corresponding harmonics yielded the measured transfer function (TFF_{meas}). A maximum of 10 harmonics were taken into account, and pressure or flow harmonics with a magnitude <1% of the first harmonic were excluded.

Fitting the model to the measured radial-carotid data. To fit the model to the measured radial-carotid pressure transfer function, we used P_{car} as an input into the model, and the computed distal model pressure ($P_{d,model}$) was fitted to the measured radial artery pressure (P_{rad}) by minimization of $\Sigma(P_{d,model} - P_{rad})^2$. We first fitted the data by changing four parameters: the characteristic impedance of the three segments ($Z_{0,p}$, $Z_{0,m}$, $Z_{0,d}$) and the modulus of the distal reflection coefficient (Γ_0). The remaining four parameters were given their reference value as obtained from fitting TFF_{Chen}. Second, we further restricted the fitting to one single parameter: the characteristic impedance of the proximal segment ($Z_{0,p}$), with the remaining seven parameters fixed at their reference value. For both fitting methods, we studied correlations between fitted model parameters and (sphygmomanometer) brachial blood pressure, subject age, heart rate, health condition (control subject or patient), and whether model parameters were different for controls and patients.

Average TFF and Maximal and Minimal Enveloping Transfer Functions

We derived an average transfer function (TFF_{avg}) for the whole group of 31 controls and 30 patients. Measured transfer functions were resampled at 0.25-Hz intervals. Averaging of all 61 transfer functions yielded TFF_{avg}. Furthermore, two TFF were selected from all fitted transfer functions, representing an upper and lower enveloping curve. Because the low frequency harmonics are most important, we chose the transfer function with the highest (TFF_{max}) and lowest (TFF_{min}) amplitude at 2 Hz.

TFF_{max}, TFF_{min}, and TFF_{avg} were used to reconstruct the carotid artery pressure ($P_{car,r}$) from measured P_{rad}, with data from all three centers included. We then calculated pulse pressure (PP = systolic − diastolic pressure) and the AIx from $P_{car,r}$ and P_{car}. AIx is calculated as $\pm(P_{sys} - P_{infl})/PP$, with P_{sys} being systolic pressure and P_{infl} as the pressure corresponding to the first inflection point on the carotid pressure wave. AIx is positive when the inflection pressure precedes systolic pressure and indicates an A-type wave (18); it is negative when the inflection point occurs after systolic pressure (C-type wave). We compared PP and AIx derived from P_{car} and $P_{car,r}$ with TFF_{min}, TFF_{avg}, and TFF_{max} using linear regression analysis. We further calculated RMS as

$$\sqrt{\frac{\Sigma (P_{car,r} - P_{car})^2}{N}}$$

with N as the number of sampling points, indicating the accuracy with which carotid pressure morphology is reconstructed. Finally, we also compared average values for PP and AIx in the control and patient group. Groups were considered statistically different if $P < 0.05$ (*t*-test; SigmaStat 2.0, Jandel Scientific).

RESULTS

Fitting Chen's Radial-Aorta Pressure Transfer Function

The agreement between the fitted model TFF_{model} and TFF_{Chen} is shown in Fig. 2. Both modulus and phase angle were well predicted by the model. The derived model parameters for the different segments are given in Table 1. The characteristic impedance for proximal, middle, and distal segment was 0.44, 1.33, and 4.08 mmHg · ml^{-1} · s^{-1}, respectively. The total length of the model was 66 cm. The distal reflection coefficient was practically constant ($\Gamma_0 = 0.86$), independent of frequency ($\tau = 0.00$).

With changing $Z_{0,p}$ (proximal segment properties) alone, transfer functions with very distinct morphologies were obtained (Fig. 3). A reduction of $Z_{0,p}$ increases the peak of the transfer function and shifts it to lower frequencies. Because of a lower wave velocity, the time delay between the proximal and distal location increases, and the phase angle becomes more negative. These effects are amplified with an overall change of Z_0. With Z_0 divided by 2, the TFF peak is still shifted to lower frequencies, but there is hardly any amplification for frequencies <3 Hz, and the higher frequencies are damped out. Vascular tone changes are modeled as changes of the reflection coefficient, Γ, being real, does not change the TFF phase angle or the location of the peak. Only its magnitude increases with a stronger reflection (vasoconstriction). The overall length of the path was changed by ±20%. A longer path length damp-

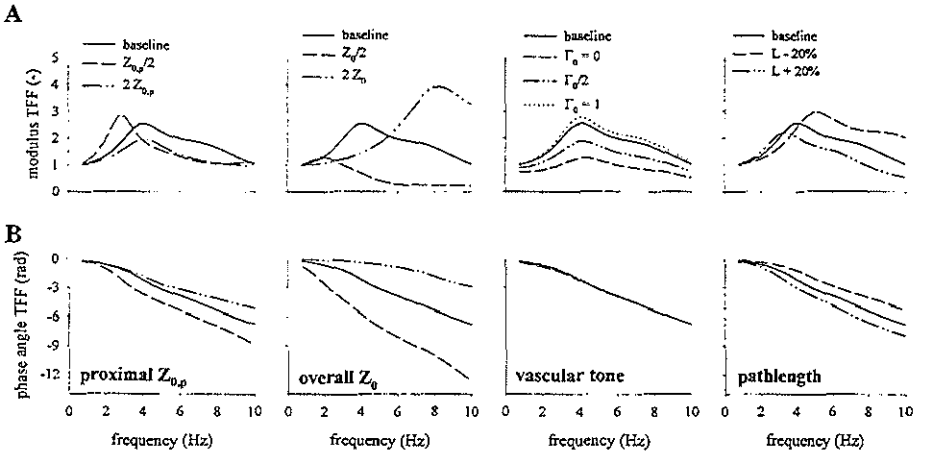

Fig. 3. Changing the model parameters yields a wide range of transfer function morphologies (*top*: TFF modulus; *bottom*: TFF phase angle). From left to right, we show the effect of changing *1*) Z_0 of the proximal segment; *2*) Z_0 of all segments; and *3*) changes in vascular tone modeled by varying Γ_0 from 0.86 (baseline) to 1, 0, and 0.43; and *4*) an ± 20% change in path L.

ens the peak, shifts it to lower frequencies, and increases the phase angle; the inverse is found for a shorter path.

Fitting Measured Radial-Carotid Pressure Transfer Functions

Hemodynamic data for the complete population are given in Table 2 as well as average values for $Z_{0,p}$, $Z_{0,m}$, $Z_{0,d}$, and Γ_0, obtained from fitting the model to measured radial-carotid transfer functions. Overall, there was good agreement between measured and fitted radial artery pressure (RMS = 3.3 ± 2.0 mmHg), but the fitting was slightly better for the control than for the patient group (RMS = 2.8 ± 1.4 vs. 3.9 ± 2.5 mmHg; $P < 0.05$). $Z_{0,p}$ and $Z_{0,m}$ were higher in the patient group, whereas $Z_{0,d}$ was higher in the control group, but differences were not significant. Γ_0 was higher in the patient group (0.85 ± 0.21 vs. 0.71 ± 0.25; $P < 0.05$). There was no correlation between any of the fitted model parameters and subject age, sphygmomanometer blood pressure (systolic, diastolic, or pulse pressure), heart rate, or the subject being classified as a patient or control.

With the model fitted to the measurements using only $Z_{0,p}$, the fitting is again better in controls (RMS = 4.6 ± 2.2 vs. 5.4 ± 3.3 mmHg). $Z_{0,p}$ is higher in patients than in controls, but the difference is not statistically significant (1.10 ± 0.64 vs. 1.22 ± 0.60 mmHg · ml^{-1} · s^{-1}). Again, there was no correlation between $Z_{0,p}$ and subject age, sphygmomanometer blood pressure (systolic, diastolic, or pulse pressure), heart rate, or the subject being classified as a patient or control.

Average TFF and Maximal and Minimal Enveloping Transfer Functions

The calculated point-to-point TFF_{avg} is shown in Fig. 4, together with TFF_{max} and TFF_{min}. The error bars indicate means ± 2 SE. TFF_{max} is the transfer function with the highest amplitude at 2 Hz (2.0) and is calcu-

Table 2. *Age, sphygmomanometric blood pressure, and heart rate in control groups and patients with known coronary artery disease*

	Controls	Patients
n	31	30
Age, yrs	35 ± 12	66 ± 12†
SBP, mmHg	129 ± 10	142 ± 18†
DBP, mmHg	81 ± 10	83 ± 10
MAP, mmHg	97 ± 10	103 ± 12*
HR, beats/min	70 ± 12	70 ± 10
PP, mmHg	48 ± 8	59 ± 12†
Fitting four parameters		
RMS, mmHg	2.8 ± 1.4	3.9 ± 2.5*
$Z_{0,p}$, mmHg · ml^{-1} · s^{-1}	0.98 ± 0.62	1.18 ± 0.60
$Z_{0,m}$, mmHg · ml^{-1} · s^{-1}	1.5 ± 0.9	1.8 ± 1.1
$Z_{0,d}$, mmHg · ml^{-1} · s^{-1}	9.2 ± 5.5	7.3 ± 5.2
Γ_0	0.71 ± 0.25	0.85 ± 0.21*
Fitting one parameter		
RMS, mmHg	4.6 ± 2.2	5.4 ± 3.3
$Z_{0,p}$, mmHg · ml^{-1} · s^{-1}	1.10 ± 0.64	1.21 ± 0.60

Values are means ± SD; n = number of controls and patients. SBP, systolic blood pressure; DBP, diastolic blood pressure, PP, pulse pressure. Mean arterial pressure (MAP) = DBP + PP/3. HR, heart rate. Root mean square (RMS) and estimated model parameters are given for the fitting algorithm, fitting 4 parameters ($Z_{0,p}$, $Z_{0,m}$, $Z_{0,d}$, and Γ_0) or 1 single parameter ($Z_{0,p}$). *$P < 0.05$; †$P < 0.01$.

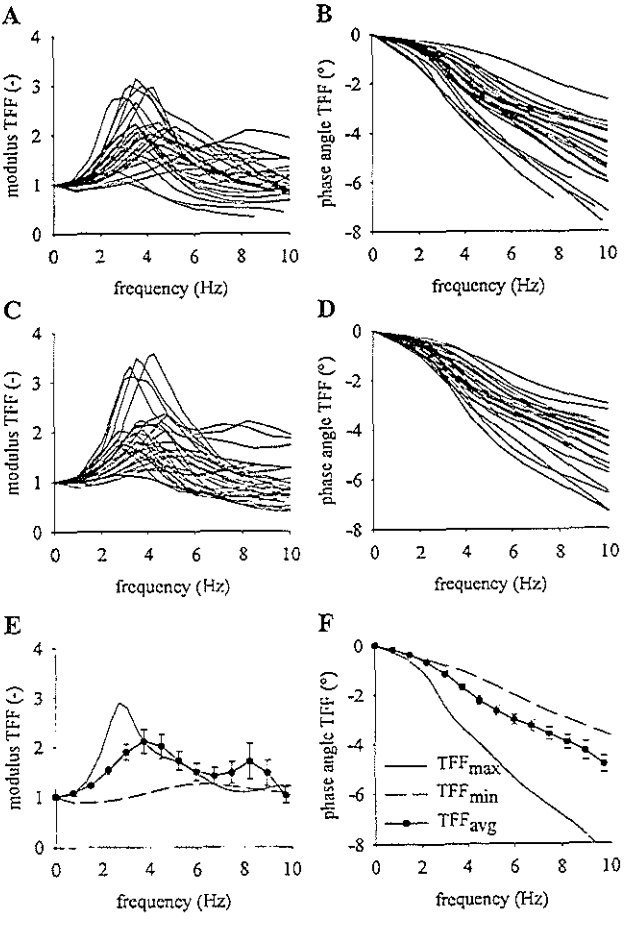

Fig. 4. The model was fitted to radial and carotid artery pressure measured in 31 controls and 30 patients and changing 4 parameters: $Z_{0,p}$, $Z_{0,m}$, $Z_{0,d}$, and Γ_0. The resulting (model) pressure transfer function is characterized by its modulus and phase angle for the control subjects (*A* and *B*) and for the patients (*C* and *D*). *E* and *F* show modulus and phase of the average of all 61 transfer functions (TFF_{avg}) and the transfer functions with the highest (TFF_{max}) and lowest (TFF_{min}) amplitude at 2 Hz. TFF_{max} and TFF_{min} are derived using the model parameters as given in the text, whereas TFF_{avg} is calculated as a point-to-point average of measured data. The bars represent 2 SE on the mean value.

lated using 0.22, 1.15, and 5.34 mmHg · ml^{-1} · s^{-1} for $Z_{0,p}$, $Z_{0,m}$, and $Z_{0,d}$, respectively, and 0.95 for Γ_0. All other parameters have reference values (Table 1). TFF_{min} is the transfer function with the lowest amplitude at 2 Hz (0.9) and is calculated with 1.12, 2.39, and 4.32 mmHg · ml^{-1} · s^{-1} for $Z_{0,p}$, $Z_{0,m}$, and $Z_{0,d}$, respectively, and 0.51 for Γ_0.

We reconstructed carotid pressure from measured radial artery pressure using TFF_{max}, TFF_{min}, and TFF_{avg}, respectively. For the whole data set, the average difference between reconstructed and measured carotid pressure, expressed as the RMS difference, was 7.8 ± 2.7, 6.9 ± 3.4, and 4.3 ± 2.3 mmHg, respectively. The correlations between PP and the AIx, derived from the reconstructed and measured carotid pressure, are given in Fig. 5. Best results are found with TFF_{avg}, yielding an average of 41.5 ± 11.8 vs. 41.1 ± 10.0 mmHg measured. A paired *t*-test indicated that both values were not significantly different ($P = 0.59$). Correlations were less good for AIx. TFF_{avg} gave the best results, with an average value of −0.02 ± 0.19 vs. 0.01 ± 0.19 mmHg measured directly on the carotid artery pressure wave. However, values were not significantly different ($P = 0.22$; paired *t*-test). PP and AIx, calculated from measured or reconstructed carotid artery pressure, were finally grouped for patients and controls (Fig. 6). PP and AIx were higher in patients than in controls, irrespective the calculation on measured or reconstructed pressures.

DISCUSSION

This study is based on a transmission line model for the aorta-radial pathway. The model is similar to the finger-carotid model of Karamanoglu and Fenely (9), consisting of three tube segments with the same values

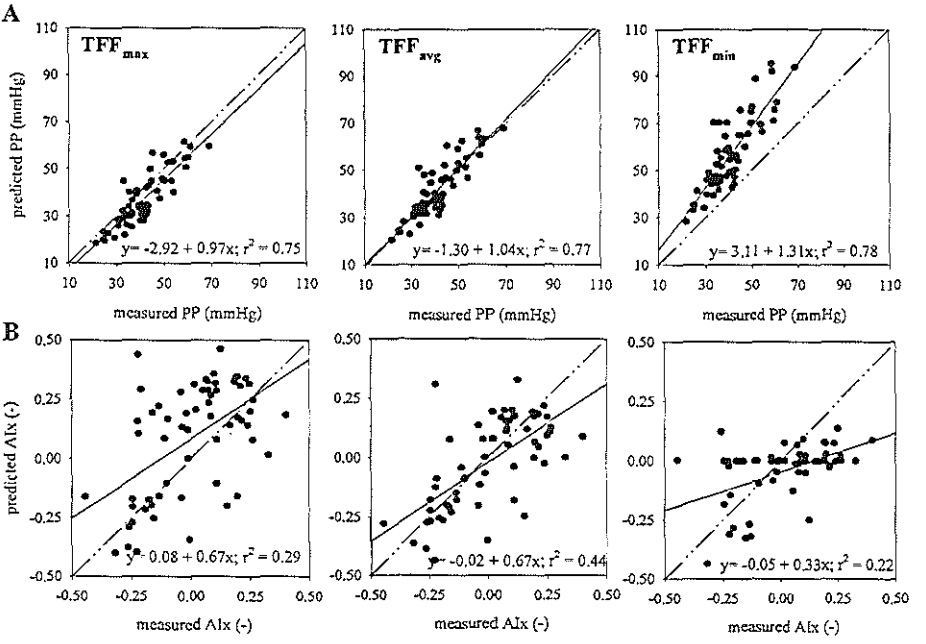

Fig. 5. Comparison of pulse pressure (PP, *A*) and augmentation index (AIx, *B*) derived from the measured carotid artery pressure and from the reconstructed carotid artery pressure using TFF_{max}, TFF_{avg}, and TFF_{min}. Solid line is the regression line; dash-dot line is the line of perfect agreement.

for tube diameters and wall viscosity. We first assessed reference model parameters by fitting the model directly to a recently invasively assessed transfer function (7, 8). The model parameters (Table 1) are within physiological ranges. The total length of the transmission line is 66 cm and is close to the average length of the arm (radial to sternum) that we measured in 13 subjects (66 ± 6 cm). Pulse-wave velocity varies between 6.5 and 8.5 m/s and is within reported ranges (9, 17). A good fit to Chen's data is obtained with a real terminal reflection coefficient, in contrast to Karamanoglu and Fenely (9). The magnitude (0.86) is higher than what Karamanoglu and Fenely (9) found at the finger level (0.64) but is close to the value of 0.8 reported for the femoral artery (15).

It was recently shown that a simple single tube with a single distal reflection site can be used to model the transfer function for "single tubelike" aortic branches such as the carotid artery and to some extent the brachial artery (21). However, such a model is too simple for the radial-aorta pathway, consisting of multiple reflection sites, and it was impossible to fit such a model to Chen's data. Using three tubes in series, three reflection sites are generated: two sites due to the impedance mismatch between the segments and a distal reflection site at the model termination. Varying

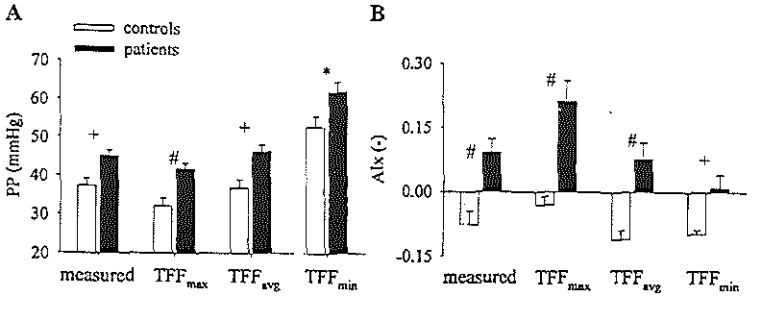

Fig. 6. Comparison of average PP (*A*) and AIx (*B*) in the control (n = 31) and patient (n = 30) population. The bars are means ± SE. Data are derived from the measured carotid artery pressure and from the reconstructed carotid artery pressure using TFF_{max}, TFF_{avg}, and TFF_{min} (*P < 0.05; +P < 0.01; #P < 0.001).

the model parameters leads to logical and expected changes in the morphology of the transfer function as shown in Fig. 3 and as summarized in RESULTS.

The model was used to fit the measured radial-carotid transfer function in 61 subjects. The fitting was first limited to $Z_{0,p}$, $Z_{0,m}$, $Z_{0,d}$, and Γ_0. Average model parameters in the control and patient group are consistent with reported physiopathological changes in arterial mechanical properties. In hypertension, for instance, the stiffness of the larger elastic arteries is increased, but the effects are far less clear for more peripheral, muscular arteries such as the radial or femoral artery (13, 20, 22). Nevertheless, individually, there was no correlation between model parameters and subject characteristics such as age, blood pressure, heart rate, or subject classification as a control or as a patient.

A whole family of TFF curves can be obtained only by changing the characteristic impedance of the proximal segment (Fig. 3). It is further expected that changes in arterial mechanical properties are most pronounced for the larger elastic vessels close to the heart (13, 20, 22). Therefore, we studied whether the fitting could be restricted to $Z_{0,p}$ and whether this improved the correlation between the fitted model parameter and the patient data. Fittings were less good than with the four parameters but still acceptable (overall mean RMS of 5.0 ± 2.8 mmHg). The resulting $Z_{0,p}$ were comparable to the values that were found when fitting four parameters (Table 2), with the same tendency for an increased $Z_{0,p}$ in the patient group. However, again, there was no correlation between $Z_{0,p}$ and subject characteristics.

$Z_{0,p}$ was not different between patients and controls (Table 2). A possible explanation is the limited number of subjects included in the study. Also, blood pressure is only slightly higher in the patient group, and the difference in arterial compliance, most prominent in the ascending aorta and aortic arch, may not be high enough to yield significant differences in $Z_{0,p}$.

The absence of a (simple) relation between model parameters and patient data inhibited the computation of individualized transfer functions. This may be due to the simplicity of the model (and the fitting procedure), with the model parameters not reflecting physiological properties. We also applied a model with reference parameter values derived for the radial-aorta transfer function on measured radial-carotid transfer functions. Still our approach is defendable. The radial-aorta and radial-carotid pathway should at least share the properties of the middle and distal segment; the differences exist in the small part of the ascending aorta and the carotid artery. We assumed the same length for these segments, but their mechanical properties are effectively different: average $Z_{0,p}$ for the radial-carotid data (4 parameter fit) is 1.08 mmHg · $ml^{-1} \cdot s^{-1}$ and is higher than $Z_{0,p}$ that was found for the radial-aorta fit (0.44 mmHg · $ml^{-1} \cdot s^{-1}$). This agrees with the smaller caliber of the carotid artery. One might think of introducing arm length as a known variable into the model. This will change the values of estimated $Z_{0,p}$, but it is unlikely that the introduction of a parameter (radial-carotid path length), which cannot be measured with great accuracy either, would change our observations. One should also consider the fact that not only the total path length but also the relative length of the three segments determines TFF.

TFF_{avg} yielded the best approximation of PP and AIx, whereas TFF_{max} or TFF_{min} gave (very) different values for PP and AIx than the values derived from the directly measured pressure wave. However, it is remarkable that when averaged over control subjects and patients, PP and AIx were different for both groups, irrespective the used transfer function. Thus, when (generalized) pressure transfer functions are used in clinical studies, comparing control subjects with patient groups or comparing different interventions, they may potentially yield reconstructed central (aorta) pressures and derived indexes, discriminating between groups or interventions. Nevertheless, individually, there are considerable differences for PP and AIx derived from the measured or reconstructed carotid artery pressure, as indicated by the (modified) Bland-Altman plot (3) in Fig. 7 (data shown for TFF_{avg} only). Furthermore, we feel that derived parameters, such as the AIx, require reconstructed waves in which enough high-frequency information is present to fully capture the details of the curve. Using other algorithms, based on autoregression models (8), may give better results than the frequency-domain approach we used.

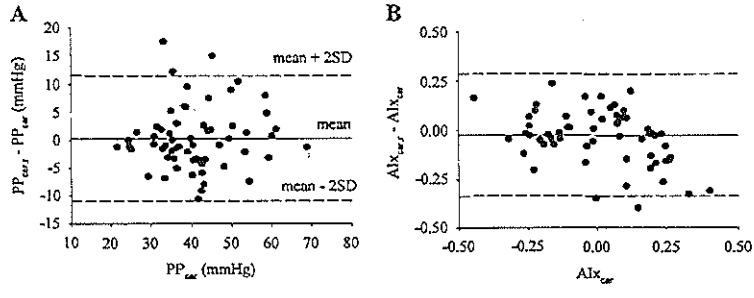

Fig. 7. Difference between PP (*A*) and AIx (*B*) derived from a reconstructed carotid artery pressure (using TFF_{avg}) and from the measured carotid artery pressure, as a function of PP and AIx derived from the measured carotid artery pressure. Solid line is the mean difference; the dashed lines are the means ± 2 SD.

This study shows that arterial pressure waves, reconstructed using (generalized) transfer functions, carry analog information as the carotid blood pressure. This, however, does not imply that these reconstructed pressures are a better approximation of central aortic pressure than carotid blood pressure. However, in clinical settings, it is easier to monitor central pressure from an easily accessible peripheral site such as the radial artery, which is more appropriate for applanation tonometry than the carotid artery. Applanation tonometry at the carotid artery is more tedious, more time consuming, and requires skilled people and averaging of the curves. Furthermore, it is better to avoid carotid applanation tonometry in people with carotid plaque. In our study, we had to exclude about 10% of patients because no reliable carotid tonometric signals could be recorded.

We conclude that using averaged, generalized TFF leads to significant discrepancies between reconstructed and measured pressure waveforms and subsequent derived indexes. Nevertheless, very distinct transfer functions (TFF_{max}, TFF_{avg}, and TFF_{min}) seem to preserve the information in the pressure wave that is needed for the computation of indexes as PP and the AIx, discriminating patients from healthy subjects.

This research is funded by a specialization grant of the Flemish Institute for the Promotion of the Scientific-Technological Research in Industry (IWT 943065–IWT 960250) and a concerted action program of the University of Gent, supported by the Flemish government (GOA-95003). S. Carlier was the recipient of a grant from the North Atlantic Treaty Organization and from the Belgian American Educational Foundation.

REFERENCES

1. **Aakhus S, Soerlie C, Faanes A, Hauger S, Bjoernstad K, Hatle L, and Angelsen B.** Noninvasive computerized assessment of left ventricular performance and systemic hemodynamics by study of aortic root pressure and flow estimates in healthy men, and men with acute and healed myocardial infarction. *Am J Cardiol* 72: 260–267, 1993.
2. **Avolio A.** Multi-branched model of the human arterial system. *Med Biol Eng Comput* 18: 709–718, 1980.
3. **Bland JM and Altman DG.** Statistical methods for assessing agreement between two methods of clinical measurement. *Lancet* 1: 307–310, 1986.
4. **Cameron JD, McGrath B, and Dart A.** Use of radial artery applanation tonometry and a generalized transfer function to determine aortic pressure augmentation in subjects with treated hypertension. *J Am Coll Cardiol* 32: 1214–1220, 1998.
5. **Carlier S, Marwick T, Segers P, Verdonck P, Van Camp G, Cosyns B, and Thomas JD.** Non-invasive estimation of left ventricular power output by simultaneous recordings of applanation tonometry and echocardiographic Doppler signals. In: *Computers in Cardiology*. IEEE Computer Society Press, 1997, p. 223–226.
6. **Chen CH, Ting CT, Nussbacher A, Nevo E, Kass D, Pak P, Wang SP, Chang MS, and Yin FC.** Validation of carotid artery tonometry as a means of estimating augmentation index of ascending aortic pressure. *Circulation* 27: 168–175, 1996.
7. **Chen C-H, Nevo E, Fetics B, Pak PH, Yin FCP, Maughan L, and Kass DA.** Estimation of central aortic pressure waveform by mathematical transformation of radial tonometry pressure: validation of generalized transfer function. *Circulation* 95: 1827–1836, 1997.
8. **Fetics B, Nevo E, Chen CH, and Kass DA.** Parametric model derivation of transfer function for noninvasive estimation of aortic pressure bt radial tonometry. *IEEE Trans Biomed Eng* 46: 698–706, 1999.
9. **Karamanoglu M and Fenely M.** On-line synthesis of the human ascending aortic pressure pulse from the finger pulse. *Hypertension* 30: 1416–1424, 1997.
10. **Karamanoglu M, Gallagher D, Avolio A, and O'Rourke M.** Pressure wave propagation in a multibranched model of the human upper limb. *Am J Physiol Heart Circ Physiol* 269: H1363–H1369, 1995.
11. **Karamanoglu M and FM.** Derivation of the ascending aorta-carotid pressure transfer function with an arterial model. *Am J Physiol Heart Circ Physiol* 271: H2399–H2404, 1996.
12. **Karamanoglu M, O'Rourke M, Avolio A, and Kelly R.** An analysis of the relationship between central aortic and peripheral upper limb pressure waves in man. *Eur Heart J* 14: 160–167, 1993.
13. **Kawasaki T, Sasayama S, Yagi S, Asakawa T, and Hirai T.** Non-invasive assessment of the age related changes in stiffness of major branches of the human arteries. *Cardiovasc Res* 21: 678–687, 1987.
14. **Kelly RP and Fitchett D.** Noninvasive determination of aortic input impedance and external left ventricular power output: a validation and repeatability study of a new technique. *J Am Coll Cardiol* 20: 952–963, 1992.
15. **Li JKJ, Melbin J, and Noordergraaf A.** Directional disparity of pulse reflection in the dog. *Am J Physiol Heart Circ Physiol* 247: H95–H99, 1984.
16. **Marcus R, Korcarz C, McCray G, Neumann A, Murphy M, Borow K, Weinert L, Bednarz J, Gretler D, Spencer K, Sareli P, and Lang R.** Noninvasive method for determination of arterial compliance using Doppler echocardiography and subclavian pulse tracings. *Circulation* 89: 2688–2699, 1994.
17. **Milnor WR.** *Hemodynamics*. Baltimore, MD: Williams & Wilkins, 1989.
18. **Murgo JP, Westerhof N, Giolma JP, and Altobelli SA.** Aortic input impedance in normal man: relationship to pressure wave forms. *Circulation* 62: 105–116, 1980.
19. **O'Rourke M.** Arterial stiffness, systolic blood pressure, and logical treatment of arterial hypertension. *Hypertension* 15: 339–347, 1990.
20. **Reneman RS, Hoeks APG, and Westerhof N.** Non-invasive assessment of artery wall properties in humans–methods and interpretation. *J Vasc Invest* 2: 53–64, 1996.
21. **Stergiopulos N, Westerhof B, and Westerhof N.** Physical basis of pressure transfer from periphery to aorta: a model-based study. *Am J Physiol Heart Circ Physiol* 274: H1386–H1392, 1998.
22. **Van Merode T, Brands P, Hoeks A, and Reneman R.** Different effects of ageing on elastic and muscular bifurcations in men. *J Vasc Res* 33: 47–52, 1996.
23. **Westerbacka J, Wilkinson I, Cockroft J, Utriainen T, Vehkavaara S, and Yji-Jarvinen H.** Diminsihed wave reflection in the aorta. A novel physiological action of insulin on large blood vessels. *Hypertension* 33: 1118–1122, 1999.
24. **Womersley JR.** *An Elastic Tube Theory of Pulse Transmission and Oscillatory Flow in Mammalian Arteries*. Wright Air Development Centre, report no. WADC-TR56-614, 1957.

Chapter 20

A simplified non-invasive index of contractile state: assessment using arterial tonometry.

SG Carlier, GP Armstrong, TH Marwick, P Segers, P Verdonck, JD Thomas.

Submitted to Circulation.

A Simplified Non-invasive Index of Contractile State: Assessment Using Arterial Tonometry.

Stephane G. Carlier, Guy P. Armstrong, Thomas H. Marwick, Patrick Segers*, Pascal Verdonck*, James D. Thomas

Department of Cardiology, The Cleveland Clinic Foundation, Cleveland, Ohio
and
*Hydraulics Laboratory - Institute of Biomedical Technology, University of Gent, Belgium

Supported in part by grant NCC9-60, National Aeronautics and Space Administration, Houston, TX. Dr Carlier is the recipient of a fellowship from the Belgian American Educational Foundation and from the North Atlantic Treaty Organization.

This work was partly presented at the 71st scientific meeting of the American Heart Association, Dallas, 1998.

Address for correspondence:
James D. Thomas, Department of Cardiology – F15, The Cleveland Clinic Foundation, 9500 Euclid Avenue, 44195 Cleveland – Ohio - USA
Tel: 216-445 63 12, Fax: 216-445 73 06, e-mail: thomasj@ccsmtp.ccf.org

Running head:
A simplified index of contractile state

Abstract

Background: *Cardiac reserve, defined as the change in maximal ventricular power output (**Pmax**) has a prognostic value in patients with ventricular dysfunction. We wanted to investigate whether (1) maximal ventricular power output and physiological cardiac reserve can be measured non invasively with echo-Doppler and tonometry during exercise: (2) a simplified index of power output (**sPmax**), the product of peak aortic flow and mean blood pressure, yields similar diagnostic value.*

Methods: *A total of 14 patients with known or suspected coronary artery disease and 11 normal control subjects underwent supine bicycle exercise echocardiography to measure aerobic exercise capacity (estimated by VO_2max). At rest and peak exercise, aortic flow was estimated from echo-Doppler, and aortic blood pressure from arterial tonometry, to calculate **Pmax** and **sPmax**. Cardiac reserve was defined as the difference between peak exercise and rest values.*

Results: *Recordings were successful in all subjects. There was a strong correlation between **Pmax** and **sPmax** (r^2=0.97). Cardiac reserve derived from Pmax and sPmax were significantly related to VO_2max (r^2=0.85 and 0.82, respectively). In a multiple logistic regression, VO_2max was independently predicted by the rate pressure product and **Pmax** or **sPmax**, but not by steady power output.*

Conclusions: *A simplified index of ventricular power output could be validated in a clinical exercise echo setting and was found strongly correlated to a more burdensome tonometric evaluation. Both indices add similar diagnostic information to conventional hemodynamic and echocardiographic parameters and could be useful for the evaluation of left ventricular contractile state of patients.*

Keywords: cardiac power output, stress echocardiography, oxygen consumption

Condensed abstract

In 25 subjects, maximal ventricular power output (Pmax) was measured non invasively with echo-Doppler and tonometry during supine bicycle exercise, and compared to a simplified index, defined as the product of peak aortic flow and mean blood pressure. Cardiac reserve was estimated by the difference of Pmax at peak exercise and baseline. Aerobic exercise capacity was estimated by expired gas analysis (VO_2max) and was found statistically correlated to Pmax. There was a strong correlation between Pmax and its simplified estimation yielding similar diagnostic value in a multiple logistic regression of VO_2max determinants. This simplified index may be useful and more practical to evaluate ventricular contractile reserve.

Background

Ventricular contractility is best assessed with invasive indices of the pressure-volume pump relationship.[1,2] However, their invasive nature precludes their widespread application. Maximal ventricular power (**Pmax**, defined as the maximum of the instantaneous product of pressure chamber and rate of volume change) has been proposed for the assessment of ventricular function. Non-invasive evaluations have been based on echocardiography and central aortic blood pressure estimation with arterial tonometry[3], pulse transduction[4] or automated cuff sphygmomanometry.[5] Contractile reserve (**CR**) might be defined as the difference of **Pmax** between peak stress and baseline conditions. In patients with heart failure, non-invasive **CR** has been demonstrated to have a better prognostic value than ejection fraction,[6] confirming earlier observations by Tan et al.[7,8] Severe exertion is the most physiological stress for evaluation of the functional reserve of the left ventricle.[9,10] We have recently reported the validation in dogs and preliminary clinical experience of a simplified index of **Pmax, sPmax**, defined as the product of mean blood pressure and peak aortic flow[11], which is easier to obtain than **Pmax** during exercise echocardiography. We present in this paper a validation of **sPmax** in a clinical setting where we evaluated "true" peak power via tonometric and echocardiographic measurements in subjects undergoing supine bicycle exercise stress with metabolic testing.

Material and methods

Rest and supine bicycle exercise echocardiography were performed in 14 patients free of significant valvulopathies and atrial fibrillation referred for evaluation of coronary heart disease, and in 11 normal control subjects. All aspects of this investigation conformed to the principles outlined in the declaration of Helsinki. Approval to conduct the study

was granted by the local Investigational Review Board and informed consent was obtained from each subject.

Exercise echocardiography: Echocardiographic examinations were performed using an ATL HDI 3000 machine (Advanced Technology Laboratories, Bothell, WA) to obtain standard views at rest, maximal exercise and immediately afterwards. Echocardiographic images were recorded on 0.5-inch VHS videotapes and also digitized on-line into a quad-screen, cine loop format, gated to the R wave of the electrocardiogram (ImageVue, Eastman Kodak Health Imaging, Allendale, NJ). All digitized images were stored on 5.25-inch optical disks. Interpretation of the images was performed by two observers using the standard 16-segments LV model.[12]

Measurement of ventilatory response: Continuous expired gas analysis was performed with a MedGraphics CardiO_2 system (Minneapolis, MN). Nose clips were used to prevent air leak from the nostrils. Breath-by-breath analysis of the expired gas was performed, and results were reported as 30-second averages. Oxygen consumption (VO_2) and carbon dioxide production (VCO_2) were measured at rest for ≥2 minutes before start of exercise and then continuously during exercise. Maximum oxygen uptake, corrected for body weight, (VO_2max) was defined as the oxygen consumption at peak exercise. The respiratory exchange ratio (RER) was calculated as the ratio of VCO_2 relative to VO_2.

Exercise testing: All subjects underwent symptom-limited exercise testing on a tiltable supine ergometer (American Echo, Kansas City, MO) using 2 minute stages, with 25 Watt workload increments. Hemodynamic response, symptom status and 12-lead electrocardiogram were monitored continuously. Brachial artery pressure was measured at the end of each stage with a mercury sphygmomanometer, based on phase 1 and 4 of the Korotkov sounds. Maximal exercise was defined by attainment of > 85% of maximum age-predicted heart rate response[13].

Estimation of aortic flow: In the absence of significant mitral regurgitation, aortic flow reflects the instantaneous rate of volume change of the left ventricle needed to calculate power. To estimate peak aortic flow, aortic annulus diameter was measured from the parasternal long axis view at rest, and assumed to remain constant with exercise[14]. At rest and at peak exercise level, or failing that, immediately on cessation of exercise, the aortic root was interrogated from the apical five-chamber view using continuous wave (CW) Doppler with optimal alignment of the ultrasound beam in the left ventricular outflow tract (LVOT). Maximal velocity, velocity-time-integral (VTI) and the RR-interval were manually measured from the videotape. Concomitantly, the audio Doppler signal output of the echocardiographic machine was digitized with a customized hardware and software interface previously described.[15] Briefly, audio Doppler signals were acquired with an analog/digital board (Wavebook/512, IOTech Inc., Cleveland, OH) and a laptop computer (Dell LM/P133, Austin, TX). Fast Fourier Transform was computed on-line to display the spectrogram, along with simultaneously acquired tonometric and ECG signals. Data were archived in binary files and processed off-line. Automatic detection of the maximal aortic velocity contour (V_{Ao}) and computation of VTI required minimal user interaction with a software developed in MatLab 4.2 (MathWorks Inc., UK). Instantaneous aortic flow (Q_{Ao}) was computed as the cross-sectional aortic annulus area times V_{Ao}. Manual and automatic measurements of peak V_{Ao} and VTI were compared following Bland and Altman.[16]

Estimation of central aortic pressure: **Pmax** should be computed with left ventricular pressure, but aortic root blood pressure (BP_{Ao}) is a valid alternative.[17,18] We performed non-invasive tonometric recordings of the carotid and radial arteries with a Millar SPT-301 pen-like transducer (Millar Instruments Inc., Houston, TX). Principles of tonometry have been extensively described.[19] Close agreement at the carotid level with invasive high-fidelity BP_{Ao}

Table 1. Rest and exercise parameters in patients and controls and their univariate correlation with VO2 max.

	Patients n=14	Controls n=11	Correlation with VO_2max r (n=25)	p
Rest:				
Ejection fraction (%)	56±13	61±6	0.178	0.440
Heart rate (min^{-1})	70±10	70±10	-0.103	0.625
Mean arterial pressure (mmHg)	106±10	104±9	0.124	0.554
Estimated aortic pulse pressure (mmHg)	45±10	32±5‡	-0.505	**0.01**
Rate pressure product (mmHg/min x 10^3)	10.1±1.7	9.2±1.2	-0.221	0.288
Cardiac output (l/min)	5.3±1.6	5.4±1.2	0.272	0.188
Maximal power (Watts)	5.9±2.0	6.3±1.7	0.468	**0.018**
Simplified maximal power (Watts)	5.0±1.4	5.5±1.5	0.524	**0.007**
Steady Power (Watts)	1.2±0.4	1.3±0.3	0.326	0.111
Peak exercise:				
Ejection fraction (%)	71±13	72±7	0.029	0.902
Maximal heart rate (min^{-1})	129±21	160±13‡	0.794	**<0.001**
Mean arterial pressure (mmHg)	134±13	137±12	0.175	0.403
Estimated aortic pulse pressure (mmHg)	68±14	80±34	0.414	**0.04**
Rate pressure product (mmHg/min x 10^3)	25.1±4.7	32.3±4.9‡	0.763	**<0.001**
Cardiac output (l/min)	9.6±3.4	13.9±3.9†	0.761	**<0.001**
Maximal power (Watts)	10.9±3.8	16.8±3.9‡	0.825	**<0.001**
Simplified maximal power (Watts)	9.3±2.8	13.2±2.9†	0.805	**<0.001**
Steady power (Watts)	2.9±1.1	4.2±1.3†	0.756	**<0.001**
VO_2max (ml/kg/min)	18±6	35±8‡		

* p≤0.05 † p≤0.01 ‡ p≤0.001, patients versus controls.

Table 2. Variation of the hemodynamic parameters (Δ peak exercise – baseline) and their univariate correlation with VO_2 max.

	Patients n=14	Controls n=11	Correlation with VO_2max r (n=25)	p
Δ ejection fraction (%)	16±5	11±4*	-0.333	0.140
Δ mean arterial pressure (mmHg)	28±10	32±7	0.106	0.614
Δ aortic pulse pressure (mmHg)	22±13	48±34*	0.577	**0.003**
Δ rate pressure product (mmHg/min x 103)	15.1±4.0	23.0±4.9‡	0.825	**<0.001**
Δ cardiac output (l/min)	4.3±2.6	8.5±3.2‡	0.788	**<0.001**
Cardiac reserve (Watts)	5.0±2.3	10.5±2.4‡	0.847	**<0.001**
Simplified cardiac reserve (Watts)	4.3±1.8	7.7±1.6‡	0.820	**<0.001**
Steady cardiac reserve (Watts)	1.6±0.9	3.0±1.1†	0.782	**<0.001**

* p≤0.05 † p≤0.01 ‡ p≤0.001, patients versus controls.

recordings has been reported.[20,21] Consecutive calibrated tonometric BP signals (ECG-gated) were displayed for visual assessment of the reproducibility and the quality of the successive recorded beats, along with the Doppler spectrogram. For calibration, diastolic and mean (obtained by integration over the heart period) tonometric BP were set equal to the diastolic and mean cuff pressure measurements at the brachial level. Mean sphygmomanometer BP was computed as (2 x Diastolic BP + Systolic BP)/3. At peak exercise, no reliable tonometric BP recording at the carotid level could be performed, due to deep respiratory movement artifacts. Consequently, BP_{Ao} was considered at rest equal to the carotid tonometric BP, but at peak exercise, BP_{Ao} was derived from the radial recordings on which a validated transfer function was applied[22]. Aortic pulse pressure (PP_{Ao}) was calculated as systolic BP_{Ao} minus diastolic BP_{Ao}. We compared carotid and transformed radial recordings at rest. Analyzed BP waves were the average of 5-7 beats giving a representative heart cycle. The standard deviation of the reconstructed systolic BP (sdSBP) was used as an index of the variability of the tonometric recordings.

Estimation of maximal power and physiological cardiac reserve: **Pmax** was determined as the peak of the instantaneous product of realigned Q_{Ao} and BP_{Ao}[23]. **sPmax** was computed as peak V_{Ao} x aortic annulus cross sectional area x mean BP. Steady (mean) power output (**mP**) was computed as the product of mean BP_{Ao} and cardiac output[7]. **CR**, simplified CR (**sCR**) and mean CR (**mCR**) were computed as the difference of peak exercise and rest values of **Pmax**, **sPmax** and **mP**, respectively.

Statistical methods: All values are expressed as mean±standard deviation. Comparison of hemodynamic variables between patients and normal subjects was performed by t-test. For multiple comparisons, analysis of variance with Bonferroni's correction was applied. Statistical significance was defined as a two-tailed p value of 0.05. Pearson's two-tailed correlation and linear regression were used to compare continuous variable. All parameters found to be significantly correlated to VO_2max by univariate analysis were included in a multiple forward stepwise linear regression in order to find the independent variables that predicted the value of VO_2max. Analyses were obtained with SPSS release 7.5.2, 1997 (SPSS Inc., Chicago, IL).

Results

Patient characteristics: Of the fourteen patients (age 64± 14 years), five were female, one had a resting ejection fraction <45%, two had moderate mitral regurgitation. Indications for evaluation were known (5) or suspected (9) coronary artery disease. The exercise echocardiograms included 6 negative tests and 3 non-diagnostic tests due to inadequate heart rate response. Five tests demonstrated rest or exercise-induced wall motion abnormalities. All eleven control subjects (age 34±5 years) were males, with normal

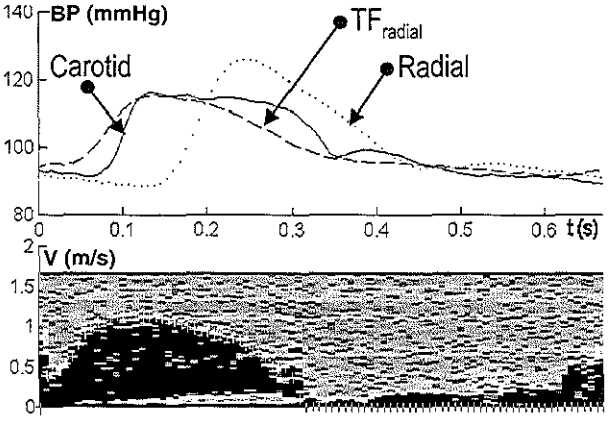

Figure 1: Upper panel: measured radial (dotted line) and carotid (solid line) calibrated tonometric pressure and the estimated aortic pressure (broken line) via a transfer function applied to the radial recording (TF_{radial}). Calibration is based on sphygmomanometric mean and diastolic pressure measurements. Radial and carotid pressure waves are the average of 5 to 7 individual beats. Lower panel: simultaneously acquired and recomputed Doppler spectrogram with the automatically detected maximal velocity contour (+).

Table 3. Rest and exercise peak aortic velocity (V_{Ao}) and velocity-time integral (VTI), at rest and peak exercise, with manual and automatic assessment of V_{Ao}.

	REST		EXERCISE	
	Patients n=14	Controls n=11	Patients n=14	Controls n=11
Manual tracing				
peak V_{Ao} (m/s)	1.21±0.20†	1.17±0.13†	1.67±0.33*	2.04±0.20
VTI (m)	0.26±0.04*	0.23±0.03†	0.28±0.06	0.29±0.05
Automatic assessment				
peak V_{Ao} (m/s)	1.11±0.20†	1.10±0.15†	1.63±0.28*	2.02±0.20
VTI (m)	0.25±0.04	0.23±0.04†	0.28±0.06	0.29±0.04

* p≤0.05, patients versus controls ; † p≤0.05, rest versus exercise

resting and exercise echocardiograms.

Hemodynamic and metabolic parameters at baseline and peak exercise: Comparison of baseline and stress parameters is shown in Table 1. With exercise, control subjects achieved a higher heart rate, rate pressure product, cardiac output, and VO_2max. Patients achieved a VO_2max of 18±6 ml/kg/min (range 11.7-27.5) corresponding to 5.1 ±1.7 metabolic equivalents (METS), with a maximum rate pressure product of 25.1±4.7 10^3 mmHg.beats/min. RER at peak exercise was 1.2±0.1, indicating good effort and maximum exercise. Three patients and one control failed to reach a RER of 1.1, three other patients and one control failed to reach 85 % of the maximum age-predicted heart rate response. Table 2 summarizes the changes from baseline to peak exercise. No difference was observed between the patients with a negative, non-diagnostic or positive exercise test.

Automated assessment of aortic flow: Comparison of automatic and manual estimation of V_{Ao} is given in table 3. Including baseline and peak exercise values, the Bland and Altman's analysis revealed a clinically non-significant bias of 0.06 m/s for peak V_{Ao}. The agreement interval was [-0.20; 0.31] m/s, for an overall mean peak V_{Ao} of 1.5 m/s (left panel of figure 2). For VTI, the bias was 0.005 m, and the agreement interval [-0.06; 0.07] m, for an overall mean VTI of 0.26 m (right panel of figure 1). The scatterplots show a random distribution of the differences lying in the agreement interval, with the exception of 2 measurements obtained at peak exercise.

Estimation of central aortic blood pressure: The upper part

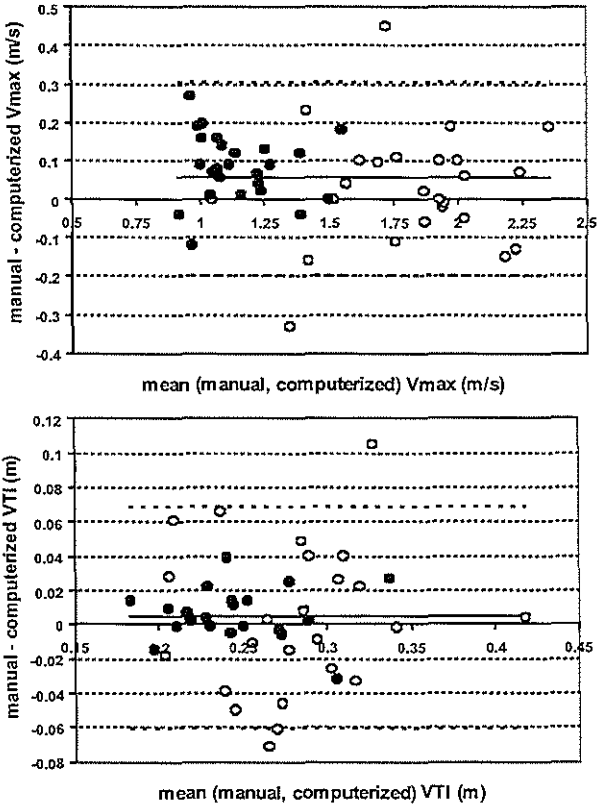

Figure 2: Bland and Altman's plots of the differences against the mean of manual and computerized assessment of: (upper panel) maximal aortic velocity (Vmax) at rest (filled circles) and at peak exercise (open circles); (lower panel) velocity time integral. Agreement interval between manual and automatic measurements is mean ± 2 sd.

Table 4. Multivariate analysis of VO_2max (forward step-wise inclusion) of the hemodynamic variables and (i) tonometric indexes of contractility (Pmax and CR), (ii) simplified indexes of contractility (sPmax and sCR) and (iii) steady power measurements (mP and mCR).

Model	Independent variables	B	SE	P	Adjusted r^2
(i)	*(with tonometric power measurements)*				**0.833**
	Cardiac reserve	0.438	0.145	0.5	
	Δ rate pressure product	2.6 10^{-3}	1 10^{-3}	<0.001	
	Rate pressure product at peak exercise	-2.1 10^{-3}	1 10^{-3}	<0.005	
	Peak power at peak exercise	1.247	0.588	<0.05	
	Constant	*16.9*	*7.2*	*0.05*	
(ii)	*(with simplified power measurements)*				**0.830**
	Δ rate pressure product	2.9 10^{-3}	1 10^{-3}	<0.001	
	Simplified cardiac reserve	0.616	1.12	0.5	
	Rate pressure product at peak exercise	-2.4.10^{-3}	1 10^{-3}	<0.05	
	Simplified peak power at peak exercise	1.792	0.828	<0.05	
	Constant	*15.5*	*7.1*	*<0.05*	
(iii)	*(with steady power measurements)*				**0.739**
	Δ rate pressure product	1 10^{-3}	0.1 10^{-3}	<0.005	
	Δ cardiac output	1.259	0.467	<0.05	
	Constant	*-0.8*	*3.9*	*0.8*	

B: unstandardized coefficients, SE= standard error.

of figure 2 illustrates, at rest, tonometric recordings at the carotid and at the radial levels and the reconstructed aortic BP via the transfer function. At the carotid level, at rest, systolic BP tended to be higher for the patients (133 ±14 mmHg) than for the controls (123±10 mmHg, p=0.06). The sdSBP was 3±2 mmHg. At the radial level, systolic BP was 140±16 mmHg, with no difference between patients and controls and sdSBP was 3±2 mmHg. At peak exercise, radial SBP reached 196±19 mmHg and 222±29 mmHg, respectively for the patients and the controls (p<0.05).

The variability of the tonometric recordings was slightly higher at peak exercise, with an average sdSBP of 5±2 mmHg. Systolic BP_{Ao} was not different among the patients and the controls: 173±15 mmHg. There was a clinically non significant bias of 2±5 mmHg between the rest carotid systolic BP and the reconstructed systolic BP_{Ao} via the transfer function.

Comparison between the tonometric and simplified peak power indexes: Figure 3 shows that there was an excellent correlation between **Pmax** and **sPmax**. The correlation between **CR** and **sCR** was also very good: **sCR** = 0.64 x **CR** +1.0, r^2=0.94, p<0.001. **Pmax**, **sPmax**, **mP**, **CR**, **sCR** and **mCR** were statistically lower for the patients (Table 1 and 2).

Correlation between hemodynamic parameters and maximal oxygen uptake: There was no correlation between rest hemodynamic parameters and VO_2max. Pearson's univariate correlation coefficients are summarized in Table 1. At maximal exercise, VO_2max was highly correlated to peak heart rate, PP_{Ao}, cardiac output, rate pressure product and maximal power indexes. With the exceptions of ejection fraction and mean arterial pressure, all the increases in the hemodynamic parameters were correlated with VO_2max (Table 2). Figure 4 shows the strong correlation found between VO_2max and both **Pmax** and **sPmax**. Table 4 summarizes the step-wise forward multivariate regression between VO_2max and hemodynamic parameters found correlated in the univariate regression, and (i) **Pmax** and **CR**, (ii) **sPmax** and **sCR**, (iii) **mP** and **mCR**. With tonometric or

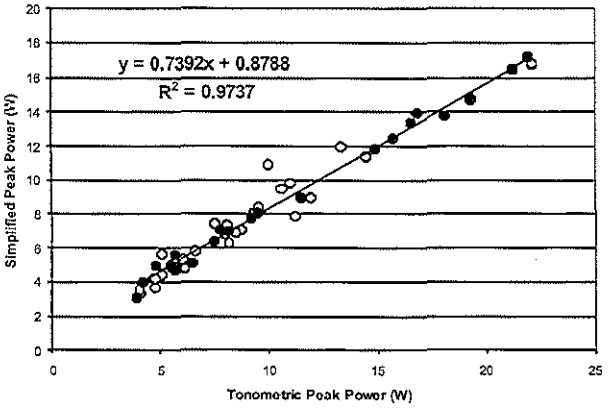

Figure 3: A plot of the simplified index of ventricular peak power output (**sPmax**), defined as peak aortic flow times mean blood pressure, against the peak power derived from the tonometric and echo-Doppler measurements (**Pmax**) during rest (filled circles) and peak exercise (open circles).

simplified derived peak power parameters, the model was similar (adjusted r^2 was 0.833 and 0.830, respectively). No steady power parameters were found independently correlated to VO_2max.

Discussion

The major findings of this study are:

(i) an index reflecting contractile state, **Pmax**, and the derived physiological cardiac reserve (**CR**), could be fully assessed non-invasively with the combined use of Doppler-echocardiography and arterial tonometry;

(ii) a simplified index, **sPmax** defined as mean arterial blood pressure times peak aortic flow, more practical to obtain in a stress-echo laboratory setting, was highly correlated to the more burdensome tonometric **Pmax**;

(iii) both measurements were strongly correlated to VO_2max, and carried additional independent information over peak exercise cardiac output and steady ventricular power output.

Non-invasive evaluation of Pmax and physiological cardiac reserve:

Mean and pulsatile powers using tonometry and Doppler-echocardiography have been invasively validated in subjects undergoing cardiac catheterization by Kelly et al.[3] A coefficient of variation of <9% has been reported. During stress-echocardiography, variability of **Pmax** evaluation might increase but it was not logistically possible to repeat these measurements performed during the daily activity of our stress-lab. Our study is the first to report rest and peak stress Pmax determinations with tonometry. Cooke et al.[10] have recently reported a coefficient of variation of 9.1% for **mP** during exercise using the CO_2 method for evaluation of cardiac output. The low standard deviation of the reconstructed systolic blood pressure (sdSBP) we report, even at peak exercise (5±2 mmHg), supports a good reproducibility of our measurements. The developed software and hardware for on-line assessment of the simultaneously recorded tonometric and Doppler signals facilitated this achievement. **Pmax** has been assessed non-invasively using an alternative to tonometry for the central BP evaluation in patient with severe heart failure. During dobutamine-induced inotropic stimulation, the preload-adjusted derived con-tractile reserve has been demonstrated predictive of the functional class,[5] and for patients in functional class III/IV following the New York Heart Association, the cardiac reserve, and not the ejection fraction, was statistically higher in those alive at the 3-year follow-up.[6] **Pmax** being preload dependent, adjustment dividing it by the square of end-diastolic volume has been proposed.[17,18] However, Nakayama et al.[24] have recently demonstrated that the optimal preload adjustment was dependent of the size of the ventricle. Since we wanted to determine the overall cardiac reserve, including the amount based on preload recruitment, we did not apply any correction based on ventricular size,

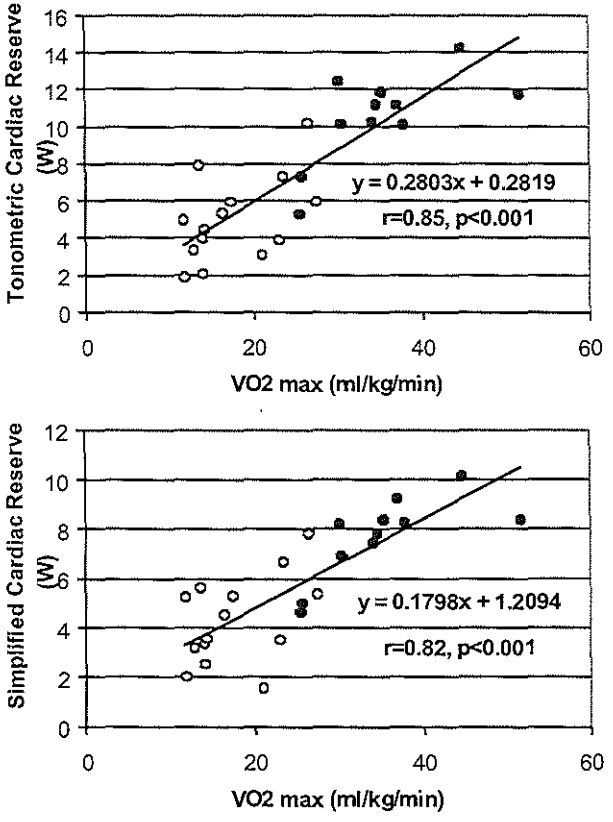

Figure 4: Plots of the linear relationship between: (upperpanel) the cardiac reserve derived from tonometric measurements (defined as **Pmax** at peak exercise minus **Pmax** at rest) and aerobic exercise capacity, VO_2max, for patients (open circles) and controls (filled circles); (lower-panel) the simplified index of contractile state (defined as **sPmax** at peak exercise minus **sPmax** at rest) and VO_2max.

similarly to Tan and colleagues[10,25].

A simplified index of Pmax:

We could perform tonometric recordings in all our patients. However, this technique requires an additional person and extra time. At peak exercise, radial recording could only be performed at the cessation of exercise. We demonstrate that **sPmax**, validated in an open-chest dog setting[11] and easier to obtain, is highly correlated to **Pmax**. Determination at peak exercise requires only a Doppler recording in the LVOT, quickly obtained during the recording of the conventional views for stress echocardiography. Off-line determination of peak aortic flow can be performed from tape recordings, or facilitated with an external setting, as the one we describe. There was a very good agreement between manual and automatic assessments of V_{Ao} and VTI. The discrepancy was slightly higher during exercise, due to the more unstable hemodynamic conditions at that time: as soon as the exercise is stopped, peak V_{Ao} decreases and measurements from the tape did not perhaps always exactly match the timing of the computerized spectrogram analysis.

Functional capacity assessed by VO_2max

The rate of maximal oxygen uptake (VO_2max) is the best test of overall functional reserve. In untrained normal people, VO_2max is determined by the cardiac output at maximal exercise[26]. For patients with heart failure or pulmonary disease, VO_2max is influenced by changes in peripheral oxygen extraction and pulmonary gas exchange, reflecting more the functional capacity of the whole organism. It is thus the best objective index of aerobic work capacity[27] that we considered as our reference physiological cardiac capacity measurement.

Although ejection fraction during exercise echocardiography has predictive value in some settings such as chronic mitral regurgitation[28], measurements of resting cardiac function do not predict functional reserve. There was no correlation between ejection fraction and VO_2max.[29] On the other hand, contractility, pressure work and heart rate are the major determinants of VO_2max[30] and are reflected in the evaluation of **Pmax**.

Respective correlation between Pmax, sPmax, mP and VO_2max

We found a direct linear relationship between VO_2max and **Pmax**, **sPmax** and **mP**, confirming previous reports[10,25]. In the univariate correlation analysis, the correlation between cardiac reserve (**CR**) and VO_2max was even higher (r=0.847) than with peak exercise **Pmax** (r=0.825). However, in the multivariate regression, **CR** was not independently correlated with VO_2max when Δ(rate pressure product), rate pressure product at peak exercise and peak exercise **Pmax** were included (table 4). With simplified power measurements, a similar model with a close adjusted r^2 was found, supporting the hypothesis that **sPmax** might yield similar diagnostic value than tonometry. Conversely, it appears that **mP** does not bring additional independent information once the rate pressure product and cardiac output are measured at rest and at peak exercise (table 4). Cooke et al.[10] reported indeed a correlation between VO_2max and cardiac output at peak exercise higher (r=0.922) than **mP** (r=0.872). The advantage of **Pmax** might be to include the pulsatile load of the ventricle, in comparison to only the steady component measured by **mP**.

Radial versus aortic blood pressure measurements:

Elevated blood pressure during submaximal exercise is predictive of cardiovascular and myocardial infarction mortality in apparently healthy male populations,[31,32] and is strongly associated with coronary risk factors.[33] The systolic radial arterial pressure can be markedly modified by summation of peripherally reflected waves, with an overestimation of systolic BP_{Ao} up to 80 mmHg during exercise.[34,35] On the other hand, mean and diastolic radial BP have been reported within 3 mmHg of aortic values[36], supporting the validity of our calibration procedure. In our population, at rest, the radial pulse pressure was statistically higher than the carotid one (55±21 mmHg vs. 39±10 mmHg, p<0.001). There was no clinically significant difference between the measured carotid pulse pressure and the one derived from the radial recordings on which we applied the transfer function published by Chen et al.[22] (41±14 mmHg). At peak exercise, the radial pulse pressure was 102±26 mmHg and PP_{Ao} was 73±25 mmHg. The use of peripheral systolic BP would lead to an overestimation of **Pmax**.

Limitations:

A supine bicycle exercise test is less physiological than walking on a treadmill and VO_2max might have been slightly lower[37], explaining perhaps that the linear relationship we found between VO_2max and cardiac output at peak exercise (CO_p (L/min) = 4.2 + 3.6 VO_2max (in L/min)) differs partly from previous reports: CO_p = 4.0 + 6.0 VO_2max for Jones et al.[38] and CO_p = 3.0 + 5.6 VO_2max for Cooke et al.[10]

There were probably too few patients in each group (negative, non-diagnostic and positive exercise tests) to find a difference in their hemodynamic parameters.

Mandarino et al. have reported on-line computation of **Pmax** based on the evaluation of the rate of change of the ventricular volume by echocardiographic automated border detection (ABD)[18] while we assess **Pmax** off-line. Increased computational processing capabilities could permit on-line V_{Ao} and **Pmax** assessment. **sPmax** might be readily performed on an echocardiographic system, with mean BP entered from the keyboard and a horizontal cursor used to visually follow peak V_{Ao}.

The noise generated during exercise is in the frequency range of the Korotkov sounds[39] and sphygmomanometer measurements are more difficult, with potential errors for the determination of the diastolic BP very important for the calibration of the tonometric measurements.

This study did not include patients with severe left ventricular dysfunction. The assessment of mean BP as (2 x Diastolic BP + Systolic BP)/3 might not be always valid in these patients, or in the presence of a modified arterial distensibility.

Finally, the transfer function used to estimate BP_{Ao} from the tonometric radial recordings has only been validated at rest.[22]

Conclusion

From simultaneously acquired tonometric and Doppler echocardiographic recordings, we describe a fully non-invasive assessment of maximal left ventricular power output during exercise echocardiography. We could validate a recently proposed simplified index easier to obtain and highly correlated with **Pmax**. Both indexes reflect contractile state and demonstrate a strong linear relationship

with VO_2max and carry additional independent information over more conventional hemodynamic parameters. Additional prospective studies in patients with congestive heart failure should be performed to further transfer bench-work pressure-volume studies to the clinical arena.

Acknowledgements. The authors would like to thank all the team of the Cardiovascular Imaging Department of the Cleveland Clinic Foundation for their expert assistance.

References

1. Suga H, Sagawa K, Shoukas AA. Load independence of the instantaneous pressure-volume ratio of the canine left ventricle and effects of epinephrine and heart rate on the ratio. *Circ Res.* 1973;32:314-322.
2. Feneley MP, Skelton TN, Kisslo KB, Davis JW, Bashore TM, Rankin JS. Comparison of preload recruitable stroke work, end-systolic pressure-volume and dP/dtmax-end-diastolic volume relations as indexes of left ventricular contractile performance in patients undergoing routine cardiac catheterization. *J Am Coll Cardiol.* 1992;19:1522-1530.
3. Kelly R, Fitchett D. Noninvasive determination of aortic input impedance and external left ventricular power output: a validation and repeatability study of a new technique. *J Am Coll Cardiol.* 1992;20:952-963.
4. Aakhus S, Soerlie C, Faanes A, Hauger SO, Bjoernstad K, Hatle L, Angelsen BAJ. Noninvasive computerized assessment of left ventricular performance and systemic hemodynamics by study of aortic root pressure and flow estimates in healthy men, and men with acute and healed myocardial infarction. *Am J Cardiol.* 1993;1993:260-267.
5. Marmor A, Raphael T, Marmor M, Blondheim D. Evaluation of contractile reserve by dobutamine echocardiography: noninvasive estimation of the severity of heart failure. *Am Heart J.* 1996;132:1195-1201.
6. Marmor A, Schneeweiss A. Prognostic value of noninvasively obtained left ventricular contractile reserve in patients with severe heart failure. *J Am Coll Cardiol.* 1997;29:422-428.
7. Tan LB. Clinical and research implications of new concepts in the assessment of cardiac pumping performance in heart failure. *Cardiovasc Res.* 1990;8:615-622.
8. Tan LB, Littler WA. Measurement of cardiac reserve in cardiogenic shock: implications for prognosis and management. *Br Heart J.* 1990;64:121-128.
9. Stelken AM, Younis LT, Jennison SH, Miller DD, Miller LW, Shaw LJ, Kargl D, Chaitman BR. Prognostic value of cardiopulmonary exercise testing using percent achieved of predicted peak oxygen uptake for patients with ischemic and dilated cardiomyopathy. *J Am Coll Cardiol.* 1996;27:345-52.
10. Cooke GA, Marshall P, Al-Timman JK, Wright DJ, Riley R, Hainsworth R, Tan LB. Physiological cardiac reserve: developments of a non-invasive method and first estimates in man. *Heart.* 1998;79:289-294.
11. Armstrong GP, Carlier SG, Fukamachi K, Cardon LA, Borden RA, Thomas JD, Marwick TH. Estimation of cardiac reserve by peak power. Validation and initial application of a simplified index. *Heart.* 1999;82:357-364.
12. Schiller NB, Shah PM, Crawford M, DeMaria A, Devereux R, Feigenbaum H, Gutgesell H, Reichek N, Sahn D, Schnittger I, et al. Recommendations for quantitation of the left ventricle by two- dimensional echocardiography. American Society of Echocardiography Committee on Standards, Subcommittee on Quantitation of Two-Dimensional Echocardiograms. *J Am Soc Echocardiogr.* 1989;2:358-67.
13. American College of Sports Medicine. ACSM's Guidelines for Exercise Testing and Prescription. *Baltimore.* 1995;Williams & Wilkins.
14. Rassi A, Jr., Crawford MH, Richards KL, Miller JF. Differing mechanisms of exercise flow augmentation at the mitral and aortic valves. *Circulation.* 1988;77:543-51.
15. Carlier S, Marwick T, Segers P, Verdonck P, Van Camp G, Cosyns B, Thomas JD. Non-invasive evaluation of left ventricular power output by simultaneous recordings of applanation tonometry and echocardiographic Doppler signals. *Computers in Cardiology.* 1997;223-226.
16. Bland IM, Altman DG. Statistical methods for assessing agreement between two methods of clinical measurement. *Lancet.* 1986;1(8476): 307-310.
17. Kass DA, Beyar R. Evaluation of contractile state by maximal ventricular power divided by the square of end-diastolic volume. *Circulation.* 1991;84:1698-1708.
18. Mandarino WA, Pinsky MR, Gorscan JIII. Assessment of left ventricular contractile state by preload-adjusted maximal power using echocardiographic automated border detection. *J Am Coll Cardiol.* 1998;31:861-868.
19. Drzewiecki GM, Melbin J, Noordergraaf A. Arterial tonometry: review and analysis. *J Biomechanics.* 1983;16:141-152.
20. Kelly R, Karamanoglu M, Gibbs H, Avolio A, O'Rourke M. Noninvasive carotid pressure wave registration as an indicator of ascending aortic pressure. *J Vasc Med Biol.* 1989;1:241-247.
21. Chen CH, Ting CT, Nussbacher A, Nevo E, Kass DA, Pak P, Wang SP, Chang MS, Yin FC. Validation of carotid artery tonometry as a means of estimating augmentation index of ascending aortic pressure. *Hypertension.* 1996;27:168-175.
22. Chen CH, Nevo E, Fetics B, Pak PH, Yin FCP, Maughan L, Kass DA. Estimation of central aortic pressure waveform by mathematical transformation of radial tonometry pressure. Validation of a generalized transfer function. *Circulation.* 1997;95:1827-1836.
23. McDonald DA. *Blood flow in arteries.* London: Edward Arnold; 1974.
24. Nakayama M, Chen CH, Nevo E, Fetics B, Wong E, Kass DA. Optimal preload adjustment of maximal ventricular power index varies with cardiac chamber size. *Am Heart J.* 1998;136:281-288.
25. Tan LB. Evaluation of cardiac dysfunction, cardiac reserve and inotropic response. *Postgrad Med J.* 1991;67 (suppl 1):S10-S20.
26. Stringer WW, Hansen JE, Wasserman K. Cardiac output estimated noninvasively from oxygen uptake during exercise. *J Appl Physiol.* 1997;82:908-12.
27. Dell'Italia LJ, Freeman GL, Gaasch WH. Cardiac function and functional capacity: implications for the failing heart. *Curr Probl Cardiol.* 1993;18:707-758.
28. Leung DY, Griffin BP, Stewart WJ, Cosgrove DM, 3rd, Thomas JD, Marwick TH. Left ventricular function after valve repair for chronic mitral regurgitation: predictive value of preoperative assessment of contractile reserve by exercise echocardiography. *J Am Coll Cardiol.* 1996;28:1198-205.
29. van den Broek SA, van Veldhuisen DJ, de Graeff PA, Landsman ML, Hillege H, Lie KI. Comparison between New York Heart Association classification and peak oxygen consumption in the assessment of functional status and prognosis in patients with mild to moderate chronic congestive heart failure secondary to either ischemic or idiopathic dilated cardiomyopathy. *Am J Cardiol.* 1992;70:359-63.
30. Rooke GA, Feigl EO. Work as a correlate of canine left ventricular oxygen consumption, and the problem of catecholamine oxygen wasting. *Circ Research.* 1982;50:273-286.
31. Filipovsky J, Ducimetiere P, Safar ME. Prognostic significance of exercise blood pressure and heart rate in middle-aged men. *Hypertension.* 1992;20:337-339.
32. Mundal R, Kjeldsen SE, Sandvik L, Erikssen G, Thaulow E, Erikssen J. Exercise blood pressure predicts mortality from myocardial infarction. *Hypertension.* 1996;27:324-329.
33. Mundal R, Kjeldsen SE, Sandvik L, Erikssen G, Thaulow E, Erikssen J. Clustering of coronary risk factors with increasing blood pressure at rest and during exercise. *J Hypertens.* 1998;16:19-22.
34. Rowell LB, Brengelmann GL, Blackmon JR, Bruce RA, Murray JA. Disparities between aortic and peripheral pulse pressures induced by upright exercise and vasomotor changes in man. *Circulation.* 1968;37:954-964.
35. Blum V, Carrière EGJ, Kolsters W, Mosterd WL, Schiereck P, Wesseling KH. Aortic and peripheral blood pressure during isometric and dynamic exercise. *Int J Sports Med.* 1997;18:30-34.
36. Pauca AL, Wallenhaupt SL, Kon ND, Tucker WY. Does radial artery pressure accurately reflect aortic pressure ? *Chest.* 1992;102:1193-1198.
37. Shephard RJ. Standard tests of aerobic power. In: Shephard RJ, ed. *Frontiers of fitness.* Springfield: Charles C Thomas; 1971.
38. Jones NL. *Clinical exercise testing.* Philadelphia: W B Saunders; 1988.
39. Ellestad MH. Reliability of blood pressure recordings. *Am J Cardiol.* 1989;63:983-985.

SUMMARY AND DISCUSSION

SUMMARY AND DISCUSSION

Intracoronary Doppler and pressure measurements (chapters 1-5):

The last few years have seen rapid advances in coronary Doppler and pressure probe technology and the development of new physiological measurements to assess the significance of coronary lesions or the results of interventions. **In chapter 1**, we have reviewed in depth these technological improvements and described methods such as the coronary flow reserve (CFR) for the assessment of a coronary lesion. We have stressed the limitations of CFR, which is dependent on an epicardial artery stenosis and on the microvascular bed. This ratio of the maximum hyperemic flow over the baseline flow can also vary with changes in the baseline conditions, as observed during coronary interventions. Most of the suboptimal CFR measurements after a balloon angioplasty are related to increased baseline velocities.[1,2] The advantages of alternative methods such as the fractional flow reserve (FFR), based on the pressure gradient across a lesion during hyperemia, have been stressed. However, from a fluid mechanics point of view, both pressure and flow are necessary to fully characterize the coronary circulation and the influence of a stenosis. Indexes like the instantaneous hyperemic diastolic pressure velocity relationship have been introduced. However, they are rather cumbersome to use and they present a large coefficient of variation that limit their clinical use.

In **chapter 2**, we show that septal hypertrophy is associated with decrements in CFR in patients with hypertrophic cardiomyopathy (HCM), and that there is also a decrease in the coronary resistance reserve, CRR, the ratio of coronary resistance during hyperemia over baseline resistance. Coronary resistance is defined as (Pao-Ped)/Vcor, where Pao is aortic pressure, Ped is end diastolic pressure and Vcor the coronary velocity. Ped corrects the extravascular compression, which cannot therefore be implied in the observed decrease of CFR and CRR. We show that capillary density tended to decrease and that there was a positive relationship between both CFR and CRR and arteriolar lumen: patients with HCM have arterioles with smaller lumen at similar wall thickness that can contribute to perfusion abnormalities. In these patients, the ratio of the slopes of the linear regression of diastolic pressure and velocity data, which reflect coronary conductance, was more sensitive than CFR to detect a decrease in coronary reserve [unpublished data]. Since this index is independent of extravascular compression, it has also the advantage to only reflect coronary vascular remodeling.

In **chapter 3**, we describe an acquisition system to simultaneously record raw Doppler signals along with pressure, ECG and other physiological signals. The off-line post-processing of the recomputed power spectrum using a fast Fourier transform permits a better determination of the true maximum velocity contour. Averaging multiple cycles increases the signal to noise ratio and further improves the detection of the maximum velocity. This system, studied initially *in vitro*, is presently used on a daily basis in our catheterization laboratory. It provides improved archiving and viewing possibilities than conventional videotapes. Studies of more complex indices of the coronary circulation such as the coronary conductance reserve are possible. A recent comparison between the on-line average peak velocity (APV) and the APV obtained by reprocessing the Doppler spectrum showed excellent agreement. The average difference among 66 measurements obtained in 11 patients was -0.7 ± 1.2 cm/s when there was an optimal on-line detection. However, in 12% of the recordings, the on-line tracking failed to recognize the true peak velocity and the

mean difference between the 2 methods was 3±8 cm/s, with a maximum difference of 15 cm/s. This was clinically significant since the average underestimation of the derived CFR was -0.4±0.3 [unpublished data].

In **chapter 4**, we demonstrate another limitation of the CFR to guide interventions: its lack of cost-effectiveness. There was no statistical difference in event-free survival at 1 year between primary stenting (86.6 %) and provisional angioplasty (85.6%). However, the costs after 1 year were significantly higher (EUR 6573 vs. EUR 5885, p=0.01) for the strategy of provisional angioplasty. Moreover, the patients with an optimal angioplasty result who received a stent in the second randomization tended to have an improved event-free survival at 1 year (93.5% vs. 84.1 %, p=0.066). These data, as well as the results of the other studies discussed in the related editorial of the Debate II study, support the ever-increasing use of stents nowadays in interventional cardiology.
FFR is an alternative physiological method, based on intracoronary pressure measurements, that has also been proposed to guide interventions. In **chapter 5**, we show that FFR fails to discriminate between optimally and suboptimally implanted stents in an *in vitro* setup. The FFR variations related to the changes of the maximal flow between 50 and 150 ml/min were 5 to 10 times higher than the variations related to the optimal or suboptimal expansion of the stents. The limitations of CFR and FFR described in chapters 1-5, as well as others, recently reviewed,[3] support the alternative method of coronary flow measurement using an IVUS catheter that is described in the next part of this thesis.

Intracoronary Flow Measurements with IVUS catheters (chapters 6-9):
Chapter 6 introduces the principles of the IVUS flow method that was originally developed by W. Li et al. in our laboratory.[4] Flow velocity is based on decorrelation estimation from sequences of radiofrequency (RF) IVUS traces.
The *in vivo* validation reported in **chapter 7** demonstrates a good agreement between the IVUS flow method and electromagnetic flowmeter (EM) recordings in a porcine carotid model (IVUS f= 1.0 EMf + 5.72 cc/min). In the early phase of the development of this technique using a single rotating IVUS crystal, good agreement was found with intracoronary Doppler measurements in 5 patients: the mean difference between the IVUS and Doppler derived CFR was –0.01±0.21, for a mean CFR of 1.9.

The study of the disturbances in the velocity profile induced by an IVUS catheter, applying computational fluid dynamics, demonstrated that secondary velocity components were in the order of 10-15 %. However, the deviation in the flow estimation was less than 1 % when flow calculation was based exclusively on the axial velocity. The presence of an IVUS catheter (diameter of ≈1 mm) in a curved tube of 3 mm in diameter induces a resistance of 10 mmHg.s/m2 for a flow entrance with a mean velocity of .4 m/s. The resistance goes up to 38 mmHg.s/m^2 in a tube of 2 mm, illustrating an important limitation of the IVUS flowmetry: a significant hemodynamic effect on the flow in small arteries during hyperemia (**chapter 8**). This limitation will be improved once new smaller IVUS catheters will be available.

Chapter 9 presents the *in vitro* evaluation of the IVUS flow method using an IVUS array catheter. Excellent linear relationships were found (all r>0.99) with a reference flow ranging from 0 to

341 cc/min, measured with a Transonics flow-meter, in tubes with a diameter ranging from 3 to 5 mm. However, an increasing offset (ranging from 6 to 182 cc/min) and a varying slope were observed. These observations are related to the inherent electronic noise picked by the IVUS catheter, and to the position of the catheter and the ring-down artifact. Nevertheless, a proposed correction, based on the determination of the offset that can be estimated in a zero flow condition, permitted the determination of a CFR in excellent agreement with the Transonic catheter. The mean difference between the two CFR estimates was 0±0.19, for a mean CFR of 2. These results warrant further in vivo investigations.

Characterization of Arterial Wall Mechanics by RF Processing (chapters 10-12):
IVUS elastography is a method for measuring the local elastic properties of coronary atherosclerotic plaques. Mechanical properties of the different tissues within a plaque are measured through the strain. We have reviewed in **chapter 10** the work of several groups working on vascular and non-vascular strain/stress assessment. We describe in detail the elastography method developed in our laboratory, and present the preliminary results obtained in tube phantoms, and in human coronary arteries. **Chapter 11** focuses on the feasibility of recording elastograms during interventional catheterization procedures. In 12 patients we obtained reproducible strain measurements at the end of diastole, where the motion of the catheter is minimal. Although these recordings were obtained with a low resolution imaging mode (64 angles of the "flow mode"), we partly validated our measurements, demonstrating a significantly lower strain in calcified than in non-calcified regions (0.20 vs. 0.51 %, respectively, $p<0.001$). A simplified, more robust and very fast real-time intravascular ultrasonic palpation system is described in **chapter 12.** Composite palpograms are created applying a one-dimensional echo tracking technique in combination with global motion compensation and multi-frame averaging of several pairs of RF echo frames obtained in diastole. The RF recording is based on digital beamed-formed RF echo data (512 lines) sampled to 12 bits at 100 MHz and directly transferred into the PC memory at full frame rate (30 fps). We demonstrated the possibility to record consistent palpograms possessing good contrast resolution and elastographic signal to noise ratio under physiological conditions. This work warrants further large-scale clinical investigations. Comparison of elastography and palpography with histology to demonstrate characterization of arterial wall mechanics is one of the ongoing studies that may validate the clinical usefulness of this new imaging modality.

Intravascular ultrasound and intracoronary brachytherapy (chapters 13-16):
In **chapter 13** we review the use of IVUS in the clinical studies of coronary brachytherapy. We have been the first to describe the methodology to compute dose volume histograms from 3-dimensional reconstruction of ECG-gated IVUS pullbacks.[5] **Chapter 14** presents the comparison, by simulation, of different treatment strategies based on either β- or γ-sources with and without a centering device. We show that among 23 patients treated in the Beta Energy Restenosis Trial, the minimum dose on 90% of the adventitial surface was 37±16 % of the prescribed dose, while 67±31% of the prescribed dose was delivered to 90% of the luminal surface. In comparison, the use of a centered device or a g-source would have increased these values, and have decreased the minimum dose on the 10% most exposed luminal and adventitial surfaces, thereby improving dose homogeneity. Although presently no clinical data support the potential benefits of an improved dose homogeneity, our pioneering work demonstrates the feasibility of assessing the dose delivered in

the arterial wall of arteries treated with brachytherapy. The importance of this work was stressed in the accompagnying editorial comments.

In **chapter 15**, we analyze a total of 206 coronary 2 mm sub-segments from 18 patients treated for de novo lesion with angioplasty followed by β-brachytherapy. We demonstrate that at 6-month follow-up, the volume of the hard plaques increased less compared to soft plaques and normal/intimal thickening regions. We also illustrate that the minimum dose deposited on 90 % of the adventitial surface (D_{90}adv) is inversely related to the plaque volume at follow-up.

In **chapter 16** we demonstrate that the 6-month angiographic outcome of 27 patients treated for a de novo lesion with angioplasty alone (no stent) followed by β-brachytherapy could partly be explained by the dose delivered in the coronary arterial wall. The minimum dose on 90% of the luminal surface (DS_{90}lum), the external elastic lamina (DS_{90}eel) and in 90% of the plaque+media volume (DV_{90}p+m) were 9.7±6.1 Gy, 5.1±3.0 Gy and 7.0±4.0 Gy, respectively. At 6-month follow-up, the patients with a DS_{90}eel greater than 5.2 Gy (n=11) had a lower angiographic loss (-0.01±0.39 vs. 0.47±0.62 mm, p=0.03) and late loss index (-0.4±58 vs. 44±56 %, p=0.06). These arteries were smaller, however the relative gain was identical and the observed difference in the loss could only reflect the remodelling of the coronary segments receiving an adequate dose.

Transthoracic echocardiography for biomechanical assessment of the left ventricle and the aorta (chapter 17-20):

Chapter 17 is an historical overview of the developments of cardiovascular echocardiography. In **chapter 18**, we show that a recursive evaluation of the total arterial compliance (Ctot) based on a 2-element windkessel model (the pulse pressure method) is feasible using transthoracic echo-Doppler and arterial tonometry. The evaluation of Ctot with the pulse pressure method is robust and give, among 14 patients with known or suspected coronary artery disease (CAD) and 9 volunteers, significantly different arterial stiffness estimation (1.2±0.4 vs. 1.6±0.2 ml/mmHg). It is also the best method to find the expected inverse relationship of total arterial compliance and age, in comparison with the area method and the ratio of the stroke volume over the pulse pressure.

Chapter 19 describes the quest for an optimized transfer function (TFF) allowing the reconstruction of aortic pressure from peripheral tonometric recordings at the level of the radial artery. We fit a three-segment transmission line model for the radial-carotid pressure TFF derived from 31 normal volunteers and 30 patients with CAD. We only find a difference, between the patients and the controls, of the distal reflection coefficient. We describe the average TFF computed, as well as the ones derived from the minimum and maximum enveloping TFF. We show the variability resulting from the use of each one on aortic derived pressure characteristics such as the central pulse pressure or the augmentation index.

Finally, in **chapter 20**, we describe the assessment of left ventricular (LV) performance and contractile reserve during supine stress echocardiography by the determination of maximum ventricular power output using simultaneous recordings of aortic flow by Doppler echocardiography and aortic pressure by arterial tonometry. We demonstrate a good agreement between the data derived from carotid recordings and from transformed radial recordings using a TFF. We also validate a

simplified index of LV power output that we first described in animal experiments[6]: the product of peak aortic flow and mean blood pressure. This surrogate of the true peak power, which is less cumbersome to obtain than invasive recordings or even arterial tonometry, showed the same correlations with the VO_2max recorded in these 25 patients.

References

1. van Liebergen RA, Piek JJ, Koch KT, de Winter RJ, Lie KI. Immediate and long-term effect of balloon angioplasty or stent implantation on the absolute and relative coronary blood flow velocity reserve. *Circulation*. 1998;98:2133-40.
2. Albertal M, Regar E, Van Langenhove G, Carlier SG, Serrano P, Boersma E, de Bruyne B, di Mario C, Piek J, Serruys PW. Flow velocity and predictors of a suboptimal coronary flow velocity reserve after coronary balloon angioplasty. *Eur Heart J*. 2001:(in press).
3. Carlier SG, Van Langenhove G, Lupotti F, Albertal M, Mastik F, Bom K, Serruys PW. Coronary flow reserve versus geometric measurements of coronary dimensions: advantages and limitations of the functional stenosis assessment. *J Intervent Cardiol*. 1999;12:411-424.
4. Li W, van der Steen AFW, Lancee CT, Cespedes I, Gussenhoven EJ, Bom N. Blood flow imaging and volume flow quantification with intravascular ultrasound. *Ultrasound Med Biol*. 1998;24:203-214.
5. Carlier SG, Marijnissen JP, Coen VL, van der Giessen WJ, Sabate M, Ligthart J, den Boer A, Cespedes IE, Li W, van der Steen AF, Levendag PC, Serruys PW. Guidance of intracoronary radiation therapy based on dose-volume histograms derived from quantitative intravascular ultrasound. *IEEE Trans Med Imaging*. 1998;17:772-8.
6. Armstrong GP, Carlier SG, Fukamachi K, Cardon LA, Borden RA, Thomas JD, Marwick TH. Estimation of cardiac reserve by peak power. Validation and initial application of a simplified index. *Heart*. 1999;82:357-364.

CONCLUSIONS AND FUTURE PERSPECTIVES

CONCLUSIONS AND FUTURE PERSPECTIVES

Miniaturized intracoronary Doppler and pressure wires offer today the possibility to study coronary physiology in the cathlab. In clinical practice, the pressure measurements are gaining interest, often in order to postpone an intervention. The assessment of the coronary flow reserve remains in a research niche. The availability of a combined wire interfaced to a fully digital processing platform would offer complete assessment of the coronary circulation.

A simultaneous morphological and physiological assessment of the coronary arteries with one IVUS catheter may be the optimal tool to assess the results of a PTCA. However, further studies of the reliability and limitations of the IVUS flow method will be necessary before full clinical implementation. IVUS flowmetry should be further investigated if we are to demonstrate that IVUS guided stent implantation combined with physiological assessment is the most effective approach for our patients.

Elastography will enter the clinical arena once it has been fully validated in vitro, with the determination of the mean strain values of different types of histology samples. When on-line robust hardware processing will be implemented to offer rapid 3-d reconstructions of the mechanical characteristics of an arterial wall segment, this technique will help us detecting rupture-prone plaques. Clinical studies will have to determine how many of these plaques are present among our patients. If they were ubiquitous, then only a systematic treatment based e.g. on high-dose statins would be applicable. If only one or two were found, one could attempt to heal these lesions by stenting. The advent of drug-coated stents could permit to do so without a risk of restenosis. If these stents are really as good as they seem to be presently, then brachytherapy will have problems competing with this easier alternative to prevent restenosis. IVUS dosimetry will then become obsolete. Currently IVUS dosimetry is utilized as a post-hoc analysis tool to understand QCA and IVUS results in brachytherapy studies. Ideally, on-line treatment planning system should become available in order to fully exploit this methodology.

There is great scope for the further development of the bioengineering technologies described in this thesis. For non-invasive pressure and flow recordings, the described acquisition systems are presently run in the Netherlands and overseas, in Brisbane, Australia. The author hopes that with further investigations they will be used to improve patient outcome, as well as to prepare other PhD's. If a few engineers can also gain some useful information from this thesis to further understand pathophysiological problems in order to develop improved diagnostic and therapeutic devices, the author will give back a very small part of what he enjoyed learning, working in close collaboration with some of their colleagues. Bioengineering is here to stay, and will hopefully remain a multidisciplinary field of expertise and exchanges.

SAMENVATTING

SAMENVATTING

Intracoronaire Doppler en drukmetingen (hoofdstukken 1-5):
Tijdens de laatste jaren is er veel vooruitgang geboekt op het gebied van coronaire Doppler en druk-meettechnieken evenals op het gebied van de ontwikkeling van nieuwe fysiologische metingen om de ernst van coronaire lesies of het resultaat van interventies te bepalen. In **hoofdstuk 1** hebben we nauwkeurig deze technologische verbeteringen nagekeken en hebben het normale coronaire debiet en methodes zoals "coronary flow reserve" (CFR) ter evaluatie van een coronaire lesie beschreven. We hebben de beperkingen van CFR welke afhangt van zowel het epicardiale als het microvasculaire bed benadrukt. Deze ratio van maximaal hyperemisch debiet over basaal debiet varieert ook met veranderingen in basale condities zoals geobserveerd gedurende coronaire interventies: de meeste van de suboptimale CFR metingen na ballonangioplastie zijn gerelateerd aan verhoogde basale bloedsnelheden.[1,2] De voordelen van alternatieve methodes zoals de "fractional flow reserve" (FFR), gebaseerd op de drukgradient over een lesie gedurende hyperemie worden naar voor gebracht. Echter, vanuit hydromechanisch standpunt, zijn zowel druk als debiet noodzakelijk om de coronaire circulatie en de invloed van stenose volledig te karakteriseren. Indices zoals de instantane hyperemische diastolische druk-snelheid relatie worden geintroduceerd. Ze zijn echter vrij omslachtig in gebruik en ze vertonen een grote variatiecoefficient welke hun klinische bruikbaarheid beperken.

In **hoofdstuk 2** hebben we aangetoond dat septale hypertrofie geassocieerd is met verminderingen in CFR in patienten met hypertrofische cardiomyopathie (HCM), en dat er ook een vermindering is in "coronaire weerstand (resistance) reserve", CRR, de ratio van coronaire weerstand gedurende hyperemie en basale weerstand. Coronaire weerstand wordt gedefinieerd als (Pao-Ped)/Vcor, waar Pao de druk in de aorta is, Ped de einddiastolische druk en Vcor de coronaire snelheid. Ped corrigeert voor de extravasculaire compressie. Deze factor kon dus niet betrokken zijn in de vastgestelde gedaalde CFR en CRR. Er werd aangetoond dat de capillaire densiteit neigde te verminderen en dat er een positief verband bestond tussen zowel CFR als CRR en het arteriolaire lumen: patienten met HCM hebben kleinere arteriolaire lumina bij een zelfde wanddikte wat kan bijdragen tot perfusiestoornissen. In deze patienten was de ratio van de hellingen van de lineaire regressie van diastolische druk- en snelheidsdata, welke coronaire conductantie weergeeft, gevoeliger dan CFR om een daling in coro-naire reserve te detecteren.[ongepubliceerde data] Gezien deze index onafhankelijk is van extravasculaire compressie, heeft het ook het voordeel enkel coronaire vasculaire "remodeling" weer te geven.

In **hoofdstuk 3** beschrijven we een acquisitiesysteem om simultaan ruwe Doppler signalen, druk-, ECG- en andere fysio-logische signalen te registreren. De "off-line" bewerking van het samengestelde power spectrum volgens een "fast" Fourier transformatie laat een betere bepaling toe van de maximale snelheidscontouren. Het middelen van verschillende cycli verhoogt de signaal-tot-ruis ratio en verbetert verder de detectie van de maximale snelheidscontour. Dit systeem, initieel bestudeerd in vitro, wordt heden dagelijks gebruikt in ons cathaterisatielab en biedt, naast verbeterde archivering en bekijk-mogelijkheden vergeleken met conventionele video, de mogelijkheid tot het bestuderen van meer complexe indices van coronaire circulatie zoals coronaire conductantie reserve. Een recente vergelijking tussen de "on-line" gemiddelde pieksnelheid

("average peak velocity", APV) en de APV bekomen via herbewerking van het Doppler spectrum toonde een excellente overeenkomst tussen de twee methodes (het gemiddelde verschil tussen 66 metingen in 11 patienten was –0.7±1.2 cm/s bij een optimale "on-line" detectie). Echter in 12% van de registraties faalde de "on-line" contourdetectie de echte pieksnelheid te herkennen waarbij het verschil tussen de 2 methodes dan gemiddeld 3±8 cm/s bedroeg, met een maximaal verschil van 15 cm/s, klinisch significant, gezien de onderschatting van de afgeleide CFR gemiddeld –0.4 ±0.3 was.[ongepubliceerde data]

In **hoofdstuk 4** tonen we een andere beperking aan van CFR om interventies te begeleiden: zijn gebrek aan kosten-effectiviteit. De strategie van provisionele angioplastie, geleid door de optimale resultaten van kwantitatieve angiografie en intracoronaire flow metingen, leidde in de 75% van de patienten die geen "bailout stenting"nodig hadden, tot een vergelijkbare "event-free" overleving na 1 jaar als de strategie van primaire stenting (85.6 vs 86.6% respectievelijk). Echter, de kosten na 1 jaar waren significant hoger (EUR 6573 vs EUR 5885, p=0.01). Bovendien neigden de patienten met een optimaal angioplastieresultaat die een stent kregen tijdens de tweede randomizatie, tot een betere "event-free" overleving na 1 jaar (93.5% vs 84.1%, p=0.066). Deze data, evenals de resultaten van andere studies samengevat in de editoriaal over de Debate II studie, ondersteunen het steeds groeiende gebruik van stents heden ten dage in de interventionele cardiologie.

In **hoofdstuk 5** tonen we in een in vitro setup aan dat de FFR, een alternatieve fysiologische methode gebaseerd op intracoronaire drukmetingen ter begeleiding van interventies, faalt om optimaal geimplanteerde van suboptimaal geimplanteerde stents te onderscheiden. De variaties van de FFR gerelateerd aan veranderingen in maximaal debiet tussen 50 en 150 ml/min waren 5 tot 10 keren hoger dan de variaties van de FFR tussen stents met een residuele diameter stenose (DS) van 35% aangetoond met QCA en met duidelijk slecht geappositioneerde struts aangetoond met IVUS en volledige ontplooide stents. De beperkingen van CFR en FFR beschreven in hoofdstukken 1 -5, evenals andere beperkingen, recent gereviseerd[3] ondersteunen de alternatieve methode van coronaire flow metingen met een IVUS catheter zoals beschreven in het volgende deel van deze thesis.

Intracoronaire debietmetingen met IVUS catheters (hoofdstukken 6-9):

Hoofdstuk 6 introduceert de principes van de "intravascular ultrasound (IVUS) flow" methode die oorspronkelijk ontwikkeld werd in ons laboratorium door W. Li et al [4]. De snelheid van de rode bloedcellen is gebaseerd op de schatting van de decorrelatie van opeenvolgende radiofrequentie (RF) tracees.

De in vivo validatie, gerapporteerd in **hoofdstuk 7**, toont een goede overeenkomst tussen de IVUS flow methode en de electromagnetische debietmeter (EM) registraties in een varken carotis model (IVUSf= 1.0 EMf + 5.72 cc/min). In de vroege fase van de ontwikkeling van deze techniek met een enkele roterende kristal IVUS catheter , werd ook een goede overeenkomst gevonden met intracoronaire Dopplermetingen in 5 patienten: het gemiddelde verschil tussen de IVUS en Doppler afgeleide CFR was -0.01±0.21, voor een gemiddelde CFR van 1.9. Studie over de storingen in snelheidsprofiel geinduceerd door een IVUS catheter, gebruikmakende van de hydrodynamica, toonde dat secundaire snelheidcomponenten in de grootte-orde van 10-15% waren, maar dat de afwijking in de schatting van het debiet kleiner was dan 1% wanneer de berekening van de flow enkel

gebaseerd was op de axiale snelheid. De aanwezigheid van deze catheter van ~1 mm in een gebogen tube van 3 mm diameter induceert een weerstand van 10 mmHg.s/m² voor een debiet die binnenkomt met een gemiddelde snelheid van 0.4 m/s. De weerstand loopt op naar 38 mmHg.s/m² in een tube van 2 mm, wat een belangrijke beperking van IVUS debietmeting illustreert: een significant hemodynamisch effect op de flow in kleine arteriën gedurende hyperemie (**hoofdstuk 8**). Deze beperking kan verbeterd worden door het beschikbaar stellen van kleinere IVUS catheters.

Hoofdstuk 9 stelt de in vitro evaluatie voor van de IVUS flow methode gebruikmakende van een IVUS array catheter. Er werden excellente lineaire verbanden gevonden (allen r>0.99) met een referentie flow gaande van 0 tot 341 cc/min, gemeten met een Transonics debietmeter, in tubes met een diameter van 3 tot 5 mm. Echter, een toenemende "offset" (gaande van 6 tot 182 cc/min) en een wisselende helling werden geobserveerd. Deze observaties waren gerelateerd aan de inherente electronische ruis opgenomen door de IVUS catheter, aan de positie van de catheter en aan "ring-down" artefact. Het "ring-down" artefact wordt veroorzaakt door het uitslingeren van de transducer nadat er een puls opgezet is. Tijdens het uitslingeren (± 1 μs) kunnen geen betrouwbare signalen worden opgenomen. Niettemin, een voorgestelde correctie, gebaseerd op de bepaling van de "offset" welke kan geschat worden bij een "zero flow" conditie, liet de bepaling toe van een CFR welke excellent overeenkwam met de gouden standaard gemeten met de Transonic catheter (het gemiddelde verschil tussen de twee CFR schattingen was 0±0.19 voor een gemiddelde CFR van 0.2). Deze resultaten beloven verder in vivo onderzoek.

Karakterisering van Arteriele Wand Mechanismen door RF Processing (hoofdstukken 10-12): IVUS elastografie is een methode voor het meten van de locale elastische eigenschappen van coronaire atherosclerotische plaques. Mechanische eigenschappen van de verschillende weefsels in een plaque worden gemeten via rek. In **hoofdstuk 10** hebben we het werk gereviseerd van verschillende groepen die werken op het domein van vasculaire en non-vasculaire rek/spanning. We beschrijven in detail de methode ontwikkeld in ons laboratorium, en de voorlopige resultaten bekomen in tube fantomen, en later in humane coronairen.

Hoofdstuk 11 handelt over preliminaire registraties in patienten, waarbij we het nut van elastogrammen tijdens catheterisatieprocedures konden aantonen. In 12 patienten konden we reproduceerbare rekmetingen bekomen in einddiastole, wanneer de beweging van de catheter minimaal is. Ofschoon deze opnames bekomen werden via beeldvorming met een lage resolutie (64 hoeken van de "flow mode"), konden we gedeeltelijk onze metingen valideren door een significant lagere rek aan te tonen in gecalcifieerde dan in non-gecalcifieerde regios (0.20 vs 0.51% respectievelijk, p<0.001). Een gesimplifieerd, meer robust en bijna "real-time" intravasculair palpatiesysteem wordt beschreven in **hoofdstuk 12**. Samengestelde palpogrammen worden gemaakt met een 1-dimensionele echo "tracking" techniek in combinatie met globale bewegingscompenstie en het "multi-frame" middelen van verschillende paren RF echo "frames" in diastole. RF registratie is nu gebaseerd op digitale "beam-formed" RF echo data (512 lijnen) verzameld tot 12 bits bij 100 MHz en direct getransfereerd naar het PC geheugen met volledige frame rate (30 fps). We konden registraties maken van consistente palpogrammen met goede contrast resolutie en elastografische signaal tot ruis ratio onder fysiologische omstandigheden, die vragen voor verder
klinische investigaties op grote schaal. Vergelijking van elastografie en palpografie met histolo-

gisch materiaal bekomen met directionele atherectomie is een van de aan de gang zijnde validatiestudies welke het klinische nut moet bewijzen van deze nieuwe beeldvormingsmodaliteit die karakterisering van de arteriele wand mechaniek toelaat.

Intravasculaire Ultrason en Intracoronaire Brachytherapie (hoofdstukken 13-16):
We hebben het gebruik van IVUS in de tot nu toe uitgevoerde klinische studies van brachytherapie gereviseerd in **hoofdstuk 13** waarin deze nieuwe therapeutische optie ook geintroduceerd wordt voor de preventie van restenose. **Hoofdstuk 14** stelt de vergelijking voor, door simulatie, van verschillende behandelingsstrategieen gebaseerd op ofwel β- of γ-bronnen met en zonder een centreringsmiddel. Het introduceert de bepaling van dosis volume histogrammen vanuit 3-dimensionele reconstructie van "ECG-gated IVUS pullbacks" welke onze groep als eerste rapporteerde.[5] We toonden in 23 patienten behandeld in the Beta Energy Restenosis Trial in ons instituut aan dat de minimale dosis op 90% van het oppervlak van de adventitia enkel 37±16 % was van de voorgeschreven dosis, terwijl het 67±31% bedroeg op 90% van het luminale oppervlak. Door simulatie zou het gebruik van een centreringsmiddel of γ-bron deze waarden verhoogd hebben evenals de mi-nimale dosis op de 10% meest blootgestelde luminale en adventitia oppervlakken verminderd hebben, daarbij de homoge-niteit van de dosis verbeterend. Ofschoon op heden geen enkele klinische data deze mogelijke voordelen ondersteunen, was het belang van ons pionierwerk dat het nut aantoont van de evaluatie van de dosis neergezet in de arteriele wand behandeld met brachytherapie, benadrukt in de editoriale commentaren van dit manuscript.

In **hoofdstuk 15** toonden we aan door het bestuderen van 206 coronaire subsegmenten van 2 mm in 18 patienten behandeld voor een de novo lesie met enkel angioplastie gevolgd door β-brachytherapie, dat na 6 maanden follow-up het volume van de plaque minder toegenomen was in harde segmenten vergeleken met zachte segmenten en segmenten met normale/intimale verdikking. We toonden eveneens aan dat de minimale dosis neergezet op 90% van het adventitia oppervlak (D_{90}adv) omgekeerd evenredig was met het volume van de plaque bij follow-up. We toonden ook aan in **hoofdstuk 16** dat de 6-maand angiografische uitkomst in 27 patienten behandeld voor de novo lesie met angioplastie alleen gevolgd door β-brachytherapie gedeeltelijk kon verklaard worden aan de hand van de dosis gedeponeerd in de coronaire wand. Minimale doses op 90% van het luminale oppervlak (DS_{90}lum), de lamina elastica externa (DS_{90}eel) en op 90% van plaque+media volume (DV_{90}p+m) waren 9.7±6.1 Gy, 5.1±3.0 Gy en 7.0±4.0 Gy respectievelijk. Na 6 maanden follow-up hadden de patienten met een DS_{90}eel groter dan 5 Gy (n=11) een lager angiografisch verlies (-0.01±0.39 vs. 0.47±0.62 mm, p=0.03) en "late loss index" (-0.4±58 vs. 44±56 %, p=0.06). Deze arteriën waren kleiner, maar de relatieve winst was identisch en het geobserveerde verschil in het verlies kon enkel de weergave zijn van de "remodelling" van de coronaire segmenten die een adekwate dosis ontvingen.

Transthoracale echocardiografie voor de biomechanische evaluatie van het linker ventrikel en de aorta (hoofdstukken 17-20):
Hoofdstuk 17 is een historisch overzicht van de ontwikkelingen van de cardiovasculaire echocardiografie waarbij studies geintroduceerd worden die gebaseerd zijn op de combinatie van simultane registratie van non-invasieve druk en flow (via transthoracale Doppler echocardiografie).
In **hoofdstuk 18** tonen we aan dat evaluatie van de totale arteriele compliantie (Ctot) gebaseerd op

een 2-element Windkessel model (de "pulse pressure method") mogelijk is gebruikmakende van transthoracale echo-Doppler en arteriele tonometrie. In een studie uitgevoerd in 14 patienten met gekend of verdacht voor coronair lijden en in 9 vrijwilligers, was de evaluatie van Ctot met de "pulse pressure method" robust en toonde een significant verschil in arteriele stijfheid (1.2±0.4 vs 1.6±0.2 ml/mmHg). Het was ook de beste methode om het verwachte omgekeerde verband te vinden tussen totale arteriele compliantie en leeftijd, in vergelijking met de "area method" en de ratio van slagvolume over polsdruk.

Hoofdstuk 19 beschrijft de zoektocht naar een geoptimaliseerde transfer functie (TFF) welke de reconstructie toelaat van aortadruk vanuit een perifeer tonometriesignaal ter hoogte van de arteria radialis. We pasten een drie-segmenten transmissielijnmodel toe voor de radialis-carotis druk TFF afgeleid uit 31 gezonde vrijwilligers en 30 patienten met coronair lijden.
Jammergenoeg konden we geen verschil aantonen in de parameters van dit model tussen patienten en controles, behalve wat betreft de distale reflectie coefficient. We beschrijven de gemiddelde berekende TFF, evenals deze afgeleid van de minimale en maximale omgevende TFF, en de variabiliteit van de afgeleide aortadruk karakteristieken zoals centrale polsdruk of augmentatie-index. resulterend uit het gebruik van elk.

Tenslotte, in **hoofdstuk 20** beschrijven we de evaluatie van de linker ventrikel (LV) functie en de contractiele reserve gedurende liggende stressechocardiografie via de bepaling van maximale ventriculaire "power output" gebruikmakende van simultane registratie van aortaflow met Doppler echocardiografie en aortadruk met arteriele tonometrie. We tonen een goede overeenkomst aan tussen de data afgeleid van carotisregistraties en van getransformeerde radialisregistraties gebruikmakende van een TFF zoals beschreven in hoofdstuk 19. We valideerden eveneens een gesimplifieerde index van linker ventrikel "power output" die we voor het eerst beschreven hadden in dierexperimenten: het product van peak aorta flow en gemiddelde bloeddruk. Dit surrogaat van de echte "peak power", minder omslachtig om te bekomen dan invasieve registraties of zelfs arteriele tonometrie, toonde dezelfde correlatie met de $V0_2$ gemeten in deze 25 patienten.

References

1. van Liebergen RA, Piek JJ, Koch KT, de Winter RJ, Lie KI. Immediate and long-term effect of balloon angioplasty or stent implantation on the absolute and relative coronary blood flow velocity reserve. *Circulation.* 1998;98:2133-40.
2. Albertal M, Regar E, Van Langenhove G, Carlier SG, Serrano P, Boersma E, de Bruyne B, di Mario C, Piek J, Serruys PW. Flow velocity and predictors of a suboptimal coronary flow velocity reserve after coronary balloon angio plasty. *Eur Heart J.* 2001:(in press).
3. Carlier SG, Van Langenhove G, Lupotti F, Albertal M, Mastik F, Bom K, Serruys PW. Coronary flow reserve versus geo metric measurements of coronary dimensions: advantages and limitations of the functional stenosis assessment. *J Intervent Cardiol.* 1999;12:411-424.
4. Li W, van der Steen AFW, Lancee CT, Cespedes I, Gussenhoven EJ, Bom N. Blood flow imaging and volume flow quantification with intravascular ultrasound. *Ultrasound Med Biol.* 1998;24:203-214.

5. Carlier SG, Marijnissen JP, Coen VL, van der Giessen WJ, Sabate M, Ligthart J, den Boer A, Cespedes IE, Li W, van der Steen AF, Levendag PC, Serruys PW. Guidance of intracoronary radiation therapy based on dose-volume histograms derived from quantitative intravascular ultrasound. *IEEE Trans Med Imaging*. 1998;17:772-8.
6. Armstrong GP, Carlier SG, Fukamachi K, Cardon LA, Borden RA, Thomas JD, Marwick TH. Estimation of cardiac reserve by peak power. Validation and initial application of a simplified index. *Heart*. 1999;82:357-364.

ACKNOWLEDGEMENTS

ACKNOWLEDGEMENTS

As a kid, I wanted to do the same as my father, professor of mathematics. A few years later I got for Christmas one of these electronic construction kits with 100+ different experiments and circuits to build. I spent hours playing with it, before later trying to repair old radios and TVs. Maths were still a passion, but that was passé and I knew I wanted to become an electronic engineer. When I explained this at home, my father tried to convince me to do medicine: "You will also build machines to measure the world, but you will help people with this. Moreover, you will be able to help your future colleagues to understand the systems they will be using." At 18, I passed the board to enter an engineering school, but followed what was probably my father's best advice ever: I started medicine. *Papa*, merci encore pour ce conseil, c'était vraiment le meilleur choix et heureusement que pour une fois je t'ai ecouté. *Maman* aussi, bien sûr, merci pour ton amour et de m'avoir aidé à y être arrivé. Et *Corine*, ma meilleure sœur, merci d'avoir veillé sur moi durant toutes ces années d'ULB, d'avoir quand même de temps en temps fait la vaiselle à l'appartement, et plus que tout encore, après tout ce que j'ai pu te faire, d'encore m'inviter à manger d'aussi bons petits plats, préparés en suffisance pour que je survive encore un jour ou deux à Rotterdam après.

During the first year of medicine, there was for me too much of biochemistry, biology,... However, there was also a great course in physics, given by a true passionate scientist: *Albert Art.* Merci encore d'avoir essayé de partager votre passion pour la physique à des carabins, et d'avoir mis sur pieds ces expos et ce musée de la science pour que les jeunes puissent toucher les théories. Second year, it got worse, with anatomy, embryology,... Fortunately, I could be quickly involved in some biomedical engineering, working on a project for the acquisition of evoked-electromyograms. *Francis Cantraine*, thank you to have taken the time to try to teach me how to write a scientific paper and to use the index medicus. I still do not write a lot and I still do too many things in the same time: there is not an ounce of improvement. *Eddy Coussaert*, thank you very much to teach me C. I am most of the time writing in Matlab now, finally pretty similar. You gave me the keys to write structured softwares, and that's probably why I cannot use these point-and-click graphical A/D softwares like Labview.

I quickly understood that cardiology was probably the best speciality for me, since a lot of physics are involved. However, the clinical assessment remains essential, and I would like to thank *professors Englert and Bernard* for their teaching in cardiology. Their talents to imitate any cardiac sound were incomparable. I want also to acknowledge the continuing support of *Jean Luc Vandenbossche.* In the beginning, I wrote some programs to process his echo-Doppler tracings. When later, a collaboration with the von Karman Institute for Fluid Dynamics was started to evaluate regurgitant jets, I could be exposed to another world, made of wind tunnels and laser Doppler anemometry. *Michel Riethmuller*, thank you for your teaching there, and to try to explain me what is upsizing to keep similar Reynolds numbers. I also had very good time whole nights long with *Eric Gailly*, when we decided to use anyhow just blood. The first attempt to get some at the slaughterhouse was perhaps not such a good idea...you should come to Rotterdam: we now manage to spend less time cleaning everything after an experiment than measuring blood flow. Jean Luc, although a leading echocardiographist, advised me to go for interventional cardiology. Merci pour cette excellente vision du futur de la cardiologie et de tes conseils de me faire partir à Rotterdam. Désolé qu'ils

étaient judicieux au point que je n'en suis pas encore revenu. Of course, not only these three successive chairmen of the department of Cardiology of the Saint Pierre hospital in Brussels forged my training, and I want to express my gratitude to the others who gave me so many hints: *Michel de Marneffe, Marc Renard, Isabelle Liebens, Willy Kostucki, Isabelle Sterling, Guy Van Camp, Bernard Cosyns, Mounia Menassel, Danielle Plein*. A special thank to *Raymond Van Herle*, our technician: do you know that I'm still using here some electronic circuits I asked you, and to *Christiane Raymond*: what would be the echo-department without you? Finally, I have a special thought for my oldest patient from Saint Pierre: *Madame Solange Hemerick*, merci pour toutes vos lettres pleines d'attention que vous m'avez écrites depuis ces 5 années. Vous resterez certainement ma plus fidèle patiente et j'espère bien vous voir devenir centenaire.

Along these years of studentship and residency one makes numerous friends. Unfortunately, we lose sight of too many. I would like to stress the chance that I have had to keep a few of them. Thank you for your continuing support and your friendship that helped me to survive in the foggy Rotterdam...most of the time by escaping to see you in Brussels. Don't you think that we should really once try to go for a party here in a coffee-shop? *Katy*, my best girlfriend and psychanalyst, I'm sure we could go even deeper in all my troubles; *Christophe*, after smoking, perhaps that you will accept that in your department, they take also care of my next book...I was thinking about a textbook of 500+ pages; *Loretto*, you could tell me if the Dutch H. is better than the Chilian one; *Patrick*, I know you don't smoke, but you should try, you will perhaps have a chance to win if we play chess; *Youssef*, that will change us from our cigars, but I'm sure we will have to take our own whisky if we really want to spend another night redoing the world; *Daniel and Virginie*, you should take for once the Thalys in the other direction, but I'm sure you would enjoy it too; *Philippe and Murielle*, now that the kids are nearly at university, I'm sure you will find a way to join us; *Christian et Rita*, on verra quel nez celui-là aura; *François, Annick, Carlo et Nathalie*, je promets cette fois d'être là avant que vous n'arriviez.

Before talking about Rotterdam, I would like to thank different very helpful friends abroad where I had the chance to spend just a few days, or much more, like in Cleveland. *Balram Bhargava and Ron Waksman* in Washington and *Tim Fox and Ian Crocker* in Atlanta: thank you for your continuing support for the dosimetry projects. *Ian*, thank you for your hospitality each time I step by Georgia. I really enjoy every time going to the fitness club, but why does this have to happen so early in the day? *Ali Hassan and Peter Fitzgerald* in Stanford: it is nice to exchange some ideas and late abstracts by e-mails, but it is always much better to work with you there: with as many IVUS to see in your place as here, but with the sun, the Bay and the wine, California wins over Rotterdam by at least 3-0. With the same score thanks to the Lac Leman, *Eric Eeckhout and Nikos Stergiopulos* are collaborating in another nice place to visit, Lausanne. Nikos, thank you to leave your own congress there to sit at my PhD defence. *Evgueni Gordov* in Tomsk: it is surely colder, but anyhow, I hope that with some of our coming EC projects, I will finally have a chance to visit you there. *Tom Marwick and Brian Haluska* in Brisbane: thanks to take care of part 5 of this thesis overseas. Next time, I will really try to stay more than 3 days there down under. In Australia, there is also my best English teacher, *Wendy Schumer*, without whom this thesis and some of my brachytherapy manuscripts and chapters would not seem written in English. Not far from there, *Guy Armtrong*, back in New Zealand, had a very important role for the non-invasive power measurements in Cleveland.

Working with him helped me also to understand our kiwi here, *Patrick Kay*. In Cleveland, I want to start to thank *Renée* for her continouous care, for the nicest bed-and-breakfast that I know, and to take me to the Amish on Sundays, when she thought I was working too much in the Clinic. Mum #2, I would have loved to see you here for my defence. I want to express my deepest gratitude to *Jim Thomas*, the busiest echocardiographist in the world, to have accepted me in the Cardiovascular Imaging Center of the Cleveland Clinic Foundation, after his continuing support, with *Dr Frederick Corhnill*, chairman of Biomedical Engineering, when I was applying for grants to go overseas. *Jim*, thank you also to stay more than 3 days in the same town and to take the time to sit in my PhD committee. *Neil Greenberg* was always very helpful in the Clinic for a Doppler connection, a driver of a color printer for a last minute poster, for a network connection... *Neil*, I'm pretty sure that you could have presented your thesis 6 months sooner, without having to take care of so many of my problems. *Murat Tuzcu, Geoffrey Vince, Pieter Vandervoort, Mario Garcia, Brian Griffin, Allan Klein, Richard Grimm, Marie Stugaard and Agnes Pasquet* were always of great support during each of my stay there. *Eddie*, even abroad, it's nice that you still think about us so often. You are definitively our best source of internet jokes. Of course, they are also very important and helpful friends who are not so far. *Patrick Segers*, you are coauthor of some of the papers of this PhD, and of many others that I could not include. Your help has been tremendous, but that we became friends, after all these different experiences conducted in Gent, is today much more important to me. I would perhaps not have met Patrick without *Pascal Verdonck*, the chairman of the IBITECH, and a real businessman. You are among the most active biomedical engineers in Belgium, but it's of course abroad that I met you and discovered the heart replicator you were developing in Gent. Thanks for your continuing support since that "Computers in Cardiology" in Washington in 1994, and to sit also in my thesis commission. *Koen and Stefaan*, it's now your turn to present your PhD and I will be happy to continue to exchange support, in the House of Blues or elsewhere. *William* et *Valeria*, notre collaboration est beaucoup plus récente mais je suis convaincu du succès de cette nouvelle aventure à Alost. Le brunch tout en haut du Hilton était génial, et merci de nous avoir laissés profiter de la vue un bon moment...*Bernard*, tes conseils de partir à Rotterdam se sont avérés les meilleurs, merci encore!

Most of this PhD has been accomplished in Rotterdam, and because I was slower than the others to finally be able to present one, I have seen and been helped by too many people to be able to acknowledge them all. I will start to express my gratitude to the small family of fellows: there was the quickest for a thesis, 15 months, *Marco Costa*; the best of all, with 7 Circulation (!), *Manel Sabate*, the most artist one, *Glen Van Langenhove*, the two who arrived 2 years after me and who are still able to present their PhD 1 week before me, *Patrick Kay* and *Ken Kozuma*. It took me some time to become the oldest fellow of the Thoraxcentre, just because *Michael Kutryk* was enjoying so much self-flagellation in the cathlab here and *Anita Dall' Agata* was, for still an unclear reason, trying to redo a complete cardiology training here after her Italian one. I'm happy to sometime see at a meeting the old ones, *Clemens von Birgelen* and *Edoardo Camenzind*. Many fellows did not spend the 2 years of a "classical" stay in the Thoraxcentre, just because it is tough to remain unpaid 2 years and raise a family, but it has always been very interesting to exchange new ideas and work on some manuscripts with them. *Pedro Serrano*, I hope you're doing well back in Spain. I will send you the reprints of chapter 5 with the version 15.1c of SPSS if you don't have it yet. *Niteen Deshpande*, I was one month ago in India, but it's just a too big country to have met with you there

by chance. *Mariano Albertal*, you've written more since you're gone than during your whole time here. You were definitively spending too much time in Rotterdam trying to find a woman. *Attila Thury*, your help on the shear stress and sonotherapy has been interrupted too early with your leave back to Hungary. With the continuous flow of fellows, a few of them arrived more recently and could not yet present their thesis before mine. I want to thank them to share the present workload in the cathlab and on Patrick's computer, preparing slides. I wish to *Giorgios Sianos, Evelyn Regar, Kengo Tanabe* and *Muzapher Degertin* to get their PhD done in less than 5 years. My Turkish friend, a particular thank to you for the Culottes business, and to let me discover the Oküzgözü here and there. I want also to thank the "native" fellows, called in the Thoraxcentre "study coordinators": *Anthonie Gijzel, Alex Wardeh* and *Marco Knook*. You have been doing a great job taking care of our study patients. CRF's were something else, but now with our new two study "nurses", *Paul Cummins* and *Arno Ruiter*, everything is under control.

Of course, no one thesis in interventional cardiology could be done without the tremendous patience of the nurses in the cathlab. I would like to thank *Tieneke van Delft, Marjo de Ronde, Jeanine Schaaf, Theo van Eeren, Stijn Swager, Marielle van Dam, Caroline Febus, Nel van de Velde, Helene Hyum and Martin Ooms* for their endeavour to balance clinical research and optimal patient care. I learned interventional cardiology with you, en bedankt voor al jullie moeite. Tieneke, you were the most difficult one to convince to prepare some adenosine, but you are also the one who taught me the most. Thanks again. *Elza Kuipers, Samantha Gibbs and Fiona Walker*, you're just arrived and you haven't seen yet what means doing an elastogram, a Doppler and an IVUS flow in the same patient for a live case...that will be another day in paradise. *Ad den Boer, Dirk van Essen, Marian Hettinga (now in ZZH), Gio Maatrijk, Anne Marie Maugenest, Ben Noorlos, Ngaire Meadows, Emile Onderwater and Jurgen Lighart*, you are everyday key-players as technicians in the cathlab, and your role is even more important when trying to interconnect all these extra devices described in this thesis. *Jurgen*, your help for the IVUS has been stressed since more than 10 years in all the thesis presented by cathlab fellows. I hope that you will continue to walk with us to stress our attention on some black holes and other potential manuscripts you are the first to recognize. *Emile*, your expertise in the computers of the cathlab has been very helpful for numerous acquisitions, and I'm sure you will come with an all-in-one-laptop integrated system to archive everything, from the electromechanical mappings to the PVloops. We would not have any patient entering in the cathlab without the careful organization run by *Laetitia Bautz*. The help of the other secretaries of the department, among them *Elles Schaap, Ilse Sadi, Marijke den Heijer*, should also be acknowledged. I address a special thank to *Marianne Eichholtz* who launched my PhD application and to *Anja van Huuksloot*: your efficiency to work for the most cited cardiologist of the world is tremendous, as high as the terror that you impose on all the new fellows... After a while, we are just happy to see that you do the same to any CEO of a large company. Actually, you protect our professor, but I know that you care a lot for his pupils too. The professor is of course *Patrick Serruys*. The first time I saw him in Brussels at a meeting of the Belgian Working Group of Interventional Cardiology, I dare to ask if it would be possible to start a fellowship in his department. I started in my best (possible) Dutch, continued in English, and said some words in French too...we still do the same, which is very strange for two native French speaking persons. I was very proud to get an interview 2 months later in the Thoraxcentre, with someone to meet every hour. I understood later that I was just entering in a very well organized system dealing with more than

100 cardiologists asking the same every year, and finally keeping 2 or 3 of them. Patrick, thank you for your continuing support of any new bioengineering development we proposed you, and not only because it was a potential good presentation in Hawai, and for your careful training in interventional cardiology. I have learned not to be tired working in the Thoraxcentre, because you are just doing 10 times more than anyone of us. Since I play tennis, I was among the lucky fellows going to work on the Sunday afternoons, playing after. That was my chance since I hate to wake up early on the Saturdays. Madame Serruys, Danielle, I am sorry that Patrick was away even more often because of me. Thank you to care so much for our professor, and to always accept us for a late dinner, or during an afternoon that could have been spent in family. Merci beaucoup pour votre gentillesse et patience.

I did my first ballon dilatation, my first stent implantation, my first total occlusion and many other premieres with Pim de Feyter. Pim, I'm sorry you became see-sick when I was learning how to drive the cathlab table, and I want to thank you for your patience, your constructive remarks, your expertise and your support during these 5 years spent in the lab learning how to do interventions. Of course, all the other senior interventionalists educated me too since I had the chance to work with all of them, and not only as the left arm/hand of the professor. I could discover many skills and tips-and-tricks that I will try to remember with *Marcel van den Brand, Arie de Vries, Wim van der Giessen and David Foley* who reviewed also carefully some of my manuscripts. I want to thank the younger ones too, *Benno Rensing, Jeroen Vos and Peter Smits* for their collaboration. The interaction with the radiotherapists, professor *Peter Levendag* and *Véronique Coen*, and the technicians from the Daniel Den Hoed Clinic has been very fruitful. Without them, no brachytherapy would have been possible in our cathlab, and no manuscripts and part 4 of this book either. Peter, thank you for your interest in this PhD and to be soon among the highly learned opponents. Finally, I want to express my gratitude to my colleagues and all the coworkers of the CCU, the 1200, the dagverpleging, the outpatient clinic, the 800 and the thorax surgery department, for their close collaboration in the day-to-day clinical work. I cannot forget to thank *professor Roelandt*, although busy trying to keep together all these frogs jumping out of the Thoraxcentre boat, as he once described me his role here, to have accepted to be the secretary of my PhD commission. Among the people in the Thoraxcentre not directly involved with patient care but with a crucial role, I want to acknowledge the help of *Eric Boersma* for statistical coaching, *Maud van Nierop and Niek van der Putten* in the computer group, *Jolanda van Wijk and Cecile Sweers* from clinical epidemiology, *Arita Ogers and Ad van Drunen* for all the money issues, and last but not least, *Paula Delfos and Jan Tuin*, for so many too lately asked videos and the cover of this thesis. In Cardialysis, the help of *Marie-Angèle Morel*, soon back, *Clemens Disco* and *Gerrit Anne van Ess* won't be forget.

I had the chance to be a bridge between the catheterization lab and the bioengineering group of the 23rd floor of the white Erasmus University tower. With only an office there the first 4 years, there have been numerous lift trips. I want to thank the unknown guardian who was stopping the lifts after 2:00 am, when I was finally ready to go home: I stayed fit thanks to him. *Klaas Bom*, who accepted to be my promotor, manages the experimental echocardiography and the bioengineering of the Thoraxcentre. From the beginning, he had the aura of the inventor, as the expert in sonar measurements who became the father of the echocardiographic phased-array probe. Klaas, you have been an example of scientific rigour and ponderability, which contrasted interestingly with my

other promotor who was willing to present at 10 different meetings the preliminary results of our experiments. I hope that I will be able to balance both influences in the future. I also want to thank you for your efforts to try to teach me diplomacy. In the department, I want to acknowledge the help of *Charles Lancée*, who was very helpful in the development of the new rf data processing methods of this thesis, and who was also always ready to fix one of my MatLab subroutines. His support, together with *Nico de Jong and Marco Voormolen*, who did the 3-D reconstruction, was crucial for the echogardiography on the back cover of this thesis. *Frans van Egmond, Wim van Alphen, Leo Bekkering and Jan Honkoop* took care of the technical developments related to the new IVUS systems. *Chris de Korte* must be acknowledged as well as for developing elastography, now with the help of *Johannes Schaar*, as for fixing my taxes reduction, or as an expert in Saab engines. Thank you also to have accepted to be one of my paranimfen. *Ignacio Cespedes* has now a managing position in the IVUS business, but we arrived nearly at the same time in the lab, with the objective to make the IVUS flow method working. Our friendship grew faster than the success of the IVUS flowmetry, but we can still hope...I mean, for the IVUS method, surely now that *Fermin Lupotti* is working hard on this. I want to stress the patience of *Frits Mastik* during all the live-cases where we demonstrated some elastography or IVUS flow. Knowing that you enjoy so much 3 weeks nearly alone in Ladakh or elsewhere in Himalaya, I can understand the burden to be in a cathlab among 15 people and 2 cameramen around one patient. Your help during these demonstrations, as well as for many parts of this thesis, has been tremendous. *Ayache and Peggy*, je tiens à vous remercier pour le French-corner que nous avons pu établir dans le labo, et c'est toujours un plaisir d'ouvrir un Chateau-Neuf au dehors. Thanks to *Ton van der Steen*'s pioneering grant and other bubble grants from Nico, we have now in the lab twice as many people as before and it will be difficult to thank them all. However, I will say a special word for *Elisabeth Brusseau*, for her new ideas on elastography and the new contour detection projects and *Roland van Lindt* for computer support. *Corrie Efting* took care, from my first day in Rotterdam, of so many administrative issues that she must be specially acknowledged. The more recent help from *Riekje Daane* was also very helpful.

On the 23rd floor, there are also all the people involved in the cutting edge research of experimental cardiology run by *professor Verdouw*, who must be thanked to have accepted to move from the small to the large PhD committee, because of some administrative issues. I think that you deserve, on the 26, to ask an extensive, rather than a small question. It is in his department that we conducted, and plan new validations experiments in pigs with the help of *Rob van Bremen, Elza van Deel, Sandra de Zeeuw, Helene van Beusekom* and many others. Among them, *Dirk Duncker* who definitively plays tennis better than I do. It's too bad that we cannot play more often. Next door, there is also the department of Hemodynamic where *Cees Slager, Jan Oomen, Hans Schuurbiers* en specially *Jolanda Wentzel* were always ready to help me for some 3-d IVUS or computational fluid dynamics issues. My second paranimph, *Rob Krams*, seats between both labs, since his impressive knowledge encompasses both animal physiology, molecular biology, cardiology and CFD expertise. I think that I could not have found a better back up for my public defence. Thank you for this, and with *Luc van Damme*, for the interesting participation in the startup of the experimental rabbit lab.

In interventional cardiology, we are interacting with many companies and many country managers and others, just asking to test new devices or to consider a new study. These interactions are most

of the time rather interesting. However, for some particular reasons, sometime these relationships evolved one step further, and I am happy to have now true friends that I see independently of their company business (which is helpful since most of them are changing every year). I want to acknowledge here, of course, *Jane Thulis* who taught me nearly everything on how to cook an IVUS catheter, cookies and truffles; *Jason Koshnitsky*, expert in dosimetry as well as in Russian vodka; *Samah Nasser* who can predict any restenosis in a cup of coffee; *Rob Eno*, who stayed too briefly in Brussels, but at least now, I have a great place to stay in the Bay area; *Joakim Eriksson*, who should come more often in Rotterdam to improve my tennis and *Heike Von Hausen*, for (too) few pieces of chance we had the pleasure to share. Besides, I want also to thank *Christophe Giot*, an old friend known before any business and interventions, who has accepted to take care of the printing of this thesis in AstraZeneca, and *Ann Vandamme* for her great help in this.

Finally, there is one extraordinary person deserving most of the acknowledgements, although coming the last one: *Tine*. Thank you for your love and support during these 5 years. You had to sleep too often in awkward places because I was finishing an abstract overnight, and you had to run too often because we were late to catch a flight, nearly missed because I was still printing a poster. However, it seems that on one of the summits that we have climbed, you could find some reasons to continue, and to go even for a new adventure, with this little one that we are just seeing by (3-d)-echo now. Thank you for everything!

CURRICULUM VITAE AND LIST OF PUBLICATIONS

CURRICULUM VITAE

Stéphane Guy Carlier was born in Ath, Belgium, on July 3, 1966. He completed his high school education in 1984 at the Athénée Royal in Ath, Belgium. In this period, he started to build strange devices to participate to the young investigators awards of the "Jeunesses Scientifiques de Belgique". He was laureate in the junior category in 1981 with a reproduction of a Bell's telephone transmitting voice using modulated-intensity light. He was laureate in the senior category in 1983 with an experimental ECG system (see cover). He was also twice the laureate of the "Fédération des Associations d'Informaticiens de Belgique" for a software solving chemical stoechiometric equations in 1982 and another one to teach music in 1984.

He started his medical school in the Free University of Brussels (ULB), Belgium, in 1984. He was awarded the Prix Fleurisse Mercier in 1984 and 1985. He started to work in 1985 as a student-assistant in the "Centre de Calcul Scientifique" under the direction of Prof. F Cantraine. The subject of his research was the development of an acquisition system of evoked electromyography for closed-loop control of curarization during anesthesia. Later, he worked in the cardiology department of the Hôpital Universitaire Saint Pierre, developing softwares for the processing of Doppler echocardiographic signals. Laureate of an IBM research and travel grant in 1986, he spent one month in the IBM Watson Research Center in Yorktown Heights, NY. With his improved experimental ECG system interfaced to a familial PC to compute vectocardiograms, he won in 1987 the prize of the "Ordre des Ingenieurs du Québec" during the Expo-Sciences Internationale in Laval, Quebec.

Doctor in Medicine, ULB, graduated in 1991 suma cum laude, he started his fellowship in Internal Medicine in 1991 at the Hôpital Universitaire Saint Pierre, Brussels, under the supervision of Profs. JC Demanet and N Clumeck. He trained in Cardiology from 1993 to 1996 in the same hospital, under the supervision of Profs. R Bernard and JL Vandenbossche. Laureate of the Belgian Society of Cardiology in 1994, he worked on an in vitro study of jets simulating mitral insufficiencies in the von Karman Institute of Fluids Dynamics, in Brussels, under the supervision of Prof. ML Riethmuller.

He obtained the special license in Cardiology from the ULB in 1996 with suma cum laude. Supported by research fellowships of the European Society of Cardiology and of the Vésale and Bekales Foundations, he started to work in the Experimental Echocardiography Department of the Erasmus University, Rotterdam, under the supervision of Prof. N Bom in 1996. Concomitantly, he started as a clinical fellow in interventional cardiology in the Catheterization Laboratory, under the supervision of Prof. PW Serruys. He served mainly as a bridge between the experimental bioengineering group and the interventionalists of the Thoraxcentre. Fellow of the Belgian American Educational Foundation and of the NATO in 1997, he studied non-invasive Doppler echocardiography at the Cleveland Clinic Foundation, under the supervision of Prof. JD Thomas. He is currently interventional cardiologist at the Thoraxcentre, Rotterdam, and collaborates closely with its biomedical engineering group on the development of new intravascular ultrasound techniques.

LIST OF PUBLICATIONS

Publications:

1. First results of PCSCOPE: one independent tool for the acquisition of biomedical signals
   *S **Carlier**, E Coussaert, F Cantraine*
   Lecture Notes in Medical Informatics, 1988; vol 35, p 394-8

2. PCSCOPE : a general purpose acquisition system. A first application in the recording of EMGs
   *S **Carlier**, E Coussaert, F Cantraine*
   Medical & Biological Engineering & Computing, 1990; vol 28, p 497-501

3. A PC based system for the acquisition and the analysis of doppler ultrasound signals
   *S **Carlier**, J-L Vandenbossche, M Englert*
   Computers in Cardiology, 1989, IEEE Computer Society Press, 1990; p 385-7

4. L'oedeme angioneurotique: un effet secondaire important des inhibiteurs de l'enzyme de conversion de l'angiotensine
   *K Crener, S **Carlier**, P Hermans, P Mols*
   Journal Européen des Urgences, 1993; vol 6, p 111-3

5. Determination of the severity of valvular regurgitation by the integral of the power spectrum: an in-vitro model
   *S **Carlier**, E Gailly, M Riethmuller, JL Vandenbossche*
   Computers in Cardiology, 1994, IEEE Computer Society Press, 1994; p 345-8

6. Lymph node perforation into the airway in AIDS-associated tuberculosis
   *T Alame, P Dierckx, S **Carlier**, R Sergysels*
   European Respiratory Journal, 1995, vol 8, p 658-60

7. Assessment of an automatic determination of left ventricular dP/dt from Doppler spectra of mitral regurgitation
   *S **Carlier**, P Verdonck, C Dimmer, JL Vandenbossche*
   Computers in Cardiology, 1995, IEEE Computer Society Press, 1995; p 321-4

8. Acquisition of raw intracoronary doppler signal for better characterization of flows
   *S **Carlier**, E Gordov, E Gailly, G Van Camp, B Cosyns, H Geschwind, JL Vandenbossche*
   Computers in Cardiology, 1996, IEEE Computer Society Press, 1996; p 221-4

9. Potentials of volumetric blood-flow measurement
   *W Li, AFW van der Steen, CT Lancée, EI Céspedes, S **Carlier**, EJ Gussenhoven, N Bom*
   Seminars in Interventional Cardiology, 1997;2: p 49-54

10. Intracoronary ultrasound during coronary interventions
    *S **Carlier***
    Journal de Cardiologie/ Tijdschrift voor cardiologie, 1997; 9(11), p 238-9

11. Débat pro/contra stents
    *S **Carlier***
    Vaisseaux, Coeur, Poumons, 1997;2(6):195-6

12. Non-invasive evaluation of left ventricular power output by simultaneous recordings of applanation tonometry and echocardiographic Doppler signals
*S **Carlier**, T Marwick, P Segers, P Verdonck, G Van Camp, B Cosyns, JD Thomas*
Computers in Cardiology, 1997, IEEE Computer Society Press, 1997 p 223-226

13. Quantification of blood volume flow by decorrelation analysis of radio-frequency intravascular echo signals
*W Li, S **Carlier**, EI Cespedes, F Mastik, AFW van der Steen, PD Verdouw, N Bom*
Computers in Cardiology, 1997, IEEE Computer Society Press, 1997 p 1-4

14. In-vivo validation of blood flow estimation using the decorrelation of radiofrequency intravascular echo signals
*AFW van der Steen, W Li, EI Céspedes, S **Carlier**, M Eberle, PD Verdouw, PW Serruys, N Bom*
IEEE Ultrasonics Symposium Proceedings, 1997; 1: p 1247-50

15. Intravascular power flow imaging: theory and potentials for planimetry
*EI Céspedes, W Li, F Mastik, AFW van der Steen, S **Carlier**, RH an Bremen, M Eberle, N Bom*
IEEE Ultrasonics Symposium Proceedings, 1997; 1: p 1273-6

16. Decreased coronary flow reserve in hypertrophic cardiomyopathy is related to remodeling of the coronary microcirculation
*R Krams, MJM Kofflard, DJ Duncker, C von Birgelen, S **Carlier**, M Kliffen, FJ ten Cate, PW Serruys*
Circulation, 1998;97: p 230-3

17. Quantification of mitral regurgitation by the automated cardiac output method: an in-vitro and in-vivo study
*G Van Camp, S **Carlier**, B Cosyns, D Plein, M Menassel, T Josse, P Segers, P Verdonck, JL Vandenbossche*
Journal of the American Society of Echocardiography, 1998; 11(6): p 643-51

18. Simultaneous morphological and functional assessment of a renal artery stent intervention with intravascular ultrasound
*S **Carlier**, W Li, EI Céspedes, AFW van der Steen, J Hamburger, K Bom, PW Serruys*
Circulation, 1998; 97: p 2575-6

19. Blood flow assessment using a mechanical intravascular ultrasound catheter: initial evaluation in vivo
*EI Céspedes, S **Carlier**, W Li, F Mastik, AFW van der Steen, N Bom, P Verdouw, PW Serruys*
Journal of Vascular Investigation, 1998; vol 4: p 39-44

20. Clinical applications of intravascular ultrasound
*EI Céspedes, S **Carlier**, J Ligthart*
Cardiología e Hipertensión, 1999; vol 3(10): p 2-8

21. Angiographically undetected stent mal-apposition resolved by intravascular ultrasound and flow imaging
*EI Céspedes, S **Carlier**, M Sabate, J Ligthart, PW Serruys, N Bom*
Journal of Vascular Investigation, 1998; vol 4 (2): p 81-84

22. Non-Doppler blood flow measurement using IVUS imaging catheter
*AFW van der Steen, EI Céspedes, **S Carlier**, W Li, F Mastik, CT Lancee, PW Serruys, JRTC Roelandt, N Bom*
The Thoraxcentre Journal, 1998; 10(1): p 27-29

23. Guidance of intracoronary radiation therapy based on dose-volume histogram derived from quantitative intravascular ultrasound
***S Carlier**, JPA. Marijnissen, VLMA Coen, WJ van der Giessen, M Sabate, J Ligthart, A den Boer, IE Céspedes, W Li, AFW van der Steen, PC Levendag, PW Serruys*
IEEE Transactions on Medical Imaging, 1998; 17: p 772-8

24. Blood flow assessment with intravascular ultrasound catheters: The ideal tool for simultaneous assessment of the coronary hemodynamics and vessel wall?
***S Carlier**, EI Céspedes, W Li, F Mastik, AFW van der Steen, N Bom, PW Serruys*
Seminars in Interventional Cardiology, 1998; 3: p 21-9

25. The pulse pressure method and the area method for the estimation of total arterial compliance in dogs: sensitivity to wave reflection intensity
*P Segers, P Verdonck, Y Deryck, S Brimioulle, S Naeije, **S Carlier**, N Stergiopulos*
Annals of Biomedical Engineering, 1998; 25: p 665-8.

26. In-vivo application of the generalized radial-aorta and carotid-aorta pressure transfer function
*P Segers, **S Carlier**, G Armstrong, P Verdonck, JD Thomas*
Computers in Cardiology, 1998; IEEE Computer Society Press, 1998; 25:669-672

27. Non-invasive characterization of total arterial compliance by simultaneous acquisition of pressure and flow: Advantages of the Pulse Pressure Method
***S Carlier**, P Segers, A Pasquet, G Armstrong, NL Greenberg, N Stergiopoulos, T Marwick, JD Thomas*
Computers in Cardiology, 1998; IEEE Computer Society Press, 1998; p 665-8

28. Intracoronary blood flow assessment with IVUS
***S Carlier**, EI Céspedes, W Li, F Mastik, AFW van der Steen, N Bom, PW Serruys*
Cardiovascular Interventions On-line, 1998, 2: p 22-24 and http://www.cvi-online.com.

29. Non Doppler blood flow measurement using an IVUS imaging catheter
*AFW van der Steen, EI Céspedes, **S Carlier**, W Li, F Mastik, CT Lancée, PW Serruys, JRTC Roelandt, N Bom*
Newsletter International Cardiac Doppler Society 1998

30. Novel developments in intravascular imaging
*AFW van der Steen, EI Céspedes, CL de Korte, **SG Carlier**, W Li, F Mastik, CT Lancee, M Eberle PW Serruys, N Bom*
IEEE Ultrasonics Symposium Proceedings, 1998; p 1733-1742

31. Stenting with a true bifurcated stent: acute and mid-term follow-up results
***S Carlier**, WJ van der Giessen, DP Foley, MJB Kutryk, BJ Rensing, ML Carleton, PW Serruys*
Catheterization & Cardiovascular Diagnosis, 1999; 47(3): p 361-9

32. Comparison of brachytherapy modalities by dose-volume histograms derived from quantitative intravascular ultrasound
S Carlier, JPA Marijnissen, VLMA Coen, WJ van der Giessen, M Sabate, J Ligthart, A den Boer, PC Levendag, PW Serruys
Cardiovascular Radiation Medicine, 1999; 1(2): p 115-24

33. Echo decorrelation estimated from signal powers
*W Li, F Mastik, EI Céspedes, **S Carlier**, AFW van der Steen*
Ultrasound in Medicine & Biology, 1999; 25(3): p 405-9

34. Effect of catheter placement on 3-D velocity profiles in curved circular tubes
*JJ Wentzel, R Krams, EI Céspedes, W Li, **S Carlier**, AFW van der Steen, CJ Slager*
Ultrasound in Medicine & Biology; 1999; 25(5): p 803-10

35. IVUS: de huidige stand van de zaken
***SG Carlier**, CL de Korte, PW Serruys, N Bom*
CardioActueel, 1999; 4(8): p 1-3

36. Estimation of cardiac reserve by peak power: Validation and clinical application of a simplified index
*G Armstrong, **S Carlier**, K Fukamachi, L Cardon, R Borden, J Thomas, T Marwick*
Heart; 1999; 82: p 357-64

37. Pulse pressure method and the area method for the estimation of total arterial compliance in dogs: sensitivity to wave reflection intensity
*P Segers, P Verdonck, Y Deryck, S Brimioulle, R Naeije, **S Carlier**, N Stergiopulos*
Annals of Biomedical Engineering, 1999; 27(4): p 480-5

38. Stroke volume changes during dobutamine-atropine stress echocardiography: the influence of heart rate and ischaemia
*D Poldermans, R Rambaldi, E Boersma, W Vletter, **S Carlier**, A Elhendy, JJ Bax, AJ Man in 't Veld, JR Roelandt*
International Journal of Cardiovascular Imaging, 1999; 15(4): p 263-9

39. Preserved endothelium-dependent vasodilation in coronary segments previously treated with balloon angioplasty and intracoronary irradiation
*Sabate M, Kay IP, van Der Giessen WJ, Cequier A, Ligthart JM, Gomez-Hospital JA, **Carlier SG**, Coen VL, Marijnissen JP, Wardeh AJ, Levendag PC, Serruys PW*
Circulation, 1999; 100(15): p 1623-9

40. Intracoronary elastography in the catheterisation laboratory: preliminary patient results
*CL de Korte, **SG Carlier**, F Mastik, AFW van der Steen, EI Céspedes, MM Doyley, PW Serruys, N Bom*
IEEE Ultrasonics Symposium Proceedings, 1999; p 1649-1652

41. Coronary flow reserve versus geometric measurements of coronary dimensions: advantages and limitations of the functional stenosis assessment
***SG Carlier**, G van Langenhove, F Lupotti, M Albertal, F Mastik, K Bom, PW Serruys*
Journal of Interventional Cardiology, 1999; (12): p 411-24

42. Intravasculaire ultrageluids diagnostiek: State of the art
SG Carlier, EI Céspedes, CL de Korte, J Ligthart, PW Serruys
Klinische Fysica, 1999; (2): p 25-9

43. Brachytherapy devices of the month: from Paris to Galileo
SG Carlier, VLMA Coen, PW Serruys
Cardiovascular Interventions On-line, 1999, 4: p 23-24 and http://www.cvi-online.com.

44. Outcome from balloon induced coronary artery dissection after intracoronary beta radiation
*Kay IP, Sabate M, Van Langenhove G, Costa MA, Wardeh AJ, Gijzel AL, Deshpande NV, **Carlier SG**, Coen VL, Levendag PC, Van der Giessen W, de Feyter PJ, Serruys PW*
Heart, 2000; 83(3): p 332-7.

45. Quantification of plaque volume, shear stress on the endothelium, and mechanical properties of the arterial wall with intravascular ultrasound imaging
*Bom N, de Korte C, Wentzel J, Krams R, **Carlier SG**, van der Steen AW, Slager C, Roelandt J*
Z Kardiologie 2000; 89 Suppl 2: p II.105-11.

46. Intravascular scanners
*Bom N, **Carlier SG**, van der Steen AF, Lancee CT*
Ultrasound in Medicine and Biology, 2000; 26 Suppl 1: p S6-S9

47. Flow estimation using an intravascular imaging catheter
*van der Steen AF, Céspedes EI, **Carlier SG**, Mastik F, Lupotti F, Borsboom JM, Li W, Serruys PW, Bom N*
Ultrasonics, 2000;38: p 363-8

48. Residual plaque burden, delivered dose, and tissue composition predict 6-month outcome after balloon angioplasty and beta-radiation therapy
*Sabate M, Marijnissen JP, **Carlier SG**, Kay IP, van der Giessen WJ, Coen VL, Ligthart JM, Boersma E, Costa MA, Levendag PC, Serruys PW*
Circulation, 2000; 101(21): p 2472-7

49. Characterization of plaque components and vulnerability with intravascular ultrasound elastography
de Korte CL, van der Steen AF, Céspedes EI, Pasterkamp G, Carlier SG, Mastik F, Schoneveld AH, Serruys PW, Bom N
Physics in Medicine and Biology, 2000; 45(6): p 1465-75

50. Cardiovascular Echography
*N Bom, AFW van der Steen, CT Lancee, **SG Carlier**, N Bruining, CL de Korte, N de Jong, JRTC Roelandt*
Klinische Fysica, 2000; (3): p 19-23

51. Distal embolization : A threat to the coronary artery?
*Van Langenhove G, Diamantopoulos L, Regar E, Foley DP, Tuin J, **Carlier SG**, Serruys PW*
Circulation, 2000; 102(13): E95

52. The Thoraxcenter brachytherapy devices big parade
SG Carlier
Cardiovascular Interventions On-line, 2000, 5: p 19-20 and http://www.cvi-online.com.

53. Individualizing the aorto-radial pressure transfer function: feasibility of a model-based approach
*P Segers, **S Carlier**, A Pasquet, SI Rabben, LR Hellevik, E Remme, T De Backer, J De Sutter, JD Thomas, P Verdonck*
American Journal of Physiology (Heart Circ Physiol), 2000; 279: p H542-9

54. Coronary stent implantation in a septal perforator artery: case report and review of the literature
*Regar E, Kozuma K, Ligthart J, **Carlier SG**, de Vries A, Serruys PW*
Japanese Circulation Journal, 2000; 64(10): p 802-4.

55. Brachytherapy in the Journal: European Cardiologists have their own forum and should use it!
*Serruys PW, **Carlier SG***
European Heart Journal, 2000; 21(24): p 1994-6

56. Relationship between tensile stress and plaque growth after balloon angioplasty treated with and without intracoronary beta-brachytherapy
*Kozuma K, Costa MA, Sabate M, Slager CJ, Boersma E, Kay IP, Marijnissen JP, **Carlier SG**, Wentzel JJ, Thury A, Ligthart JM, Coen VL, Levendag PC, Serruys PW*
European Heart Journal, 2000; 21(24): p 2063-70

57. IVUS based dosimetry and treatment planning
*Crocker I, Fox T, **Carlier SG***
Journal of Invasive Cardiology, 2000; 12(12): p 643-8

58. Randomized comparison of primary stenting and provisional balloon angioplasty guided by flow velocity measurement
*Serruys PW, de Bruyne B, **Carlier S**, Sousa JE, Piek J, Muramatsu T, Vrints C, Probst P, Seabra-Gomes R, Simpson I, Voudris V, Gurne O, Pijls N, Belardi J, van Es GA, Boersma E, Morel MA, van Hout B*
Circulation, 2000; 102(24): p 2930-7

59. The role of intravascular ultrasound imaging in vascular brachytherapy
***SG Carlier**, VLMA Coen, M Sabate, IP Kay, JMR Ligthart, WJ van der Giessen, PC Levendag, K Bom, PW Serruys*
International Journal of Cardiovascular Interventions, 2000; 3(1): p 3-12

60. Intravasculaire ultrageluidsdiagnostiek: State of the Art
***SG Carlier**, EI Céspedes, CL de Korte, J Ligthart, PW Serruys*
Technologie in de gezondheidszorg, 2000; (3): p 28-33

61. Advancing intravascular palpography towards clinical application
*MM Doyley, CL de Korte, F Mastik, **SG Carlier**, AFW van der Steen*
Acoustical Imaging, 2000; (25): p 493-500

62. High resolution IVUS elastography in patients
*CL de Korte, MM Doyley, **SG Carlier**, F Mastik, AFW van der Steen, PW Serruys, N Bom*
IEEE Ultrasonics Symposium Proceedings, 2000; p 1767-1770

63. An automated approach for clinical intravascular ultrasound palpation
*MM Doyley, CL de Korte, F Mastik, **SG Carlier**, AFW van der Steen, PW Serruys, N Bom*
IEEE Ultrasonics Symposium Proceedings, 2000; p 1779-1782

64. Recent developments in IVUS
*AFW van der Steen, CL de Korte, F Mastik, MM Doyley, **SG Carlier**, FL Lupotti, EI Céspedes PW Serruys, N Bom*
BMUS Bulletin, 2000: 8(4): p 24-27

65. Application of beta-irradiation through the struts of a previously deployed stent
*G Sianos, IP Kay, **SG Carlier**, J Ligthart, AL Wardeh, VLMA Coen, PC Levendag, PW Serruys*
International Journal of Cardiovascular Interventions, 2000; 3: p 121-5

66. Intracoronary vascular brachytherapy: what have we learnt from our personal experience?
*PW Serruys, **SG Carlier**, IP Kay*
Vascular Radiotherapy Monitor, 2000; 2(3), p 97-103

67. Peripheral 'oscillatory' compliance is associated with aortic augmentation index
*P Segers, A Quasem, T De Backer, **S Carlier**, P Verdonck, A Avolio*
Hypertension, 2001; 37:1434-1439

68. LV hydraulisch vermogen, gecorrigeerd voor eind-diastolisch volume, is een maat voor LV contractiliteit. Een mathematische model studie
*P Segers, **S Carlier**, N Westerhof, J Poelaert, P Verdonck*
Tijdschrift voor Cardiologie / Journal de Cardiologie,2001 (in press)

69. Value of coronary stenotic flow velocity acceleration on the prediction of long-term improvement in functional status after angioplasty
*M Albertal, E Regar, JJ Piek, G Van Langenhove, **SG Carlier**, A Thury, G Sianos, E Boersma, B de Bruyne, C Di Mario, PW Serruys*
Am Heart J, 2001; 142:81-6

70. Flow velocity and predictors of a suboptimal coronary flow velocity reserve after balloon angioplasty
*M Albertal, E Regar, G Van Langenhove, **SG Carlier**, P Serrano, E Boersma, B de Bruyne, C Di Mario, J Piek, PW Serruys*
European Heart Journal, 2001 (in press)

71. Current management of primary pulmonary hypertension
*TLM De Backer, JP Smedema, **SG Carlier***
Biodrugs, 2001 (in press)

72. Uncomplicated moderate coronary artery dissections after balloon angioplasty: good outcome without stenting
*M Albertal, G Van Langenhove, E Regar, IP Kay, D Foley, G Sianos, K Kozuma, T Beijsterveldt, **SG Carlier**, JA Belardi, E Boersma, JE Sousa, B de Bruyne, PW Serruys*
Heart, 2001; 86:193-198

73. In vitro study of FFR, QCA and IVUS for the assessment of optimal stent deployment
*K Matthys, **SG Carlier**, P Segers, J Ligthart, G Sianos, P Serrano et al.*
Catheterization & Cardiovascular Diagnosis, 2001 (in press)

74. Morphologic and mechanic information of coronary arteries obtained by intravascular elastography: feasability study in vivo
*CL De Korte, **SG Carlier**, F Mastik, MM Doyley, AFW van der Steen, PW Serruys, K Bom*
European Heart Journal, 2001 (in press)

75. Review in depth: intravascular ultrasound elastography
***SG Carlier**, CL De Korte, E Brusseau, PW Serruys, AFW van der Steen*
Journal of Cardiovascular Risk, 2001 (in press)

Abstracts:

1. Left ventricular architecture and diastolic function in ultraendurance athletes.
*J-M Gregoire, J-L Vandenbossche, **S Carlier**, M Englert*
In: *3rd International Congress on Cardiac Doppler, Frankfurt 1989*

2. Methodologic variability of cardiac doppler measurements of peak aortic pressure gradient and peak systolic tricuspid gradient.
*J-L Vandenbossche, W Kostuki, P Decroly, E Contu, **S Carlier**, M Englert*
Acta Cardiologica, 1989, vol 44 (1), p 61
In: *9th Meeting of the Belgian Society of Cardiology, Brussels*, 1989

3. Relevance of plasma norepinephrine to assess sympathetic activity at rest and during exercise: importance of sampling site.
*I Blankoff, M Renard, **S Carlier**, M Hoylaert, R Bernard*
Acta Cardiologica, 1991, vol 46 (6), p 664-665
In: *12th Meeting of the Belgian Society of Cardiology, Brussels*, 1992

4. Alinidine to reduce dobutamine induced tachycardia in cardiac patients.
*I Blankoff, H Dereppe, Y Chami, **S Carlier**, M Renard, R Bernard*
Acta Cardiologica, 1992, vol 46 (6), p 665-666
In: *12th Meeting of the Belgian Society of Cardiology, Brussels*, 1992

5. Intravenous piroximone versus dobutamine in heart failure secondary to acute myocardial infarction.
*I Blankoff, M Renard, C Henuzet, **S Carlier**, R Bernard*
European Heart Journal, 1992, vol 13, p 256
In: *14th Congress of the European Society of Cardiology, Barcelona*, 1992

6. Influence de la méthode de mesure utilisée sur la valeur de la pression artérielle en consultation.
***S Carlier**, JC Demanet*
Archives des maladies du coeur et des vaisseaux, 1992, vol 85, p 36
In: *Société Francaise d'Hypertension Arterielle, Paris*, 1992

7. Cheyne-Stokes breathing and sleep architecture in patients with congestive heart failure.
***S Carlier**, R Sergysels, V Ninane, I Blankoff, M Renard, R Bernard*
Acta Cardiologica, 1993, vol 48, p 87-88
In: *13th Meeting of the Belgian Society of Cardiology, Brussels*, 1993

8. Intravenous piroximone versus dobutamine in heart failure secondary to acute myocardial infarction.
*I Blankoff, M Renard, **S Carlier**, Ch Henuzet, R Bernard*
Acta Cardiologica, 1993, vol 48, p 110-111
In: *13th Meeting of the Belgian Society of Cardiology, Brussels*, 1993

9. Detection of viable myocardium following acute myocardial infarction using SPECT with 99mTc labeled Mibi and 15-(ortho-123I-phenyl)-pentadecnoic acid.
***S Carlier**, P Bourgeois, M Renard, I Blankoff, R Bernard, HR Ham*
Acta Cardiologica, 1993, vol 48, p109-110
In: *13th Meeting of the Belgian Society of Cardiology, Brussels*, 1993

10. Hemodynamic adaptation to exercise in chronic heart failure patients with atrial fibrillation or sinus rhythm.
*I Blankoff, **S Carlier**, L Alvarez, M Renard, R Bernard*
European Heart Journal, 1993, vol 14, p 379
In: *15th Congress of the European Society of Cardiology, Nice*, 1993

11. Cheyne-Stokes breathing and sleep architecture in patients with congestive heart failure.
***S Carlier**, B Dachy, V Ninane, I Blankoff, M Renard, R Sergysels*
European Heart Journal, 1993, vol 14, p 374
In: *15th Congress of the European Society of Cardiology, Nice*, 1993

12. Assessment of the prediction of myocardial recovery after myocardial infarction using SPECT with 15-(ortho-123I- phenyl)-pentadecanoic acid.
***S Carlier**, P Bourgeois, L Alvarez, M Renard, I Blankoff, R Bernard, HR Ham*
European Heart Journal, 1993, vol 14, p 29
In: *15th Congress of the European Society of Cardiology, Nice*, 1993

13. Etude épidémiologique de l'hypertension artérielle à Bruxelles. Evaluation de la prise en charge des hypertendus par le corps médical sur une période de 10 ans.
***S Carlier**, JC Demanet*
Archives des Maladies du Coeur et des Vaisseaux, 1993, vol 86, p 51
In: *Société Francaise d'Hypertension Arterielle, Paris*, 1993

14. Evaluation de l'efficacité et de la tolérance de la nicardipine intraveineuse dans l'urgence hypertensive.
*Ph Robert, **S Carlier**, E Beaucarne, A Elgariani, JP Flamand, P Mols*
Archives des Maladies du Coeur et des Vaisseaux, 1993, vol 86, p 72
In: *Société Francaise d'Hypertension Arterielle, Paris*, 1993

15. The effect of night O_2 breathing on Cheyne-Stokes respiration in patient with congestive heart failure.
*R Sergysels, V Ninane, B Dachy, **S Carlier**, G Art, R Peche*
The European Respiratory Journal, 1993, Vol 6, p 392s
In: *Annual Congress of the Europan Respratory Society, Firenze*, 1993

16. Correlation between integral of power spectrum of doppler signals and flows in an in-vitro model of valvular regurgitation.
***S Carlier**, E Gailly, M Riethmuller, JL Vandenbossche*
Acta Cardiologica, 1994, vol 49 (6), p 83-84
In: *14th Meeting of the Belgian Society of Cardiology, Brussels*, 1994

17. Hemodynamic adaptation to exercise in chronic heart failure patients with atrial fibrillation or sinus rythm.
*I Blankoff, **S Carlier**, L Alvarez, M Renard, R Bernard*
Acta Cardiologica, 1994, vol 49 (6), p77
In: *14th Meeting of the Belgian Society of Cardiology, Brussels*, 1994

18. Immediate reproducibility of signal-averaged electrocardiogram and incidence of false positive or negative LA potentials in a high risk population.
*I Blankoff, **S Carlier**, L Alvarez, D Plein, B Cosyns, M Renard, R Bernard*
Acta Cardiologica, 1994, vol 49 (6), p 517
In: *14th Meeting of the Belgian Society of Cardiology, Brussels*, 1994

19. In vitro correlation between integral of power spectrum of pulsed doppler signals and flows in a model of valvular regurgitation.
***S Carlier**, E Gailly, M Riethmuller, JL Vandenbossche*
European Heart Journal, 1994, vol 15, p 518
In: *16th Congress of the European Society of Cardiology, Berlin*, 1994

20. Immediate reproducibility of signal-averaged electrocardiogram and incidence of false positive late potentials in a high risk population.
*I Blankoff, **S Carlier**, L Alvarez, D Plein, B Cosyns, M Renard, R Bernard*
European Heart Journal, 1994, vol 15, p 495
In: *16th Congress of the European Society of Cardiology, Berlin*, 1994

21. Correlation between flow and integrated power spectrum of Doppler signal in a simple in vitro model of coronary artery.
***S Carlier**, N Greenberg, P Vandervoort, JD Thomas, JL Vandenbossche*
European Heart Journal, 1995, vol 16, p 54
In: *17th Congress of the European Society of Cardiology, Amsterdam*, 1995

22. Quantification of mitral regurgitation: correlation between echocardiographic and contrast angiographic.
*C Dimmer, **S Carlier**, B Cosyns, G Van Camp, JL Vandenbossche*
Acta Cardiologica, 1996, vol 1:
In: *16th Meeting of the Belgian Society of Cardiology, Brussels*, 1996

23. Doppler derived dP/dt measurements in patients with mitral regurgitation: utility in the evaluation of left ventricular
systolic function.
*C Dimmer, **S Carlier**, B Cosyns, G Van Camp, JL Vandenbossche*
Acta Cardiologica, 1996, vol 1:
In: *16th Meeting of the Belgian Society of Cardiology, Brussels*, 1996

24. New insight into Ballistocardiography: results of an experiment in microgravity.
***S Carlier**, N Pettiaux, D Padeken, H Hamacher, K Prisk, M Paiva*
Acta Cardiologica, 1996, vol 1:
In: *16th Meeting of the Belgian Society of Cardiology, Brussels*, 1996

25. First in vitro study for the evaluation of the Automated Cardiac Output Measurement system for prosthetic mitral valve flow
*P Verdonck, G Van Camp, **S Carlier**, P Segers*
In: *8th International Postgraduate Course on Advances in Cardiac Ultrasound, Davos*, 1996

26. Automatic dP/dt estimation from doppler spectra of mitral regurgitation for the assessment of myocardial systolic function and reserve.
S Carlier, C. Dimmer, P. Verdonck, G. Van Camp, B. Cosyns, J.L. Vandenbossche
European Heart Journal, 1996, vol
In: *18th Congress of the European Society of Cardiology, Birmingham*, 1996

27. Comparison of aortic and pulmonary flow in children, measured with the automatic cardiac output method.
*G Van Camp, M Menassel, D Plein, A Farhati, Y Bouhdid, B Cosyns, **S Carlier**, JL Vandenbossche*
Circulation, 1996, 94:8, p I-491
In: *69th Scientific Sessions of the American Heart Association, New Orleans*, 1996

28. Assessment of the optimal atrioventricular delay in dual chamber pacing by a new color Doppler automated method.
*G Van Camp, F Delhaye, Y Bouhdid, **S Carlier**, M Menassel, D Plein, JL Vandenbossche*
Acta Cardiologica, 1996, 6: p 566
In: *17th Meeting of the Belgian Society of Cardiology, Brussels*, 1997

29. A new method for the evaluation of the severity of mitral regurgitation
S Carlier, G Van Camp, B Cosyns, M Menassel, D Plein, Y Bouhdid, JL Vandenbossche
Acta Cardiologica, 1996, 6: p 576
In: *17th Meeting of the Belgian Society of Cardiology, Brussels*, 1997

30. Automated cardiac output measurement using color Doppler velocity profiles obtained with the multibeam Doppler method: in vivo validation in the intensive care unit.
*G Van Camp, M Menassel, D Plein, Y Bouhdid, B Cosyns, **S Carlier**, JL Vandenbossche*
Acta Cardiologica, 1996, 6: p 597
In: *17th Meeting of the Belgian Society of Cardiology, Brussels*, 1997

31. Clinical relevance of abnormal echoes at transesophageal echocardiography early after valve replacement: a two years follow-up study.
*B Cosyns, A Farhati, G Van Camp, M Derluyn, A Brunet, **S Carlier**, JL Vandenbossche*
Acta Cardiologica, 1996, 6: p 597
In: *17th Meeting of the Belgian Society of Cardiology, Brussels*, 1997

32. Assessment of mitral regurgitation severity with ACM
S Carlier, G Van Camp, B Cosyns, P Verdonck, P Segers, M Menassel, D Plein, Y Bouhdid, JL Vandenbossche
The Thoraxcentre Journal, 1997:June, p 14
In: *12th Symposium on Echocardiology, Rotterdam*, 1997

33. Flow estimation using intravascular imaging catheter
*AFW van der Steen, W Li, EI Céspedes, **S Carlier**, CT Lancée, PD Verdouw, PW Serruys, N Bom*
The Thoraxcentre Journal, 1997:June, p 10
In: *12th Symposium on Echocardiology, Rotterdam*, 1997

34. Principles of intravascular velocity imaging and quantitative flow measurements
*EI Céspedes, W Li, AFW van der Steen, **S Carlier**, CT Lancée, N Bom, PD Verdouw, PW Serruys*
The Thoraxcentre Journal, 1997:June, p 14
In: *12th Symposium on Echocardiology, Rotterdam*, 1997

35. Improvement of coronary flow studies by the acquisition of raw Doppler signals and the use of echocontrast enhancement.
***S Carlier**, P Frinking, R Krams, E Gailly, PW Serruys*
European Heart Journal, 1997:18, p 151
In: *19th Congress of the European Society of Cardiology, Stockholm*, 1997

36. Assessment of stroke volume changes during dobutamine-atropine stress echocardiography using three different non-invasive methods: ACM, Finapress model flow and biplane discs method.
*D Poldermans, R Rambaldi, WJW Bos, E Boersma, W Vletter, **S Carlier**, JRTC Roelandt*
European Heart Journal, 1997:18, p 211
In: *19th Congress of the European Society of Cardiology, Stockholm*, 1997

37. New intracoronary volumetric blood flow measurement method with intravascular ultrasound: in-vitro assessment and first in vivo results.
***S Carlier**, W Li, F Mastik, J Honkoop, AFW van der Steen, CT Lancée, S de Zeeuw, R van Bremen, EI Céspedes, PW Serruys, N Bom*
European Heart Journal, 1997:18, p 376
In: *19th Congress of the European Society of Cardiology, Stockholm*, 1997

38. Intravascular ultrasound blood flowmetry and velocity imaging: preliminary experience in vivo
*EI Céspedes, **S Carlier**, W Li, AFW van der Steen, JR van Meegen, PW Serruys, N Bom*
Ultrasound in Medicine and Biology, 1997:23 (Suppl 1), p S71
In: *8th Congress of the World Federation for Ultrasound in Medicine & Biology, Buenos Aires* 97

39. Intravascular power flow imaging: initial experience in-vitro and in-vivo
*EI Céspedes, F Mastik, W Li, **S Carlier**, AFW van der Steen, M Eberle, PW Serruys*
Ultrasound in Medicine and Biology, 1997:23 (Suppl 1), p S71
In: *8th Congress of the World Federation for Ultrasound in Medicine & Biology, Buenos Aires* 97

40. Quantification of mitral regurgitation by the automated cardiac output method: in-vitro and in-vivo evaluation.
***S Carlier**, G Van Camp, B Cosyns, D Plein, M Menassel, T Josse, P Verdonck, P Segers, JL Vandenbossche*
Circulation, 1997;96(8):I-471
In: *70th Scientific Sessions of the American Heart Association, Orlando*, 1997

41. In-vivo validation of a new intracoronary volumetric blood flow measurement method with intravascular ultrasound
***S Carlier**, EI Céspedes, W Li, AFW van der Steen, JR van Meegen, F Mastik, J Honkoop, PW Serruys, N Bom*
Circulation, 1997;96(8):I-703
In: *70th Scientific Sessions of the American Heart Association, Orlando*, 1997

42. New intracoronary volumetric blood flow measurement method with intravascular ultrasound: in-vivo validation and preliminary clinical experience
S Carlier, EI Céspedes, W Li, AFW van der Steen, JR van Meegen, K Blom, PW Serruys
Acta Cardiologica, 1997; 52(6): p 544-5
In: *18th Meeting of the Belgian Society of Cardiology, Brussels*, 1998

43. Intracoronary brachytherapy: gamma and beta source dosimetry and dose-volume histograms from intravascular ultrasound.
JPA Marijnissen, PC Levendag, V Coen, AG Visser, S Carlier, J Ligthart, PW Serruys
Cardiovascular Radiation Therapy II, 1998, p 29
In: *Cardiovascular Radiation Therapy II, Washington DC*, 1998

44. Evaluation du flux endocoronaire en cardiologie interventionnelle
S Carlier
Revue Medicale de Bruxelles, 1998, 19 (2): p 97-98
In: *Journée de Cardiologie de l'ULB, Limellette*, 1997

45. Assessment of left ventricular contractile reserve by simultaneous acquisition of echo-Doppler and tonometric
recordings at rest and at peak exercise.
S Carlier, G Armstrong, RA Borden, N Greenberg, TH Marwick, JD Thomas
Journal of the American College of Cardiology, 1998; p 283A
In: *47th Annual Scientific Session of the American College of Cardiology, Atlanta*, 1998

46. Cardiac power can be readily estimated: validation of a simple index.
G Armstrong, K Fukamuchi, S Carlier, L Cardon, JD Thomas, TH Marwick
Journal of the American College of Cardiology, 1998; p 56A
In: *47th Annual Scientific Session of the American College of Cardiology, Atlanta*, 1998

47. Cardiac power reserve: a novel simple index correlates with VO_2
G Armstrong, S Carlier, R Borden, TH Marwick
Journal of the American College of Cardiology, 1998; p 256A
In: *47th Annual Scientific Session of the American College of Cardiology, Atlanta*, 1998

48. The Pulse Pressure Method versus the area method: non-invasive in vivo validation
S Carlier, P Segers, G Armstrong, N Stergiopoulos, P Verdonck, JD Thomas
Journal of Cardiovascular Diagnosis and Procedures, 1998, vol 15 (2): p 149
In: *XIII Congress of the Cardiovascular System Dynamics Society, Gent*, 1998

49. Coronary flow assessment using intravascular ultrasound: method and initial experience in the catheterization laboratory
EI Cespédes, S Carlier, F Mastik, W Li, AFW van der Steen, PW Serruys, M Eberle, N Bom
Houston Society for Engineering in Medicine and Biology, 1998, p 168
In: *16th Annual Houston Conference on Biomedical Engineering Research, Houston*, 1998

50. Assessment of stiffness and elevated mechanical stress in atherosclerotic plaques by intravascular ultrasound: in vitro experience.
CL de Korte, EI Céspedes, S Carlier, AFW van der Steen, G Pasterkamp, D Thompson, JD Thomas, N Bom, PW Serruys
European Heart Journal, 1998:19, p 620
In: *20th Congress of the European Society of Cardiology, Vienna*, 1998

51. The use of dose-volume histograms based on quantitative intravascular ultrasound imaging in intra coronary brachytherapy.
*JPA Marijnissen, AG Visser, VLMA Coen, WJ van der Giessen, **S Carlier**, M Sabate, J Ligthart, PC Levendag, PW Serruys*
European Heart Journal, 1998:19, p 620
In: *20th Congress of the European Society of Cardiology, Vienna*, 1998

52. A new intracoronary measurement catheter, Metricath, compared to IVUS and QCA in a stented porcine coronary model.
*WJ vander Giessen, SC Krabbendam, HMM van Beusekom, DF Foley, PW Serruys, PD Verdouw, **S Carlier**, H Boersma, R Wolthuis*
European Heart Journal, 1998:19, p 390
In: *20th Congress of the European Society of Cardiology, Vienna*, 1998

53. Initial clinical experience with a volumetric coronary blood flow assessment method based on conventional intravascular ultrasound imaging catheters
***S Carlier**, EI Céspedes, W Li, F Mastik, J Honkoop, AFW van der Steen, CT Lancée, N Bom, PW Serruys*
European Heart Journal, 1998:19, p 390
In: *20th Congress of the European Society of Cardiology, Vienna*, 1998

54. Evaluation of Intracoronary Radiation Therapy Based on Dose-Volume Histograms Derived from 3-D Quantitative Intravascular Ultrasound
***S Carlier**, JPA Marijnissen, V Coen, M Sabate, A den Boer, W van der Giessen, PC Levendag*
Circulation, 1998
In: *71th Scientific Sessions of the American Heart Association, Dallas*, 1998

55. Clinical Validation of a Simplified Index of Left Ventricular Peak Power.
***S Carlier**, G Armstrong, R Borden*
Circulation, 1998
In: *71th Scientific Sessions of the American Heart Association, Dallas*, 1998

56. Coronary Blood Flow Imaging and Volume Flow Quantitation with a Intravascular Ultrasound Imaging Catheter: Initial Clinical Experience.
***S Carlier**, EI Céspedes, W Li, F Mastik, AFW van der Steen, N Bom, PW Serruys*
Circulation, 1998
In: *71th Scientific Sessions of the American Heart Association, Dallas*, 1998

57. Intravascular ultrasound flow quantification and imaging using an array catheter
*EI Céspedes, F Mastik, W Li, **S Carlier**, J Honkoop, AFW. van der Steen, PW Serruys, N Bom*
Ultrasonic Imaging 1998; 20: p 44

58. The pulse pressure method: a new golden standard for arterial compliance estimation?
***S Carlier**, A Pasquet, P Segers*
Acta Cardiologica; 1998:293
In: *Joint Scientific Meeting of the Dutch and Belgian Society of Hypertension. Mondorf*, 1998

59. Dosimetry by IVUS – is it feasible.
S Carlier
Cardiovascular Radiation Therapy III, 1999, p 91-2
In: *Cardiovascular Radiation Therapy III, Washington DC*, 1999

60. Relationship between myocardial viability at dobutamine echocardiography and late potentials early after acute myocardial infarction
*E Akseki, B Cosyns, I Liebens, D Plein, T Mnif, T Josse, G Van Camp, S **Carlier**, JL Vandenbossche*
Journal of the American College of Cardiology, 1999; 1178-108
In: *48th Annual Scientific Session of the American College of Cardiology, New Orleans*, 1999

61. IVUS elasticity imaging and quantitative flow
*AFW van der Steen, **SG Carlier**, CL de Korte, F Mastik, FL Lupotti, MM Doyley, CT Lancée, EI Céspedes, W Li, PW Serruys, N Bom*
In: *13th Rotterdam Symposium on Echocardiology, Rotterdam, The Netherlands* 1999

62. A higher average shear stress is paradoxically predictive of restenosis and/or MACE after balloon angioplasty in human coronary arteries
*G Van Langenhove, **S Carlier**, M Albertal, E Boersma, PW Serruys*
European Heart Journal, 1999, vol 20 (abst suppl): p 507
In: *21th Congress of the European Society of Cardiology, Barcelona*, 1999

63. DEBATE II: analysis of the flow velocity profile in the stented and non-stented, optimal and suboptimal groups
*M Albertal, G Van Langenhove, P Serrano, **SG Carlier**, M Costal, J Guermonprez, P Schoefield, E Verna, J Belardi, PW Serruys*
European Heart Journal, 1999, vol 20 (abst suppl): p 372
In: *21th Congress of the European Society of Cardiology, Barcelona*, 1999

64. Dose volume histograms offer new insights into the IVUS and angiographic follow-up after coronary brachytherapy
***S Carlier**, JPA Marijnissen, M Sabate, VLMA Coen, A Wardeh, W van der Giessen, PC Levendag, PW Serruys*
European Heart Journal, 1999, vol 20 (abst suppl): p 407
In: *21th Congress of the European Society of Cardiology, Barcelona*, 1999

65. In vivo assessment of instantaneous wall shear stress with the IVUS flow method
***S Carlier**, G Van Langenhove, F Mastik, R Krams, EI Cespedes, AFW van der Steen, K Bom, PW Serruys*
European Heart Journal, 1999, vol 20 (abst suppl): p 406
In: *21th Congress of the European Society of Cardiology, Barcelona*, 1999

66. Persisting coronary dissection after intracoronary beta-radiation
*Kay IP, Sabate M, **Carlier SG**, Gijzel AL, M Albertal, Wardeh AJ, van der Giessen W, Coen VL, Levendag PC, de Feyter PJ, Serruys PW*
European Heart Journal, 1999, vol 20 (abst suppl): p 407
In: *21th Congress of the European Society of Cardiology, Barcelona*, 1999

67. Predictors of coronary flow reserve before and after balloon angioplasty
*M Albertal, G Van Langenhove, P Serrano, **SG Carlier**, M Costa, RT van Domburg, C Di Mario, E Verna, C Hanet, PW Serruys*
European Heart Journal, 1999, vol 20 (abst suppl): p 490
In: *21th Congress of the European Society of Cardiology, Barcelona*, 1999

68. Regional analysis of dosimetry and volumetric morphological changes in coronary segments treated with beta-radiation following successful balloon angioplasty
*Sabate M, Marijnissen JP, **Carlier SG**, Kay IP, van der Giessen WJ, Coen VL, Ligthart JM, den Boer A, Levendag PC, Serruys PW*
European Heart Journal, 1999, vol 20 (abst suppl): p 490
In: *21th Congress of the European Society of Cardiology, Barcelona*, 1999

69. Late loss after coronary brachytherapy is minimal when 90% of coronary media receives more than 4 Gray
***S Carlier**, I Crocker, M Sabate, D Meerkin, T Fox, V Coen, J Marijnissens, A Arsenault, J Ligthart, W van der Giessen, P Levendag, R Bonan, PW Serruys*
In: *European Society for Therapeutic Radiology and Oncology, Brussels*, 1999

70. Intravascular ultrasound elastography: preliminary clinical experience
*CL de Korte, **SG Carlier**, F Mastik, AFW van der Steen, EI Céspedes, N Bom*
Circulation, 1999; 100(18): I-229
In: *72th Scientific Sessions of the American Heart Association, Atlanta*, 1999

71. Correlation between dose deposited to the vessel wall and outcomes following intracoronary beta-radiation
***S Carlier**, I Crocker, M Sabate, D Meerkin, T Fox, V Coen, J Marijnissens, A Arsenault, W van der Giessen, P Levendag, R Bonan, PW Serruys*
Circulation, 1999; 100(18):I-516
In: *72th Scientific Sessions of the American Heart Association, Atlanta*, 1999

72. Debate II: a randomized comparison of cost-effectiveness of primary versus provisional stenting
*B De Bruyne, PW Serruys, **S Carlier**, B van Hout, JM van Sonsbeek, O Gurne, NHJ Pijls, JA Belardi, JL Guermonprez, P Schofield, CDJ Ilsley, GJ Laarman*
Circulation, 1999; 100(18): I-790
In: *72th Scientific Sessions of the American Heart Association, Atlanta*, 1999

73. Regional analysis of dosimetry and volumetric morphological changes in coronary segments treated with beta-radiation following successful balloon angioplasty
*Sabate M, Marijnissen JP, **Carlier SG**, Kay IP, van der Giessen WJ, Coen VL, Ligthart JM, A den Boer, Levendag PC, Serruys PW*
Circulation, 1999; 100(18):I-516
In: *72th Scientific Sessions of the American Heart Association, Atlanta*, 1999

74. Dose volume histograms determined by IVUS
SG Carlier
Cardiovascular Radiation Therapy IV, 2000, p 116
In: *Cardiovascular Radiation Therapy IV, Washington DC*, 2000

75. Novel intravascular imaging
*AFW van der Steen, TG van Leeuwen, A van der Laarse, SWE van der Poll, CL de Korte, MM Doyley, F Mastik, FL Lupotti, **SG Carlier**, FJ van der Meer, DJ Faber, J Perree*
In: *Arterial remodeling, Amsterdam* 2000

76. Combined morphological and mechanical assessment of plaques with IVUS Elastography: Validation and preliminary experiments in vivo
CL de Korte, AFW van der Steen, ***SG Carlier****, F Mastik, MM Doyley, G Pasterkamp, PW Serruys, N Bom*
In: *Arterial remodeling, Amsterdam* 2000

77. Value of postprocedural stenotic flow velocity acceleration in the invasive prediction of restenosis after coronary angioplasty
M Albertal, ***SG Carlier****, G Van Langenhove, E Regar, A Thury, G Sianos, PW Serruys*
European Heart Journal, 2000, vol 21 (abst suppl): p 34
In: *22th Congress of the European Society of Cardiology, Amsterdam*, 2000

78. Assessment of dose-effect relationship of intracoronary brachytherapy by the marginal loss/gain coefficient
SG Carlier*, V de Valk, T Fox, I Crocker, M Sabate, D Meerkin, A Arsenault, V Coen, R Bonan, PW Serruys*
European Heart Journal, 2000, vol 21 (abst suppl): p 34
In: *22th Congress of the European Society of Cardiology, Amsterdam*, 2000

79. Assessment of the determinants of maximal and total left ventricular power based on a computerized heart-arterial model
P Segers, ***S Carlier****, N Westerhof, P Verdonck*
European Heart Journal, 2000; vol 21 (abst suppl): p 62
In: *22th Congress of the European Society of Cardiology, Amsterdam*, 2000

80. Geographical miss: a cause of treatment failure after catheter based intracoronary beta-radiation therapy using the BetaCath 90Sr/Y system
G Sianos, IP Kay, M Costa, MA Morel, ***SG Carlier****, J Ligthart, A Wardeh, M Albertal, R Bonan, PW Serruys*
European Heart Journal, 2000; vol 21 (abst suppl): p 401
In: *22th Congress of the European Society of Cardiology, Amsterdam*, 2000

81. Intracoronary blood flow velocity analysis of optimal balloon angioplasty versus stent implantation: a subanalysis of the DEBATE II trial
JJ Piek, M Albertal, E Boersma, B de Bruyne, ***S Carlier****, JE Sousa, T Muramatsu, C Vrints, M Meuwissen, PW Serruys*
European Heart Journal, 2000; vol 21 (abst suppl): p 35
In: *22th Congress of the European Society of Cardiology, Amsterdam*, 2000

82. In vitro study of FFR, QCA and IVUS for the assessment of optimal stent deployment
P Segers, ***S Carlier****, K Matthys, J Ligthart, G Sianos, P Serrano, P Verdonck, PW Serruys*
European Journal of Heart Failure, 2000; 2(2): p 112-113
In: *Heart Failure 2000 meeting, Venice*, 2000

83. Determinants of maximal and total left ventricular power : a mathematical model study
P Segers, ***S Carlier****, N Westerhof, P Verdonck*
BME, 2000; p 9
In: *2nd European Symposium in BME and MP, Patras*, 2000.

84. Individualizing the aorto-radial pressure transfer function: feasibility of a model-based approach
*P Segers, **S Carlier**, A Pasquet, SI Rabben, LR Hellevik, E Remme, T De Backer, J De Sutter, JD Thomas, P Verdonck*
Heart and Vessels, 2000; S13: p 44

85. In vitro study of FFR, QCA and IVUS for the assessment of optimal stent deployment
*P Segers, **S Carlier**, K Matthys, J Ligthart, G Sianos, P Serrano, P Verdonck, PW Serruys*
Circulation, 2000; 102(18): p II-365.
In: *73th Scientific Sessions of the American Heart Association, New Orleans*, 2000

86. Is the low-dose radiation deleterious in catheter-based beta-radiation therapy? A result from dose-volume histogram and 3-dimensional volumetric analysis.
*K Kozuma, M Costa, M Sabate, JPA Marijnissen, IP Kay, WJ van der Giessen, E Regar, **SG Carlier**, VLMA Coen,*
J Ligthart, PC Levendag, PW Serruys
Circulation, 2000; 102(18): p II-752.
In: *73th Scientific Sessions of the American Heart Association, New Orleans*, 2000

87. The dose-effect of intracoronary beta-brachytherapy on in-stent neointimal hyperplasia inhibition.
***SG Carlier**, A Hassan, K Kozuma, M Costa, DP Lee, H Okura, VLMA Coen, PC Levendag, PJ Fitzgerald, PW Serruys*
Circulation, 2000; 102(18): p II-569.
In: *73th Scientific Sessions of the American Heart Association, New Orleans*, 2000

88. Individialilzing the aorto-radial pressure transfer function
*P Segers, **S Carlier**, T De Backer, J De Sutter, JD Thomas, P Verdonck*
International Angiology, 2000; 19, p 108

89. The pulse pressure method for non-invasive evaluation of total arterial compliance
***S Carlier**, P Segers, T De Backer, N Stergiopulos, JD Thomas*
Journal of Hypertension, 2000; 18(supp 4): p S197
In: *18th Scientific meeting of the International Society of Hypertension, Chicago*, August 20 -24, 2000

90. Individualizing the aorto-radial pressure transfer function: feasibility of a model-based approach
*P Segers, **S Carlier**, A Pasquet, SI Rabben, LR Hellevik, E Remme, T De Backer, J De Sutter, JD Thomas, P Verdonck*
In: *Cardiovascular System Dynamics Society, Baltimore*, 2000

91. High shear stress after successful balloon angioplasty is associated with restenosis and target lesion revascularization
*A Thury, G van Langenhove, **SG Carlier**, M Albertal, K Kozuma, E Regar, JJ Wentzel, R Krams, CJ Slager, JJ Piek, PW Serruys*
J Am Coll Cardiol 2001; 37(2) Suppl A, p 16A
In: *50th Annual Scientific Session of the American College of Cardiology*

92. Intracoronary blood flow velocity analysis of suboptimal balloon angioplasty versus stent implantation: a subanalysis of the DEBATE-II trial
*JJ Piek, M Voskuil, M Albertal, E Boersma, B de Bruyne, S **Carlier**, JE Sousa, T Muramatsu, C Vrints, M Meuwissen, S Chamuleau, PW Serruys*
J Am Coll Cardiol 2001; 37(2) Suppl A, p 21A
In: *50th Annual Scientific Session of the American College of Cardiology*

93. Geographical miss: impact on the restenosis rate in relation to the type of injury. Insights from the beta radiation in Europe (BRIE) study
*G Sianos, M Costa, K Kozuma, PI Kay, **SG Carlier**, MA Morel, PW Serruys*
J Am Coll Cardiol 2001; 37(2) Suppl A, p 29A
In: *50th Annual Scientific Session of the American College of Cardiology*

94. Initial experience with intravascular sonotherapy for prevention of in-stent restenosis: safety and feasibility
*A Thury, G Sianos, K Kozuma, AMH Knook, AJ Wardeh, E Regar, **SG Carlier**, WJ van der Giessen, DP Foley, PW Serruys*
J Am Coll Cardiol 2001; 37(2) Suppl A, p 85A
In: *50th Annual Scientific Session of the American College of Cardiology*

95. In vitro validation of coronary flow reserve measurement with a array IVUS transducer.
***SG Carlier**, F Lupotti, F Mastik, T van der Steen, K Bom, PW Serruys*
European Heart Journal, 2001 (in press)
In: *23th Congress of the European Society of Cardiology, Stockholm*, 2001

96. An increased wall shear stress inhibits neointimal hyperplasia after stent implantation: preliminary in vivo experience of the ARED flow divider in a rabbit model of restenosis.
***SG Carlier**, LCA van Damme, CP Blommerde, G. van Langenhove, JJ Wentzel, PD Verdouw, CJ Slager, R Krams, PW Serruys*
European Heart Journal, 2001 (in press)
In: *23th Congress of the European Society of Cardiology, Stockholm*, 2001

97. Stenting of bifurcational coronary lesions: results of the multicentric European culottes registry.
***SG Carlier**, A Colombo, I De Scheerder, B Reimers, W Rutsch, K Dawkins, H Surryapranata, V Legrand, C Macaya, PW Serruys*
European Heart Journal, 2001 (in press)
In: *23th Congress of the European Society of Cardiology, Stockholm*, 2001

98. Three dimensional palpography: a new tool for detection of vulnerable plaque, a feasibility and reproducibility in vitro.
*J Schaar, F Mastik, C De Korte, MM Doyley, S **Carlier**, N Bom, PW Serruys, T van der Steen*
European Heart Journal, 2001 (in press)

Book Chapters:

1. Cardiovascular flow measurements with IVUS
N Bom, W Li, **S Carlier**, EI Céspedes, AFW van der Steen
JHC Reiber and EE van der Wall (eds), What's new in Cardiovascular Imaging, 1998; p 149-58

2. Intracoronary Doppler and Pressure Monitoring
S Carlier, C di Mario, M Kern, PW Serruys
E Topol (ed), Textbook of Interventional Cardiology, 1998, p 748-781

3. Foreword
PW Serruys, **SG Carlier**
R Bonan and R Waksman (eds),Vascular Brachytherapy: State of the Art, 1999; p 1-3

4. The Scope of the Problem of Vascular Restenosis
PW Serruys, **SG Carlier**
PC Levendag (ed), Vascular Brachytherapy: New Perspectives, 1999, p 4-7

5. IVUS based dosimetry
SG Carlier, T. Fox, I. Crocker, P.C. Levendag, P.W. Serruys
R Waksman (ed), Vascular Brachytherapy, 2001 (in press)

6. Technical aspects of intravascular imaging
N Bom, AFW van der Steen, N Bruining, C L de Korte, **SG Carlier**, CT Lancee
P Lanzer (ed), Theory and Practice of Vascular Medicine (in press)